THE MOLECULAR PATHOGENESIS AND DIAGNOSIS OF PHAEOCHROMOCYTOMA: ROLES FOR PRIMARY CILIA AND ADRENAL VENOUS SAMPLING?

Samuel Matthew O'Toole

A thesis submitted in partial fulfilment of the requirements of the degree of Doctor of Philosophy

April 2019

Queen Mary University of London

Mile End Road

E1 4NS

London

UK

Statement of originality

I, Samuel Matthew O'Toole, confirm that the research included within this thesis is my own work or that where it has been carried out in collaboration with, or supported by others, that this is duly acknowledged below and my contribution indicated. Previously published material is also acknowledged below.

I attest that I have exercised reasonable care to ensure that the work is original, and does not to the best of my knowledge break any UK law, infringe any third party's copyright or other Intellectual Property Right, or contain any confidential material.

I accept that the College has the right to use plagiarism detection software to check the electronic version of the thesis.

I confirm that this thesis has not been previously submitted for the award of a degree by this or any other university.

Date: 28th April 2019

Details of collaboration and publications:
RNA sequencing was performed at The Barts and The London Genome Centre and its analysis was conducted in collaboration with David Watson.

Oncometabolite induced primary cilia loss in pheochromocytoma. O'Toole SM, Watson DS, Novoselova TV, Romano LEL, King PJ, Bradshaw TY, Thompson CL, Knight MM, Sharp TV, Barnes MR, Srirangalingam U, Drake WM, Chapple JP. Endocrine Related Cancer 2019; 26(1): 165-180.

Adrenal Vein Catecholamine Levels and Ratios: Reference Intervals Derived from Patients with Primary Aldosteronism. Sze CWC*, O'Toole SM*, Tirador RK, Akker SA, Matson M, Perry L, Druce MR, Dekkers T, Deinum J, Lenders JWM, Eisenhofer G, Drake WM. Hormone and Metabolic Research 2017; 49(6): 418-423.

Abstract

Primary cilia are microtubule-based cellular organelles that project into the extracellular space. They subserve a wide range of sensory stimuli, co-ordinate and modulate a number of signalling pathways and are intrinsically linked to the cell cycle and its progression. Cilia loss is frequently observed in tumours; yet, the responsible mechanisms and consequences for tumourigenesis remain unclear.

The aim of this thesis is to examine the role of primary cilia in the pathogenesis of phaeochromocytomas (life-threatening catecholamine-producing neuroendocrine tumours of the adrenal medulla).

We demonstrate that primary cilia are lost in phaeochromocytomas compared to adjacent non-cancerous tissue. These structural changes are associated with transcriptional alterations within cilia-mediated signaling pathways that are associated with tumorigenesis generally and phaeochromocytomas specifically. Importantly, cilia loss is most dramatic in patients with germline mutations in the pseudohypoxia-linked genes *SDHx* and *VHL*.

Using a phaeochromocytoma-derived cell line, we show that hypoxia and oncometabolite-induced pseudohypoxia are key drivers of cilia loss and identify that this is dependent on activation of the Aurora-A/HDAC6 cilia resorption pathway. We also show that cilia loss drives transcriptional changes associated with proliferation and tumourigenesis.

Our data provide evidence for primary cilia dysfunction contributing to phaeochromocytoma pathogenesis through a hypoxic/pseudohypoxic mechanism and implicate oncometabolites as ciliary regulators. These findings have relevance beyond phaeochromocytomas as hypoxia is a general feature of the tumour microenvironment and the resultant ciliary resorption can be pharmacologically inhibited, suggesting a potential therapeutic target.

Further studies demonstrate that additional features of the phaeochromocytoma microenvironment, namely catecholamines, also impact on primary cilia expanding our understanding of the role of this organelle.

Finally, we provide normative reference intervals for adrenal venous catecholamines facilitating accurate diagnosis of phaeochromocytomas for use in situations where localisation cannot be reliably achieved by standard imaging approaches alone.

Acknowledgements

First and foremost, my thanks go to all the patients who consented to their tissue use and without whom this project would not have been possible. I am similarly indebted to Barts Charity for their generous funding of my Clinical Research Training Fellowship (MRD0191).

I would like to thank my supervisors Profs Paul Chapple, Tyson Sharp and William Drake for their continued support, education and patience. My particular thanks to Paul for hosting me and making me so welcome in the unfamiliar settings of the lab and to Professor Drake for his ongoing clinical mentorship.

My gratitude goes to everyone at the Centre for Endocrinology who helped make these three years fly by. It is impossible to name everyone who contributed to my time there but especial thanks goes to the members of the Chapple group past and present (Suran, Teisha, Emma and Lisa) as well as Sri who introduced me to Paul and VHL.

It goes without saying that without the support of my friends and family I would not have been able to do this and I am eternally grateful to them. It is a great regret to me that my father was not able to see the completion of this project. He was an advocate for scholarship and free thought and I hope he would have liked to read the completed work.

Last, but never least, my thanks to Helen, who perhaps more than anyone else has witnessed the evolution of this thesis and has been at my side every step of the way, always with a helpful word, particularly when punctuation was involved.

Table of contents

Table of figures

Table of tables

List of abbreviations

3-MT	3-methoxytyramine
AC	Adenylyl cyclase
ACTH	Adrenocorticotropic hormone
ADPKD	Autosomal dominant polycystic kidney disease
APC	Anaphase-promoting complex
Arl13b	ADP-ribosylation factor-like protein 13B
ATRX	Alpha thalassemia/mental retardation syndrome
ANOVA	Analysis of variance
ASC	Adipose-derived mesenchymal stem cells
AURKA	Aurora kinase A
AVS	Adrenal venous sampling
BMSC	Bone marrow-derived mesenchymal stem cells
BSA	Bovine serum albumin
CALK	Chlamydomonas aurora-like protein kinase
cAMP	Cyclic adenosine monophosphate
CCHD	Cyanotic congenital heart disease
ccRCC	Clear cell renal cell carcinoma
CCRK	Cell cycle-related kinase
CDKN2C	Cyclin dependent kinase inhibitor 2C
cDNA	Complementary DNA
Cep164	Centrosomal protein 164
CHD	Congenital heart disease
CK1ε	Casein kinase 1 isoform epsilon
CNS	Central nervous system
CSDE1	Cold-shock domain-containing E1
CSM	Cell surface membrane
CT	Computed tomography
CVD	Cyclophosphamide, vincristine and dacarbazine
DAG	Diacylglycerol
DAPI	4’,6-diamidino-2-phenylindole dihydrochloride
DBH	Dopamine beta-hydroxylase
Dhh	Desert hedgehog
DMEM	Dulbecco’s Minimum Eagle Medium
DMOG	Dimethyloxalylglycine, N-(methoxyoxoacetyl)-glycine methyl ester
DMSO	Dimethyl sulfoxide
DNA	Deoxyribonucleic acid
dsDNA	Double stranded DNA
Dvl	Dishevelled
EDA	Exploratory data analysis
EDTA	Ethylenediaminetetraacetic acid
ELST	Endolymphatic sac tumour
EM	Electron microscopy
EMT	Epithelial-to-mesenchymal transition

ER	Endoplasmic reticulum or oestrogen receptor
ERK (MAPK)	Extracellular signal-regulated kinase
ETC	Electron transport chain
F-12K	Kaighn's modification of Ham's F-12 medium
FBS	Foetal bovine serum
FDG	Fluorodeoxyglucose
F-DOPA	Fluorodopa
FGFR	Fibroblast growth factor receptor
FH	Fumarate hydratase
GAP	GTPase-activating protein
GAPDH	Glyceraldehyde 3-phosphate dehydrogenase
GAPP	Grading of Adrenal Phaeochromocytoma and Paraganglioma
GBM	Glioblastoma multiforme
GIST	Gastrointestinal stromal tumour
Gli	Glioma associated oncogene protein
GO	Gene ontology
GPCR	G-protein coupled receptor
GSK3β	Glycogen synthase kinase-3β
GTP	Guanosine triphosphate
H&E	Haemotoxylin and eosin
HB	Haemangioblastoma
HDAC	Histone deacetylase
HEF1	Human enhancer of filamentation 1
HIF	Hypoxia inducible factor
HIF-PHD	HIF-prolyl hydroxylase
HLRCC	Hereditary leiomyomatosis and renal cell cancer
HNPGL	Head and neck paraganglioma
HRE	Hypoxia response element
Hsp90	Heat shock protein 90
ICC	Immunocytochemistry
ICK	Intestinal cell kinase
IDH	Isocitrate dehydrogenase
IF	Immunofluorescence
IFT	Intraflagellar transport
IFT#	Intraflagellar transport protein <number>
IGF-1R	Insulin-like growth factor 1 receptor
IHC	Immunohistochemistry
Ihh	Indian hedgehog
INPP5E	Inositol polyphosphate 5-phosphatase
IP3	Inositol trisphosphate
IPA	Ingenuity Pathway Analysis
IVC	Inferior vena cava
KIF	Kinesin family member
L-DOPA	L-3,4-dihydroxyphenylalanine
LOH	Loss of heterozygosity

LPA	Lysophosphatidic acid
MAPK (ERK)	Mitogen activated protein kinase
MAD	MAX dimerisation protein
MAML3	Mastermind-like transcriptional coactivator 3
MAX	Myc-associated factor X
MDH	Malate dehydrogenase
MEK	Mitogen-activated protein kinase kinase
MEN2	Multiple Endocrine Neoplasia
MGMT	O^6-alkylguanine DNA methyltransferase
MIBG	Metaiodobenzylguanidine
MIP	Maximum intensity projection
MMF	Monomethyl fumarate
MN	Metanephrine
MPC	Mouse phaeochromocytoma cell line
MRI	Magnetic resonance imaging
MTC	Medullary thyroid cancer
MTT	Mouse tumour tissue cell line
mTOR	Mammalian target of rapamycin
mTORC	Mammalian target of rapamycin complex
MXI	MAX-interacting protein
NEK	NIMA-related kinase
NET	Neuroendocrine tumour
NF1	Neurofibromatosis type 1, neurofibromin 1
NGS	Normal goat serum
NIH	National Institute of Health
NIMA	Never in mitosis gene A
NMN	Normetanephrine
NudE	Nuclear distribution gene E
OCT	Optimal cutting temperature
OMIM	Online Mendelian inheritance in man
PASS	Phaeochromocytoma of the Adrenal Scaled Score
PET	Positron emission tomography
PA	Primary aldosteronism
PBS	Phosphate buffered saline
PBST	Phosphate buffered saline with 0.1% Tween 20
PC12	Phaeochromocytoma 12 cell line
PCA	Principal component analysis
PCP	Planar cell polarity
PCR	Polymerase chain reaction
PDGFRα	Platelet-derived growth factor alpha
PIP_2	Phosphatidylinositol bisphosphate
PIP_3	Phosphatidylinositol trisphosphate
PGL	Paraganglioma
PGL#	Familial paragangliomas type #
PHD	(HIF)-prolyl hydroxylase

PI3K	Phosphatidylinositol-3-kinase
PKA	Protein kinase A
PKC	Protein kinase C
PKD	Polycystic kidney disease
PLC	Phospholipase C
Plk1	Polo-like kinase 1
PNMT	Phenylethanolamine N-methyltransferase
PPGL	Phaeochromocytoma and paraganglioma
PPIA	Peptidylpropyl isomerase A
PRRT	Peptide receptor radionuclide therapy
Ptch	Patched
PTH	Parathyroid hormone
pVHL	von-Hippel Lindau protein
PyT	Pythagoras' Theorem
QMUL	Queen Mary University London
qRT-PCR	Quantitative real time PCR
RCC	Renal cell carcinoma
RET	Rearranged during transfection
RIN	RNA integrity number
RIPA	Radioimmunoprecipitation assay
RNA	Ribonucleic acid
ROI	Region of interest
RPE	Retinal pigment epithelium
SDH	Succinate dehydrogenase
SDHAF2	Succinate dehydrogenase assembly factor 2
SDHx	Succinate dehydrogenase subunit x
SDS-PAGE	Sodium dodecyl sulphate polyacrylamide gel electrophoresis
SEM	Standard error of the mean
Shh	Sonic hedgehog
siRNA	Short interfering RNA
Smo	Smoothened
SPECT	Single photon emission computed tomography
SR-SIM	Super resolution structured illumination
SSA	Somatostatin analogue
SSTR	Somatostatin receptor
SuFu	Suppressor of fused
SULT1A3	Sulfotransferase 1A3/1A4
TAE	Tris-acetate-EDTA
TCA	Tricarboxylic acid
TH	Tyrosine hydroxylase
TKI	Receptor tyrosine kinase inhibitors
TKR	Tyrosine kinase receptor
TMEM127	Transmembrane protein 127
TP53	Tumour protein 53
TSA	Trichostatin A

TSC	Tuberous sclerosis complex
t-SNE	t-distributed stochastic neighbour embedding
TTL	Tubulin glycylases
ULN	Upper limit of normal
UV	Ultraviolet
VEGF	Vascular endothelial growth factor
VHL	von Hippel-Lindau
WB	Western blot
Wnt	Wingless/Integrated

CHAPTER 1

The primary cilium

1.1 Structure

Primary, non-motile, cilia are near ubiquitous singular microtubule-based organelles. First observed in mammalian cells over 100 years ago (Zimmermann 1898), the term 'primary cilium' was coined in 1968 (Sorokin 1968). Long considered a vestigial by-product of evolution from lower order flagellated organisms, primary cilia were generally felt to be functionless for the majority of the 20th century. This perception was transformed by the discovery of intraflagellar transport (IFT)(Kozminski *et al.* 1993) and the finding that ciliary defects occurred in a range of disease states that subsequently became known as 'ciliopathies' (reviewed in (Tobin & Beales 2009)). Although structurally related to motile cilia, primary cilia differ in that they are non-motile, singular and present in virtually all nucleated mammalian cells (Figure 1.1A).

1.1.1 Axoneme

The ciliary axoneme consists of a core of nine microtubule doublets that is covered by the ciliary membrane and extends into the extracellular space (Figure 1.1A) (Sorokin 1968). In motile cilia, there is also a central pair of microtubules that together with additional structures (e.g. dynein arms) confer motility; these are lacking in primary cilia (Figure 1.1A) (Fawcett & Porter 1954). Primary cilia axonemes are thus said to have a '9+0' structure compared to the '9+2' structure of motile cilia. The axoneme provides structural support for the primary cilium and also serves as a transport platform to facilitate IFT (Kozminski *et al.* 1993).

Axonemal microtubules are α/β tubulin dimers that are subject to extensive post-translational modifications which define microtubule stability, direct protein complex recruitment and influence transport processing through alterations in kinesin motor function (Reed *et al.* 2006; Gaertig & Wloga 2008; Hammond *et al.* 2010). Acetylation of α-tubulin is particularly enriched within the axoneme resulting in microtubule stabilisation (Piperno *et al.* 1987) and providing an invaluable experimental target for cilia identification.

1.1.2 Basal body

The basal body is a cylindrical structure that sits at the base of the axoneme. It is comprised of nine microtubule triplets, two of which are contiguous with the doublet microtubules of the axoneme (Figure 1.1A).

The basal body is derived from the elder of the cell's two centrioles (the mother centriole). This, in addition to other factors, means that there is only one primary cilium per cell, except in certain

ciliopathies and cancers in which multiple centrioles can result in more than one primary cilium (Kinzel *et al.* 2010).

The basal body has two main functions: it anchors the cilium to the cell membrane and cytoskeleton through fibrous distal appendages and acts as a docking site for IFT particles through transition fibres (Deane *et al.* 2001; Williams *et al.* 2011). Transition fibres also form a physical barrier to ciliary entry (Doolin & Birge 1966; Hagiwara *et al.* 2008) and are discussed further below.

1.1.3 Transition zone

The transition zone is an evolutionary conserved ciliary sub-domain and is the point at which the triplet microtubules of the basal body become the doublets of the axoneme (Figure 1.1A). It is characterised by Y-shaped linkers that connect the microtubule doublets to the membrane-associated ciliary necklace (Figure 1.1A).

The transition zone functions as a gatekeeper for entry and exit of membrane-bound proteins into and from the axoneme (Garcia-Gonzalo *et al.* 2011; Chih *et al.* 2012), but not soluble cytoplasmic proteins (Kee *et al.* 2012; Najafi *et al.* 2012). In addition, it has been suggested that a ciliary pore complex analogous to the nuclear pore complex exists. Evidence for this includes the presence of components of the nuclear localisation machinery in cilia and the presence of a ciliary RanGTP gradient akin to that seen across the nuclear membrane (Fan *et al.* 2007, 2011; Dishinger *et al.* 2010; Hurd *et al.* 2011).

1.1.4 Ciliary membrane

The ciliary membrane, although contiguous with the cell surface membrane, is separated from it by the ciliary necklace (Gilula & Satir 1972). This consists of multiple circumferential rows of membranous particles which sit adjacent to the Y-linkers of the transition zone (Figure 1.1A). It thus forms a physical barrier as part of the transition zone's 'ciliary gate' and is required for insertion of specific ciliary membrane components (Deane *et al.* 2001).

The ciliary membrane, like the cell surface membrane (CSM), is a phospholipid bilayer, but has a different composition. It has a higher composition of sterols and lipid rafts than the cell membrane (Chailley & Boisvieux-Ulrich 1985; Tyler *et al.* 2009). In addition, its protein composition is different with inclusion or exclusion of a range of receptors observed (Ostrowski *et al.* 2002; Teilmann & Christensen 2005; Teilmann *et al.* 2005).

The ciliary pocket is an invagination of the CSM at the base of the cilium which can envelop varying portions of the axoneme.

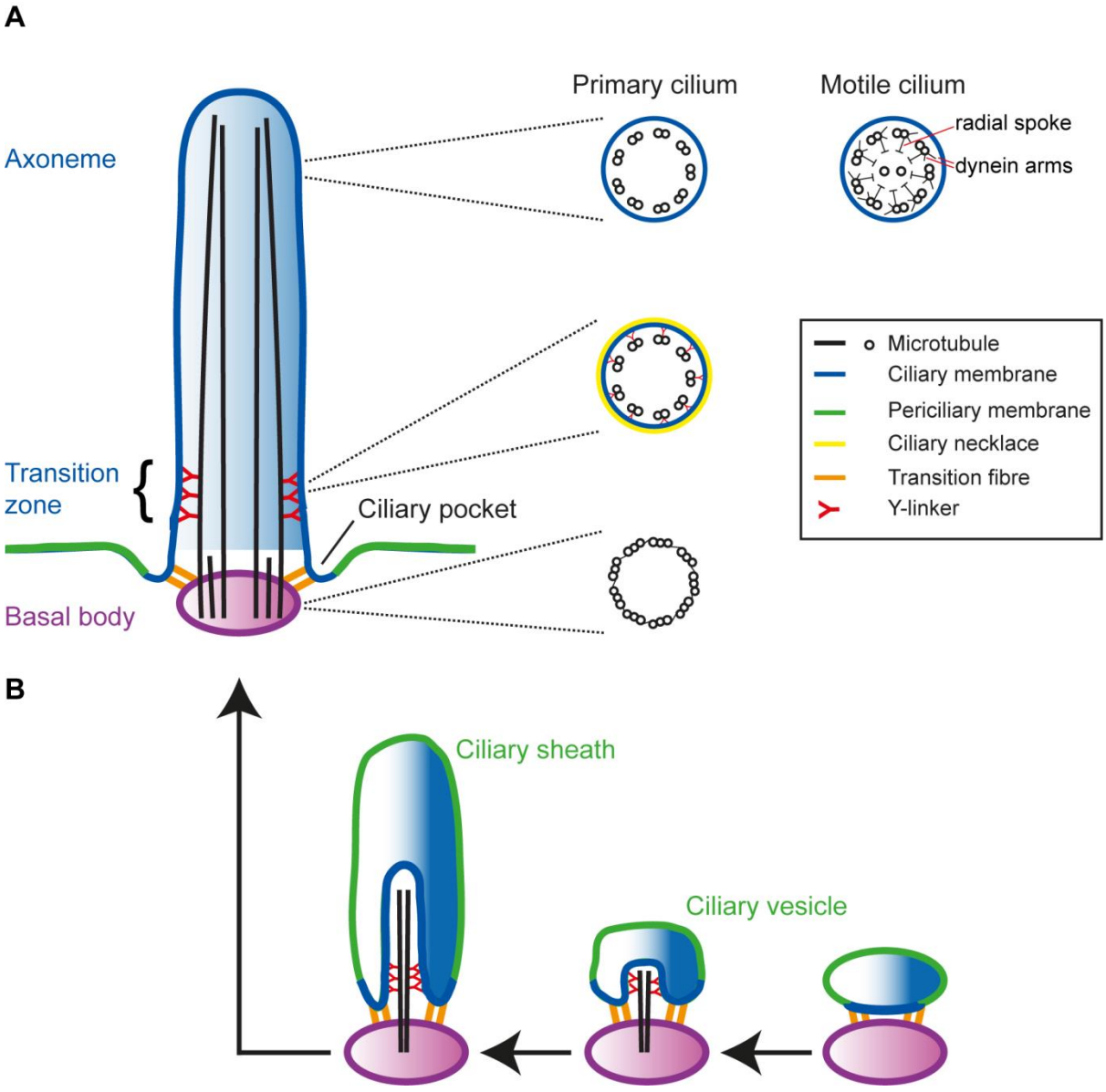

Figure 1.1 Schematic representation of the structure and formation of a primary cilium

(A) Cross-sections of a primary ('9+0') cilium at the level of the axoneme, transition zone and basal body are shown, in addition to a motile ('9+2') cilium for comparison.

(B) Stages of ciliogenesis

1.2 Cilia length control

Although primary cilia are non-motile, they are dynamic structures, elongating and resorbing during the cell cycle as a result of IFT and activation of ciliary disassembly pathways. IFT is an evolutionarily conserved, selective, bidirectional, microtubule-based mechanism by which protein transport modules (IFT particles or trains) are trafficked along the ciliary axoneme in a process that is vital for ciliary function (Kozminski *et al.* 1993; Huangfu & Anderson 2005; Berbari *et al.* 2009) (Figure 1.2).

It is apparent that ciliary length is regulated and is not merely limited by resource availability (Rosenbaum *et al.* 1969). The rate of ciliary and flagellar assembly is not constant and reduces with increasing axonemal length (Rosenbaum & Child 1967), due to a reduction in IFT transport capacity (Engel *et al.* 2009). The axoneme shortens in the absence of IFT due to constant tubulin turnover (Stephens 1997; Song & Dentler 2001). This disassembly rate is constant and length independent, unlike assembly (Marshall *et al.* 2005). Therefore, a specified length set point exists (which varies between cells and with conditions) at the point at which the declining assembly rate is equal to the disassembly rate resulting in an equilibrium. These observations have given rise to the balance point model of ciliary length control (Marshall *et al.* 2005).

Cilia length is important as it both determines sensitivity to extracellular cues (Resnick & Hopfer 2007) and influences the amplitude of ciliary-mediated signalling pathways. For example, it has been shown that lithium chloride-induced elongation of chondrocyte primary cilia attenuates Hedgehog (Hh) signalling amplitude (Thompson *et al.* 2016). For these reasons, it is commonly used as an experimental readout for cilia function.

1.2.1 Ciliogenesis

The formation of a primary cilium requires the mother centriole and is thus intimately associated with centriole duplication and the cell cycle. Ciliogenesis occurs during G1/G0.

Following dissociation of the centrosome from mitotic spindles, the mother centriole attaches to a Golgi-derived vesicle via transition fibres (Sorokin 1962, 1968; Deane *et al.* 2001) en route to the cell membrane (Figure 1.1B). Within this vesicle, a ciliary bud emerges and elongates to form the axoneme which projects within the vesicle lumen (Boisvieux-Ulrich *et al.* 1989). The ciliary vesicle then fuses with the cell membrane in an exocytotic process in which the outer vesicle membrane becomes the periciliary membrane.

Tubulin incorporation into microtubules results in axoneme lengthening and occurs at the distal tip corresponding to the fast growing '+' end (Johnson & Rosenbaum 1992). As cilia do not contain the necessary machinery for protein synthesis, delivery of the requisite building blocks relies on IFT (Rosenbaum & Child 1967).

Anterograde IFT describes the transport of IFT particles and their associated cargo proteins from the ciliary base to the ciliary tip (Figure 1.2). The first stage is recruitment of the necessary IFT components by transition fibres at the ciliary base (Deane *et al.* 2001; Graser *et al.* 2007). Here, IFT particles are formed which consist of a kinesin-2 motor element and an IFT-B complex. The kinesin-2 element comprises a heterodimer of motor subunits of kinesin family members (KIF3A and KIF3B) and an accessory subunit (KAP) (Cole 1999). The IFT-B complex consists of multiple IFT proteins (IFT-20, 21, 22, 25, 27, 46, 52, 54, 57, 70, 72, 74, 80, 88, 172), the loss of any of which inhibits ciliogenesis (Pazour *et al.* 2000; Huangfu *et al.* 2003; Hou *et al.* 2007). These IFT particles are transported to the ciliary tip along axonemal microtubules by the kinesin-2 motor complex (Iomini *et al.* 2001; Qin *et al.* 2004) at speeds of approximately 2μm/s (Kozminski *et al.* 1993). At the ciliary tip, kinesin-2 is inactivated thereby releasing its cargo (Shih *et al.* 2013).

Return of IFT particles to the ciliary base is through retrograde IFT which is achieved by cytoplasmic dynein 2 (Pazour *et al.* 1999) at a speed of approximately 3.5μm/s (Kozminski *et al.* 1993). The dynein 2 complex contains heavy, intermediate, light intermediate and light chains and is associated with the 6 proteins of the IFT-A complex (IFT-43, 121, 122, 139, 140, 144) (Hirano *et al.* 2017). Ciliogenesis can still occur following loss of these proteins, unlike the IFT-B complex, but cilia are malformed with prominent bulges (Piperno *et al.* 1998; Iomini *et al.* 2001).

In addition to transporting ciliary assembly components to the distal tip, IFT is also responsible for the passage of some components of the signal transduction machinery of cilia-mediated signalling pathways along the axoneme. An example of this is the Hh pathway (discussed further later), which requires IFT for transit of a number of its signalling components and the activity of which is attenuated when IFT is defective (Huangfu & Anderson 2005; Liu *et al.* 2005; Ocbina & Anderson 2008). In this situation, IFT is assisted by the BBSome, which consists of seven highly conserved core Bardet-Biedl Syndrome (BBS) proteins (1, 2, 4, 5, 7, 8, 9) (Nachury *et al.* 2007) and promotes the trafficking of membrane proteins to the cilium (Händel *et al.* 1999; Berbari *et al.* 2008a).

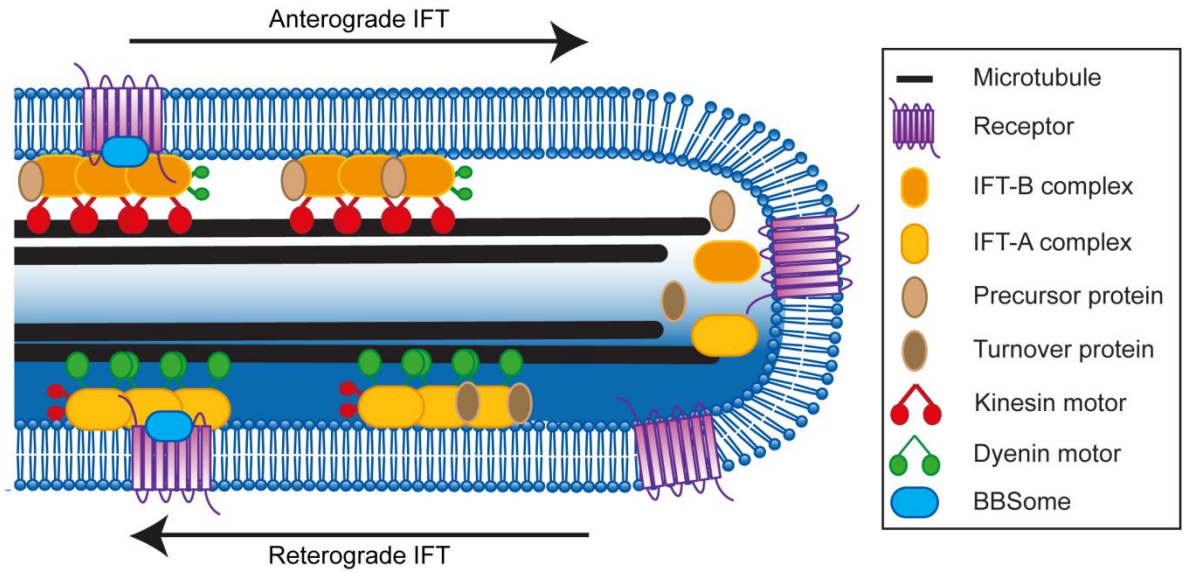

Figure 1.2: Schematic representation of intraflagellar transport

Anterograde intraflagellar transport (IFT) is subserved by the kinesin motor/IFT-B complex with the dynein motor/IFT-A complex being responsible for retrograde IFT. Receptors and other ciliary proteins are trafficked in association with the BBSome (BBS Bardet-Biedl Syndrome).

1.2.2 Ciliary disassembly

Once formed, primary cilia are disassembled prior to mitotic entry through a variety of different mechanisms.

1.2.2.1 Aurora kinase A/histone deacetylase 6

Aurora kinase A (AURKA) is a mitotic serine/threonine protein kinase and is an orthologue of the *Chlamydomonas* protein CALK (Chlamydomonas aurora-like protein kinase), the phosphorylation of which regulates and is a marker of flagellar length (Luo *et al.* 2011). Amongst its many functions, AURKA localises to the basal body and phosphorylates, thereby activating, histone deacetylase 6 (HDAC6) (Pugacheva *et al.* 2007). HDAC6 is a member of the class II HDAC family and although predominantly cytoplasmic also localises to the axoneme (Pugacheva *et al.* 2007), where it deacetylates α-tubulin (Hubbert *et al.* 2002), destabilising axonemal microtubules and thus promoting ciliary disassembly (Pugacheva *et al.* 2007). Inhibition of HDAC6 does not in itself alter ciliary length (Sharma *et al.* 2011), highlighting its role in ciliary disassembly in response to disassembly cues, for example serum stimulation (Pugacheva *et al.* 2007). In addition to tubulin,

HDAC6 has a number of other substrates including histones (Grozinger *et al.* 1999), heat shock protein 90 (Hsp90) (Kovacs *et al.* 2005) and cortactin (Zhang *et al.* 2007).

Activation of AURKA at the basal body can be achieved through a variety of different mechanisms (Figure 1.3), which subserve different ciliary disassembly cues and have differential roles within the cell cycle.

The pro-metastatic scaffolding protein human enhancer of filamentation 1 (HEF1, also known as CAS-L and NEDD-9) binds and activates AURKA (Pugacheva & Golemis 2005). HEF1 stabilisation is achieved through the non-canonical Wnt pathway, in which Wnt5a ligand binds the frizzled receptor, activating casein kinase 1 isoform epsilon (CK1ε) resulting in phosphorylation of dishevelled 2 (Dvl2) and ultimately interaction with polo-like kinase 1 (Plk1) (Lee *et al.* 2012a). Additional regulation of AURKA/HDAC6 occurs via hypoxic signalling as HEF1 is a hypoxia inducible factor 1α (HIF1α) target gene (Xu *et al.* 2010).

Calmodulin activates AURKA in response to calcium release from the endoplasmic reticulum (ER) both directly (Plotnikova *et al.* 2010) and indirectly by promoting interaction between AURKA and HEF1 (Plotnikova *et al.* 2012). Cellular entry of extracellular calcium also stimulates ciliary disassembly (Tucker *et al.* 1979).

Inositol polyphosphate 5-phosphatase (INPP5E) is another activator of AURKA and although there is a direct interaction between the two, its activation is indirect. INPP5E dephosphorylates phosphatidylinositol trisphosphate (PIP_3) to phosphatidylinositol bisphosphate (PIP_2) and it is through this second messenger that AURKA is activated (Plotnikova *et al.* 2015). The relationship between INPP5E and AURKA is further complicated by reciprocal activation of INPP5E which, in addition to its role in AURKA activation, inhibits the Akt signalling pathway resulting in a reduction in *AURKA* transcription (Plotnikova *et al.* 2015).

Other activators of AURKA include pitchfork (Kinzel *et al.* 2010) and the keratin intermediate filament scaffold protein trichoplein (Inoko *et al.* 2012), which is protected from degradation by nuclear distribution element-like 1 (Inaba *et al.* 2016).

In addition to phosphorylating HDAC6, AURKA has a number of other protein targets. These include polycystin 2 and p53. Phosphorylation of the calcium-permeable non-selective cation channel polycystin 2 reduces its activity resulting in a reduction of ER calcium release and thereby a reduction in calmodulin-induced AURKA activation (Plotnikova *et al.* 2011). AURKA-mediated phosphorylation at two distinct serine residues of p53 both inhibits its DNA binding and

transcriptional activity (serine 215) (Liu *et al.* 2004) and targets it for ubiquitination and proteolysis by mouse double minute 2 homolog (serine 315) (Katayama *et al.* 2004).

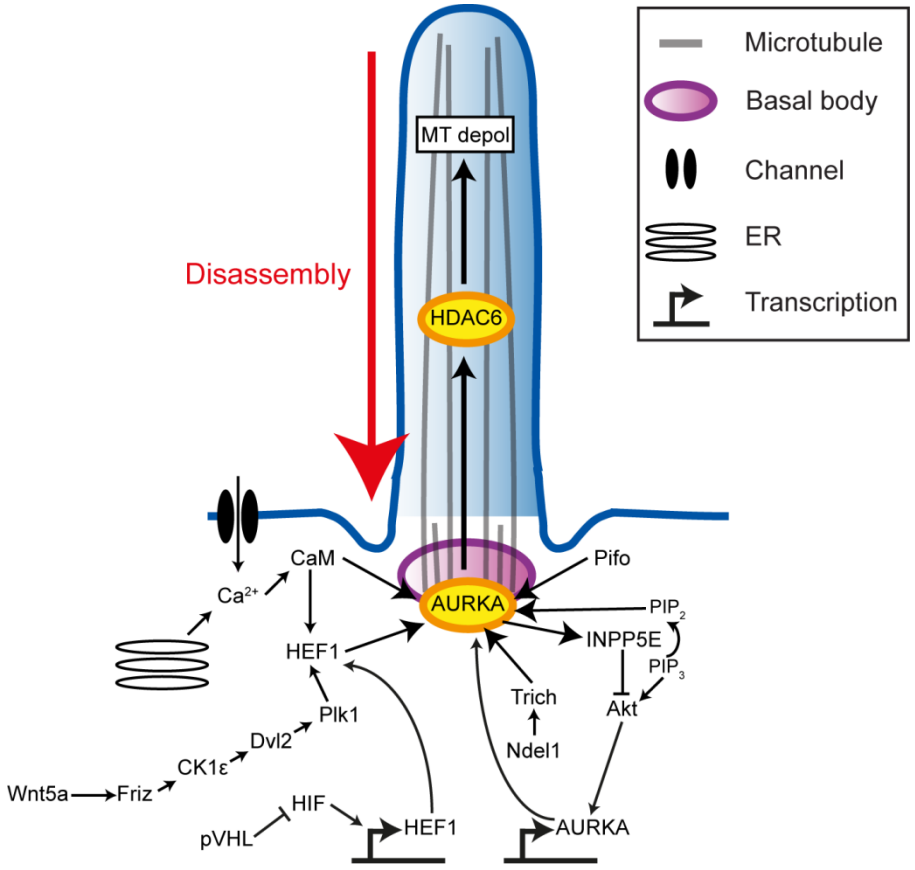

Figure 1.3: Schematic representation of the AURKA/HDAC6 ciliary disassembly pathway

Aurora kinase A (AURKA) is activated by a variety of mechanisms and in turn activates histone deacetylase 6 (HDAC6) which deacetylates and depolymerises (depol) axonemal microtubules (MT) resulting in ciliary disassembly.

CaM – calmodulin, HEF1 – human enhancer of filamentation 1, Friz – frizzled, CK1ε – casein kinase 1 isoform epsilon, Dvl2 – dishevelled 2, Plk1 – polo-like kinase 1, pVHL – protein von Hippel-Lindau, HIF – hypoxia inducible factor, Ndel1 – nuclear distribution element-like 1, Trich – trichoplein, INPP5E – inositol polyphosphate 5-phosphatase, PIP_2 – phosphatidylinositol bisphosphate, PIP_3 – phosphatidylinositol trisphosphate, Akt – protein kinase B, Pifo – pitchfork.

1.2.2.2 Tctex-1

The dynein light chain Tctex-1 (also known as DYNLT1) appears to have a dual role in promoting ciliary resorption. It is a component of the dynein 2 complex and is therefore involved in retrograde IFT (Palmer *et al.* 2011; Asante *et al.* 2014). In addition, Tctex-1 modulates actin dynamics (Chuang *et al.* 2005) and promotes ciliary disassembly through interactions with several actin-binding proteins and stimulation of ciliary pocket membrane endocytosis (Li *et al.* 2011; Saito *et al.* 2017). Inhibition of actin polymerisation prevents both serum- and Tctex-1-induced ciliary resorption (Li *et al.* 2011). This Tctex-1 ciliary disassembly pathway is activated by the insulin-like growth factor 1 receptor (IGF-1R) pathway in which Gβγ signalling promotes release of dynein-bound Tctex1 and recruits it to the ciliary base (Yeh *et al.* 2013).

1.2.2.3 Nde1

Nde1, the mammalian orthologue of NudE (nuclear distribution gene E) is a centrosomal phosphoprotein, knockdown of which results in cilia elongation (Kim *et al.* 2011a; Doobin *et al.* 2016). It is degraded by the E3 ubiquitin ligase F-box/WD repeat-containing protein 7 after priming by CDK5; loss of either of these results in Nde1 persistence and resultant cilia shortening (Maskey *et al.* 2015). The mechanism by which Nde1 causes ciliary disassembly has not been elucidated, although it is known to interact with the dynein light chain LC8 (also known as DYNLL1) (Feng & Walsh 2004).

1.2.2.4 NIMA-related kinases (NEKs)

Never in mitosis gene A (NIMA)-related kinases (NEKs) are a family of serine/threonine protein kinases that have a multi-faceted role in cilia length control. Some members elongate cilia and their loss results in a reduction in ciliary length, for example NEK1 (Thiel *et al.* 2011) and NEK4 (Coene *et al.* 2011). Others play a role in ciliary disassembly.

NEK2 loss results in a reduction in ciliary resorption and its overexpression results in reduced ciliary incidence and length (Spalluto *et al.* 2012). Its role in ciliary disassembly is complex and appears to involve both AURKA/HDAC6 dependent and independent mechanisms. NEK2 activates the microtubule depolymerising kinase Kif24, thereby promoting ciliary disassembly independent of AURKA/HDAC6 (Kim *et al.* 2015). In addition, there is a functional interaction between AURKA and NEK2, which act co-operatively (DeVaul *et al.* 2017), and leads to ciliary resorption following NEK2 overexpression (Endicott *et al.* 2015). Furthermore, HEF1 inhibits NEK2 whilst activating AURKA (Pugacheva & Golemis 2005).

Similarly to NEK2, NEK8 is involved in ciliary disassembly through interactions with a number of ciliary and centrosomal proteins including inversin (Fukui *et al.* 2012), polycystin 2 (Manning *et al.* 2013), nephrocystin 3 (Frank *et al.* 2013) and ankyrin repeat and sterile alpha motif domain-containing protein 6 (Hoff *et al.* 2013). Loss of NEK8 results in cilia elongation (Smith *et al.* 2006; Sohara *et al.* 2008) whilst its proteosomal degradation occurs during ciliogenesis (Zalli *et al.* 2012). The exact mechanism by which NEK8 promotes ciliary disassembly has not been fully elucidated, but a role in transcriptional regulation has been suggested. NEK8 loss results in increased expression of foxj1a, a transcriptional regulator of ciliary genes (Hellman *et al.* 2010), and it interacts with the Hippo pathway effector transcription factors TAZ and YAP (Habbig *et al.* 2012; Grampa *et al.* 2016). Furthermore, NEK8 is a hypoxia responsive gene and its transcription is therefore downregulated by the tumour suppressor gene product von-Hippel Lindau protein (pVHL) (Ding *et al.* 2015), which itself contributes to ciliary stabilisation (discussed later).

1.2.2.5 Others

A number of additional pathways that are involved in ciliary disassembly have been identified.

The centrosomal protein CPAP is a scaffolding protein that forms part of the ciliary disassembly complex alongside AURKA and Nde-1, and its loss has been associated with ciliary elongation (Gabriel *et al.* 2016). Its role appears more complex, however, as it is also required for ciliary formation (Wu & Tang 2012) and its levels reduce following serum stimulation and ciliary resorption (Kim *et al.* 2016). CPAP binds tubulin at different sites; different mutations in its C-terminal domain result in differential changes in tubulin binding and its own tertiary structure with opposite effects on ciliary microtubules (Zheng *et al.* 2016).

Other centrosomal proteins that suppress ciliogenesis have been identified. Cep 97 and CP110 interact (Spektor *et al.* 2007) and activate Kif24 resulting in microtubule depolymerisation (Kobayashi *et al.* 2011). Plk1, in addition to activating the AURKA/HDAC6 pathway via HEF1, phosphorylates Kif2A in the subdistal appendages of the mother centriole thereby activating its microtubule depolymerisation activity (Miyamoto *et al.* 2015).

Loss of function of tuberous sclerosis complex (TSC) results in cystic renal disease and elongated primary cilia through an unknown mechanism which is independent of its binding partners mammalian target of rapamycin (mTOR) and polycystin 1 (Hartman *et al.* 2009).

Certain cilia-mediated signalling pathways, discussed further below, alter ciliary length through their own signalling. Anaphase-promoting complex (APC), a component of the canonical Wnt pathway,

stimulates ciliary disassembly as a result of both destabilising ciliary microtubules, in a process that required its co-activator Cdc20, and by targeting the cilia assembly factor NEK1 for proteolysis (Wang *et al.* 2014). Glycogen synthase kinase-3β (GSK3β) phosphorylates β-catenin, the Wnt pathway effector, resulting in its degradation. Inhibition of GSK3β by lithium chloride results in ciliary elongation (Miyoshi *et al.* 2009).

Other intra-cellular signalling molecules appear to result in varied ciliary responses. Cyclic AMP (cAMP) results in cilia elongation in some situations (Besschetnova *et al.* 2010; Abdul-Majeed & Nauli 2011) whilst reduction in cAMP formation by inhibition of adenylyl cyclase (AC) can also result in cilia lengthening (Ou *et al.* 2009). Cilia elongation can occur in response to reductions in intra-cellular calcium (Besschetnova *et al.* 2010) or through calcium-mediated activation of protein kinase C (PKC) (Abdul-Majeed *et al.* 2012).

1.3 Cilia functions

1.3.1 Cilia and the cell cycle

The presence of a primary cilium is closely associated with cell cycle stage (Figure 1.4) (Sorokin 1962). Ciliary assembly occurs during G1/G0 with disassembly necessary prior to mitotic entry in order to release the basal body to participate in mitotic spindle assembly as part of the centrosome. Ciliary disassembly occurs in two stages: prior to G1/S transition and before M phase (which is the main contributor) (Rieder *et al.* 1979; Jensen *et al.* 1987). This co-ordination between the primary cilium and the cell cycle is mediated through the temporal control of factors that alter the balance between ciliary assembly and disassembly.

Ciliary assembly (discussed previously) is suppressed by the CP110-Cep97 inhibitory complex which is localised to the mother centriole and subsequently the basal body (Spektor *et al.* 2007). Release of this inhibition is therefore required for ciliogenesis to occur (during G1/G0) and is achieved through protein kinases including Tau tubulin kinase 2 and microtubule affinity-regulating kinase 4 (Goetz & Anderson 2010; Kuhns *et al.* 2013). CP110-Cep97 further suppresses ciliogenesis through its maintenance of Kif24, which depolymerises axonemal microtubules (Kobayashi *et al.* 2011). Kif24 is also involved in ciliary disassembly at the S/G2 transition when it is induced by Nek2 (Kim *et al.* 2015). In *Chlamydomonas*, a NEK family member is necessary both for ciliary resorption and cell cycle progression from G2 to M phase (Mahjoub *et al.* 2004).

The timing of ciliary resorption (again discussed previously) is governed by the temporal activation throughout the cell cycle of a variety of different disassembly mechanisms. AURKA activates HDAC6

following its own activation by pitchfork (Kinzel *et al.* 2010) and HEF1 (Pugacheva *et al.* 2007) during cell cycle re-entry and G2/M transition (Pugacheva & Golemis 2005). Kif2 depolymerises ciliary tubulin and is upregulated by Plk1 and downregulated by AURKA (Jang *et al.* 2009; Miyamoto *et al.* 2015). The dynein light chain Tctex-1 stimulates both ciliary disassembly and S phase (Li *et al.* 2011). Nde1, which has low expression during quiescence, interacts with another dynein light chain and stimulates cilia disassembly. Loss of Nde1 results in elongated cilia and delayed re-entry into the cell cycle (Kim *et al.* 2011a). Control of Nde1 is maintained by ubiquitin-mediated degradation in a cell cycle dependent fashion by CDK5 (Maskey *et al.* 2015).

Further elements that link primary cilia stability to the cell cycle include cell-cycle related post-translational modifications of tubulin by the mitotic spindle associated protein CEP41, which is required for tubulin glutamylation and microtubule organisation (Lee *et al.* 2012b). The ciliary disassembly factor APC is sequestered to the primary cilium by the cell cycle regulator cdc20 (Wang *et al.* 2014) and cilia-mediated Hippo signalling is an important regulator of the cell cycle (Praskova *et al.* 2008; Zanconato *et al.* 2015).

It has therefore been suggested that a ciliary checkpoint exists within the cell cycle opposing cellular proliferation (Mans *et al.* 2008) and elongation of the primary cilium is associated with suppression of cell division (Kim *et al.* 2011a; Li *et al.* 2011). Whether this is an absolute requirement is all cells remains under debate as, although centrosome ablation results in failure of cell cycle progression (Uetake *et al.* 2007) and deformed cilia (Mikule *et al.* 2007), cells can undergo mitosis (Mahoney *et al.* 2006). Overexpression of Ift88 in HeLa cells results in failure of cells to enter S phase, whilst its depletion results in failure to progress into G2 (Robert *et al.* 2007). It was argued that this was due to a non-ciliary role of Ift88 as HeLa cells were believed to be non-ciliated (Robert *et al.* 2007), although this is not actually the case (Kowal & Falk 2015).

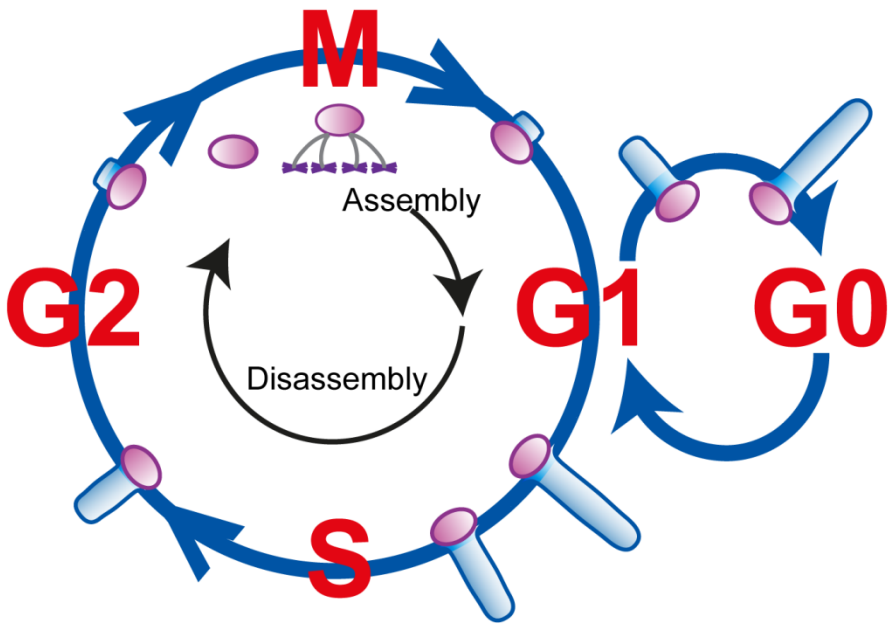

Figure 1.4: Cilia assembly and disassembly throughout the cell cycle

Cilia are assembled through G1 and G0 and disassembled at G1/S and G2/M.

1.3.2 Cilia-mediated signalling pathways

Primary cilia respond to a range of extracellular stimuli. This includes physical factors such as the mechanotransduction of luminal fluid flow (Nauli *et al.* 2003) or joint loading (Wann *et al.* 2012), temperature (Prodromou *et al.* 2012) and hypoxia (Proulx-Bonneau & Annabi 2011; Wann *et al.* 2013; Brown *et al.* 2014). They also respond to a variety of secreted paracrine and endocrine signalling molecules, for example platelet-derived growth factor alpha (PDGFRα) (Schneider *et al.* 2005), IGF-1 (Zhu *et al.* 2009), parathyroid hormone (PTH) (Xiang *et al.* 2014), Wingless/Integrated (Wnt) (Lancaster *et al.* 2011) and Hh (Huangfu *et al.* 2003).

A number of effector signalling pathways are either entirely subserved by primary cilia or modified by them. We will consider three that are of particular importance to normal embryonic development: Hh, Wnt and Notch. Disruption of these pathways can result in defective development in embryos and are frequently seen in a variety of cancers.

1.3.2.1 Hedgehog signalling

The Hedgehog signalling pathway is central to tissue patterning and embryogenesis during both vertebrate and invertebrate development. Named after the hedgehog-like appearance of *Drosophila*

larvae lacking the *Hh* gene, key components of the pathway are conserved between vertebrates and invertebrates. However, significant differences also exist; vertebrate Hh requires the primary cilium whilst invertebrate Hh signalling does not (Huangfu *et al.* 2003).

Three mammalian Hh ligands exist: Sonic (Shh), Indian (Ihh) and Desert (Dhh). They share signal transduction machinery and their effects and biological roles are generated through their differential temporal and spatial expression throughout development. Shh, the best studied, plays a key role in axis patterning and subsequently organogenesis (Wilson *et al.* 2009). Ihh, in combination with Shh, is critical in skeletogenesis (Vortkamp *et al.* 1996), whilst Dhh is largely confined to the gonads where it regulates spermatogenesis (Bitgood & McMahon 1995).

Native Shh ligand is auto-cleaved to produce an N-terminal fragment (ShhN) with signalling capabilities and a C-terminal fragment (ShhC) which is degraded by the ER (Porter *et al.* 1996). Post-cleavage modification of ShhN by cholesterol and palmitate is required for its function (Chamoun *et al.* 2001; Traiffort *et al.* 2004). Modified ShhN can then be released from the cell in a process involving Dispatched A and signal peptide, CUB domain and EGF-like domain-containing protein 2 (Burke *et al.* 1999; Tukachinsky *et al.* 2012).

In the absence of Hh ligand, its receptor Patched-1 (Ptch1) inhibits the function of another transmembrane protein, Smoothened (Smo) (Rohatgi *et al.* 2007). Through their interaction, Ptch1 and Smo regulate the activity of a group of three glioma associated oncogene proteins (Gli1-3) (Ingham 2001). Full length Gli2 (Gli2FL) and Gli3 (Gli3FL) are transcriptional activators which in the absence of Hh ligand are cleaved to truncated forms that act as transcriptional repressors (Gli2R and Gli3R) (Dai *et al.* 1999; Sasaki *et al.* 1999). Gli1 lacks the repressor domain and acts only as a transcriptional activator (Dai *et al.* 1999; Sasaki *et al.* 1999). There is substantial cross-talk between components of the Hh signalling pathway: Gli1 is a Gli3 target gene (Dai *et al.* 1999) whilst Ptch1 expression is induced by Gli1, suggesting that it is itself a negative regulator of Hh signalling (Buttitta *et al.* 2003).

Primary cilia are required for mammalian Hh signalling as defects in key components of primary cilia result in truncated or absent cilia and dysregulated Hh signalling (Huangfu *et al.* 2003; Huangfu & Anderson 2005; Delous *et al.* 2007; Weatherbee *et al.* 2009). This has been observed with loss of function of the IFT-B particle proteins Ift88 and Ift172 (Huangfu *et al.* 2003; Huangfu & Anderson 2005), the anterograde IFT motor Kif3a (Huangfu *et al.* 2003; Huangfu & Anderson 2005), the retrograde IFT motor Dnchc2 (Huangfu & Anderson 2005) and basal body proteins (Delous *et al.* 2007; Weatherbee *et al.* 2009). The situation is more complex, however, as primary cilia are also

required for formation of Gli3R, and IFT mutants can result in either loss or gain of Hh signalling depending on body site. For example, in the neural tube where Gli activators are the major contributors to pattern formation, IFT mutants result in loss of Hh signalling, whilst in the limbs where Gli3R is most important, they result in a gain of Hh signalling (Huangfu & Anderson 2005).

In the absence of Hh ligand, key components of the Hh signalling pathway are localised to or excluded from the primary cilium with the net result that repressor forms of Gli prevail and Hh signalling is turned off (Figure 1.5A). Ptch1 localises to the primary cilium and prevents ciliary entry of Smo (Rohatgi *et al.* 2007). Gli is complexed with suppressor of fused (SuFu) and the kinesin family member Kif7 at the ciliary base (Liem *et al.* 2009). SuFu is a negative regulator of Gli and promotes its cytoplasmic sequestration and degradation via multiple mechanisms (Ding *et al.* 1999; Barnfield *et al.* 2005; Tuson *et al.* 2011). In the absence of Hh ligand, axonemal enrichment of Gli is prevented and processing to GliR is promoted (Liem *et al.* 2009).

In the presence of Hh ligand (Figure 1.5B), Ptch1 exits the cilium allowing entry of Smo (Corbit *et al.* 2005; Haycraft *et al.* 2005; Rohatgi *et al.* 2007). Within the axoneme, Smo forms a complex with the ciliary proteins Evc and Evc2 which localises to a distinct ciliary region distal to the transition zone (Dorn *et al.* 2012; Yang *et al.* 2012). This Smo-Evc/Evc2 complex results in dissociation of Gli-SuFu complexes, thereby liberating full length Gli which is transported out of the cilium by IFT (Dorn *et al.* 2012; Caparrós-Martín *et al.* 2013). Gli-SuFu complexes are transported past Smo-Evc/Evc2 by the motor protein Kif7 which relocates from its basal ciliary position along the axoneme to the ciliary tip following Hh ligand stimulation (Endoh-Yamagami *et al.* 2009; Liem *et al.* 2009).

Thus, mammalian Hh signalling is dependent on primary cilia through restrictive but modifiable compartmentalisation of the downstream signal transduction machinery.

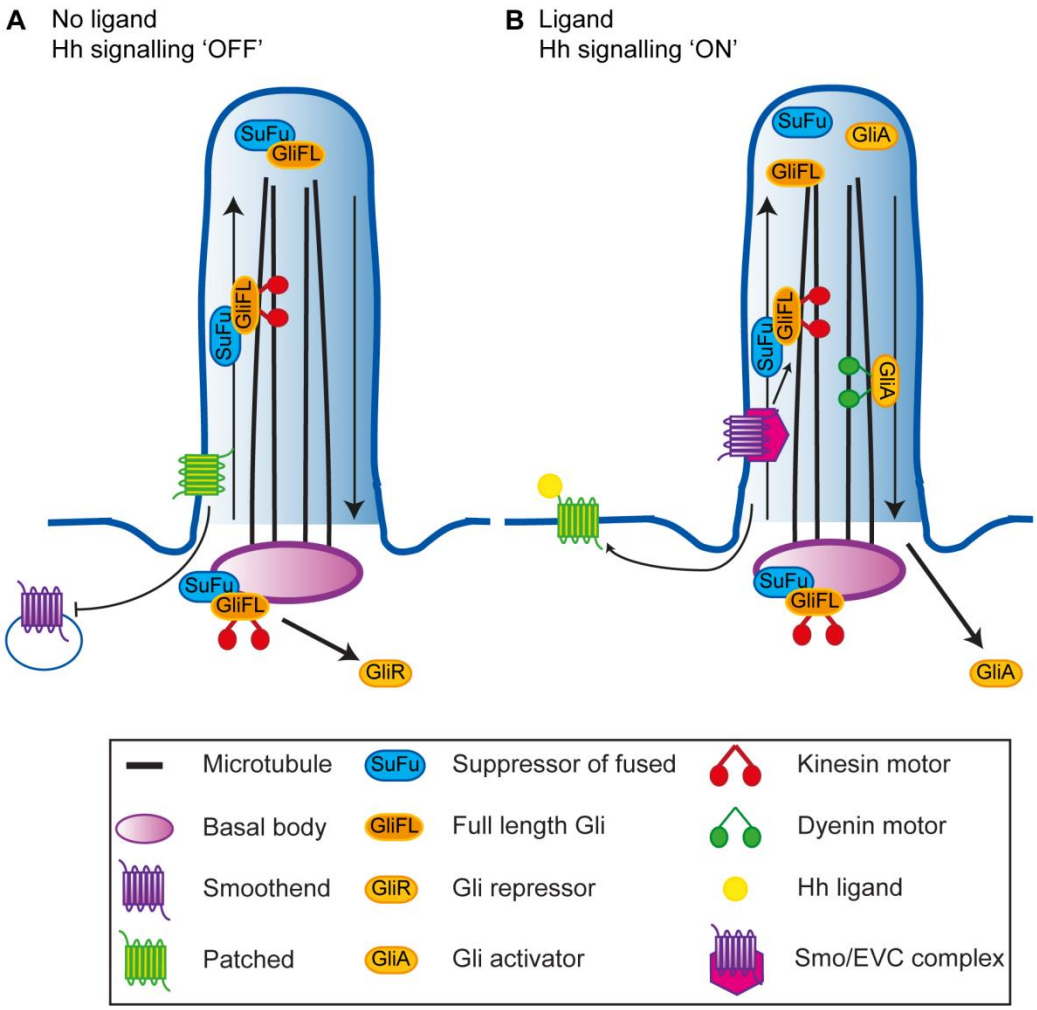

Figure 1.5: Vertebrate Hedgehog signalling requires a primary cilium

(A) In the absence of Hedgehog (Hh) ligand, Patched prevents ciliary entry of Smoothened and full length Gli (GliFL) is cleaved into its repressor (GliR).
(B) In the presence of Hh ligand, Patched leaves the cilium allowing Smoothened to enter and complex with EVC. This results in dissolution of the SuFu-GliFL complex with subsequent activation of Gli (GliA) at the ciliary tip. GliA is transported out of the cilium and translocates to the nucleus.

1.3.2.2 Wnt signalling

The Wnt signalling pathways, like Hh signalling, are central to axis patterning and embryonic development. Wnt ligands (of which there are 19 in humans) bind the Frizzled family of G-protein coupled receptors (GPCRs) which in turn activate the intra-cellular phosphoprotein Dvl. Different Wnt pathways are subserved by different Frizzled co-receptors and intracellular machinery.

1.3.2.2.1 Canonical Wnt signalling

The canonical Wnt pathway regulates the β-catenin transcription factor. In the absence of Wnt ligand, β-catenin is targeted for ubiquitin-mediated proteosomal degradation by the multimeric axin-APC-PP2A-GSK3-CK1 destruction complex. In the presence of Wnt ligand, Frizzled in combination with its co-receptor LRP5/6 activates Dvl disrupting the β-catenin destruction complex and promoting its survival. β-catenin translocates into the nucleus where it activates the TCF/LEF1 transcription complex.

The role of primary cilia in canonical Wnt signalling is debated. In some studies, IFT mutant zebrafish (Huang & Schier 2009) and mice (Ocbina *et al.* 2009) have absent cilia but normal canonical Wnt signalling. In others, cilia loss due to organ-specific inactivation of Kif3a (Lin *et al.* 2003), Ift88 (Cano *et al.* 2004) and Mks1 (Wheway *et al.* 2013) are associated with increased β-catenin expression.

It has been suggested that primary cilia might act as a means of dampening canonical Wnt signalling through spatial compartmentalisation of some of its signalling components (Figure 1.6). The ciliary protein inversin binds Dvl and targets it for degradation, thereby preventing β-catenin accumulation. Again, *in vivo* evidence regarding inversin is conflicting as no defects in canonical Wnt signalling were observed in inversin mutated mice (Sugiyama *et al.* 2011), whilst human mutations can result in nephronophthisis and β-catenin accumulation (Bellavia *et al.* 2010). Nephrocystin-3, another ciliary protein, interacts with inversin and inhibits canonical Wnt signalling (Bergmann *et al.* 2008). Jouberin binds β-catenin promoting its nuclear accumulation. In cells with primary cilia, Jouberin is sequestered to the basal body and axoneme resulting in downregulation of Wnt signalling (Lancaster *et al.* 2011).

The situation is further complicated as a number of BBSome proteins have differential modifying effects on β-catenin. Reductions in Bbs1, 4 and 6 all result in stabilisation of β-catenin and transcription of its target genes (Gerdes *et al.* 2007), whilst overexpression of Bbs3 results in an augmented Wnt response (Wiens *et al.* 2010). Furthermore, components of the β-catenin destruction complex directly influence primary cilia. APC stimulates ciliary disassembly through microtubule destabilisation and proteolytic targeting of the ciliary assembly factor NEK1 (Wang *et al.* 2014). Inhibition of GSK3β results in ciliary elongation (Miyoshi *et al.* 2009), whilst CK1ε is integral to HEF1 stabilisation and therefore AURKA/HDAC6 activation (Lee *et al.* 2012a).

1.3.2.2.2 Non-canonical Wnt signalling

Non-canonical Wnt signalling is unrelated to β-catenin and consists of the pathways involved in planar cell polarity (PCP) and cellular calcium entry. PCP is specified through actin polymerisation and cytoskeletal rearrangement following activation of Rho-associated kinase, whilst calcium release is stimulated by the phospholipase C (PLC)/IP_3 pathway.

PCP signalling requires the establishment of cell polarity and the presence of a ciliary basal body to define apico-basal polarity (Jones *et al.* 2008). PCP signalling requires Dvl (Wallingford *et al.* 2000; Park *et al.* 2008) in addition to the IFT components Ift88 and Kif3a (Jones *et al.* 2008), the transition zone proteins TMEM67, TMEM216 (Dawe *et al.* 2007, 2009; Valente *et al.* 2010), the basal body protein meckelin (Adams *et al.* 2012) and BBSome proteins (Seo *et al.* 2010). Whilst Ift20 and Bbs8 knockdown result in defects in both cilia and PCP, a non-ciliary role in cytoskeletal organisation has been postulated (May-Simera *et al.* 2015). The ciliary protein inversin, which facilitates the degradation of β-catenin, stimulates non-canonical Wnt signalling and has been proposed as a molecular switch between the canonical and non-canonical Wnt pathways (Simons *et al.* 2005).

The relationship between primary cilia and non-canonical Wnt signalling is, at least in part, reciprocal. The PCP effector Fuzzy displays ciliary localisation and is a requisite for ciliogenesis (Zilber *et al.* 2013).

1.3.2.3 Notch signalling

Notch signalling is another important development signalling pathway and is particularly relevant in neurogenesis. Notch ligands are transmembrane proteins that bind the extracellular domain of the single-pass transmembrane Notch receptor. This cell-cell interaction triggers proteolytic cleavage of the Notch receptor by γ-secretase, releasing the intracellular domain which translocates to the nucleus and results in transcriptional activation of Notch target genes.

A number of components of the Notch signalling pathway localise to primary cilia including the Notch-3 receptor and presenilin-2 (the catalytic subunit of γ-secretase) (Ezratty *et al.* 2011). Ciliary loss through Ift88 knockdown results in reduced Notch signalling with resultant increased proliferation and abnormal differentiation (Ezratty *et al.* 2011; Grisanti *et al.* 2016). This effect appears to result from a reduction in the cleaved intracellular Notch receptor domain (Grisanti *et al.* 2016). Localisation of presenilin-2 to the basal body is required for Notch-receptor cleavage and depends on a conserved VxPx C-terminal motif and the small GTPase ARF4 (Ezratty *et al.* 2016).

Primary cilia are therefore facilitatory to Notch signalling. In addition, cross-talk with other cilia-mediated signalling pathways occurs. Activation of Notch signalling in the developing neural tube results in cilia elongation and regulates ciliary localisation of the Hh signalling components Patched, Smoothened and full length Gli (Kong *et al.* 2015; Stasiulewicz *et al.* 2015).

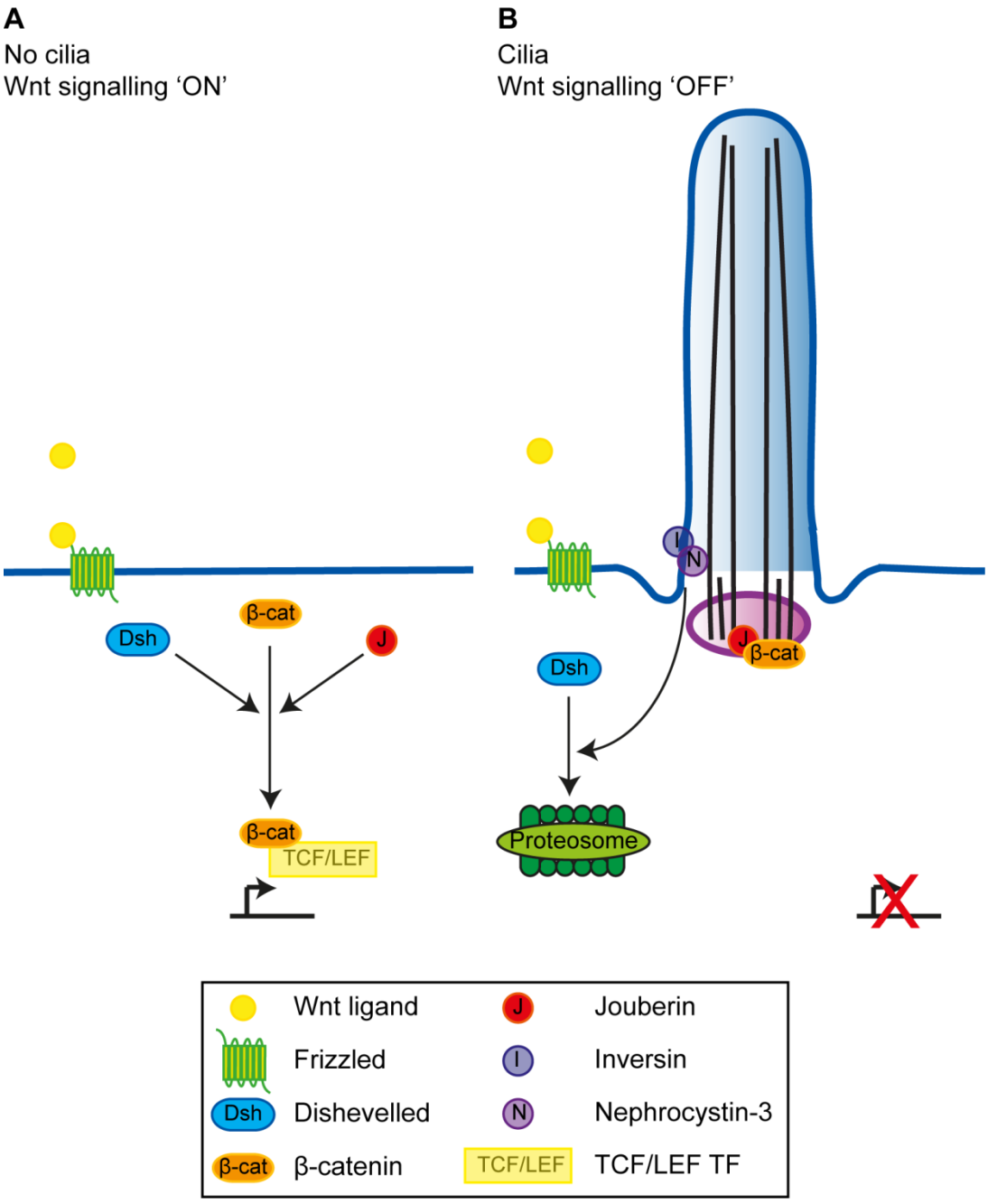

Figure 1.6: Canonical Wnt signalling is negatively regulated by primary cilia

(A) In the absence of a primary cilium, Wnt ligand binds the Frizzled receptor resulting in translocation of β-catenin into the nucleus in a process involving Dishevelled and Jouberin. Once there, activation of the T-cell factor/lymphoid embryonic factor (TCF/LEF) transcription factor (TF) results in Wnt target gene transcription.
(B) In the presence of a primary cilium, nuclear translocation of β-catenin is reduced even in the presence of Wnt ligand. Dishevelled is targeted for proteosomal degradation by the ciliary proteins Inversin and Nephrocytsin-3 whilst Jouberin is sequestered to the basal body.

1.4 Primary cilia in cancer

Given the role primary cilia play in normal developmental signalling, it is unsurprising that disruption of ciliary function can result in significant abnormalities. Mutations in genes that encode ciliary proteins have been described in conjunction with a range of human diseases collectively termed 'ciliopathies' [reviewed in (Novarino *et al.* 2011)]. These diseases include Bardet-Biedl syndrome, Autosomal Dominant Polycystic Kidney Disease (ADPKD), nephronophthisis and Leber congenital amaurosis amongst others. Although ciliopathies are distinct clinical entities with a defined genetic basis, a number of features are variably shared and overlap including retinal degeneration, renal cysts and polydactyly.

Beyond these monogenic Mendelian ciliopathies, ciliary disruption has been increasingly reported in a range of multi-factorial diseases including osteoarthritis (McGlashan *et al.* 2008), obesity (Ansley *et al.* 2003), diabetes mellitus (Hearn *et al.* 2005) and cancer (Seeley *et al.* 2009; Wong *et al.* 2009). Whether these observed changes in primary cilia contribute to such multi-faceted disease processes remains to be elucidated and it is unlikely that ciliary disruption in isolation would be sufficient for their development. Proposed mechanisms by which cilia disruption might be considered oncogenic include dysregulation of tumorigenic signalling pathways and disruption of normal cell cycle control.

Structural abnormalities in primary cilia (generally in their incidence and/or length) have been reported in tumours arising from all three germ cell layers (Figure 1.7). In the majority of tumour types, cilia are lost in tumour cells compared to adjacent non-cancerous tissue (Figure 1.7). Whether this contributes to tumorigenesis, or is merely reflective of the increased rate of cellular proliferation in neoplasms, remains under debate (and is addressed in this thesis). In a smaller subset of tumour types, cilia remain present on tumour cells and are required for tumour development (Figure 1.7). In such instances, the presence or absence of primary cilia is associated with histological subtype. For example, in craniopharyngiomas, primary cilia are near ubiquitous in the adamantinomatous subtype, whilst they are absent in the papillary subtype (Coy *et al.* 2016). In tumours that are dependent on ciliary-mediated signalling, for example Hh signalling in medulloblastomas, the presence or absence of primary cilia is dependent on whether the initiating oncogenic event occurs upstream or downstream of primary cilia (Han *et al.* 2009; Wong *et al.* 2009). In this context, cilia can be either requisite or inhibitory to tumour development, which highlights the broad and cell-specific role primary cilia play in tumourigenesis. We will consider the mechanistic details further in the setting of specific tumour types.

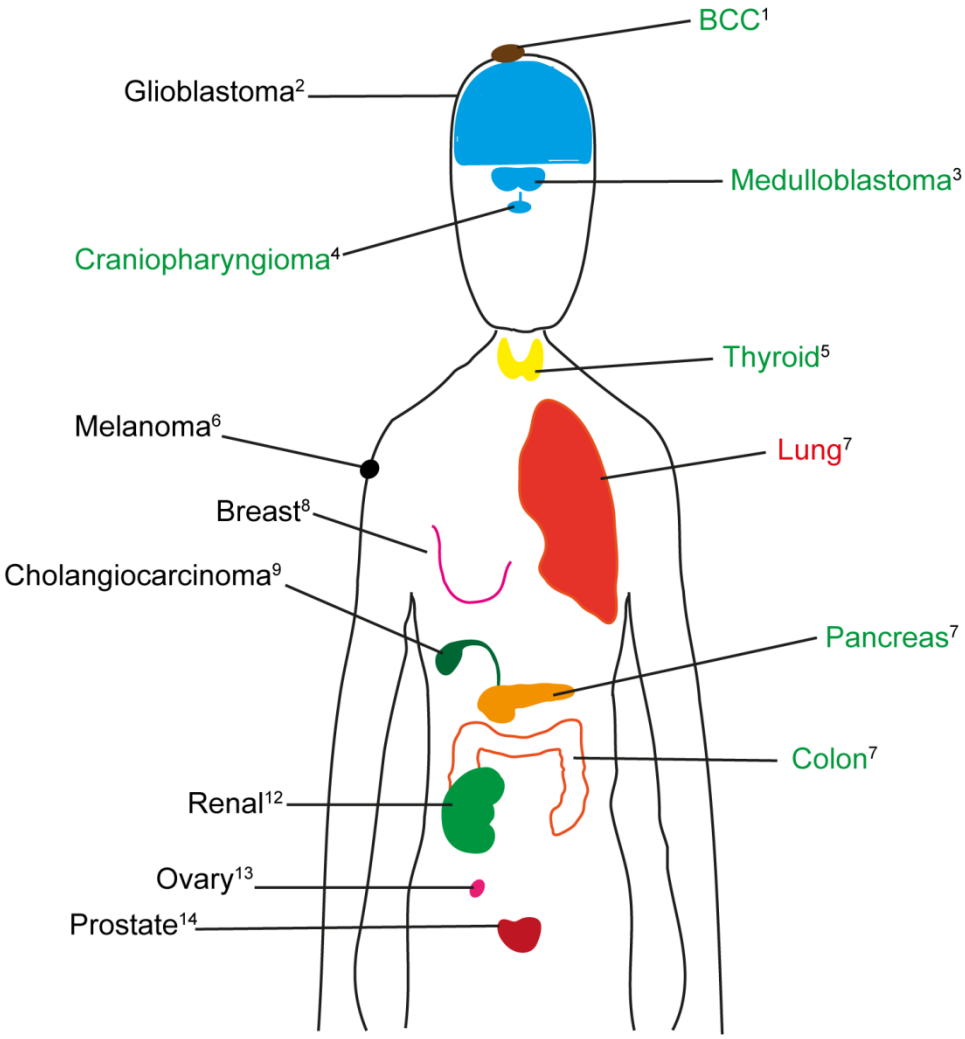

Figure 1.7 Cancers in which alterations in primary cilia have been observed

Cancers in which cilia loss relative to adjacent tissue has been observed are depicted with black text, those in which cilia are preserved are in red and those in which both cilia loss and preservation have been observed are in green.

1 - (Wong *et al.* 2009), 2 - (Moser *et al.* 2009), 3 - (Han *et al.* 2009), 4 - (Coy *et al.* 2016), 5 - (Lee *et al.* 2016), 6 - (Kim *et al.* 2011b), 7 - (Yasar *et al.* 2017), 8 - (Menzl *et al.* 2014), 9 - (Gradilone *et al.* 2013), 10 - (Seeley *et al.* 2009), 11 - (Rocha *et al.* 2014), 12 - (Schraml *et al.* 2009), 13 - (Egeberg *et al.* 2012), 14 - (Hassounah *et al.* 2013)

1.4.1 Primary cilia dysregulation in cancers

1.4.1.1 Breast cancer

Relative to normal breast epithelium, primary cilia incidence is severely reduced in breast cancer (Yuan *et al.* 2010; Menzl *et al.* 2014; Nobutani *et al.* 2014). This is also the case for the precursor lesion carcinoma *in situ* (Menzl et al. 2014), which suggests that primary cilia dysfunction is an early feature in breast cancer development. Cilia loss is also observed in cancer-associated stromal cells compared with stromal cells in normal tissue (Menzl *et al.* 2014).

Similar observations are seen in cell culture. Breast fibroblasts and epithelial cells are readily ciliated (Yuan *et al.* 2010; Spann *et al.* 2015), while breast cancer cell lines normally lack cilia. If they do not, they belong to the basal subtype of breast cancer (Yuan *et al.* 2010; Nobutani *et al.* 2014; Spann *et al.* 2015). Cilia loss is progressive with increasing degrees of transformation in the human MCF isogenic breast cancer cell series, providing further evidence that structural and functional alterations in primary cilia occur during breast cancer development and progression (Yuan *et al.* 2010). Xenografts of human breast cancer cells (both primary and cell line) result in orthotopic and metastatic tumours in immunodeficient mice, but cilia remain rare suggesting that this is an intrinsic cell characteristic and not overly influenced by environment or cell cycle (Nobutani *et al.* 2014).

Numerous cilia genes are down-regulated in breast cancer (Menzl *et al.* 2014; Shpak *et al.* 2014). They include genes important in ciliogenesis (e.g. IFT46, BBS2, TTC8 and DYNC2H1) and those that code for cilia-localised receptors (e.g. PKD2), although their precise role in breast cancer pathogenesis remains to be determined. The oncogene NEK2 is overexpressed in breast cancer (Hayward *et al.* 2004), resulting in increased ciliary disassembly via Kif24 (Kim *et al.* 2015). Knockdown of either NEK2 or Kif24 in the MCF breast cancer cell series restores cilia and reduces proliferation. However, this is not the case in the most invasive MCF cell types, suggesting that additional mechanisms are involved in cilia loss (Kim *et al.* 2015). NEK8 is also overexpressed in breast cancer (Bowers & Boylan 2004) and modulates ciliary length through the oncogenic Hippo signalling pathway (Habbig *et al.* 2012). Furthermore, a number of cilia-associated genes are commonly mutated in breast cancer: for example *Gli1*, *RPGRIP1* and *DNAH9* (Sjoblom *et al.* 2006; Wood *et al.* 2007). Expression of Kif3a, assessed by immunohistochemistry, is higher in breast cancer tissue compared to adjacent non-cancerous tissue and is correlated with a number of clinical parameters including pathological grade, Ki67 index and presence of lymph node metastases. Higher Kif3a expression is correlated with improved survival (Xia *et al.* 2018).

Primary cilia play an important role in breast development when they are present on luminal epithelial, myoepithelial and stromal cells. Luminal cells lose primary cilia once early branching morphogenesis is complete (McDermott *et al.* 2010). This differential pattern of cilia expression is conserved in healthy human adult breast epithelium with myoepithelial (or basal) cells more frequently possessing primary cilia than luminal cells (Yuan *et al.* 2010; Menzl *et al.* 2014; Nobutani *et al.* 2014). The importance of primary cilia in co-ordinated breast development is exemplified by the *Ift88* mutant Tg737^{ORPK} mouse. These mice display significant cilia loss in developing breast tissue with resultant increases in canonical Wnt and Hh signalling and duct branching defects (McDermott *et al.* 2010).

Thus, luminal breast cancer, derived from the rarely ciliated luminal epithelium, lacks cilia while basal breast cancer (which includes the poor prognosis triple-negative subtype) which originates from the ciliated myoepithelial cells still displays cilia. This illustrates the diverse role that primary cilia can play in cancer.

1.4.1.2 Ovarian cancer

Bioinformatic studies of cancer databases identify that numerous cilia genes are differentially expressed in ovarian cancer compared with normal tissue (Shpak *et al.* 2014) but *in vivo* studies examining cilia in ovarian cancer are lacking. The ovarian cancer cell lines SK-OV3 and OVCAR3 are ciliated (Egeberg *et al.* 2012; Spann *et al.* 2015), although less frequently than primary healthy ovarian surface epithelial cells due to increased AURKA-mediated ciliary disassembly (Egeberg *et al.* 2012). Both Hh and PDGRα signalling are dysregulated in ovarian cancer. Hh signalling is activated due to increased activator and reduced repressor forms of Gli which occurs in a Smo-independent manner despite Smo localisation to the primary cilia (Egeberg *et al.* 2012; Spann *et al.* 2015).

Primary cilia are present on healthy rodent (Teilmann *et al.* 2005) and human (Egeberg *et al.* 2012) ovarian surface epithelium and contain the necessary functional components for Hh and PDGFRα signal transduction (Egeberg *et al.* 2012). Cilia are also present on ovarian hormone producing granulosa cells (Herman & Albertini 1983; Teilmann *et al.* 2005; Johnson *et al.* 2008) and are sensitive to the pituitary hormone prolactin (Herman & Albertini 1983). Depletion of primary cilia in ovarian granulosa cells in a conditional *Ift88* knockout mouse results in alterations in the oestrus cycle, impaired ovulation and delayed breast development, which can be rescued by exogenous oestrogen (Johnson *et al.* 2008). Therefore, primary cilia are important in ovarian endocrine function.

Thus, it appears likely that primary cilia play a role in ovarian cancer development, although this still requires definitive experimental validation.

1.4.1.3 Prostate cancer

A single study has examined primary cilia in human prostate cancer specimens (Hassounah *et al.* 2013). Primary cilia frequency and length was reduced in both prostatic intra-epithelial neoplasia and prostate cancer compared with noncancerous tissue. Of note, while frequency was unchanged, cilia were shorter in the stromal cells surrounding tumours than in normal prostate tissue, suggesting the possibility of a 'field effect' or cilia shortening being an early event in prostate tumourigenesis. In addition, primary cilia frequency in the 'normal' tissue surrounding prostate cancer correlated with many clinical outcomes, including tumour size, stage and risk of recurrence.

The cilia-mediated Hh signalling pathway plays a pivotal role in prostatic development and is required for normal budding and duct formation (Podlasek *et al.* 1999; Wang *et al.* 2003). Paracrine signalling between the epithelium, which secretes Hh ligand, and the stroma, which expresses the Hh receptor Ptch, inhibits proliferation and promotes differentiation (Wang *et al.* 2003). As is expected for a system reliant on Hh signalling, primary cilia are present on both mesenchymal and epithelial prostate cells (Zhang *et al.* 2009). This is further reflected in the presence of functional primary cilia on the UGSM2 (murine urogenital sinus mesenchyme) and WPMY-1 (human prostate myofibroblast) cell lines (Zhang *et al.* 2009) and prostatic fibroblasts (Wilkinson *et al.* 2013). Interestingly, primary cilia are absent on a range of prostate cancer cell lines derived from prostate and metastatic sites (Zhang *et al.* 2009), but are present on prostate cancer-associated fibroblasts, which are dependent on Hh signalling for survival and proliferation (Wilkinson *et al.* 2013).

1.4.1.4 Renal cancer

Primary cilia frequency is reduced in all subtypes of renal cancer compared to adjacent non-cancerous renal tissue (Schraml *et al.* 2009; Basten *et al.* 2013). Ciliary loss is most pronounced in clear cell renal cell carcinoma (ccRCC), the most common subtype of renal cancer, in which von Hippel-Lindau (VHL) is inactivated (Moore *et al.* 2011).

Von Hippel–Lindau (VHL) disease is a familial cancer syndrome caused by mutations in the VHL gene and is discussed in detail in Chapter 2. Affected individuals are at risk of developing a range of tumours, including endocrine malignancies of the pancreas and adrenal medulla. In addition, renal and pancreatic cysts are a feature of VHL, which can be considered an atypical ciliopathy (Schraml *et al.* 2009).

Primary cilia loss is a feature of renal cysts in VHL patients (Esteban *et al.* 2006), as well as in sporadic ccRCC (Schraml *et al.* 2009; Basten *et al.* 2013). VHL-deficient RCC cell lines display no or very few cilia (Esteban *et al.* 2006; Lutz & Burk 2006; Schermer *et al.* 2006; Lolkema *et al.* 2008), and *Vhl* knockdown in murine renal cells results in cilia loss (Schermer *et al.* 2006). Expression of wild-type pVHL in these RCC cells restores cilia (Esteban *et al.* 2006; Lutz & Burk 2006; Schermer *et al.* 2006), but this is not the case with disease-causing pVHL mutations (Lutz & Burk 2006). Frew *et al.* (Frew *et al.* 2008) found that VHL loss in retinal pigment epithelial (RPE) cells and primary mouse embryonic fibroblasts did not affect cilia formation, but resulted in an accelerated rate of cilia disassembly upon challenge with serum, a stimulus to ciliary disassembly. However, others have observed reduced ciliary formation in VHL knockdown RPE cells (Dere *et al.* 2015).

Thus, pVHL appear to play an important role in maintenance of primary cilia. The canonical function of pVHL is as an E3-ubiquitin ligase that targets HIF for proteasomal-mediated degradation. The mechanisms by which pVHL loss results in cilia ablation have been reported to involve both HIF-dependent (Esteban *et al.* 2006) and HIF-independent pathways (Lutz & Burk 2006).

pVHL localises to primary cilia (Schermer *et al.* 2006; Lolkema *et al.* 2008) where it binds to and stabilises microtubules (Okuda *et al.* 1999; Hergovich *et al.* 2003, 2006; Schermer *et al.* 2006; Lolkema *et al.* 2007). This is achieved via a microtubule-binding domain in pVHL that is distinct from the HIF-binding domain. Interestingly, this microtubule-binding domain is a mutational hotspot (Hergovich *et al.* 2003) in VHL. VHL–microtubule interactions are mediated by the Par3-Par6-aPKC (Okuda *et al.* 1999; Schermer *et al.* 2006) and kinesin-2/KIF3A (Lolkema *et al.* 2007) complexes. Thus, the role of pVHL in microtubule stabilisation provides a clear mechanism for its function in ciliary maintenance.

In addition, pVHL loss results in increased expression of both HDAC6 and AURKA. This occurs due to both HIF-dependent (Xu *et al.* 2010) (both *HEF1* and *NEK8* are HIF- responsive genes (Xu *et al.* 2010; Ding *et al.* 2015)) and HIF-independent (Dere *et al.* 2015) mechanisms and it should be noted that HIF accumulation is insufficient in itself to cause RCC development (Kim *et al.* 2006a).

The situation is more complex, however, as VHL inactivation alone may be insufficient to alter cilia *in vivo*. Evidence to support this comes from human data in which VHL inactivation in single renal tubular cells gives rise to a different ciliary phenotype than VHL inactivation in cyst-lining cells (Montani *et al.* 2010). Mouse models of VHL do not recapitulate the renal phenotype (Haase *et al.* 2001; Ma *et al.* 2003) and additional genetic inactivations are required for cilia loss and cyst formation — for example, mutations in glycogen synthase kinase-3β (Thoma *et al.* 2007),

phosphatase and tensin homologue (Frew *et al.* 2008), transformation-related protein 53 (Albers *et al.* 2013), Kif3a (Guinot *et al.* 2016) and retinoblastoma 1 (Harlander *et al.* 2017). In addition to its direct interaction with AURKA (Fumoto *et al.* 2008; Dar *et al.* 2009), GSK3β regulates the microtubule binding function of VHL (Hergovich *et al.* 2006) such that simultaneous loss of both VHL and GSK3β results in intensified serum-induced ciliary disassembly (Thoma *et al.* 2007).

Thus, pVHL and primary cilia are important in renal cyst and ccRCC formation. We can speculate that primary cilia may also play a role in the pathogenesis of other VHL-associated cancers, although this is yet to be demonstrated.

1.4.1.5 Medulloblastoma

Medulloblastomas, the most common paediatric brain tumour, arise from cerebellar granule neuron precursors and are dependent on Hh signalling for their proliferation and tumorigenesis (Huangfu & Anderson 2005). Primary cilia play a dual role in either supporting or inhibiting medulloblastoma development dependent on the location of the initiating oncogenic event within the Hh pathway (Han *et al.* 2009). In medulloblastomas driven by the upstream activator of Hh signalling Smo, tumour formation was prevented by ablation of primary cilia. When the oncogenic event was distal to primary cilia, for example in Gli2-driven tumours, absence of cilia was required for tumour development. This molecular dissection of medulloblastoma aetiology in mice correlates with human medulloblastoma subtypes: primary cilia are present on classic and desmoplastic medulloblastomas associated with Ptch1 mutations, but are absent on anaplastic medulloblastomas (Han *et al.* 2009). Furthermore, a number of key ciliary proteins and regulators have been identified as central to medulloblastoma formation including Kif3a (Han *et al.* 2009; Barakat *et al.* 2013), INPP5E (Conduit *et al.* 2017) and ADP-ribosylation factor-like protein 13B (Arl13b) (Bay *et al.* 2018).

Remarkably, the importance of primary cilia in medulloblastomas extends beyond their development. In Hh-dependent medulloblastomas, loss of primary cilia confers and correlates with resistance to Smo inhibitors (Zhao *et al.* 2017) thus identifying cilia as potential therapeutic targets.

1.4.2 Mechanisms of ciliary dysfunction in cancer

Tumoural alterations in primary cilia result from dysregulation of the balanced control of ciliary assembly and disassembly.

Activation of the AURKA/HDAC6 ciliary disassembly pathway is seen in many tumours in which cilia loss occurs. AURKA is overexpressed in ovarian (Egeberg *et al.* 2012) and renal cancer (Schraml *et al.* 2009; Basten *et al.* 2013; Dere *et al.* 2015), whilst HDAC6 overexpression is a feature of cholangiocarcinomas (Gradilone *et al.* 2013; Mansini *et al.* 2018) and chondrosarcomas (Xiang *et al.* 2017). In cholangiocarcinomas, this is achieved through alterations in microRNA processing (Mansini *et al.* 2018). Inhibition of HDAC6 by tubacin restores primary cilia and reduces proliferation and cellular invasion (Gradilone *et al.* 2013; Xiang *et al.* 2017).

This mechanism is not universal, however, as HDAC6 depletion and inhibition have no effect on ciliation of pancreatic cancer cells (Kobayashi *et al.* 2017). Broader HDAC inhibition with trichostatin A did have an impact and led to the identification of HDAC2 as a ciliary disassembly factor through its positive regulation of AURKA expression (Kobayashi *et al.* 2017). K-ras signalling is also upregulated in pancreatic cancer cells and similarly upregulates AURKA expression (Seeley *et al.* 2009) through the transcription factor ETS2 (Furukawa *et al.* 2006).

Enhanced ciliary disassembly also occurs in breast cancer due to Nek2 over-expression (Hayward *et al.* 2004; Cappello *et al.* 2014). Depletion of Nek2 or its effector Kif24 in a variety of breast cancer cell lines restores cilia (Kim *et al.* 2015). Cell cycle-related kinase (CCRK) and its substrate intestinal cell kinase (ICK) appear to suppress cilia formation (Yang *et al.* 2013) and are over-expressed in glioblastoma multiforme (GBM) (Ng *et al.* 2007). The mechanism by which this results in cilia loss has not been elucidated with data from a mouse developmental model suggesting a role in ciliogenesis (Snouffer *et al.* 2017), which does not explain the role observed in GBM.

Reductions in cilia assembly are also responsible for cilia loss in cancer. The oestrogen receptor alpha (ERα) co-repressor split ends regulates the expression of a number of genes involved in ciliary biology and its knockdown results in ciliary loss (Légaré *et al.* 2017). Intriguingly, tumoural split ends RNA levels are predictive of metastasis risk in human ER negative breast cancer (the subtype which lacks cilia) (Légaré *et al.* 2017). Post-translational glycylation of microtubules by tubulin glycylases (TTLs) contributes to axonemal stability. TTL3 knockout mice display aberrant colonic cilia formation and increased epithelial turnover; low TTL3 levels are associated with human colorectal cancer development (Rocha *et al.* 2014).

Alterations in cilia-mediated signalling pathways also potentially contribute to ciliary dysregulation in cancer. The Wnt pathway component APC promotes ciliary disassembly whilst inhibiting ciliogenesis and is mutated in the hereditary cancer syndrome familial adenomatous polyposis (Jimbo *et al.* 2002; Jaulin & Kreitzer 2010). If the β-catenin binding protein Jouberin loses its ciliary localisation signal, nuclear β-catenin accumulates resulting in increased cellular proliferation compared to wild type Jouberin (Lancaster *et al.* 2011).

1.4.3 Mechanisms by which ciliary dysfunction contributes to tumourigenesis

In tumour types in which cilia loss occurs, it does so early in tumourigenesis, as it is a feature of a range of pre-invasive precursor lesions. For example, cilia loss has been observed in pancreatic intraepithelial neoplasia (Seeley *et al.* 2009; Schimmack *et al.* 2016), prostatic intraepithelial neoplasia (Hassounah *et al.* 2013), breast carcinoma in situ (Menzl *et al.* 2014) and melanoma in situ (Kim *et al.* 2011b; Snedecor *et al.* 2015).

In addition to cilia loss being an intrinsic feature of tumoural cells, there is growing evidence that features of the local tumour microenvironment influence primary cilia. Whilst pancreatic cancer cells generally lack primary cilia, tumour-associated stromal cells display primary cilia (Bailey *et al.* 2009; Schimmack *et al.* 2016) and are crucial in sustaining oncogenic paracrine Hh signalling in this context (Bailey *et al.* 2009). Endocrine factors can also play a role; PTH suppresses cilia formation and promotes proliferation and invasion of chondrosarcoma cells (Xiang *et al.* 2014). Furthermore, the human carcinogens ochratoxin A and potassium bromide induce ciliary loss in renal tubular epithelial cells (Radford *et al.* 2012). The inflammatory cytokine tissue necrosis factor alpha causes cilia loss through NF-κB signalling (Vézina *et al.* 2014) and expression of programmed cell death protein-1 receptor is associated with primary cilia frequency in colorectal cancers (Dvorak *et al.* 2017). Cilia are sensory organelles and changes in luminal fluid flow and composition (Mansini *et al.* 2019) and oxygen tension (Proulx-Bonneau & Annabi 2011) can result in disease-relevant alterations in primary cilia.

Primary cilia loss, achieved through a variety of independent mechanisms, results in increased cellular proliferation providing evidence for cilia playing a cell-cycle gatekeeper role. Overexpression of HDAC6 in cholangiocytes results in ciliary loss and increased proliferation and is prevented by HDAC6 inhibition (Gradilone *et al.* 2013). This is dependent on primary cilia being present and is prevented by IFT88 knockdown, arguing against a non-ciliary mechanism (Gradilone *et al.* 2013). Similarly, depletion or inhibition of HDAC6 in chondrosarcoma cells restores cilia, reduces proliferation and invasion and inhibits tumour growth *in vivo* (Xiang *et al.* 2017). Depletion of Nek2

or Kif24 in breast cancer cell lines also restores primary cilia and reduces cellular proliferation (Kim *et al.* 2015), whilst TTL3 loss promotes colonic epithelial proliferation & tumour formation (Rocha *et al.* 2014). Primary cilia loss in human astrocytes stimulates cell growth in a lysophosphatidic acid (LPA) dependent manner (Loskutov *et al.* 2018). When present, the primary cilium sequesters the LPA receptor, thereby preventing its interaction with relevant G proteins that are excluded from cilia. In the absence of a cilium, as is the case in GBM, this interaction occurs with resultant proliferation (Loskutov *et al.* 2018). CCRK and ICK directly link primary cilia to the cell cycle: loss of either results in ciliary elongation and a reduction in G1/S progression which is prevented by Kif3 knockdown (Yang *et al.* 2013). Conversely, increasing cilia length through a variety of means in a range of cancer cell lines can slow cellular proliferation in a process that requires primary cilia (Khan *et al.* 2016).

Cilia dysfunction results in dysregulation of a number of cilia-mediated oncogenic signalling pathways. Hh signalling is disrupted in multiple cancers in which cilia loss and retention is a feature, including pancreatic (Nielsen *et al.* 2008; Bailey *et al.* 2009), medulloblastoma (Han *et al.* 2009), basal cell carcinoma (Wong *et al.* 2009; Yang *et al.* 2017) and ovarian cancer (Egeberg *et al.* 2012). Activation of Hh signalling, in addition to being pro-proliferative, contributes to the key oncogenic process of epithelial-to-mesenchymal transition (EMT) in a cilia-dependent manner (García-Zaragoza *et al.* 2012; Guen *et al.* 2017). Wnt signalling is a feature of prostate cancer (Lancaster *et al.* 2011; Hassounah *et al.* 2013) and is attenuated by a shortened cilium and activated by ciliary ablation (Lancaster *et al.* 2011; Oh & Katsanis 2013). Aberrant Notch signalling is a feature of choroid plexus tumours (Li *et al.* 2016), is dependent on primary cilia and plays a crucial role in cellular differentiation (Ezratty *et al.* 2011).

It has also been proposed that cilia contribute to tumourigenesis through altered proteosomal activity (Gerhardt *et al.* 2016) and dysregulation of autophagy (Cao & Zhong 2015). Alterations in activity of the E3 ubiquitin ligase component of the ubiquitin-proteasome system are a common feature of cancers (Kitagawa *et al.* 2009) and multiple BBSome and transition zone proteins interact with proteosomal components (Gerdes *et al.* 2007; Sang *et al.* 2011; Liu *et al.* 2014; Gerhardt *et al.* 2015). The cellular homeostatic process of autophagy is bi-directionally linked to primary cilia and is dysregulated in cancers in which ciliary dysfunction occurs (Perera *et al.* 2015; Lee *et al.* 2016). Autophagy itself promotes and restricts processes involved in ciliary assembly and disassembly (Pampliega *et al.* 2013; Tang *et al.* 2013) and cilia-mediated Hh signalling promotes autophagy (Pampliega *et al.* 2013).

Beyond its role in tumour development, features of tumoural primary cilia are associated with prognosis and treatment susceptibility and resistance. Cilia loss is associated with an increased risk of perineural invasion in prostate cancer (Hassounah *et al.* 2013), distant metastases in melanoma (Snedecor *et al.* 2015) and overall survival in colorectal adenocarcinoma (Dvorak *et al.* 2016). Further indirect evidence of the link between cilia loss and prognosis is provided by HEF1 which stimulates the AURKA/HDAC6 pathway and is pro-metastatic in breast cancer (Minn *et al.* 2005) and melanoma (Kim *et al.* 2006b) and is associated with increased aggressiveness of GBM (Natarajan *et al.* 2006). Interestingly in pancreatic cancer, in which cilia loss is a feature, those tumours that retained cilia had an increased risk of lymph node metastasis and a poorer prognosis (Emoto *et al.* 2014).

In Hh-dependent medulloblastomas, loss of tumoural primary cilia may confer resistance to Smo inhibitors (Zhao *et al.* 2017; Bay *et al.* 2018), whilst AURKA overexpression leads to taxol resistance (Anand *et al.* 2003). Cilia presence and length is associated with resistance to a variety of kinase inhibitors in a range of cancer cell lines and drug sensitivity can be restored through shortening of primary cilia (Jenks *et al.* 2018).

CHAPTER 2
Phaeochromocytomas and paragangliomas

2.1 Definition and demographics

Phaeochromocytomas and paragangliomas (PGL; collectively termed PPGLs) are neuroendocrine tumours (NETs). They are of neural crest origin and have the potential to secrete catecholamines. Phaeochromocytomas arise from chromaffin cells of the adrenal medulla, a modified ganglion of the sympathetic nervous system which receives innervation from preganglionic fibres. PGL arise from chromaffin cells of the autonomic nervous system, either from the paravertebral sympathetic chain or parasympathetic ganglia in the neck and skull base, in which case they are termed head and neck PGL (HNPGL) (Figure 2.1). Phaeochromocytomas form around 70-75% of PPGLs with PGL comprising the remainder(Lenders *et al.* 2005).

The first published clinical description of a phaeochromocytoma was in 1800 (Sugrue 1800; Cronin 2008), although it was not until 1886 that the associated histopathology was documented, including the characteristic tumoural colour change from red to dark brown with the addition of chromate salts (Fränkel 1886). It is this 'chromaffin reaction', caused by catecholamine oxidation, which led to the naming of the condition, literally meaning 'dark coloured tumour'.

The actual prevalence of PPGLs in the general population is difficult to determine given that the diagnosis is often only made in retrospect post mortem. Autopsy studies suggest a prevalence rate of 0.05% with 50% of these deaths being directly attributable to PPGLs (Lo *et al.* 2000; McNeil *et al.* 2000). Prevalence is unsurprisingly enriched in certain clinical populations and reaches 0.6% in the hypertensive outpatient population (Omura *et al.* 2004) and 5% of patients with adrenal incidentalomas (radiological abnormalities identified on examinations performed for other reasons) (Mansmann *et al.* 2004). It is much higher in certain genetic conditions, discussed later in this chapter. There is no identified difference in prevalence between the sexes.

The overall malignancy rate for all PPGLs approaches 20% (Plouin *et al.* 2012), but is higher in certain patient groups and is up to 40% in patients with mutations in succinate dehydrogenase B (SDHB) (Brouwers *et al.* 2006; Amar *et al.* 2007).

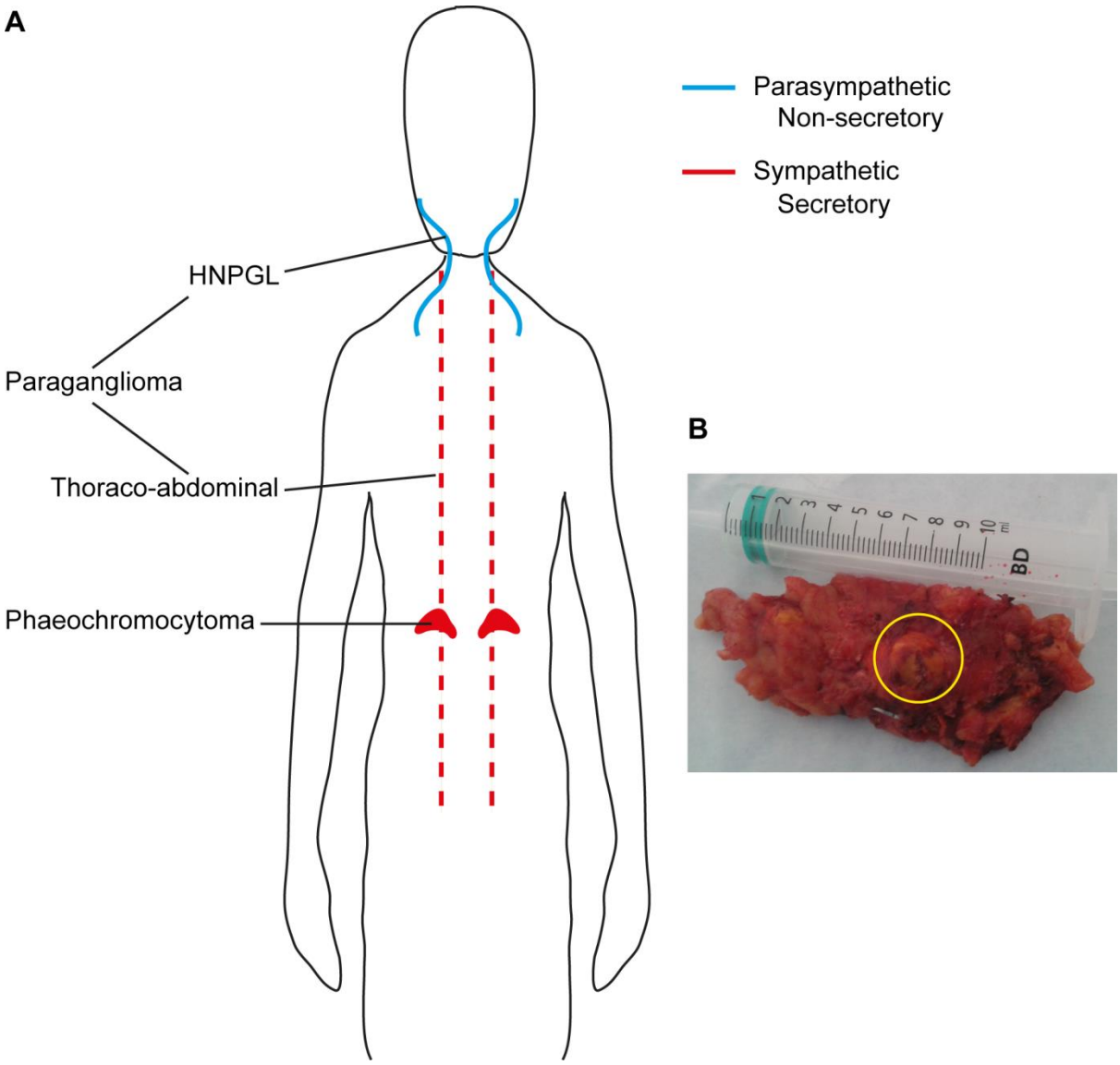

Figure 2.1: Location and secretory pattern of phaeochromocytomas and paragangliomas

(A) Schematic demonstrating the possible location of phaeochromocytomas (arising from the adrenal medulla) and paragangliomas (arising from the autonomic nervous system). Locations of tumours of sympathetic origin (which are almost always secretory) are marked in red and those of parasympathetic origin (which are rarely secretory) in blue. HNPGL – head and neck paraganglioma.

(B) A photograph of an adrenalectomy specimen containing a phaeochromocytoma (circled in yellow) with a 10ml syringe for scale.

2.2 Clinical features

The symptoms and signs associated with PPGLs result from either the action of uncontrolled catecholamine release or due to tumour mass effect of the primary lesion or secondary deposits when metastatic.

The majority of PPGLs are secretory, although some, particularly HNPGL (van Duinen *et al.* 2013), are not. Patients with secretory PPGs are subject to autonomous, excessive and episodic catecholamine secretion which, through their adrenoreceptor action, gives rise to the classical symptoms and signs of hypertension, palpitations, sweating, anxiety, headaches and hyperglycaemia (discussed later in this chapter). These features are often paroxysmal, reflecting stochastic catecholamine release, which can either be spontaneous or precipitated; precipitants of catecholamine release include trauma, tumoural infarction and a wide range of drugs (e.g. dopamine receptor antagonists, β-adrenoceptor antagonists, opiates, glucocorticoids and neuromuscular blocking agents). The most severe manifestation of catecholamine excess is a 'phaeochromocytoma crisis' in which severe hypertension is immediately life-threatening due to the risks of stroke, myocardial infarction and acute pulmonary oedema. In the context of PPGL, these clinical effects are due to adrenaline and noradrenaline with minimal effect from dopamine. The cardiovascular burden of catecholamine excess is high with significant associated morbidity and mortality (Khorram-Manesh *et al.* 2004; Zelinka *et al.* 2012).

PPGLs can also cause clinical symptoms and signs due to local mass effect from infiltration and obstruction of adjacent structures, which can either be due to the primary tumour itself or metastatic deposits. Due to the diffuse distribution of chromaffin cells throughout the body and the potential for multifocality, the diagnosis of metastases within PPGLs is restricted to tumours found in nonchromaffin tissue (De Lellis *et al.* 2004).

2.3 Pathogenesis

2.3.1 Catecholamine production

The catecholamines dopamine, noradrenaline and adrenaline are monoamines formed of a catechol group linked to an amine group by an ethyl chain (Figure 2.2B). They are produced from the precursor amino acids phenylalanine and tyrosine in the adrenal medulla, postganglionic sympathetic nervous system and specific areas of the brain (e.g. ventral tegmental area and substantia nigra) with the type of catecholamine being regulated by the presence or absence of

certain enzymes in the catecholamine synthesis pathway (Figure 2.2A). In the rate-limiting step of this anabolic pathway, tyrosine is converted to L-3,4-dihydroxyphenylalanine (L-DOPA) by tyrosine hydroxylase (TH), a cytosolic enzyme present only in catecholamine producing cells (Nagatsu *et al.* 1964). L-DOPA is subsequently converted to dopamine by aromatic L-amino acid decarboxylase (also known as DOPA decarboxylase), a widely expressed enzyme which, unlike TH, has other non-catecholamine related functions. Dopamine beta-hydroxylase (DBH), which is confined to catecholamine producing cells, converts dopamine to noradrenaline. Noradrenaline is subsequently converted to adrenaline in cells containing phenylethanolamine N-methyltransferase (PNMT), which is predominantly expressed in the adrenal medulla.

Catecholamine release, whether from the adrenal medulla (predominantly adrenaline), sympathetic nerves (noradrenaline) or dopaminergic pathways of the central nervous system (dopamine), is episodic and results from exocytosis of pre-formed catecholamine-containing vesicles into the synaptic cleft or vasculature. Noradrenaline is released following action potential arrival at the pre-synaptic terminal with depolarisation of the neural membrane, a process that is inhibited by a wide range of factors including reciprocal innervation from cholinergic parasympathetic neurons, dopamine, serotonin, histamine and noradrenaline itself through the action of pre-synaptic α_2-adrenoceptors. In contrast, noradrenaline release is augmented by adrenaline through its effect on the stimulatory β_2-adrenoceptor. In health, circulating noradrenaline levels are low and represent 'over-spill' from the synapses of the sympathetic nervous system and it therefore has limited systemic effect. Adrenaline, the predominant circulating catecholamine, is released by the adrenal medulla in response to stimulation from sympathetic preganglionic neurons carried by the splanchnic nerves. Unlike catecholamines, metanephrines are released continuously and independently of vesicle-mediated catecholamine release, which has important clinical implications in PPGL diagnosis.

Catecholamines function both as neurotransmitters and hormones and exert their wide ranging physiological effects though GPCRs: adrenaline and noradrenaline via adrenoreceptors and dopamine via dopamine receptors.

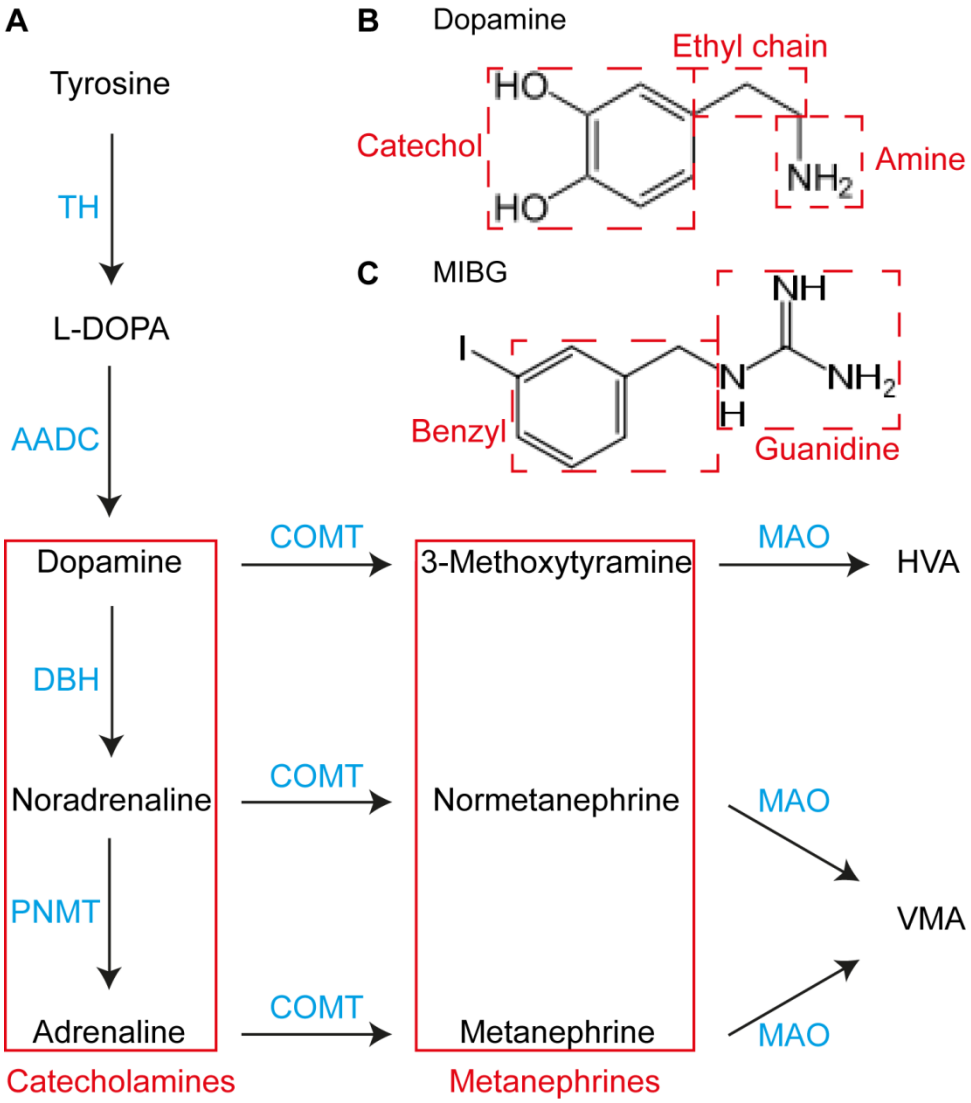

Figure 2.2: Catecholamine structure, synthesis and degradation pathways

(A) A schematic representation of the key stages in catecholamine and metanephrine synthesis and degradation. Enzymes are represented in blue.

TH – tyrosine hydroxylase, AADC – aromatic L-amino acid decarboxylase, DBH – DOPA beta-hydroxylase, PNMT – phenylethanolamine N-methyltransferase, COMT – catechol-*O*-methyltransferase, MAO – monoamine oxidase, HVA – homovanillic acid, VMA – vanillylmandelic acid.

(B) The three constituent chemical components of a catecholamine are demonstrated, using dopamine as an example.

(C) Metaiodobenzylguanidine (MIBG) consists of iodinated benzyl and guanidine groups and is structurally similar to catecholamines.

There are two subgroups of adrenoceptor (α- and β-) which enact a diverse, and sometimes paradoxical, range of tissue responses through their different tissue localisations, associated G proteins and ligand sensitivities (Figure 2.3). Activation of the G_q linked α_1-adrenoceptor results in activation of PLC with resultant cellular calcium influx and smooth muscle contraction, amongst other effects. By contrast the α_2-adrenoceptor, through G_i, reduces cAMP and calcium entry and thus confers relaxation of smooth muscle and inhibition of neurotransmitter release. Stimulation of the G_s coupled β-adrenoceptors results in cAMP generation and subsequent increases in heart muscle contraction (via the β_1-adrenoceptor), widespread relaxation of smooth muscle (β_2) and thermogenesis (β_3) based on differential tissue expression of receptor subtypes.

Dopamine acts via its own GPCR, which has five subtypes divided into two subgroups. The D_1-like family (D_1 and D_5) is coupled to G_s and stimulation results in activation of AC and cAMP generation. The D_2- like family (D_2, D_3 and D_4) is conversely linked to G_i and inhibits AC and reduces cAMP. Dopamine receptors are widespread throughout the central nervous system with particular importance in the mesolimbic, mesocortical, nigrostriatal and tuberoinfundibular pathways where they play roles in reward-related cognition, executive functioning, learning and the inhibition of pituitary prolactin release. The cardiovascular effects of dopamine are limited, but it does increase myocardial contractility as well as having a vasodilatory effect.

Figure 2.3: Adrenoceptor pharmacology (overleaf)

PLC – phospholipase C, AC – adenylyl cyclase, IP_3 – inositol trisphosphate, DAG – diacylglycerol, cAMP – cyclic adenosine monophosphate, SM – smooth muscle, GI – gastrointestinal. Arrow size represents relative ligand receptor affinity.

1 – Constriction of blood vessels, bronchi, GI and bladder sphincters, uterus, seminal tract, iris. 2 – Both constriction and dilatation. 3 – Reduced release at adrenergic and cholinergic nerve terminals and inhibition of brainstem sympathetic outflow. 4 – Dilatation of blood vessels and bronchi, relaxation of GI tract, uterus, bladder detrusor, seminal tract and ciliary muscle. 5 – Hepatic and muscular. 6 – Increased release at adrenergic nerve terminals.

The β_3-adrenoceptor is not shown for clarity. It is linked to G_s and results in increased cAMP with resultant skeletal muscle thermogenesis, adipose tissue lipolysis and thermogenesis.

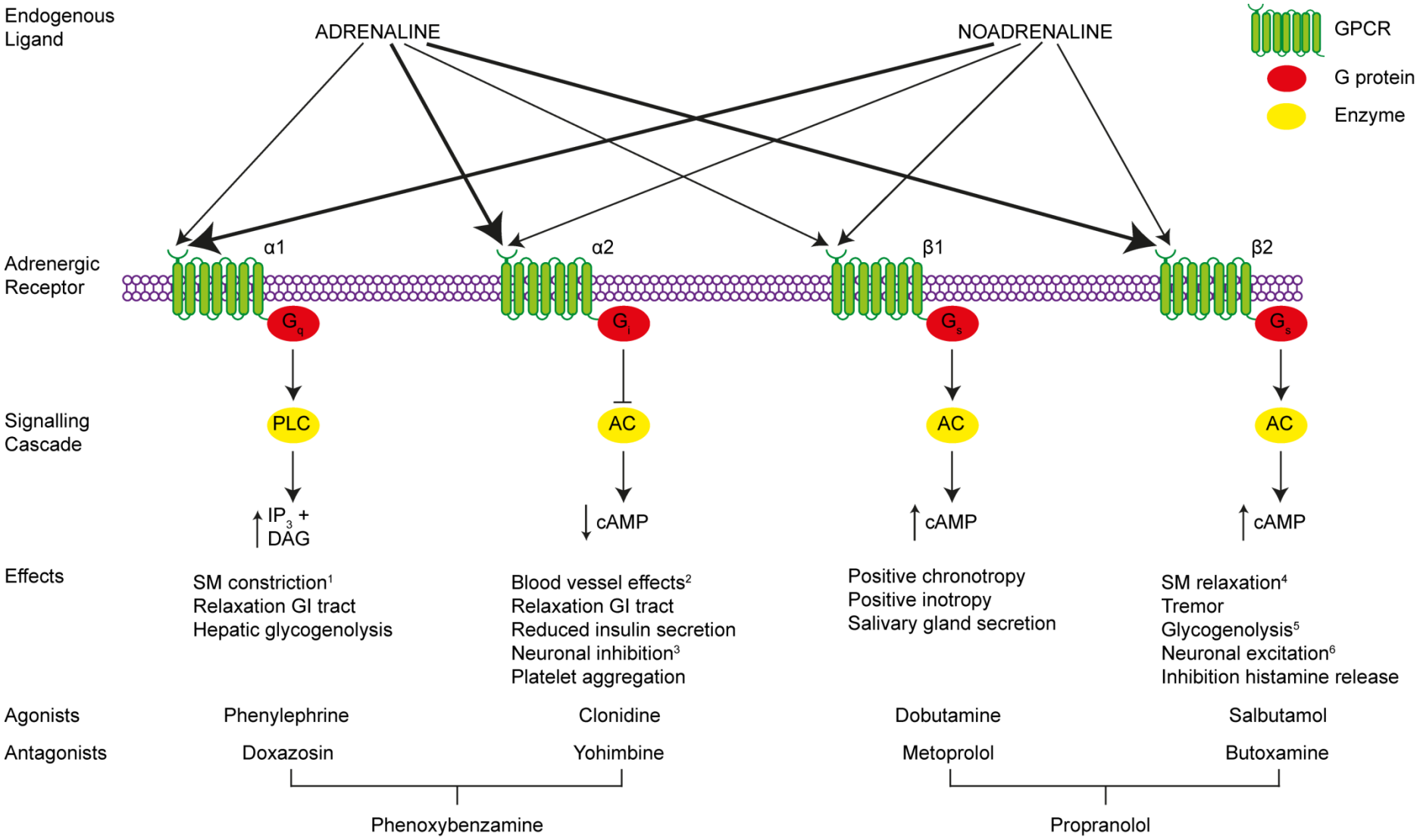
Endogenous Ligand
ADRENALINE
NOADRENALINE
GPCR
G protein
Enzyme
Adrenergic Receptor
α1
α2
β1
β2
G_q
G_i
G_s
G_s
Signalling Cascade
PLC
AC
AC
AC
↑ IP_3 + DAG
↓ cAMP
↑ cAMP
↑ cAMP
Effects
SM constriction[1]
Relaxation GI tract
Hepatic glycogenolysis
Blood vessel effects[2]
Relaxation GI tract
Reduced insulin secretion
Neuronal inhibition[3]
Platelet aggregation
Positive chronotropy
Positive inotropy
Salivary gland secretion
SM relaxation[4]
Tremor
Glycogenolysis[5]
Neuronal excitation[6]
Inhibition histamine release
Agonists
Phenylephrine
Clonidine
Dobutamine
Salbutamol
Antagonists
Doxazosin
Yohimbine
Metoprolol
Butoxamine
Phenoxybenzamine
Propranolol

2.3.2 Aetiology

2.3.2.1 Environmental factors

Exposure to chronic hypoxia increases the risk of PPGL development and is the only known environmental risk factor.

2.3.2.1.1 Altitude

The chemoreceptor type I cells of the carotid body are sensitive to the partial pressure of oxygen and undergo hyperplasia in response to hypobaric hypoxia in a range of mammals, including humans residing at high altitude (Edwards *et al.* 1971, 1972; Arias-Stella & Bustos 1976; Arias-Stella & Valcarcel 1976). This response was also seen in rats after just one month's exposure to simulated high altitude in a hypobaric chamber (Laidler & Kay 1975, 1978). These changes result in increased urinary, venous and arterial noradrenaline in rats (Johnson *et al.* 1983; Hui *et al.* 2003) and humans (Cunningham *et al.* 1965; Mazzeo *et al.* 1994) at altitude without changes in adrenaline production (Cunningham *et al.* 1965; Johnson *et al.* 1983; Mazzeo *et al.* 1994).

The frequency of carotid body tumours (a type of HNPGL) appears to be elevated in cows (Arias-Stella & Bustos 1976) and humans (Saldana *et al.* 1973; Pacheco-Ojeda *et al.* 1988; Rodríguez-Cuevas *et al.* 1998) residing at high altitude, although these data are observational and could potentially be explained by an increased prevalence of predisposing germline mutations in susceptibility genes in geographically isolated populations (Enríquez-Vega *et al.* 2019). There is also a suggestion that altitude could potentially modify phenotypic severity of genetic predispositions as high altitude dwelling was associated with increased tumour number within an SDHD cohort (Astrom *et al.* 2003).

2.3.2.1.2 Congenital cyanotic heart disease

Congenital cyanotic heart disease (CCHD) has been associated with PPGL development through retrospective case studies. The largest series, which was an international collaboration, identified 18 individuals with both CCHD and PPGL (Opotowsky *et al.* 2015). Patients were young (median age of diagnosis 31.5 years) with a noradrenergic phenotype and a high frequency of multiple tumours and extra-adrenal disease. These case descriptions were combined with analysis of a US national discharge database which demonstrated that hospitalised CCHD patients had a significantly increased risk of having a PPGL compared to patients without CCHD (adjusted odds ratio 6.0). Non-cyanotic CHD did not confer an increased risk of PPGL development.

Given the importance of hypoxic signalling in PPGL development, it has been suggested that the prolonged and severe hypoxia in CCHD is an aetiological factor. For example, in the previously mentioned international series the median duration of cyanosis prior to PPGL diagnosis was 20 years with a mean oxygen saturation of 87.4% (Opotowsky *et al.* 2015). However, hypoxic signalling has not been directly examined in these tumours.

2.3.2.1.3 Chronic lung disease

Studies by the US National Toxicology Program have identified a wide range of inhaled toxins as risk factors for phaeochromocytoma development in rodents. Implicated agents include talc, nickel oxide, nickel subsulfide and cobalt sulphate (National Toxicology Progam 1993, 1996a, b, 1998). When these studies are considered together, there is a strong correlation between lung pathology, specifically inflammation and fibrosis, and the development of phaeochromocytoma in rats (Ozaki *et al.* 2002), suggesting that the mechanism is hypoxia-mediated due to toxin-induced lung disease rather than due to specific toxic or carcinogenic effects. There is no evidence in humans that any of these toxins result in phaeochromocytoma.

Autopsy studies suggest that carotid body hyperplasia occurs in individuals with chronic hypoxia due to a range of chronic pulmonary conditions including cystic fibrosis and chronic obstructive pulmonary disease (Lack 1977, 1978). There are no data suggesting that PPGLs are more prevalent in these patient groups however.

2.3.2.2 Germline genetic mutations

A heritable role in PPGL development had long been suspected (Marchand 1883) and formed part of the textbook 'rule of tens', in which 10% of PPGLs were thought to be hereditary (Warrell *et al.* 2003). This original estimation has proved to be an underestimate and germline mutations in PPGL predisposition genes are known to occur in up to 40% of tumours (Dahia 2014; Favier *et al.* 2015). Indeed, Fränkel's original patient, who was 18 and had bilateral phaeochromocytomas almost certainly had multiple endocrine neoplasia type 2 (MEN2) based on genetic analysis of their descendants (Fränkel 1886; Neumann *et al.* 2007).

Advances in genetic technology and understanding over the past 30 years have resulted in the identification of an ever expanding list of PPGL predisposition genes, which currently number 16 (Table 2.1, Figure 2.4). These genes have traditionally been classified according to their function and role in PPGL pathogenesis into two groups, or clusters. Cluster 1 is characterised by pseudohypoxic

signalling, whilst in cluster 2 tumours kinase signalling is activated (Figure 2.5). A recent comprehensive molecular characterisation of PPGLs from the Cancer Genome Atlas has affirmed this taxonomy and identified two additional distinct groups of PPGLs termed 'Wnt-altered' and 'cortical admixture' (Fishbein *et al.* 2017).

In this section, we will consider genetic syndromes and germline mutations associated with PPGL development. The role of somatic mutations will be discussed later in the chapter.

2.3.2.2.1 Cluster 1

Under normal cellular conditions, the transcriptional activity of the HIFs are repressed through the constant targeting of their alpha subunit (HIFα) for proteosomal degradation by the protein von Hippel-Lindau (pVHL)-containing E3 ubiquitin ligase complex (Kibel *et al.* 1995) (Figure 2.5). pVHL forms the recognition component of this complex and hydroxylation at specific proline residues is required to allow HIFα binding. This HIF hydroxylation is catalysed by HIF-prolyl hydroxylases (HIF-PHDs or PHDs) in a process that requires oxygen (Maxwell *et al.* 1999; Cockman *et al.* 2000; Ivan *et al.* 2001; Jaakkola *et al.* 2001). Therefore, when oxygen is limited, HIFα hydroxylation is reduced with its resultant escape from the degradation pathway. Persistent HIFα is then available to dimerise with its constitutively expressed partner HIF1β. This HIFα-HIF1β complex is imported into the nucleus where it binds to specific hypoxia response elements (HREs) on DNA with resultant transcriptional activation (Wenger *et al.* 2005; Schodel *et al.* 2011). HIF is a master transcription factor resulting in the expression of hundreds of genes involved in diverse cellular processes including proliferation, apoptosis, differentiation, energy metabolism, growth factor production and angiogenesis (Elvidge *et al.* 2006; Hu *et al.* 2006; Choi *et al.* 2008; Ortiz-Barahona *et al.* 2010). Hypoxic signalling therefore plays an important physiological role in embryonic development and adaptation to altitude; its inappropriate activation, however, contributes to the pathophysiology of many disease states including cancer (Pouysségur *et al.* 2006; Bertout *et al.* 2008; Kaelin 2008).

Activation of hypoxic signalling in the presence of oxygen, so called pseudohypoxia, is the defining feature of cluster 1 PPGLs. This situation arises either from loss of function of pVHL or HIF-PHDs, which can occur either directly or indirectly (Figure 2.5). Cluster 1 genes can be further subdivided into two groups based on differential tumour methylation profiling, which is present in type 1a (SDHx, FH, MDH2) and absent in type 1b (VHL, HIF2α, HIF-PHD) (Letouzé *et al.* 2013).

The associated clinical characteristics of cluster 1 tumours are diverse and gene specific, although elevated normetanephrine (NMN) is characteristic (Eisenhofer *et al.* 2011).

2.3.2.2.1.1 Succinate dehydrogenase

The succinate dehydrogenase (SDH) complex consists of four subunits A, B, C and D. The hydrophilic A and B subunits form the catalytic core of the enzyme and contain the substrate binding site for succinate whilst the hydrophobic C and D subunits anchor the complex to the inner mitochondrial membrane as mitochondrial complex II. SDH is part of both the tricarboxylic acid (TCA) cycle and the electron transport chain (ETC). It catalyses the succinate to fumarate step of the TCA cycle and transfers electrons to the ubiquinone pool. Disruption of SDH function results in succinate accumulation, which inhibits HIF-PHDs, with resultant persistence of HIFα and activation of pseudohypoxic signalling (Selak *et al.* 2005). Succinate accumulation also results in inhibition of additional 2-oxoglutarate-dependent enzymes, including histone and DNA demethylases (Smith *et al.* 2007), leading to epigenetic modification through DNA hypermethylation. Loss of function of SDH results in altered methylation of specific genes and is associated with increased cell migration and EMT (Letouzé *et al.* 2013; Hoekstra *et al.* 2015). Disrupting the ETC results in superoxide generation which also contributes to HIF-PHD inhibition (Gerald *et al.* 2004), although is insufficient to be genotoxic in its own right (Smith *et al.* 2007).

Mutations in any of the four genes encoding the SDH subunits (SDHx; SDHA, SDHB, SDHC, SDHD) or its associated assembly factor (SDHAF2) can result in familial paraganglioma syndromes (PGL1-5; Table 2.1). Inheritance occurs in an autosomal dominant fashion with variable penetrance and maternal imprinting in the cases of SDHD and SDHAF2. In addition to PPGLs, SDHx mutations can be associated with other neoplasia: RCCs (Dwight *et al.* 2013), gastrointestinal stromal tumours (GISTs) (Gill *et al.* 2010; Janeway *et al.* 2011) and pituitary adenomas (López-Jiménez *et al.* 2008; Xekouki *et al.* 2012; Dwight *et al.* 2013; Papathomas *et al.* 2014). SDHx mutations are also responsible for some cases of Carney-Stratakis syndrome (McWhinney *et al.* 2007) and polymorphisms have been related to Cowden-like syndrome, although this association requires further elucidation (Ni *et al.* 2008).

Despite their shared pathological mechanism, the clinical spectrum of SDHx-related PPGLs is varied, particularly tumour location and metastatic risk, and is further discussed with reference to each constituent gene below. Functional SDHx PPGLS are, like all cluster 1 tumours, predominantly NMN secreting with the addition of 3-methoxytyramine (3-MT) (Eisenhofer *et al.* 2011).

2.3.2.2.1.1.1 Familial paragangliomas type 1 (SDHD)

SDHD, the gene responsible for PGL1 (OMIM 16800), was the first component of the SDH complex to be associated with PPGL development (Baysal *et al.* 2000). The syndrome has a high prevalence of HNPGLs (Baysal *et al.* 2000; Neumann *et al.* 2004; Ricketts *et al.* 2010) and also features sympathetic PGLs (Gimm *et al.* 2000) and phaeochromocytomas (Astuti *et al.* 2001a). It is maternally imprinted, resulting in a paternal pattern of inheritance (Yeap *et al.* 2011), and malignancy is uncommon. SDHD mutations can also result in development of RCCs (Ricketts *et al.* 2010) and rarely pituitary adenomas (Xekouki *et al.* 2012; Papathomas *et al.* 2014).

2.3.2.2.1.1.2 Familial paragangliomas type 2 (SDHAF2)

PGL2 (OMIM 601650) consists almost exclusively of HNPGL. Described clinically in 1982 (van Baars *et al.* 1982), SDHAF2 was identified as the responsible gene in 2009 (Hao *et al.* 2009). SDHAF2 is necessary for flavination and therefore function of the SDH complex (Hao *et al.* 2009) and is maternally imprinted, resulting in a paternal pattern of inheritance with high penetrance (~75%) (Kunst *et al.* 2011).

2.3.2.2.1.1.3 Familial paragangliomas type 3 (SDHC)

PGL3 (OMIM 605373), like PGL2, consists almost entirely of HNPGL in addition to some sympathetic PGLs and results from mutations in SDHC (Niemann & Müller 2000; Schiavi *et al.* 2005; Andrews *et al.* 2018).

2.3.2.2.1.1.4 Familial paragangliomas type 4 (SDHB)

Mutations in SDHB result in PGL4 (OMIM 115310), which features phaeochromocytomas and PGLs (sympathetic and HNPGL) (Astuti *et al.* 2001b; Timmers *et al.* 2007a; Ricketts *et al.* 2010). Metastatic disease is seen in approximately one third of patients, making SDHB mutations the greatest risk factor for malignancy in PPGLs (Brouwers *et al.* 2006; Amar *et al.* 2007; Timmers *et al.* 2007a), which is putatively linked to the degree of hypermethylation seen in these tumours (Letouzé *et al.* 2013). Penetrance is around 40% by age 40 (Schiavi *et al.* 2010). Uncommonly, SDHB mutations can be associated with RCC, GISTs and pituitary adenomas (Benn *et al.* 2006; Ricketts *et al.* 2010; Xekouki *et al.* 2012; Dénes *et al.* 2015). SDHB expression can be easily and routinely assessed in tumours by immunohistochemistry (IHC) with lack of expression being seen with mutations in any subunit of the SDH complex (van Nederveen *et al.* 2009). This can be used to help triage genetic analysis in resource limited settings.

2.3.2.2.1.1.5 Familial paragangliomas type 5 (SDHA)

SDHA was identified as the final SDHx PPGL predisposition gene in 2010 (PGL5; OMIM 614165) (Burnichon *et al.* 2010). It is associated with phaeochromocytomas and PGLs as well as GIST and pituitary adenomas. Penetrance is low (10% by age 70) and therefore most disease appears sporadic (Korpershoek *et al.* 2011; van der Tuin *et al.* 2018). Similarly to SDHB, lack of tumoural SDHA expression can be identified by IHC (Korpershoek *et al.* 2011).

2.3.2.2.1.2 Fumarate hydratase

Fumarate hydratase (FH) follows SDH as the next enzyme in the TCA cycle and catalyses the conversion of fumarate to malate (Figure 2.5). Loss of FH function results in accumulation of the TCA cycle intermediate fumarate which, like succinate, inhibits 2-oxoglutarate-dependent enzymes including HIF-PHDs (Isaacs *et al.* 2005). Indeed, FH was first identified as a PPGL predisposition gene in an SDH wildtype tumour that clustered with SDHx mutant tumours (Clark *et al.* 2014). Consistent with this original report, FH deficient PPGLs share the same epigenetic dysregulation (Castro-Vega *et al.* 2014; Hoekstra *et al.* 2015) and EMT (Sciacovelli *et al.* 2016) phenotypes as SDHB-deficient tumours. Likewise, FH IHC can be used diagnostically (Udager *et al.* 2018).

FH is a rare cause of PPGLs, but phaeochromocytomas, sympathetic PGLs and HNPGLs have all been described (Castro-Vega *et al.* 2014; Clark *et al.* 2014). Mutations in FH also give rise to hereditary leiomyomatosis and renal cell cancer (HLRCC; OMIM 150800), which is characterised by cutaneous and uterine leiomyomas and type 2 papillary RCCs. PPGL prevalence in HLRCC is low (2/34 patients in the largest series published to date) and it remains unclear what drives tissue-specific tumourigenesis in this condition (Muller *et al.* 2017).

2.3.2.2.1.3 Malate dehydrogenase 2

Malate dehydrogenase (MDH) is another TCA cycle gene implicated in PPGL predisposition (Figure 2.5). The index case had multiple malignant PGLs and a germline *MDH2* mutation (Cascón *et al.* 2015). Loss of heterozygosity (LOH) was observed in four tumours indicating biallelic inactivation and was associated with reduced levels of MDH2 protein and activity and a methylation phenotype similar to SDH-deficient PPGLs (Cascón *et al.* 2015). The upstream intermediaries malate and fumarate accumulate following *MDH2* knockdown (Cascón *et al.* 2015) and result in inhibition of 2-oxoglutarate-dependent enzymes (Dalgard *et al.* 2004; Hewitson *et al.* 2007; Koivunen *et al.* 2007). Further cases have been reported and are associated with a noradrenergic phenotype, although a

more complete understanding of MDH2 PPGL clinical characteristics is currently limited (Calsina *et al.* 2018).

2.3.2.2.1.4 von Hippel-Lindau disease

Von Hippel-Lindau disease (VHL; OMIM 193300) is a dominantly inherited cancer syndrome characterised by haemangioblastomas (HB) of the central nervous system (CNS), retinal haemangiomas, renal cysts and ccRCC, pancreatic cysts and pancreatic NETs and endolymphatic sac tumours (ELSTs) in addition to PPGLs. The syndrome was coined 'VHL' in 1964 (Melmon & Rosen 1964) and is named after the German ophthalmologist Eugen von Hippel who described the retinal lesions of the condition (von Hippel 1904) and the Swedish pathologist Arvind Lindau who associated these with CNS HBs (Lindau 1927). Phaeochromocytomas are commonly bilateral and have a low rate of malignancy. Penetrance is almost complete by 65 years of age.

VHL is classified according to the range of manifestations individuals develop. In type 1, PPGLs are absent, but other visceral manifestations may exist (Neumann & Wiestler 1991). In type 2, ccRCC are a feature of type 2B (Hoffman *et al.* 2001), but not of type 2A (Brauch *et al.* 1995). In type 2C, PPGLs are the only manifestations of the condition (McNeill *et al.* 2009).

Following the identification of the VHL gene (Latif *et al.* 1993), it became apparent that this clinical variation resulted from a close genotype-phenotype relationship in which type 1 disease resulted from deletions and truncating mutations whilst missense mutations were responsible for type 2 disease (Zbar *et al.* 1996; Clifford *et al.* 2001; Hoffman *et al.* 2001). Tumour pathogenesis results from inappropriate activation of HIF signalling as previously described. The situation is more complicated, however, in type 2C disease in which mutant forms of pVHL retain the ability to degrade HIF (Clifford *et al.* 2001; Hoffman *et al.* 2001). This finding suggests that alternative, HIF-independent, functions of VHL must be at least partly responsible for PPGL development. pVHL plays a role in directly modulating apoptosis, through interactions with p53 and the nuclear factor κB and Jun pathways (Lee *et al.* 2005; Roe *et al.* 2006; Yang *et al.* 2007), and senescence (Young *et al.* 2008). In addition to its role in primary cilia maintenance (discussed in Chapter 1), pVHL is involved in cell-cell adhesion through regulation of β1 integrin adhesions (Esteban-Barragán *et al.* 2002) and extracellular matrix formation via its role in fibronectin assembly (Ohh *et al.* 1998). Mutant pVHL displays defective binding to fibronectin and collagen IV (Bishop *et al.* 2004; Tang *et al.* 2006).

2.3.2.2.1.5 Prolyl hydroxylase

Germline mutations in both *PHD1* (Yang *et al.* 2015) and *PHD2* (Ladroue *et al.* 2008; Yang *et al.* 2015) are rare, but identified, causes of PPGLs in combination with congenital eythrocytosis.

2.3.2.2.1.6 Hypoxia Inducible Factor 2α

A germline gain of function mutation in *HIF2A* has been described in a single patient with a multifocal secretory PPGL and polycythaemia (Lorenzo *et al.* 2013). Somatic mutations in the same gene have also been found in PPGLs in combination with polycythaemia and somatostatinomas and have been termed the 'Pacak-Zhuang syndrome' (Zhuang *et al.* 2012). *HIF2A* is the only cluster 1 PPGL predisposition gene in which a gain, rather than loss, of function mutation is responsible.

2.3.2.2.2 Cluster 2

Cluster 2 PPGLs are characterised by abnormal activation of a range of kinase signalling cascades, which collectively result in alterations in cell growth, proliferation and survival (Klesse & Parada 1998; Dasgupta *et al.* 2003; Lee *et al.* 2005) (Figure 2.5).

The central pathways involved are the phosphatidylinositol-3-kinase/Akt/mammalian target of rapamycin (PI3K/Akt/mTOR) and Ras/Raf/mitogen-activated protein kinase kinase/extracellular signal-regulated kinase (Ras/Raf/MEK/ERK). They are activated through mutations either in genes at receptor level (e.g. *RET*) or that modify the downstream intracellular cascade (e.g. *NF1*, *MAX*, *TMEM127*). Specific features are discussed in relation to each gene below.

Phaeochromocytomas dominate in cluster 2 and the secretory profile, in contrast to cluster 1, is predominantly of increased metanephrine (MN) (Eisenhofer *et al.* 2001, 2011) with the exception of Myc-associated factor X (MAX)-associated tumours. Malignancy is less likely than with cluster 1 (Table 2.1).

2.3.2.2.2.1 Multiple Endocrine Neoplasia Type 2 (MEN2)

MEN2A (OMIM 171400) and 2B (162300) are syndromes that are inherited in an autosomal dominant manner and result from gain-of-function mutations in the rearranged during transfection (RET) proto-oncogene on chromosome 10q11, which is also responsible for Familial Medullary Thyroid Carcinoma (OMIM 155240). MEN2A and 2B consist of medullary thyroid cancer (MTC), PPGL and hyperparathyroidism in addition to Marfanoid features and mucosal neuromas in MEN2B (also previously known as MEN3).

PPGLs are almost entirely adrenal phaeochromocytomas with a high rate of bilateral disease and a low risk of malignancy (Pacak *et al.* 2009). The penetrance of PPGLs in MEN2 is around 50% compared to almost 100% for MTC, which tends to occur many decades before the diagnosis of PPGL (Gagel *et al.* 1988; Ponder *et al.* 1988). First described as a distinct entity in 1961 as 'Sipple's syndrome' (Sipple 1961), mutations in *RET* were identified as the cause in 1993 making it one of the first PPGL syndromes to have an established genetic basis (Mulligan *et al.* 1993). There is a close genotype-phenotype correlation in MEN2; specific mutations are associated with risk of PPGL development and of MTC aggressiveness and are therefore used to govern the timing of prophylactic thyroidectomy (Brandi *et al.* 2001; Mucha *et al.* 2017).

The RET protein is a tyrosine kinase receptor (TKR) for the glial cell line-derived neutrophic factor family of ligands. Ligand binding results in recruitment of a co-receptor and subsequent heterodimerisation with a second RET molecule. Autophosphorylation of specific tyrosine residues within the tyrosine kinase domain occurs with resultant activation in downstream signalling cascades, which include the oncogenic MAPK/ERK and PI3K/Akt pathways (Richardson *et al.* 2006).

2.3.2.2.2.2 Neurofibromatosis type 1 (NF1)

Neurofibromatosis type 1 (NF1, OMIM 162200) is a neurocutaneous syndrome caused by mutations in the neurofibromin 1 (*NF1*) gene. NF1 has an autosomal dominant pattern of inheritance and features café au lait spots, Lisch nodules, neurofibromas and optic pathway gliomas. Originally described by von Recklinghausen in 1882 (von Recklinghausen 1882), its association with phaeochromocytomas was first established in 1910 (Suzuki 1910). PPGLs are relatively uncommon in NF1, occurring in less than 5% of patients (Gutmann *et al.* 1997; Gruber *et al.* 2017). Disease is almost exclusively adrenal with bilateral disease in up to 30% of cases and metastatic disease in up to 10% (Bausch *et al.* 2006, 2007; Gruber *et al.* 2017). Germline mutations in *NF1* account for only 3% of PPGLs (Bausch *et al.* 2006), but it is the most commonly somatically mutated gene (20.8%) in PPGLs (Evenepoel *et al.* 2017).

Identified in 1990 (Cawthon *et al.* 1990), the *NF1* gene contains 62 exons meaning clinical rather than genetic diagnosis of NF1 predominates the literature. The *NF1* gene product, neurofibromin, contains a GTPase-activating protein (GAP) domain which interacts with and negatively regulates the GTPase Ras (Martin *et al.* 1990). Mutations in *NF1* therefore result in aberrant activation of the Ras signalling cascade, which includes the MEK/MAPK/ERK and PI3K/Akt/mTOR signalling pathways. Collectively these pathways play crucial roles in the control of cellular proliferation and apoptosis (Klesse & Parada 1998; Dasgupta *et al.* 2003; Lee *et al.* 2005).

The phaeochromocytoma-derived cell lines MPC ('mouse phaeochromocytoma') and MTT ('mouse tumour tissue') were generated from heterozygous *Nf1* knockout mice (Powers *et al.* 2000; Martiniova *et al.* 2009).

2.3.2.2.2.3 Transmembrane protein 127 (TMEM127)

Transmembrane protein 127 (TMEM127) was identified as a PPGL predisposition gene (OMIM 171300) in 2010 through interrogation of familial phaeochromocytoma kindreds without a known genetic cause (Qin *et al.* 2010). It is a classical tumour suppressor gene with LOH observed in associated tumours and follows an autosomal dominant pattern of inheritance with incomplete penetrance (32% by age 65 years) (Qin *et al.* 2010; Toledo *et al.* 2015). It accounts for approximately 1-2% of PPGLs without a previously identified genetic cause (Abermil *et al.* 2012; Bausch *et al.* 2017). Disease is almost entirely confined to the adrenals with bilateral and multifocal disease in 50% of affected individuals (Yao *et al.* 2010; Toledo *et al.* 2015), although PGLs have also been reported (Neumann *et al.* 2011). Metastatic disease has been observed in up to 10% of patients (Bausch *et al.* 2017). Germline mutations also predispose to renal cancer with confirmatory LOH data (Qin *et al.* 2014; Hernandez *et al.* 2015). Other organ tumours (colonic, pancreatic, melanoma, parathyroid adenoma, acute myeloid leukaemia) have also been reported in association with TMEM127, however experimental evidence suggesting causality is lacking (Bausch *et al.* 2017).

The transcriptome of TMEM127-associated PPGLs are similar to that seen in NF1-associated tumours with enrichment in various kinase signalling pathways. TMEM127 is a negative regulator of mTOR complex 1 (mTORC1) (Figure 2.5) and its knockdown resulted in increased mTOR signalling and cellular proliferation (Qin *et al.* 2010).

2.3.2.2.2.4 Myc-associated factor X (MAX)

MAX is a transcription factor that contains the basic helix-loop-helix and leucine zipper motif which heterodimerizes with its partners Myc (Landschulz *et al.* 1988; Murre *et al.* 1989), Mad (MAX dimerisation protein 1; MXD1) (Ayer *et al.* 1993) and MXI1 (MAX-interacting protein 1) (Zervos *et al.* 1993). These complexes bind and compete for specific 'E-box Myc site' DNA sequences within the promoter regions of a multitude of genes (Blackwell *et al.* 1990, 1993). The Myc-MAX complex is a transcriptional activator (Kerkhoff *et al.* 1991; Amin *et al.* 1993), which promotes cellular transformation (Amati *et al.* 1993a), cell cycle progression (Amati *et al.* 1993b) and apoptosis (Askew *et al.* 1991). MAD-MAX and MXI1-MAX are transcriptional repressors (Ayer *et al.* 1993;

Zervos *et al.* 1993) and antagonise Myc-dependent transcription through competition for MAX, which is a central component in the regulation of this transcription system.

The first evidence that MAX was implicated in PPGL development was the identification that the rat phaeochromocytoma-derived PC12 cell line possessed mutant forms of Max that lacked the dimerisation domain and were thus incapable of repressing transcription from an E-box element (Hopewell & Ziff 1995). Reintroduction of functional MAX resulted in repression of E-box-dependent transcription and reduced proliferative rate (Hopewell & Ziff 1995).

Despite this observation, it was not for another 16 years until MAX was identified as a PPGL predisposition gene in humans (OMIM 154950) (Comino-Méndez *et al.* 2011). Pathogenesis was confirmed through demonstration of a lack of full length protein and LOH within tumours. Inheritance is autosomal dominant with paternal transmission of disease (Comino-Méndez *et al.* 2011) and a 73% penetrance rate by the age of 40 (Bausch *et al.* 2017). MAX mutations account for around 1% of otherwise genetically negative PPGLs (Burnichon *et al.* 2012; Bausch *et al.* 2017). Disease is almost exclusively adrenal with a very high proportion of bilateral or multifocal disease and a malignancy rate of approximately 10% (Burnichon *et al.* 2012; Bausch *et al.* 2017). Unlike other cluster 2 genes, normetanephrine is frequently elevated (Burnichon *et al.* 2012). Single cases have implicated MAX mutations in the pathogenesis of renal cell carcinomas (Casey *et al.* 2017) and renal oncocytomas (Korpershoek *et al.* 2016) in combination with PPGLs.

2.3.2.2.2.5 Kinesin family member 1B

During normal development, sympathetic neuronal precursor cells undergo apoptosis when growth factors become limiting in a process that is dependent on c-Jun (Estus *et al.* 1994), HIF-PHD3 (Lee *et al.* 2005) and the beta splice variant of kinesin family member 1B (KIF1Bβ) (Schlisio *et al.* 2008) (Figure 2.5). Insertion of HIF-PHD3 into a variety of neuronal cell lines (including PC12) results in apoptotic cell death, which is prevented by knockdown of KIF1Bβ resulting in cells resistant to the apoptotic cue of growth factor withdrawal (Schlisio *et al.* 2008). In addition to its pro-apoptotic function, KIF1B is a molecular motor function and transports synaptic vesicles and mitochondria (Nangaku *et al.* 1994; Zhao *et al.* 2001).

Pathogenic mutations in KIF1B (OMIM 605995) have been identified in five individuals from a single kindred with phaeochromocytomas, neuroblastomas and other non-neuronal tumours (a leiomyosarcoma and lung adenocarcinoma) (Schlisio *et al.* 2008; Yeh *et al.* 2008). Transcriptome analysis of the phaeochromocytomas revealed similarity to NF1 and RET associated tumours,

thereby placing KIF1B in cluster 2 (Yeh *et al.* 2008). Interestingly, LOH was not identified in the associated neuronal tumours, suggesting a role for haploinsufficiency or methylation effects, but was in the lung adenocarcinoma (Schlisio *et al.* 2008; Yeh *et al.* 2008).

KIF1B's locus, on 1p36, is frequently deleted in tumours of neural crest origin (Schwab *et al.* 1996), including phaeochromocytomas (Dannenberg *et al.* 2000). This, taken together with the high prevalence (20.4%) of somatic KIF1B mutations seen in PPGLs (Evenepoel *et al.* 2017) and the previously described molecular evidence, supports the role for KIF1B and failure of neuronal apoptosis as a contributor to PPGL pathogenesis. However, no further germline mutation cases have been identified in the ten years since its description as a PPGL predisposition gene.

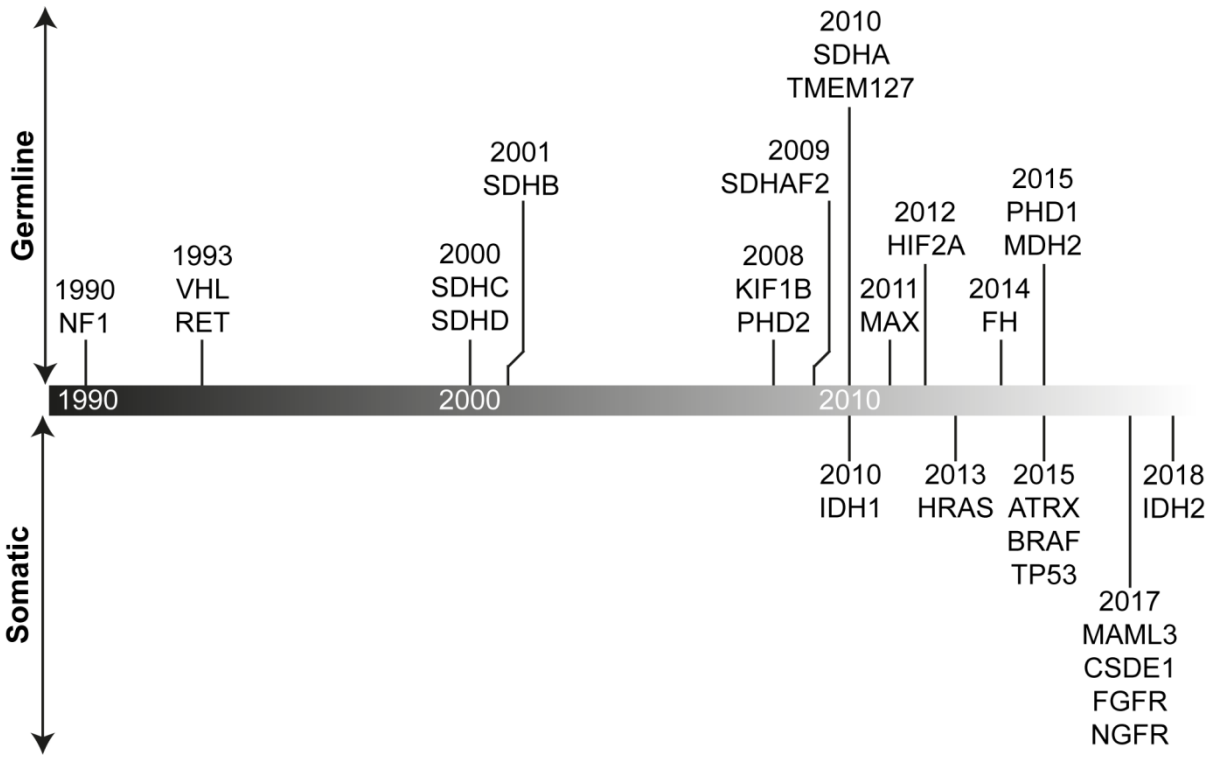

Figure 2.4: Timeline of discovery of genetic drivers of PPGL formation

NF1 – neurofibromatosis type 1, VHL – von Hippel-Lindau, RET – rearranged during transfection, SDHx – succinate dehydrogenase, KIF1B – kinesin family member 1β, PHD – prolyl hydroxylase, TMEM127 – transmembrane protein 127, MAX – myc-associated factor X, HIF – hypoxia inducible factor, FH – fumarate hydratase, MDH – malate dehydrogenase, IDH – isocitrate dehydrogenase, TP53 – tumour protein 53, MAML3 – mastermind-like 3, CSDE1 – cold-shock domain-containing E1, FGFR – fibroblast growth factor receptor, NGFR – nerve growth factor receptor.

Table 2.1: Summary of genes in which germline mutations result in PPGL predisposition (overleaf)

PGL – familial paraganglioma syndrome, HLRCC – hereditary leiomyomatosis and renal cell carcinoma, VHL – von Hippel-Lindau, MEN2 – multiple endocrine neoplasia type 2, NF1 – neurofibromatosis type 1, SDH – succinate dehydrogenase, FH – fumarate hydratase, MDH – malate dehydrogenase, PHD – prolyl hydroxylase, HIF – hypoxia inducible factor, RET – rearranged during transfection, TMEM – transmembrane protein, MAX – Myc-associated factor X, KIF – kinesin family member, phaeo – phaeochromocytoma, TA – thoraco-abdominal, PGL – paraganglioma, HNPGL – head and neck PGL, RCC – renal cell carcinoma, GIST – gastrointestinal stromal tumour, PA – pituitary adenoma, HB – haemangioblastoma, ccRCC – clear cell RCC, pNET – pancreatic neuroendocrine tumour, ELST – endolymphatic sac tumour, MTC – medullary thyroid cancer, PHPTH – primary hyperparathyroidism.

†Refers to the year the gene was identified as a cause of PPGL development.

Cluster	Syndrome	Gene	Locus	Year identified†	PPGL				Associated clinical features
					Phaeo	TA PGL	HNPGL	Behaviour	
1a	PGL1	SDHD	11q23	2000	+	+	+++	Maternal imprinting, multifocal, rarely malignant	RCC, GIST, PA
	PGL 2	SDHAF2	11q13	2009	-	-	+++	Maternal imprinting, ~75% penetrance	Nil
	PGL3	SDHC	1q23	2000	-	+	+++	-	GIST
	PGL4	SDHB	1p36	2001	+	++	+	~40% penetrance ~30% malignant	RCC, GIST, PA
	PGL 5	SDHA	5p15	2010	+	+	+	Low penetrance	GIST, PA
	HLRCC	FH	1q43	2014	++	+	+	Malignancy similar to SDHB	Cutaneous & uterine leiomyomas, RCC
	Nil	MDH2	7q11	2015	+	+	-	-	Nil
1b	VHL	VHL	3p25	1993	+++	+	-	Low malignancy rate	HB, ccRCC, pNET, ELST
	Nil	PHD1	19q13	2015	-	+	-	-	Polycythaemia
	Nil	PHD2	1q42	2008	-	+	-	-	Polycythaemia
	Nil	HIF2A	2p21	2012	-	++	-	-	Somatostatinoma, polycythaemia
2	MEN2	RET	10q11	1993	+++	-	-	50-80% bilateral Low malignancy rate	2A: MTC, PHPTH 2B: MTC, Marfanoid habitus, mucosal ganglioneuromas
	NF1	NF1	17q11	1990	+++	+	-	30% bilateral Low malignancy rate MPC/MTT cells	Neurofibromas, café au lait spots, Lisch nodules, optic pathway gliomas
	Nil	TMEM127	2q11	2010	+++	+	+	10% malignant	RCC
	Nil	MAX	14q23	2011	+++	+	-	10% malignant, NMN PC12 cells	RCC, renal oncocytoma
	Nil	KIF1B	1p36	2008	+++	-	-	Single kindred only	Leiomyosarcoma, lung adenocarcinoma

Table 2.1: Summary of genes in which germline mutations result in PPGL predisposition (legend on previous page)

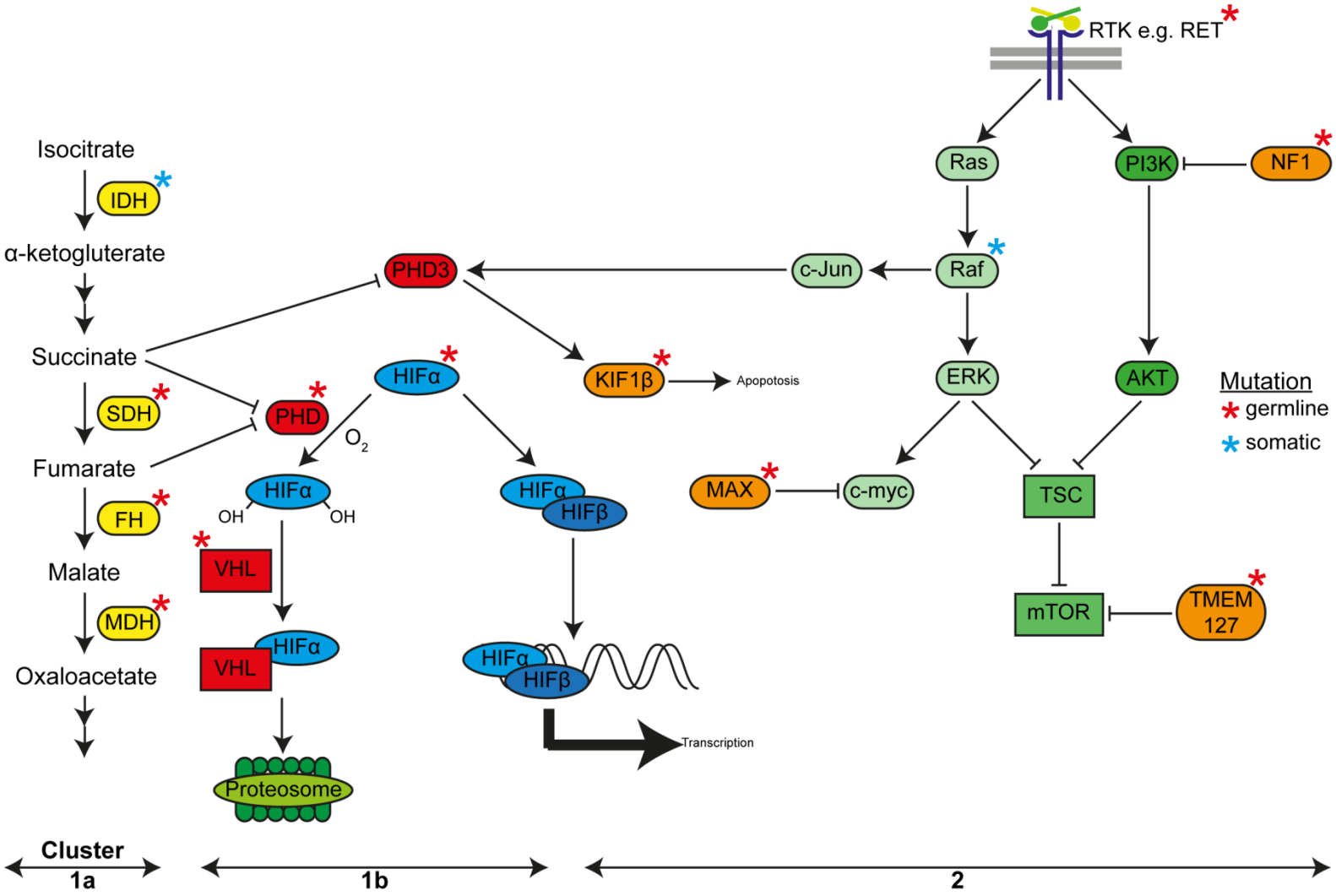

Figure 2.5: Schematic representation of cluster 1 and 2 PPGL predisposition genes and their function (legend overleaf)

Figure 2.5: Schematic representation of cluster 1 and 2 PPGL predisposition genes and their function (figure overleaf)

IDH – isocitrate dehydrogenase, SDH – succinate dehydrogenase, FH – fumarate hydratase, MDH – malate dehydrogenase, PHD – prolyl hydroxylase, HIF – hypoxia inducible factor, VHL – von Hippel-Lindau, KIF1β – kinesin family member 1β, MAX – myc-associated factor X, ERK – extracellular signal-regulated kinase, TSC – tuberous sclerosis complex, mTOR – mammalian target of rapamycin, NF1 – neurofibromatosis type 1, PI3K – phosphatidylinositol-3-kinase, TMEM127 – transmembrane protein 127.

Red stars indicated genes in which germline mutations predispose to PPGL formation. Blue stars indicate genes which have been found to be mutated in PPGLs, but not the germline.

2.3.2.4 Somatic mutations

The molecular pathogenic mechanisms at the heart of PPGL development have been discussed above and centre on pseudohypoxic signalling and activation of RTK pathways (Figure 2.5). Two additional subtypes that have recently been characterised through a comprehensive multi-modal process are 'Wnt-altered' and 'cortical admixture' and highlight the role of somatic mutations in PPGLs (Fishbein *et al.* 2017). Taken together, germline and somatic mutations in identified driver genes occur in upwards of 80% of PPGLs (Burnichon *et al.* 2011; Comino-Méndez *et al.* 2013; Crona *et al.* 2013; Fishbein *et al.* 2015, 2017). Somatic mutations occur in the same genes that germline mutations occur in (with the notable exception of *SDHx*) as well as in a number of additional genes.

Wnt-altered PPGLs are distinctive in that activation of the Wnt and Hh pathways is prominent and the tumours are associated with novel somatic mutations and gene fusion products. Cold shock domain-containing E1 (*CSDE1*) modulates a number of key cellular processes including translation initiation, RNA stability, apoptosis, cellular differentiation and neuronal development (Mihailovich *et al.* 2010; Kobayashi *et al.* 2013) and is somatically mutated in Wnt-altered PPGLs (Fishbein *et al.* 2017). Tumoural fusion genes resulting in upregulation of mastermind-like transcriptional coactivator 3 (MAML3) are also found in this subtype and result in a distinct methylation profile and overexpression of Wnt and Hh target genes. The cortical admixture subtype is represented by an overexpression of adrenal cortical markers perhaps implying impure tumour sampling, although it is not merely defined by this and has a PPGL, rather than cortical, DNA methylation profile (Fishbein *et al.* 2017).

Somatic mutations in PPGLs occur in genes within both the cluster 1 and 2 pathways in which germline mutations have not been identified. Isocitrate dehydrogenase (IDH) is a TCA cycle enzyme, loss of function of which results in HIF-PHD inhibition (Dalgard *et al.* 2004; Hewitson *et al.* 2007; Koivunen *et al.* 2007). Somatic mutations in both I*DH1* (Gaal *et al.* 2010; Fishbein *et al.* 2015; Remacha *et al.* 2017) and *IDH2* (Richter *et al.* 2019) have been identified in PPGLs with the same clinical phenotype and methylation profile as SDHx/FH associated tumours. Somatic mutations also result in activation of the cluster 2 Ras/Raf/MEK/ERK pathway. *H-RAS* is one of the most frequently somatically mutated genes in PPGLs (Crona *et al.* 2013), whilst mutations in *BRAF* have also been identified (Luchetti *et al.* 2015; Fishbein *et al.* 2017).

Somatic mutations also occur in genes outside of the confines of the established PPGL predisposition clusters. Mutations in alpha thalassemia/mental retardation syndrome (*ATRX*) result in alternative lengthening of telomeres with resultant genome instability and alterations in the DNA damage response (Lovejoy *et al.* 2012; Fishbein *et al.* 2015). In addition to being common (they occur in over 10% of PPGLs), *ATRX* mutations are associated with clinically aggressive behaviour (Fishbein *et al.* 2015). Other notable genes that undergo somatic mutation in PPGLs are the cell cycle genes: tumour protein 53 (*TP53*) (Luchetti *et al.* 2015; Fishbein *et al.* 2017), cyclin dependent kinase inhibitor 2C (*CDKN2C*) (van Veelen *et al.* 2009) and the RTKs fibroblast growth factor receptor 1 (*FGFR1*) (Fishbein *et al.* 2017; Welander *et al.* 2018) and nerve growth factor (NGFR) (Fishbein *et al.* 2017).

2.4 Investigations

The sensitivity and specificity of the available diagnostic tests for PPGLs are generally very good and the largest hurdle to diagnosis remains lack of its consideration in the differential. Investigation should be prompted in individuals with suggestive signs and symptoms (particularly if episodic or provoked by medications associated with crisis precipitation), an adrenal incidentaloma, a personal history of PPGL or a known or suspected hereditary predisposition (Lenders *et al.* 2014).

2.4.1 Biochemistry

Once suspected, diagnosing PPGL relies on the demonstration of elevated circulating catecholamines or their metabolites (Figure 2.2).

Historical testing for VMA, catecholamines and other metabolites has been replaced by metanephrine assessment, which offers increased sensitivity and specificity (Manu & Runge 1984) due to their constant, rather than episodic, tumoural release (Eisenhofer *et al.* 1998). Assessment of

metanephrines in plasma compared to urine appears to confer slightly greater sensitivity (Lenders *et al.* 1995) and specificity (Lenders *et al.* 2002), although either method is deemed acceptable in consensus guidelines (Lenders *et al.* 2014). The terminology associated with metanephrine measurement can be confusing: 'total metanephrines' refers both to the sum of the individually fractionated metanephrines, metanephrine and normetanephrine, as well as the combination of free and conjugated metanephrines. Free circulating metanephrines are sulphate-conjugated by sulfotransferase 1A3/1A4 (SULT1A3) (Dajani *et al.* 1999), predominantly in the gastrointestinal tract (Eisenhofer *et al.* 1996), and represent only a small proportion of measured 'total metanephrines'.

Metanephrine measurement should be by liquid chromatography with electrochemical detection or with tandem mass spectrometry and not immunoassay due to their reduced accuracy and increased variability (Mullins *et al.* 2012). For plasma assessment, blood should be taken with patients in the resting supine position as this is how the diagnostic reference intervals were defined (Lenders *et al.* 1995) and because upright posture increases neuronal noradrenaline release and sampling in this position dramatically increases the false positive rate (Lenders *et al.* 2007). There is evidence that normal circulating metanephrines increase with age, but age-defined reference intervals are not commonly utilised in clinical practice (Eisenhofer *et al.* 2013). Falsely elevated test results for urine and plasma metanephrines can result from a range of medications either through pharmacodynamic interference that affects all measurement methods or through analytical interference of certain methodologies (summarised in (Lenders *et al.* 2014)). If this is suspected, repeat testing following discontinuation of the offending medication is necessary. 3-MT is the only metanephrine influenced by a catecholamine-rich diet (de Jong *et al.* 2009).

Given the extremely high sensitivity (in excess of 95%) and specificity (over 90%) of plasma free metanephrines for PPGL detection, additional confirmatory testing is rarely necessary (Lenders *et al.* 2002; Hickman *et al.* 2009).

In some circumstances, the clonidine suppression test can be a useful adjunct in the diagnosis of PPGLs (Eisenhofer *et al.* 2003). Clonidine, an α_2-adrenoceptor agonist, inhibits neuronal noradrenaline release and therefore will reduce circulating noradrenaline and normetanephrine in individuals without PPGLs. Blood is taken prior to clonidine administration and three hours after with a positive result considered if the normetanephrine concentration remains elevated at three hours and has fallen by less than 40% compared to baseline, reflecting autonomous tumoural production. Given its reliance on normetanephrine, the clonidine suppression test is only useful in noradrenaline secreting PPGLs.

Circulating chromogranin A, a non-specific neuroendocrine secretory protein, is inferior to plasma metanephrines in PPGL detection (Algeciras-Schimnich *et al.* 2008), but could play a role as a diagnostic adjunct in combination with metanephrines (Giovanella *et al.* 2006) or in instances when metanephrines are not elevated (Zuber *et al.* 2014).

2.4.2 Imaging

Once the biochemical detection of catecholamine excess has been secured, the next step is to localise the PPGL by imaging. In keeping with all endocrine conditions, imaging should follow diagnostic biochemistry to reduce the risk of discovery of incidental radiological abnormalities of uncertain significance. The exception to this rule would be in non-secretory PPGL, for example HNPGLs which might present due to local mass effect, and in surveillance of patients with mutations in PPGL predisposing genes (Maher *et al.* 2011; Jasperson *et al.* 2014).

2.4.2.1 Cross sectional imaging

First line imaging is either by computed tomography (CT) or magnetic resonance imaging (MRI), both of which have diagnostic sensitives exceeding 90% for adrenal phaeochromocytomas (Jalil *et al.* 1998; Lumachi *et al.* 2006). CT findings of adrenal lesions that are suggestive of an adenoma include a pre-contrast mean attenuation of less than ten Hounsfield Units or a contrast washout exceeding 60% (Caoili *et al.* 2002), although neither of these criteria are absolute (Blake *et al.* 2003). CT has the advantage of greater spatial resolution in the thorax, abdomen and pelvis, whilst MRI is better for HNPGL. CT is quicker, more readily available and better tolerated by patients whilst MRI has the advantage of not involving ionising radiation and so is preferable in groups in whom radiation exposure should be minimised (for example, children, during pregnancy and those with genetic predisposition syndromes).

The choice of initial imaging modality and extent is at the discretion of the treating clinician and is influenced by the pre-test likelihood of PPGL location, disease extent and probability of syndromic disease.

2.4.2.2 Nuclear medicine imaging

A range of radioisotope scans are available as adjunctive imaging techniques in the diagnosis and staging of PPGLs.

Metaiodobenzylguanidine (MIBG) consists of an iodinated benzyl group and a guanidine group and is structurally similar to catecholamines (Figure 2.2C) (Nakajo *et al.* 1983). MIBG actively enters neuroendocrine cells via the adrenaline transporter and is stored in neurosecretory granules, resulting in its concentration in these cells compared to other tissues. Labelling MIBG with the gamma-emitter ^{123}I allows for its detection by a gamma camera, which can be combined with single photon emission computed tomography (SPECT) to improve anatomical localisation. The sensitivity of ^{123}I-MIBG reaches almost 90% for phaeochromocytomas but is significantly lower for paragangliomas (Bhatia *et al.* 2008; Wiseman *et al.* 2009), in recurrent (Rufini *et al.* 2011) and metastatic (Ilias *et al.* 2008) disease and in patients with *SDHB* mutations (Fonte *et al.* 2012). False negative results can be seen in necrotic or haemorrhagic tumours (Bhatia *et al.* 2008) and following administration of a wide range of medications (Solanki *et al.* 1992). MIBG has the advantage of the availability of a therapeutic isotope ^{131}I-MIBG and therefore diagnostic imaging with ^{123}I-MIBG should be considered in patients with confirmed or suspected recurrent or metastatic disease, in whom ^{131}I-MIBG might be a therapeutic option.

Fluorodeoxyglucose (^{18}F-FDG) is an alternative radioisotope that is widely used in positron emission tomography (PET). It is taken up by all cells, with greatest uptake by those that are most metabolically active. In accordance with its mechanism of action, its sensitivity for benign phaeochromocytomas is low (58%), but is much higher (88%) for metastases (Shulkin *et al.* 1999). ^{18}F-FDG-PET is of particular use in metastatic SDHB-associated PPGLs where its sensitivity approaches 100% and comfortably outperforms ^{123}I-MIBG (Timmers *et al.* 2007b). An alternative positron emitter is the catecholamine fluorodopa (^{18}F-DOPA) which enters chromaffin cells via the L-type amino acid transporter system and has very high sensitivities (>90%) for detecting recurrent or metastatic PPGLs (Rufini *et al.* 2011; Gabriel *et al.* 2013), although its utility in SDHB-associated PPGLs is more limited (Gabriel *et al.* 2013). Thus, both ^{18}F-FDG-PET and ^{18}F-DOPA-PET are very sensitive at identifying metastatic disease, although they do not offer a therapeutic option.

Unlike the previous radioisotopes, the somatostatin analogue (SSA) ^{68}Ga-DOTATATE's specificity is conferred by its affinity for cell surface somatostatin receptor (SSTRs), particularly $SSTR_2$, which are widely expressed on NETs including PPGLs. The sensitivity for detection of PPGLs, particularly metastases, exceeds 90% and is superior to any other available cross sectional or nuclear medicine imaging modality (Janssen *et al.* 2015; Gild *et al.* 2018; Han *et al.* 2018). Its performance appears to be maintained in SDHB-associated PPGLs (Janssen *et al.* 2015), unlike the other radioisotopes, in accordance with the increased $SSTR_2$ expression in these tumours (Elston *et al.* 2015). Like MIBG, a therapeutic radiopharmaceutical, ^{177}Lu-DOTATATE, is available.

2.4.3 Histopathology

On haemotoxylin and eosin (H&E) staining, PPGLs classically demonstrate a 'Zellballen' pattern comprised of nests of tumour cells separated by peripheral capillaries. At the periphery of these nests lie sustentacular cells. The role of the sustentacular cell in tumours is unclear; they are thought to play a glial-like support role, although they may contain a stem cell contingent (Schmid *et al.* 1994). Although various 'subtypes' of PPGLs have been proposed based on their histological appearance, they do not correlate with tumour genetics, biology, natural history or prognosis and are not routinely used (Tischler & deKrijger 2015). PPGLs can form composite tumours with neuroblastomas, ganglioneuroblastomas and malignant peripheral nerve sheath tumours (Tischler 2000).

Although the histological diagnosis of PPGL can usually be made on H&E sections alone, IHC can be informative. The sustentacular cell population is usually positive for S100, whilst chromogranin A and synaptophysin usually label phaeochromocytes. Tyrosine hydroxylase is more specific than these generic neuroendocrine markers, although can be negative in non-secretory PPGLs, especially HNPGL. In addition to diagnostic confirmation, IHC can provide early insight into the likelihood of an underlying genetic mutation. Negative IHC for SDHB is highly suggestive of a mutation in an SDHx complex gene and due to the lack of SDHx somatic mutations in PPGLs, in contrast to GISTs, is predictive of a germline mutation (Gill *et al.* 2010; Korpershoek *et al.* 2011; Papathomas *et al.* 2015).

Malignant disease in PPGLs is defined by the World Health Organisation as the presence of metastatic disease in an organ which does not have chromaffin cells (usually bone or lymph node) (De Lellis *et al.* 2004). Unlike other cancers, there is no reliable pathological staging system that correlates with prognosis. Two scoring systems have been proposed: Phaeochromocytoma of the Adrenal Scaled Score (PASS) (Thompson 2002) and Grading of Adrenal Phaeochromocytoma and Paraganglioma (GAPP) (Kimura *et al.* 2014) (Table 2.2). The PASS is limited to phaeochromocytomas and is subject to significant inter-observer variation (Wu *et al.* 2009). Both were retrospectively compiled and have not been prospectively validated and are intrinsically limited by the lack of correlation between histological appearances and the largest predictor of malignancy, SDHB mutation status (Brouwers *et al.* 2006; Amar *et al.* 2007; Blank *et al.* 2010).

Phaeochromocytoma of the Adrenal Scale Score (PASS)[1]		Grading of Adrenal Phaeochromocytoma and Paraganglioma (GAPP)[2]	
Parameter	Score	Parameter	Score
Large nests or diffuse growth	2	Histological pattern	
		Zellballen	0
Central or confluent tumour necrosis	2	Large and irregular cell nest	1
		Pseudorosette	1
High cellularity	2	Cellularity†	
		Low (<150)	0
Cellular monotony	2	Moderate (150-200)	1
		High (>250)	2
Tumour cell spindling	2	Comedo necrosis	
		Absent	0
Mitotic count >3/10 HPF	2	Present	2
		Vascular or capsular invasion	
Atypical mitotic figures	2	Absent	0
		Present	2
Extension into adipose tissue	2	Ki67 index (%)	
		<1	0
Vascular invasion	1	1-3	1
		>3	2
Capsular invasion	1	Catecholamine type	
		Adrenaline	0
Profound nuclear pleomorphism	1	Noradrenaline	1
Nuclear hyperchromasia	1	Non-functioning	0
Maximum	20	Maximum	10

Table 2.2: Comparisons of the PASS and GAPP scores for predicting PPGL malignancy

[1] (Thompson 2002), [2] (Kimura *et al.* 2014), HPF high power field

† Number of tumour cells in a square of a 10mm micrometer observed under high power magnification

2.4.4 Genetic testing

Genetic testing should be considered in all patients with a PPGL due to the high frequency with which they occur in patients with germline mutations in predisposition genes. Positive results should prompt cascade genetic screening of at risk family members, enrolment in appropriate surveillance programmes and allow a more meaningful discussion regarding management options and prognosis given the overall clinical heterogeneity in PPGLs. Factors that increase the *a priori* likelihood of a germline mutation include a positive family history, previous personal history of PPGL, multifocal,

extra-adrenal and malignant disease as well as the presence of other syndromic associations (Table 2.1).

Like all genetic testing, the relative benefits and likelihoods of a positive result must be balanced against potential costs (financial and otherwise) in the context of the wider health economy. This has led to a range of different approaches to genetic testing for PPGLs. The Endocrine Society suggests a step-wise decisional algorithm for all patients based on the presence or absence of metastases, site of disease and secretory profile (Lenders *et al.* 2014). This is intellectually satisfying and limits unnecessary testing of genes unlikely to be responsible, however risks both delay to diagnosis if the first set of testing is negative and may not convert to a lower cost. The UK Genetic Testing Network (https://ukgtn.nhs.uk/) adopts a blanket 10 gene (*FH, MAX, RET, SDHA-D, SDHAF2, TMEM127, VHL*) panel-based approach to patients who have one of the following risk factors: PGL, family history, age under 45, syndromic features, malignant or multifocal disease.

2.4.5 Others

Employing the aforementioned techniques, uncertainty regarding PPGL localisation is uncommon, particularly in patients with sporadic and syndromic disease. The situation is different in patients with a genetic predisposition to PPGL development, who are enrolled in biochemical and radiological surveillance programmes which aim to diagnose small, pre-symptomatic tumours (Maher *et al.* 2011; Jasperson *et al.* 2014). Occasionally, radiological abnormalities are detected which are too small to characterise by either cross sectional or nuclear medicine imaging and the situation is further complicated by the possibility of incidentaloma detection, particularly with advancing age.

In such circumstances, there is a potential role for a technique that provides functional information to assist anatomical localisation. Selective venous sampling with measurement of catecholamines is one such approach that has been used for over 60 years (Von Euler *et al.* 1955), although uncertainty regarding its utility remains (Freel *et al.* 2010). This technique is examined in Chapter 6.

2.5 Management

Once a PPGL is diagnosed, the immediate priority is to render the patient safe from the end organ effects of catecholamine excess. This is equally relevant as pre-treatment before surgical intervention or as long-term therapy in patients with incurable disease.

2.5.1 Medical therapy

Initial medical management of a PPGL with α-adrenoceptor antagonists is established endocrine practice and uniformly recommended by society guidelines, although the underlying evidence base is limited (Lenders *et al.* 2014; Whelton *et al.* 2018). Traditional teaching mandates that alpha blockade must precede beta blockade due to the risk of unopposed alpha stimulation and resultant paradoxical hypertension or precipitation of a catecholamine crisis, although evidence for this is limited to case reports and small case series (Briggs *et al.* 1978; Sibal *et al.* 2006). The non-selective α_1 and α_2 receptor antagonist phenoxybenzamine is generally the first line choice, partly due to its non-competitive mechanism of action being felt to be protective from catecholamine surges. Thus, receptor re-synthesis is required to overcome blockade, which although helpful when the source of catecholamine excess is *in situ*, can result in significant postoperative hypotension following its removal. The reversible and selective α_1 receptor antagonist doxazosin has therefore been proposed as an alternative agent. Direct comparison between the two is limited to retrospective series with varied results suggesting either no difference between intra-operative blood pressure control (Kocak *et al.* 2002; Prys-Roberts & Farndon 2002) or inferior blood pressure control with doxazosin (Weingarten *et al.* 2010). A prospective head-to-head trial has recently been completed and the results are awaited (PRESCRIPT; NCT01379898).

Alpha blockade often results in a reflex tachycardia due to the direct effects of catecholamines on β-adrenoceptors and excess noradrenaline produced at cardiac adrenergic nerve endings (an α_2-mediated effect that is also used as an argument for doxazosin over phenoxybenzamine). This tachycardia can be treated with non-selective β-antagonists such as propranolol, introduced only after sufficient α-antagonist exposure (Lenders *et al.* 2014). Patients with PPGLs are volume contracted due to α_1-mediated vasoconstriction and are at risk of significant hypotension upon initiation of α-antagonists. This can be reduced by expanding circulating volume though increased oral fluid and salt intake or intravenous fluid administration (Pacak 2007).

A variety of other anti-hypertensive agents have also been used in patients with PPGLs peri-operatively or during a crisis. The tyrosine hydroxylase inhibitor metyrosine can be a useful adjunct

to phenoxybenzamine, but its side effects restrict it to immediate pre-operative use (Perry *et al.* 1990; Steinsapir *et al.* 1997). Some units do not use alpha blockers even when available. A large French centre utilises the dihydropyridine calcium-channel blocker nicardipine (Lebuffe *et al.* 2005), which acts by preventing catecholamine-stimulated calcium influx into arterial smooth muscle. Perioperative complications (specifically myocardial infarction and death) in a single large volume centre in Germany were no different regardless of whether alpha blockers were used, although maximal intraoperative blood pressure was higher in patients not treated with an α antagonist pre-operatively (Groeben *et al.* 2017). The combined α_1 and β antagonist labetalol has also been used (Poopalalingam & Chin 2001), however, like all beta blockers, concerns exist regarding the risk of paradoxical hypertension in spite of its α_1 activity and adverse events have been reported (Kuok *et al.* 2011). Other drugs that also have a role are magnesium (James 1989), sodium nitroprusside (Boutros *et al.* 1990) and glyceryl trinitrate (Emerson & Rainbird 2003).

2.5.2 Surgery

Surgical resection represents the only possibility of PPGL cure. There are no data advocating the survival benefit of any single operative approach or technique, but retrospective and historical comparisons between open and laparoscopic adrenalectomies suggest the latter to be associated with reduced pain, blood loss, hospital stay and morbidity (Shen *et al.* 2010; Agarwal *et al.* 2012). Laparoscopic adrenalectomy can be achieved by either the trans- or retro-peritoneal approach with the former allowing assessment of the abdominal cavity, whilst the latter avoids it and is thus of use in patients with adhesions from previous surgery (Walz *et al.* 2006). The operation choice is surgeon and patient dependent and the potential benefits of a less invasive procedure must be balanced against the risk of incomplete resection and recurrence (Li *et al.* 2001). The Endocrine Society suggests that open adrenalectomy should be undertaken in tumours exceeding 6cm and those that are invasive (Lenders *et al.* 2014).

In patients with, or who are at risk of, bilateral phaeochromocytomas, there is an argument for partial (cortical-sparing) rather than complete adrenalectomy with the aim of preserving adrenal cortical function and avoiding hypoadrenalism and its associated mortality. The risk is leaving residual medullary tissue in which a recurrent phaeochromocytoma could develop in an already operated surgical field, increasing the risk of operative complications. In a large study of nearly 100 patients with VHL and MEN2 who underwent partial adrenalectomies for phaeochromocytomas, the 3 year recurrence rate was 7% with 78% of patients remaining steroid independent (Grubbs et al. 2013). Longer term follow up detailing recurrence risk in this situation is currently lacking.

2.5.3 Radiotherapy (external beam and radionuclide)

Conventional external beam radiotherapy can be an effective treatment in metastatic PPGLs and provides local disease control in approximately 80% of lesions at 5 years (Breen *et al.* 2018).

Radionuclide therapy provides an alternative approach to delivering targeted radiotherapy to PPGL cells whilst minimising damage to normal surrounding tissues.

^{131}I-MIBG has a longer half-life than ^{123}I-MIBG (8 days compared to 13 hours), which, together with its emission of beta particles, makes it well suited for radionuclide therapy. A meta-analysis of 17 studies containing 243 patients found complete radiological response in 3%, partial response in 27% and stable disease in 52% (van Hulsteijn *et al.* 2014). The response of soft tissue metastases to ^{131}I-MIBG appears better than that of bone metastases (Loh *et al.* 1997). Despite being 'targeted' radiotherapy, ^{131}I-MIBG is associated with significant side effects, including a long-term risk of haematological malignancy in 15% of treated patients (Sze *et al.* 2013).

In peptide receptor radionuclide therapy (PRRT), the high expression rate of $SSTR_2$ on PPGLs is exploited for therapeutic benefit. Somatostatin analogues are coupled to a radioactive ligand (usually ^{177}Lu) to deliver targeted radiotherapy. Although less established than ^{131}I-MIBG, initial comparisons suggest that PRRT may prove more effective (Nastos *et al.* 2017).

2.5.4 Chemotherapy and other agents

The Averbuch regime of cyclophosphamide, vincristine and dacarbazine (CVD) is the single most widely used chemotherapy regime for PPGLs (Keiser *et al.* 1985). Overall response rates are generally disappointing with only 37% of patients achieving a partial tumour volume response and 40% a partial catecholamine response (Niemeijer *et al.* 2014). The response rate to CVD, however, appears to be far higher in SDHB-associated PPGLs (Jawed *et al.* 2018).

Temozolamide, the oral precursor of dacarbazine, monotherapy similarly shows a greater response rate in SDHB-associated PPGLs, which is potentially explained by its mechanism of action (Hadoux *et al.* 2014). It is an alkylating agent that exerts its chemotherapeutic effect through DNA adduction, the generation of double strand breaks and subsequent cellular apoptosis. This process is opposed by O^6-alkylguanine DNA methyltransferase (MGMT), expression of which is downregulated due to hypermethylation of its promoter in SDHx-associated PPGLs (Hadoux *et al.* 2014).

Increasing understanding of PPGL biology and the responsible molecular mechanisms has presented

multiple potential therapeutic targets, with receptor tyrosine kinase inhibitors (TKIs) being the preferred agents. Current evidence is generally limited to small, retrospective series with many prospective trials in progress. The first TKI utilised was the multi-RTK targeting sunitinib, which through its actions against vascular endothelial growth factor (VEGF) and RET was a promising candidate to treat both cluster 1 and cluster 2 PPGLs. The single largest series to date contained 17 patients, of whom 57% had a partial response or stable disease, with a suggestion of improved response in SDHB-associated tumours (Ayala-Ramirez *et al.* 2012). A multi-centre, prospective, placebo-controlled trial is currently underway (FIRSTMAPP, NCT01371201). The mTOR inhibitor everolimus does not appear to be effective in monotherapy (Druce *et al.* 2009) and is currently being trialled in combination with the multi-targeting TKI vatalanib (NCT00655655). Pazopanib has no evidence of benefit and serious cardiovascular adverse effects led to early trial termination (Jasim *et al.* 2017). TKIs currently in clinical trials for PPGLs include the VEGFR and RET targeting cabozantinib (NCT02302833), axitinib (NCT01967576), the VEGFR inhibitor lenvatinib (NCT03008369) and the FGFR targeting dovitinib (NCT01635907). Such trials are desperately needed given the generally poor response rates of metastatic PPGLs to currently available therapies and the limited, predominantly retrospective, evidence base on which they are used.

2.6 Thesis aims and objectives

Alterations in primary cilia have been observed in a range of different cancers; most commonly cilia are absent or reduced in tumours compared to their tissue of origin (Schraml *et al.* 2009; Hassounah *et al.* 2013). Whether ciliary loss is merely a consequence of the enhanced cellular proliferation seen in tumours, or whether it might contribute to tumourigenesis itself, remains under debate.

Renal cysts and ccRCCs associated with von Hippel-Lindau disease are devoid of primary cilia (Basten *et al.* 2013). Despite the identified role pVHL plays in microtubule and ciliary stabilisation (Okuda *et al.* 1999; Schermer *et al.* 2006), it is unknown whether primary cilia loss is a feature of other VHL-associated tumours such as PPGLs. The overarching aim of this thesis was to investigate whether alterations in primary cilia contribute to PPGL pathogenesis.

The first objective was to determine whether primary cilia are altered in PPGLs and in particular those associated with VHL. This was addressed through analysis of primary cilia structure and transcriptome in human phaeochromocytomas compared to adjacent non-cancerous adrenal medullas. In order to address whether cilia loss contributes to PPGL tumourigenesis, genetic manipulation of a phaeochromocytoma-derived cell line to impair ciliogenesis was performed and cellular proliferation and gene expression were analysed.

Primary cilia are sensory organelles that are ideally placed to interact with the tumour microenvironment. Hypoxia is a cardinal feature of the tumour microenvironment in general, and has particular relevance to cluster 1 PPGLs. The effect of hypoxia on primary cilia appears complex, variable and cell lineage dependent (Proulx-Bonneau & Annabi 2011; Wann *et al.* 2013; Brown *et al.* 2014; Lavagnino *et al.* 2016) and has not been well studied in the context of cancer.

The second objective of this thesis was to investigate whether features of the tumour microenvironment directly relevant to PPGLs influenced primary cilia. Utilising phaeochromocytoma-derived cell lines, we investigated the effect hypoxia and pseudohypoxia (achieved in a variety of PPGL-relevant manners) had on primary cilia and demonstrated the responsible mechanism. The effects of catecholamines on primary cilia were also examined.

Next, our attention turns from phaeochromocytoma pathogenesis to diagnosis. Adrenal venous sampling is an established, but now rarely required, technique for phaeochromocytoma localisation in the event of equivocal imaging findings, particularly in the context of inherited PPGL syndromes. Uncertainty remains regarding its use (Freel *et al.* 2010), largely due to the lack of robust reference intervals for catecholamine values in adrenal venous effluent.

The third objective of this thesis was to define a diagnostic cut-off for adrenal venous catecholamine concentrations in phaeochromocytomas. This was achieved by determining reference intervals in patients without phaeochromocytomas and comparing these to patients with phaeochromocytomas.

CHAPTER 3
Materials and methods

3.1 Patient recruitment and ethical approval

3.1.1 Primary cilia in phaeochromocytoma and paraganglioma

Consecutive patients who were due to undergo surgery for phaeochromocytoma or paraganglioma (diagnosed on the basis of preoperative biochemistry and imaging) at St Bartholomew's Hospital, University College London Hospital and the National Hospital for Neurology and Neurosurgery (all London, UK) were approached for involvement in this study between 2014 and 2016. All participants gave written informed consent for this study, which was approved by Cambridge East Research Ethics Committee (REC: 06/Q0104/133). Clinical data was obtained from participants' medical records.

3.1.2 Adrenal venous catecholamine measurement

Successive patients who underwent adrenal venous sampling (AVS) for the localisation of established primary aldosteronism (PA) at St Bartholomew's Hospital, London and the Radboud University Medical Center, Nijmegan, The Netherlands between 2006 and 2015 were included in this analysis.

A second group of six patients at St Bartholomew's Hospital were identified who had undergone AVS for the diagnosis and localisation of phaeochromocytomas, with subsequent histological confirmation of the diagnosis.

It is standard clinical practice to routinely measure adrenal venous catecholamines at both centres to provide reassurance and confirmation of adrenal vein cannulation. Individualised patient consent was not required, but the protocol received institutional board review at both centres.

3.2 Cell culture

All materials were obtained from Sigma Aldrich (Haverhill, UK) unless otherwise stated. All work was conducted in the Centre for Endocrinology, William Harvey Research Institute, Queen Mary University of London (QMUL) unless otherwise stated.

3.2.1 PC12 cells

PC12 Adh rat phaeochromocytoma cells were obtained from the American Type Culture Collection (ATCC CRL-1721.1 ^{TM}) and were cultured in F-12K (Kaighn's modification of Ham's F-12 medium) medium supplemented with 15% horse serum (v/v), 2.5% foetal bovine serum (FBS; v/v) and 50U/ml penicillin and 50µg/ml streptomycin (final concentration in media 1%).

3.2.2 MPC and MTT cells

MPC and MTT mouse phaeochromocytoma cells were a gift from Prof Karel Pacak (National Institute of Health, Bethesda, Maryland, USA) via Prof Marta Korbonits (QMUL). They were cultured in Dulbecco's Minimum Eagle Medium (DMEM) supplemented with 10% FBS (v/v) and 50U/ml penicillin and 50 µg/ml streptomycin (final concentration in media 1%).

3.2.3 Cell culture conditions

All cells were cultured at 37 ^{o}C, 5% CO_2. For standard conditions cells were cultured in an incubator at standard atmospheric conditions. For hypoxic experiments, cells were cultured in a hypoxic workstation set to an oxygen concentration of 1%, with nitrogen as the balancing gas. Hypoxia experiments were conducted in the Barts Cancer Institute, QMUL.

Cells were seeded in complete media at a density of 30,000 cells/cm^2 onto 15mm glass coverslips (VWR, Lutterworth, UK) or plastic culture dishes for 24 hours until approximately 70-80% confluent. For cilia experiments, they were then washed thrice with phosphate buffered saline (PBS) and transferred to serum-free medium for a further 24 hours or otherwise specified in order to induce growth arrest and promote ciliogenesis.

Drug treatments, dissolved in the relevant solvent, were applied to cells for the duration described in the text with vehicle-only samples being used as controls (Table 3.1).

Cells were confirmed to be mycoplasma free by regular testing using the MycoAlert Mycoplasma Detection Kit (Lonza, Slough, UK).

Drug	Manufacturer	Catalogue number	Solvent
α-ketoglutaric acid	Sigma	K1128	Water
Adrenaline hydrochloride	Sigma	E4642	Water
Antimycin A	Seahorse Bioscience[1]	103015-100	DMSO
DMOG	Sigma	D3695	Water
Dopamine hydrochloride	Sigma	H8502	Water
FM19G11	Sigma	F8807	DMSO
Lithium chloride	Sigma	L9650	Water
Malonate[2]	Sigma	M1875	Water
Metoclopramide hydrochloride	Sigma	M0763	Water
MMF	Sigma	651419	DMSO
Noradrenaline	Sigma	A7256	Water
Octreotide[3]	Novartis	n/a	DMSO
Pasireotide[3]	Novartis	n/a	DMSO
PHA-680632	Selleck Chemicals[4]	S1454	DMSO
Phenoxybenzamine hydrochloride	Sigma	B019	Ethanol
Propranolol hydrochloride	Sigma	P0884	Ethanol
Rotenone	Seahorse Bioscience[1]	103015-100	DMSO
Salbutamol	Sigma	S8260	Methanol
Trichostatin A	Sigma	T1952	DMSO
Tubacin	Sigma	SML0065	DMSO

Table 3.1: Cell culture drugs used in this thesis

DMOG – dimethyloxalylglycine, N-(methoxyoxoacetyl)-glycine methyl ester, DMSO – dimethyl sulfoxide, MMF – mono-methyl fumarate, n/a – not applicable.

1 – Seahorse Bioscience, Massachusetts, USA
2 – Sodium malonate dibasic monohydrate
3 – Octreotide and pasireotide were gifts from Novartis, Camberley, UK.
4 – Selleck Chemicals, Houston, Texas, USA

3.2.4 Trypan blue dye exclusion assay

Following passage, an aliquot of cell suspension was mixed with an equal volume of 0.4% trypan blue solution (Sigma Aldrich) in order to assess cell viability. This mixture was applied to a haemocytometer and examined with a light microscope at x10 magnification. Trypan blue is unable to cross an intact cell membrane and therefore cells containing it (as assessed by blue cytoplasm) are non-viable. Cells were counted to determine the solution concentration, with in excess of 95% cells being viable in a healthy suspension.

3.2.5 siRNA-mediated knockdown

PC12 cells were transfected with either targeted or non-targeted control siRNAs using Lipofectamine 3000 (Thermo Fisher Scientific) according to the manufacturer's instructions. Pre-designed Silencer Select (Ambion, Inchinnan, UK) or SMARTpool (Dharmacon, Lafayette, Colorado, USA) siRNAs were utilised. All siRNAs were used at a total concentration of 30nM. For gene knockdown, multiple distinct siRNAs were used: two for Silencer Select, four for SMARTpool (Table 3.2).

PC12 cells were plated in complete media. Once 70-90% confluent, the medium was removed, the cells washed with PBS and replaced with fresh media. Lipofectamine-siRNA complexes were prepared as below and added to the fresh media. Cells were processed 48 hours after transfection.

Lipofectamine mix (/well)	24 well plate	6 well plate
OptiMEM	25µl	125µl
Lipofectamine 3000	0.75µl	3.75µl
siRNA mix (/well)		
OptiMEM	25µl	125µl
siRNA (total)	15pmol	60pmol
Lipofectamine-siRNA mix (/well)		
Lipofectamine mix	25µl	125µl
siRNA mix	25µl	125µl

Target	Manufacturer	ID	Target sequence (5' → 3')
Cep164	Dharmacon	J-101005-09	CCAAAUUAGAGCCGAGCAA
		J-101005-10	GUGAUGAGCACUACCGGAA
		J-101005-19	AGGAGGAGAACAUGCGGAA
		J-101005-20	AGACCAAGCACCUGGACGA
Fh	Ambion	s127738	CAAGAACGGAUCAACCUUA
		s127739	GGUCCCAACCGAUAAGUA
Hif1α	Dharmacon	J-091718-05	UGAGAGAAAUGCUUACACA
		J-091718-06	GGAAACGAGUGAAAGGAUA
		J-091718-07	UUACUGAGUUGAUGGGUUA
		J-091718-08	CUGAUAACGUGAACAAAUA
Ift88	Ambion	s157132	GGACCUAACCUACUCCGUU
		s157133	CUAUGAGUCAUAUAGGUAU
Sdhb	Ambion	s151576	GCAAAGUCUCGAAAAUAUA
		S151577	CGGACAAGGCUGGAGAUAA
Vhl	Ambion	s128583	CCAAAUGUGCGGAAAGACA
		s128584	GGACUUCUGGUUAACCAAA
Negative control #1	Ambion	4390843	Proprietary

Table 3.2: siRNAs used in this thesis

Cep164 – centrosomal protein 164, Fh – fumarate hydratase, HIF – hypoxia inducible factor, Ift88 – intraflagellar transport protein 88, Sdhb – succinate dehydrogenase subunit B, Vhl – von Hippel-Lindau, n/a – not applicable.

3.3 Tissue preparation

Samples of phaeochromocytomas, paragangliomas and adrenal medullas were obtained at the time of operation and immediately placed into either 4% (w/v) formaldehyde or RNA later. Samples in RNA later were stored at -20^{o}C until the time of RNA extraction.

Samples were kept in formaldehyde overnight at 4^{o}C and then washed in PBS for one hour. They were then suspended in 30% (w/v) sucrose in water at 4^{o}C until they had fallen to the bottom of the collecting tube. They were then embedded in optimal cutting temperature (OCT) compound (VWR) on dry ice and stored at -80^{o}C until the time of cryosectioning.

3.4 Immunofluorescence (IF)

3.4.1 Immunocytochemistry (ICC) in cultured cells

PC12, MPC and MTT cells were cultured on 15mm glass coverslips (VWR) in 12 and 24 well plates. Culture media was removed and the coverslips were washed three times with PBS. Cells were then fixed with 4% (w/v) formaldehyde in PBS for 10 minutes. The formaldehyde was then removed and the coverslips again washed three times for five minutes with PBS. Cells were then permeabilised with 0.25% (v/v) triton-X 100 for five minutes, which was then removed, followed by three further 5 minute PBS washes. Cells were then blocked with 3% (w/v) bovine serum albumin (BSA), 5% (v/v) normal goat serum (NGS) in PBS (IF blocking buffer) for one hour in order to reduce non-specific antibody interactions.

Cells were then incubated with the desired primary antibodies (Table 3.3) in IF blocking buffer for two hours. Coverslips were washed three times for 10 minutes with PBS and then incubated in the dark for one hour with species-specific fluorescent secondary antibodies (Table 3.4) in IF blocking buffer. After removal of the secondary antibody solution, 1µg/ml 4',6-diamidino-2-phenylindole (DAPI) was applied for one minute to label cell nuclei. The coverslips were washed three further times with PBS for 5 minutes and mounted on SuperFrost slides (VWR) with fluorescence mounting medium (Dako) for confocal imaging and with Fluoromount-G (Southern Biotech) for super resolution imaging. Coverslip edges were sealed with nail varnish to prevent them drying out and were stored at 4^{o}C.

All steps were conducted at room temperature. Antibody concentrations were determined following optimisation experiments (not shown).

Target	Clonality	Clone	Species	Supplier	Cat No	Use	Dilution
Acetylated α-tubulin	Mono	6-11B-1	Mouse	Sigma	T6793	ICC, IHC	1:2000
Arl13b	Poly	n/a	Rabbit	Proteintech	17711-1-AP	ICC, IHC	1:500
β-actin	Mono	AC-15	Mouse	Abcam	ab6276	WB	1:10,000
FH	Mono	EPR11648	Rabbit	Abcam	ab171948	WB	1:1000
GAPDH	Poly	n/a	Rabbit	Abcam	ab9485	WB	1:5000
IFT88	Poly	n/a	Rabbit	Proteintech	13967-1-AP	ICC WB	1:50 1:1000
Ki67	Mono	EPR3610	Mouse	Abcam	ab92742	ICC	1:600
SDHB	Mono	21A11AE7	Mouse	Abcam	ab14714	WB	1:1000
VHL	Poly	n/a	Rabbit	Santa Cruz	Sc-5575	ICC WB	1:250 1:1000

Table 3.3: Primary antibodies used in this thesis

Cat No – catalogue number, Arl13b – ADP ribosylation factor like protein 13b, ICC – immunocytochemistry, IHC – immunohistochemistry, n/a – not applicable, WB – Western blot, FH – fumarate hydratase, GAPDH – glyceraldehyde 3-phosphate dehydrogenase, IFT88 – intraflagellar transport protein 88, SDHB – succinate dehydrogenase subunit B, VHL – von Hippel-Lindau.

Fluorophore	Target	Clonality	Species	Supplier	Cat No	Use	Dilution
Alexa Fluor 488	Mouse IgG	Poly	Goat	Invitrogen[1]	A-11029	ICC, IHC	1:1000
	Rabbit IgG	Poly	Goat	Invitrogen[1]	A-11034	ICC, IHC	1:1000
Alexa Fluor 568	Mouse IgG	Poly	Goat	Invitrogen[1]	A-11031	ICC, IHC	1:1000
	Rabbit IgG	Poly	Goat	Invitrogen[1]	A-11036	ICC, IHC	1:1000
IR Dye 680LT	Mouse IgG	Poly	Goat	Li-Cor[2]	ABIN2169640	WB	1:5000
	Rabbit IgG	Poly	Goat	Li-Cor[2]	ABIN2169643	WB	1:5000
IR Dye 800CW	Mouse IgG	Poly	Goat	Li-Cor[2]	ABIN2169616	WB	1:5000
	Rabbit IgG	Poly	Goat	Li-Cor[2]	ABIN2169624	WB	1:5000
DAPI	n/a	n/a	n/a	Sigma	D9542	ICC, IHC	1:5000

Table 3.4: Fluorescent molecules and secondary antibodies used in this thesis

ICC – immunocytochemistry, IHC – immunohistochemistry, WB – Western blotting, DAPI – 4',6-diamidino-2-phenylindole dihydrochloride

1 – Invitrogen, Inchinnan, UK
2 – LI-COR, Cambridge, UK

3.4.2 Immunohistochemistry (IHC) in tissue sections

A microtome-cryostat set at -20 ^{o}C was used to cut frozen section tissue samples embedded in OCT compound. 10µm sections were obtained and placed in room temperature PBS to dissolve the OCT compound.

Tissue sections were treated in the same manner as ICC of cultured cells (above) using a free floating technique by which they were sequentially transferred to wells containing the relevant reagents, with the exception that the primary antibody incubation stage occurred overnight at 4^{o}C. Tissue sections were mounted on SuperFrost Plus adhesion slides (VWR) with fluorescence mounting medium (Dako) and covered by glass coverslips. Slide edges were sealed with nail varnish and stored at 4^{o}C.

3.5 Western blotting

3.5.1 Cell lysate preparation

For protein extraction, cells were cultured in 6 well plastic culture dishes (surface area 9.6 cm^2/well) and all steps were performed on ice. The media was removed and cells were washed twice with 2ml of ice cold PBS. Cells were then lysed with 100µl of ice cold radioimmunoprecipitation assay (RIPA) buffer containing protease and phosphodiesterase inhibitors (Roche, Welwyn Garden City, UK) and the culture dish repeatedly scraped with a cell scraper. The lysate was collected and homogenised by passing it through a 21G needle 10 times and then incubated on ice for 30 minutes before being centrifuged for 12 minutes (13000g, 4^oC). The protein-containing supernatant was collected and either used immediately or stored at -80^oC for later use.

3.5.2 Protein quantification

Sample protein concentration was calculated using a Bradford assay against stock concentrations of BSA. 10µl of each sample and BSA standards were plated in duplicate onto a 96 well plate and mixed with 200µl of protein assay reagent (1 part reagent: 4 parts ddH_20). After 5 minutes at room temperature, the Wallac 1420 multilabel counter was used to quantify absorbance at 595nm. From this readout, sample protein concentrations were calculated against that of the stock concentrations of BSA. Sample protein concentrations were then equalised prior to sodium dodecyl sulphate polyacrylamide gel electrophoresis (SDS-PAGE).

3.5.3 SDS-PAGE

Cell lysates were mixed with an equal volume of 2x Laemelli buffer, vortexed and centrifuged before boiling at 100^oC for 10 minutes. Samples were again vortexed and centrifuged prior to loading onto precast 4-12% gradient NuPage Bis-Tris gels (Invitrogen).

Gels were loaded with 25µl/well for 10 well gels and 20µl/well for 15 well gels. The Novex Sharp pre-stained protein standard (Invitrogen) was used as a molecular weight marker. Gels were run at 150V for 1-2 hours depending on the protein under examination.

3.5.4 Immunoblotting and band quantification

Following electrophoresis, samples were transferred to nitrocellulose membrane (Whatman, Maidstone, UK) by semi-dry transfer using a Trans-Blot SD semi-dry transfer cell (Bio-Rad, Watford,

UK). The transfer buffer consisted of 20mM Tris, 120mM glycine and 10% methanol (v/v). Proteins were transferred at 15V at room temperature for 40 minutes for one gel and 50 minutes for two gels.

After transfer, membranes were cut to size and blocked in 5ml 5% (w/v) non-fat milk in PBS with 0.1% Tween 20 (PBST) for one hour at room temperature. Following blocking, membranes were incubated with 5ml 5% (w/v) non-fat milk in PBST (blocking solution) containing the appropriate primary antibodies (Table 3.3) overnight at 4^{o}C. The membranes were subsequently washed thrice with PBST for 10 minutes and then incubated with the appropriate species-specific infra-red secondary antibodies (Table 3.4) in blocking solution for one hour at room temperature in the dark. The membrane was then washed three times with PBST for 10 minutes at room temperature and a final wash with PBS.

Membranes were imaged using the Li-Cor Odyssey infra-red scanner and densitometry was performed using Odyssey software to quantify band intensity.

3.6 RNA

3.6.1 RNA isolation and quantification

3.6.1.1 RNA isolation from cultured cells

Total RNA was isolated from cells using an RNeasy kit (Qiagen, Manchester, UK) according to manufacturer's instructions.

Cells were quickly washed three times with PBS and then placed onto ice. They were then lysed with 350µl RLT buffer, which contains guanidine-thiocyanate which inhibits RNAses, and scraped by a cell scraper. The lysate was then transferred to a chilled Eppendorf where it was homogenised five times with a 20 gauge needle. 350µl 70% (v/v) ethanol was added and mixed well before 700µl was transferred to a silica based spin column within a collection tube. This was centrifuged for 15s at 8000g and the flow through discarded, leaving the RNA bound to the column. This was washed with 700µl RW1 buffer followed by centrifugation at 8000g for 15 seconds with the flow through again discarded. Next, 500µl RPE buffer was added to the column which was again spun (8000g, 15 seconds) and the flow through discarded. This step was repeated followed by a 2 minute spin (8000g). The spin column was then transferred into a new collection tube and centrifuged for one minute at 14000g before transferring it to a fresh Eppendorf. 30µl RNAse free water was added to

the spin column membrane to elute the RNA. It was left to stand on ice for one minute and then centrifuged at 8000g for one minute. RNA was then used immediately or stored at -80^{o}C.

3.6.1.2 RNA isolation from tissue

Tissue samples stored in RNA later were homogenised in 350µl RLT buffer in 2ml tubes prefilled with ceramic beads using the Precellys 24 tissue homogeniser (Bertin Instruments, Montigny-le-Bretonneux, France). Set at a speed of 3000, 20 second runs were completed until the tissue was homogenised.

Once homogenised, tissue RNA was processed in the same way as from cultured cells using the RNeasy kit as above.

3.6.1.3 RNA quantification

The Nanodrop ND-1000 spectrophotometer (Thermo Fisher Scientific, Loughborough, UK) was used to measure RNA concentration (based on specimen optical density at 260nm) and purity (from the A260/280 absorbance ratio).

3.6.2 RNA sequencing

Isolated total RNA was sent to the Genome Centre, QMUL for RNA sequencing. There, RNA integrity was confirmed using the Bioanalyser Automated Electrophoresis System (Agilent Technologies) with samples of RNA integrity number (RIN) exceeding seven proceeding for further processing (see appendix). 100ng of RNA was used as the input in the KAPA Stranded RNA-Seq with RiboErase (Roche) as per manufacturer's instructions to generate libraries. Libraries were quantified by spectrophotometry using a Nanodrop ND-1000 and library fragment size estimated by Tapestation (Agilent Technologies). Three equal library pools were made and 12pM loaded onto three Illumina NextSeq 500 flow cells and sequenced to 75bp Paired End, as per manufacturer's instructions.

3.6.2.1 RNA sequence data and pathway analyses

Following RNA sequencing, reads were pseudo-aligned using kallisto (Bray *et al.* 2016). Transcript-level counts were aggregated to gene-level with the tximport package (Soneson *et al.* 2015). Prior to exploratory data analysis (EDA), low count genes were filtered based on previous guidelines (Robinson & Oshlack 2010), libraries were normalised using the relative log expression method (Anders & Huber 2010) and counts transformed to $\log_2$-counts per million, which stabilises variance for unsupervised analysis. This matrix was also used to test for pathway enrichment (see below), but not for differential expression. Each gene was tested for differential expression between adrenal and

tumour tissue using tools from the DESeq2 analysis pipeline (Love *et al.* 2014). We filtered genes and estimated *q*-values using the package's independent hypothesis weighting method (Ignatiadis *et al.* 2016).

To detect pathway enrichment in gene sets associated with cilia regulation, we implemented a modified version of the QuSAGE algorithm (Yaari *et al.* 2013; Turner *et al.* 2015) designed for modelling RNA-seq data. This method tests for overexpression in the residual matrix among user supplied gene sets, following the same filtering, normalisation and transformation steps described above for EDA. Pathway *q*-values were calculated using Storey's method (Storey & Tibshirani 2003). Gene sets were summarised to vectors of length 24 (sample size) by taking the first principal component of each, i.e. by calculating the module eigengene. Cilia structure and cilia-mediated signalling gene sets were curated from the Broad Institute's Molecular Signatures Database v6.0 (http://software.broadinstitute.org/gsea/msigdb).

Functional analysis of differential gene expression between control and *Ift88*-knockdown cells was performed using Ingenuity Pathway Analysis (IPA; Ingenuity Systems), using all genes with log fold change ≥ 2 and *q*-value ≤ 0.01 as input. For all gene set enrichment analyses, a right-tailed Fisher's exact test was used to calculate a pathway *P*-value determining the probability that each biological function assigned to that data set was due to chance alone. All enrichment scores were calculated in IPA using all transcripts that passed quality control as the background data set.

Further details or the transcriptome and pathway analysis are included in the appendix and are uploaded at GitHub (https://github.com/C4TB/markdown-chapple_pcc).

3.6.3 Polymerase chain reaction (PCR)

3.6.3.1 cDNA synthesis

RNA was converted to cDNA using the QuantiTect Reverse Transcription kit (Qiagen) according to the manufacturer's instructions. First, genomic DNA was eliminated by incubating RNA with gDNA wipe out buffer at 42^{o}C for 2 minutes in the following reaction.

gDNA wipe out buffer	1µl
1µg RNA	Variable
RNase free water	Variable
	7µl

Next, the genomic DNA elimination reaction was incubated with reverse transcriptase, RT buffer and RT primer mix for 15 minutes at 45^{o}C.

Quantiscript reverse transcriptase	0.5µl
Quantiscript RT buffer	2µl
RT primer mix	0.5µl
Genomic DNA elimination reaction	7µl
	10µl

The reaction mixture was then incubated at 95^{o}C for 3 minutes. The cDNA was quantified using the Nanodrop ND-1000 spectrophotometer and diluted in equal volumes of nuclease free water. It was either used immediately or stored at -20^{o}C for future use.

3.6.3.2 Reverse Transcription PCR (RT-PCR)

RT-PCR reactions were performed using *Taq* polymerase (New England Biolabs) according to the following reaction:

DNA template	1µl
Primer (10µM)	0.5µl
dNTPs (10mM)	0.5µl
Taq polymerase	0.125µl
10X Taq reaction buffer	1µl
Nuclease free water	6.875µl
	10µl

The cycling conditions were:

	94°C 5mins	
Denaturation	94°C 30s	x25 cycles
Annealing	60°C 30s	
Extension	72°C 30s	
	72°C 10mins	
	4 °C	

3.6.3.3 Primer design

Primers were designed using Primer-3 software and synthesised in Sigma Genosys. Primers were designed to target specific regions of target genes, for the amplicon length to be 100-250bp and to avoid gDNA amplification through location in different exons or across exon-exon boundaries. Amplicon size and reaction specificity were confirmed by agarose gel electrophoresis. Primer details are presented in Table 3.5.

Gene	Accession no.	Sequence	Size (bp)	Annealing temperature (°C)
Cep164	XM_017596023.1	F – GAATCTGCATCTAGACCTTGG R – CACTACTGTCTGCACCCTGG	158	60
HIF1α	NM_001530.4	F – CATTGAAGATGAAATGAAAGC R – CATTTCTGTGTGTAAGCATTTC	221	60
PPIA	NM_017101	Proprietary	106	60

Table 3.5: Primers used in this thesis

Cep164 – centrosomal protein 164, HIF – hypoxia inducible factor, PPIA – peptidylpropyl isomerase A, Vhl – von Hippel-Lindau, bp base pairs

3.6.3.4 Gel electrophoresis

Following amplification, samples were combined with 2µl 6X DNA loading dye (New England Biolabs) containing bromophenol blue and subjected to agarose gel electrophoresis. Samples were loaded onto 2% agarose gel made up in Tris-acetate-EDTA (TAE) buffer (40mM Tris pH8, 20mM glacial acetic acid, 1mM EDTA) containing 0.5µg/ml ethidium bromide. Samples were electrophoresed for 45 minutes at 90V in TAE buffer and then visualised using a UVP UV transilluminator. Amplicon size was confirmed against a reference molecular weight marker.

3.6.3.5 Quantitative real time PCR (qRT-PCR)

The syber-green system, in which a fluorescent dye preferentially binds dsDNA, was used to quantify PCR product accumulation with each cycle. Real time PCR was performed using the MX3000p thermal cycler and analysed using MXPro QPCR software (Agilent, Santa Clara, USA).

qRT-PCR reaction mixtures contained:

cDNA	1µl
Primer (5µM)	1µl
qPCRBIO SyGreen Mix	5µl
Nuclease free water	3µl
	10µl

qRT-PCR programme:

	94°C 3min	
Amplification:	94°C 30s	x40 cycles
	60°C 30s	
	72°C 30s	
	Collect end point fluorescence values	
Dissociation:	95°C 1min	
	55°C 30s	
	Collect all fluorescence values from 55-95°C	
	95°C 30s	

Standard curves for each target gene were generated from serial dilution of the amplified PCR product prepared in nuclease-free water. Relative gene expression was calculated from these standard curves, using peptidylpropyl isomerase A (PPIA) as the reference gene.

3.7 Microscopy techniques

Imaging was performed with LSM510 or LSM880 laser scanning confocal microscopes (Zeiss). Super resolution structured illumination (SR-SIM) was on LSM710 with Elyra PS1 (Zeiss) at The School of Engineering, QMUL.

3.7.1 Measurement of primary cilia incidence and length in 2D cell culture

Primary cilia incidence was quantified using the confocal microscopes listed above with a x63 oil-immersion objective. Cilia incidence was defined as the number of cells with a cilium (identified by dual-labelled IF against the axonemal markers acetylated α-tubulin and Arl13b) divided by the number of nuclei (identified by DAPI) in a given field of view. For each experimental condition, ten representative fields of view were counted for each of three biological replicates. The number of cells scored for ciliary incidence for each experiment is included in the relevant figure legend.

For measurement of primary cilia length, cilia were identified as above and sequential z-stacked sections were imaged (section thickness 0.5µm). The image format was set to 1024x1024 pixels with a zoom of 1 and line averaging of 4 per slice. Two dimensional maximum intensity projections (MIPs) were created using Zen software (Zeiss) and individual cilia length was traced and measured using ImageJ software (NIH). For each experimental condition, five representative Z-stacks were scored for each of three biological replicates. The number of cells scored for ciliary length for each experiment is included in the relevant figure legend.

Quantification of cilia incidence and length was performed blinded to experimental status.

3.7.2 Measurement of primary cilia incidence and length in 3D tissue sections

Primary cilia incidence and length were quantified from MIPs created as for 2D cell culture. Five representative MIPs were scored from each of three distinct sections per tissue specimen. The numbers of cells scored for cilia incidence and length for each sample type is included in the relevant figure legend. In addition, the surpass module of Imaris 7.1 image processing and analysis software (Bitplane) was used to surface render 3D images.

3.7.3 Quantification of pVHL axoneme intensity

PC12 cells were fixed and subjected to immunolabelling as above for detection of acetylated α-tubulin and pVHL and imaged as above (settings x4 zoom, line averaging 8). Regions of interest (ROI) of the ciliary axoneme were defined by immunolabelling for acetylated α-tubulin using Zen software and levels of pVHL localised within this area were determined by analysis of fluorescent intensity.

3.8 Adrenal venous catecholamine measurement

3.8.1 Adrenal venous sampling

AVS was performed one hour after the commencement of an intravenous adrenocorticotropic hormone (ACTH) infusion (rate 50μg/hour). Samples were obtained sequentially from both adrenal veins under fluoroscopic guidance by an experienced interventional radiologist. A third sample was taken from the infra-renal inferior vena cava (IVC) as a peripheral sample (Figure 6.1), as previously described (Lau *et al.* 2012; Sze *et al.* 2014).

Successful cannulation of each adrenal vein was defined by an adrenal vein to peripheral cortisol ratio exceeding five to one (Webb *et al.* 2012) and only samples meeting these criteria were included for analysis.

In PA patients, aldosterone antagonists and potassium sparing diuretics were discontinued for at least four weeks, whilst beta-blockers and angiotensin converting enzyme inhibitors were withheld for at least two weeks prior to AVS.

3.8.2 Cortisol and catecholamine measurement

Serum cortisol was measured by electrochemiluminescence immunoassay (Roche) at both centres. Plasma catecholamines were measured using high performance liquid chromatography with electrochemical detection at both St Bartholomew's Hospital (Chromsystems, Gräfelfing, Germany) and at the University of Dresden (in house method (Eisenhofer *et al.* 1986)) for the Nijmegan samples.

3.9 Statistics

All data are presented as mean ± standard deviation (SD) unless otherwise stated. For cilia length box and whisker plots, the box represents the interquartile range with the centre line the median and the whiskers represent the 10^{th} and 90^{th} centiles. Statistical significance was determined using two-tailed Student's t-test, one-way Analysis of Variance (ANOVA) or The Wilcoxon signed rank test as appropriate. Centile values for adrenal vein noradrenaline to adrenaline ratios were calculated by counting. Analyses were performed using Prism version 7 (GraphPad, San Diego, California). For RNA-sequencing, analyses were conducted in the R statistical environment, version 3.4.0, using software from the Bioconductor repository (Huber *et al.* 2015).

CHAPTER 4

Primary cilia loss is a feature of human phaeochromocytomas and contributes to tumourigenesis

The RNA sequencing detailed in this chapter was performed at The Barts and The London Genome Centre. Its analysis was conducted in collaboration with David Watson.

Work in this chapter has been published in the following article, which is included in the appendix of this thesis.

Oncometabolite induced primary cilia loss in pheochromocytoma. O'Toole SM, Watson DS, Novoselova TV, Romano LEL, King PJ, Bradshaw TY, Thompson CL, Knight MM, Sharp TV, Barnes MR, Srirangalingam U, Drake WM, Chapple JP. Endocrine Related Cancer 2019; 26(1): 165-180.

4.1 Introduction

Primary cilia are directly linked to cell cycle progression through the basal body/mother centriole and it has been suggested that their presence might act as a checkpoint opposing mitotic cell division (Izawa *et al.* 2015). Alterations in primary cilia have been observed in a range of different cancers. Most commonly, cilia are absent or reduced in tumours compared to their tissue of origin (Schraml *et al.* 2009; Hassounah *et al.* 2013).

Whether ciliary loss is merely a consequence of the enhanced cellular proliferation seen in tumours, or whether it might contribute to tumourigenesis itself, remains under debate. In addition to its cell cycle link, primary cilia modulate a number of signalling pathways that can be dysregulated in cancer (Berbari *et al.* 2009; Wong *et al.* 2009; Goetz & Anderson 2010; Lancaster *et al.* 2011; Oh & Katsanis 2013). This, combined with the intriguing observation that primary cilia are required for certain tumours to develop (Wong *et al.* 2009), suggests a more complex role.

pVHL plays a role in primary cilia stabilisation (Okuda *et al.* 1999; Schermer *et al.* 2006) and its loss of function in the familial cancer syndrome von Hippel-Lindau disease results in renal cyst and ccRCC formation, which are devoid of primary cilia (Basten *et al.* 2013). It is unknown whether primary cilia disruption in VHL is limited to ccRCCs or is a more generalised feature of other VHL-associated cancers, which include PPGLs.

4.2 Aims and Objectives

The aim of this chapter was to investigate whether primary cilia were altered in phaeochromocytomas.

Based on cilia alterations in other tumours of neural origin and in ccRCC in which the PPGL predisposition gene *VHL* is inactivated, we hypothesised that primary cilia would be altered in phaeochromocytomas, particularly those associated with VHL.

The first objective was to determine whether primary cilia incidence or length was altered in phaeochromocytomas compared to adjacent normal adrenal medullas.

The second objective was to determine whether there were any identifiable clinical variables that impacted on phaeochromocytoma primary cilia incidence and length.

The third objective was to determine if the observed changes in primary cilia structure resulted in alterations in cilia-mediated signalling in phaeochromocytomas.

The fourth objective was to determine whether phaeochromocytoma-derived cells displayed primary cilia in 2D culture.

The fifth objective was to determine whether inhibition of ciliogenesis in phaeochromocytoma-derived cells resulted in changes in cellular proliferation or gene expression.

4.3 Results

4.3.1 Primary cilia loss and alterations in cilia-mediated signalling are features of human phaeochromocytomas

4.3.1.1 Primary cilia incidence and length is reduced in phaeochromocytomas relative to adjacent normal adrenal medullas

Paired tissue samples from phaeochromocytomas and adjacent macroscopically normal adrenal medullas were collected from 25 sequential consenting patients who underwent adrenalectomy between April 2014 and September 2016. Two patients had bilateral disease, giving a total of 27 paired samples; the clinical details are presented in Tables 4.1 & 4.2. Following processing, tissues were immunostained for the axonemal proteins acetylated α-tubulin and Arl13b, imaged with a confocal microscope and analysed for primary cilia (Figure 4.1A; see Chapter 3 for full methodology).

Primary cilia incidence was lower in phaeochromocytomas (3.06% $\pm$ 0.14) compared to adjacent adrenal medullas (8.42% $\pm$ 0.03; $p=4.7x10^{-11}$) (Figure 4.1B) within the cohort as a whole and between every paired sample (Figure 4.1E). Cilia length was also reduced in phaeochromocytomas (1.48µm $\pm$ 0.34) compared to adrenal medullas (2.02 µm $\pm$ 0.39; $p=8.2x10^{-11}$) (Figure 4.1C) and was lower in the phaeochromocytoma of each sample pair in all but one instance (Figure 4.1F). There was a correlation between the incidence and length of primary cilia measured in individuals in both phaeochromocytomas ($p=1.1x10^{-7}$, $r^2=0.6828$) and adjacent adrenal medullas ($p=0.0008$, $r^2=0.3668$) (Figure 4.1D).

Thus, primary ciliary loss is a feature of phaeochromocytomas. This finding is consistent with observations in other tumours of neuroectodermal origin: GBM (Loskutov *et al.* 2018), medulloblastoma (Han *et al.* 2009) and melanoma (Kim *et al.* 2011b; Snedecor *et al.* 2015).

	Paired	Unpaired	All
Samples (n)	27	20	47
Patients (n)	25	15	40
Sex			
Male; n (%)	12 (48%)	7 (47%)	19 (47.5%)
Female; n (%)	13 (52%)	8 (53%)	21 (52.5%)
Age (years)			
- Mean ± SEM	46.8 ± 4.0	46.2 ± 3.4	46.6 ± 2.8
- Range	12 - 78	15 - 68	12 – 78
Size (mm)			
- Mean ± SEM	49 ± 4	47 ± 7	48 ± 4
- Range	8 - 87	13 - 120	8 – 120
Location			
- Adrenal	27 (100%)	7 (35%)	34 (72%)
- PGL	0 (0%)	13 (65%)	13 (28%)
Mode of diagnosis			
- Symptomatic	9 (33%)	9 (45%)	18 (38%)
- Incidental	14 (52%)	7 (35%)	21 (45%)
- Screening	4 (15%)	4 (20%)	8 (17%)
Germline mutation (patients)	5 (25%)	8 (53%)	13 (33.5%)
SDHA	0	1	1
SDHB	1	4	5
VHL	3	2	5
MEN2	1	1	2
Germline mutation (tumours)	7 (26%)	13 (65%)	20 (42.6%)
SDHA	0	3	3
SDHB	1	5	6
VHL	5	4	9
MEN2	1	1	2

Table 4.1: Summary table of patient and sample clinical details

SEM – standard error of the mean, PGL – paraganglioma, SDH – Succinate Dehydrogenase, VHL – von Hippel-Lindau, MEN2 – Multiple Endocrine Neoplasia type 2.

Mode of diagnosis: symptomatic = diagnosis due to symptoms or signs of catecholamine excess leading to diagnosis, incidental = diagnosis due to investigation for another unrelated condition, screening = diagnosis during a screening programme in individuals with known PPGL predisposition.

Sample ID (RNAseq ID)	Sex	Age at operation	Phaeo/PGL	Location	Mode of diagnosis	Syndromic	Genetics screening	Gene mutation	Max size/mm	NMN	MN	3-MT
1[A] (H1-2)	M	49	Phaeo	Right	Symptomatic	No	No		36	-	+	-
2[A] (H3-4)	F	71	Phaeo	Right	Incidental	No	No		32	+	+	-
3[A] (H5-6)	M	12	Phaeo	Left	Symptomatic	No	Yes	Negative	58	+++	-	+
4[A, B] (H7-10)	M	37	Phaeo	Left	Screening	Yes	Yes	MEN2	14	-	+	-
5[A] (H11-12)	F	31	Phaeo	Left	Symptomatic	No	Yes	Negative	49	+++	-	+
6[A] (H13-14)	M	18	Phaeo	Left	Screening	Yes	Yes	VHL	32	++	-	+
7[A] (H15-16)	M	69	Phaeo	Right	Incidental	No	No		80	+++	+++	+
8[A] (H17-18)	M	39	Phaeo	Left	Incidental	No	Yes	SDHB	48	+	-	-
9[A] (H19-20)	F	34	Phaeo	Right	Symptomatic	No	Yes	Negative	76	+++	-	+
10[A] (H21-22)	M	64	Phaeo	Left	Incidental	No	Yes	Negative	33	+	-	-
11[A, C] (H23-24) 12	M	14 14	Phaeo	Right Left	Screening Screening	Yes Yes	Yes Yes	VHL VHL	14 8	+ +	- -	+ -
13	F	27	Phaeo	Right	Symptomatic	No	Yes	Negative	54	+++	-	+
14	F	66	Phaeo	Right	Incidental	No	No		47	+	-	-
15	F	69	Phaeo	Right	Incidental	No	No		57	+	-	-
16 17	F	13 13	Phaeo	Left Right	Symptomatic Symptomatic	Yes Yes	Yes Yes	VHL VHL	23 49	+++ +++	- -	- -
18	F	35	Phaeo	Right	Incidental	No	Yes	Negative	73	++	+++	+
19	F	78	Phaeo	Left	Incidental	No	No		45	+	++	-
20	M	63	Phaeo	Right	Incidental	No	No		35	+	++	-
21	F	52	Phaeo	Right	Symptomatic	No	No		30	+	+	-
22	M	43	Phaeo	Right	Incidental	No	No		56	++	+++	-
23	M	46	Phaeo	Right	Symptomatic	No	Yes	Negative	75	++	-	+
24	F	74	Phaeo	Left	Incidental	No	No		76	++	+++	++
25	F	50	Phaeo	Right	Incidental	No	Yes	Negative	80	++	+++	+
26	F	60	Phaeo	Right	Incidental	No	No		87	+++	+++	+
27	M	56	Phaeo	Right	Incidental	No	No		55	+	++	-

Table 4.2: Clinical details of 27 paired samples of tumour and adjacent adrenal samples from 25 individuals

Table 4.2: Clinical details of 27 paired samples of tumour and adjacent adrenal samples from 25 individuals (previous page)

F – female, M – male, Phaeo – phaeochromocytoma, PGL – paraganglioma, SDHB – succinate dehydrogenase B, VHL – von Hippel-Lindau, MEN2 – Multiple Endocrine Neoplasia Type 2, NMN - normetanephrine, MN – metanephrine, 3-MT – 3-methoxytramine.

Mode of diagnosis: symptomatic = diagnosis due to symptoms or signs of catecholamine excess leading to diagnosis, incidental = diagnosis due to investigation for another unrelated condition, screening = diagnosis during a screening programme in individuals with known PPGL predisposition.

For metanephrines: - not elevated, + elevated 1-5x upper limit of normal (ULN), ++ elevated 5-10x ULN, +++ elevated >10x ULN.

[A] Samples included in the RNAseq analysis (RNAseq sample ID in brackets; odd number adrenal medulla, even number pheochromocytoma)

[B] Patient 4 had synchronous bilateral disease which was included in RNAseq analysis but immunochemistry was only available in the left pheochromocytoma

[C] Patient 11 had metachronous bilateral disease and RNAseq was performed on one set of paired samples only

Figure 4.1: Primary cilia incidence and length is reduced in phaeochromocytomas relative to adjacent adrenal medullas (next page)

(A) Maximum intensity projections (MIP) of confocal Z-stacks of phaeochromocytoma (phaeo) and adjacent adrenal medulla. Tissue sections were processed for dual-immunofluorescent detection of the ciliary markers acetylated α-tubulin (green) and Arl13b (red) and counterstained with DAPI (blue) to detect nuclei. A single confocal section from the area demarked by the dashed box is shown zoomed (XY zoom). Individual cilia, indicated by arrows, are further enlarged in insets 1-6 and are shown as surface rendered D images in the panels on the right. Scale bars = 10 μm.

Quantification of primary cilia incidence (B, E) and length (C, F) in 27 paired phaeochromocytomas and adjacent adrenal medullas (adrenal) following treatment as per (A). In (E) and (F), paired samples are linked by a solid line. Linear regression (D) demonstrates a relationship between cilia incidence and length in both tissue types.

Number of cells scored per sample for incidence: 2039 $\pm$ 551 for adrenal medulla and 2359 $\pm$ 841 for phaeochromocytoma. Number of cilia measured per sample for length: 186 $\pm$ 108 for adrenal medulla and 75 $\pm$ 55 for phaeochromocytoma. Statistical significance was assessed using a paired t-test (B, C) and linear regression (D). *** $p<0.001$.

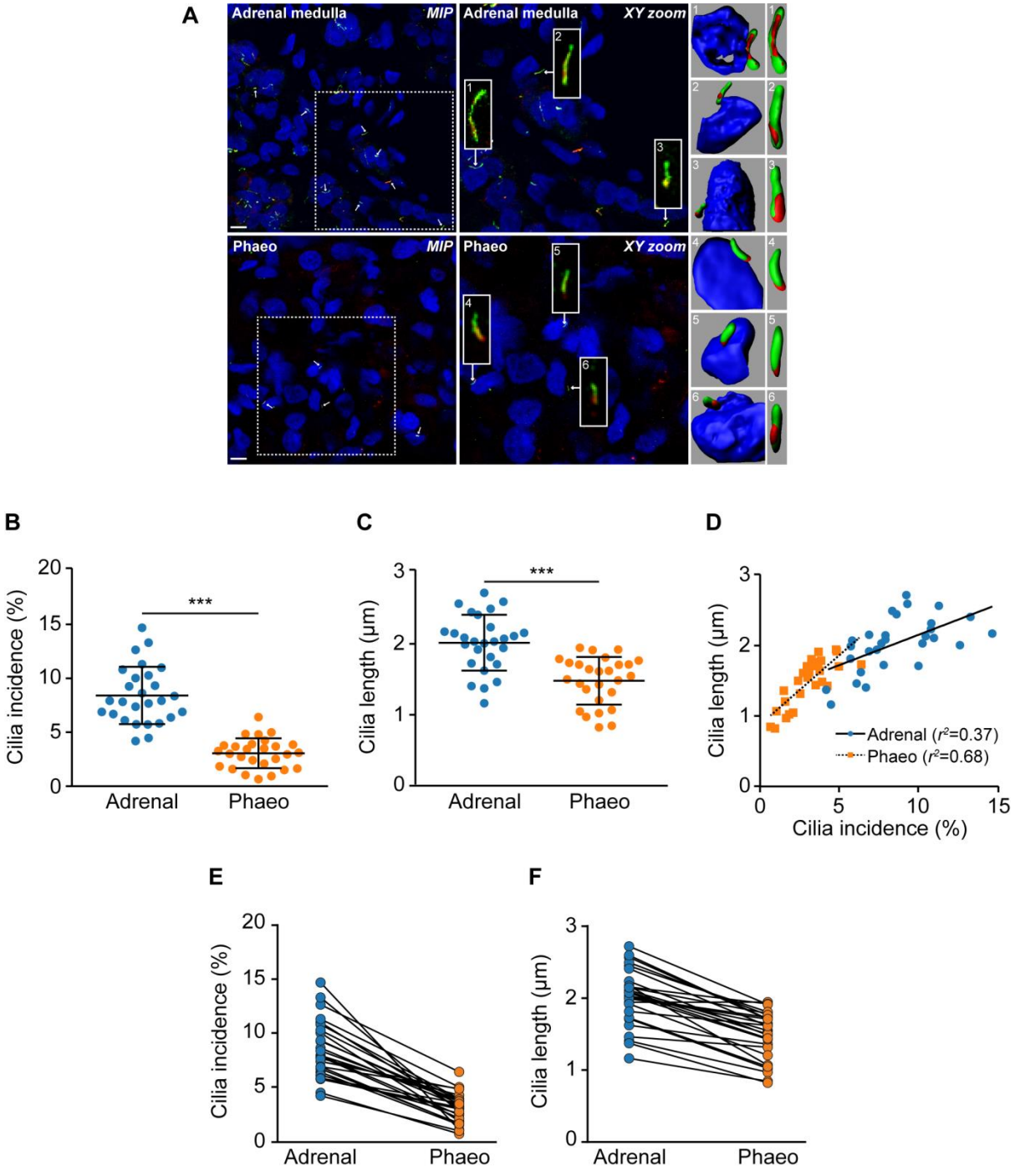

Figure 4.1: Primary cilia incidence and length is reduced in phaeochromocytomas relative to adjacent adrenal medullas

Legend on previous page

4.3.1.2 Primary cilia loss is a particular feature of cluster 1 phaeochromocytomas and paragangliomas

We next sought to investigate whether there were any identifiable factors that correlated with ciliary phenotype. As discussed in Chapter 1, it has previously been reported that the tumour suppressor pVHL plays a role in ciliogenesis (Schermer *et al.* 2006) and VHL-associated ccRCCs have severely reduced primary cilia (Schraml *et al.* 2009; Basten *et al.* 2013). VHL is a known PPGL predisposition gene (discussed in Chapter 2), but whether primary cilia are implicated in the pathogenesis of PPGL or any other VHL-associated tumour is unknown.

We thus examined cilia incidence and length in phaeochromocytomas and adjacent normal adrenal medullas in five specimens from patients with von Hippel-Lindau disease in comparison to 22 specimens from patients without this syndrome (Tables 4.1 & 4.2). There was no difference between either cilia incidence (8.6% $\pm$ 5.0 v. 8.4% $\pm$ 2.0; p=0.86) or length (1.77µm $\pm$ 0.55 v. 2.09µm $\pm$ 0.34; p=0.10) in the adrenal medullas of patients with or without VHL. Cilia incidence was, however, reduced in phaeochromocytomas in patients with VHL compared to those without (1.40% $\pm$ 0.82 v. 3.4% $\pm$ 1.2; p=0.0101), as was cilia length (1.15µm $\pm$ 0.35 v. 1.58µm $\pm$ 0.31; p=0.0101) (Figure 4.2A & B). This reduction in cilia incidence and length in VHL-associated phaeochromocytomas is further illustrated by waterfall plots showing their relative changes between adrenal medulla and tumour (Figure 4.2C & D). For incidence, relative reduction in primary cilia between adrenal medulla and phaeochromocytoma was greater in patients with VHL than those without (-82.3% $\pm$ 3.0 v. -58.0% $\pm$ 3.0; p=0.001).

These findings suggest that cilia loss and shortening in VHL-associated phaeochromocytomas occurs during tumourigenesis and is not a pre-existing or pre-malignant feature. This is in contrast to other tumour types in which cilia loss occurs in pre-neoplastic lesions including pancreatic intraepithelial neoplasia (Seeley *et al.* 2009; Schimmack *et al.* 2016), melanoma *in situ* (Kim *et al.* 2011b; Snedecor *et al.* 2015) and breast carcinoma *in situ* (Menzl *et al.* 2014). Unlike these malignancies, however, PPGL do not have a recognised pre-neoplastic stage.

In order to further evaluate whether enhanced tumoural cilia loss was specific to VHL or was a wider feature of other pseudohypoxic phaeochromocytomas, we extended our analysis to include an additional 20 tumours from 15 patients from whom a paired adrenal sample was unavailable (total 47 PPGL from 40 patients; Tables 4.1 & 4.3).

We compared PPGLs from patients with germline mutations in *VHL*, to tumours from patients with germline mutations in *SDHx* and those without a known germline mutation in a pseudohypoxia-linked gene. Cilia incidence was reduced in PPGLs from patients with germline mutations in *VHL* (1.4% $\pm$ 0.8; $p=1.5x10^{-6}$) and *SDHx* (2.2% $\pm$ 0.7; p=0.0211) relative to PPGLs from patients without a known germline cluster 1 mutation (4.0% $\pm$ 0.2) (Figure 4.2E). Cilia length was also reduced in VHL- (1.22 µm $\pm$ 0.30) and SDHx- (1.39 µm $\pm$ 0.38) PPGLs relative to non-cluster 1 tumours (1.65 µm $\pm$ 0.28), although this was only significant for VHL (p=0.0007 for VHL, p=0.24 for SDHx) (Figure 4.2F). There was no significant difference between cilia incidence or length in VHL- and SDHx- associated PPGLs.

Therefore, cilia loss and shortening appears to be a more generalised feature of cluster 1 PPGLs and not merely limited to VHL, suggesting the presence of additional mechanisms beyond the microtubule stabilising ability of pVHL.

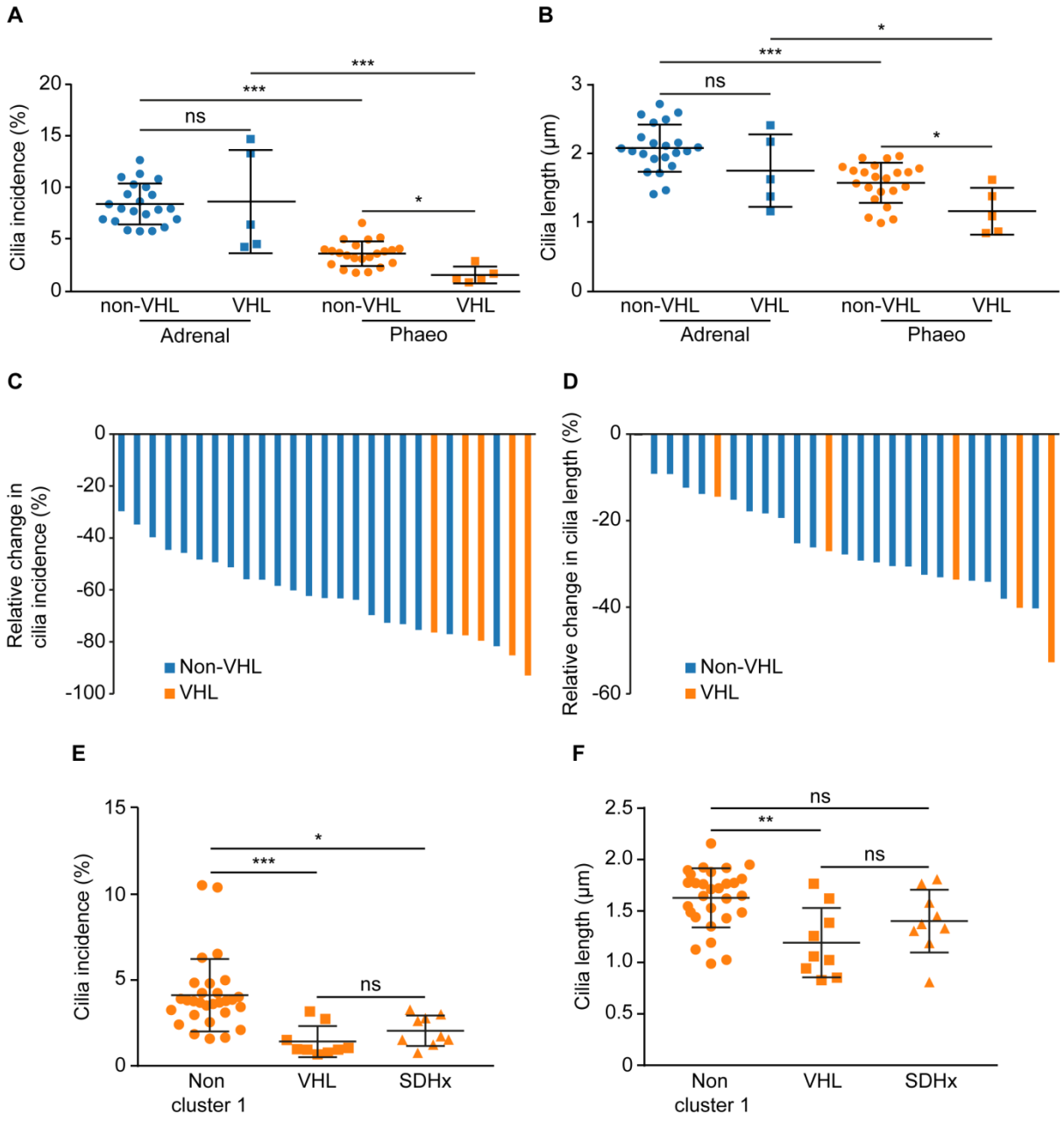

Figure 4.2: Loss of primary cilia is a particular feature of cluster 1 PPGL

Quantification of primary cilia incidence (A) and length (B) in 27 paired phaeochromocytoma and adjacent adrenal medulla (adrenal) according to VHL mutation status. Waterfall plots demonstrating change in cilia incidence (C) and length (D) in tumours compared to adjacent adrenal medulla according to VHL mutation status. Number of cells scored and cilia measured as per Figure 4.1.

Quantification of primary cilia incidence (E) and length (F) in 47 PPGLs with germline mutations in VHL (n=9), SDHx (n=9) and without a cluster 1 mutation (Non cluster 1; n=29). Cells scored for incidence: 2618 $\pm$ 893 per sample; number of cilia measured for length: 84 $\pm$ 67 per sample.

Statistical significance was assessed using a one-way ANOVA. ns not significant, * $p<0.05$, ** $p<0.01$, *** $p<0.001$.

ID	Sex	Age at operation	Phaeo/PGL	Location	Mode of diagnosis	Syndromic	Genetics screening	Gene mutation	Max size/mm	NMN	MN	3-MT
28	M	43	PGL	H&N	Symptomatic	Yes	Yes	SDHB	20	-	-	-
29	F	44	PGL	H&N	Symptomatic	Yes	Yes	SDHB	18	-	-	-
30	F	68	PGL	Bladder	Symptomatic	Yes	Yes	SDHB	45	+	-	+++
31 32 33	F	49	PGL	Thoracic	Symptomatic	Yes Yes Yes	Yes Yes Yes	SDHA SDHA SDHA	58	+	-	++
34 35 36	M	15	Phaeo	Right	Screening Screening Screening	Yes Yes Yes	Yes Yes Yes	VHL VHL VHL	35	+	-	-
37	F	43	Phaeo	Right	Incidental	No	Yes	Negative	60	+++	+	-
38	F	53	PGL	Abdo	Incidental	No	No	[redacted]	56	+	-	-
39	M	45	Phaeo	Right	Symptomatic	No	No	[redacted]	110	+++	+++	+
40	M	66	Phaeo	Right	Incidental	No	Yes	Negative	120	+++	-	++
41	F	50	PGL	Abdo	Incidental	No	No	[redacted]	52	++	-	-
42	F	36	PGL	Abdo	Symptomatic	Yes	Yes	VHL	25	+	-	-
43	M	65	PGL	Abdo	Incidental	No	No	[redacted]	45	+	-	-
44	M	39	PGL	H&N	Symptomatic	No	Yes	Negative	20	-	-	-
45	M	37	Phaeo	Right	Screening	Yes	Yes	MEN2	13	-	+	-
46 47	F	40	PGL	Abdo	Incidental	Yes	Yes	SDHB	39 33	+	-	-

Table 4.3: Clinical details of 20 tumour samples from 15 individuals

F – female, M – male, Phaeo – phaeochromocytoma, PGL – paraganglioma, H&N – head and neck, abdo – abdominal, SDH – succinate dehydrogenase, VHL - von Hippel-Lindau, MEN2 – Multiple Endocrine Neoplasia Type 2, NMN – normetanephrine, MN – metanephrine, 3-MT – 3-methoxytramine.

Mode of diagnosis: symptomatic = diagnosis due to symptoms or signs of catecholamine excess leading to diagnosis; incidental = diagnosis due to investigation for another unrelated condition; screening = diagnosis during a screening programme in individuals with known PPGL predisposition.

Metanephrines: - not elevated, + elevated 1-5x ULN, ++ elevated 5-10x ULN, +++ elevated >10x ULN.

4.3.1.3 PPGL primary cilia incidence is associated with a number of clinical parameters

Having established that ciliary loss was most pronounced in individuals with cluster 1 mutations, we sought to examine whether other clinical variables might also be associated with ciliary incidence and length. The previously described 47 PPGLs were thus classified according to a range of clinical parameters (Figure 4.3).

Patient sex did not alter ciliary incidence (p=0.059) or length (p=0.77) (Figure 4.3A & B) and no relationship was observed when menopausal status was considered (as a surrogate for oestrogen exposure) (p=0.65; data not shown). As expected, phaeochromocytoma laterality was not associated with changes in primary cilia (Figure 4.3E & F; p=0.15 for incidence, p=0.53 for length), nor was tumour site (Figure 4.3G & H; p=0.40 for incidence, p=0.28 for length). Maximal tumour dimension was also independent of primary cilia incidence (Figure 4.3M; p=0.11) and length (Figure 4.3N; p=0.20).

When age at time of surgery was considered, no correlation between cilia incidence (p=0.45) or length (p=0.14; data not shown) was observed. However, patients under the age of 18 had tumour cells with fewer (1.6% $\pm$ 0.9 v. 4.0% $\pm$ 2.1; p=0.0097) and shorter (1.18µm $\pm$ 0.32 v. 1.61µm $\pm$ 0.31; p=0.0040) cilia (Figure 4.3 C & D), suggesting an association between cilia loss and age at time of operation.

PPGLs can generally be diagnosed in one of three ways: when there is a clinical suspicion due to signs and symptoms, as an incidental finding on imaging or as part of a screening programme in individuals with a known PPGL predisposition. Tumours from patients diagnosed on screening had fewer cilia than those diagnosed incidentally (2.0% $\pm$ 1.2 v. 4.1% $\pm$ 2.1; p=0.04; Figure 4.3I) and a non-significant tendency towards shorter cilia (1.40µm $\pm$ 0.35 v. 1.66µm $\pm$ 0.29; p=0.16; Figure 4.3J). There was no difference between symptomatic patients and those diagnosed incidentally (p=0.55 for incidence, p=0.08 for length) or on screening (p=0.31 for incidence, p=0.16 for length).

Tumours that secreted metanephrine had increased cilia incidence (Figure 4.3K; 4.1% $\pm$ 1.8 v. 2.3% $\pm$ 1.5, p=0.0007) and length (Figure 4.3L; 1.64m $\pm$ 0.31 v. 1.38µm $\pm$ 0.31, p=0.0074) compared to those that didn't. This finding is explored further in Chapter 5.

Thus, a younger age at operation, the method of diagnosis and the secretory profile all appear to be associated with primary cilia incidence and length. Whether these are independent of one another remains to be determined and could potentially be explained by the confounding effect of cluster 1 mutations. Individuals with *VHL* and *SDHx* mutations develop PPGLs at a younger age and are more

likely to be enrolled in screening programmes. In addition, cluster 1 PPGLs are predominantly normetanephrine producing and therefore the positive effect of metanephrine may be a reflection of the negative genetic influence on cilia in these tumours.

As the presence of a primary cilium is potentially a checkpoint for cell division, we tested if cilia loss correlated with cellular proliferation in PPGLs. This was measured through routine clinical quantification of the percentage of cells displaying positive immunohistochemistry for Ki67, a marker of proliferative activity. Ki67 index has previously been correlated with malignant potential in PPGLs (Clarke *et al.* 1998) and is used in the GAPP histological grading system (Kimura *et al.* 2014). Cilia incidence was reduced in PPGLs with a Ki67 index of 3% of higher (Figure 4.3O; 2.8% $\pm$ 1.1 v. 4.4% $\pm$ 2.2; p=0.034) and there was a non-significant tendency towards shorter cilia (Figure 4.3P; 1.51µm $\pm$ 0.38 v. 1.67µm $\pm$ 0.20; p=0.13). This observation suggests that ciliary incidence may be reduced in tumours with an increased rate of cellular proliferation.

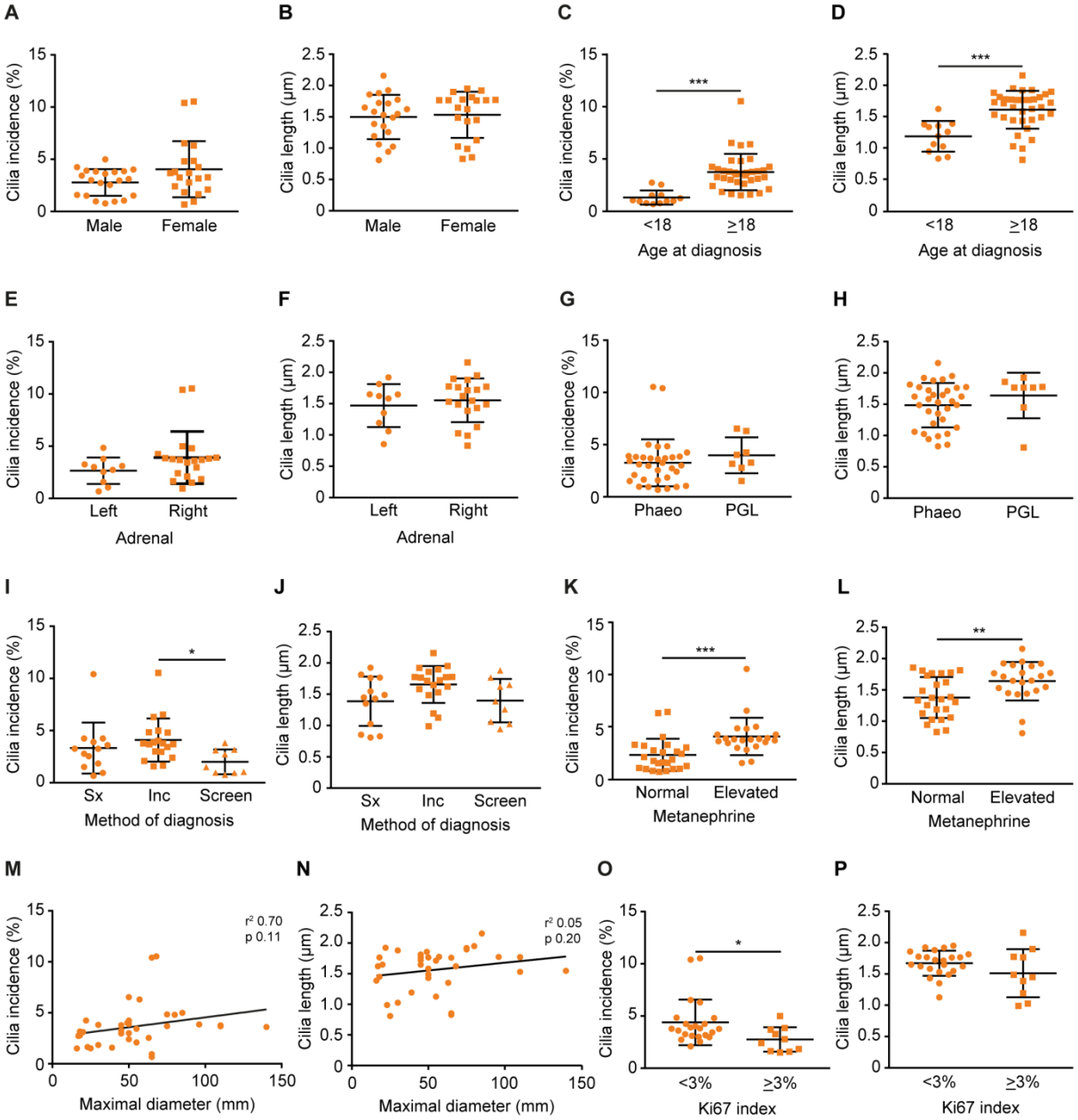

Figure 4.3: PPGL primary cilia incidence and length is correlated with clinical and pathological parameters

Quantification of tumoural cilia incidence (A, C, E, G, I, K, M, O) and length (B, D, F, H, J, L, N, P) according to sex (A, B), age at diagnosis (C, D), laterality if a phaeochromocytoma (E, F), location (G, H), method of diagnosis (I, J), metanephrine secretion (K, L), maximal diameter (M, N) and Ki67 labelling index (O, P) in 47 PPGLs from 40 patients.

Phaeo – phaeochromocytoma, PGL – paraganglioma, sx – symptomatic, inc – incidental, screen – screening.

Statistical tests: unpaired t-test (A-H, K, L, O, P), one-way ANOVA (I, J), linear regression (M, N). * p< 0.05, ** p<0.01, *** p<0.001. Where no star is evident, p>0.05.

4.3.1.4 RNA sequencing transcriptome analysis reveals that cilia-mediated signalling pathways are disrupted in phaeochromocytomas

Having identified that primary cilia loss and shortening is a feature of phaeochromocytomas relative to adrenal medullas, we next sought to examine whether these structural changes were associated with alterations in cilia-mediated signalling.

RNA was extracted and sequenced from 12 paired samples of phaeochromocytomas and adjacent adrenal medullas at the time of adrenalectomy (Table 4.2). Reads were pseudo-aligned, aggregated to gene-level, filtered, normalised and transformed to leave 17,198 genes for exploratory data analysis (please see Chapter 3 and appendix for detailed methodology). These pre-processing steps resulted in data that were approximately normally distributed (see appendix) and enabled generation of a sample similarity matrix by calculating the pairwise Euclidean distance between all samples, visualised as a heatmap and hierarchical clustering dendrogram (Figure 4.4A). This shows perfect sample separation by tissue type, with the exception of sample H21, which is incorrectly grouped with the tumour samples; interestingly this sample clusters closely with H22, its matching tumour sample.

Principal component analysis (PCA; Figure 4.4B) revealed that principal component 1, which accounts for over 40% of variation in the data, clearly separated the samples by tissue type. Again, the adrenal sample H21 is a clear outlier from the other adrenal samples, although it does remain separated from the tumour samples by principal component 1 and its closest data point remains its matched tumour partner H22. Phaeochromocytoma samples are spread along the second principal component, which accounts for over 10% of variation, indicating a heterogeneity in this group that is absent in the adrenal medulla samples. An alternate approach to projecting high-dimensional datasets with just two axes is t-distributed stochastic neighbour embedding (t-SNE; Figure 4.4C) which explicitly aims to preserve local structure when mapping a large matrix onto a low-dimensional subspace. This approach clearly separates tumour and adrenal samples, although the tumour sample heterogeneity evident on the PCA plot is lost due to the algorithm's emphasis on preserving each data point's proximity to its nearest neighbour. Again, sample H21 is misclassified and this is particularly apparent, although it remains close to its paired sample.

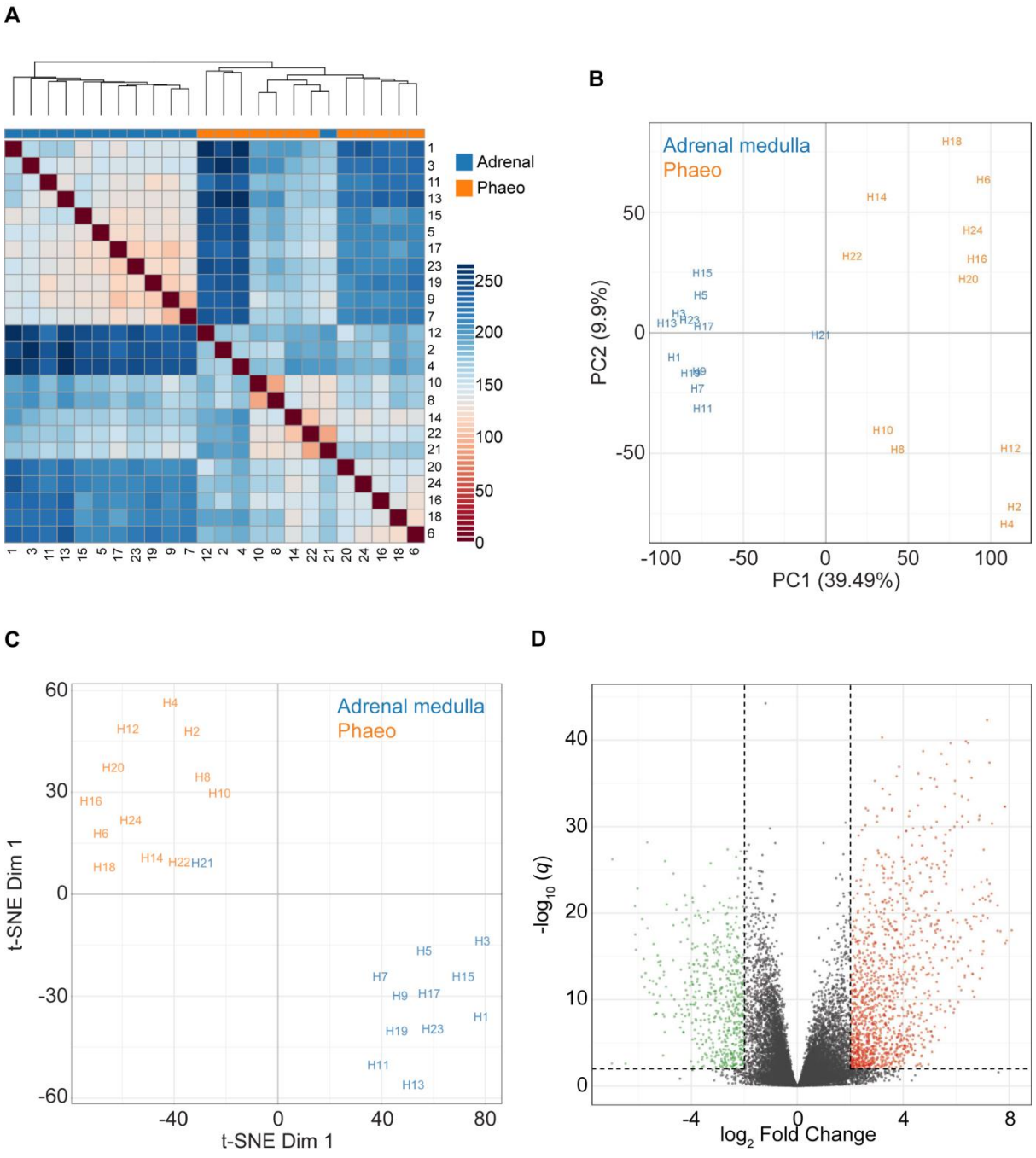

Figure 4.4: Transcriptomic differences between phaeochromocytomas and adrenal medullas

Sample similarity matrix **(A)**, principal component analysis **(B)** and t-distributed stochastic neighbour embedding **(C)** of RNA-seq expression data from 12 paired phaeochromocytomas and adjacent adrenal medulla tissue samples. **(D)** Volcano plot showing $\log_{10}$ FDR-adjusted *q* values versus $\log_2$ fold change between phaeochromocytomas and adjacent adrenal medullas. The vertical and horizontal dotted lines indicates 2x or -2x fold change and $q = 0.01$, respectively.

Differential expression analysis was performed using the DESeq2 software package (Love *et al.* 2014). We defined a gene as differentially expressed if its absolute log fold change was ≥ 2 and its *q*-value was ≤ 0.01, imposing a 1% false discovery rate (FDR). This strict threshold ensured high specificity. Overall, 1839 genes met these criteria, representing 8% of the transcriptome after filtering (Figure 4.4D).

To test whether cilia function was altered in phaeochromocytomas relative to adjacent adrenal medullas, we curated a collection of 32 cilia-related gene sets from public databases including Gene Ontology (http://geneontology.org/), the Kyoto Encyclopedia of Genes and Genomes (https://www.genome.jp/kegg/), Biocarta (https://cgap.nci.nih.gov/Pathways/BioCarta_Pathways), The Pathway Interaction Database (Schaefer *et al.* 2009) and the Hallmark Gene Set Collection (Liberzon *et al.* 2015). Pathway enrichment was tested using a modified version of the QuSAGE algorithm (Yaari *et al.* 2013; Turner *et al.* 2015) and was significant in 14 pathways (44%). To visualise these pathway-level differences, we created a matrix of eigengenes by taking the first principal component of each pathway across all samples and plotting this as a heatmap (Figure 4.5). Using this approach, hierarchical clustering now classifies all samples by tissue type, including H21.

Altered gene modules include those associated both with cilia structure and cilia-mediated signalling pathways.

Both gene modules associated with cilia structure demonstrate altered expression in phaeochromocytomas relative to adrenal medullas: GO_NONMOTILE_PRIMARY_CILIUM ($q = 2.6 \times 10^{-13}$) and GO_NONMOTILE_PRIMARY_CILIUM_ASSEMBLY ($q = 6.1 \times 10^{-9}$), suggesting that changes in gene expression may contribute to the observed cilia loss in phaeochromocytomas.

Hierarchical clustering analysis of the expression of the 137 component genes that make up the GO_NONMOTILE_PRIMARY_CILIUM module (Figure 4.6) correctly classifies all samples, with one exception (H21).

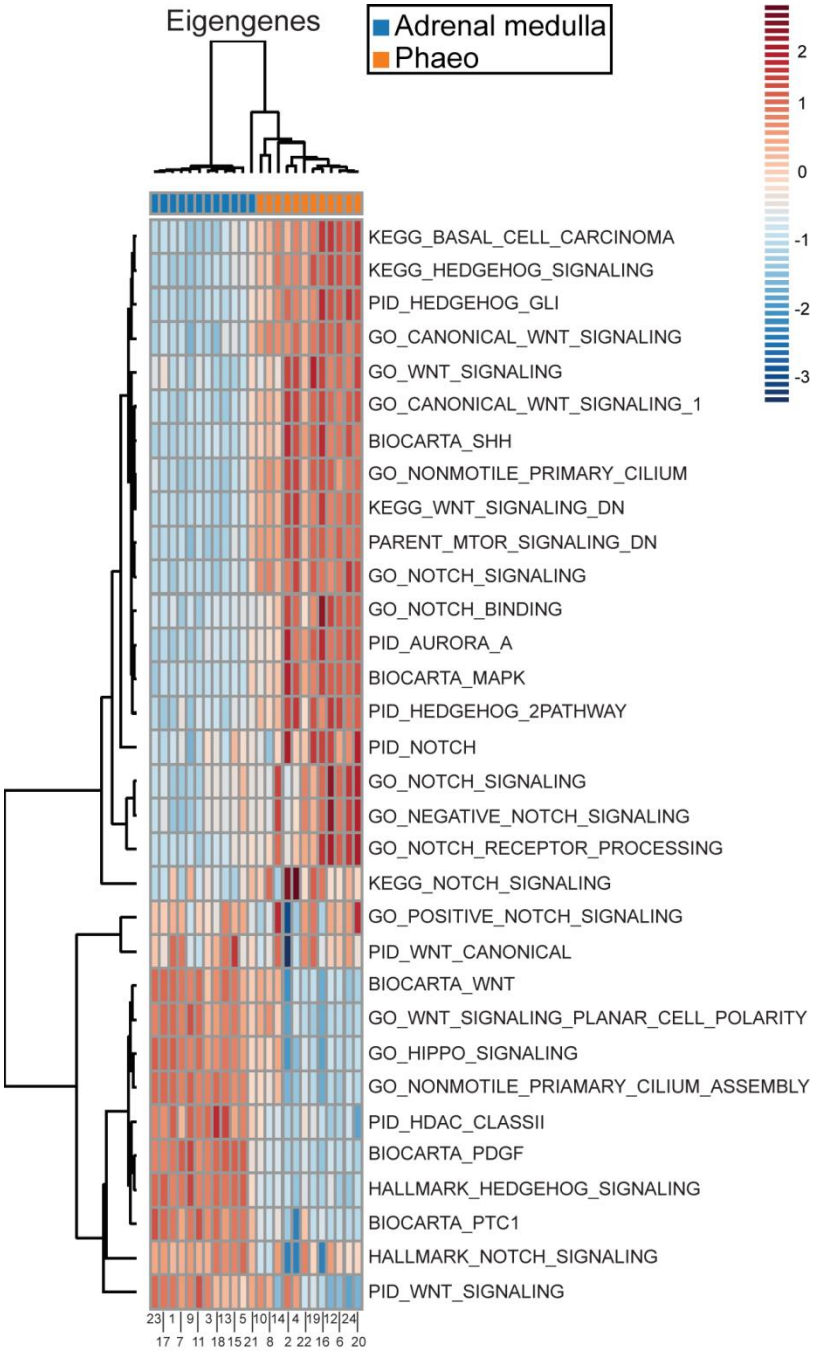

Figure 4.5: Cilia-associated gene networks are differently expressed between phaeochromocytoma and adrenal medullas

Heat map and hierarchical clustering dendrogram depicting differently expressed module eigengenes, between phaeochromocytomas and adrenal medullas, from a collection of 32 gene sets known to be associated with cilia structure and cilia-mediated signalling.

Numbers correspond with sample IDs as per Table 4.2.

A number of gene modules associated with cilia-mediated signalling are also altered between phaeochromocytomas and adrenal medullas. They include gene modules associated with Hedgehog, Wnt and Notch signalling, for example HALLMARK_HEDGEHOG_SIGNALING (q = 1.66 x10^{-7}), BIOCARTA_WNT_PATHWAY (q = 1.52 x10^{-6}) and GO_NEGATIVE_REGULATION_OF_NOTCH_SIGNALING_ PATHWAY (q = 1.58 x10^{-6}). Analyses of these gene modules revealed significant upregulation and downregulation of individual genes (absolute log fold change $\geq$ 2, $q \leq$ 0.01) while hierarchical clustering analyses separately grouped tumours and adrenal medulla samples in each of these pathways with the exception of one medulla sample (H21) in the Hedgehog and Notch pathways and two tumour samples (H10 and H22) in the Wnt pathway (Figure 4.7A-C). These data are consistent with cilia-mediated signalling pathways being disrupted in phaeochromocytomas.

In addition, expression of the Aurora-A gene module was altered between the two sample groups (q = 0.00036), suggesting a possible mechanistic role for Aurora-A, which is known to play a role in the regulation of ciliary disassembly. Furthermore, modulation of mTOR signalling, which in addition to its ciliary association is also implicated in PPGL pathogenesis, was also altered (q = 0.00061).

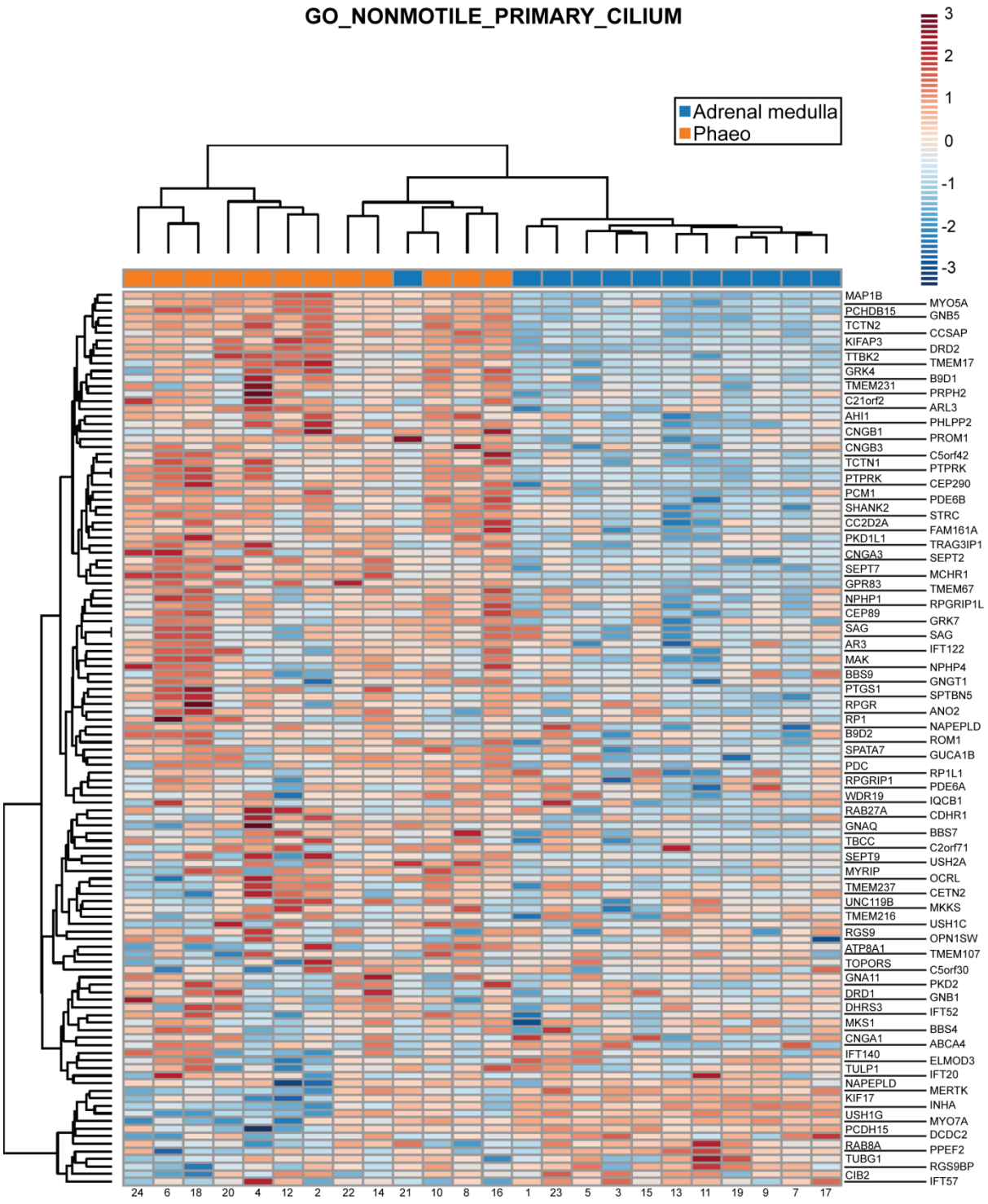

Figure 4.6: Differential expression of primary cilia related genes between phaeochromocytomas and adrenal medullas

Heat map and hierarchical clustering dendrogram depicting differentially expressed genes in the GO_NONMOTILE_PRIMARY_CILIUM pathway, comparing phaeochromocytoma and adjacent adrenal medulla samples.

Numbers correspond with sample IDs as per Table 4.2.

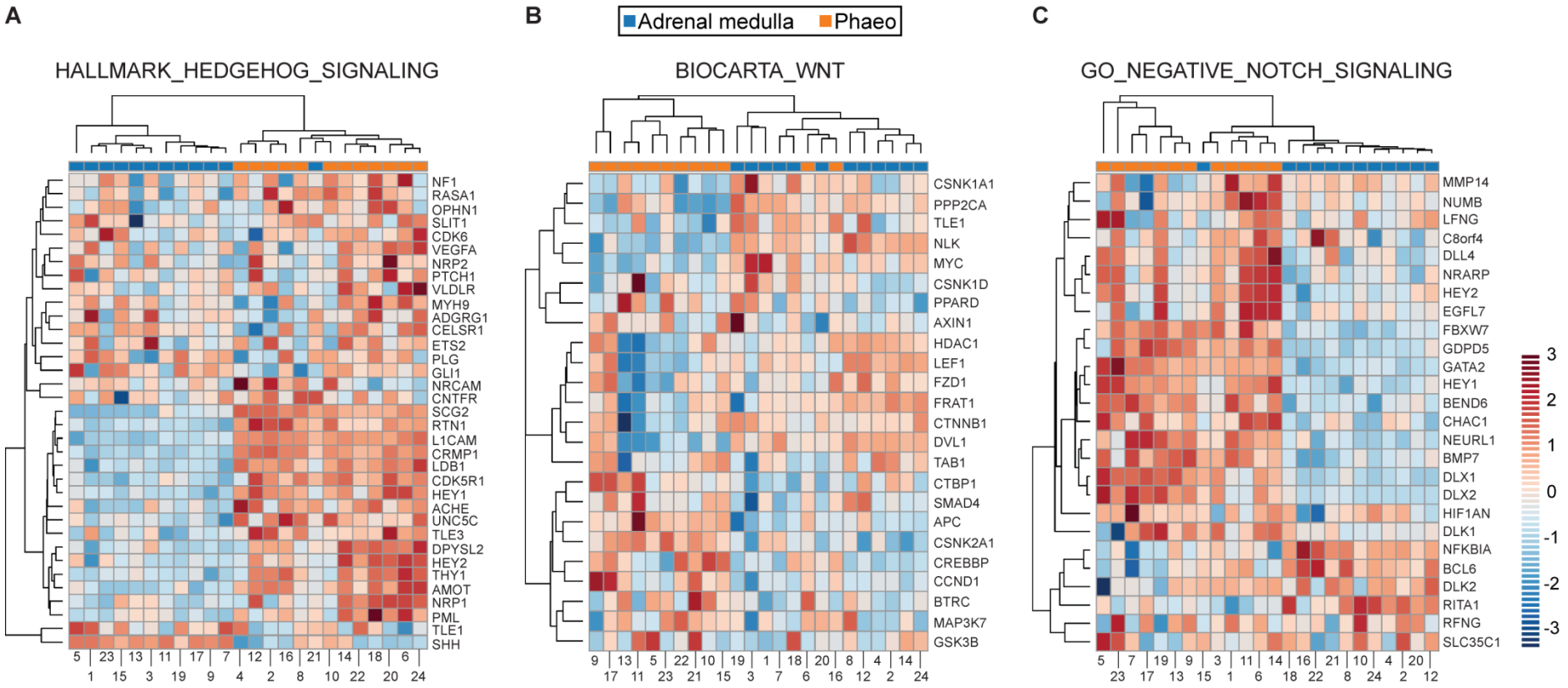

Figure 4.7: Differential expression of primary cilia-mediated signalling pathways between phaeochromocytomas and adrenal medullas

Heat map and hierarchical clustering dendrogram depicting differentially expressed genes in three cilia-associated signalling pathways that are altered in phaeochromocytomas relative to adjacent adrenal medullas: **(A)** HALLMARK_HEDGEHOG_SIGNALLING, **(B)** BIOCARTA_WNT_PATHWAY, **(C)** GO_NEGATIVE_EREGULATION_OF_NOTCH_SIGNALLING_PATHWAY.

Numbers correspond with sample IDs as per Table 4.2.

4.3.2 Primary cilia loss in phaeochromocytoma-derived cells results in cellular proliferation and alters expression of tumourigenesis-linked gene networks

There remains ongoing debate as to whether primary cilia loss in cancer is a driver or merely an observed consequence of tumourigenesis. In the previous section, we have demonstrated that primary cilia loss and shortening is a feature of phaeochromocytomas *in vivo* and is associated with alterations in the transcription of cilia-associated gene networks. We next sought to examine whether primary cilia might contribute to PPGL pathogenesis and if so, the underlying pathophysiology.

4.3.2.1 Phaeochromocytoma-derived cells are able to form primary cilia

Experiments to address this important question would require *in vitro* cellular manipulation and thus a cell line was required. No commercially available human phaeochromocytoma cell line exists and repeated attempts to grow primary cultures from the surgical specimens described above were short lived due to fibroblast overgrowth. Therefore, murine and rat phaeochromocytoma-derived cell lines were utilised.

The PC12 cell line was established from a rat phaeochromocytoma. It expresses all enzymes of the catecholamine synthesis pathway with the exception of PNMT and therefore can secrete dopamine and noradrenaline but not adrenaline (Greene & Tischler 1976). It has subsequently been identified that PC12 cells possess mutant forms of the PPGL predisposition gene *Max* which are incapable of repressing Myc-dependent transcription. This can be prevented by reintroduction of functional Max with resultant reduction in cellular proliferation (Hopewell & Ziff 1995).

The MPC cell line was generated from a phaeochromocytoma in a heterozygous *Nf1* knockout mouse, in which neurofibromin remains expressed. Unlike PC12 cells, PNMT is expressed and therefore MPC cells can synthesise adrenaline (Powers *et al.* 2000). The MTT line is a subclone of MPC generated from a liver metastasis following inoculation of athymic nude mice with MPC cells. When injected into mice, MTT cells result in larger and earlier tumour development than MPC cells and are therefore considered a model for more aggressive disease (Martiniova *et al.* 2009).

Dual labelled immunofluorescence was performed on PC12, MPC and MTT cells in two dimensional culture in order to confirm primary cilia expression and to validate and optimise antibodies for their detection. Primary cilia were readily detected on all cell types using the dual axonemal markers acetylated α-tubulin and Arl13b (Figure 4.8A). Using confocal microscopy the localisation of both

proteins clearly overlapped assisting in the identification of cilia and facilitating axonemal length measurements (Figure 4.8A). When super-resolution imaging using structured illumination microscopy was employed, however, acetylated α-tubulin localised to the microtubule core of the axoneme whilst Arl13b was associated with the ciliary membrane (Figure 4.8B). Use of an antibody against the intraflagellar transport protein IFT88 also identified cilia with increased inter-cellular variation: some axonemes were labelled diffusely, others only towards the base (Figure 4.8C). The basal body markers pericentrin and γ-tubulin were also trialled (data not shown), but the results were not as consistent or as easily identifiable as the combination of acetylated α-tubulin and Arl13b which were used for ongoing experiments.

Figure 4.8: Phaeochromocytoma-derived cells display primary cilia (overleaf)

PC12, MPC and MTT cells were fixed and immunolabelled with antibodies directed against acetylated α-tubulin and Arl13b (A, B) or acetylated α-tubulin and IFT88 (C). Nuclei were counter-stained with DAPI. Imaging was performed with either a confocal (A, C) or structured illumination (B) microscope.

Acet α-tubulin acetylated α-tubulin. Scale bars: 5μm (A, C), 2μm (B). In C, arrow denotes axonemal distribution of IFT88; arrowhead denotes localisation at axoneme base.

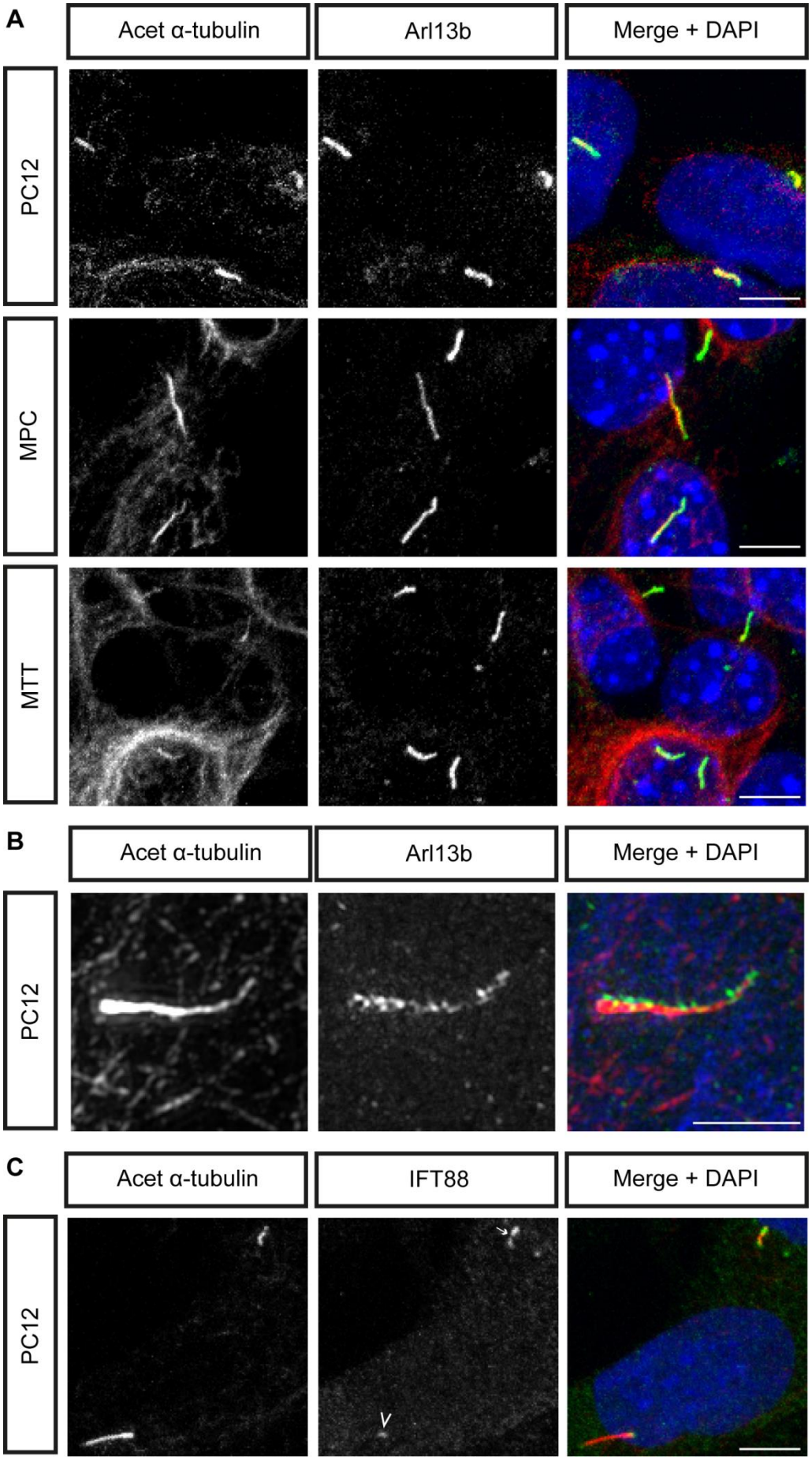
A
Acet α-tubulin
Arl13b
Merge + DAPI
PC12
MPC
MTT
B
Acet α-tubulin
Arl13b
Merge + DAPI
PC12
C
Acet α-tubulin
IFT88
Merge + DAPI
PC12

In order to identify and accurately measure primary cilia, it is important to consider their orientation. PC12 cells were grown in monolayer culture before fixation and processing for primary cilia detection with antibodies against acetylated α-tubulin and Arl13b. Confocal Z-stacks were obtained and primary cilia could be classified as either arising from the cell's basal or apical surface through examination of their orthogonal projections (Figure 4.9A). Over 80% of primary cilia in PC12 cells were basal with similar results for both MPC and MTT cells (Figure 4.9B). This facilitates cilia length measurement from maximum intensity projections as basal cilia are more limited to the XY dimension than apical cilia (discussed in Chapter 7).

Ciliogenesis can be experimentally stimulated by forcing cells into S-phase, for example by serum-starvation or contact inhibition (Wheatley *et al.* 1996; Alieva *et al.* 1999). PC12 cells were plated in complete media for 24 hours to allow attachment before the media was changed to serum-free media. Cells were fixed and processed as previously described at a variety of time points (Figure 4.9C). At baseline, only a small proportion of PC12 cells displayed a primary cilium (8.4% $\pm$ 0.75) and they were short (1.49 µm $\pm$ 0.41). Cilia incidence increased with increasing duration of serum starvation (Figure 4.9D). This effect was seen after 8 hours (30.0% $\pm$ 2.3; p=0.0010) and persisted to 72 hours (77.0% $\pm$ 2.3; $p=2.3x10^{-34}$). Cilia length also increased with increasing duration of serum starvation (Figure 4.9E). Again, this effect was observed after 8 hours (1.79µm $\pm$ 0.53; p=0.0022) and continued to 72 hours (2.08 µm $\pm$ 0.64; $p=2.7x10^{-6}$). Beyond 72 hours of serum starvation, cell death began to occur.

A common experimental approach is to deliberately maximise cilia prevalence by growing cells to confluence in serum-free media for a prolonged period of time (Wheatley *et al.* 1996; Alieva *et al.* 1999). This however limits interpretation of the dynamics of ciliary assembly and disassembly; the 24 hour time point, which sits within the 'dynamic range' of ciliogenesis, was chosen for further experiments for this reason.

MPC and MTT cells were plated for 24 hours in complete media to allow attachment before a further 24 hours of culture in either serum-free or serum-containing media (Figure 4.9F). In MPC cells, cilia incidence was greater in serum-free conditions (Figure 4.9G; 76.1% $\pm$ 10.1 v. 60.4% $\pm$ 14.8; $p=.2\ x10^{-6}$), as was cilia length (Figure 4.9H; 2.87µm $\pm$ 0.78 v. 2.25µm $\pm$ 0.70; $p=8.5\ x10^{-16}$). The same effect was seen in MTT cells, with serum-starvation increasing cilia incidence (64.5% $\pm$ 12.2 v. 54.3% $\pm$ 12.1; p=0.018) and length (2.77µm $\pm$ 0.62 v. 2.30µm $\pm$ 0.60; $p=1.6x10^{-7}$). There was no difference between MPC and MTT cilia incidence and length in serum-containing media (p=0.99 and 0.74 respectively), but there was following serum-starvation (p=0.0031 and 0.00065 respectively).

Thus, phaeochromocytoma-derived cells have the potential to display primary cilia, which can be stimulated by serum starvation.

Figure 4.9: Primary cilia on phaeochromocytoma-derived cells are predominantly basal and are stimulated by serum starvation (overleaf)

Confocal images of PC12 **(A, C)**, MPC and MTT **(F)** cells cultured in the absence of serum for between 0 and 72 hours (24 hours if not specified). Cells were immunolabelled with anti-acetylated α-tubulin (green) and anti-Arl13b (red) for detection of primary cilia. Nuclei were stained with DAPI (blue). Cilia are either numbered and shown in orthogonal section in the corresponding boxes **(A)** or are indicated by arrows, or arrowheads, where they are also shown zoomed in the insets **(A, F)**. Scale bars = 10μm.

(B) Quantification of primary cilia cellular position in PC12, MPC and MTT cells following treatment as per **(A)**.

Quantification of primary cilia incidence **(D, G)** and axonemal length **(E, H)** following treatment as per **(A)**. Error bars indicate $\pm$ SEM, boxes 25th, 50th and 75th centiles and whiskers the 10th and 90th centiles. Number of cells scored for incidence: 2186 $\pm$ 379 per condition. Number of cilia measured for length: 256 $\pm$ 23.

Statistical tests: one-way ANOVA. * $p<0.05$, ** $p<0.01$, *** $p<0.001$.

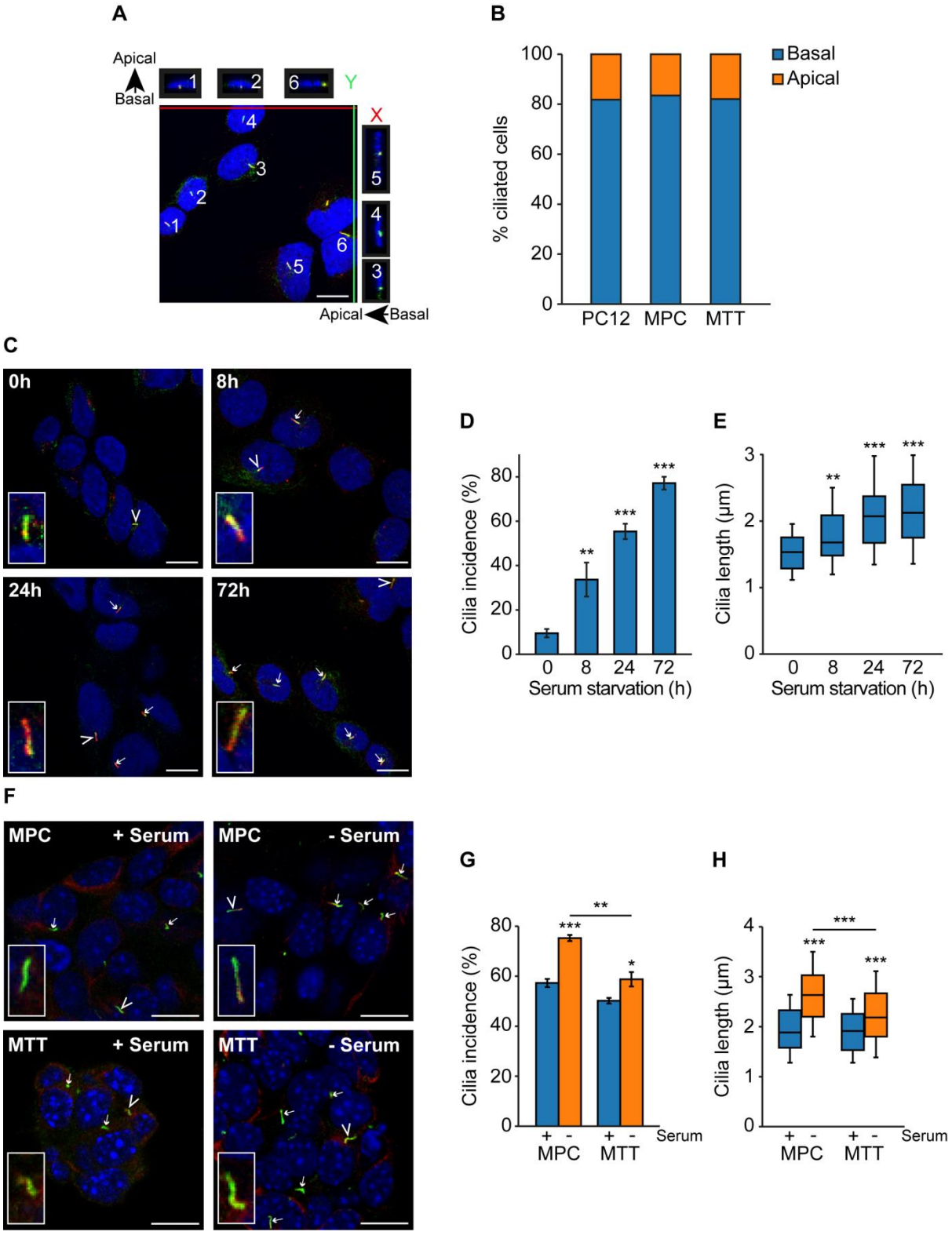

Figure 4.9: Primary cilia on phaeochromocytoma-derived cells are predominantly basal and are stimulated by serum starvation

Legend on previous page

4.3.2.2 Loss of primary cilia in phaeochromocytoma-derived cells promotes cellular proliferation

Having established that PC12 cells can form primary cilia, we set out to investigate the effect of primary cilia loss. We hypothesised that siRNA-mediated knockdown of key contributors to ciliary assembly would result in reduced cilia formation and would therefore provide insight into its consequences.

PC12 cells were transfected with *Ift88*, *centrosomal protein 164* (*Cep164)* or non-targeting control siRNAs for 48 hours prior to processing. IFT88 is a central component of the intraflagellar transport complex (Pazour *et al.* 2000), whilst Cep164 contributes to microtubule organisation and maintenance during ciliary formation (Graser *et al.* 2007). Loss of either would be expected to result in reduced cilia formation.

Knockdown of *Ift88* was confirmed at protein level by immunoblot (Figure 4.10A & B) and at transcript level by qPCR for *Cep164* (Figure 4.10E).

Primary cilia incidence (Figure 4.10C & F) was reduced following knockdown of *Ift88* (8.9% $\pm$ 5.2 v. 32.2% $\pm$ 9.7; $p=3.9\times10^{-15}$) and *Cep164* (21.1% $\pm$ 7.5 v. 43.6% $\pm$ 6.8; p=0.0022) compared to non-targeting controls. Cilia length (Figure 4.10 D & G) was also reduced following *Ift88* (1.48µm $\pm$ 0.42 v. 1.96µm $\pm$ 0.46; $p=3.0\times10^{-12}$) and *Cep164* (2.15µm $\pm$ 0.39 v. 2.99µm $\pm$ 0.49; $p=1.8\times10^{-9}$) knockdown compared to non-targeting control siRNAs.

In addition to immunolabelling to detect primary cilia, transfected cells were exposed to antibodies against the proliferation marker Ki67 (Figure 4.10H). The percentage of PC12 cells positive for Ki67 was greater following both *Ift88* ($p=4.4\times10^{-12}$) and *Cep164* (p=0.039) knockdown compared to non-targeting controls (Figure 4.10I & K). Moreover, cells that had nuclear accumulation of Ki67 did not have a primary cilium (Figure 4.10H) supporting a role for primary cilia opposing cell division. Increased cellular proliferation following *Ift88* and *Cep164* knockdown, relative to non-targeting controls, was further confirmed through quantification of cell numbers 48 hours after siRNA transfection (Figure 4.10J & L).

Thus, increased cellular proliferation is a direct consequence of primary cilia loss, achieved by reducing ciliogenesis, in phaeochromocytoma-derived cells.

Figure 4.10 Loss of primary cilia in PC12 cells promotes cellular proliferation (overleaf)

(A) Immunoblot of total cell lysates from PC12 cells transfected with siRNAs targeting IFT88 or non-targeting control siRNAs (Con). Cell lysates were generated 48 hours after transfection and immunoblots probed with an anti-IFT88 antibody and anti-β-actin as a loading control.
(B) Densitometric analyses were performed and mean relative IFT88 protein levels calculated (n=6). Data were normalised to β-actin.
(C, D) Quantification of cilia incidence (C) and length (D) in cells 48h following treatment as in (A).
(E) Relative RNA expression of Cep164 in PC12 cells 48 hours after transfection with siRNAs targeting this transcript. Cep164 levels are expressed relative to those in cells transfected with non-targeting control siRNAs (arbitrary units). Data was normalized to levels of peptidylpropyl isomerase A.
(F, G) Quantification of cilia incidence (F) and length (G) in cells 48h following treatment as in (A).
(H) Confocal images of PC12 cells cultured for 48 h after transfection with siRNA targeting IFT88, Cep164 or non-targeting control siRNAs (Con). Cells were immunolabelled to detect cilia (Arl13b, green) and the proliferation marker Ki67 (red). Nuclei were stained with DAPI (blue). Cilia are indicated by arrows and Ki67 positive cells by arrowheads. Scale bars = 10 μm.
(I-L) Quantification of the percentage of Ki67 positive cells (I, K), and relative cell numbers (J, L), 48 h after transfection with siRNA targeting IFT88 (I, J) or Cep164 (K, L) compared to non-targeting controls.
Error bars indicate $\pm$ SEM, boxes 25th, 50th and 75th centiles and whiskers the 10th and 90th centiles. Number of cells scored for incidence: 1430 $\pm$ 130 per condition. Number of cilia measured for length: 108 $\pm$ 15 per condition. Ki67 scoring was performed in ten randomly selected fields for each experimental condition in three biological replicates. Cell counting was performed on six samples from three biological replicates.
Statistical tests: *t*-test (B-G, I, K), one-way ANOVA (J, L). * $p<0.05$, ** $p<0.01$, *** $p<0.001$.

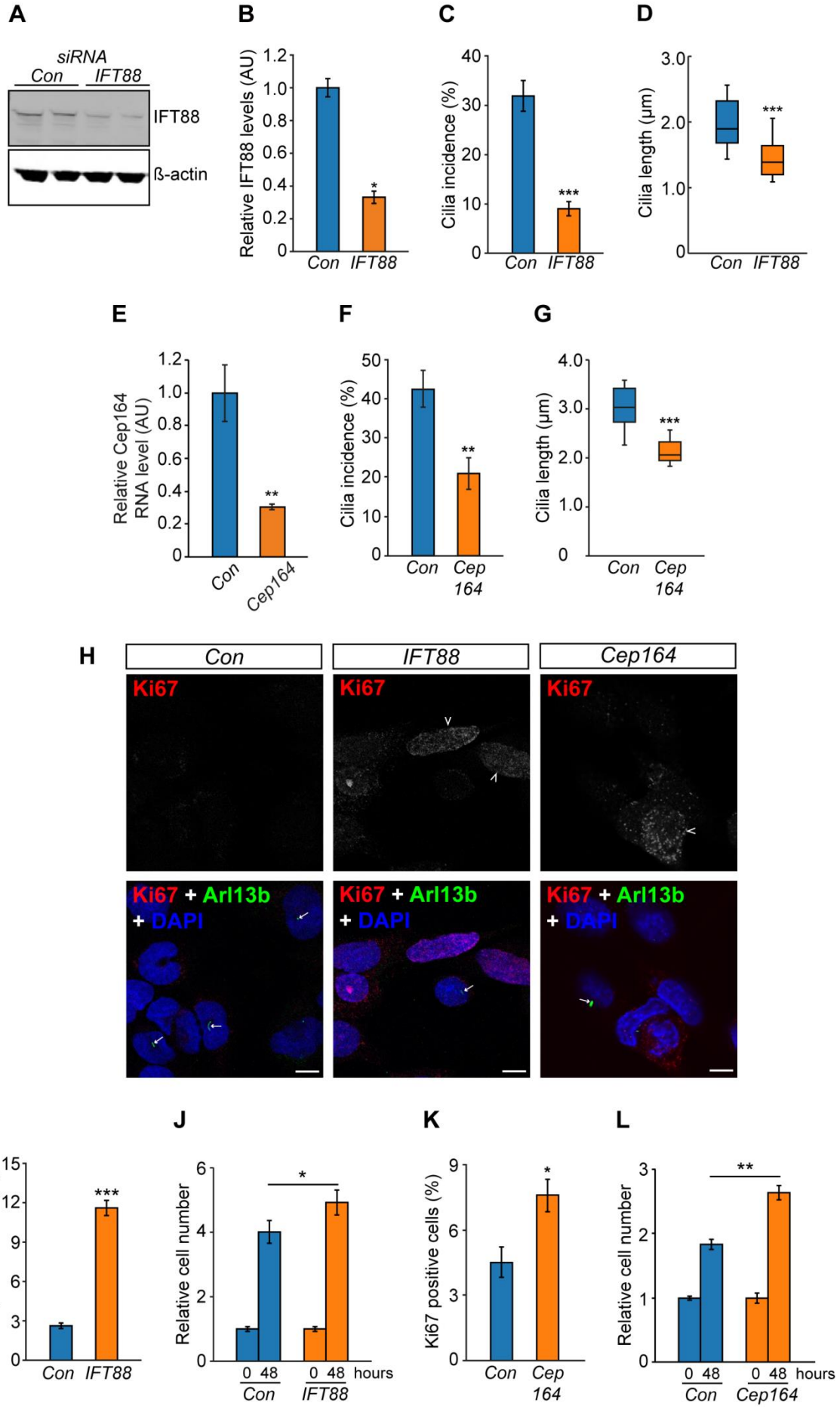
A
siRNA
Con
IFT88
IFT88
ß-actin
B
Relative IFT88 levels (AU)
Con
IFT88
C
Cilia incidence (%)
Con
IFT88
D
Cilia length (µm)
Con
IFT88
E
Relative Cep164 RNA level (AU)
Con
Cep164
F
Cilia incidence (%)
Con
Cep 164
G
Cilia length (µm)
Con
Cep 164
H
Con
IFT88
Cep164
Ki67
Ki67 + Arl13b + DAPI
I
Ki67 positive cells (%)
Con
IFT88
J
Relative cell number
0 48
Con
0 48
IFT88
hours
K
Ki67 positive cells (%)
Con
Cep 164
L
Relative cell number
0 48
Con
0 48
Cep164
hours

4.3.2.3 Loss of primary cilia in phaeochromocytoma-derived cells promotes transcriptional changes associated with tumourigenesis

Having identified that *Ift88* knockdown in PC12 cells results in cilia loss and increased cellular proliferation, we sought to examine how cilia function might further impact on cellular processes in this context by comparing the transcriptomes of cells in which primary cilia had been reduced.

RNA was extracted and sequenced from PC12 cells that had been transfected with *Ift88* or non-targeting siRNAs. Reads were pseudo-aligned and subjected to the same pre-processing steps as the human tissue samples described earlier in this chapter (also see Chapter 3). Principal component analysis was performed and principal component 1, which accounted for over 30% of variation, clearly separated the *Ift88* knockdown and control cells (Figure 4.11A). 662 genes, representing 6% of the transcriptome after filtering, were differentially expressed at log fold change ≥ 2 and $q < 0.01$ (Figure 4.11B).

Functional analysis of the observed differential gene expression between *Ift88* knockdown and control cells was performed using Ingenuity Pathway Analysis (Ingenuity Systems). This gene ontology (GO) analysis revealed that the top ten biological processes of these genes were related to cell death, cell proliferation and tumourigenesis. Moreover, activation z-scores suggested that cell death pathways (cell death, necrosis, apoptosis, cell death of tumour cells) were inhibited, while proliferation and tumourigenesis pathways were induced (tumourigenesis of tissue, cell proliferation of tumour cells, non-melanoma solid tumour, gastrointestinal neoplasia) (Figure 4.11C).

Hierarchical cluster analysis of gene modules described by the GO terms ‘cell death’, ‘tumorigenesis of tissues’ and ‘cell proliferation of tumour cells’ clearly separates IFT88 knockdown samples from controls (Figure 4.11D-F).

These data suggest that cilia loss promotes cellular proliferation in phaeochromocytoma-derived PC12 cells.

In combination with the observation that primary cilia loss is a feature of human phaeochromocytomas, this provides evidence that primary cilia loss in phaeochromocytomas contributes to cellular proliferation and tumourigenesis rather than merely reflecting it.

Figure 4.11: IFT88 knockdown in PC12 cells promotes transcriptional changes associated with tumourigenesis (overleaf)

(A) Principal component analysis (PCA) of RNA-seq expression data from IFT88 knockdown (R10-R12) and control cells (R13-R15; n=3 per condition).
(B) Volcano plot showing log10 FDR-adjusted q-values versus log2 fold change between IFT88 knockdown and control cells. The vertical and horizontal dotted lines indicate 2x or -2x fold change and p = 0.01, respectively.
(C) Gene Ontology (GO) analysis of the transcriptome of PC12 cells transfected with siRNA targeting IFT88 or non-targeting control siRNAs showing the top-ranking altered biological processes identified by Ingenuity Pathways Analysis. *q* values are depicted in red (*E* = 10 to the power of the following number).
(D-F) Heat map and hierarchical clustering dendrograms of differentially expressed genes in altered pathways with the GO terms cell death **(D)**, tumorigenesis of tissues **(E)** and cell proliferation of tumor cells **(F)**. Numbers shown at the bottom of the heat maps correspond to sample IDs as in **(A)**.

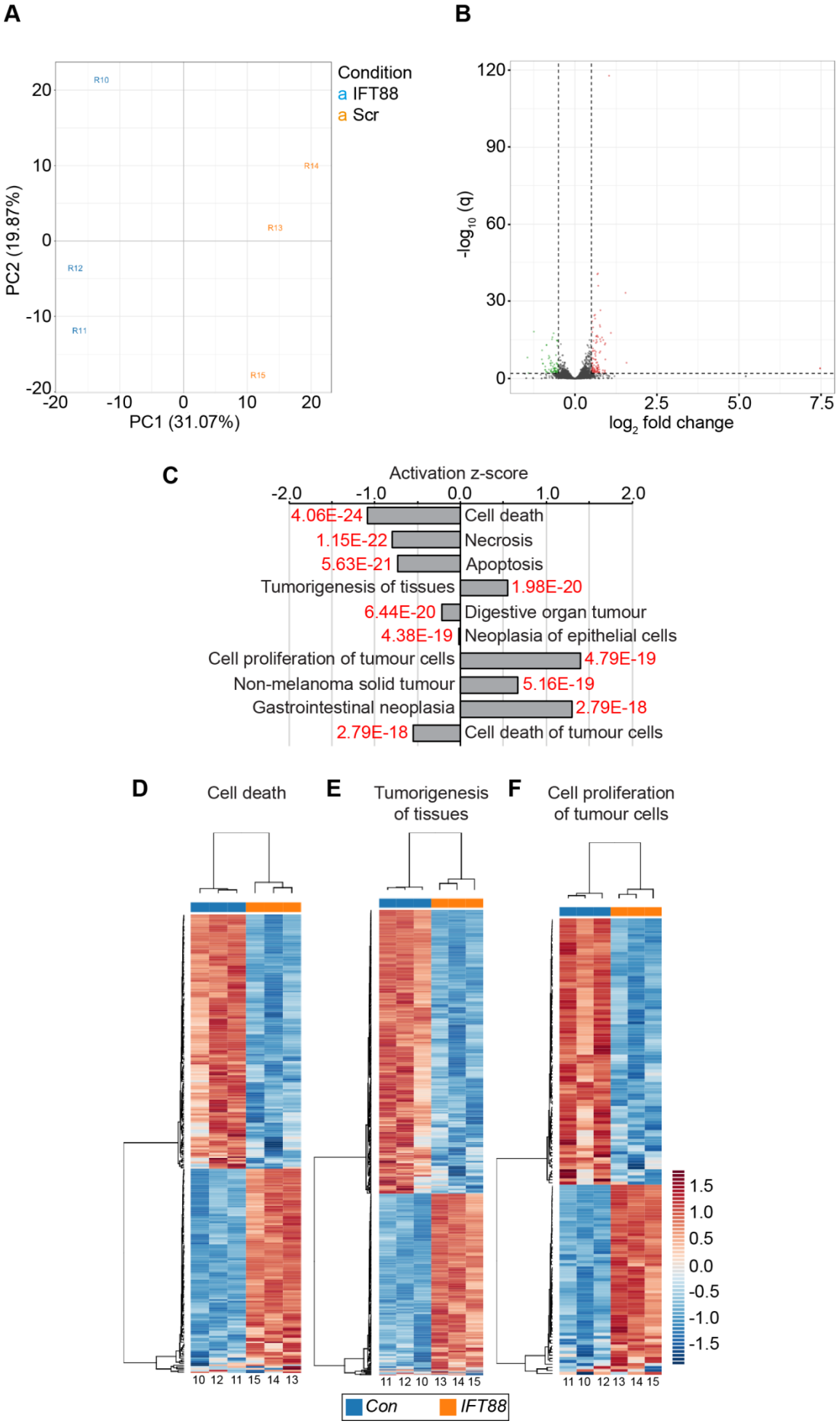
A
B
Condition
a IFT88
a Scr
R10
R14
R13
R12
R11
R15
PC2 (19.87%)
PC1 (31.07%)
-log10 (q)
log2 fold change
C
Activation z-score
-2.0
-1.0
0.0
1.0
2.0
4.06E-24 Cell death
1.15E-22 Necrosis
5.63E-21 Apoptosis
Tumorigenesis of tissues 1.98E-20
6.44E-20 Digestive organ tumour
4.38E-19 Neoplasia of epithelial cells
Cell proliferation of tumour cells 4.79E-19
Non-melanoma solid tumour 5.16E-19
Gastrointestinal neoplasia 2.79E-18
2.79E-18 Cell death of tumour cells
D
Cell death
E
Tumorigenesis of tissues
F
Cell proliferation of tumour cells
10 12 11 15 14 13
11 12 10 13 14 15
11 10 12 13 14 15
1.5
1.0
0.5
0.0
-0.5
-1.0
-1.5
Con
IFT88

4.4 Discussion

In this chapter, I have demonstrated that primary cilia incidence and length are reduced in phaeochromocytomas compared to adjacent normal adrenal medullas. This alteration is most pronounced in cluster 1 pseudohypoxic tumours and appears to be associated with a variety of clinical and pathological variables including proliferation index. Utilising the PC12 cell line, I have subsequently demonstrated that cilia loss directly results in increased cellular proliferation and transcriptional changes which are oncogenic.

4.4.1 Primary cilia loss in human phaeochromocytomas

We observed that primary cilia incidence and length were reduced in 27 phaeochromocytomas relative to paired adjacent normal adrenal medullas (Figure 4.1A-C).

Although primary cilia have been detected by electron microscopy (EM) in the rat adrenal medulla (Coupland 1965) and on a single HNPGL (Murata *et al.* 1984), the data presented here are the first to demonstrate that primary cilia loss is a feature of phaeochromocytomas. This finding is consistent with observations in other tumours that arise from the embryonic neuroectoderm (Han *et al.* 2009; Kim *et al.* 2011b; Loskutov *et al.* 2018), as well as those of endodermal (Nielsen *et al.* 2008; Hassounah *et al.* 2013) and mesodermal (Schraml *et al.* 2009; Basten *et al.* 2013; Ho *et al.* 2013) origin.

Interestingly, the presence or absence of primary cilia in medulloblastoma is variable and is governed by the initiating oncogenic event (Han *et al.* 2009). Primary cilia persist in cells of classical and desmoplastic variants, in which Wnt and Hh signalling activation requires primary cilia, but not in the anaplastic variants, where Hh activation occurs downstream of primary cilia and is repressed by their presence (Han *et al.* 2009). In phaeochromocytomas, cilia were universally lost and there was no suggestion of a dual role for primary cilia in this context (Figure 4.1E & F).

Primary cilia loss was enhanced in phaeochromocytomas from patients with germline mutations in the PPGL predisposition gene *VHL* (Figure 4.2A & B). Primary cilia loss is a feature of renal cysts (Esteban *et al.* 2006) and ccRCC (Schraml *et al.* 2009; Basten *et al.* 2013) in which VHL has been inactivated and thus our findings expand the range of VHL-associated pathologies in which primary cilia are implicated. pVHL localises to primary cilia (Schermer *et al.* 2006; Lolkema *et al.* 2008) where it binds and stabilises microtubules (Okuda *et al.* 1999; Hergovich *et al.* 2003, 2006; Schermer *et al.* 2006; Lolkema *et al.* 2007). Disruption of this process by VHL loss or through mutations in the

microtubule-binding domain, which is a mutational hotspot in VHL (Hergovich *et al.* 2003), might therefore explain the ciliary loss in VHL through reduced ciliary assembly (Dere *et al.* 2015) or enhanced disassembly (Frew *et al.* 2008).

No difference was observed between cilia in normal adrenal medullas in patients with VHL and those without (Figure 4.2A & B), suggesting that cilia loss and shortening occurs during tumourigenesis and is not a pre-existing feature of VHL. In other tumour types, cilia loss often occurs early in the disease process and is typically seen in pre-malignant conditions, for example in pancreatic intraepithelial neoplasia (Seeley *et al.* 2009; Schimmack *et al.* 2016), melanoma *in situ* (Kim *et al.* 2011b; Snedecor *et al.* 2015) and breast carcinoma *in situ* (Menzl *et al.* 2014). Unlike these examples, phaeochromocytomas do not have a generally recognised pathological pre-malignant stage, although adrenal medullary hyperplasia has been proposed as a precursor lesion. The distinction between medullary hyperplasia and phaeochromocytoma has historically been based on size criteria alone (Carney *et al.* 1975), which seems biologically unlikely. Indeed, molecular analysis suggests there is no difference between phaeochromocytomas and medullary 'hyperplasia' and that it would be better termed and thought of as a micro-phaeochromocytoma (Korpershoek *et al.* 2014).

PPGL cilia loss was equally pronounced in patients with *SDHx* mutations as it was in those with VHL and was greater in both groups than in those without a cluster 1 predisposition (Figure 4.2E & F). This raises the possibility that the mechanism of ciliary loss is not entirely due to pVHL-microtubule interactions. Loss of VHL's canonical function as an E3-ubiquitin ligase results in HIF accumulation and activation of pseudohypoxic signalling, which includes increased expression of components of the AURKA/HDAC6 cilia disassembly pathway (Xu *et al.* 2010). This is the first report of *SDHx* mutations resulting in changes in primary cilia in any context. It is interesting to note that SDH is also implicated in the pathogenesis of GISTs (Janeway *et al.* 2011), a tumour type in which the ciliary-mediated signalling pathways Hh and PDGFRA play important roles (Tang *et al.* 2016). Purely descriptive work has observed primary cilia on GISTs (Dvorak *et al.* 2014), without any meaningful comparison or analysis. Therefore, it is possible that primary cilia may play a role in GIST formation.

PPGL cilia incidence and length appeared to be associated with a number of clinical and pathological parameters (Figure 4.3). Tumours from patients aged less than 18 years old and those that were screen detected displayed fewer cilia compared to those aged over 18 and those who were diagnosed due to symptoms or as an incidental finding respectively. This is likely explained by the high degree of overlap between these groups and those patients with VHL (8/9 and 6/8 respectively). Cilia incidence and frequency was increased in metanephrine secreting tumours. This could also be a confounding effect of the relatively greater loss of cilia in cluster 1 tumours that are

predominantly normetanephrine secreting. However, it is a plausible biological effect as adrenaline increases primary cilia incidence in pancreatic ductal cancer cells (Khan *et al.* 2016). This is explored further in Chapter 5.

Cilia incidence was reduced in PPGLs with a higher Ki67 proliferation index (Figure 4.3O), suggesting a link between cilia loss and cellular proliferation, although the directionality of this cannot be ascertained from these data. Despite the proposed role for cilia as a cell cycle checkpoint (Izawa *et al.* 2015), no association between Ki67 index and primary cilia was found in either breast (Menzl *et al.* 2014) or prostate (Hassounah *et al.* 2013) cancer.

Increased prevalence of primary cilia has been associated with improved survival in pancreatic ductal adenocarcinoma (Emoto *et al.* 2014) and colorectal adenocarcinoma (Dvorak *et al.* 2016). None of our PPGL patients had metastatic disease and so this question remains unanswered in PPGL. Primary cilia have also been linked to drug resistance and subsequent tumour evolution. In medulloblastomas which require a primary cilium, ciliary loss confers resistance to Smo inhibitors (Zhao *et al.* 2017). In a variety of tumour cell lines, Jenks *et al* demonstrated that primary cilia confer resistance to a range of kinase inhibitors in a length-dependent manner and intriguingly that drug-resistant cells could be sensitised by disrupting ciliogenesis (Jenks *et al.* 2018).

Transcriptome analysis identified altered expression of gene modules associated with cilia-mediated signaling in phaeochromocytomas relative to adjacent adrenal medullas (Figure 4.5). Altered cilia-mediated signaling pathways included Hh, Wnt and Notch signaling (Figure 4.7).

The role of cilia in the regulation of cancer-linked signaling pathways is complex and context dependent (Oh & Katsanis 2013). For example, Wnt signaling, which is generally considered to be attenuated by the presence of a cilium, can be decreased in cells with shortened cilia yet activated by ablation of cilia (Lancaster *et al.* 2011; Oh & Katsanis 2013). However, for Hh signaling, the cilium activates the pathway in the presence of the sonic hedgehog ligand (Shh) and restrains signaling when Shh is absent (Wong *et al.* 2009; Hassounah *et al.* 2012). There is also crosstalk between cilia-mediated signaling pathways, such as Notch signaling modulating Shh signaling by regulating the ciliary localization of the Hh signal transduction proteins patched and smoothened (Kong *et al.* 2015). This complexity makes it difficult to interpret how alterations in cilia incidence and length may impact on specific pathways. Nevertheless, hierarchical clustering analyses separately grouped tumor and adrenal medulla samples based on changes of gene expression in multiple cilia-linked signaling pathways (Figure 4.5). This is consistent with loss of cilia correlating with dysregulation of cilia-mediated signaling in PCCs. Disruption of Wnt and Hh signaling is particularly relevant to PPGLs

with Wnt-altered tumors classified as one of four molecularly defined PPGL subtypes (Fishbein *et al.* 2017).

4.4.2 Primary cilia loss in phaeochromocytoma-derived cell lines is oncogenic

Cells derived from rat (PC12) and mouse (MPC, MTT) phaeochromocytomas are capable of forming primary cilia in two-dimensional culture (Figures 4.8 & 4.9).

PC12 cells have been previously shown to form primary cilia which express ACIII and elongate in response to lithium chloride treatment (Ou *et al.* 2009). This is the first report demonstrating that MPC and MTT cells can form primary cilia. MTT cells have fewer, shorter cilia which are less easily stimulated by serum starvation than MPC cells (Figure 4.9G & H). MTT cells, a subclone of MPC, display a more aggressive phenotype than MPC cells when injected into athymic mice (Martiniova *et al.* 2009) and we can therefore postulate that this altered behaviour might contribute to the observed ciliary changes. This is the case with the MCF isogenic breast cancer cell series, in which progressive cilia loss follows increasing degrees of transformation (Yuan *et al.* 2010). It should be borne in mind that all three cell lines used are non-human and harbour mutations in cluster 2 PPGL predisposition genes; *Max* in the case of PC12 (Hopewell & Ziff 1995) and *Nf1* in MPC and MTT (Powers *et al.* 2000).

We observed that disruption of cilia structure and function, achieved by knockdown of *Ift88* or *Cep164*, correlated with increased cellular proliferation of PC12 cells (Figure 4.10). IFT88, as a central component of the IFT complex B, is required for cilia formation. Its loss is associated with cilia loss and increased proliferation in some tissues (e.g. kidney (Delaval *et al.* 2011) and pancreas (Cano *et al.* 2004)) and failure of progenitor cell expansion in others, including cerebellar neurons (Chizhikov *et al.* 2007). In addition, IFT88 has functions independent of cilia, including a role in cell migration (Boehlke *et al.* 2015). IFT88 depletion in HeLa cells promotes progression through the cell cycle and this has been proposed as a cilia-independent function (Robert *et al.* 2007). This conclusion is based on the assertion that HeLa cells are not ciliated, although the original article did not specifically examine this and subsequent reports have established that HeLa cells can form primary cilia (Kowal & Falk 2015). Although we cannot completely exclude a contribution from cilia-independent mechanisms, the observed concordance of effect achieved by knockdown of two separate genes central to ciliogenesis points towards a cilia-dependent effect.

In addition to increased cellular proliferation, *Ift88* knockdown in PC12 cells resulted in changes in gene expression that inhibited cell death pathways while activating cell proliferation and tumour-

linked pathways (Figure 4.11). IFT88 has recently been implicated as a tumour suppressor in hepatocellular carcinoma with low levels of expression being associated with poor prognosis in patients and enhanced invasion and migration of liver cancer stem cells *in vitro* (Huang *et al.* 2017; You *et al.* 2017). Although cilia were not examined in these studies, they provide further support for a role for ciliary dysfunction in tumourigenesis.

The effect of IFT88 loss is not universal across cancer types; its depletion in thyroid cancer cells did not alter cellular proliferation, migration or invasion but did confer oncogenic changes in glycolysis and lipid biosynthesis (Lee *et al.* 2018). These changes in cellular metabolism and respiration are also seen in a murine model of ADPKD (Podrini *et al.* 2018) and highlight the varied and multi-faceted roles primary cilia might play in tumourigenesis.

Together, our data are consistent with cilia acting as a checkpoint for cell division in PC12 cells and suggest cilia loss promotes proliferation and perhaps tumourigenesis in PCC/PGL.

4.5 Summary

In this chapter I have demonstrated that primary cilia structure is altered in phaeochromocytomas compared to adjacent normal adrenal medullas and that this is accompanied by changes in transcription related both to ciliary assembly/disassembly and cilia-mediated signalling pathways. Pseudohypoxic cluster 1 tumours had the most pronounced ciliary phenotype and this is investigated mechanistically in Chapter 5. Through knockdown of key ciliary proteins in phaeochromocytoma-derived cells, I have shown that cilia loss as the primary insult results in increased cellular proliferation and oncogenic transcriptional changes, providing further evidence that primary cilia loss is a contributor and not merely a consequence of PPGL tumourigenesis.

CHAPTER 5

The influence of features of the tumour microenvironment on primary cilia in phaeochromocytomas

Work in this chapter has been published in the following article, which is included in the appendix of this thesis.

Oncometabolite induced primary cilia loss in pheochromocytoma. O'Toole SM, Watson DS, Novoselova TV, Romano LEL, King PJ, Bradshaw TY, Thompson CL, Knight MM, Sharp TV, Barnes MR, Srirangalingam U, Drake WM, Chapple JP. Endocrine Related Cancer 2019; 26(1): 165-180.

5.1 Introduction

Primary cilia function as sensory organelles to a wide range of extracellular stimuli (discussed in Chapter 1) and, through the projection of the axoneme into the extracellular space, are ideally placed to interact with the tumour microenvironment. This is the complex physical, chemical and cellular *milieu* in which tumour cells exist and interact and to which they must adapt to survive (Balkwill *et al.* 2012).

Despite this, there is sparse experimental evidence examining the effect on primary cilia of features of the tumour microenvironment. Perhaps the cardinal feature of this environment is hypoxia, and this is of particular importance in cluster 1 pseudohypoxic phaeochromocytomas. The effect of hypoxia on primary cilia appears complex, variable and cell lineage dependent (Proulx-Bonneau & Annabi 2011; Wann *et al.* 2013; Brown *et al.* 2014; Lavagnino *et al.* 2016). It has not been well studied in the context of cancer.

Limited studies have shown that cancer cell primary cilia can be modulated by other features of the tumour microenvironment, namely endocrine (Xiang *et al.* 2014) and paracrine (Bailey *et al.* 2009; Mansini *et al.* 2019) factors, external carcinogens (Radford *et al.* 2012) and inflammation (Vézina *et al.* 2014; Dvorak *et al.* 2017).

Having observed ciliary loss to be a feature of human phaeochromocytomas in Chapter 4, this chapter examines whether specific phaeochromocytoma-relevant components of the tumour microenvironment might be responsible.

5.2 Aims and Objectives

The aim of this chapter was to investigate whether features of the tumour microenvironment influenced primary cilia in phaeochromocytomas. The choice of elements of the tumour microenvironment for study priority was governed by those with an established role in phaeochromocytoma and neuroendocrine tumour aetiology, pathophysiology and treatment.

We hypothesised that primary cilia would be influenced by certain features of the tumour microenvironment.

The first objective was to determine whether hypoxia altered primary cilia incidence or length in phaeochromocytoma-derived cells, and if so, by what mechanism.

The second objective was to determine whether pseudohypoxia altered primary cilia incidence or length in phaeochromocytoma-derived cells, and if so, by what mechanism.

The third objective was to determine whether circulating catecholamines in patients with phaeochromocytomas led to alterations in primary cilia incidence or length.

The fourth objective was to determine whether catecholamines altered primary cilia incidence or length in phaeochromocytoma-derived PC12 cells, and if so, by what mechanism.

The fifth objective was to determine whether other chemical features of the tumour microenvironment, namely somatostatin receptor stimulation, led to changes in primary cilia incidence and length.

5.3 Results

In the previous chapter, we have demonstrated that cilia loss and shortening in human phaeochromocytomas is most pronounced in patients with germline mutations in *VHL* and *SDHx* (Figure 4.2). Loss of function of the associated VHL and SDHx proteins results in pseudohypoxia due to failure of destruction of HIF (discussed in detail in Chapter 2). We thus sought to examine whether hypoxia and pseudohypoxia influenced phaeochromocytoma primary cilia and, if so, by what mechanism.

5.3.1 The effects of hypoxia on phaeochromocytoma primary cilia

5.3.1.1 Hypoxia impairs ciliogenesis in PC12 cells in a reversible manner

Hypoxia, a cardinal feature of the tumour microenvironment, has previously been shown to alter primary cilia in a variable and tissue-dependent manner (Proulx-Bonneau & Annabi 2011; Wann *et al.* 2013; Brown *et al.* 2014; Lavagnino *et al.* 2016).

We sought to investigate the effect hypoxia had on primary cilia in the rat PC12 phaeochromocytoma-derived cell line. First, we examined whether or not it altered the ability of cells to form a primary cilium in response to the ciliogenesis cue of serum starvation. PC12 cells were plated in complete media for 24 hours to allow attachment before being washed and the media exchanged with serum-free media. Cells were then exposed either to standard tissue culture conditions (atmospheric oxygen, 21%) or a hypoxic chamber (1% oxygen) for a variety of time intervals prior to fixation and immunolabelling for detection of primary cilia (Figure 5.1A).

Cilia incidence was lower in cells cultured in the absence of serum in 1% oxygen compared to 21% oxygen (Figure 5.1B). This difference was observed after only four hours of exposure to differential oxygen concentrations (40.0% $\pm$ 10.3 v. 31.2% $\pm$ 0.08; p=0.046) and was maintained and increased after up to 24 hours exposure (70.7% $\pm$ 14.7 v. 51.3% $\pm$ 9.5; $p=1.1 \times 10^{-9}$). Similarly, cilia length was lower in cells cultured in the absence of serum in 1% oxygen compared to 21% oxygen (Figure 5.1C). This effect, although seen after four hours, was not statistically significant until eight hours (2.43µm $\pm$ 0.84 v. 2.02µm $\pm$ 0.64; $p=4.2 \times 10^{-5}$).

Thus, ciliogenesis was reduced in PC12 cells cultured under conditions of hypoxia (1% oxygen) compared to normoxia (21% oxygen). This observation is consistent with previous reports in primary rat tenocytes (Lavagnino *et al.* 2016) and murine bone marrow derived mesenchymal stem cells (Proulx-Bonneau & Annabi 2011) cultured in 1% oxygen. Interestingly, no effect on cilia incidence

was seen in murine bone marrow derived mesenchymal stem cells cultured in 5% oxygen (Brown *et al.* 2014), whilst 2% oxygen resulted in longer cilia in primary bovine articular chondrocytes (Wann *et al.* 2013). In these studies, hypoxia-induced ciliary changes were associated with alterations in cilia-mediated functions including mechanoresponsiveness (Lavagnino *et al.* 2016) and Wnt (Proulx-Bonneau & Annabi 2011) and Hh (Brown *et al.* 2014) related gene expression.

We next sought to determine whether the effect of hypoxia on PC12 primary cilia was reversible. PC12 cells were exposed to serum-free media for 24 hours in a hypoxic chamber (1% oxygen) prior to return to atmospheric oxygen for a variety of time intervals before fixation and immunolabelling for detection of primary cilia (Figure 5.2A).

Cilia incidence increased with time following return to 21% oxygen (Figure 5.2B). After 24 hours of recovery, primary cilia incidence was significantly greater than after hypoxic exposure (59.5% $\pm$ 10.2 v. 51.3% $\pm$ 9.3; p=0.048), although it took 48 hours recovery for ciliary incidence to be at a comparable level with cells cultured in atmospheric oxygen alone (64.2% $\pm$ 11.0 v. 70.7% $\pm$ 14.7; p=0.21). Likewise, cilia length increased with increasing recovery time post hypoxic exposure (Figure 5.2C). This effect was first seen after 24 hours return to atmospheric oxygen conditions (2.54µm $\pm$ 0.80 v. 2.26µm $\pm$ 0.70; p=0.017), at which point cilia length was indistinguishable from that of cells not exposed to 1% oxygen (2.54µm $\pm$ 0.80 v. 2.51µm $\pm$ 0.59; p=0.99).

Thus, ciliogenesis is impaired by hypoxia in PC12 cells in a reversible manner, with full recovery being observed following return to standard atmospheric oxygen. Given the differential effects of hypoxia on primary cilia previously observed with other cell types, we next sought to examine whether this was consistent with the response in other phaeochromocytoma cell lines.

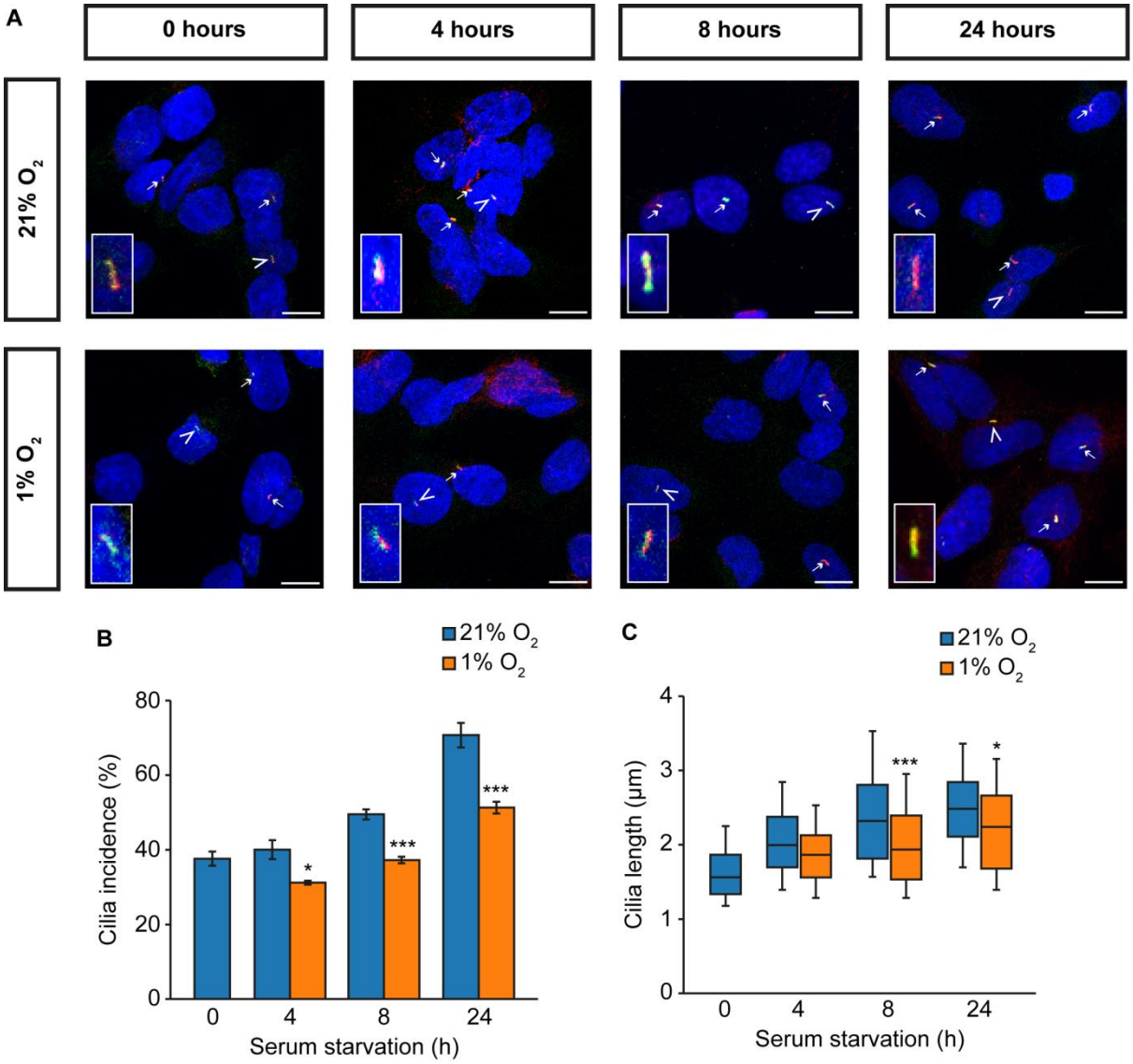

Figure 5.1: Hypoxia reduces cilia formation in PC12 cells

(A) Confocal images of PC12 cells exposed to serum-free media either at 1% or 21% oxygen for the time periods indicated. Cells were immunolabelled with anti-acetylated α-tubulin (red) and anti-Arl13b (green) for detection of primary cilia. Nuclei were stained with DAPI (blue). Cilia are indicated by arrows, or arrowheads where they are also shown zoomed in the insets. Scale bars = 10 µm.

Quantification of primary cilia incidence (B) and length (C) following treatment as per (A). Error bars indicate $\pm$ SEM, boxes 25th, 50th and 75th centiles and whiskers the 10th and 90th centiles. Number of cells scored for incidence: 1222 $\pm$ 185 per condition. Number of cilia measured for length: 156 $\pm$ 26 per condition. Statistical significance was assessed using a one-way ANOVA. * $p < 0.05$, *** $p < 0.001$. Stars indicate comparison between the two oxygen concentrations tested. Where no stars are evident, $p > 0.05$.

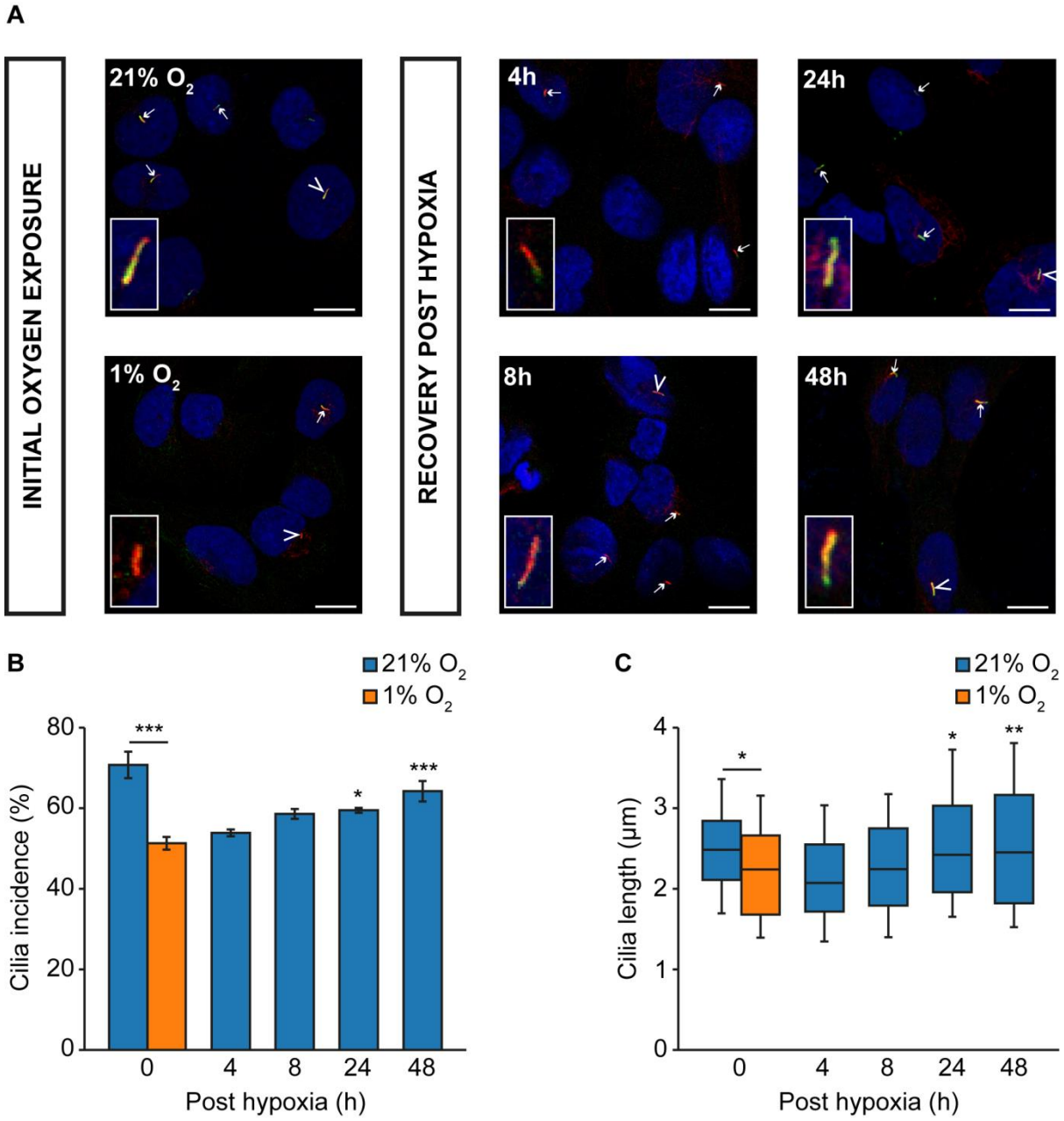

Figure 5.2: Hypoxia induced ciliary loss in PC12 cells recovers following return to normoxia

(A) Confocal images of PC12 cells exposed to serum-free media at 1% oxygen for 24 hours prior to return to atmospheric (21%) oxygen for the time periods indicated. Cells were immunolabelled with anti-acetylated α-tubulin (red) and anti-Arl13b (green) for detection of primary cilia. Nuclei were stained with DAPI (blue). Cilia are indicated by arrows, or arrowheads where they are also shown zoomed in the insets. Scale bars = 10 µm.

Quantification of primary cilia incidence (B) and length (C) following treatment as per (A). Error bars indicate ± SEM, boxes 25th, 50th and 75th centiles and whiskers the 10th and 90th centiles. Number of cells scored for incidence: 1015 ± 175 per condition. Number of cilia measured for length: 147 ± 29 per condition. Statistical test used: one-way ANOVA. * p <0.05, ** p<0.01, *** p< 0.001. Stars above error bars indicate comparison to 24 hours exposure to 1% oxygen and above horizontal lines between the two columns linked.

5.3.1.2 The effect of hypoxia on ciliogenesis in MPC and MTT cells

MPC and MTT are related mouse phaeochromocytoma-derived cell lines that harbour mutations in the *nf1* gene (Powers *et al.* 2000). Beyond PC12 cells, they represent the only other phaeochromocytoma-derived cell lines that have been used in more than one peer-reviewed publication.

In order to test whether hypoxia had the same effect on ciliogenesis as was observed in PC12 cells, MPC and MTT cells were subjected to the same test conditions (namely culture in serum-free media either in 1% or atmospheric oxygen; Figure 5.3).

In accordance with the observations in PC12 cells, cilia incidence was reduced in both MPC (64.1% $\pm$ 8.7 v. 76.1% $\pm$ 1.8; p=0.002) and MTT cells (54.3 % $\pm$ 6.1 v. 64.5% $\pm$ 4.0; p=0.0351) exposed to hypoxic conditions (Figure 5.3B). The same pattern of reduced ciliary length following exposure to hypoxia was also observed in both MPC (2.25µm $\pm$ 0.76 v. 2.77µm $\pm$ 0.78; p=1 $x10^{-15}$) and MTT cells (1.99µm $\pm$ 0.56 v. 2.23µm $\pm$ 0.66; p=0.00011; Figure 5.3C).

Thus, hypoxia impairs ciliary formation in all three established phaeochromocytoma-derived cell lines suggesting that its effect is conserved and consistent and not merely cell line specific.

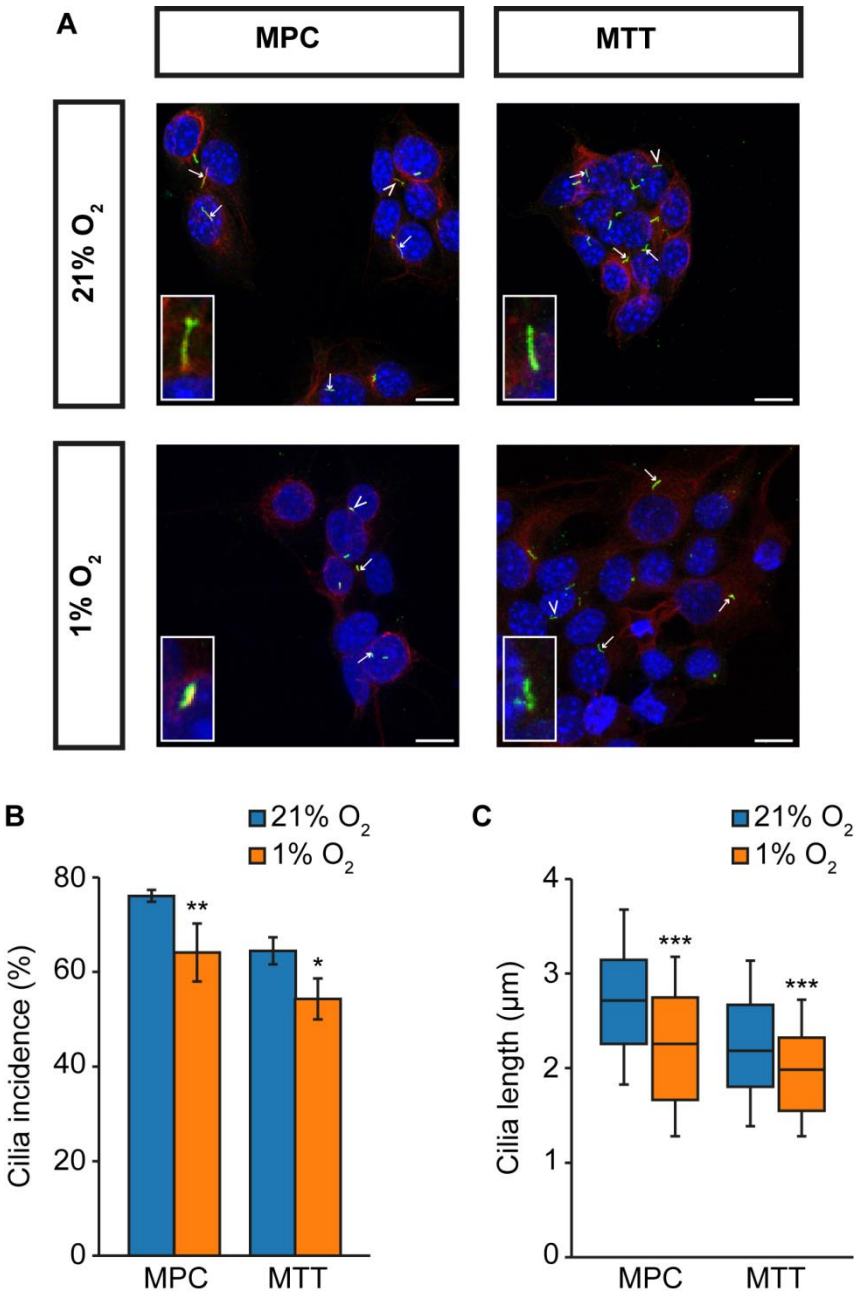

Figure 5.3: Hypoxia impairs ciliogenesis in MPC and MTT cells

(A) Confocal images of MPC and MTT cells exposed to serum-free media either at 1% or 21% oxygen for 24 hours. Cells were immunolabelled with anti-acetylated α-tubulin (red) and anti-Arl13b (green) for detection of primary cilia. Nuclei were stained with DAPI (blue). Cilia are indicated by arrows, or arrowheads where they are also shown zoomed in the insets. Scale bars = 10 µm.

Quantification of primary cilia incidence (B) and length (C) following treatment as per (A). Error bars indicate $\pm$ SEM, boxes 25th, 50th and 75th centiles and whiskers the 10th and 90th centiles. Number of cells scored for incidence: 1954 $\pm$ 338 per condition. Number of cilia measured for length: 295 $\pm$ 34 per condition. Statistical significance was assessed using a one-way ANOVA. * $p < 0.05$, ** $p < 0.01$, *** $p < 0.001$.

5.3.1.3 Hypoxia-induced cilia loss in PC12 cells is dependent on HIF-mediated signalling

Having established that hypoxia reduced ciliary formation, we next sought to determine whether this was mediated by HIF signalling or an alternate mechanism.

First, we utilised the HIFα inhibitor FM19G11 (Moreno-Manzano *et al.* 2010). PC12 cells were plated in complete media for 24 hours to allow attachment before being washed and the media exchanged with serum-free media containing either FM19G11 or DMSO as a vehicle-only control. Cells were then incubated for a further 24 hours in 1% oxygen prior to processing. Two concentrations of FM19G11 were tested (500nM and 1μM) based on previous demonstrations of efficacy (Moreno-Manzano *et al.* 2010) that did not show toxic effects on PC12 cells in preliminary experiments.

Treatment of hypoxia-exposed PC12 cells with FM19G11 (Fig 5.4A) resulted in significantly increased cilia incidence compared to vehicle-only treated controls (Fig 5.4B). This effect was seen at both FM19G11 concentrations tested; 500nM (51.0% $\pm$ 0.13 v. 38.6% $\pm$ 0.14; p=0.0013) and 1μM (56.0% $\pm$ 0.13 v 38.6% $\pm$ 0.14; p=2.8 $x10^{-6}$). There was no significant difference between the effect seen with either dose (p=0.42).

FM19G11 also resulted in increased cilia length compared to vehicle-only treated controls (Fig 5.4C). Again this effect was seen at both 500nM (2.91μm $\pm$ 0.92 v. 2.37μm $\pm$ 0.73; p=2.4 $x10^{-6}$) and 1μM (2.85μm $\pm$ 0.91 v. 2.37μm $\pm$ 0.73; p=2.7 $x10^{-5}$) and there was no difference in effect between these concentrations (p=0.97).

Thus, the inhibition of HIFα function by FM19G11 prevents hypoxia-induced reductions in ciliary incidence and length. In order to further test this, we performed siRNA-mediated knockdown of *HIF1α*.

PC12 cells were plated in complete media for 24 hours before being exchanged and transfected with siRNA targeting either *HIF1α* or a non-targeting control. After 48 hours, cells were transferred either to 1% oxygen or maintained in 21% oxygen for a further 24 hours before being processed.

Successful knockdown of *HIF1α* was confirmed by qPCR (Fig 5.5A). Knockdown of *HIF1α* (Fig 5.5B) resulted in a significantly greater ciliary incidence in PC12 cells exposed to hypoxia compared to those treated with non-targeting siRNA (Fig 5.5C; 49.7% $\pm$ 16.2 v. 33.8% $\pm$ 13.3; p=0.014). Ciliary length was similarly increased in PC12 cells exposed to 1% oxygen that had been transfected with siRNA against *HIF1α* (Fig 5.5D; 1.92μm $\pm$ 0.55 v. 1.50μm $\pm$ 0.48; p=8.2$x10^{-7}$). There was no significant difference between cilia length in the *HIF1α* siRNA treated group and the non-targeted siRNA group

not exposed to hypoxia (p=0.74), however cilia incidence remained lower (52.0% ± 12.3 v. 64.8% ± 10.7; p=0.017).

Thus, we have demonstrated that both pharmacological and siRNA-mediated attenuation of HIF signalling rescues hypoxia-induced ciliary loss in PC12 cells. Taken together, these results provide evidence that hypoxia-induced ciliary loss in PC12 cells is HIF-dependent.

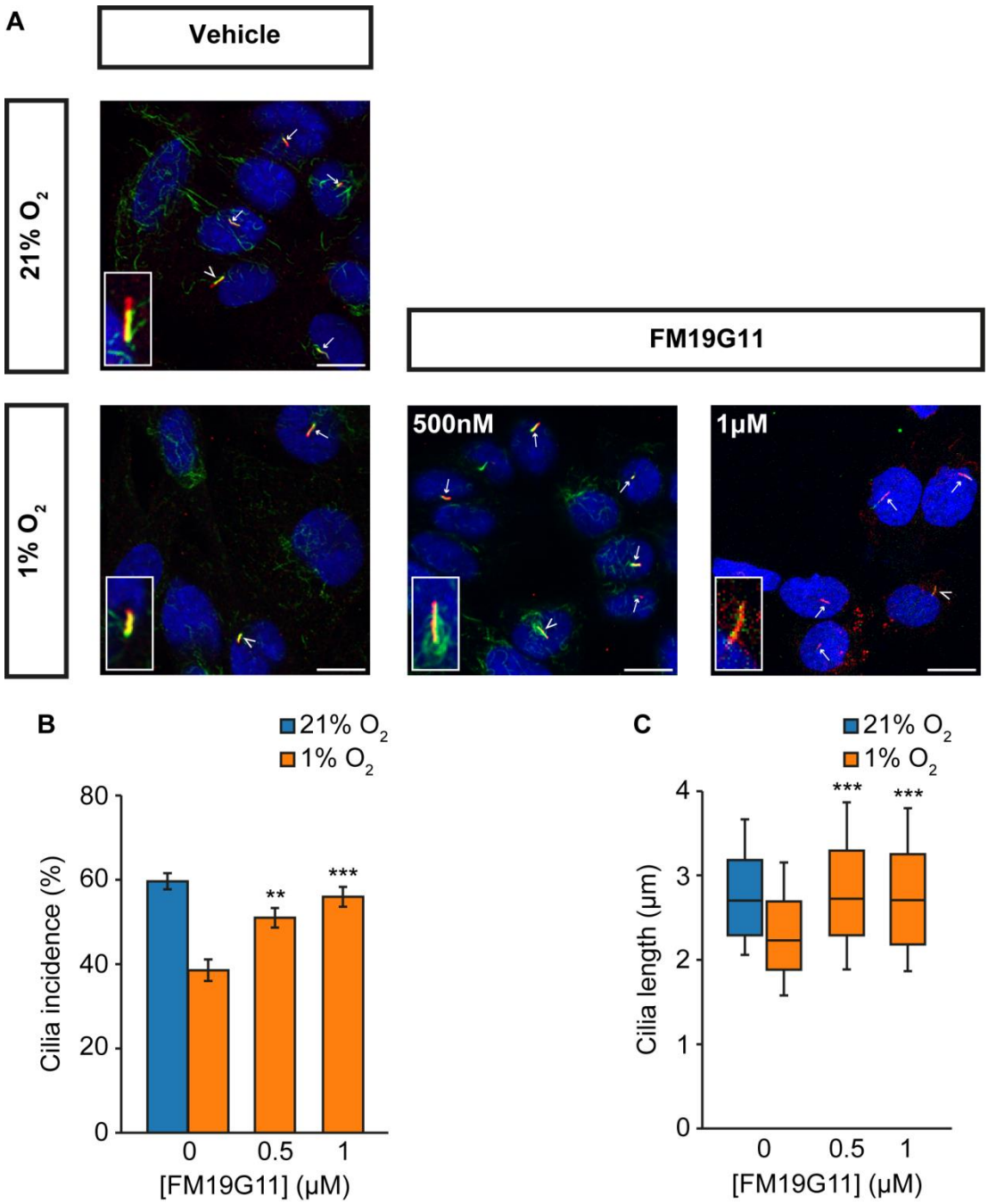

Figure 5.4: Hypoxia-induced ciliary loss in PC12 cells is prevented by FM19G11
(A) Confocal images of PC12 cells exposed to serum-free media containing either FM19G11 or vehicle-only control at 1% or 21% oxygen for 24 hours. Cells were immunolabelled with anti-acetylated α-tubulin (red) and anti-Arl13b (green) for detection of primary cilia. Nuclei were stained with DAPI (blue). Cilia are indicated by arrows, or arrowheads where they are also shown zoomed in the insets. Scale bars = 10 µm.

Quantification of primary cilia incidence **(B)** and length **(C)** following treatment as per **(A)**. Error bars indicate ± SEM, boxes 25th, 50th and 75th centiles and whiskers the 10th and 90th centiles. Number of cells scored for incidence: 1016 ± 93 per condition. Number of cilia measured for length: 124 ± 30 per condition. Statistical significance was assessed using a one-way ANOVA compared to vehicle-only control in 1% O_2. ** $p < 0.01$, *** $p < 0.001$.

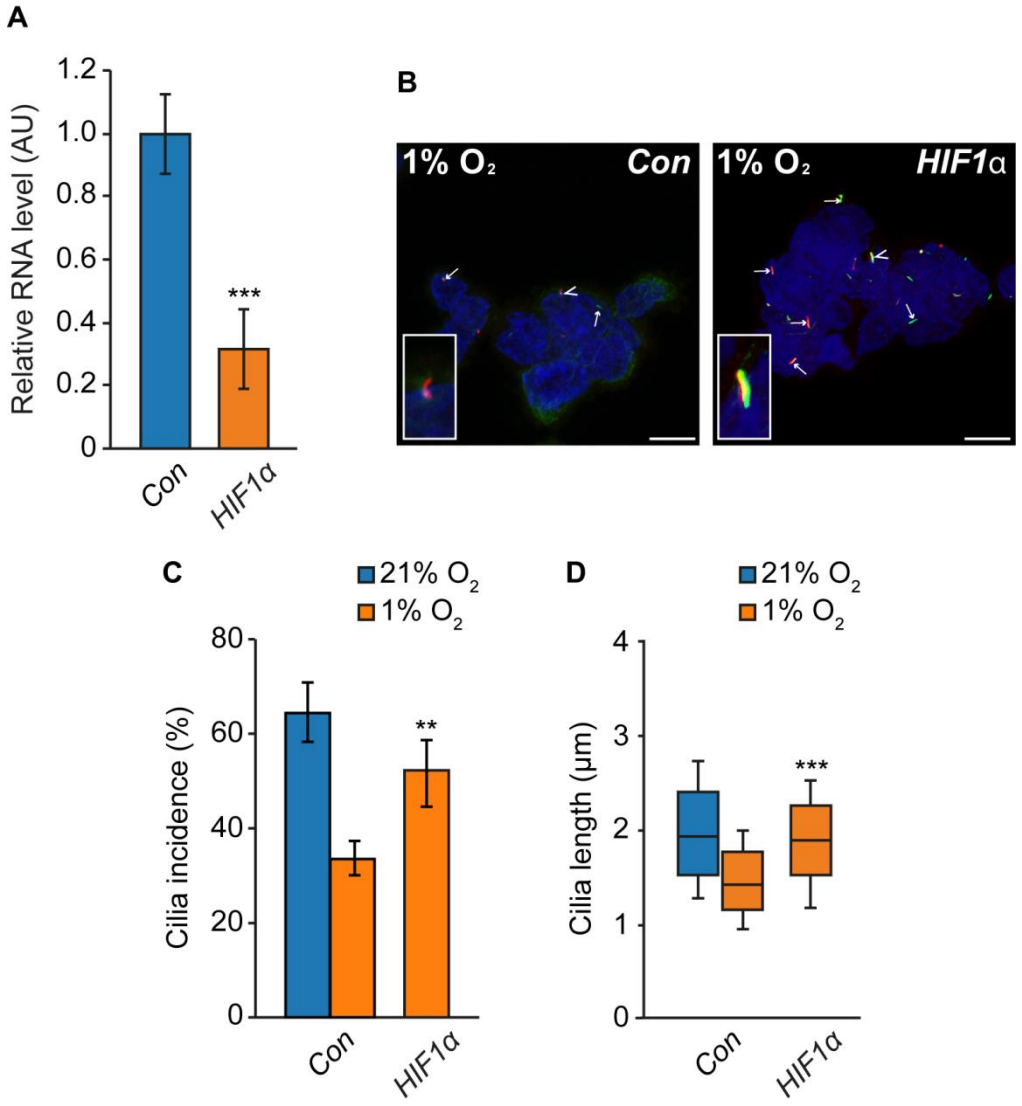

Figure 5.5: siRNA mediated knockdown of HIF1α prevents hypoxia-induced ciliary loss in PC12 cells

(A) Quantification of relative RNA expression (AU, arbitrary units) assessed by qPCR of HIF1α in PC12 cells 48 hours after transfection with siRNAs targeting HIF1α or non-targeting controls (Con). Data were normalised to peptidylpropyl isomerase A. Statistical significance was assessed using an unpaired t-test. *** $p<0.001$.

(B) Confocal images of PC12 cells cultured for 24 hours in 1% oxygen after transfection as per (A). Cells were immunolabelled with anti-acetylated α-tubulin (red) and anti-Arl13b (green) for detection of primary cilia. Nuclei were stained with DAPI (blue). Cilia are indicated by arrows, or arrowheads where they are also shown zoomed in the insets. Scale bars = 10 µm.

Quantification of primary cilia incidence **(C)** and length **(D)** following treatment as per (B). Error bars indicate $\pm$ SEM, boxes 25th, 50th and 75th centiles and whiskers the 10th and 90th centiles. Number of cells scored for incidence: 3810 $\pm$ 373 per condition. Number of cilia measured for length: 96 $\pm$ 12 per condition. Statistical significance was assessed using a one-way ANOVA compared to non-targeting control in 1% oxygen. ** $p<0.01$, *** $p< 0.001$.

5.3.1.4 Hypoxia-induced cilia loss in PC12 cells is dependent on AURKA/HDAC6 pathway activation

We next set out to understand the mechanism by which HIF-mediated signalling might result in the observed ciliary loss in PC12 cells and hypothesised that the AURKA/HDAC6 pathway (discussed in Chapter 1) might be responsible.

Activation of the AURKA/HDAC6 pathway results in deacetylation of ciliary tubulin and destabilisation of the axonemal microtubules resulting in ciliary disassembly (Pugacheva *et al.* 2007). Overexpression of components of this pathway with resultant ciliary loss has been observed in a range of human cancers including renal (Schraml *et al.* 2009; Basten *et al.* 2013; Dere *et al.* 2015; Ding *et al.* 2015), ovarian (Egeberg *et al.* 2012), cholangiocarcinoma (Gradilone *et al.* 2013; Razumilava *et al.* 2014) and chondrosarcoma (Xiang *et al.* 2017).

In order to test this hypothesis, hypoxia-exposed PC12 cells were treated with a variety of pharmacological inhibitors. PC12 cells were plated and grown in serum-containing media for 24 hours prior to exchange for serum-free media containing either inhibitor or vehicle-only control. Cells were then exposed to 1% oxygen for 24 hours prior to processing for cilia (Figure 5.6A).

Treatment of PC12 cells exposed to hypoxia with the specific AURKA inhibitor PHA-680632 resulted in significantly increased cilia incidence (Figure 5.6B; 61.3% $\pm$ 11.3 v. 38.6% $\pm$ 14.1; $p=1.1 \times 10^{-10}$) compared to vehicle-only treated controls. The same pattern of increased cilia incidence was also seen with inhibition by the mammalian class I and II HDAC inhibitor trichostatin A (TSA) (60.1% $\pm$ 10.2; $p=1.0 \times 10^{-9}$) and the selective HDAC6 inhibitor tubacin (53.8% $\pm$ 15.0; $p=4.0 \times 10^{-5}$). In all cases, cilia incidence was increased to levels comparable to cells cultured in 21% oxygen and not exposed to hypoxia (59.6% $\pm$ 10.6; p=0.99 for PHA-680632, p=0.99 for TSA, p=0.49 for tubacin). Lithium chloride was utilised for comparison as an agent known to increase ciliary length by an alternative mechanism (Ou *et al.* 2009). Treatment with lithium chloride also resulted in increased ciliary incidence (48.0% $\pm$ 9.9; p=0.045) albeit to a lesser degree than the specific pathway inhibitors (p=0.0005 for PHA-680632, p=0.002 for TSA, p=0.49 for tubacin) and it did not completely rescue hypoxia-induced cilia loss (p=0.004 compared to 21% oxygen).

Cilia length (Figure 5.6C) was also significantly increased by treatment with PHA-680632 (2.80µm $\pm$ 0.80 v. 2.37µm $\pm$ 0.73; $p=7.7 \times 10^{-6}$) and TSA (2.88µm $\pm$ 0.70; $p=2.7 \times 10^{-7}$). Cilia length was also increased with tubacin (2.54µm $\pm$ 0.67; p=0.44) and lithium chloride (2.48µm $\pm$ 0.70; p=0.90), although this was a trend only with significance not achieved. In keeping with this, cilia length was

restored to that seen in 21% oxygen following treatment with PHA-680632 ($p=0.99$) and TSA ($p=0.99$) but not tubacin ($p = 0.03$) or lithium ($p = 0.004$).

These data suggest that reduced oxygen levels lead to cilia resorption in PC12 cells by a mechanism that includes HIF signalling and activation of the AURKA/HDAC6 pathway.

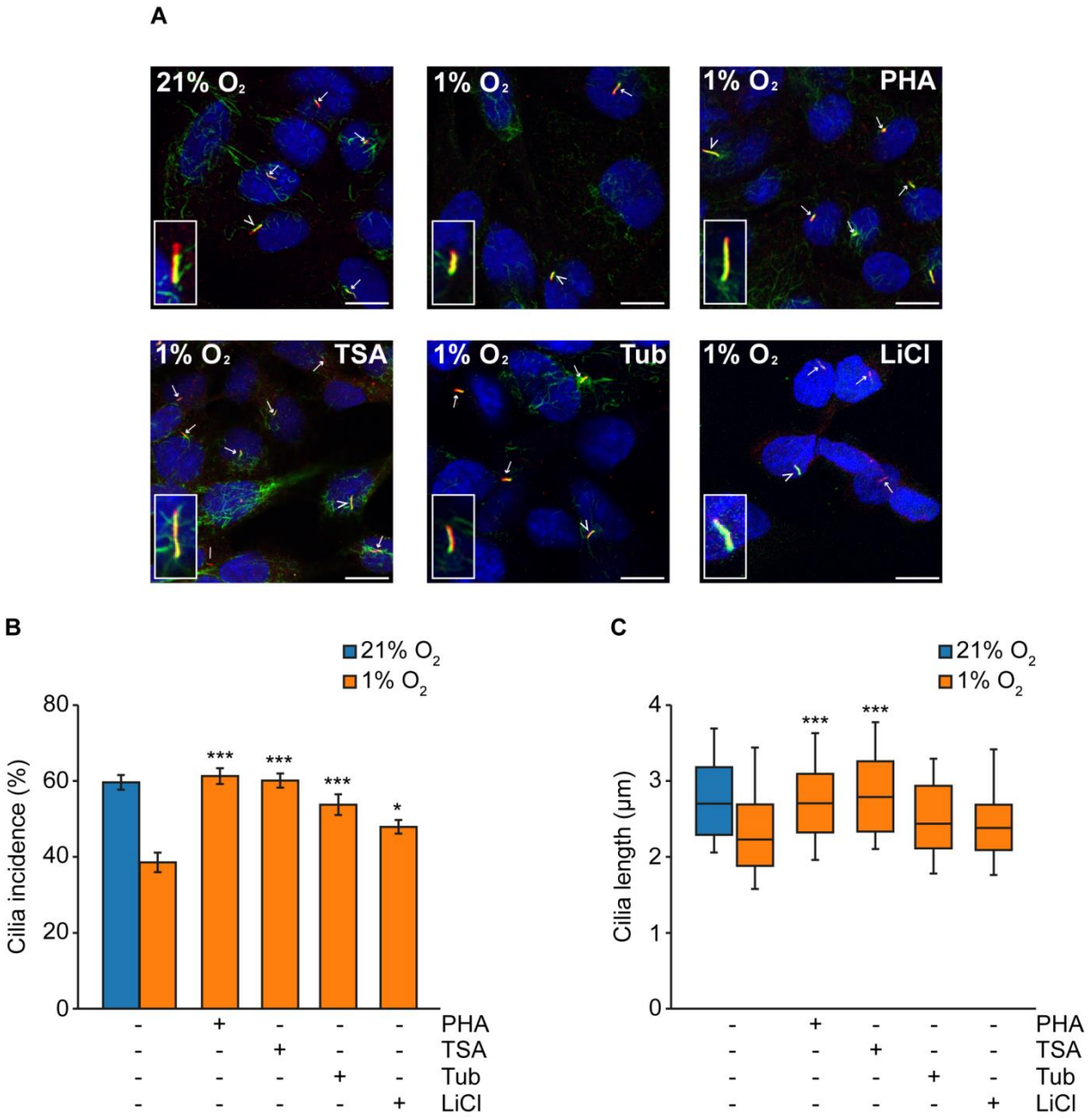

Figure 5.6: Hypoxia-induced ciliary loss in PC12 cells is prevented by AURKA/HDAC6 inhibition

(A) Confocal images of PC12 cells immunolabelled for detection of primary cilia (anti-acetylated α-tubulin (red), anti-Arl13b (green), DAPI (blue)). Cells were cultured in 21% or 1% oxygen for 24 hours in the presence or absence of the inhibitors PHA-680632 (PHA), trichostatin A (TSA), tubacin (Tub) and lithium chloride (LiCl), or vehicle only controls. Cilia are indicated by arrows, or arrowheads where they are also shown zoomed in the insets. Scale bars = 10 µm.

Quantification of primary cilia incidence **(B)** and length **(C)** following treatment as per **(A)**. Error bars indicate $\pm$ SEM, boxes 25th, 50th and 75th centiles and whiskers the 10th and 90th centiles. Number of cells scored for incidence: 1034 $\pm$ 91 per condition. Number of cilia measured for length: 127 $\pm$ 24 per condition. Statistical significance was assessed using a one-way ANOVA compared to vehicle-only control in 1% O_2. * $p < 0.05$, *** $p < 0.001$.

5.3.2 The effects of pseudohypoxia on phaeochromocytoma primary cilia

Having identified that phaeochromocytoma primary cilia are modulated by hypoxia, we sought to test whether the effect was also seen with pseudohypoxia. The persistence of HIF mediated signalling in the presence of oxygen is the hallmark feature of cluster 1 phaeochromocytomas due to mutations in *VHL*, *SDHx*, and *FH*. It arises through functional inactivation of either HIF-PHDs or pVHL and results in persistence of HIFα and transcription of HIF target genes.

5.3.2.1 Pseudohypoxia achieved by HIF-PHD inhibition results in cilia loss and shortening

In order to establish whether pseudohypoxia impacted primary cilia, we first targeted HIF-PHD by treating PC12 cells with the inhibitor dimethyloxalylglycine, N-(methoxyoxoacetyl)-glycine methyl ester (DMOG) (Jaakkola *et al.* 2001). DMOG is an experimental hypoxia mimetic that reduces proteosomal degradation of HIF by inhibiting HIF-PHD mediated hydroxylation of HIFα which is required for pVHL binding. In addition to providing mechanistic information as to whether pseudohypoxia impacted primary cilia, targeting HIF-PHD has direct relevance to PPGL because germline mutations in both *PHD1* (Yang *et al.* 2015) and *PHD2* (Ladroue *et al.* 2008; Yang *et al.* 2015) are rare, but identified, causes of PPGL in combination with congenital eythrocytosis.

PC12 cells were grown in serum-containing media for 24 hours to allow attachment before the media was changed to serum-free media containing either DMOG or vehicle only control for a further 24 hours (Fig 5.7A).

Exposure to DMOG for 24 hours resulted in a significant reduction in primary cilia incidence (Fig 5.7B) at both 10μM (58.3% $\pm$ 12.2 v. 68.5% $\pm$ 12.6, p=0.0046) and 100μM (45.4% $\pm$ 11.6, $p=2.3\times10^{-11}$) compared to control. A similar pattern was observed regarding cilia length (Fig 5.7C). Cilia length was reduced in PC12 cells exposed to DMOG at both 10 μM (2.10μm $\pm$ 0.75 v. 2.72μm $\pm$ 0.70, $p=8.0\times10^{-14}$) and 100μM (2.32μm $\pm$ 0.79, $p=3.9\times10^{-7}$) compared to vehicle only control.

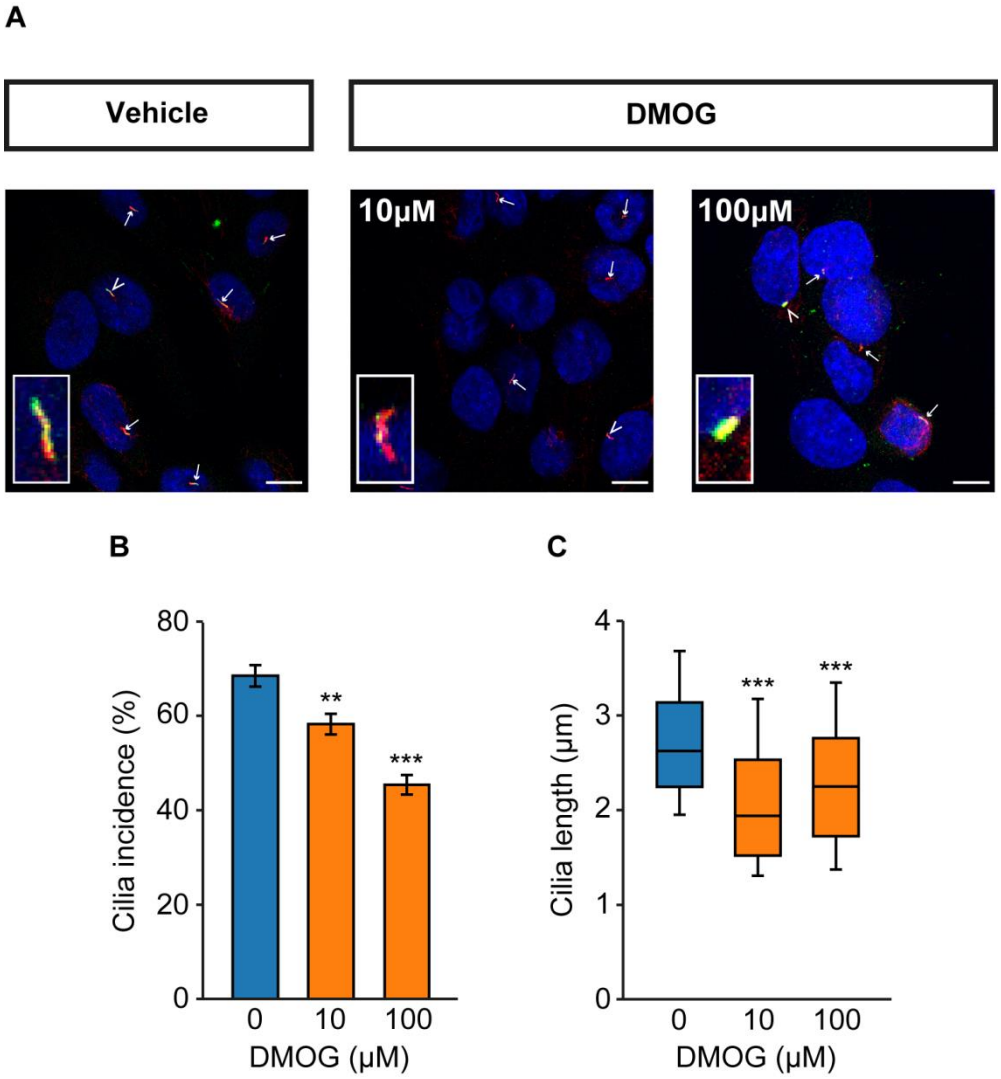

Figure 5.7: Treatment of PC12 cells with the HIF-PHD inhibitor DMOG results in reduced ciliary formation

(A) Confocal images of PC12 cells exposed to serum-free media containing DMOG at the concentrations indicated (or vehicle only control) for 24 hours. Cells were immunolabelled with anti-acetylated α-tubulin (red) and anti-Arl13b (green) for detection of primary cilia. Nuclei were stained with DAPI (blue). Cilia are indicated by arrows, or arrowheads where they are also shown zoomed in the insets. Scale bars = 10 µm.

Quantification of primary cilia incidence **(B)** and length **(C)** following treatment as per **(A)**. Error bars indicate $\pm$ SEM, boxes 25th, 50th and 75th centiles and whiskers the 10th and 90th centiles. Number of cells scored for incidence: 1100 $\pm$ 64 per condition. Number of cilia measured for length: 200 $\pm$ 22 per condition. Statistical significance was assessed using a one-way ANOVA compared to control. ** $p<0.01$, *** $p< 0.001$.

5.3.2.2 Pseudohypoxia achieved by loss of SDH function results in cilia loss and shortening

Having demonstrated that direct inhibition of HIF-PHD impaired ciliary formation, we sought to examine whether doing so indirectly recapitulated this observation. As previously discussed, mutations in *SDHx* are an important cause of cluster 1 PPGL development. Loss of enzyme activity (Figure 2.5) results in succinate accumulation which in turn inhibits HIF-PHD (Selak *et al.* 2005) resulting in HIF accumulation and pseudohypoxia.

First, we pharmacologically inhibited SDH with malonate, which competes with succinate for active sites of SDH, resulting in succinate accumulation (Webb 1966). PC12 cells were exposed to serum-free media containing malonate or vehicle-only control for 24 hours (Figure 5.8A).

Exposure to malonate for 24 hours resulted in a significant reduction in primary cilia incidence (Figure 5.8B) at both 10μM (76.2% $\pm$ 10.4 v. 56.1% $\pm$ 9.0; $p=3.7\times10^{-10}$) and 100μM (57.2% $\pm$ 10.8; $p=6.9\times10^{-10}$). No difference was observed between the two concentrations tested (p=0.91).

Cilia length was also reduced in PC12 treated with malonate (Figure 5.8C). Again, this effect was observed at both 10μM (2.49μm $\pm$ 0.65 v. 1.98μm $\pm$ 0.67; $p=3.0\times10^{-8}$) and 100μM (1.99μm $\pm$ 0.64; $p=9.2\times10^{-8}$). As with incidence, no difference with length was observed between the two concentrations (p=0.98).

We next sought to confirm that this effect was due to malonate inhibition of SDH. The TCA cycle intermediate α-ketoglutarate prevents inhibition of SDH by malonate through binding site competition (MacKenzie *et al.* 2007). PC12 cells were exposed to serum-free media containing 100μM malonate alone or with 100μM α-ketoglutarate or vehicle-only control for 24 hours (Figure 5.9A).

As before, malonate only reduced cilia incidence (Figure 5.9B; 42.5% $\pm$ 7.7 v. 64.0% $\pm$ 9.0; $p=9.0\times10^{-6}$). However, when α-ketoglutarate was also applied, there was no significant change in ciliary incidence compared to vehicle-only control (57.0% $\pm$ 6.6; p=0.16 compared to vehicle-only control; p=0.0013 compared to malonate-only).

Similarly, malonate again resulted in cilia shortening (Figure 5.9C; 2.07μm $\pm$ 0.67 v. 2.47μm $\pm$ 0.50; p=0.15). This effect was not evident when cells were co-incubated with α-ketoglutarate (2.62μm $\pm$ 0.64; p=0.57 compared to vehicle-only control; $p=2.5\times10^{-5}$ compared to malonate-only).

Thus, α-ketoglutarate rescued malonate-induced changes in primary cilia.

SDH is a multimeric complex compromised of four subunits (A-D). Mutations in each subunit are associated with a predisposition to PPGL development (Table 2.1). In clinical practice, mutations in *SDHB* are particularly important as they are the most frequent and are associated with the highest malignancy rate (Benn *et al.* 2015).

We next performed siRNA-mediated knockdown of *SDHB* (Figure 5.10). PC12 cells were transfected with either *SDHB* targeting or non-targeting control siRNAs in serum-containing media and processed after 48 hours. SDHB protein expression was assessed in whole cell lysates by Western blot using antibodies against SDHB and glyceraldehyde 3-phosphate dehydrogenase (GAPDH) as a loading control (Figure 5.10A). SDHB protein expression was quantified relative to GAPDH (Figure 5.10B) and this confirmed knockdown relative to control siRNAs (0.30 AU $\pm$ 0.04 v. 1.00 AU $\pm$ 0.19; p=0.0035).

PC12 cells underwent transfection as above in serum-containing media and were processed for detection of primary cilia after 48 hours (Figure 5.10C). *SDHB* knockdown resulted in a reduction in both cilia incidence (Figure 5.10D; 20.1% $\pm$ 8.5 v. 46.6% $\pm$ 14.1; p=1.2x10^{-8}) and length (Figure 5.10E; 1.78µm $\pm$ 0.80 v. 2.20µm $\pm$ 0.62; p=0.0012).

In addition to its enzymatic function, SDH forms complex II of the ETC and its inhibition can result in uncoupling of the ETC and superoxide generation. Previous data in murine kidneys and liver have suggested that stimulation of superoxide formation alters primary cilia length, although not in a consistent manner (Kim *et al.* 2013; Han *et al.* 2016, 2017; Kong *et al.* 2019). We thus sought to examine whether the observed effect of SDH loss of function on PC12 primary cilia was due to superoxide formation.

PC12 cells were treated with either rotenone (a complex I inhibitor), antimycin A (a complex III inhibitor) or vehicle-only control (Figure 5.11A) in serum-free medium for 24 hours. Cilia incidence (Figure 5.11B) was not altered following administration of rotenone at either 0.05µM (64.8% $\pm$ 9.8 v. 69.6% $\pm$ 8.9; p=0.44) or 0.1µM (66.7% $\pm$ 9.7; p=0.84) or antimycin A at either 1µM (62.1% $\pm$ 14.5; p=0.07) or 10µM (65.8 $\pm$ 11.4; p=0.68). Likewise, cilia length (Figure 5.11C) was unaltered following treatment with rotenone at 0.05µM (2.27µm $\pm$ 0.61 v. 2.35µm $\pm$ 0.68; p=0.89) or 0.1µM (2.15µm $\pm$ 0.70; p=0.12) or antimycin A at either 1µM (2.28µm $\pm$ 0.70; p=0.93) or 10µM (2.22µm $\pm$ 0.76; p=0.46).

Thus, in PC12 cells, loss of SDH function appears to influence primary cilia dynamics due to pseudohypoxia and not due to superoxide formation.

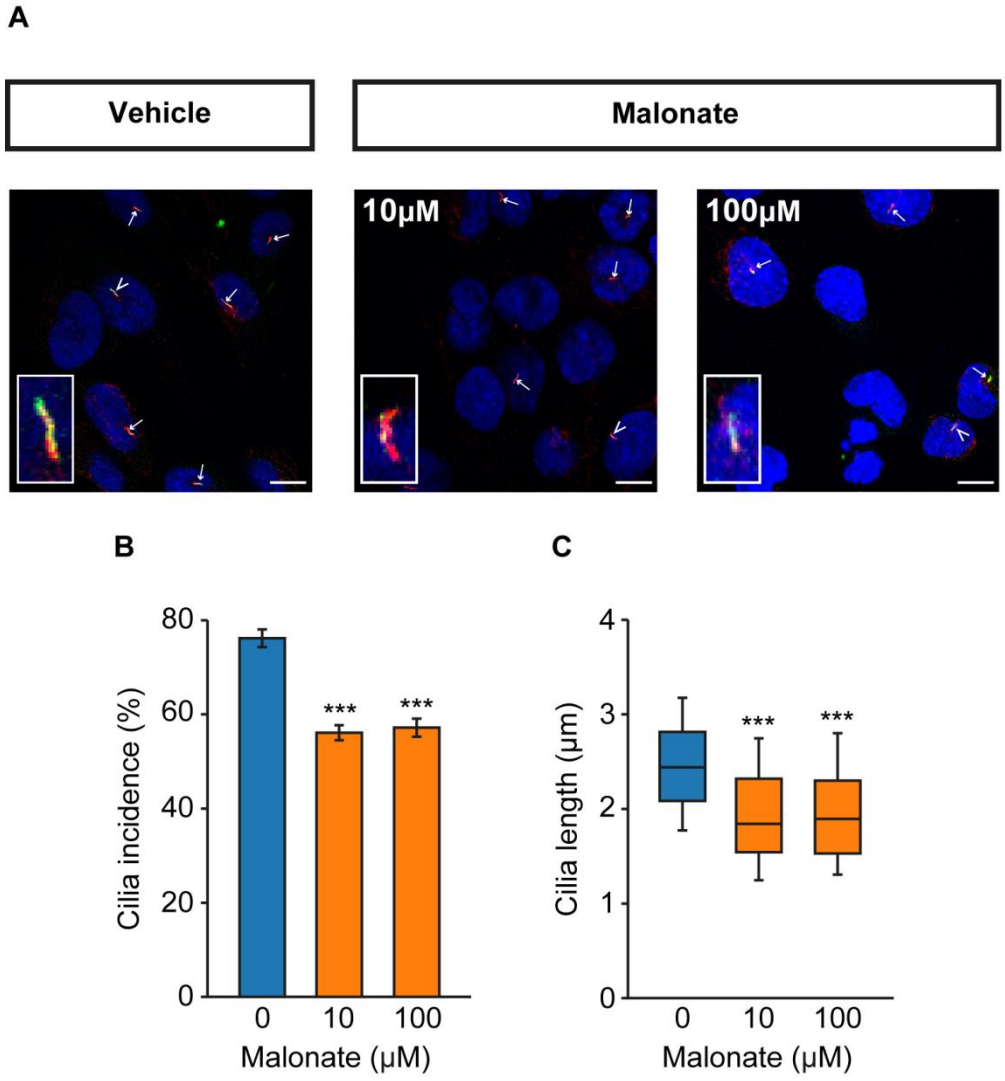

Figure 5.8: Inhibition of SDH by malonate results in reduced ciliary formation in PC12 cells

(A) Confocal images of PC12 cells exposed to serum-free media containing malonate at the concentrations indicated (or vehicle only control) for 24 hours. Cells were immunolabelled with anti-acetylated α-tubulin (red) and anti-Arl13b (green) for detection of primary cilia. Nuclei were stained with DAPI (blue). Cilia are indicated by arrows, or arrowheads where they are also shown zoomed in the insets. Scale bars = 10 μm.

Quantification of primary cilia incidence **(B)** and length **(C)** following treatment as per **(A)**. Error bars indicate $\pm$ SEM, boxes 25th, 50th and 75th centiles and whiskers the 10th and 90th centiles. Number of cells scored for incidence: 1288 $\pm$ 112 per condition. Number of cilia measured for length: 120 $\pm$ 7 per condition. Statistical significance was assessed using a one-way ANOVA compared to control. *** $p < 0.001$.

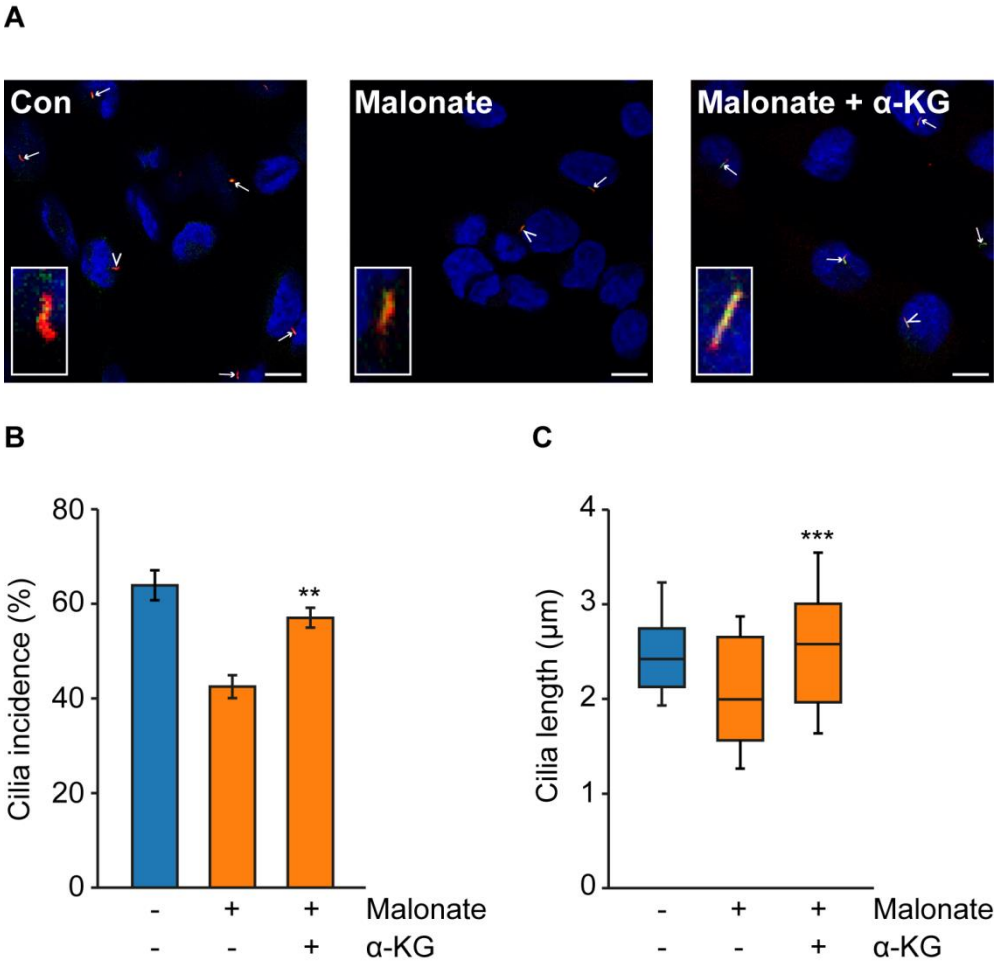

Figure 5.9: α-ketoglutarate prevents malonate induced changes in PC12 primary cilia

(A) Confocal images of PC12 cells exposed to serum-free media containing 100 µM malonate, 100 µM malonate and 100 µM α-ketoglutarate (α-KG) or vehicle only control (con) for 24 hours. Cells were immunolabelled with anti-acetylated α-tubulin (red) and anti-Arl13b (green) for detection of primary cilia. Nuclei were stained with DAPI (blue). Cilia are indicated by arrows, or arrowheads where they are also shown zoomed in the insets. Scale bars = 10 µm.

Quantification of primary cilia incidence **(B)** and length **(C)** following treatment as per **(A)**. Error bars indicate $\pm$ SEM, boxes 25th, 50th and 75th centiles and whiskers the 10th and 90th centiles. Number of cells scored for incidence: 1384 $\pm$ 275 per condition. Number of cilia measured for length: 126 $\pm$ 31 per condition. Statistical significance was assessed using a one-way ANOVA compared to malonate-only treatment. ** $p < 0.01$, *** $p < 0.001$.

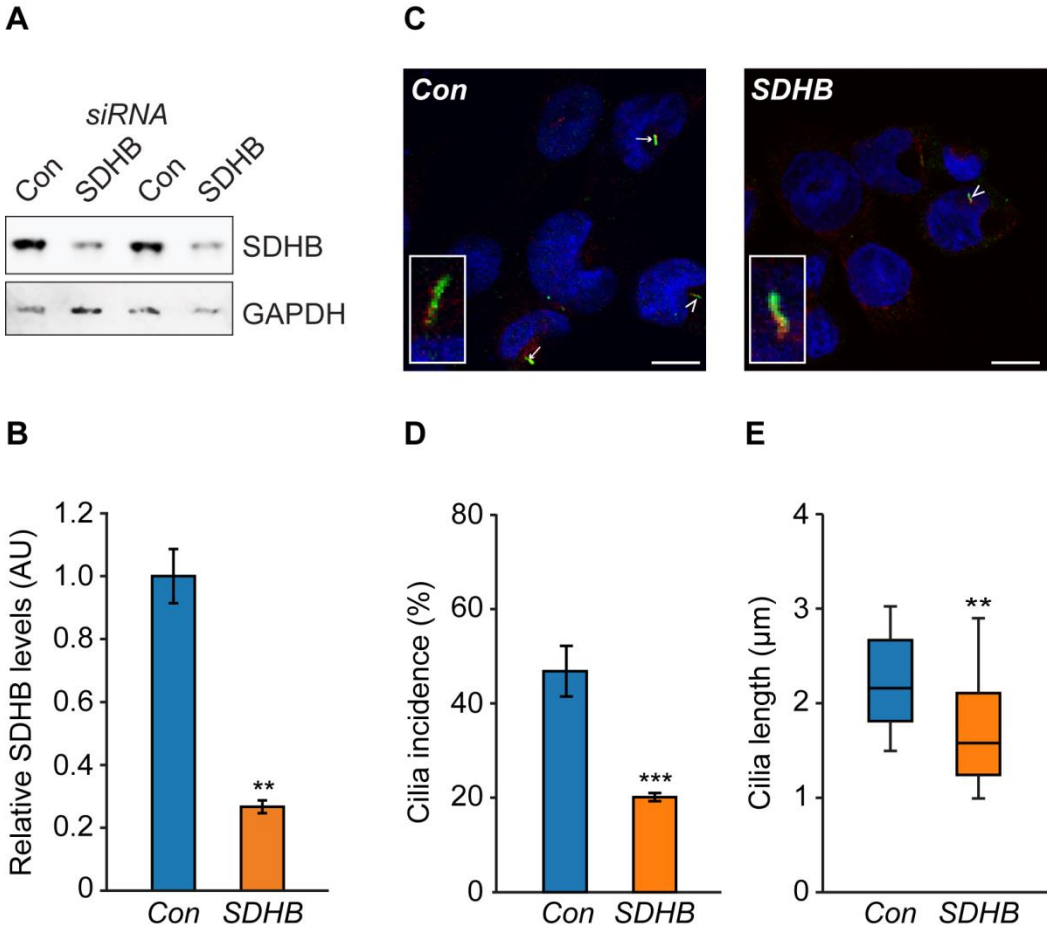

Figure 5.10: SDHB knockdown in PC12 cells reduces primary cilia incidence and length

Immunoblot **(A)** and densitometric analyses **(B)** of total cell lysates from PC12 cells transfected with SDHB targeting or non-targeting control siRNAs (Con) and probed with antibodies against SDHB and GAPDH as a loading control. SDHB protein level was normalised to GAPDH as arbitrary units (AU); n = 6.

(C) Confocal images of PC12 cells following treatment as per **(A)**. Cells were immunolabelled with anti-acetylated α-tubulin (red) and anti-Arl13b (green) for detection of primary cilia. Nuclei were stained with DAPI (blue). Cilia are indicated by arrows, or arrowheads where they are also shown zoomed in the insets. Scale bars = 10 µm.

Quantification of primary cilia incidence **(D)** and length **(E)** following treatment as per **(A)**. Error bars indicate $\pm$ SEM, boxes 25th, 50th and 75th centiles and whiskers the 10th and 90th centiles. Number of cells scored for incidence: 1342 $\pm$ 31 per condition. Number of cilia measured for length: 115 $\pm$ 35 per condition. Statistical significance was assessed using a Student's t test. ** p<0.01, *** p<0.001.

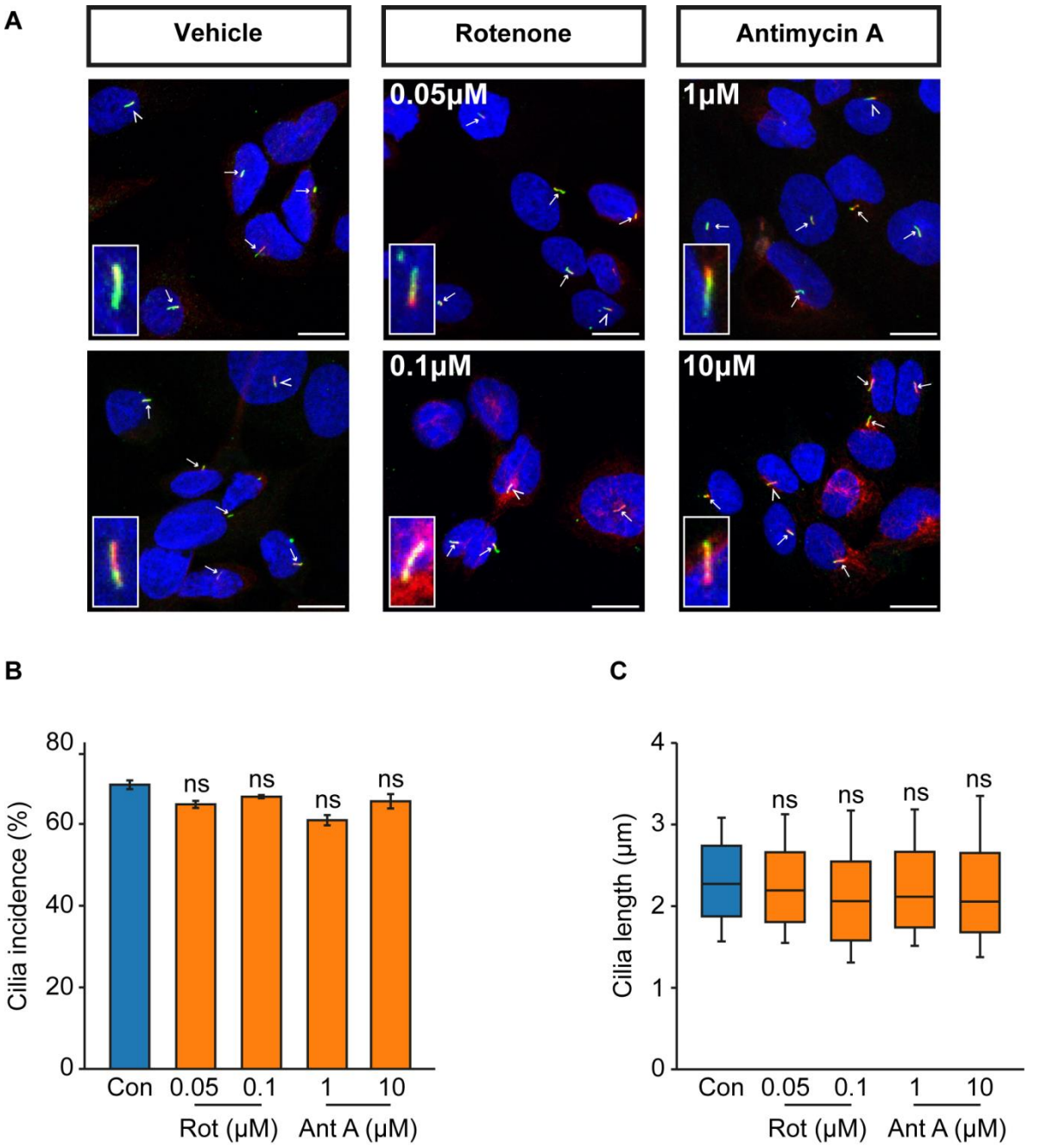

Figure 5.11: Inhibition of the electron transport chain does not affect PC12 primary cilia

(A) Confocal images of PC12 cells exposed to rotenone (Rot), antimycin A (Ant A) or vehicle-only control (Con) at the concentrations indicated for 24 hours. Cells were immunolabelled with anti-acetylated α-tubulin (red) and anti-Arl13b (green) for detection of primary cilia. Nuclei were stained with DAPI (blue). Cilia are indicated by arrows, or arrowheads where they are also shown zoomed in the insets. Scale bars = 10 µm.

Quantification of primary cilia incidence **(B)** and length **(C)** following treatment as per **(A)**. Error bars indicate ± SEM, boxes 25th, 50th and 75th centiles and whiskers the 10th and 90th centiles. Number of cells scored for incidence: 1199 ± 107 per condition. Number of cilia measured for length: 142 ± 18 per condition. Statistical significance was assessed using a one-way ANOVA compared to vehicle-only treatment. ns = not significant.

5.3.2.3 Pseudohypoxia achieved by loss of FH function results in cilia loss and shortening

Having demonstrated that pseudohypoxia due to loss of SDH function influenced primary cilia we sought to investigate whether other disease-relevant mechanisms also did so.

Fumarate hydratase (FH) follows SDH as the next enzyme in the TCA cycle and catalyses the conversion of fumarate to malate (Figure 2.5). Similarly to SDH, loss of FH function results in accumulation of a TCA cycle intermediate (fumarate) with resultant inhibition of HIF-PHDs. *FH* is a cluster 1 phaeochromocytoma predisposing gene (Castro-Vega *et al.* 2014).

First, PC12 cells were treated with serum-free media containing the cell-permeable derivative of fumarate, monomethyl fumarate (MMF), or vehicle-only control for 24 hours (Figure 5.12A).

Cilia incidence was reduced in PC12 cells treated with MMF (Figure 5.12B) at both 100μM (71.1% $\pm$ 12.8 v. 78.7% $\pm$ 11.6; p=0.028) and 200μM (66.2% $\pm$ 8.6; p=0.00011). There was no significant difference between the two concentrations tested (p=0.20). Cilia length was also reduced in MMF treated PC12 cells (Figure 5.12C) at both 100μM (2.30μm $\pm$ 0.77 v. 2.94μm $\pm$ 0.71; $p=3.9x10^{-14}$) and 200μM (2.22μm $\pm$ 0.87; $p=2.3x10^{-17}$). Again, no difference was observed between the two MMF concentrations (p=0.46).

In order to confirm these findings, we next performed siRNA-mediated knockdown of *FH* (Figure 5.13). PC12 cells were transfected with either *FH* targeting or non-targeting control siRNAs in serum-containing media and processed after 48 hours. FH protein expression was assessed in whole cell lysates by Western blot using antibodies against FH and β-actin as a loading control (Figure 5.13A). FH protein expression was quantified relative to β-actin (Figure 5.13B) and this confirmed knockdown relative to control siRNAs.

PC12 cells underwent transfection as above in serum-containing media and were processed for detection of primary cilia after 48 hours (Figure 5.13C). *FH* knockdown resulted in a reduction in both cilia incidence (Figure 5.13D; 39.7% $\pm$ 9.4 v. 55.7% $\pm$ 14.1; $p=3.1x10^{-6}$) and length (Figure 5.13E; 2.15μm $\pm$ 0.60 v. 2.34μm $\pm$ 0.68; $p=5.75x10^{-19}$).

Taken together, these results suggest that loss of FH function results in a reduction in primary cilia incidence and length. That the findings are consistent with those observed with loss of HIF-PHD and SDH function suggests that the underlying mechanism involves pseudohypoxia.

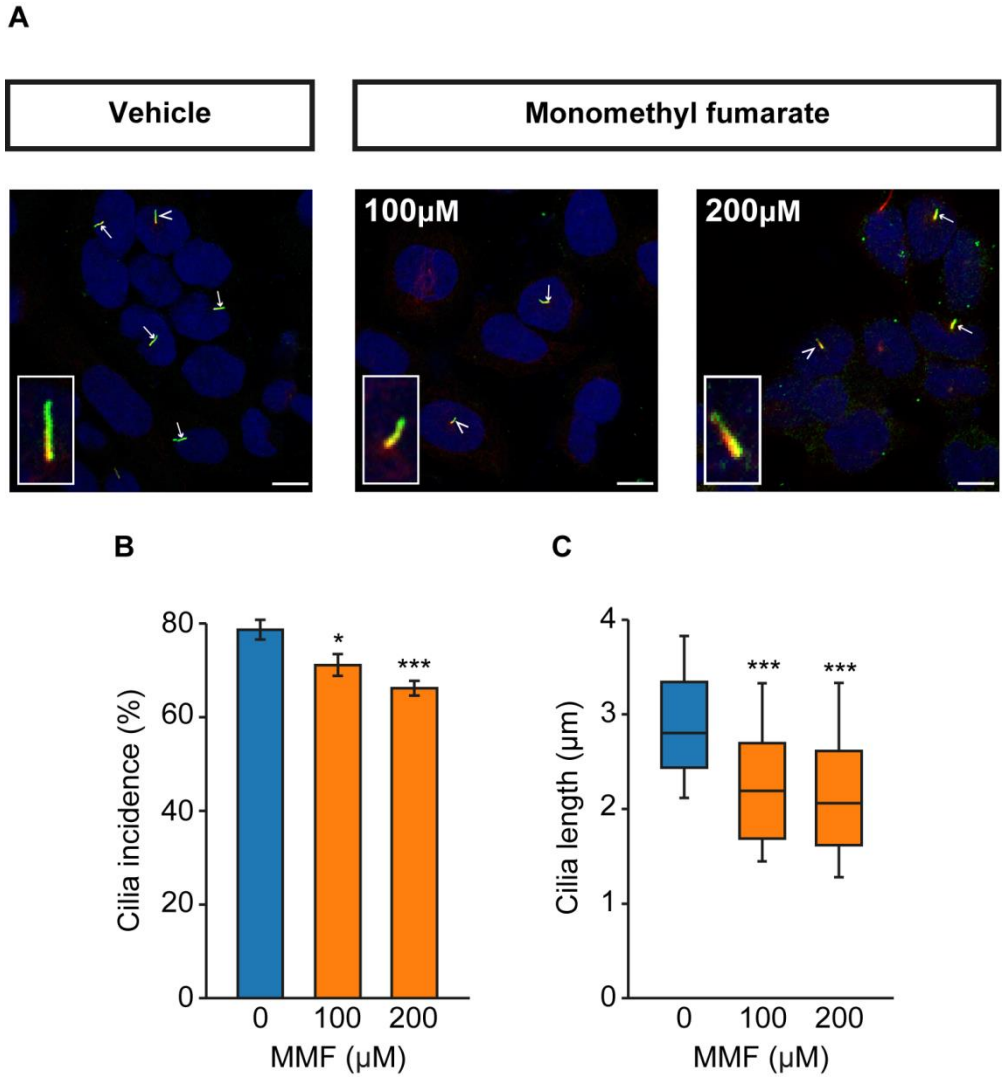

Figure 5.12: Monomethyl fumarate causes reduced ciliary formation in PC12 cells

(A) Confocal images of PC12 cells exposed to serum-free media containing monomethyl fumarate (MMF) at the concentrations indicated (or vehicle only control) for 24 hours. Cells were immunolabelled with anti-acetylated α-tubulin (red) and anti-Arl13b (green) for detection of primary cilia. Nuclei were stained with DAPI (blue). Cilia are indicated by arrows, or arrowheads where they are also shown zoomed in the insets. Scale bars = 10 µm.

Quantification of primary cilia incidence **(B)** and length **(C)** following treatment as per **(A)**. Error bars indicate $\pm$ SEM, boxes 25th, 50th and 75th centiles and whiskers the 10th and 90th centiles. Number of cells scored for incidence: 1706 $\pm$ 423 per condition. Number of cilia measured for length: 212 $\pm$ 61 per condition. Statistical significance was assessed using a one-way ANOVA compared to control. * $p<0.05$, *** $p<0.001$.

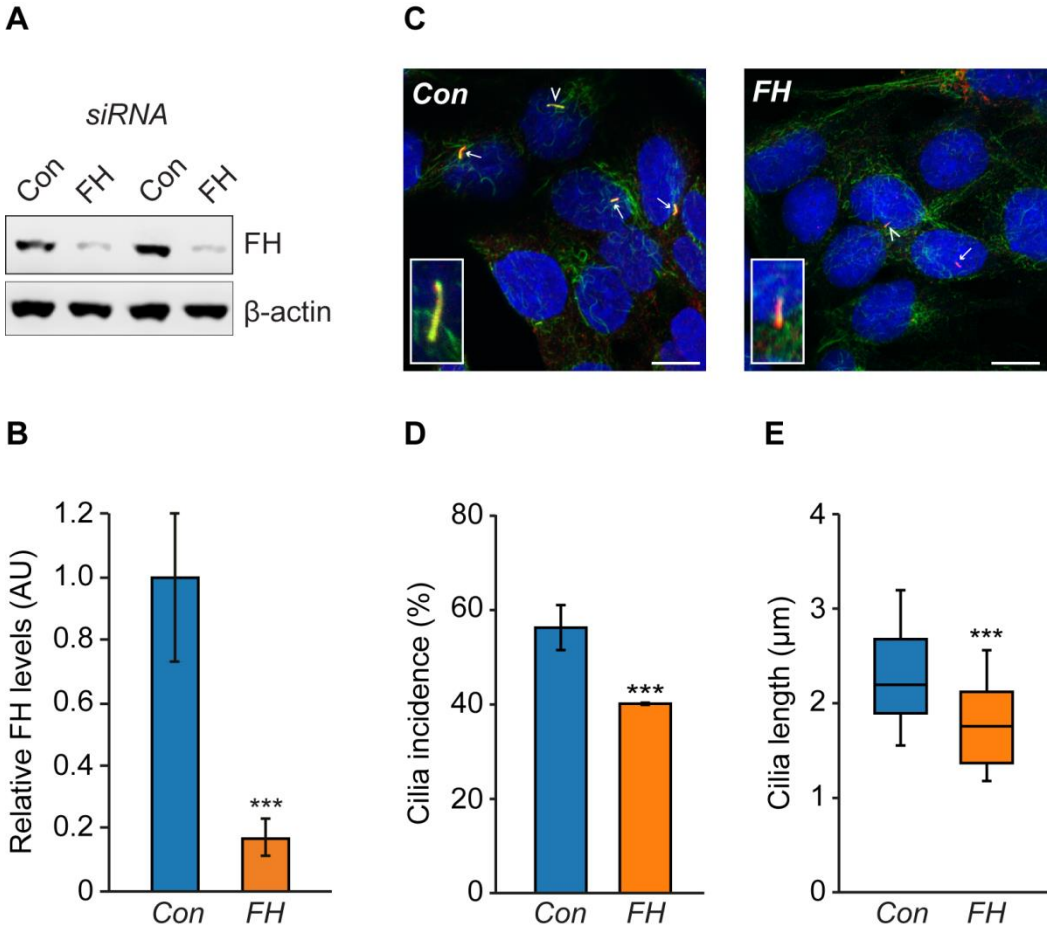

Figure 5.13: FH knockdown in PC12 cells reduces primary cilia incidence and length

Immunoblot **(A)** and densitometric analyses **(B)** of total cell lysates from PC12 cells transfected with FH targeting or non-targeting control siRNAs (Con) and probed with antibodies against FH and β-actin as a loading control. FH protein level was normalised to β-actin as arbitrary units (AU); n = 6.

(C) Confocal images of PC12 cells following treatment as per **(A)**. Cells were immunolabelled with anti-acetylated α-tubulin (red) and anti-Arl13b (green) for detection of primary cilia. Nuclei were stained with DAPI (blue). Cilia are indicated by arrows, or arrowheads where they are also shown zoomed in the insets. Scale bars = 10 µm.

Quantification of primary cilia incidence **(D)** and length **(E)** following treatment as per **(A)**. Error bars indicate $\pm$ SEM, boxes 25th, 50th and 75th centiles and whiskers the 10th and 90th centiles. Number of cells scored for incidence: 1669 $\pm$ 209 per condition. Number of cilia measured for length: 253 $\pm$ 21 per condition. Statistical significance was assessed using a Student's t test. *** $p<0.001$.

5.3.2.4 Pseudohypoxia achieved by loss of VHL function results in cilia loss and shortening

Having observed that loss of function of various upstream enzymes in the HIF degradation pathway influenced primary cilia, we next sought to investigate the final common effector in the pathway, namely VHL.

pVHL binds hydroxylated HIF and targets it for proteosomal-mediated degradation (Ivan *et al.* 2001; Jaakkola *et al.* 2001). Perturbations in primary cilia structure have been observed in renal cysts (Esteban *et al.* 2006) and ccRCCs (Schraml *et al.* 2009; Basten *et al.* 2013) in which VHL function has been lost.

PC12 cells were transfected with either *VHL* targeting or non-targeting control siRNAs in serum-containing media and processed after 48 hours. VHL protein expression was assessed in whole cell lysates by Western blot using antibodies against VHL and β-actin as a loading control (Figure 5.14A). VHL protein expression was quantified relative to β-actin (Figure 5.14B) and this confirmed knockdown relative to control siRNAs.

PC12 cells underwent transfection as above in serum-containing media and were processed for detection of primary cilia after 48 hours (Figure 5.14C). *VHL* knockdown resulted in a reduction in both cilia incidence (Figure 5.14D; 49.8% $\pm$ 8.8 v. 71.6% $\pm$ 9.6; $p=6.9\times10^{-13}$) and length (Figure 5.14E; 2.01μm $\pm$ 0.68 v. 2.56μm $\pm$ 0.72; $p=8.1\times10^{-14}$).

In summary, these data demonstrate that cilia loss in PC12 cells was induced by a number of different conditions that impair HIFα degradation, including those that lead to accumulation of oncometabolites.

In addition to its canonical function of HIF degradation, pVHL stabilises microtubules and plays a role in cilia maintenance (Okuda *et al.* 1999; Hergovich *et al.* 2003; Schermer *et al.* 2006). It has been reported previously that pVHL loss alone does not affect cilia structure, but may sensitise cells to lose pre-established cilia (Thoma *et al.* 2007). pVHL has been shown to localise to the ciliary axoneme (Schermer *et al.* 2006; Lolkema *et al.* 2008) and this was also the case in PC12 cells (Figure 5.15A). We hypothesised that hypoxia might result in changes in ciliary pVHL localisation.

In order to test this, PC12 cells were grown in serum-free media at 1% or 21% oxygen for 24 hours prior to fixation and immunofluorescence detection of acetylated α-tubulin and pVHL. Regions of interest of the ciliary axoneme were defined by immunolabelling for acetylated α-tubulin and levels of pVHL that localised within this area were determined by analysis of fluorescent intensity (Figure

5.15A). pVHL fluorescent intensity was reduced in the cilium of PC12 cells maintained at 1% oxygen compared to those at 21% (Figure 5.15B; 0.81AU $\pm$ 0.28 v. 1AU $\pm$ 0.37; p=0.023).

Thus, activation of hypoxic signalling may also destabilise cilia through a mechanism where pVHL is reduced in the ciliary axoneme.

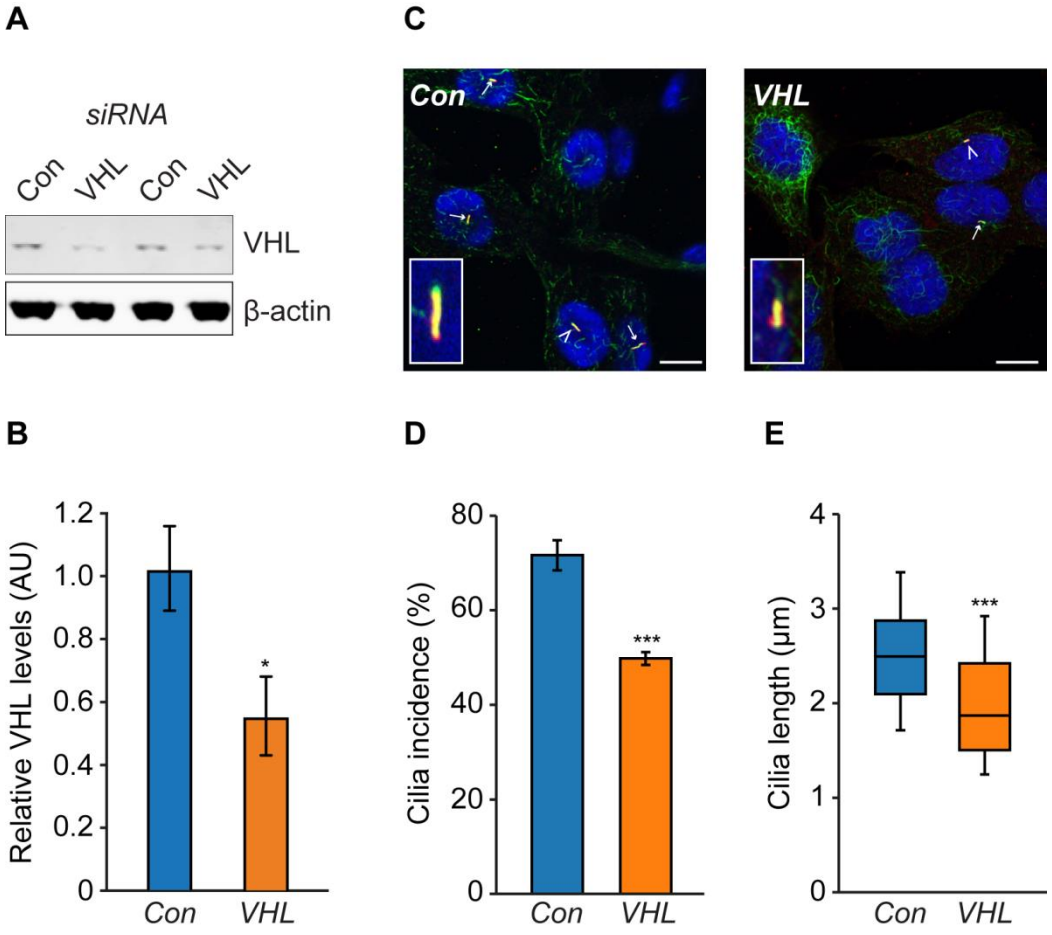

Figure 5.14: VHL knockdown in PC12 cells reduces primary cilia incidence and length

Immunoblot **(A)** and densitometric analyses **(B)** of total cell lysates from PC12 cells transfected with VHL targeting or non-targeting control siRNAs (Con) and probed with antibodies against FH and β-actin as a loading control. VHL protein level was normalised to β-actin as arbitrary units (AU); n = 6.

(C) Confocal images of PC12 cells following treatment as per **(A)**. Cells were immunolabelled with anti-acetylated α-tubulin (red) and anti-Arl13b (green) for detection of primary cilia. Nuclei were stained with DAPI (blue). Cilia are indicated by arrows, or arrowheads where they are also shown zoomed in the insets. Scale bars = 10 µm.

Quantification of primary cilia incidence **(D)** and length **(E)** following treatment as per **(A)**. Error bars indicate $\pm$ SEM, boxes 25th, 50th and 75th centiles and whiskers the 10th and 90th centiles. Number of cells scored for incidence: 1934 $\pm$ 65 per condition. Number of cilia measured for length: 193 $\pm$ 7 per condition. Statistical significance was assessed using a Student's t test. * $p<0.05$, *** $p<0.001$.

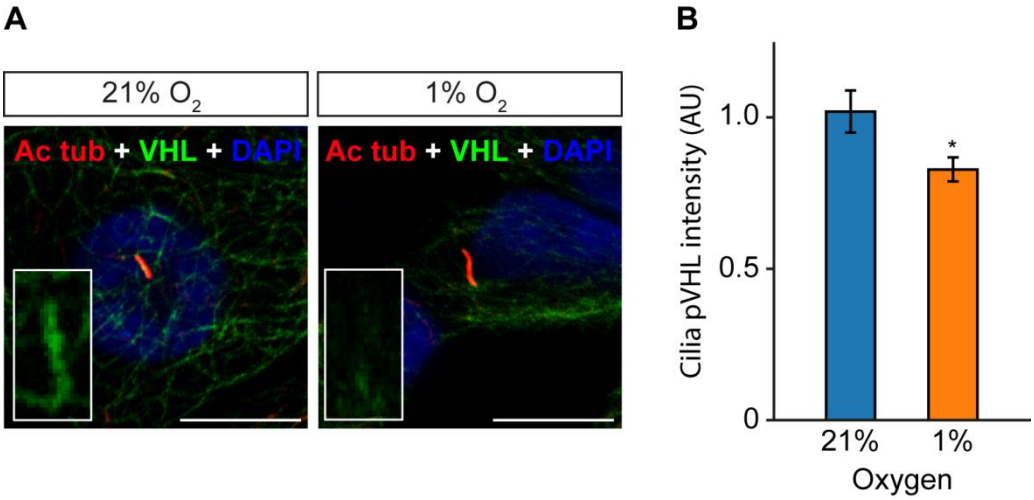

Figure 5.15: Ciliary localisation of pVHL is reduced by hypoxia

(A) Confocal images of PC12 cells that were cultured in 21% or 1% oxygen for 24 hours prior to fixation and immunolabelling for detection of primary cilia (anti-acetylated α-tubulin, red) and pVHL (green). Nuclei were counter-stained with DAPI (blue). Scale bars: 10µm.
(B) Quantification of the intensity of pVHL staining in axonemes (defined by the ciliary area of acetylated α-tubulin) in ciliated cells cultures as in **(A)**. AU arbitrary intensity. Number of cilia scored: 31 $\pm$ 3 per condition. Statistical significance was assed using a Student's t-test. * $p<0.05$.

5.3.2.5 Loss of SDHB and VHL in PC12 cells results in increased cellular proliferation

Thus we have demonstrated separately that loss of function of SDHB and VHL results in cilia loss and that cilia loss itself increases cellular proliferation in PC12 cells (Figure 4.10). We next sought to confirm that cilia loss due to knockdown of *SDHB* and *VHL* directly resulted in increased cellular proliferation.

PC12 cells were transfected as previously with siRNAs targeting *SDHB, VHL* or non-targeting controls. 48 hours after transfection cells were either fixed and immunolabelled for Ki67 (Figure 5.16A, B) or counted (Figure 5.16C).

The prevalence of Ki67 positive cells (Figure 5.16B) was increased by knockdown of both *VHL* (20.1% $\pm$ 4.0 v. 6.9% $\pm$ 1.0; $p=4.6\times10^{-6}$) and *SDHB* (24.5% $\pm$ 4.2; $p=2.7\times10^{-8}$). Cell number relative to time of transfection (Figure 5.16C) was also increased by knockdown of *VHL* (3.74 $\pm$ 0.09 v. 2.84 $\pm$ 0.15; p=0.027) and *SDHB* (4.20 $\pm$ 0.05; p=0.0086) compared to non-targeting controls.

These observations are consistent with pseudohypoxia-induced cilia loss contributing to increased cellular proliferation.

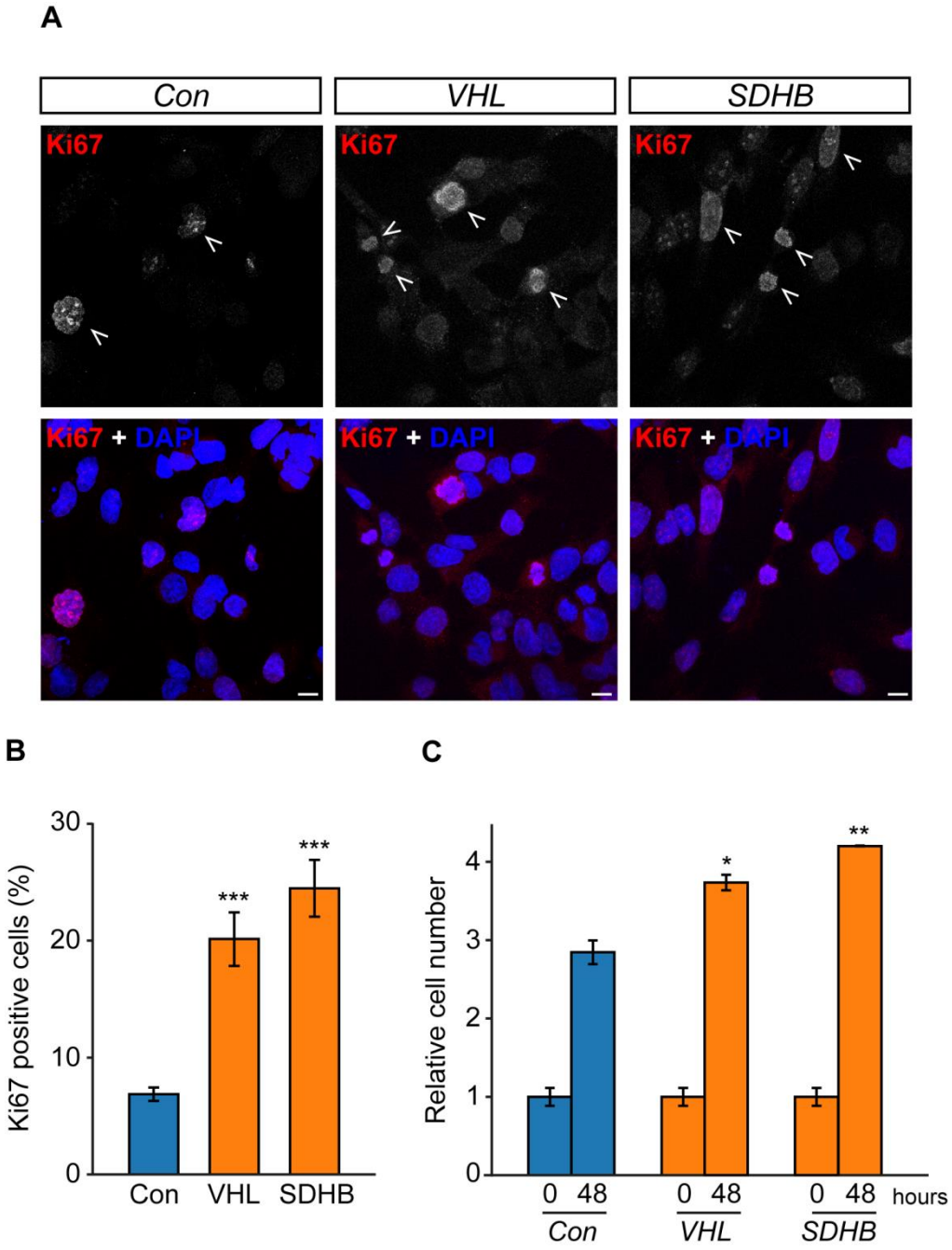

Figure 5.16: Knockdown of SDHB and VHL in PC12 cells results in increased proliferation

(A) Confocal images of PC12 cells 48 hours after transfection with siRNA against non-targeting control (Con), VHL or SDHB. Cells were immunolabelled with anti-Ki67 (red) and nuclei were stained with DAPI (blue). Arrowheads indicate Ki67 positive cells. Scale bars = 10 µm.

Quantification of Ki67 positive cells **(B)** and relative cell numbers **(C)** following treatment as per (A). Number of cells scored for Ki67 positivity: 1177 $\pm$ 403 per condition. Cell counting was performed on six samples from three biological replicates. Error bars indicate SEM. Statistical significance was assessed using a one-way ANOVA compared to control. * $p<0.05$, ** $p<0.05$ *** $p<0.001$.

5.3.2.6 Inhibition of both the AURKA/HDAC6 cilia resorption pathways and of hypoxic signalling prevents cilia loss in SDHB and VHL knockdown cells

We next hypothesised that the mechanism by which cilia incidence and length was reduced upon depletion of SDHB or VHL was the same as that seen with hypoxia.

First, we tested whether inhibition of HIF signalling prevented cilia loss in SDHB and VHL depleted cells. PC12 cells were transfected with siRNAs targeting *SDHB*, *VHL* or non-targeting controls as previously and then cultured in media containing FM19G11 or vehicle only control. 48 hours after transfection, cells were fixed and cilia immunolabelled for confocal microscopy (Figure 5.17A).

Following *SDHB* knockdown, cilia incidence was significantly increased in cells treated with FM19G11 compared to those treated with vehicle-only control (Figure 5.17B; 72.0% $\pm$ 11.5 v. 47.7% $\pm$ 10.2; $p=1.5x10^{-13}$). FM19G11 similarly increased cilia incidence in PC12 cells in which *VHL* had been knocked down (Figure 5.17D; 77.0% $\pm$ 10.2 v. 43.8% $\pm$ 8.7; $p=1.6x10^{-19}$). Cilia length was also increased by FM19G11 compared to vehicle-only control following knockdown of *SDHB* (Figure 5.17C; 2.65µm $\pm$ 0.83 v. 1.87µm $\pm$ 0.65; $p=1.2x10^{-28}$) and *VHL* (Figure 5.17E; 2.69µm $\pm$ 0.70 v. 2.03µm $\pm$ 0.66; $p=5.9x10^{-13}$).

Thus, in PC12 cells depleted of SDHB or VHL, cilia loss and shortening is ameliorated by inhibition of hypoxic signalling.

Next, we tested whether inhibition of the previously described AURKA/HDAC6 pathway prevented cilia loss in this context. PC12 cells were again transfected with siRNAs targeting *SDHB*, *VHL* or non-targeting controls and then cultured in media containing TSA, tubacin or PHA-680632 or vehicle only control. 48 hours after transfection, cells were fixed and cilia immunolabelled for confocal microscopy (Figure 5.17A).

Following *SDHB* knockdown, cilia incidence was significantly increased compared to vehicle-only control (Figure 5.17B) in PC12 cells treated with TSA (70.1% $\pm$ 9.6 v. 47.7% $\pm$ 10.2; $p=2.6x10^{-11}$), tubacin (70.1% $\pm$ 9.6; $p=7.4x10^{-12}$) and PHA-680632 (72.0% $\pm$ 11.5; $p=3.0x10^{-14}$). No significant difference was observed between the effect seen with any of the drug treatments (p=0.99 for TSA v. tubacin, p=0.87 for TSA v. PHA-680632, p=0.94 for tubacin v. PHA-680632).

The same pattern was observed with cilia incidence following AURKA/HDAC6 pathway inhibition in *VHL* knockdown cells (Figure 5.17D). Cilia incidence was increased by TSA (74.7% $\pm$ 10.0 v. 43.8% $\pm$ 9; $p=2.2x10^{-18}$), tubacin (67.9% $\pm$ 8.5; $p=4.2x10^{-14}$) and PHA-680632 (70.9% $\pm$ 12.2; $p=1.5x10^{-13}$).

Likewise with SDHB, there were no significant differences between these three drug treatments (p=0.14 for TSA v. tubacin, p=0.73 for TSA v. PHA-680632, p=0.90 for tubacin v. PHA-680632).

Cilia length was also increased compared to vehicle-only controls (Figure 5.17C) in SDHB depleted PC12 cells treated with TSA (2.56µm $\pm$ 0.65 v. 1.87µm $\pm$ 0.65; $p=7.5x10^{-25}$), tubacin (2.64µm $\pm$ 0.74; $p=1.2x10^{-28}$) and PHA-680632 (2.59µm $\pm$ 0.80; $p=3.8x10^{-27}$). Again, no between group differences were observed (p=0.80 for TSA v. tubacin, p=0.99 for TSA v. PHA-680632, p=0.97 for tubacin v. PHA-680632).

The same pattern was observed with regard to cilia length following AURKA/HDAC6 pathway inhibition in *VHL* knockdown cells (Figure 5.17E). Cilia length was increased compared to vehicle-only controls by TSA (2.44µm $\pm$ 0.70 v. 2.03µm $\pm$ 066; $p=2.0x10^{-7}$), tubacin (2.67µm $\pm$ 0.70; $p=5.8x10^{-13}$) and PHA-680632 (2.69µm $\pm$ 0.70; $p=5.8x10^{-13}$). There was no difference between tubacin and PHA-680632 treatment (p=0.99) but there was between TSA treated cells and tubacin (p=0.38) and PHA-680632 (p=0.16).

Taken together, these data indicate that the AURKA/HDAC6 pathway is a modulator of cilia loss in PC12 cells depleted for SDHB or VHL and that this process appears to be dependent on HIF signalling.

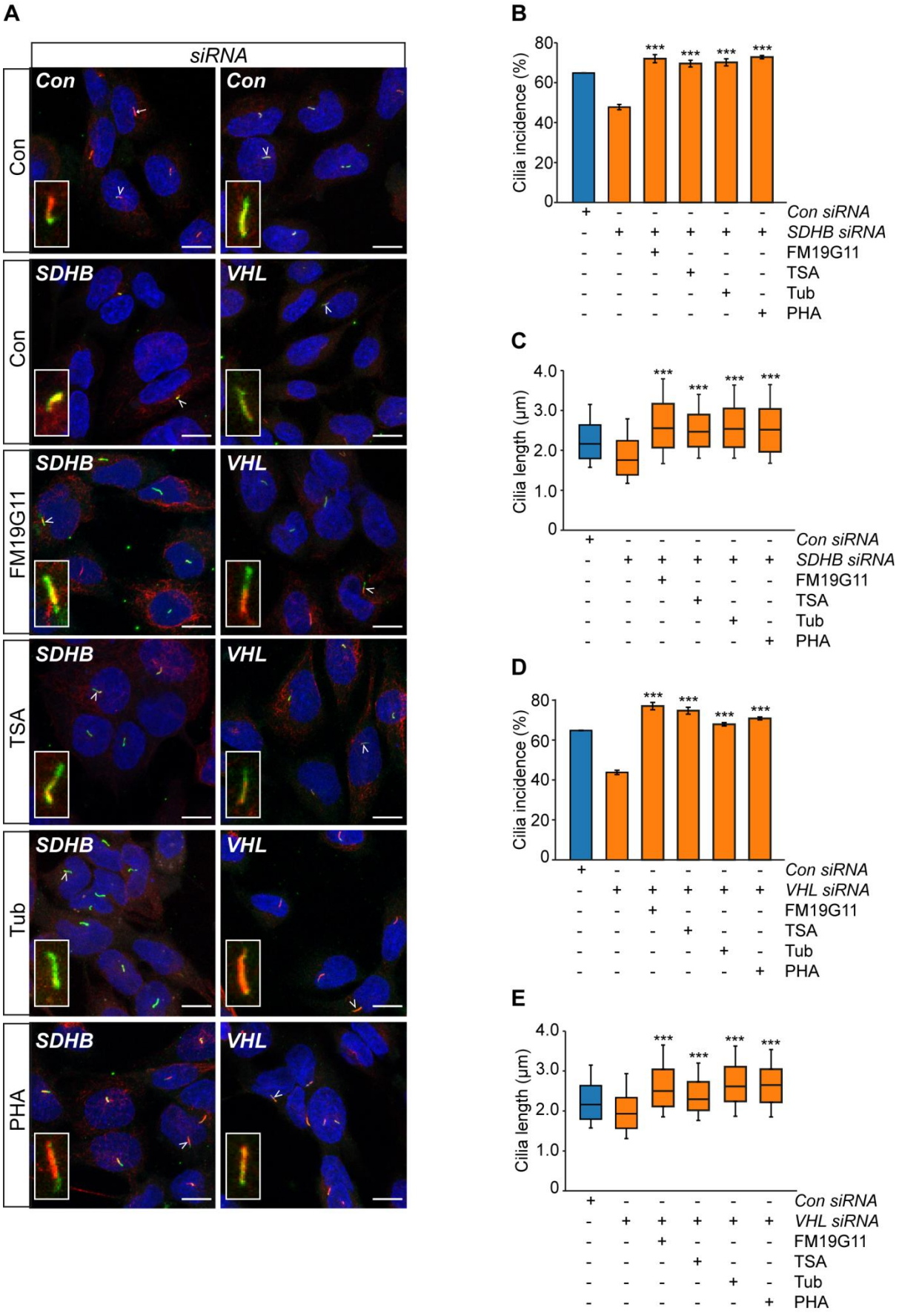
A
siRNA
Con
Con
Con
SDHB
VHL
FM19G11
SDHB
VHL
TSA
SDHB
VHL
Tub
SDHB
VHL
PHA
SDHB
VHL
B
Cilia incidence (%)
0
20
40
60
80
***
Con siRNA
SDHB siRNA
FM19G11
TSA
Tub
PHA
C
Cilia length (μm)
0
1.0
2.0
3.0
4.0
***
Con siRNA
SDHB siRNA
FM19G11
TSA
Tub
PHA
D
Cilia incidence (%)
0
20
40
60
80
***
Con siRNA
VHL siRNA
FM19G11
TSA
Tub
PHA
E
Cilia length (μm)
0
1.0
2.0
3.0
4.0
***
Con siRNA
VHL siRNA
FM19G11
TSA
Tub
PHA

Figure 5.17: Inhibition of cilia resorption and hypoxic signalling prevents cilia loss caused by knockdown of SDHB and VHL

(A) Confocal images of PC12 cells 48 hours after transfection with siRNAs targeting SDHB or VHL in the presence or absence of the inhibitors FM19G11, TSA, tubacin (Tub) and PHA-680632 (PHA), or vehicle only controls. Cells were immunolabelled with anti-acetylated α-tubulin (red) and anti-Arl13b (green) for detection of primary cilia. Nuclei were stained with DAPI (blue). Cilia are indicated by arrows, or arrowheads where they are also shown zoomed in the insets. Scale bars = 10 μm

Quantification of primary cilia incidence **(B, D)** and length **(C, E)** 48 hours after transfection with siRNAs targeting SDHB **(B, C)** or VHL **(D, E)** and drug treatments as per **(A)**. Error bars indicate $\pm$ SEM, boxes 25th, 50th and 75th centiles and whiskers the 10th and 90th centiles. Number of cells scored for incidence: 1873 $\pm$ 200 per condition. Number of cilia measured for length: 231 $\pm$ 50 per condition. Statistical significance was assessed using a one-way ANOVA compared to control. *** $p<0.001$.

5.3.3 The effects of catecholamines and metanephrines on phaeochromocytoma primary cilia

Having identified that two key components of the phaeochromocytoma tumour microenvironment (namely hypoxia and pseudohypoxia) influenced primary cilia, we sought to examine other features. We first considered the secretory product of these tumours: catecholamines and metanephrines.

5.3.3.1 The effect of circulating metanephrines on human phaeochromocytoma primary cilia incidence and length

For the patients previously described in chapter 4, we obtained available diagnostic pre-operative biochemistry and analysed whether the type or magnitude of metanephrine secretion influenced phaeochromocytoma primary cilia incidence or length. Patients were recruited from a number of different centres with differing clinical practices including whether measurement of metanephrines was in urine or plasma and with different reference ranges depending on the method of quantification. In order to allow magnitude comparisons between patients from different centres, magnitude was expressed as a proportion compared to the upper limit of the normal reference range (ULN).

Using linear regression analysis, cilia incidence and length were compared with the magnitude of elevation for each individual metanephrine (normetanephrine, metanephrine and 3-methoxytyramine), as displayed in Figure 5.18. There was no statistically significant relationship between tumoural cilia incidence and concentration of normetanephrine, metanephrine or 3-methoxytyramine (Figure 5.18A, C, E; p = 0.71, 0.19 and 0.65 respectively). Similarly, p values did not reach significance when comparing cilia length and normetanephrine and 3-methoxytyramine (Figure 5.18B, F; p =0.74 and 0.71 respectively). However, pre-operative metanephrine elevation was positively correlated with tumoural cilia length (Figure 5.18D, r^2 = 0.0868, p=0.0445).

The absolute magnitude of each individual metanephrine is not constant due to variable tumoural secretion. Furthermore, commonly used medications in the care of patients with phaeochromocytomas can alter measured metanephrine concentrations due to either analytical interference in some assays (e.g. paracetamol) or pharmacodynamic interference regardless of the methodology of measurement (e.g. phenoxybenzamine) (Lenders *et al.* 2014). Given these variables and the unpredictable degree with which they might alter absolute metanephrine concentrations on a given day, we also considered whether tumoural cilia incidence and length might be related to any elevation of circulating metanephrine.

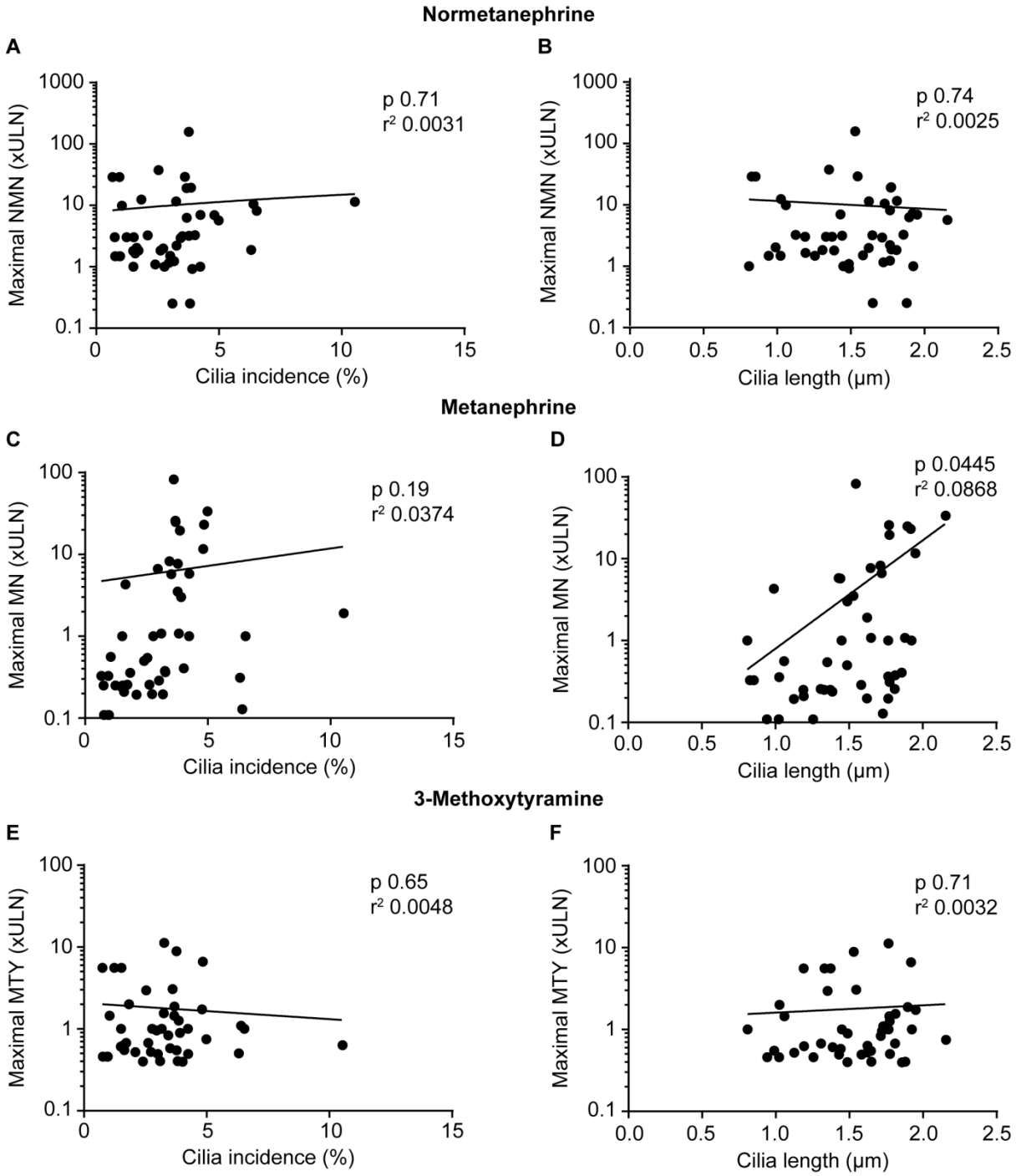

Figure 5.18: Phaeochromocytoma primary cilia length is correlated with circulating metanephrine concentration.

Data are presented from the 47 phaeochromocytomas and paragangliomas previously described in chapter 4. Cilia incidence **(A, C, E)** and length **(B, D, F)** were calculated and plotted against the pre-operative concentration of normetanephrine (NMN; **A, B**), metanephrine (MN; **C, D**) and 3-methoxytyramine (MTY; **E, F**) expressed as a proportion of the upper limit of normal (ULN) of the reference range. N = 47 tumours for NMN and MN (**A-D**) and 45 for MTY (**E, F**). r^2 values were calculated using linear regression analysis. Only cilia length and MN (**D**) reached a statistically significant p value (p=0.0445).

All tumours were classified according to whether each constituent metanephrine (measured in the urine or plasma) was within or above the assay-specified reference range. Using this approach, in accordance with the findings in Figure 5.18, cilia length was significantly higher in those tumours with any elevation of metanephrine (Figure 5.19D; 1.64µm ± 0.31 compared to 1.38µm ± 0.31, p=0.0074). In addition, cilia incidence was also greater in those tumours with elevated metanephrine (Figure 5.19C; 4.06% ± 1.80 compared to 2.29% ± 1.54, p=0.0007).

There was no significant difference in cilia incidence or length in tumours associated with elevated normetanephrine (Figure 5.19A, B; p=0.64 and 0.37 respectively) or 3-methoxytyramine (Figure 5.19E, F; p=0.66 and 0.30 respectively). It should be noted that there were only three tumours with non-elevated normetanephrine and this small group size makes meaningful comparisons difficult.

Phaeochromocytomas often produce more than one type of metanephrine. In the group studied, 24 of 47 tumours (51.1%) produced multiple metanephrines (70.8% of which produced two and the remaining 29.2% produced all three). Having identified that tumours with elevated metanephrine had increased cilia incidence and length compared to those with elevated normetanephrine and 3-methoxytyramine, we wanted to see whether this effect was preserved in tumours that produced multiple metanephrines.

There was no significant difference between cilia incidence or length depending on the predominant metanephrine produced (Figure 5.20 A, B), although in accordance with previous results, there was a trend towards metanephrine-predominant tumours to have more abundant (3.63% ± 0.79 v. 3.10% ± 2.32, p=0.8234) and longer cilia (1.69µm ± 0.28 v. 1.43µm ± 0.34, p=0.0925) compared to normetanephrine-predominant tumours. It should be noted that the other two subgroups (non-secretory and 3-methoxytyramine-predominant tumours) both had small sample sizes (3 and 4 respectively).

Similarly, when the profile of metanephrine production was considered (Figure 5.20 C-F), no statistically significant difference between groups was identified. There was, however, a trend towards increasing cilia incidence (3.55% ± 2.03 v. 2.64% v. 1.68, p=0.2494) and length (1.57µm ± 0.31 v. 1.43µm ± µm ± 0.35, p=0.36) in tumours producing multiple compared to a single metanephrine only.

Taken together, these results suggest that adrenaline or its metabolite metanephrine may be correlated with primary cilia incidence and length in human phaeochromocytomas, although any relationship is clearly complex with multiple potential confounders.

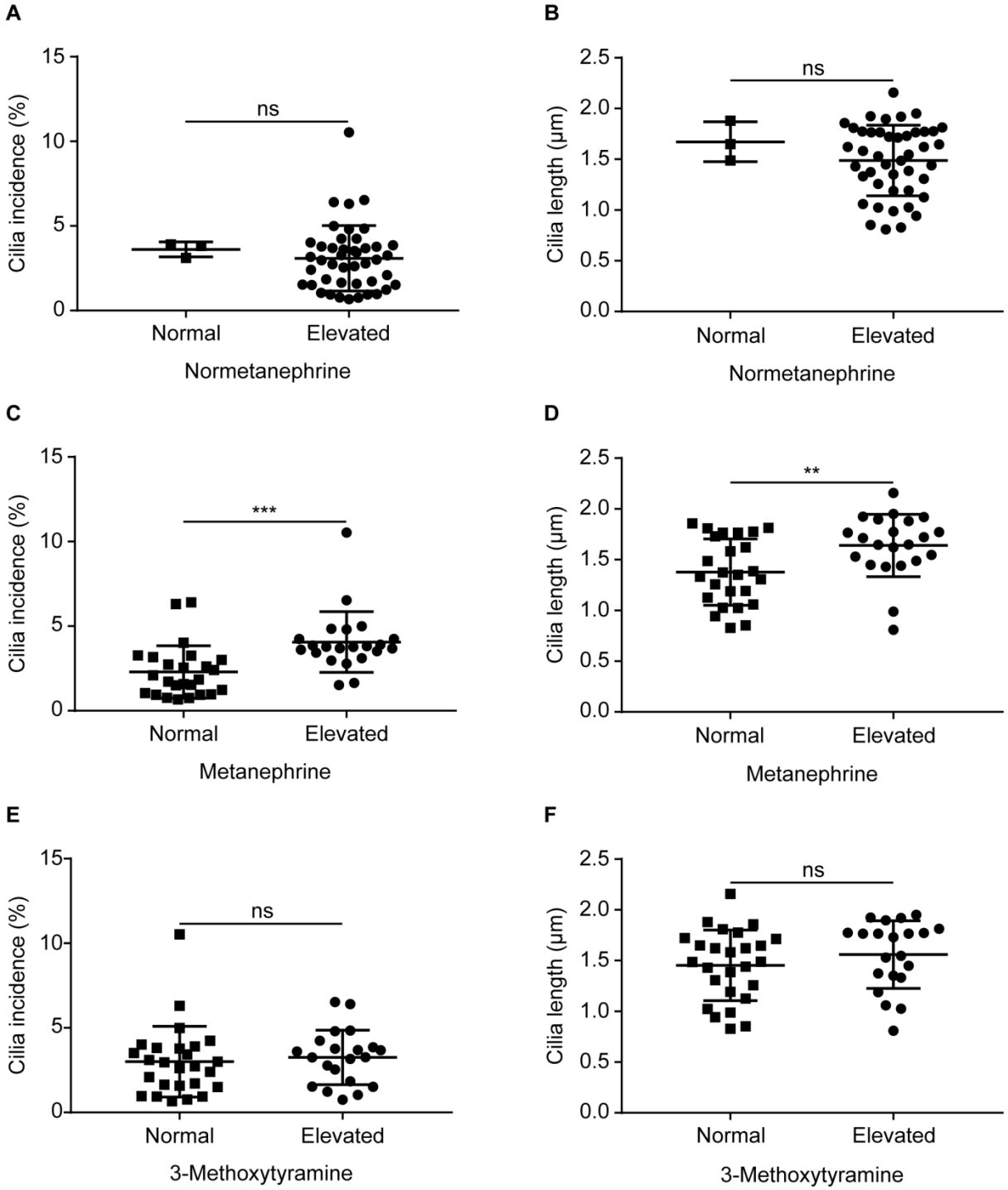

Figure 5.19: Phaeochromocytoma primary cilia incidence and length is correlated with elevated circulating metanephrine.

Data are presented from the 47 phaeochromocytomas and paragangliomas previously described in Chapter 4. Cilia incidence **(A, C, E)** and length **(B, D, F)** were calculated and plotted against normetanephrine **(A, B)**, metanephrine **(C, D)** and 3-methoxytyramine **(E, F)** and whether they were elevated or within the reference range. N = 47 tumours for normetanephrine and metanephrine **(A-D)** and 45 for 3-methoxytyramine **(E, F)**. Centre bar represents mean, error bars standard deviation. Statistical significance was assessed using an unpaired two-tail t test. Ns = not significant, ** $p<0.01$, *** $p<0.001$.

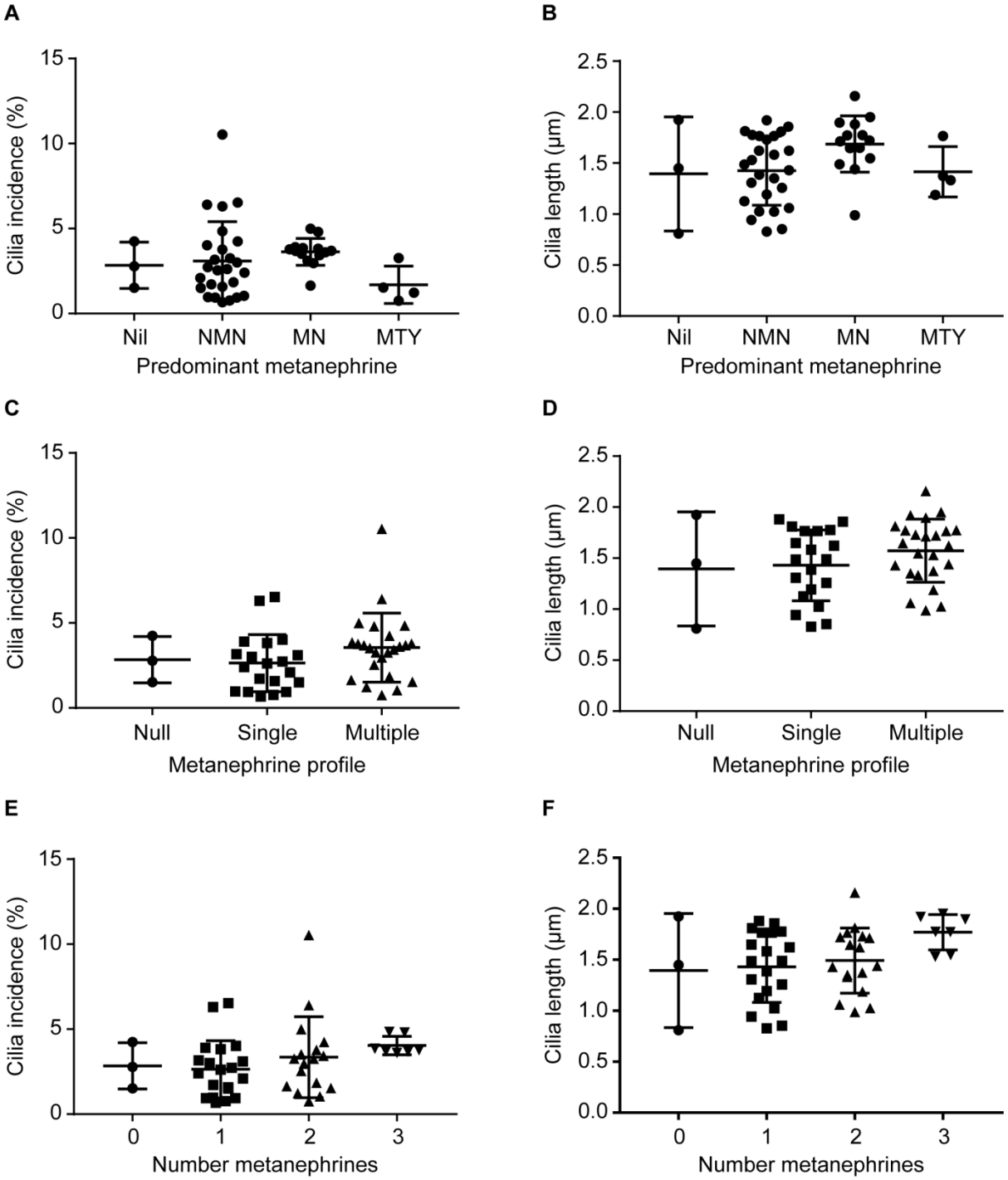

Figure 5.20: Phaeochromocytoma primary cilia incidence and length in vivo is not related to predominant or number of metanephrines secreted

Data are presented from the 47 phaeochromocytomas and paragangliomas previously described in chapter 4. Cilia incidence **(A, C, E)** and length **(B, D, F)** were calculated and plotted according to the predominant metanephrine **(A, B)** or the number of different metanephrines produced **(C-F)**. NMN = normetanephrine, MN = metanephrine, MTY = 3-methoxytyramine. N = 47. Centre bar represents mean, error bars standard deviation. Statistical significance was assessed using a one-way ANOVA.

5.3.3.2 The effect of catecholamines on primary cilia incidence and length in rat phaeochromocytoma-derived PC12 cells

Having observed that circulating metanephrine was correlated with phaeochromocytoma primary cilia incidence and length, we sought to further investigate the effects of catecholamines on primary cilia.

5.3.3.2.1 Adrenaline increases incidence and length of primary cilia in PC12 cells via the beta adrenoceptor

The catecholamines adrenaline and noradrenaline exert their action via the alpha and beta adrenoceptors. These are G-protein coupled receptors with a number of subtypes defined by their coupled G-protein and agonist sensitivity which have a range of differing tissue localisations and physiological functions (Figure 2.3).

There is extremely limited data about the effect of adrenaline and noradrenaline on primary cilia. The β_2-adreneroceptor has been shown to localise to primary cilia in murine neurons (Yao *et al.* 2016), whilst it is excluded from primary cilia in murine inner medullary collecting duct cells (Marley *et al.* 2013). Although little has been published on the effects of catecholamines on primary cilia, they are known to be stimulatory to the related motile cilia in bronchial (Weiterer *et al.* 2015) and tracheal (Bailey *et al.* 2014) epithelium.

Given the observation that ciliary incidence and length were increased in phaeochromocytomas that secreted metanephrine (Figure 5.19 C-D), the metabolite of adrenaline, we first sought to evaluate the effect of adrenaline on primary cilia in the context of the rat PC12 phaeochromocytoma cell line. PC12 cells were exposed to increasing concentrations of adrenaline in serum-free media for 24 hours prior to fixation and immunolabelling to detect primary cilia (Figure 5.21A).

Cilia incidence was increased in PC12 cells exposed to all concentrations of adrenaline tested (1nM – 100µM) compared to vehicle only control (Figure 5.21B; e.g. 67.2% $\pm$ 11.6 for 1nM compared to 44.8% $\pm$ 12.5; $p=3.4x10^{-5}$) with the greatest effect being observed at 100 nM (68.2% $\pm$ 10.7; $p=1.2x10^{-5}$). No difference was seen between the different concentrations of adrenaline tested. Increased cilia length was observed at most concentrations tested (2.36µm $\pm$ 0.70 compared to 2.76µm $\pm$ 0.90 for 1nM, p=0.047; 2.90µm $\pm$ 1.17 for 100nM, p=0.0002; 2.72µm $\pm$ 0.92 for 1µM, p=0.0034; 2.89µm $\pm$ 0.88 for 100µM, p=0.0011). In the two concentrations where significance was not reached, there was a trend to increased cilia length (p= 0.16 for 10nM; 0.28 for 10µM). Again, no difference was observed between the different adrenaline concentrations tested.

Thus, the administration of extracellular adrenaline to PC12 cells resulted in increases in ciliary incidence and length. Activation of both alpha and beta adrenoceptors are linked to mechanisms that have previously been shown to influence cilia length (Figure 2.3). Stimulation of alpha receptors results in intracellular calcium influx and activation of PKC via the G_q/PLC/IP3/DAG signalling cascade (reviewed in (Insel 1989)), whilst beta receptor activation results in increases in cAMP and Protein Kinase A (PKA) activity via the G_s/AC cascade (reviewed in (Wallukat 2002)). Therefore we utilised non-selective alpha and beta receptor antagonists in order to delineate the receptor subtype responsible for the observed adrenaline-mediated ciliary changes in PC12 cells.

Phenoxybenzamine is a non-selective irreversible alpha adrenoceptor antagonist whilst propranolol is a non-selective beta adrenoceptor antagonist. Together they form the cornerstone of medical treatment of phaeochromocytomas in preparation for surgery or when inoperable to reduce the risk of catecholamine-mediated surges and vascular events. PC12 cells were exposed to either phenoxybenzamine or propranolol at varying concentrations for one hour prior to washing and exposure to 1µM adrenaline for 24 hours in serum-free conditions. Cells were then fixed and immunolabelled to detect primary cilia (Figure 5.22A). Adrenaline and vehicle only controls were utilised for comparison.

There was no difference between cilia incidence in cells that had been pre-treated with phenoxybenzamine at all concentrations tested (10nM – 1µM) compared to those exposed to adrenaline alone (Figure 5.22B; p=0.87 for 10nM, 0.99 for 100nM and 0.98 for 1µM). However, when PC12 cells were exposed to propranolol prior to adrenaline, cilia incidence was significantly shorter at all concentrations tested (10nM – 1µM) compared to those exposed to adrenaline alone (Figure 5.22B; 60.2% $\pm$ 13.2 compared to 48.4 % $\pm$ 6.2 for 10nM, p=0.0105; 49.4 % $\pm$ 12.7 for 100nM, p=0.0300; 45.3 % $\pm$ 12.6 for 1µM, p=0.0035). There was no difference between cilia incidence in cells exposed to propranolol and adrenaline and those exposed to neither (p=0.99 for 10nM, 0.97 for 100nM and 0.99 for 1µM).

Cilia length was not significantly different in PC12 cells pre-treated with phenoxybenzamine compared to those without pre-treatment (Figure 5.22C; 2.72µm $\pm$ 0.92) at concentrations of 10nM (2.39µm $\pm$ 0.64, p=0.073) and 1µM (2.39µm $\pm$ 0.55, p=0.092) but not at 100nM when cilia were significantly shorter (2.34µm $\pm$ 0.52, p=0.023). In the same pattern as was observed with cilia incidence, PC12 pre-treated with propranolol had significantly shorter cilia than those without (Figure 5.22C; 2.72µm $\pm$ 0.92 compared to 2.29µm $\pm$ 0.72 for 10nM, p=0.024; 2.03µm $\pm$ 0.71 for 100nM, p=2.3 $x10^{-8}$; 2.16µm $\pm$ 0.66 for 1µM, p=4.5 x 10^{-6}). Similarly, there was no difference

between cilia length in cells exposed to propranolol and adrenaline and those exposed to neither (p=0.99, 0.10 and 0.70 respectively).

Thus, beta but not alpha adrenoceptor blockade prevents adrenaline-induced increases in cilia incidence and length, suggesting that the mechanism by which this occurs is dependent on the beta adrenoceptor.

Thus, we hypothesised that activation of the beta receptor by an alternative means would also result in increases in ciliary incidence and length. In order to test this, we utilised the β_2 receptor agonist salbutamol. PC12 cells were exposed to salbutamol or vehicle only control in serum-free conditions for 24 hours prior to fixation and immunolabelling for primary cilia (Figure 5.23A).

Cilia incidence was increased in PC12 cells treated with salbutamol at both concentrations tested (1 and 10nM) compared to vehicle only control (Figure 5.23B; 50.3% $\pm$ 7.0 compared to 64.7% $\pm$ 14.3 for 1nM, p=0.032; 60.6% $\pm$ 12.3 for 10 nM, p = 0.041). There was no significant difference between the effects seen at 1 and 10nM (p=0.84). Cilia length was similarly increased in PC12 cells exposed to salbutamol compared to vehicle only control (Figure 5.23C; 1.87µm $\pm$ 0.39 compared to 2.50µm $\pm$ 0.55 for 1nM, p=1.35 $x10^{-6}$; 2.30µm $\pm$ 0.45 for 10nM, p=0.00363). Again, there was no difference between the two salbutamol concentrations (p=0.21).

Taken together, these observations suggest that adrenaline increases cilia incidence and length in PC12 cells via action on the beta adrenoceptor, probably subtype 2. This is the first record of the effect of adrenaline on primary cilia, although the proposed mechanism is in keeping with that seen in motile cilia (Bailey *et al.* 2014; Weiterer *et al.* 2015) and is supported by ciliary localisation of the β_2-adrenoceptor (Yao *et al.* 2016).

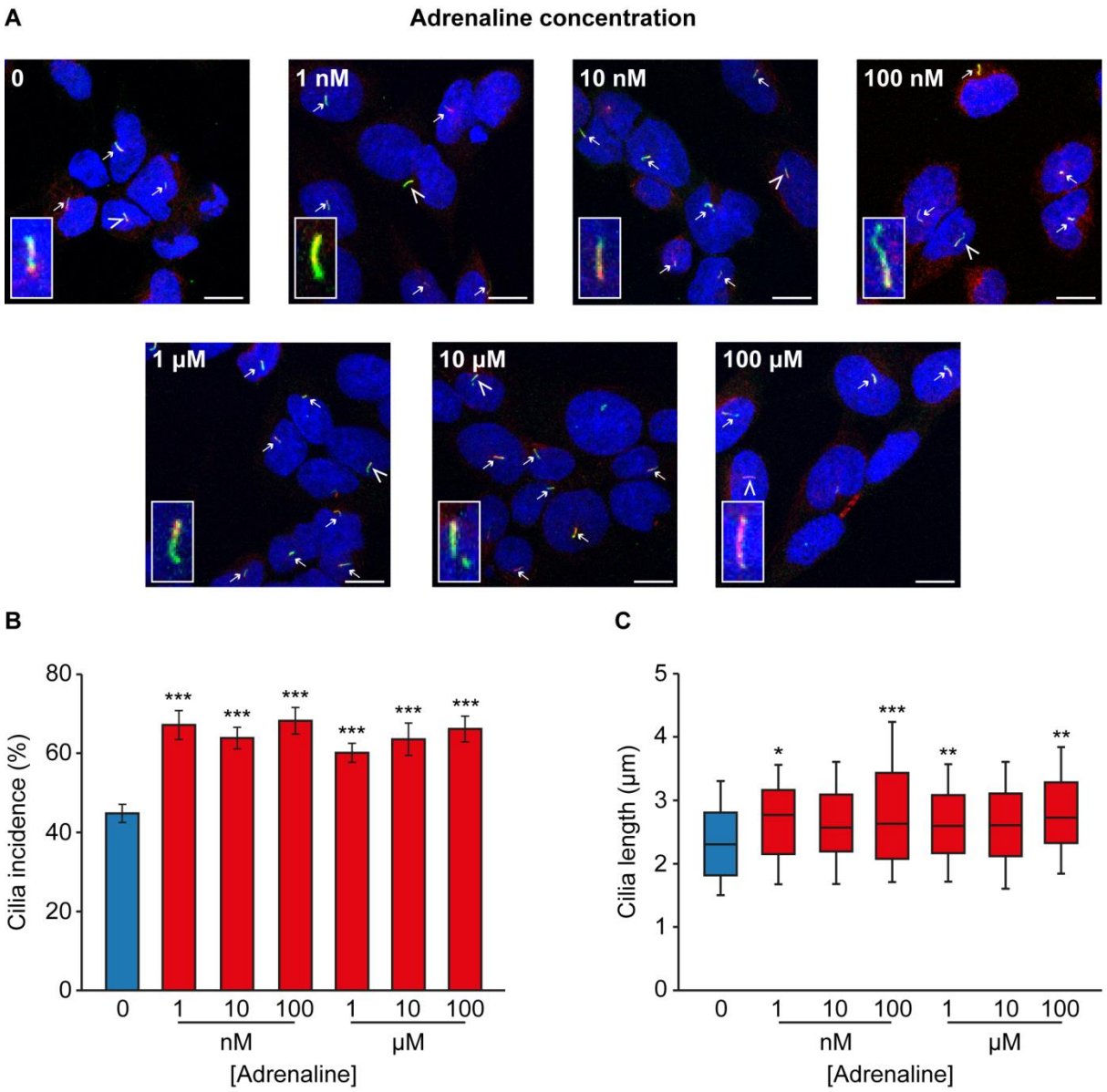

Figure 5.21: Adrenaline increases PC12 cell primary cilia incidence and length

(A) Confocal images of PC12 cells exposed to adrenaline at the concentrations indicated (or vehicle only control) for 24 hours. Cells were immunolabelled with anti-acetylated α-tubulin (red) and anti-Arl13b (green) for detection of primary cilia. Nuclei were stained with DAPI (blue). Cilia are indicated by arrows, or arrowheads where they are also shown zoomed in the insets. Scale bars = 10 µm.

Quantification of primary cilia incidence **(B)** and length **(C)** following treatment as per **(A)**. Error bars indicate $\pm$ SEM, boxes 25th, 50th and 75th centiles and whiskers the 10th and 90th centiles. Number of cells scored for incidence: 1698 $\pm$ 138 per condition. Number of cilia measured for length: 193 $\pm$ 40 per condition. Statistical significance was assessed using a one-way ANOVA comparing to control. * $p< 0.05$, * $p<0.01$, *** $p< 0.001$.

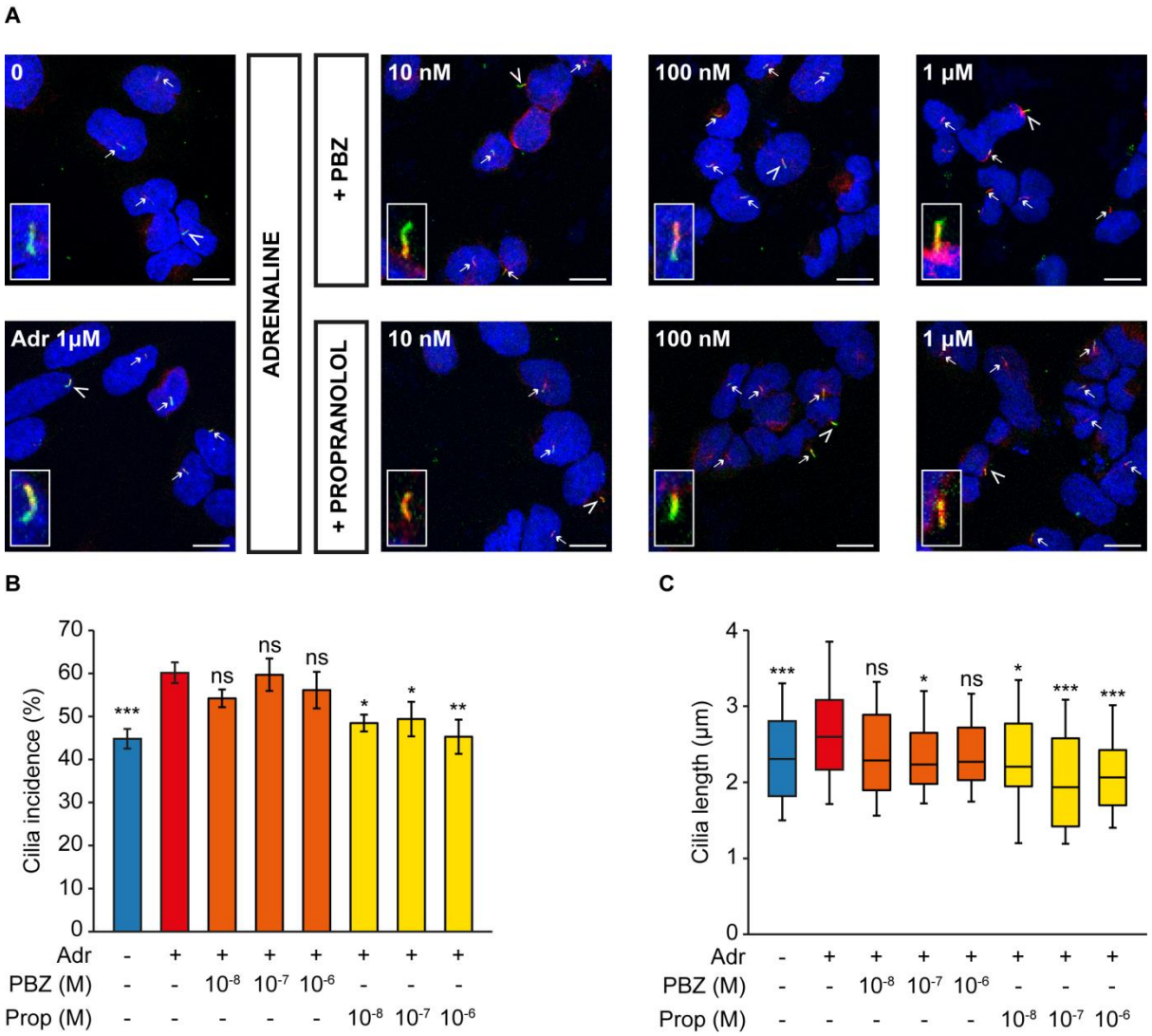

Figure 5.22: The beta adrenergic receptor antagonist propranolol prevents adrenaline-mediated increases in primary cilia incidence and length in PC12 cells

(A) Confocal images of PC12 cells exposed to phenoxybenzamine (PBZ) or propranolol (prop) at the concentrations indicated (or vehicle only control) for one hour prior to washing and incubation with 1uM adrenaline (Adr) for 24 hours. Cells were immunolabelled with anti-acetylated α-tubulin (red) and anti-Arl13b (green) for detection of primary cilia. Nuclei were stained with DAPI (blue). Cilia are indicated by arrows, or arrowheads where they are also shown zoomed in the insets. Scale bars = 10 µm.

Quantification of primary cilia incidence **(B)** and length **(C)** following treatment as per (A). Error bars indicate $\pm$ SEM, boxes 25th, 50th and 75th centiles and whiskers the 10th and 90th centiles. Number of cells scored for incidence: 1641 $\pm$ 220 per condition. Number of cilia measured for length: 167 $\pm$ 21 per condition. Statistical significance was assessed using a one-way ANOVA comparing to adrenaline treatment only (Adr; red bar). Ns = not significant, * p< 0.05, * p<0.01, *** p< 0.001.

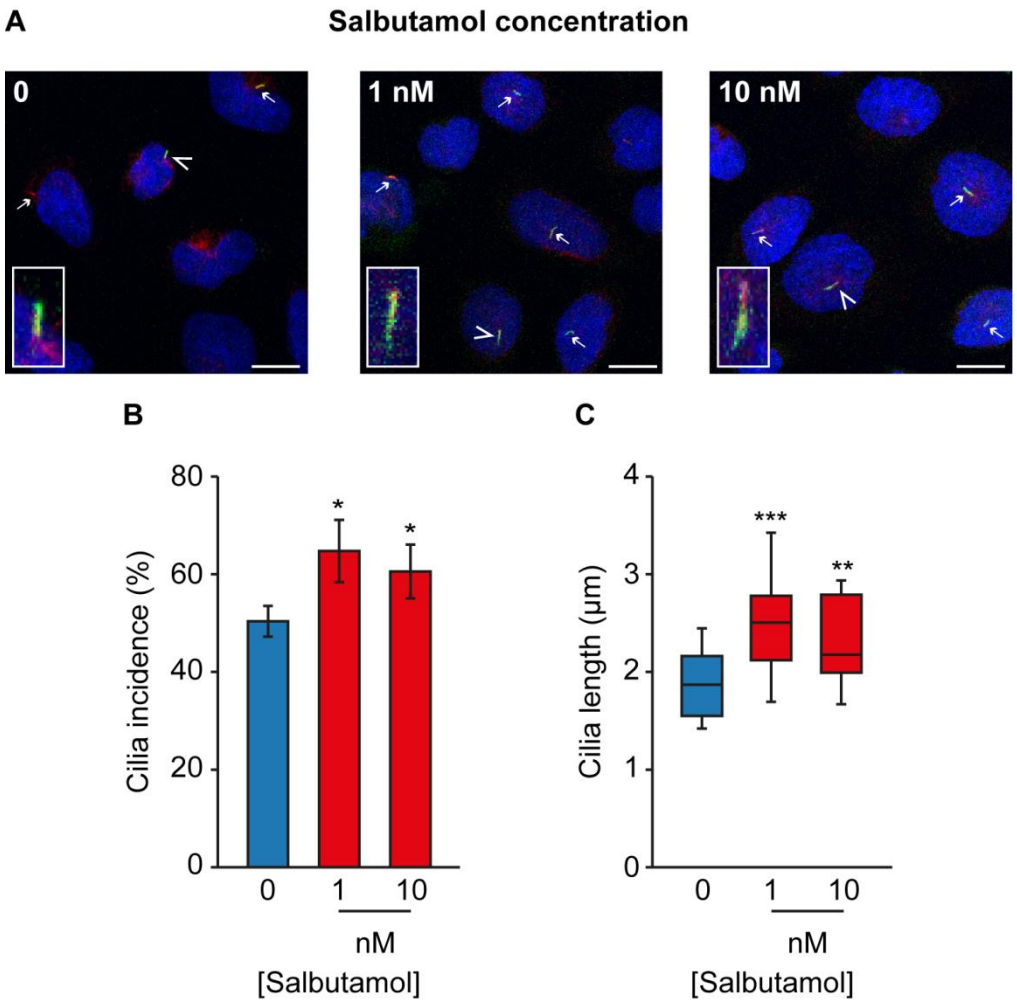

Figure 5.23: The beta adrenergic receptor agonist salbutamol increases primary cilia incidence and length in PC12 cells

(A) Confocal images of PC12 cells exposed to salbutamol at the concentrations indicated (or vehicle only control) for 24 hours. Cells were immunolabelled with anti-acetylated α-tubulin (red) and anti-Arl13b (green) for detection of primary cilia. Nuclei were stained with DAPI (blue). Cilia are indicated by arrows, or arrowheads where they are also shown zoomed in the insets. Scale bars = 10 µm.

Quantification of primary cilia incidence **(B)** and length **(C)** following treatment as per **(A)**. Error bars indicate $\pm$ SEM, boxes 25th, 50th and 75th centiles and whiskers the 10th and 90th centiles. Number of cells scored for incidence: 542$\pm$ 98 per condition. Number of cilia measured for length: 98 $\pm$ 19 per condition. Statistical significance was assessed using a one-way ANOVA comparing to control. * $p< 0.05$, * $p<0.01$, *** $p< 0.001$.

5.3.3.2.2 Noradrenaline increases incidence and length of primary cilia in rat phaeochromocytoma cells

We next examined whether noradrenaline had the same effect as adrenaline on primary cilia. PC12 cells were exposed to increasing concentrations of noradrenaline in serum-free media for 24 hours prior to fixation and immunolabelling for cilia detection (Figure 5.24A).

Primary cilia incidence was increased by noradrenaline at all concentrations tested (1nM – 100μM) compared to vehicle only control (Figure 5.24B). The greatest effect was seen with 1μM noradrenaline (70.9% $\pm$ 3.7 v. 44.8% $\pm$ 2.3; $p=1.9\times10^{-8}$). There was no significant difference in effect between any of the noradrenaline concentrations tested.

The relationship between noradrenaline and cilia length was less clear (Figure 5.24C). Ciliary length was increased following noradrenaline treatment at some but not all concentrations: 10nM (2.36μm $\pm$ 0.70 v. 2.64μm $\pm$ 0.68; p=0.038), 1μM (3.04 μm $\pm$ 1.12; $p=2.5\times10^{-10}$) and 100μM (2.74μm $\pm$ 0.89; p=0.0032). Cilia length was longest following treatment with 1μM noradrenaline and was significantly longer when compared to all other concentrations of noradrenaline with the exception of 100μM (p=0.09).

Thus, both adrenaline and noradrenaline increase PC12 primary cilia incidence and length.

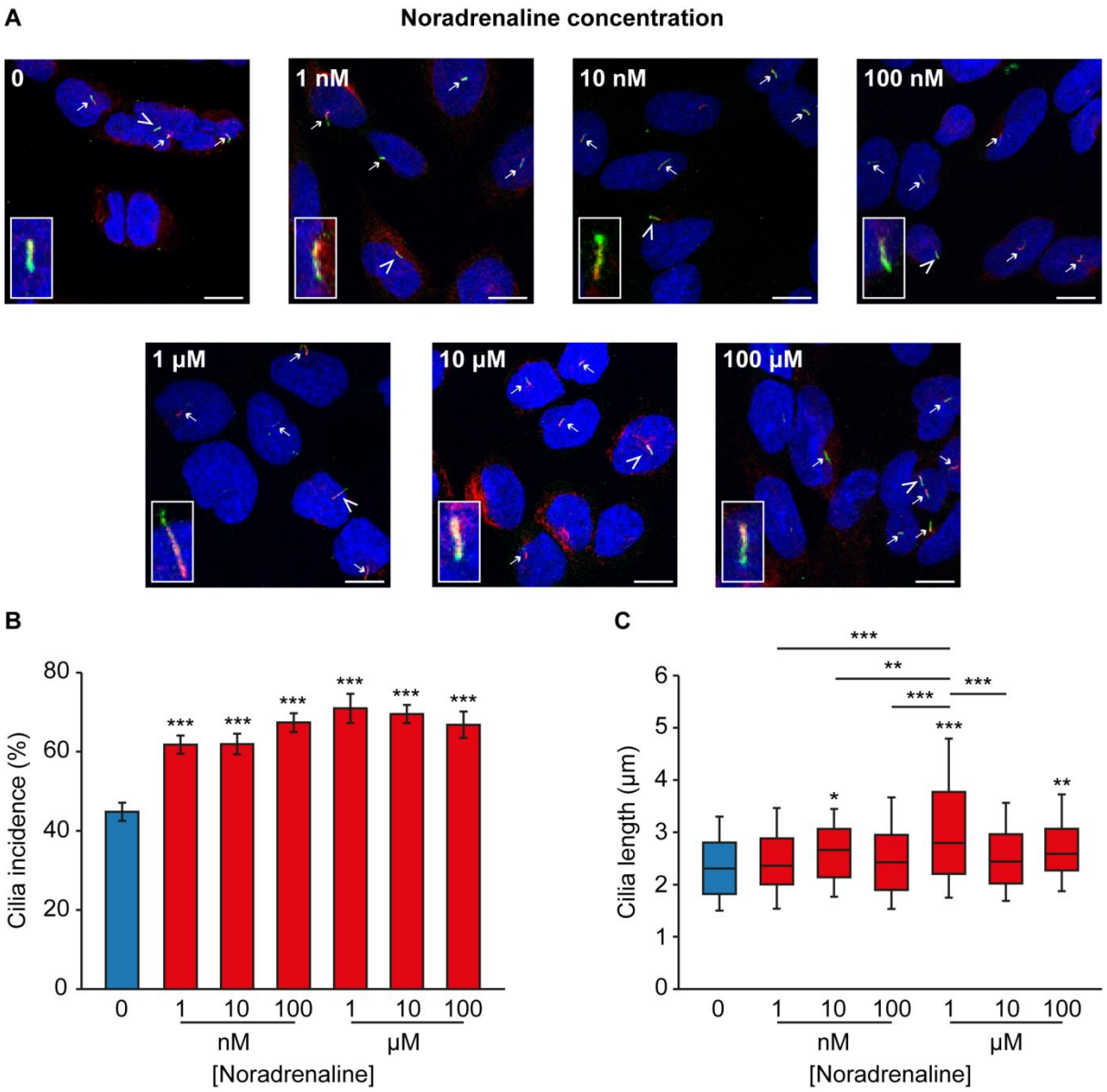

Figure 5.24: Noradrenaline increases PC12 cell primary cilia incidence and length

(A) Confocal images of PC12 cells exposed to noradrenaline at the concentrations indicated (or vehicle only control) for 24 hours. Cells were immunolabelled with anti-acetylated α-tubulin (red) and anti-Arl13b (green) for detection of primary cilia. Nuclei were stained with DAPI (blue). Cilia are indicated by arrows, or arrowheads where they are also shown zoomed in the insets. Scale bars = 10 µm.

Quantification of primary cilia incidence **(B)** and length **(C)** following treatment as per **(A)**. Error bars indicate ± SEM, boxes 25th, 50th and 75th centiles and whiskers the 10th and 90th centiles. Number of cells scored for incidence: 1532 ± 125 per condition. Number of cilia measured for length: 161 ± 17 per condition. Statistical significance was assessed using a one-way ANOVA comparing to control. * $p< 0.05$, * $p<0.01$, *** $p< 0.001$.

5.3.3.2.3 Dopamine increases incidence and length of primary cilia in rat phaeochromocytoma cells via dopamine receptors

The catecholamine dopamine, unlike adrenaline and noradrenaline, exerts its action via the dopamine receptor. Dopamine receptors have been shown to be expressed on primary cilia in a variety of tissue and cell types (Abdul-Majeed & Nauli 2011; Domire *et al.* 2011; Iwanaga *et al.* 2011a; Avasthi *et al.* 2012; Marley & von Zastrow 2012; Marley *et al.* 2013; Jin *et al.* 2014; Upadhyay *et al.* 2014; Omori *et al.* 2015) and their activation or loss causes tissue-specific changes in primary cilia (Abdul-Majeed & Nauli 2011; Marley *et al.* 2013; Jin *et al.* 2014; Kathem *et al.* 2014; Miyoshi *et al.* 2014; Upadhyay *et al.* 2014).

Given the established role of dopamine on primary cilia, we sought to evaluate this in the context of the rat PC12 phaeochromocytoma cell line. PC12 cells were exposed to increasing concentrations of dopamine in serum-free media for 24 hours prior to fixation and immunolabelling to detect primary cilia as previously described (Figure 5.25A).

Cilia incidence was increased in PC12 cells exposed to all concentrations of dopamine tested (1nM – 100µM) compared to vehicle only control (Figure 5.25B; e.g. 60.9% $\pm$ 10.2 for 1nM compared to 44.8% $\pm$ 12.5; p=0.0039), however no difference was observed between different concentrations of dopamine tested (e.g. 60.9% $\pm$ 10.2 for 1nM compared to 68.2% $\pm$ 6.1 for 100nM; p=0.7758). Increased cilia length was observed in cells exposed to dopamine at concentrations exceeding 10µM (Figure 5.25C; 2.81µm $\pm$ 0.77 for 10µM compared to. 2.36µm $\pm$ 0.70; p=0.0012).

Thus, the administration of extracellular dopamine to PC12 cells resulted in increases in ciliary incidence at all concentrations tested (Figure 5.25B) and length at concentrations above 10µM (Figure 5.25C). These observations are consistent with previous findings in mouse endothelium (Abdul-Majeed & Nauli 2011; Kathem *et al.* 2014) and porcine renal cells (Upadhyay *et al.* 2014). The mechanism by which dopamine increases cilia length in these cell types appears to be via action on the D_1-like subfamily of dopamine receptors (D_1 and D_5). Evidence for this includes that cilia lengthening was observed following exposure to the D_1-like receptor agonist fenoldopam (Kathem *et al.* 2014; Upadhyay *et al.* 2014) and transfection of a constitutively active D_1 receptor (Avasthi & Marshall 2012). Knockdown of the D_5 receptor results in cilia shortening and insensitivity to fluid flow in vascular endothelium (Abdul-Majeed & Nauli 2011).

Interestingly, the opposite response was observed in primary cilia in striatal neurons in rats and mice that had lost dopaminergic input (Miyoshi *et al.* 2014). In this paradigm, lack of dopamine due to

stereotactic lesions, pharmacological depletion (via reserpine) or inhibition of synthesis (by the tyrosine hydroxylase inhibitor alpha-methyl-p-tyrosine) resulted in increases in cilia length. This effect was mediated by the D_2 receptor. Receptor activation by the agonists bromocriptine and quinpirole attenuated reserpine-induced cilia lengthening, whilst receptor blockade (by the antagonist haloperidol) or loss (in D_2 null mice) resulted in ciliary lengthening.

Thus, it appears that there is differential ciliary responsiveness to dopamine in different tissue types mediated by different dopamine receptor subtypes.

In order to begin to determine the mechanisms by which dopamine might influence cilia incidence and length in PC12 cells, they were exposed to increasing concentrations of the D_2 receptor antagonist metoclopramide in serum-free media for 24 hours prior to fixation and immunolabelling to detect primary cilia (Figure 5.26A). Metoclopramide was chosen due to a combination of its receptor specificity, its widespread clinical use as an anti-emetic and its association with precipitation of phaeochromocytoma crises (Guillemot *et al.* 2009).

Cilia incidence was reduced in PC12 cells exposed to metoclopramide at concentrations at and exceeding 1µM compared to vehicle only control (Figure 5.26B; 33.1% $\pm$ 6.5 at 1µM compared to 46.3% $\pm$ 12.3; $p = 0.0091$). Cilia length was also reduced in cells exposed to metoclopramide at 1µM and 10µM (Figure 5.26C; 1.91µm $\pm$ 0.50 for 1µM compared to 2.35µm $\pm$ 0.67; $p = 0.015$).

Thus, antagonism of the D_2 receptor in PC12 cells results in cilia loss and shortening. Although the effect of metoclopramide on primary cilia has not been reported previously, it is interesting to note that the direction of effect is the reverse of that observed in striatal neurons.

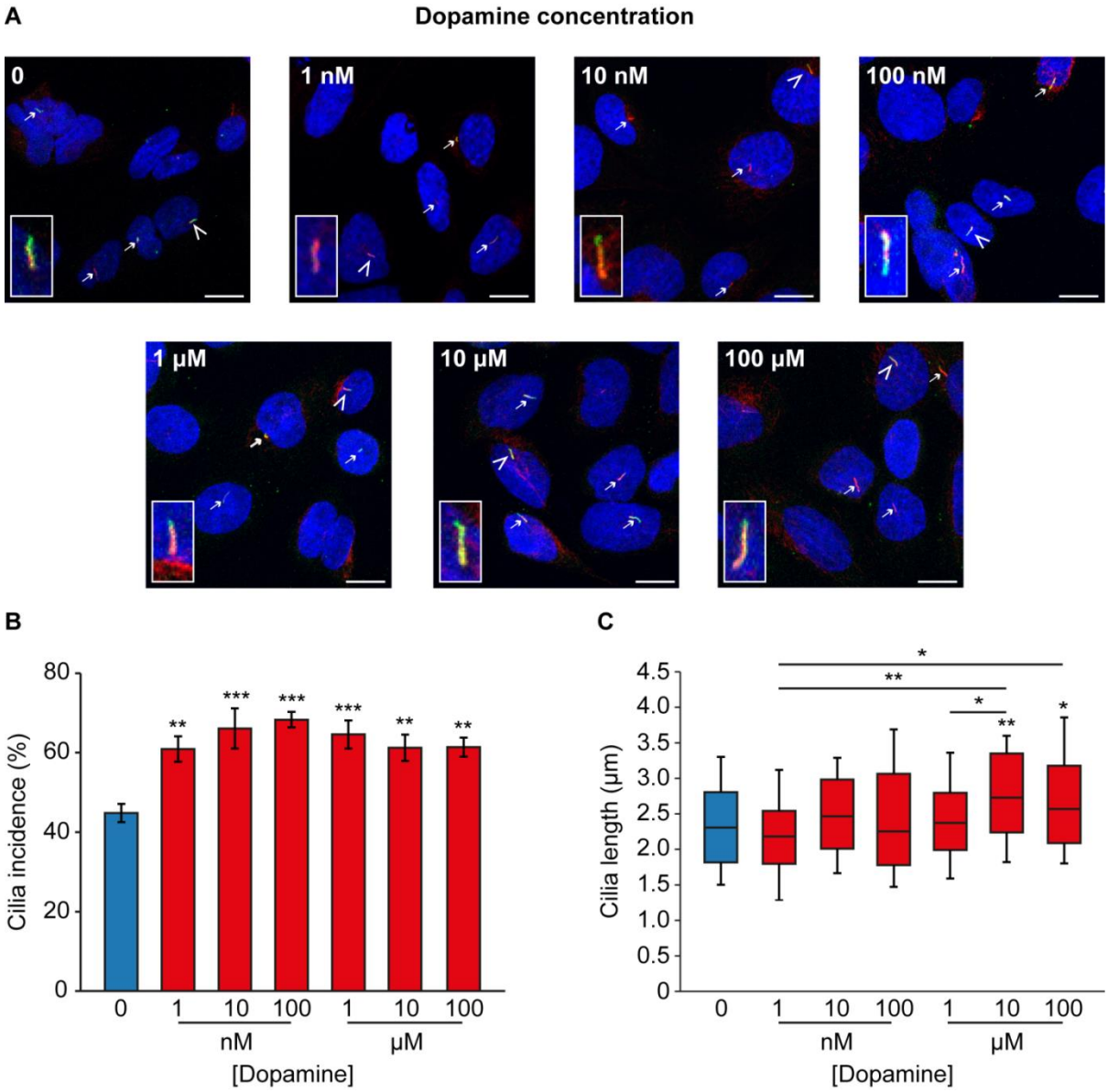

Figure 5.25: Dopamine increases PC12 cell primary cilia incidence and length

(A) Confocal images of PC12 cells exposed to dopamine at the concentrations indicated (or vehicle only control) for 24 hours. Cells were immunolabelled with anti-acetylated α-tubulin (red) and anti-Arl13b (green) for detection of primary cilia. Nuclei were stained with DAPI (blue). Cilia are indicated by arrows, or arrowheads where they are also shown zoomed in the insets. Scale bars = 10 µm.

Quantification of primary cilia incidence **(B)** and length **(C)** following treatment as per **(A)**. Error bars indicate $\pm$ SEM, boxes 25th, 50th and 75th centiles and whiskers the 10th and 90th centiles. Number of cells scored for incidence: 1882 $\pm$ 205 per condition. Number of cilia measured for length: 209 $\pm$ 28 per condition. Statistical significance was assessed using a one-way ANOVA. * $p < 0.05$, ** $p < 0.01$, *** $p < 0.001$. Stars above error bars represent comparison to control and above horizontal lines comparison between the two linked bars. Where no stars are evident, $p > 0.05$.

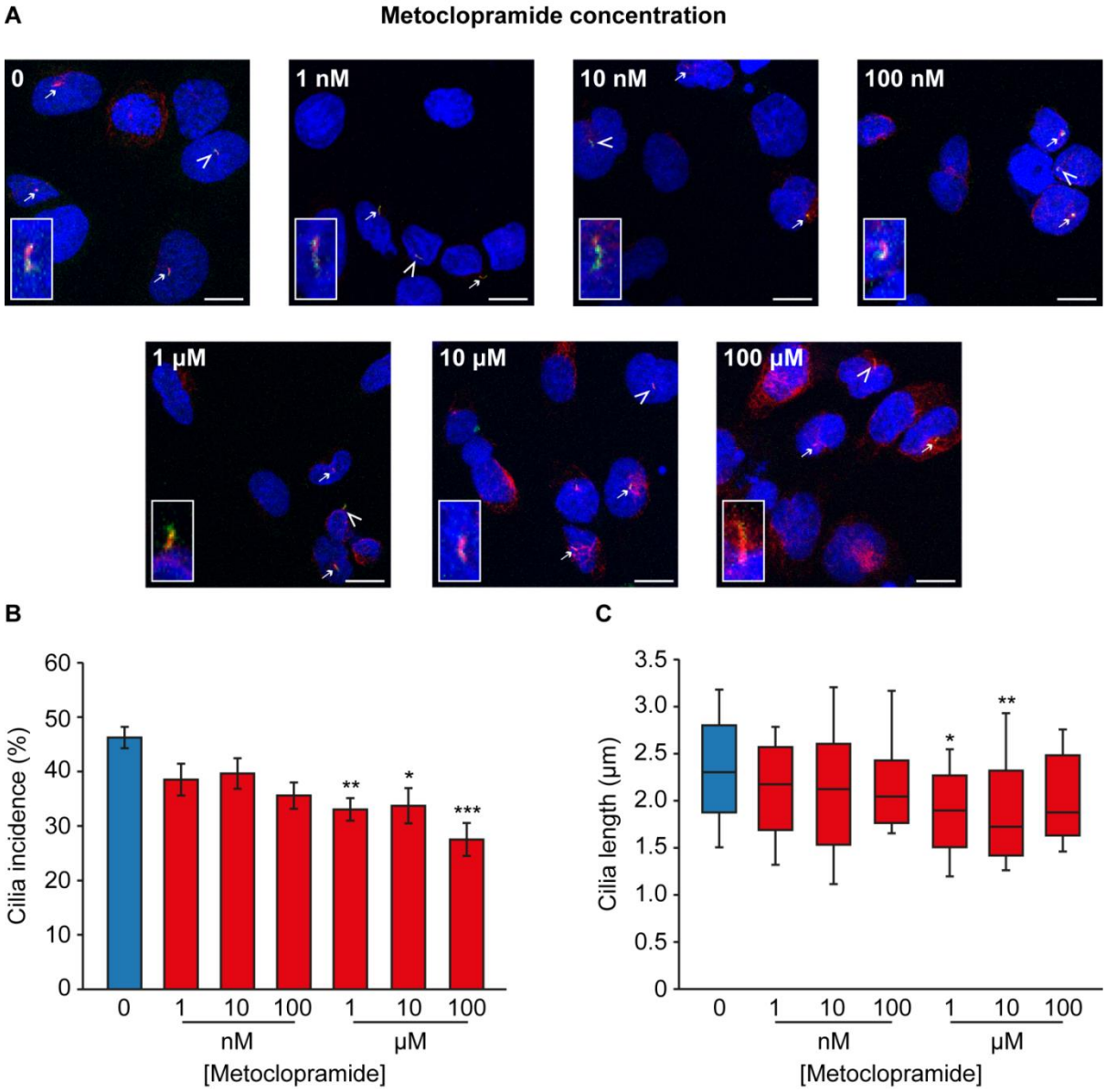

Figure 5.26: Metoclopramide decreases PC12 cell primary cilia incidence and length

(A) Confocal images of PC12 cells exposed to metoclopramide at the concentrations indicated (or vehicle only control) for 24 hours. Cells were immunolabelled with anti-acetylated α-tubulin (red) and anti-Arl13b (green) for detection of primary cilia. Nuclei were stained with DAPI (blue). Cilia are indicated by arrows, or arrowheads where they are also shown zoomed in the insets. Scale bars = 10 µm.

Quantification of primary cilia incidence **(B)** and length **(C)** following treatment as per **(A)**. Error bars indicate $\pm$ SEM, boxes 25th, 50th and 75th centiles and whiskers the 10th and 90th centiles. Number of cells scored for incidence: 1552 $\pm$ 125 per condition. Number of cilia measured for length: 109 $\pm$ 29 per condition. Statistical significance was assessed using a one-way ANOVA comparing to control. * $p < 0.05$, ** $p < 0.01$, *** $p < 0.001$.

5.3.4 The effect of other non-cellular features of the phaeochromocytoma microenvironment on primary cilia

Having demonstrated that hypoxia and catecholamines, specific features of the phaeochromocytoma microenvironment, influenced primary cilia structure in both human tumours and the rat PC12 phaeochromocytoma-derived cell line, we postulated that other chemical features of the tumour microenvironment might also do so.

5.3.4.1 Somatostatin analogues increase PC12 cell primary cilia incidence and length

Somatostatin receptors are expressed in both normal adrenal medulla (Kimura *et al.* 2001; Reubi *et al.* 2001; Unger *et al.* 2012) and phaeochromocytomas (Kubota *et al.* 1994; Reubi *et al.* 2000; Pasquali *et al.* 2008; Unger *et al.* 2008; Ziegler *et al.* 2009; Elston *et al.* 2015). The relative expression of receptor subtype appears to be highly variable between series and the methodology employed, with one large study of 180 tumours reporting increased $SSTR_3$ expression in SDH deficient PPGL (Elston *et al.* 2015). $SSTR_3$ alone of all the SSTRs is known to have a ciliary localisation in a variety of tissues including brain (Händel *et al.* 1999; Berbari *et al.* 2008a), pituitary (Iwanaga *et al.* 2011b), pancreatic islet cells (Iwanaga *et al.* 2011b) and kidney (O'Connor *et al.* 2013). Ciliary localisation of $SSTR_3$ is dependent on a consensus sequence within its third intracellular loop (Berbari *et al.* 2008b) and requires a variety of ciliary proteins including Bbs2 and 4 (Berbari *et al.* 2008a), tubby (Sun *et al.* 2012) and Arl6 (Jin *et al.* 2010). Mutations in the genes encoding these proteins result in lack of ciliary localisation of $SSTR_3$.

We thus sought to test whether treatment of PC12 cells, which express SSTRs (Traina *et al.* 1998), with somatostatin analogues led to changes in primary cilia. These drugs and their derivatives have multi-faceted clinical uses in PPGL, predominantly as diagnostic (Taïeb *et al.* 2012) and therapeutic (Kong *et al.* 2017) radiolabelled peptides, but also on occasion as systemic therapy (Koriyama *et al.* 2000; Tonyukuk *et al.* 2003; van Hulsteijn *et al.* 2013; Elshafie *et al.* 2014). PC12 cells were exposed to increasing concentrations of octreotide or pasireotide in serum-free media for 24 hours prior to fixation and immunolabelling to detect primary cilia (Figure 5.27A).

Treatment with octreotide did not significantly alter cilia incidence, although there was a trend towards an increase (Figure 5.27B; 51.1% $\pm$ 7.7 compared to 57.8% $\pm$ 7.2 at 1µM, $p = 0.25$). Cilia length was increased in cells exposed to octreotide at concentrations of 100nM and above (Figure 5.27C; 1.99µm $\pm$ 0.51 compared to 2.30µm $\pm$ 0.67 at 100nM, $p = 0.0054$).

Pasireotide also resulted in an increase in PC12 ciliary length at all concentrations tested (Figure 5.27C; 1.99µm $\pm$ 0.51 compared to 2.38µm $\pm$ 0.62 at 100nM, $p=5.8x10^{-5}$). In addition, ciliary incidence was increased from concentrations of 100nM and above (Figure 5.27B; 51.1% $\pm$ 7.7 compared to 63.5% $\pm$ 11.2 at 100nM, p = 0.0002).

Thus, somatostatin receptor stimulation by the analogues octreotide and pasireotide results in increases in ciliary incidence (with pasireotide only; Figure 5.27A) and length (Figure 5.27B). The observed differences in effect may relate to pasireotide's greater affinity for $SSTR_3$ and $_5$ (Lesche *et al.* 2009) and are discussed further later in this chapter.

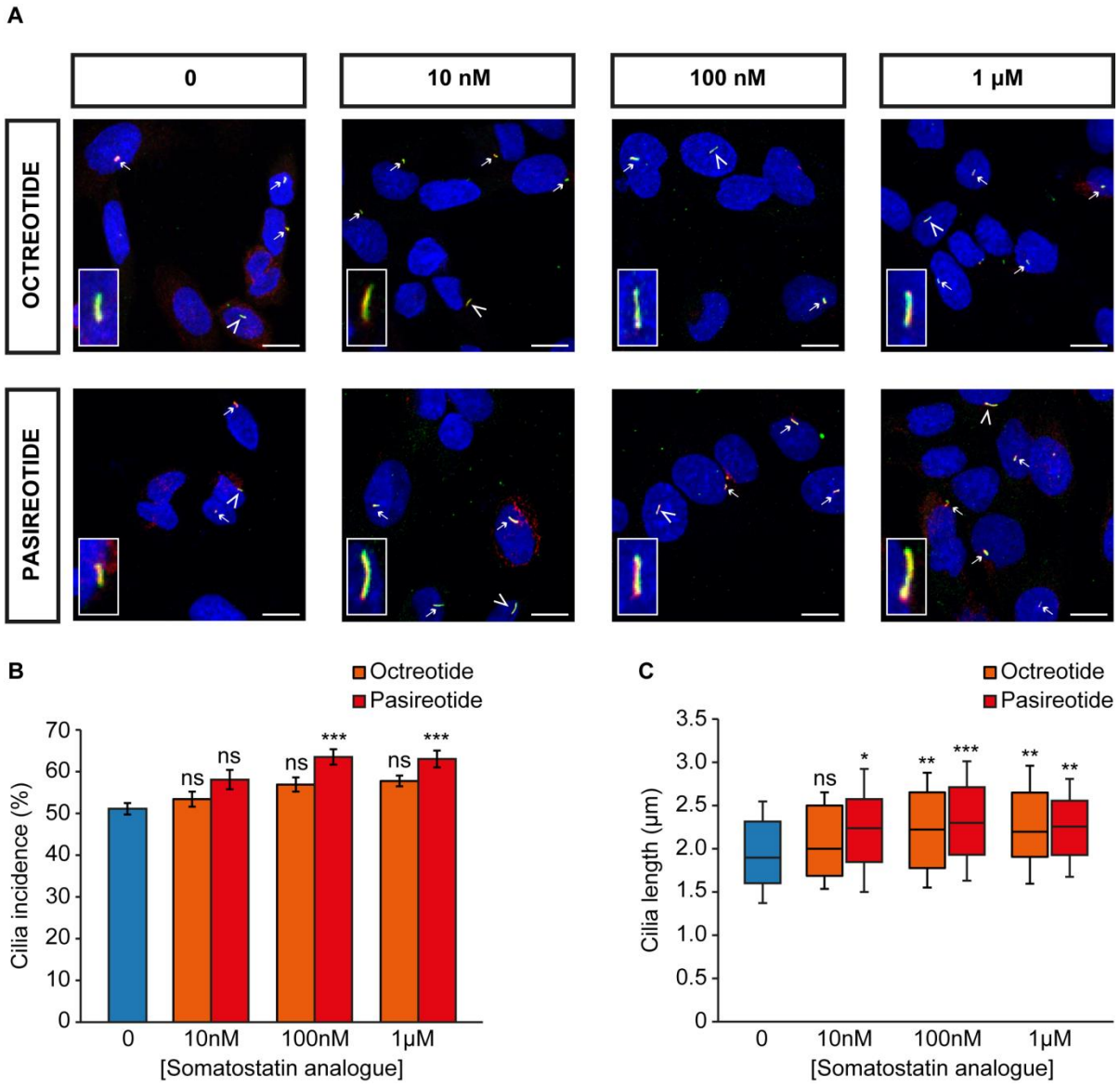

Figure 5.27: Somatostatin analogues increase PC12 cilia incidence and length

(A) Confocal images of PC12 cells exposed to the somatostatin analogues octreotide or pasireotide at the concentrations indicated (or vehicle only control) for 24 hours. Cells were immunolabelled with anti-acetylated α-tubulin (red) and anti-Arl13b (green) for detection of primary cilia. Nuclei were stained with DAPI (blue). Cilia are indicated by arrows, or arrowheads where they are also shown zoomed in the insets. Scale bars = 10 µm.

Quantification of primary cilia incidence **(B)** and length **(C)** following treatment as per **(A)**. Error bars indicate $\pm$ SEM, boxes 25th, 50th and 75th centiles and whiskers the 10th and 90th centiles. Number of cells scored for incidence: 1344 $\pm$ 137 per condition. Number of cilia measured for length: 111 $\pm$ 10 per condition. Statistical significance was assessed using a one-way ANOVA comparing to control. Ns not significant, * $p< 0.05$, ** $p<0.01$, *** $p< 0.001$. There was no significant difference between octreotide and pasireotide at each concentration tested.

5.4 Discussion

In this chapter, I have demonstrated that primary cilia on phaeochromocytoma-derived cells are sensitive to a variety of features of the phaeochromocytoma tumour microenvironment, including hypoxia, pseudohypoxia and catecholamines, and therapeutic agents, namely somatostatin analogues. Both hypoxia and pseudohypoxia result in cilia loss via a mechanism that is HIF and AURKA/HDAC6 dependent. Primary cilia elongate in response to catecholamines via a mechanism mediated by the β-adrenoceptor and in response to somatostatin receptor stimulation.

5.4.1 Hypoxia results in primary cilia loss in phaeochromocytoma-derived cells

Culture of all three available phaeochromocytoma-derived cell lines (PC12, MPC and MTT) in hypoxic (1% oxygen) conditions resulted in a reduction in cilia incidence and length compared to normoxic (21% oxygen) conditions (Figures 5.1-5.3).

The response of primary cilia to hypoxia in other tissues is varied (Table 5.1). Consistent with our observations, cilia incidence was reduced by short (twenty four hours) periods of hypoxic exposure (1-1.2% oxygen) in murine bone marrow-derived mesenchymal stem cells (Proulx-Bonneau & Annabi 2011), primary rat tenocytes (Lavagnino *et al.* 2016) and human lean adipose-derived stem cells (ASCs) (Ritter *et al.* 2018). Chronic exposure to hypoxia (as 5% oxygen) did not affect cilia incidence in murine bone marrow-derived mesenchymal stem cells (BMSCs) (Brown *et al.* 2014), although the exact duration of hypoxic culture was not stated. The only study to examine this relationship *in vivo* did not demonstrate a difference in cilia incidence in ovine renal tubules from animals reared at sea level or those exposed to hypobaric hypoxia at altitude (Shamloo *et al.* 2017).

Hypoxia's effect on ciliary length is equally varied and interpretation is hampered as many studies examine only length or incidence. Twenty four hours of 1.2% oxygen shortened cilia in human ASCs (Ritter *et al.* 2018), whilst the same duration of 2% oxygen lengthened bovine articular chondrocyte cilia (Wann *et al.* 2013). Longer term exposure of mouse BMSCs to 5% oxygen also lengthened cilia in basal conditions, however no effect was seen with serum starvation (Brown *et al.* 2014). Longer cilia were also seen in ovine fetal renal tubules of sheep raised at altitude, but not in the kidneys of adult animals (Shamloo *et al.* 2017).

Reference	Cell type	Hypoxia conditions	Incidence effect	Length effect
(Proulx-Bonneau & Annabi 2011)	Mouse BMSCs	24h 1% O_2	Reduced (data not presented)	ND
(Wann *et al.* 2013)	Bovine primary articular chondrocytes	24h 2% O_2	ND	Increased (18%)
(Brown *et al.* 2014)	Mouse BMSCs	'Chronic' (hypoxia duration not stated) 0h SF 5% O_2 24h SF 5% O_2 48h SF 5% O_2	 Unchanged (60-70%) Unchanged (91.5% ± 4.8 v. 85.5% ± 9.1) Unchanged (data not presented)	 Increased (1.8 µm v. 2.15 µm) Unchanged (2.4 µm v. 2.2 µm) Unchanged (1.9 µm v. 2.1 µm)
(Lavagnino *et al.* 2016)	Rat tail tenocytes	24h 1% O_2	Reduced (54.1% ± 12.2 v. 71.7% ± 6.32)	ND
(Shamloo *et al.* 2017)	Ovine renal proximal tubules and distal collecting ducts	110 days at sea level (19.6 kPa) or 3801m (12.6 kPa)	Unchanged (data not presented)	Adults – no change Fetal – increased
(Ritter *et al.* 2018)	Human lean ASC	24h 1.2% O_2	Reduced	Reduced
This thesis	Rat phaeo (PC12) Mouse phaeo (MPC) Mouse phaeo (MTT)	24h 1% O_2	Reduced (51.3% ± 9.5 v. 70.7% ± 14.7) Reduced (64.1% ± 8.7 v. 76.1% ± 1.8) Reduced (54.3% ± 6.1 v. 64.5% ± 4.0)	Reduced (2.02µm ± 0.64 v. 2.43µm ± 0.84) Reduced (2.25µm ± 0.76 v. 2.77µm ± 0.78) Reduced (1.99µm ± 0.56 v. 2.23µm ± 0.66)

Table 5.1: The effect of hypoxia on primary cilia

BMSC – bone marrow-derived mesenchymal stem cells, ND – not done, SF – serum free, ASC – adipose-derived mesenchymal stem cells, phaeo – phaeochromocytoma. Incidence – mean +/- SD, length – median or mean +/- SD.

Whether these observed differences are tissue-specific or related to the different experimental conditions utilised (specifically duration and extent of hypoxia) is uncertain and these factors have not been systematically evaluated.

A key concept to consider in the interpretation of these findings is the definition of 'normoxia' and how experimental conditions relate to the physiological situation they are trying to evaluate. Atmospheric oxygen at sea level (160 mmHg, 21.1%) might be considered 'normoxia' and this is the situation (allowing for altitude) under which the vast majority of laboratory cell biology studies are performed. This oxygen tension, however, is actually supraphysiological when compared to tissue level oxygenation, which ranges between 30 and 70 mmHg (3.8-9.5%) (Bylund-Fellenius *et al.* 1981; Müller *et al.* 1998). At a cellular level, normal oxygen tension is lower still, in the range 9.9-19 mmHg (1.3-2.5%) (Gleadle & Ratcliffe 2001). Thus, normoxia in our experiments (as in all others) is actually hyperoxia and a lower oxygen tension would be a more physiologically matched control. It should be noted that some of the 'hypoxic' oxygen tensions used previously could be considered either tissue-level normoxic (Wann *et al.* 2013) or hyperoxic (Brown *et al.* 2014).

Having shown that the effect of hypoxia on primary cilia is conserved across PC12, MPC and MTT cell lines, this supports the finding that hypoxia results in cilia loss in the context of phaeochromocytomas. It must be considered, however, that these cell lines contain mutations in phaeochromocytoma-predisposing genes. PC12 cells harbour a *MAX* mutation (Hopewell & Ziff 1995), whilst MPC and MTT are deficient in *NF1* (Powers *et al.* 2000). These are all cluster 2 phaeochromocytoma-predisposing genes, in which hypoxic signalling is not considered to be a salient feature. There is, however, some evidence that inactivation of *NF1* results in increased expression of HIF1α and its target VEGF (Kawachi *et al.* 2013).

We have demonstrated through prevention of HIF-mediated transcription and via HIF1α knockdown that the mechanism by which hypoxia induces cilia loss in phaeochromocytoma cells is HIF1 dependent (Figure 5.5).

This mechanism is the same as that identified in BMSCs in which exposure to 1% oxygen reduced cilia incidence. Consistent with our findings, HIF1α knockdown prevented hypoxia-induced cilia changes and expression of a constitutively active HIF1α phenocopied the ciliary response to hypoxia (Proulx-Bonneau & Annabi 2011). One study suggests that it is HIF2α and not HIF1α that is responsible for hypoxia-induced cilia changes (Wann *et al.* 2013). The evidence for this is indirect, however, relying on the effect on cilia and HIF2α caused by IL1b treatment. In addition, they argue the fact this effect is prevented by echinomycin (which blocks HIF DNA binding akin to FM19G11)

supports the HIF2α mechanism, whilst the original data for echinomycin surrounds HIF1α and not HIF2α (Kong *et al.* 2005).

We found that inactivation of the AURKA/HDAC6 ciliary disassembly pathway prevented hypoxia-induced ciliary changes in PC12 cells (Figure 5.6).

Activation of the AURKA/HDAC6 pathway results in deacetylation of ciliary tubulin and destabilisation of the axonemal microtubules resulting in ciliary disassembly (Pugacheva *et al.* 2007). Consistent with our experimental findings, expression of both *AURKA* (Klein *et al.* 2008) and *HDAC6* (Kaluza *et al.* 2011) are upregulated by hypoxia and specifically HIF1α in the case of AURKA (Cui *et al.* 2013).

5.4.2 Pseudohypoxia results in primary cilia loss in phaeochromocytoma-derived cells

Similarly to the response to hypoxia, pseudohypoxia in PC12 cells, achieved via a variety of disease-relevant mechanisms, resulted in a reduction in cilia incidence and length (Figures 5.7, 5.8, 5.10, 5.12-14).

Again, the response of primary cilia to pseudohypoxia in other tissues is varied (Table 5.2) and evaluation is similarly hampered due to the analysis of incidence or length data in isolation.

In keeping with our observations in PC12 cells, pseudohypoxia achieved by HIF1α overexpression in murine BMSCs (Proulx-Bonneau & Annabi 2011) and by knockdown of PHD1 in human retinal pigment epithelial cells (Moser *et al.* 2013) resulted in a reduction in cilia incidence. Other studies found no impact of pseudohypoxia on ciliary incidence (Lutz & Burk 2006; Verghese *et al.* 2011; Resnick 2016).

Converse to our findings, inhibition of HIF-PHD by DMOG (Wann *et al.* 2013) and cobalt chloride (Verghese *et al.* 2011; Wann *et al.* 2013) in canine renal cells (Verghese *et al.* 2011) and bovine articular chondrocytes (Wann *et al.* 2013) resulted in cilia elongation.

This raises the question as to whether the effect of hypoxic signalling on primary cilia is tissue dependent and/or cell type specific. It should be noted that the manner in which pseudohypoxia was achieved in these studies are varied and were limited to examining a singular mechanism of action.

In PC12 cells, the mechanism of cilia loss and shortening again appears to be dependent on HIF signalling and the AURKA/HDAC6 pathway (Figure 5.17). This is consistent with the observed effects

of HIF1α overexpression (Moser *et al.* 2013), and that cobalt chloride-mediated inhibition of HIF-PHD (Romain *et al.* 2014) and VHL inactivation (Xu *et al.* 2010) induce AURKA expression. In this experimental paradigm, therefore, this mechanism appears to explain the observed ciliary effect of pseudohypoxia.

However, alternative mechanisms may also be involved, particularly in the context of von Hippel-Lindau disease, which unlike the other cluster 1 predisposition genes, has an established functional role in primary cilia.

pVHL appears to have a crucial role in ciliary maintenance in the kidney. Primary cilia loss is a feature of VHL-deficient renal cysts (Esteban *et al.* 2006), ccRCC (Schraml *et al.* 2009; Basten *et al.* 2013), renal cancer cell lines (Esteban *et al.* 2006; Lutz & Burk 2006; Schermer *et al.* 2006; Lolkema *et al.* 2008) and wildtype murine renal cells in which *Vhl* has been knocked down (Schermer *et al.* 2006). The effect of VHL loss in other cell types, notably RPE cells, is less clear with conflicting reports of reduced ciliary formation (Dere *et al.* 2015) or enhanced ciliary disassembly (Frew *et al.* 2008). The responsible mechanisms appear to be multi-factorial. pVHL loss results in increased expression of HDAC6 and AURKA by both HIF-dependent (Xu *et al.* 2010) and HIF-independent (Dere *et al.* 2015) mechanisms. In addition, pVHL itself localises to primary cilia (Schermer *et al.* 2006; Lolkema *et al.* 2008) where it binds to and stabilises microtubules (Okuda *et al.* 1999; Hergovich *et al.* 2003, 2006; Schermer *et al.* 2006; Lolkema *et al.* 2007) via a microtubule-binding domain that is distinct from the HIF-binding domain. Through AURKA/HDAC6 inhibition, our data supports pseudohypoxia causing accelerated ciliary disassembly in phaeochromocytomas, although we also demonstrate that hypoxia reduces ciliary localisation of pVHL, potentially priming it for disassembly (Figure 5.15).

These experiments are the first to examine the effects on primary cilia of oncometabolite accumulation due to loss of function of SDH. In addition to causing pseudohypoxia, loss of function of SDH potentially results in superoxide generation due to decoupling of the ETC. Others have suggested that superoxide generation can alter primary cilia length, although the effect is inconsistent between studies. Ischaemia-reperfusion injury shortens primary cilia in both murine kidney (Kim *et al.* 2013) and liver (Han *et al.* 2017), whilst a unilateral nephrectomy increases superoxide formation in the remaining kidney and increases cilia length (Han *et al.* 2016). We did not find that inhibition of other ETC complexes altered primary cilia incidence or length (Figure 5.11), suggesting this was not the responsible mechanism in PC12 cells.

We did not directly compare the relative effects on cilia of the different mechanisms of causing pseudohypoxia. This has the potential to be informative mechanistically and provide disease insight.

For example, cluster 1 tumours behave differently depending on the affected gene with *SDHB* and *FH* mutated tumours having an increased risk of malignancy compared to *VHL* mutated tumours. Part of this difference is explained by oncometabolite inhibition of additional α-ketoglutarate dependent enzymes including histone demethylases (Smith *et al.* 2007) with resultant epigenetic modification (Letouzé *et al.* 2013), but this does not satisfactorily explain the differences within the genes of the *SDHx* complex.

Collectively, these findings suggest that the reduction in cilia frequency and length in phaeochromocytomas is likely to be mediated by both HIF signalling and the AURKA/HDAC6 cilia resorption pathway, although involvement of other regulators of cilia dynamics is also possible. Hypoxia is not only a driver of PPGL formation (Rodriguez-Cuevas *et al.* 1986; Opotowsky *et al.* 2015), but is also a salient feature of many solid tumours, and may therefore modulate cilia presence in cancers more generally.

Reference	Cell type	Pseudohypoxia conditions	Incidence effect	Length effect
(Lutz & Burk 2006)	Renal cell carcinoma line 786-0 (VHL+)	18h 250uM $CoCl_2$ 18h 200uM Desferrioxamine	Unchanged (data not presented)	ND
(Verghese *et al.* 2011)	Canine MDCK cells	100µM $CoCl_2$	Unchanged (data not presented)	Increased
(Proulx-Bonneau & Annabi 2011)	Mouse BMSCs	HIF1α overexpression	Reduced (data not presented)	ND
(Moser *et al.* 2013)	Human retinal pigment epithelial cells	PHD1 KD	Reduced (data not presented)	ND
(Wann *et al.* 2013)	Bovine primary articular chondrocytes	0-24h 100µM $CoCl_2$ 0-24h 10 µM DMOG	ND ND	Increased Increased (doubled)
(Resnick 2016)	Canine MDCK cells	24h 100uM $CoCl_2$ 24h 100uM Desferrioxamine	Unchanged (data not presented)	ND
This thesis	Rat phaeo (PC12)	24h 100µM DMOG 24h 100µM malonate SDHB knockdown 24h 200µM MMF FH knockdown VHL knockdown	Reduced (45.4% $\pm$ 11.6 v. 68.5% $\pm$ 12.6) Reduced (57.2% $\pm$ 10.8 v. 76.2% $\pm$ 10.4) Reduced (20.1% $\pm$ 8.5 v. 46.6% $\pm$ 14.1) Reduced (66.2% $\pm$ 8.6 v. 78.6% $\pm$ 11.6) Reduced (39.7% $\pm$ 9.4 v. 55.7% $\pm$ 14.1) Reduced (49.8% $\pm$ 8.8 v. 71.6% $\pm$ 9.6)	Reduced (2.32µm $\pm$ 0.79 v. 2.72µm $\pm$ 0.70) Reduced (1.99µm $\pm$ 0.64 v. 2.49µm $\pm$ 0.65) Reduced (1.78µm $\pm$ 0.80 v. 2.20µm $\pm$ 0.62) Reduced (2.22µm $\pm$ 0.87 v. 2.99µm $\pm$ 0.71) Reduced (2.15µm $\pm$ 0.60 v. 2.34µm $\pm$ 0.68) Reduced (2.01µm $\pm$ 0.68 v. 2.56µm $\pm$ 0.72)

Table 5.2: The effect of pseudohypoxia on primary cilia

VHL – von Hippel Lindau, $CoCl_2$ – cobalt chloride, ND – not done, MDCK – Madin-Darby canine kidney, BMSC – bone marrow-derived mesenchymal stem cells, HIF – hypoxia inducible factor, PHD – prolyl hydroxylase, DMOG – dimethyloxalylglycine, MMF – monomethyl fumarate, SDHB – succinate dehydrogenase B, FH – fumarate hydratase.

5.4.3 Catecholamines modulate phaeochromocytoma primary cilia

In patients with phaeochromocytomas, circulating metanephrine appeared to influence primary cilia structure. A positive relationship between maximal metanephrine concentration and primary cilia length was observed (Figure 5.18). When any elevation in metanephrine concentration was considered, tumoural primary cilia incidence and length was increased in patients with elevated circulating metanephrines compared to those without (Figure 5.19). Normetanephrine and 3-methoxytyramine did not appear to alter phaeochromocytoma primary cilia incidence or length in *vivo*. In PC12 cells, adrenaline similarly increased primary cilia incidence and length by a mechanism that appeared to be dependent on the β-adrenoreceptor (Figures 5.21 & 5.22).

Although adrenaline is known to be stimulatory to motile cilia in bronchial (Weiterer *et al.* 2015) and tracheal (Bailey *et al.* 2014) epithelium, there is a paucity of experimental data with respect to primary cilia. Consistent with our findings, a single high content screening analysis of a human pancreatic ductal cancer cell line (CFPAC-1) identified that 10μM adrenaline, but not noradrenaline, increased primary cilia incidence (Khan *et al.* 2016). Other structural studies have identified that the β2-adrenoeceptor is localised to primary cilia in murine neurons (Yao *et al.* 2016), whilst it is excluded from primary cilia in murine inner medullary collecting duct cells (Marley *et al.* 2013).

Relative receptor selectivity is one possible explanation for the observed difference between the effects in the tumour samples and is supportive of a β_2-mediated effect (Insel 1989; Wallukat 2002). Numerous other variables might also play a role, including the duration of disease and whether catecholamine release is sustained or episodic. A key confounder is the fact that cluster 1 tumours have a predominantly noradrenergic phenotype (Srirangalingam *et al.* 2008, 2009) and therefore any effect seen with noradrenaline may be mitigated by the negative regulatory effect of hypoxic signalling in these tumours.

A ciliary response to as little as 1nM adrenaline was observed in PC12 cells and this concentration is dwarfed by both that in adrenal venous effluent in patients without phaeochromocytomas (Table 6.2) and in phaeochromocytoma homogenate (Eisenhofer *et al.* 1998). This effect is thus seen within the physiological concentration range. It is important to consider, however, that PC12 cells are able to synthesise and secrete noradrenaline and dopamine, but not adrenaline (Greene & Tischler 1976). Under basal conditions, the mean concentration of noradrenaline in media that PC12 cells have been grown in is 6.1 nmol/mg (Greene & Tischler 1976) and this additional tumoural production may explain the more varied response observed with noradrenaline.

Antagonism of the beta receptor by propranolol prevents adrenaline-induced changes in PC12 primary cilia (Figure 5.22), whilst stimulation of the β_2 receptor by salbutamol phenocopies the adrenaline response (Figure 5.23). Together these results suggest that the ciliary response to adrenaline in PC12 cells is likely to be mediated by the β_2 receptor. Stimulation results in activation of AC, production of cAMP and activation of PKA. This pathway is an established promoter of ciliogenesis due to increasing anterograde IFT (Besschetnova *et al.* 2010) with a number of its components localising to primary cilia (Händel *et al.* 1999; Bishop *et al.* 2007; Ou *et al.* 2009).

Dopamine increased cilia incidence and length in PC12 cells. Unlike adrenaline and noradrenaline, it exerts its action via the dopamine receptor and has an established role in primary cilia dynamics. There are five dopamine receptor subtypes, three of which display ciliary localisation in a range of tissues: 1 (Domire *et al.* 2011; Avasthi *et al.* 2012; Marley & von Zastrow 2012; Marley *et al.* 2013; Omori *et al.* 2015), 2 (Iwanaga *et al.* 2011a; Marley & von Zastrow 2012; Omori *et al.* 2015) and 5 (Abdul-Majeed & Nauli 2011; Marley & von Zastrow 2012; Jin *et al.* 2014; Upadhyay *et al.* 2014). Activation of dopamine receptors appears to convey differential ciliary responsiveness in different tissue types mediated by different receptor subtypes. In murine endothelial cells (Abdul-Majeed & Nauli 2011; Kathem *et al.* 2014) and porcine renal cells (Upadhyay *et al.* 2014), dopamine increases cilia length via action on the D1-like receptor subfamily (which includes D1 and D5) (Abdul-Majeed & Nauli 2011; Avasthi & Marshall 2012; Kathem *et al.* 2014; Upadhyay *et al.* 2014). In contrast, dopamine appears to shorten primary cilia in rodent striatal neurons via action on the D2 receptor (Miyoshi *et al.* 2014). In PC12 cells, metoclopramide (a D2 receptor antagonist) appeared to reduce and shorten primary cilia, presumably by preventing dopamine's autocrine action. Although this response is in keeping with previous reports, it is somewhat unexpected as it is the reverse of that seen in other tissues of neural origin. Furthermore, the D2 receptor is coupled to $G_{\alpha i}$ and activation results in a reduction in cAMP and PKA activity, which would not be expected to increase cilia length. The observed mechanism requires further delineation studies and it should be borne in mind that metoclopramide also has 5-HT4 activity (Guillemot *et al.* 2009), which can increase ciliary length (Khan *et al.* 2016).

These data provide preliminary evidence for modulation of primary cilia by circulating catecholamines within the context of phaeochromocytomas. Further studies will define the underlying mechanism and whether this effect is seen in a broader range of tissues.

5.4.4 Somatostatin analogues result in elongation of primary cilia

Somatostatin is a pan-inhibitory peptide hormone that acts predominantly on the pituitary gland and gastrointestinal system via five different GPCRs ($SSTR_{1-5}$). $SSTR_2$ (Kimura *et al.* 2001; Reubi *et al.* 2001), $SSTR_3$ and $SSTR_5$ (Unger *et al.* 2012) are all expressed in human adrenal medulla. SSTRs are also expressed in phaeochromocytomas, although the relative expression of each receptor subtype is highly variable between cohorts (Kubota *et al.* 1994; Reubi *et al.* 2000; Pasquali *et al.* 2008; Unger *et al.* 2008; Ziegler *et al.* 2009; Elston *et al.* 2015). Although the physiological role of somatostatin in the adrenal medulla is not well characterised, SSAs have a well-established role in the diagnosis (Taïeb *et al.* 2012) and treatment (Kong *et al.* 2017) of PPGL and other neuroendocrine tumours (Rinke *et al.* 2009; Caplin *et al.* 2014).

The SSA pasireotide increased ciliary incidence and length in PC12 cells, which express SSTRs (Traina *et al.* 1998), whilst the SSA octreotide increased cilia length only, and at higher concentrations (Figure 5.27). Pasireotide has greater affinity for $SSTR_3$ and $SSTR_5$ than octreotide (Lesche *et al.* 2009) and we may therefore postulate that the observed difference might be due to these receptor subtypes. Interestingly $SSTR_3$ is the only SSTR known to localise to primary cilia (Händel *et al.* 1999; Berbari *et al.* 2008a; Iwanaga *et al.* 2011b; O'Connor *et al.* 2013). There is little direct experimental evidence regarding the effect of SSAs on primary cilia. A single study found that pasireotide increased primary hepatocyte cilia length and reduced cyst formation in a rat model of PKD and that this effect was augmented with concurrent HDAC6 inhibition (Lorenzo Pisarello *et al.* 2018). SSAs retard progression of cystic liver disease in the ciliopathy ADPKD (van Keimpema *et al.* 2009) in humans, providing further indirect clinical evidence.

5.5 Summary

In this chapter I have demonstrated that phaeochromocytoma primary cilia are influenced both by internal (for example, pseudohypoxia in the case of cluster 1 tumours) and external (components of the tumour microenvironment, including hypoxia and catecholamines) factors. In the case of hypoxia and pseudohypoxia, cilia loss occurs in a HIF and AURKA/HDAC6 dependent manner and can be prevented by inhibition of these pathways. This raises the possibility that primary cilia play a complex and multi-factorial interactive role with the tumour microenvironment and are potential modifiable targets.

CHAPTER 6

Adrenal venous catecholamine measurement as an adjunct in the diagnosis of phaeochromocytoma, with particular reference to syndromic disease

The work performed in this chapter was conducted in collaboration with others as part of routine clinical care. All analysis and interpretation are my own work.

At St Bartholomew's Hospital, London, UK, Dr Candy Sze was responsible for maintenance of the Conn's database, Dr Matthew Matson performed the AVS, and clinical care of the patients was the responsibility of Dr Scott Akker, Prof Maralyn Druce and Prof William Drake.

Data from Radboud University Medical Center, Nijmegan, The Netherlands, was provided by Prof Jacques Lender and Prof Graeme Eisenhofer, Technische Universität Dresden, Dresden, Germany.

Work in this chapter has been published in the following article, which is included in the appendix of this thesis.

Adrenal Vein Catecholamine Levels and Ratios: Reference Intervals Derived from Patients with Primary Aldosteronism. Sze CWC*, O'Toole SM*, Tirador RK, Akker SA, Matson M, Perry L, Druce MR, Dekkers T, Deinum J, Lenders JWM, Eisenhofer G, Drake WM. Hormone and Metabolic Research 2017; 49(6): 418-423.

* denotes equal contribution

6.1 Introduction

In this chapter, we move from the pathophysiology of phaeochromocytoma development to its diagnosis. The largest barrier to phaeochromocytoma detection is its lack of consideration in the differential. Once suspected, the biochemical diagnosis is confirmed by demonstration of elevated free metanephrines in plasma or fractionated metanephrines in urine (Lenders *et al.* 2014). These tests have very high sensitivities and specificities consistently exceeding 90% (Raber *et al.* 2000; Lenders *et al.* 2002, 2014) such that dynamic testing, for example with the clonidine suppression test, has a very limited clinical role (Lenders *et al.* 2014).

Once the biochemical diagnosis has been made and metanephrine excess has been confirmed, the source must be identified and localised by cross-sectional imaging techniques e.g. CT or MRI. Functional imaging modalities e.g. ^{123}I-MIBG or ^{18}F-FDG may be used if further confirmation is required and are of particular use in the setting of metastatic disease, when PRRT is a therapeutic option.

Taking this approach, uncertainty regarding PPGL localisation is unusual; particularly in patients with sporadic and symptomatic disease. The situation is different, however, in patients with a genetic predisposition to PPGL development e.g. VHL and SDHx. Such patients are often asymptomatic and enrolled within screening programmes in which biochemical and radiological surveillance runs concurrently and aims to diagnose small, pre-symptomatic PPGL when the risk of disseminated disease is lower (Maher *et al.* 2011; Jasperson *et al.* 2014). On occasion, this can lead to the detection of small radiological abnormalities which can be too small to characterise fully by cross-sectional modalities and are below the limit of detection of nuclear medicine techniques. Bilateral radiological abnormalities are also a consideration in these patient groups, particularly with advancing age when incidentaloma incidence increases. This presents difficulties in decision-making in a group of patients who are often at risk of developing other tumours requiring multiple abdominal interventions. Correct identification of one or other adrenal gland as the source of catecholamine excess would be treated by a unilateral adrenalectomy (thereby avoiding, for a time at least, the need for adrenal replacement therapy) whereas a secure diagnosis of bilateral phaeochromocytoma could facilitate surgery at a single sitting.

Thus, there is a potential role for a technique that could assist with anatomical localisation in cases which are unclear following a conventional imaging approach. One such technique is AVS, which although now most commonly used for the lateralisation of primary aldosteronism (PA), was originally developed in the pre-CT era for the diagnosis and localisation of catecholamine-secreting

tumours (Von Euler *et al.* 1955). In this procedure (Figure 6.1), venous access is established via the common femoral vein and an intra-venous catheter is advanced under fluoroscopic guidance. Blood samples are obtained sequentially from both adrenal veins and the infra-renal IVC as a peripheral sample. Location of the catheter tip is confirmed in real time with fluoroscopy and successful cannulation is subsequently confirmed by the demonstration of a significant gradient in cortisol concentration between the adrenal vein and the periphery (Funder *et al.* 2016). The magnitude of the requisite gradient depends on whether AVS is carried out with (5:1) or without (2:1) ACTH stimulation of adrenal cortisol release (Funder *et al.* 2016).

Historically, caval catheters and AVS have been used for the diagnosis (Von Euler *et al.* 1955; Jones *et al.* 1979; Palublnskas *et al.* 1980; Allison *et al.* 1983) and lateralisation of adrenal phaeochromocytomas (Davies *et al.* 1979; Nobin *et al.* 1982; Chew *et al.* 1994; Srirangalingam *et al.* 2010) as well as the localisation of abdominal (Crout & Sjoerdsma 1960; Fleisher *et al.* 1964; Grim *et al.* 1967; Moss *et al.* 1980; Chew *et al.* 1994; Pacak *et al.* 2001; Srirangalingam *et al.* 2010), bladder (Miller *et al.* 1983) and head and neck paragangliomas (Crout & Sjoerdsma 1960; Cockcroft *et al.* 1987). Interpretation of these venous sampling studies depended on either the use of non-standardised gradient cut-offs, comparison with the contralateral adrenal or assumptions surrounding the noradrenaline: adrenaline ratio. Adrenaline is the predominantly secreted adrenal catecholamine (Wurtman & Axelrod 1965) and an excess of noradrenaline, expressed as a noradrenaline: adrenaline ratio exceeding one, has been proposed as being pathological (Newbould *et al.* 1991), although there are limited normative data to support this. Uncertainty remains in the field (Freel *et al.* 2010), largely due to the lack of robust reference intervals for catecholamine values in adrenal venous effluent.

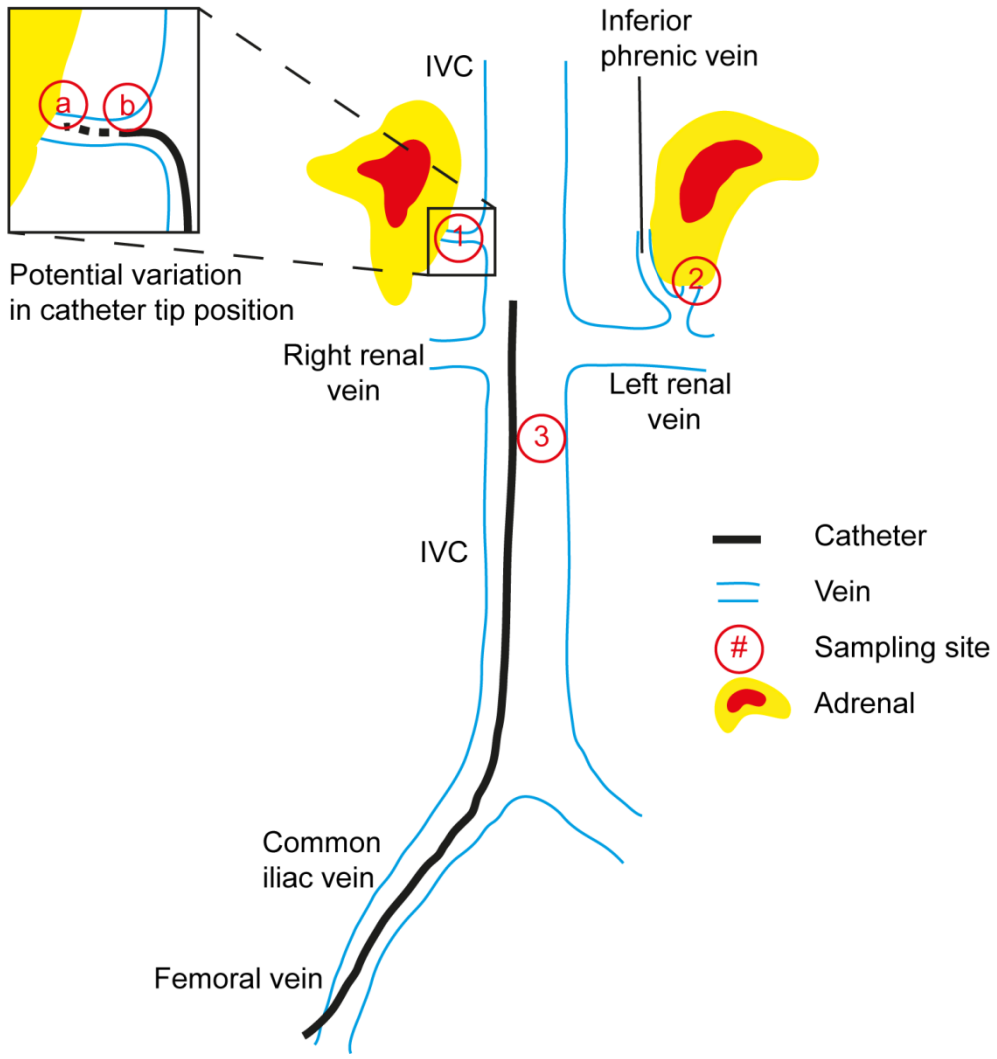

Figure 6.1: Schematic diagram of adrenal venous sampling

Venous access is established via the right femoral vein and the catheter advanced through the common iliac vein and infra-renal inferior vena cava (IVC). Blood samples are taken under gravity without the application of negative pressure from each adrenal vein (1 and 2) and the infra-renal IVC as a peripheral sample (3). Adrenal venous anatomy is different on either side; the right adrenal vein (1) drains directly into the IVC, whilst the left (2) first drains into the left renal vein. This makes the right adrenal vein technically more difficult to cannulate, whilst samples from the left adrenal vein are susceptible to dilution from the inferior phrenic vein. In both adrenal veins, there is potential variation in the distance the catheter tip is from the adrenal gland at the time of sampling (inset; a and b) which might impact on the magnitude of the measured adrenal hormones. It is for this reason that cortisol is used as a 'correction factor' in the evaluation of primary aldosteronism.

6.2 Aims and Objectives

The aim of this chapter was to investigate whether AVS for catecholamines has a potential role in assisting the localisation of phaeochromocytoma in selected cases.

We hypothesised that the adrenal venous noradrenaline: adrenaline ratio would differ significantly in patients with phaeochromocytoma compared to those without.

The first objective was to determine normal circulating adrenal vein catecholamine concentrations in patients without phaeochromocytoma, who had undergone AVS due to PA.

The second objective was to determine circulating adrenal vein catecholamine concentrations in patients with histologically confirmed phaeochromocytoma.

The third objective was to define a diagnostic cut-off that would differentiate patients with and without phaeochromocytoma.

6.3 Results

6.3.1 Normal adrenal venous catecholamine concentrations in patients with primary aldosteronism

6.3.1.1 Clinical characterisation of PA cohort

One hundred and seventy-two patients (88 male, 84 female, age 51.5 years ± 0.5) underwent AVS under conditions of ACTH stimulation for the localisation of biochemically confirmed PA at two international centres (Table 6.1); St Bartholomew's Hospital, London and the Radboud University Medical Centre, Nijmegan, The Netherlands. The mean age of patients (p = 0.43) and bilateral adrenal vein cannulation success (p = 0.15) was similar at both centres. The St Bartholomew's cohort had significantly more male patients (59.2% compared to 32.7%, p=0.0014).

	All	SBH	RUMC	p value
Patients (n)	172	120 (69.8)	52 (30.2)	
AVS (n)	177	125 (70.6)	52 (29.4)	
Sex				
Male (n)	88 (51.2)	71 (59.2)	17 (32.7)	0.0014
Female (n)	84 (48.9)	49 (40.8)	35 (67.3)	
Age (years)				
Mean ± SEM	51.5 ± 0.8	51.1 ± 0.9	52.5 ± 1.5†	0.43
Range	21 – 76	21-76	24-72†	
Bilateral cannulation (%)	130 (72.6)	87 (67.4)	43 (82.7)	0.15

Table 6.1: Clinical characteristics of 172 patients with PA who underwent AVS

Figures in brackets represent percentage figures. SBH = St Bartholomew's Hospital, RUMC = Radboud University Medical Center, AVS = adrenal venous sampling, SEM = standard error of the mean. Statistical significance assessed by the chi-squared test for sex and cannulation success and an unpaired t-test for age.

† Age at time of AVS unavailable for three patients.

6.3.1.2 Adrenal venous catecholamine concentrations in patients with PA

Technically successful cannulation of the adrenal vein was defined by the adrenal vein cortisol concentration exceeding that of the infra-renal IVC by a factor of five. Using these strict criteria, samples for catecholamine analysis were available from a total of 289 adrenal veins (130 right, 159 left). Catecholamine concentrations from both adrenal veins were available from 113 patients.

First, we considered only the 113 patients with technically successful bilateral adrenal vein cannulation with available catecholamine concentrations (Table 6.2 and Figure 6.2).

As expected, adrenaline exceeded noradrenaline in both veins. In addition, a discrepancy between left and right was observed. The median adrenaline (64.1 nmol/L compared to 35.1, $p=1.7 \times 10^{-7}$) and noradrenaline (16.3 nmol/L compared to 10.6, $p=2.4 \times 10^{-6}$) concentrations were both higher in the right adrenal vein than in the left. Conversely, the noradrenaline to adrenaline ratio was greater on the left (0.31) than the right (0.26, $p=8.3 \times 10^{-6}$).

	Left adrenal vein	Right adrenal vein	p-value
Adrenaline (nmol/L)			
Minimum	4.0	4.0	1.7×10^{-7}
1st quartile	19.5	31.5	
Median	35.1	61.4	
3rd quartile	72.8	126.7	
Maximum	301.4	571.0	
Noradrenaline (nmol/L)			
Minimum	0.7	0.9	2.4×10^{-6}
1st quartile	6.6	8.8	
Median	10.6	16.3	
3rd quartile	18.7	31.8	
Maximum	74.1	160.5	
Adrenaline: noradrenaline			
Minimum	0.09	0.08	8.3×10^{-6}
1st quartile	0.20	0.18	
Median	0.31	0.26	
3rd quartile	0.51	0.38	
Maximum	3.10	4.35	

Table 6.2: Paired adrenal venous catecholamine concentrations in patients who underwent adrenal venous sampling for the diagnosis of PA with successful bilateral cannulation

Data are presented from the 113 patients with successful bilateral adrenal vein cannulation. P values were calculated using the Wilcoxon signed rank test.

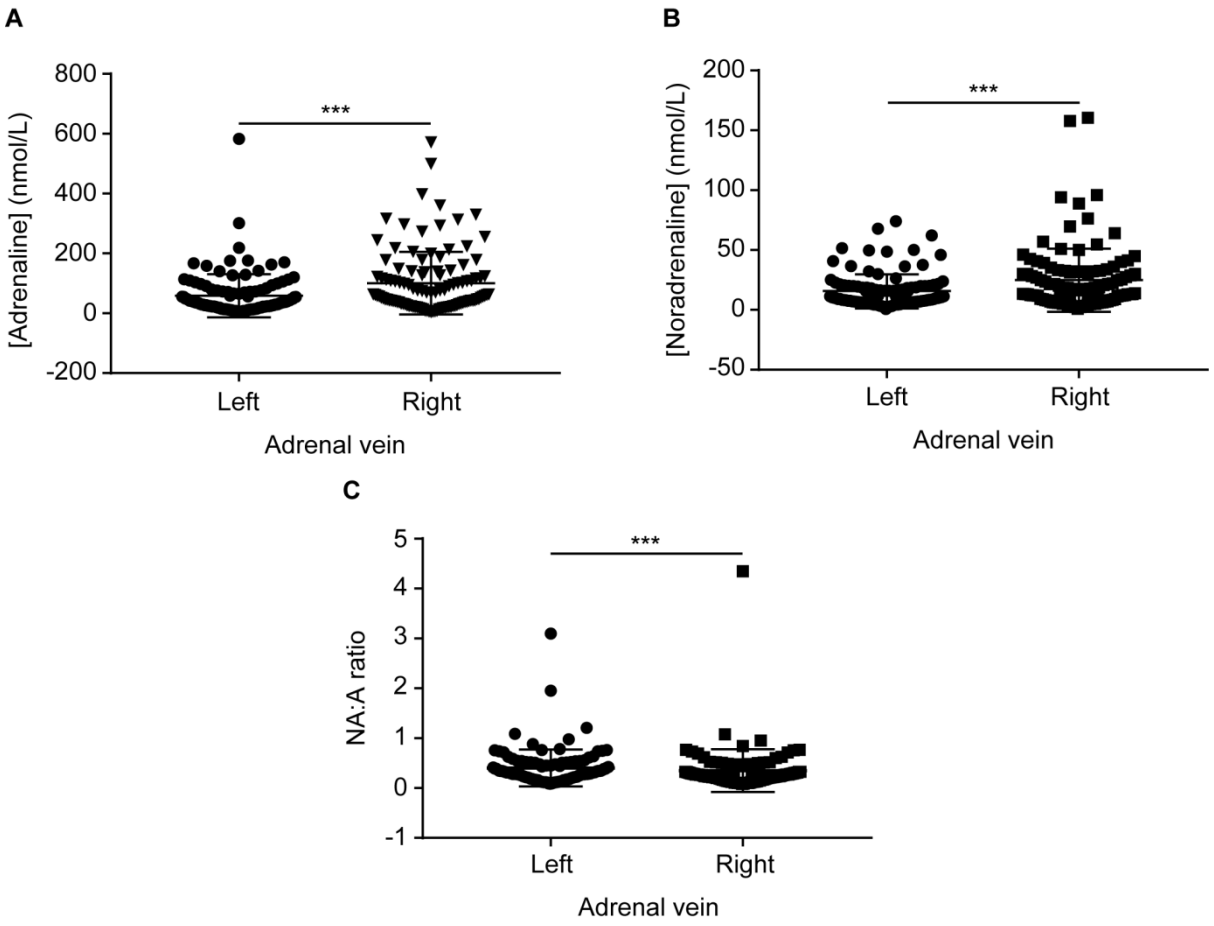

Figure 6.2: Adrenal venous catecholamine concentrations in patients who underwent adrenal venous sampling for the diagnosis of PA

113 patients with PA had successful bilateral adrenal vein cannulation (defined as an adrenal vein: peripheral cortisol ratio exceeding 5:1). Adrenal venous adrenaline **(A)** and noradrenaline **(B)** were measured and the noradrenaline: adrenaline ratio **(C)** was calculated for each adrenal vein. Centre bar represents mean, error bars standard deviation. Statistical significance was assessed using the Wilcoxon signed rank test. *** $p<0.001$.

Given the large degree of intra-individual variability in absolute adrenal venous catecholamine concentrations (up to a factor of 178 on the right and 106 on the left), we considered whether a 'correction' factor would reduce this. In the lateralisation of PA, adrenal venous aldosterone is typically 'normalised' to ipsilateral adrenal venous cortisol to provide an aldosterone: cortisol ratio which is used for comparison with the contralateral adrenal vein (Funder *et al.* 2016). This approach is employed to correct for variations in the distance from the adrenal gland that the blood test is taken with the assumption being that the concentration of all adrenal hormones will be highest closest to the adrenal gland and will reduce the further from it (Figure 6.1). This is of particular importance in lateralisation studies as there is significant anatomical difference between the right adrenal vein (which is short and drains directly into the IVC) and the left adrenal vein (which is longer and drains into the left renal vein before reaching the IVC).

Thus, we 'normalised' the absolute catecholamine concentration in the adrenal veins by 'correcting' for ipsilateral adrenal venous cortisol concentration (Table 6.3 and Figure 6.3). This did not reduce inter-individual variability (factors ranging from 129 to 922), but did eliminate the observed differences between left and right adrenal venous adrenaline (Figure 6.3A; median 0.00253 compared to 0.00285 p=0.31) and noradrenaline (Figure 6.3B; median 0.00081 compared to 0.00074, p=0.96). The noradrenaline: adrenaline ratio remained higher in the left adrenal vein than the right (Figure 6.3C; median 0.00002 compared to 0.000016, $p=6.1x10^{-9}$).

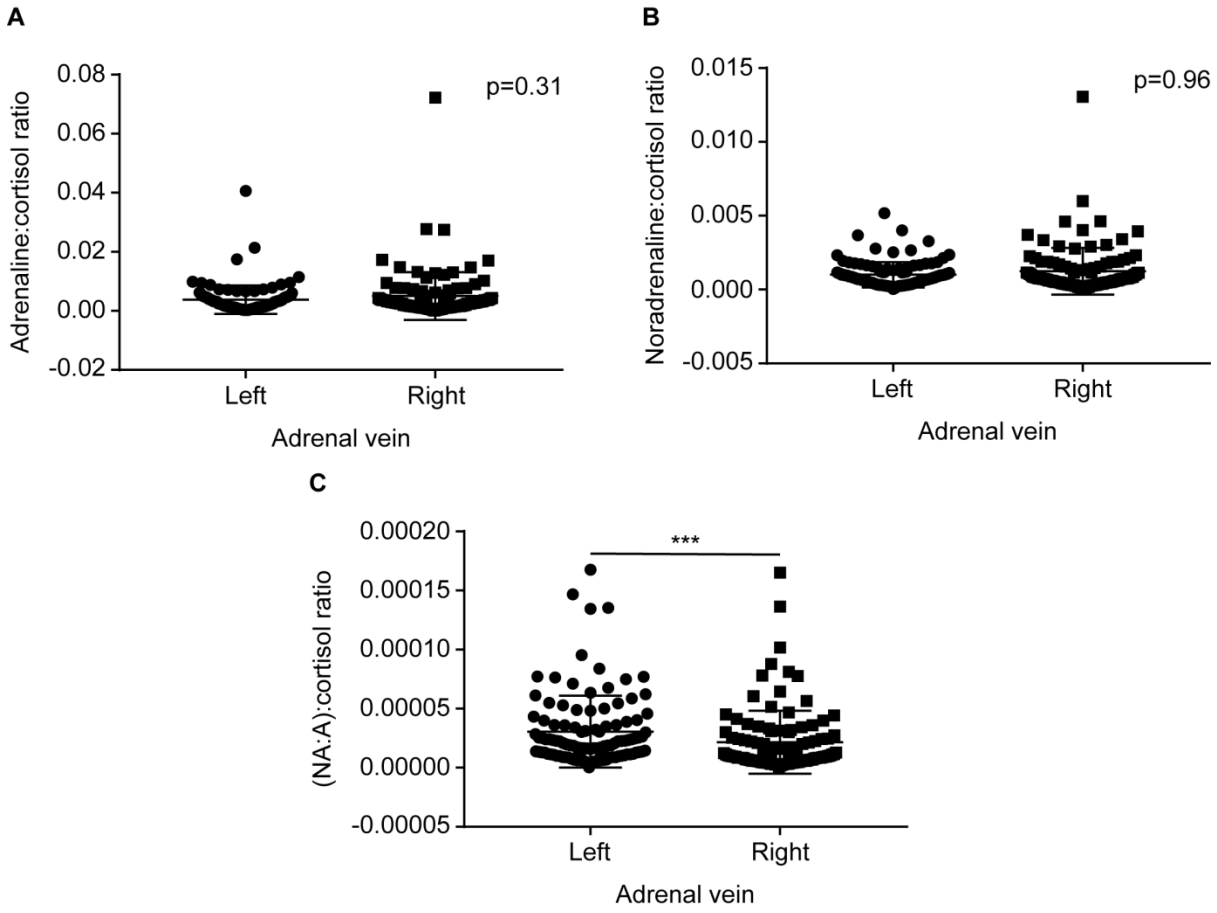

Figure 6.3: Adrenal venous catecholamine concentrations divided by ipsilateral cortisol concentrations in patients who underwent adrenal venous sampling for the diagnosis of PA

113 patients with PA had successful bilateral adrenal vein cannulation (defined as an adrenal vein: peripheral cortisol ratio exceeding 5:1). Adrenal venous adrenaline **(A)** and noradrenaline **(B)** were measured and the noradrenaline: adrenaline ratio **(C)** was calculated for each adrenal vein and divided by ipsilateral adrenal venous cortisol concentration. Centre bar represents mean, error bars standard deviation. Statistical significance was assessed using the Wilcoxon signed rank test. *** $p<0.001$.

	Left adrenal vein	Right adrenal vein	p value
Adrenaline/cortisol			
Minimum	0.00029	0.00011	0.31
1st quartile	0.00131	0.00149	
Median	0.00253	0.00285	
3rd quartile	0.00471	0.00520	
Maximum	0.04064	0.07223	
Noradrenaline/cortisol			
Minimum	0.00002	0.00005	0.96
1st quartile	0.00043	0.00043	
Median	0.00081	0.00074	
3rd quartile	0.00121	0.00143	
Maximum	0.00517	0.01306	
NA:A/cortisol			
Minimum	$2.5x10^{-7}$	$1.8x10^{-7}$	$6.1x10^{-9}$
1st quartile	0.000012	0.000006	
Median	0.000020	0.000016	
3rd quartile	0.000036	0.000025	
Maximum	0.000168	0.000165	

Table 6.3: Adrenal vein catecholamine: cortisol ratios in patients who underwent adrenal venous sampling for the diagnosis of PA

Data are presented from the 113 patients with successful bilateral adrenal vein cannulation. P values were calculated using the Wilcoxon signed rank test.

Given that the patients were from two different centres in two different countries, we considered whether differences existed between the two cohorts (Figure 6.4 and Table 6.4). Adrenal venous adrenaline concentrations were similar in patients from each centre (median concentrations 31.8 nmol/L and 31.2 nmol/L on the left, p = 0.464; 62.8 nmol/L and 69.9 nmol/L on the right, p = 0.974). However, adrenal venous noradrenaline concentrations were significantly higher in the St Bartholomew's cohort (median 11.1 nmol/L compared to 9.6 nmol/L on the left, $p = 8.2x10^{-6}$; 17.7 nmol/L compared to 13.8 nmol/L on the right, p = 0.0178). This resulted in a higher noradrenaline: adrenaline ratio in the St Bartholomew's cohort (0.35 compared to 0.23 on the left, p = 0.0003; 0.29 compared to 0.21 on the right, p = 0.0013).

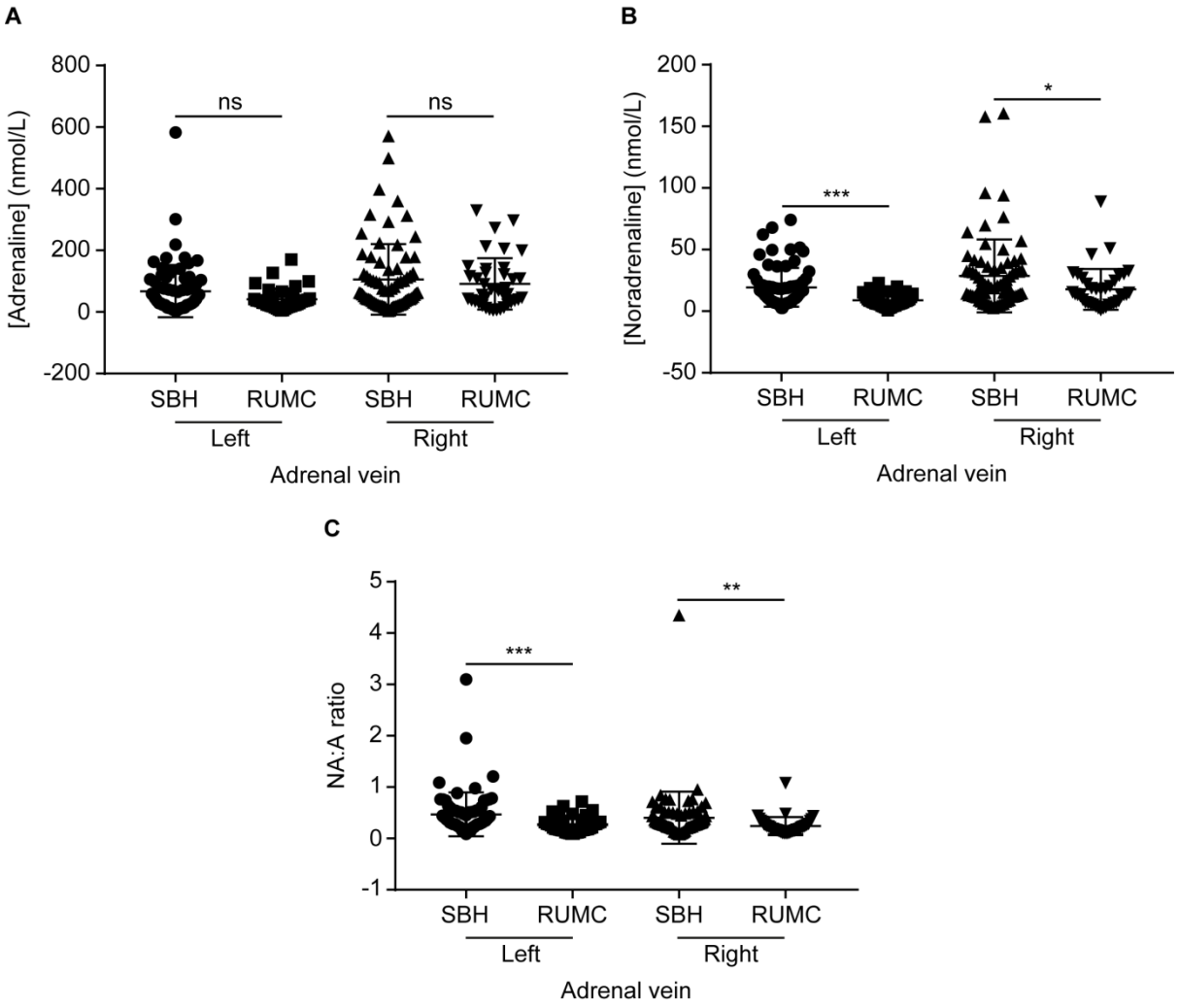

Figure 6.4: Adrenal venous catecholamine concentrations in patients who underwent AVS for the diagnosis of PA according to centre

113 patients with PA (74 at St Bartholomew's Hospital (SBH), 39 at Radbound University Medical Center (RUMC)) had successful bilateral adrenal vein cannulation, defined as an adrenal vein: peripheral cortisol ratio exceeding 5:1. Adrenal venous adrenaline **(A)** and noradrenaline **(B)** were measured and the noradrenaline: adrenaline ratio **(C)** was calculated for each adrenal vein. Centre bar represents mean, error bars standard deviation. Statistical significance between centres was assessed using the Mann Whitney U test. NA = noradrenaline, A = adrenaline, ns = not significant, * $p<0.05$, ** $p<0.01$, *** $p<0.001$.

	Median (IQR)		
	St Bartholomew's	Radboud UMC	p-value
Left adrenal vein			
Adrenaline (nmol/L)	31.8 (17.5-76.9)	31.2 (18.9-51.9)	0.464
Noradrenaline (nmol/L)	11.1 (6.9-20.7)	9.6 (5.2-11.4)	$8.2x10^{-6}$
Noradrenaline: adrenaline ratio	0.35 (0.24-0.55)	0.23 (0.16-0.35)	0.0003
Right adrenal vein			
Adrenaline (nmol/L)	62.8 (28.6-131.9)	69.6 (33.4-133.3)	0.974
Noradrenaline (nmol/L)	17.7 (11.6-32.9)	13.8 (6.6-25.8)	0.0178
Noradrenaline: adrenaline ratio	0.29 (0.21-0.51)	0.21 (0.15-0.30)	0.0013

Table 6.4: Adrenal venous catecholamine concentrations in patients who underwent AVS for the diagnosis of PA according to centre

Data are presented from the 113 patients (74 St Bartholomew's, 39 Radbound UMC) with successful bilateral adrenal vein cannulation as median and interquartile ranges. P values were calculated using the Mann Whitney U test. IQR = Interquartile range, UMC = University Medical Center.

Given that the only demographic difference between the cohorts was the significantly higher proportion of males in the St Bartholomew's group (Table 6.1), we sought to examine whether this was the cause of the observed difference in adrenal venous noradrenaline concentration.

The St Bartholomew's group consisted of 71 males and 49 females (Table 6.1). There was no significant difference between the sexes and concentration of adrenaline (p=0.68 left, p=0.45 right), noradrenaline (p=0.36 left, p=0.93 right) or the noradrenaline: adrenaline ratio (p=0.85 left, p=0.36 right) in either adrenal vein (Table 6.5 and Figure 6.5). This was as expected given the lack of need for gender-specific reference intervals for catecholamines and is suggestive of another factor being responsible for the observed inter-cohort differences.

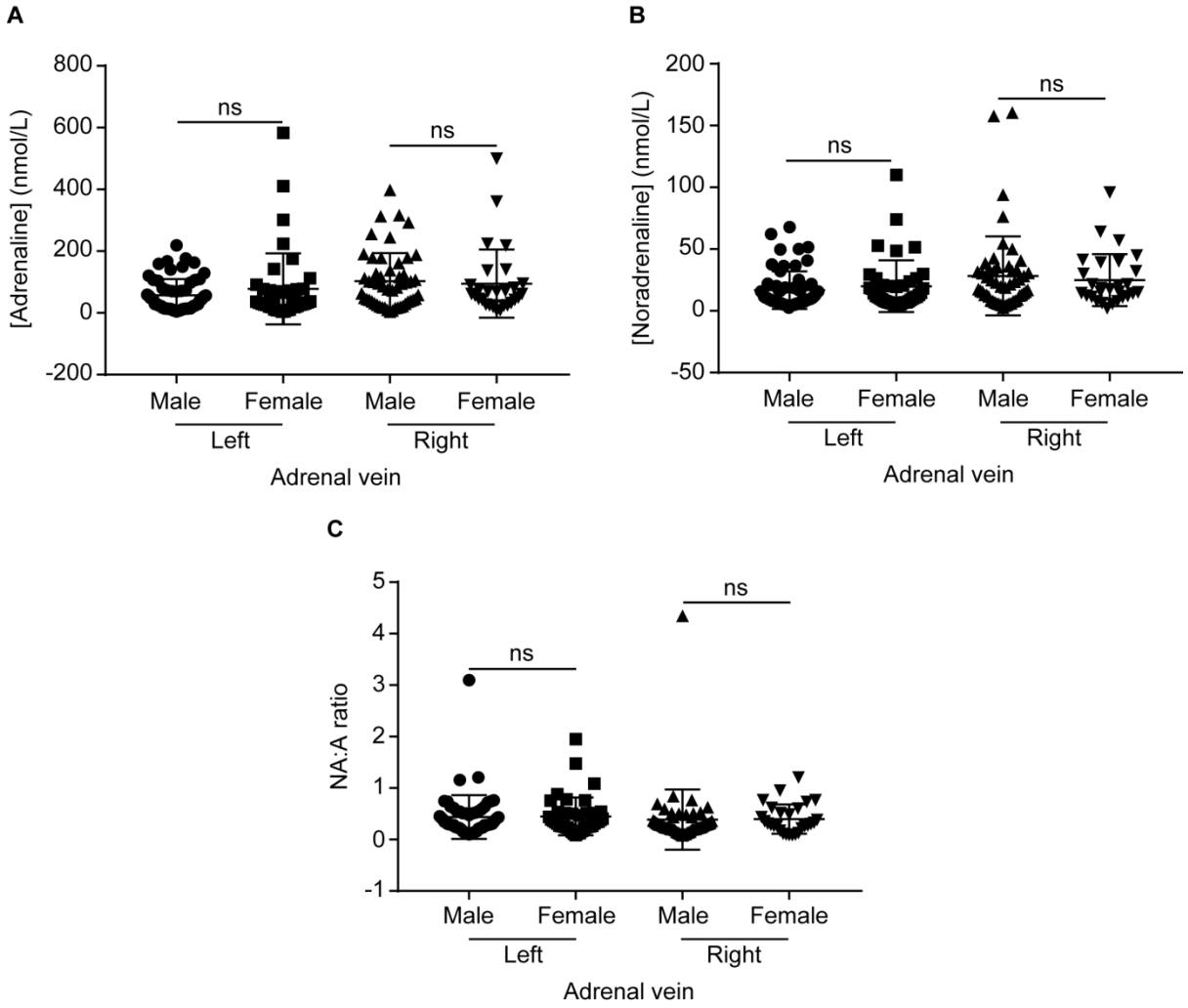

Figure 6.5: Adrenal venous catecholamine concentrations in patients who underwent AVS for the diagnosis of PA at St Bartholomew's Hospital according to sex

120 patients with PA (71 male, 49 female) underwent AVS at St Bartholomew's Hospital. Data are presented from all successfully cannulated adrenal veins (108 on the left, 86 on the right; defined as an adrenal vein: peripheral cortisol ratio exceeding 5:1). Adrenal venous adrenaline **(A)** and noradrenaline **(B)** were measured and the noradrenaline: adrenaline ratio **(C)** was calculated for each adrenal vein. Centre bar represents mean, error bars standard deviation. Statistical significance between sexes was assessed using the Mann Whitney U test. NA = noradrenaline, A = adrenaline, ns = not significant.

	Median (IQR)		
	Male	Female	p-value
Left adrenal vein			
Adrenaline (nmol/L)	39.5 (13.7 – 79.9)	36.0 (19.7 – 76.4)	0.68
Noradrenaline (nmol/L)	10.3 (6.9 – 19.8)	12.2 (7.4 – 22.4)	0.36
Noradrenaline: adrenaline ratio	0.31 (0.23 – 0.54)	0.34 (0.24 – 0.52)	0.85
Right adrenal vein			
Adrenaline (nmol/L)	84.1 (32.7 – 135.2)	61.4 (28.1 – 93.4)	0.45
Noradrenaline (nmol/L)	19.2 (8.6 – 32.9)	16.7 (11.5-37.4)	0.93
Noradrenaline: adrenaline ratio	0.27 (0.20 – 0.42)	0.31 (0.18 – 0.58)	0.36

Table 6.5: Adrenal venous catecholamine concentrations in patients who underwent AVS for the diagnosis of PA at St Bartholomew's Hospital according to sex

Data are presented from the 120 patients with PA who underwent AVS at St Bartholomew's Hospital as per Figure 6.5 as median and interquartile ranges. P values were calculated using the Mann Whitney U test. IQR = Interquartile range.

It is well established that a number of anti-hypertensive medications can interfere with the laboratory measurement of catecholamines (Lenders *et al.* 2014) either due to analytical interference depending on the method used (e.g. certain beta adrenergic receptor antagonists) or due to pharmacodynamic interference irrespective of the analytical methodology (e.g. alpha adrenergic receptor antagonists). In the PA patients who had undergone AVS, the range of prescribed anti-hypertensives was strictly limited to those classes that are known not to interfere with aldosterone measurement – namely alpha adrenoceptor antagonists and calcium-channel receptor antagonists. We thus sought to determine whether these medications might alter adrenal venous catecholamine concentrations and whether this might explain the observed differences between the two centres. All patients who underwent AVS at St Bartholomew's Hospital were on the alpha adrenergic receptor antagonist doxazosin at the time of AVS. However, this was not the case in Nijmegan, where only 22 or 52 patients (42.3%) were. Taking advantage of this fact, we compared the adrenal venous catecholamine concentrations in Dutch patients according to whether or not they were taking doxazosin at the time of AVS (Figure 6.6 and Table 6.6).

There was no significant difference in adrenal venous adrenaline concentration on either side in those taking doxazosin compared to those who weren't (Figure 6.6A; p=0.56 for left, p=0.87 for right). Noradrenaline concentration was significantly higher in patients taking doxazosin in the left adrenal vein (Figure 6.6B; 9.7 nmol/L compared to.6.1 nmol/L, p=0.0087). However, this did not

result in a significant change in the noradrenaline: adrenaline ratio on the left (Figure 6.6C; p=0.138) and no difference in noradrenaline concentration was seen on the right (p=0.234). Interestingly, the observed noradrenaline: adrenaline ratio in the right adrenal vein was higher (0.27 v 0.17, p=0.013) in those on doxazosin despite a lack of significant change in either catecholamine concentration on that side. It would be expected that any effect of alpha adrenoceptor blockade on circulating catecholamines would be systemic and thus this unilateral observation is unexpected and is discussed in detail later in this chapter.

	Median (IQR)		
	Alpha-blocker	No alpha-blocker	p-value
Left adrenal vein			
Adrenaline (nmol/L)	32.8 (27.0-46.3)	30.6 (15.6-57.0)	0.555
Noradrenaline (nmol/L)	9.7 (7.3-15.1)	6.1 (4.3-9.6)	0.0087
Noradrenaline: adrenaline ratio	0.29 (0.19-0.46)	0.19 (0.15-0.34)	0.138
Right adrenal vein			
Adrenaline (nmol/L)	57.5 (38.1-138.9)	73.6 (36.2-118.2)	0.874
Noradrenaline (nmol/L)	17.6 (9.5-29.2)	12.7 (5.4-23.1)	0.234
Noradrenaline: adrenaline ratio	0.27 (0.18-0.38)	0.17 (0.13-0.24)	0.013

Table 6.6: Adrenal venous catecholamine concentrations in patients who underwent AVS for the diagnosis of PA at Radboud UMC according to whether they were taking an alpha adrenergic receptor antagonist at the time of AVS

Data are presented from 52 patients (22 on doxazosin, 30 who were not) from Radboud UMC with at least one adrenal vein successfully cannulated as median and interquartile ranges. P values were calculated using the Wilcoxon signed rank test. All patients at St Bartholomew's Hospital were on an alpha receptor antagonist at the time of AVS and are not included in this analysis.

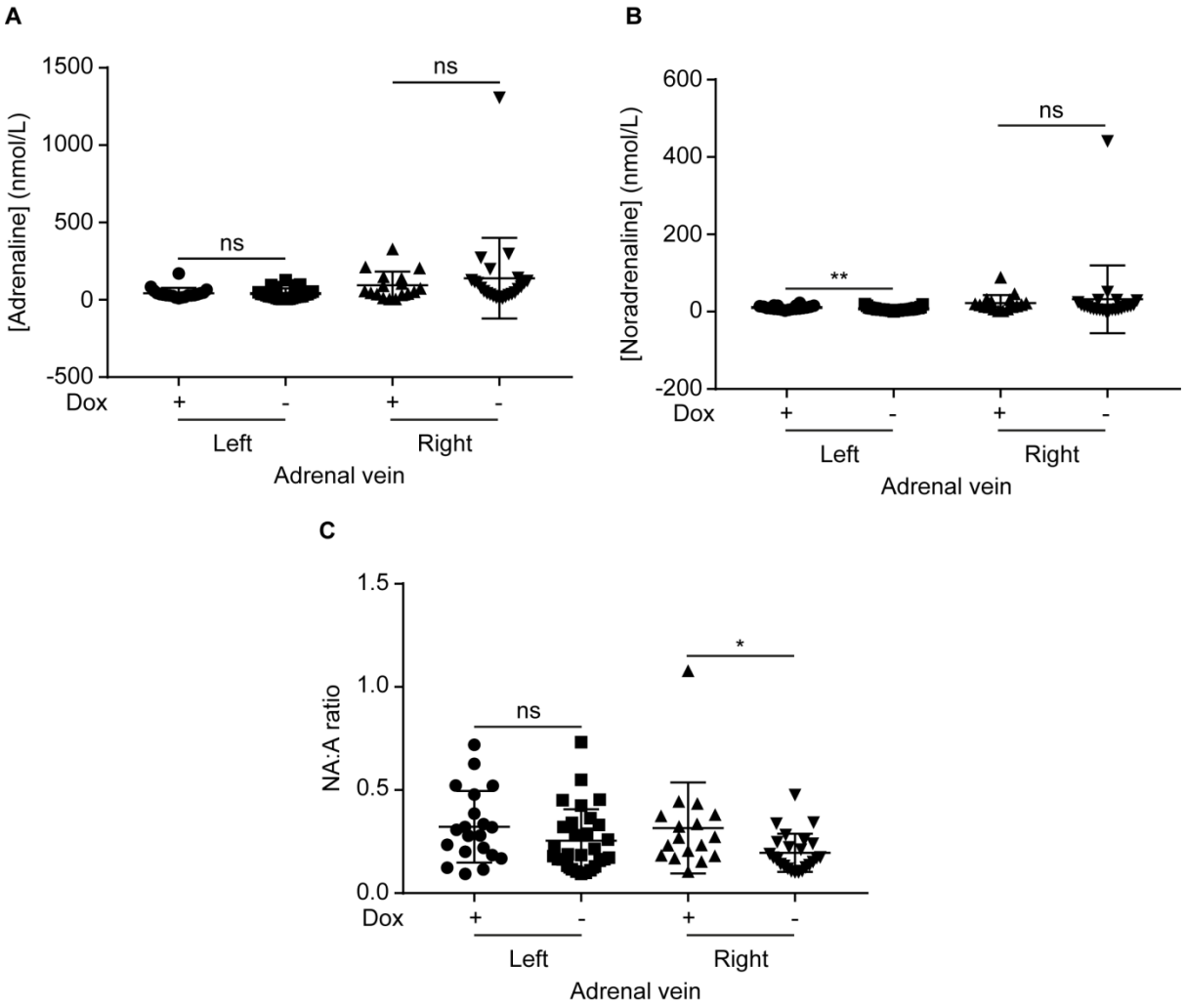

Figure 6.6: Adrenal venous catecholamine concentrations in patients who underwent AVS for the diagnosis of PA at Radbound University Medical Center according to whether they were taking an alpha adrenergic receptor antagonist at the time of AVS

52 patients with PA (22 on doxazosin, 30 who were not) had at least one adrenal vein successfully cannulated (adrenal venous cortisol greater than five times the periphery; n=49 on the left, 41 on the right). Adrenal venous adrenaline **(A)** and noradrenaline **(B)** were measured and the noradrenaline: adrenaline ratio **(C)** was calculated for each adrenal vein. Centre bar represents mean, error bars standard deviation. Statistical significance between groups was assessed using the Mann Whitney U test. Dox = doxazosin, NA = noradrenaline, A = adrenaline, ns = not significant, * $p < 0.05$.

Thus, in keeping with previous reports (Kahaly *et al.* 1985; Freel *et al.* 2010; Baba *et al.* 2013), absolute concentrations of catecholamines in the adrenal veins vary widely between individuals. This variation is reduced when considering the noradrenaline: adrenaline ratio, with a ratio exceeding one having previously been proposed as pathological (Newbould *et al.* 1991) as adrenaline is the predominant adrenal catecholamine (Wurtman & Axelrod 1965).

Considering all 172 patients with PA who underwent AVS, the left adrenal vein was successfully cannulated 159 times (92.4%) and the right 130 times (75.6%). Using all successfully cannulated adrenal veins samples, even if success was only unilateral, centile values for the left and right adrenal venous adrenaline: cortisol, noradrenaline: cortisol and noradrenaline: adrenaline ratios were calculated and are shown in Table 6.7. The noradrenaline: adrenaline ratio for the 97.5th centile was 1.21 on the left and 1.04 on the right.

Centile	Adrenal vein					
	Left			Right		
	A:cortisol	NA:cortisol	NA:A	A:cortisol	NA:cortisol	NA:A
1	0.000299	0.000105	0.09	0.000381	$8.8x10^{-5}$	0.07
2.5	0.000323	0.000189	0.10	0.000475	0.000123	0.09
5	0.000345	0.000215	0.11	0.000587	0.000175	0.10
10	0.000643	0.000266	0.13	0.000921	0.000275	0.11
25	0.001313	0.000438	0.20	0.001485	0.000430	0.17
50	0.002529	0.000811	0.31	0.002847	0.000737	0.26
75	0.004713	0.001213	0.51	0.005196	0.001435	0.40
90	0.007280	0.001864	0.74	0.011220	0.002903	0.62
95	0.009491	0.002595	0.88	0.014735	0.003820	0.77
97.5	0.012952	0.003371	1.21	0.019827	0.004613	1.04
99	0.020971	0.003972	2.41	0.027653	0.005857	3.38

Table 6.7: Centile values for the adrenaline (A): cortisol, noradrenaline (NA): cortisol and noradrenaline: adrenaline ratio in the right and left adrenal veins in patients with PA (n = 159 on the left, 130 on the right)

6.3.2 Adrenal venous catecholamine concentrations in patients with phaeochromocytoma

As a comparative group, six patients (three male, three female) with the clinical and biochemical suspicion of catecholamine excess who had undergone AVS as part of the diagnostic process were identified from the phaeochromocytoma database at St Bartholomew's Hospital (Table 6.8). Mean patient age was 31.3 $\pm$ 6.9 years (range 13 – 67 years) and five of the six had a genetic predisposition to phaeochromocytoma development (all VHL).

In the five VHL patients, surgery was indicated due to the presence of a confirmed secretory phaeochromocytoma (mean diameter 41.25 $\pm$ 9.6 mm) and AVS was undertaken either to confirm bilateral disease (patients 1 – 4) or to exclude phaeochromocytoma below the limit of resolution of imaging techniques (patient 5). AVS data guided surgical decision making: in patients 1 – 4, bilateral disease was confirmed due to an elevated adrenal venous noradrenaline: adrenaline ratio (minimum ratio 2.96) and these patients underwent a bilateral adrenalectomy at a single sitting. Bilateral phaeochromocytomas were confirmed histologically in all cases and it should be noted that in patient 1 there was no discernible radiological abnormality in the left adrenal despite histological confirmation of a phaeochromocytoma. In cases 2 – 4, a contralateral adrenal abnormality was identified radiologically, however they were small (5 – 10 mm) and radiologically indeterminate and did not display I^{123}-MIBG-uptake. Patient 5 had a left renal cell carcinoma and left para-aortic mass which was impossible to distinguish from the left adrenal gland on imaging. He was committed to surgical resection of both lesions and AVS was undertaken pre-operatively to exclude disease in the contralateral adrenal, which, if present, would have been tackled at the same operation. Given the reassuring right adrenal vein noradrenaline: adrenaline ratio (0.8), he underwent resection of the left renal lesion and para-aortic mass only. It was not possible surgically to spare the left adrenal gland and histological evaluation confirmed a paraganglioma with a normal adrenal gland. The left adrenal vein noradrenaline: adrenaline ratio was 0.5.

Patient 6 was older (67 years) and did not have VHL or any other phaeochromocytoma-predisposing syndrome. She had elevated circulating catecholamines and bilateral adrenal lesions (14 and 19mm respectively). There was a low clinical suspicion of bilateral disease and the smaller lesion did not display I^{123}-MIBG avidity; however it could not be categorically characterised as being benign on radiological criteria. She therefore underwent AVS to determine whether a unilateral or bilateral adrenalectomy was required with a unilateral procedure being ultimately performed due to a left adrenal vein noradrenaline: adrenaline ratio of 0.85. Histology confirmed a phaeochromocytoma in

the resected gland and post-operative metanephrine measurements were normal excluding the presence of a phaeochromocytoma in the left adrenal gland which remained in situ.

It should be noted that all six patients were on an alpha receptor antagonist (phenoxybenzamine) at the time of AVS and there were no haemodynamic or other adverse effects following AVS.

The lowest adrenal vein noradrenaline: adrenaline ratio in a confirmed phaeochromocytoma was 2.96 on the left and 1.75 on the right, although this figure is the minimum possible ratio and may have been higher as unfortunately insufficient sample was available for further determination of the noradrenaline concentration.

Adrenal venous noradrenaline: adrenaline ratios for patients with PA and those with phaeochromocytoma are displayed in Figure 6.7. Using a cut-off defined by the 97.5th centile of the PA cohort (1.21 on the left, 1.04 on the right), the false negative rate in the phaeochromocytoma cohort was 0%.

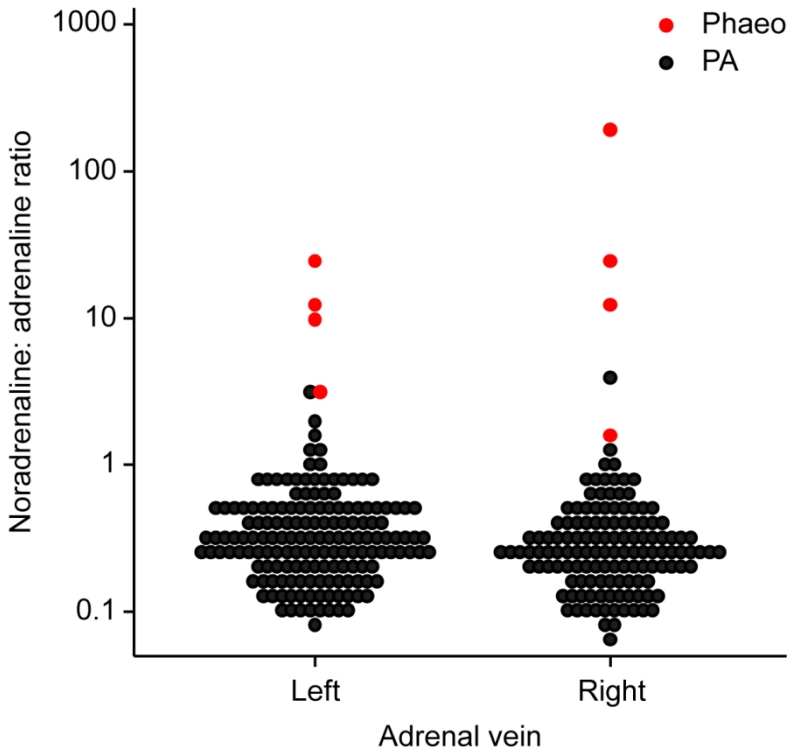

Figure 6.7: Adrenal venous noradrenaline: adrenaline ratios in patients undergoing AVS for PA (black) or with histologically confirmed phaeochromocytoma (red)

Adrenal venous noradrenaline: adrenaline ratios are presented from 172 patients with PA (black circles; left 159, right 130) and six patients with phaeochromocytomas (red circles; left 4, right 4). Phaeo = phaeochromocytoma, PA = primary aldosteronism.

Centre bar represents mean, error bars standard deviation. Statistical significance between groups was assessed using the Mann Whitney U test. Dox = doxazosin, NA = noradrenaline, A = adrenaline, ns = not significant, * $p < 0.05$, ** $p<0.01$.

Patient	Age	Sex	Genetic syndrome	Radiology*		MIBG		NA:A ratio		Operation	Histology
				Right	Left	Right	Left	Right	Left		
1	13	M	VHL	45	0	+	-	NC	2.96	Bilateral adrenalectomy	Bilateral phaeochromocytoma
2	29	M	VHL	45	10	+	-	210	9	Bilateral adrenalectomy	Bilateral phaeochromocytoma
3	25	F	VHL	25	5	+	-	26	11	Bilateral adrenalectomy	Bilateral phaeochromocytoma
4	24	F	VHL	10	50	-	+	11	26	Bilateral adrenalectomy	Bilateral phaeochromocytoma
5	30	M	VHL	0	0	-	-	0.8	0.5	Resection of left kidney, adrenal and para-aortic mass	Renal carcinoma, para-aortic paraganglioma Normal adrenal histology
6	67	F	Nil	19	14	+	-	1.75†	0.85	Right adrenalectomy	Phaeochromocytoma

Table 6.8: Clinical, radiological, biochemical and pathological description of six patients who underwent AVS for the diagnosis of phaeochromocytoma

MIBG = Metaiodobenzylguanidine, NA = noradrenaline, A = adrenaline, VHL = von Hippel-Lindau, + = positive, - = negative, NC = not cannulated.

* Maximum dimension (mm) of an adrenal abnormality visualised by any imaging modality.

† This is the minimum possible ratio as unfortunately insufficient sample was available for further determination of the noradrenaline concentration.

6.4 Discussion

In this chapter, I have defined side-specific normative reference intervals of adrenal venous catecholamines and their ratio in patients with PA. Using these, I have proposed a diagnostic cut-off based on the 97.5th centile value and have demonstrated that this provides a 0% false positive detection rate in a cohort of six patients with phaeochromocytoma who underwent AVS.

6.4.1 Normal adrenal venous catecholamine concentrations in patients with primary aldosteronism

This series is the largest to date of catecholamine concentrations in the adrenal veins. In keeping with previous studies (Kahaly *et al.* 1985; Freel *et al.* 2010; Baba *et al.* 2013), we observed wide variation in absolute catecholamine concentrations (up to a factor of 178 on the right and 106 on the left); a fact which has been used to argue against the utility of AVS in the diagnosis of phaeochromocytoma (Freel *et al.* 2010). This variation was reduced when considering the noradrenaline to adrenaline ratio in each adrenal vein (variation up to a factor of 54 on the right and 34 on the left), but not by 'correcting' for adrenal vein cortisol.

As hypothesised, adrenal venous adrenaline concentration exceeded that of noradrenaline bilaterally, resulting in a noradrenaline to adrenaline ratio of less than one. Interestingly, both adrenaline and noradrenaline concentrations were higher in the right than the left adrenal vein. This effect was seen at both centres and is most likely explainable by proximity of the catheter tip to the adrenal gland (which will be closer by necessity on the right due to normal anatomical variation) at the time of sampling as the effect was not seen when 'corrected' for adrenal vein cortisol. The noradrenaline: adrenaline ratio, however, persisted to be greater on the left after correction for cortisol. The most likely explanation being that this reflects a degree of dilution from the inferior phrenic vein (in which noradrenaline would be the predominant catecholamine), although caution must be applied to the interpretation of these data as it contains a double correction.

Studies that have examined adrenal venous catecholamines in healthy individuals are lacking and are unlikely ever to be performed due to the invasive nature of AVS and the inherent risks, albeit small, of contrast administration and radiation exposure from fluoroscopic screening. Three studies have examined this area in the context of hypertension or non-phaeochromocytoma adrenal lesions (summarised in Table 6.9), although they are generally small and direct comparison between them is difficult. Different patient subgroups were included in each: patients with essential hypertension in one (Kahaly *et al.* 1985), predominantly ACTH-independent Cushing's syndrome in another (Freel *et*

al. 2010) and a mixture of causes of secondary hypertension and non-functional adrenal adenomas in the third (Baba *et al.* 2013). AVS was performed under a variety of different conditions, including without stimulation (Baba *et al.* 2013) and following dexamethasone suppression (Freel *et al.* 2010), which might impact on catecholamine concentration and are discussed later. In all previous series, adrenal venous cannulation success is very unclear as either criteria were not reported (Kahaly *et al.* 1985) or venography only was used (Baba *et al.* 2013). In the Mayo series, a non-standardised, non-verified and unpublished adrenal vein to peripheral catecholamine gradient was used, as cortisol was uninterpretable in the context of dexamethasone suppression, although it is reasonable to assume successful cannulation given the historic success at that centre (Freel *et al.* 2010).

These differences notwithstanding, adrenal vein adrenaline concentrations exceeded noradrenaline in all series. In accordance with our findings, adrenal venous adrenaline and noradrenaline concentrations were greater in the right adrenal vein than the left and the noradrenaline: adrenaline ratio was greater on the right in the Mayo Clinic series (Freel *et al.* 2010). No statistically significant differences between sides were observed in a heterogeneous cohort (Baba *et al.* 2013).

When comparing between the two centres in our cohort, there was no significant difference in adrenal venous adrenaline concentrations on either side. Noradrenaline, however, was greater in patients from St Bartholomew's Hospital and this resulted in an increased noradrenaline: adrenaline ratio bilaterally. One potential explanation for this observed difference could be due to differences in measurement methodology as there was not a single 'reference' laboratory for this study. Both centres used high performance liquid chromatography with electrochemical detection: a technique that is far less susceptible to inter-laboratory variation than immunoassays. In addition, the fact that no difference was seen with adrenaline, which was measured by the same method, suggests an alternative explanation is more likely.

The only demographic difference between the two centres was sex, with a higher proportion of male patients in the St Bartholomew's group. Sex-specific reference ranges for catecholamines are not utilised in clinical practice and so it might be assumed that this is unlikely to be the cause for the observed difference. However, urinary noradrenaline excretion is higher in men than women (Lehmann & Keul 1986; Gerlo *et al.* 1991). The situation with plasma noradrenaline is less clear cut, with studies showing either no difference between the sexes (Brecht & Schoeppe 1978) or higher levels in women (Davidson *et al.* 1984). A sex-specific effect on adrenal vein catecholamines was not examined in any of the three previous series (Kahaly *et al.* 1985; Freel *et al.* 2010; Baba *et al.* 2013). In the St Bartholomew's cohort, no difference between any adrenal vein catecholamine was

Reference	N	AVS details	Catecholamine (nmol/L)	Median (interquartile range)		p-value
				Left adrenal vein	Right adrenal vein	
(Kahaly *et al.* 1985)†	57 essential hypertension	Conditions of AVS and cannulation criteria not stated				
			Adrenaline	16.7 (0.5-295.5)‡		ns
			Noradrenaline	15.4 (1.0-278.3)‡		ns
			NA:A ratio	Ns	ns	ns
(Freel *et al.* 2010)	17 Cushing's 1 PA	Dexamethasone suppression AV: IVC catecholamine gradient				
			Adrenaline	6.2 (2.2-15.4)	18.1 (8.1-18.1)	<0.02
			Noradrenaline	3.0 (2.0-7.3)	4.5 (3.1-10.3)	<0.09
			NA:A ratio	0.54 (0.3-1.1)	0.3 (0.2-0.5)	0.02
(Baba *et al.* 2013)	8 PA 5 Cushing's 2 NFA	No ACTH Venography				
			Adrenaline	77.4 (0.09-148.7) ‡	53.5 (0.2-959.7) ‡	0.63
			Noradrenaline	18.1 (0.9-54.7) ‡	8.1 (0.6-189.7) ‡	0.58
			NA:A ratio	Ns	ns	ns
This thesis	113 PA	ACTH stimulation AV:IVC cortisol >5:1				
			Adrenaline	35.1 (19.5-72.8)	61.4 (31.5-126.7)	1.7×10^{-7}
			Noradrenaline	10.6 (6.6-18.7)	16.3 (8.8-31.8)	2.4×10^{-6}
			NA:A ratio	0.31 (0.20-0.51)	0.26 (0.18-0.38)	8.3×10^{-6}

Table 6.9: Summary of published reports of adrenal venous catecholamine concentrations and ratios

AVS – adrenal venous sampling, PA – primary aldosteronism, AV – adrenal vein, IVC – inferior vena cava, NFA – non-functioning adenoma, NA – noradrenaline, A – adrenaline, ns – not stated.

† Data were not presented for each individual adrenal vein

‡ Data for range but not interquartile range were presented and are displayed

observed between men and women (Figure 6.5) and the most plausible explanation for this difference between the two centres is chance.

This led us to consider whether the alpha adrenoceptor antagonist doxazosin might be responsible for the observed difference due to variations in prescription between the two centres. Patients with PA on doxazosin had higher adrenal venous noradrenaline concentrations in the left adrenal vein, although this did not result in an alteration in the noradrenaline: adrenaline ratio in spite of an unchanged adrenaline. A trend to a higher noradrenaline concentration on the right in patients on doxazosin was observed, although statistical significance was not reached. Interestingly, in spite of this, the noradrenaline: adrenaline ratio was higher on the right. Doxazosin, an α_1-adrenoceptor specific antagonist, has previously been shown to increase urinary noradrenaline excretion resulting in false positive results in the diagnosis of phaeochromocytoma (Eisenhofer *et al.* 2003). The proposed mechanism by which this occurs is via reflexive sympathetic activation and is distinct to that seen with non-selective alpha adrenergic receptor antagonists, such as phenoxybenzamine. In these instances, inhibition of the presynaptic α_2-receptor reduces noradrenaline reuptake and results in increased peripheral noradrenaline (Lenders *et al.* 2014). The interpretation of these observations is difficult as any effect of doxazosin would reasonably be expected to be systemic. An increase in noradrenaline in the left adrenal vein, as was observed, is consistent with relative dilution from the inferior phrenic vein, which as a peripheral vein would be expected to have an excess of noradrenaline compared to the adrenal vein and as such any effect of doxazosin on noradrenaline would be exaggerated. The fact that the noradrenaline: adrenaline ratio is not elevated as a result calls into question whether this observation is maintained and consistent. Evaluation in other distinct cohorts would be informative to further answer this question.

One limitation of the approach employed to define reference intervals was the use of patients with PA, however the use of healthy normotensive individuals would not be justifiable given the invasive nature and contrast and radiation exposure of AVS. Aldosterone stimulated the central nervous system in animals (Gomez-Sanchez 1986), but there is contradictory evidence as to whether sympathetic nervous system activity is increased (Kontak *et al.* 2010) or attenuated (Miyajima *et al.* 1991) in individuals with PA and whether this alters adrenal venous catecholamine levels is unknown. Alpha blockade, as discussed, has the potential to elevate circulating noradrenaline (Lenders *et al.* 2014); however both the PA and phaeochromocytoma groups were treated with alpha receptor antagonists prior to AVS (although with different agents). Prior to this report, the group at the Mayo Clinic reported AVS catecholamine results in 18 patients being evaluated for autonomous cortisol production (Freel *et al.* 2010). These patients had cortisol excess, suppressed

ACTH in all but one case and the AVSs were performed under dexamethasone suppression. All of these factors have the potential to influence adrenal catecholamine production via effects on enzymes of the catecholamine synthesis pathway (Wurtman & Axelrod 1965; Thoenen *et al.* 1969; Gewirtz *et al.* 1971). The evidence for this in humans is limited and conflicting with reports of reduced peripheral adrenaline (Cameron *et al.* 1995), noradrenaline (Krsek *et al.* 2006) or both (Mannelli *et al.* 1994) in patients with Cushing's syndrome. One study found that chronic administration of ACTH to normal subjects did not affect peripheral noradrenaline, whilst dexamethasone at a dose of 6mg over three days reduced noradrenaline (Stene *et al.* 1980). Another study found no significant difference between the adrenal venous noradrenaline: adrenaline ratio in eight patients with Cushing's compared to 12 controls (Mannelli *et al.* 1994). Our reported patients were also hypercortisolaemic, albeit temporarily, due to infusion of cosyntropin at the time of AVS and this has been shown to increase adrenal vein adrenaline and noradrenaline in one small series (Valenta *et al.* 1986).Thus, although use of a PA cohort to define reference intervals has its limitations, it is the best available option.

Normal catecholamine secretion is variable and episodic, whilst their metanephrine metabolites are released in a continuous process that is independent of episodic catecholamine release and relatively unaffected by stress (Eisenhofer *et al.* 1995a, b, 1998). Due to these advantages, use of adrenal venous metanephrines has been proposed as an alternate to adrenal venous cortisol for assessment of adrenal vein cannulation in patients with PA (Dekkers *et al.* 2013). In this study, adrenal vein metanephrine concentration was greater than in the periphery, but side-specific results were not reported. The reported use of AVS for metanephrines in the diagnosis of phaeochromocytoma is limited to two case reports which made empirical judgements based on non-normative metanephrine gradients (Pacak *et al.* 2001; Därr *et al.* 2011). We considered the use of adrenal vein metanephrines in our cohort, however only catecholamine results were available for the patients with phaeochromocytoma, so a meaningful comparison between the two groups would not have been possible.

6.4.2 Adrenal venous noradrenaline: adrenaline ratio in patients with phaeochromocytoma

Using the PA cohort, we have presented centile values for the adrenal venous noradrenaline: adrenaline ratio in each adrenal vein (Table 6.7). The 97.5th centile values were 1.21 on the left and 1.04 on the right. Comparing these cut offs with data from six patients with histologically proven phaeochromocytomas, in whom a conventional imaging only approach could either not confirm the

site of abnormality or could not refute bilateral disease, the false negative rate was 0%. The lowest adrenal vein noradrenaline: adrenaline ratio in a confirmed phaeochromocytoma was 2.96 on the left and 1.75 on the right.

AVS has previously been a widely used adjunct in the diagnosis (Von Euler *et al.* 1955; Jones *et al.* 1979; Palublnskas *et al.* 1980; Allison *et al.* 1983) and lateralisation (Davies *et al.* 1979; Nobin *et al.* 1982; Chew *et al.* 1994; Srirangalingam *et al.* 2010) of phaeochromocytoma. However, interpretation of these studies depended either on the use of non-standardised concentration gradient cut-offs, comparisons with the contralateral adrenal or assumptions regarding the noradrenaline: adrenaline ratio. Furthermore, the criteria used to define successful adrenal venous cannulation is either not stated or based on sub-optimal criteria e.g. venography.

An adrenal venous noradrenaline: adrenaline ratio exceeding one has previously been suggested to be pathological (Newbould *et al.* 1991) because adrenaline is the predominant adrenal catecholamine (Wurtman & Axelrod 1965) and that an excess of noradrenaline is therefore pathological. This assertion, however has limited normative data to support it and was based on data from only three patients with phaeochromocytoma and five without (Newbould *et al.* 1991). This previously proposed cut-off is close to what was observed in the PA cohort presented in this chapter, particularly on the left.

In all phaeochromocytoma patients presented, the noradrenaline: adrenaline ratio significantly exceeded these specified cut-offs (1.21 on the left, 1.04 on the right). This was also the case in the five previously reported cases in which it was possible to calculate the adrenal venous noradrenaline: adrenaline ratio (minimum ratio 2.1) (Davies *et al.* 1979; Nobin *et al.* 1982). Four of the 18 patients with non-phaeochromocytoma adrenal conditions in the Mayo cohort underwent an adrenalectomy on the basis of an adrenal vein noradrenaline: adrenaline ratio exceeding one (Freel *et al.* 2010). In none of these instances was a phaeochromocytoma diagnosed histologically and this has been used as an argument against the use of AVS in the diagnosis of phaeochromocytoma. However, it could be argued that this approach was inappropriate and unnecessary as all of the patients had normal urinary metanephrines and so the diagnosis of phaeochromocytoma was effectively excluded.

It should be noted that the bulk of the published literature surrounding venous sampling for the diagnosis of phaeochromocytoma heralds from a time when cross-sectional and nuclear medicine imaging quality and availability were much more limited than in contemporary practice. As a result AVS has a more limited role in the diagnosis of phaeochromocytoma and paraganglioma than

previously. One situation in which it may still play a role is in patients with predisposing genetic syndromes such as VHL and SDHx. Participation in modern screening programmes means that catecholamine excess may be identified early, often in asymptomatic individuals who might have bilateral radiological abnormalities. In this context, identification of a single adrenal gland as the source of catecholamine excess would facilitate a unilateral adrenalectomy, postponing the need for adrenal replacement therapy and its associated morbidity and mortality. Conversely, a secure diagnosis of bilateral phaeochromocytoma would allow surgery at a single sitting. In the context of bilateral disease or a predisposing syndrome, adrenal preserving surgery is an option, but long term follow-up data are limited and there is a significant risk of recurrence (Grubbs *et al.* 2013) and a more difficult second operation.

These benefits are illustrated by the cases of phaeochromocytoma presented here (Table 6.8). In the patients with VHL, use of AVS either confirmed or refuted bilateral secretory disease and therefore allowed all five individuals to have definitive and curative surgery in a single sitting. In the single non-syndromic patient with bilateral adrenal abnormalities, AVS was utilised to confirm unilateral disease and thus facilitated a curative surgical strategy that preserved her adrenal reserve. AVS has previously been used in a 15 year-old with an *SDHD* mutation to inform a surgical approach that allowed preservation of his left adrenal gland when a right phaeochromocytoma and a left abdominal paraganglioma were resected (Srirangalingam *et al.* 2010).

An advantage of the use of the adrenal vein noradrenaline: adrenaline ratio is that it does not rely on comparison with the contralateral adrenal gland, which, in the clinical settings outlines, has a high pre-test probability of being abnormal. One disadvantage is the issue of a purely adrenaline secreting phaeochromocytoma which would not be identified using the noradrenaline: adrenaline ratio. However, such cases are rare, particularly within the context of VHL and SDHx (Srirangalingam *et al.* 2008, 2009) and would be identified prior to AVS by urine and plasma catecholamine and metanephrine analysis.. It should be noted that adrenaline secreting phaeochromocytoma are a feature of both MEN2 and NF1 (Eisenhofer *et al.* 2011) and this should be borne in mind when interpreting AVS results in these syndromes.

6.5 Summary

In summary, I have presented data from a large group of patients with PA and suggest that it could serve as a reference interval for adrenal vein catecholamines in non-phaeochromocytoma patients. We acknowledge that with advanced cross-sectional and nuclear medicine imaging, AVS is not required in the routine diagnosis of phaeochromocytoma. However, in some patients with known germline mutations of genes that predispose to the formation of phaeochromocytomas, screening programs may detect the presence of bilateral radiological abnormalities (with or without abnormal urine/plasma biochemistry) that present diagnostic difficulties. In such selected situations, AVS, performed in an experienced centre and interpreted in the context of the reference intervals presented here, remains a useful complementary tool for determining treatment strategies in this challenging group of patients.

CHAPTER 7

Discussion and future work

This thesis has demonstrated that primary cilia loss is a feature of PPGLs and that ciliary loss is associated with increased cellular proliferation and oncogenic alterations in cilia-mediated signalling. Ciliary alterations are most pronounced in PPGLs in which hypoxic signalling is activated due to increased ciliary disassembly through the AURKA/HDAC6 pathway. This demonstrates how cilia are modified both by intrinsic cellular properties (e.g. cluster 1 gene mutations) as well as by the extracellular environment (e.g. tissue hypoxia). In addition to hypoxia, we have presented evidence that other features of the tumour microenvironment (e.g. catecholamines) modify primary cilia.

7.1 Primary cilia loss in cancer

7.1.1 Primary cilia loss in PPGLs

Primary cilia incidence has been examined in 17 tumour types in 27 published studies prior to this one (Table 7.1). The observed prevalence of primary cilia in non-cancerous tissue varies widely between tissues from <1% of lymphoid cells (Yasar *et al.* 2017) to over 90% of renal tubular cells (Schraml *et al.* 2009). Whilst variation by tissue is expected, there is often significant discrepancy within the same tissue in different studies. For example, over 90% of renal tubular cells were ciliated in one study (Schraml *et al.* 2009) compared to a median of 5% in another (Basten *et al.* 2013). This may partly be explained by the different methods of cilia identification employed, but it also raises concerns around the issues of reproducibility and comparability. In the two studies mentioned previously, cilia incidence in ccRCC was either a median of 0.41% or a mean of 7.8%, a figure higher than cilia incidence in normal renal tubules in the other study (Schraml *et al.* 2009; Basten *et al.* 2013).

We found that primary cilia were present on 8.42 $\pm$ 0.03% and 3.06 $\pm$ 0.14% of cells of the adrenal medulla and phaeochromocytomas respectively (Figure 4.1B). These incidences are in keeping with those reported in other tissues and tumours (Table 7.1). Phaeochromocytomas consist of two main cell populations: phaeochromocytes and sustentacular cells. We did not examine how tumoural cilia were distributed between these cell subpopulations and this could provide additional insight into the functional role of primary cilia in phaeochromocytomas. In pancreatic cancer, tumour-associated stromal cells retain cilia whilst they are lost from tumoural cells; this divergence plays a vital role in mediating paracrine Hh signalling (Bailey *et al.* 2009; Schimmack *et al.* 2016).

A gradient of cilia loss from normal to pre-invasive lesion to cancer is seen in melanoma (Kim *et al.* 2011b; Snedecor *et al.* 2015), breast (Menzl *et al.* 2014), prostate (Hassounah *et al.* 2013) and pancreatic (Schimmack *et al.* 2016) cancer. This finding suggests, in these tumours at least, that cilia

are lost early in tumour development. Progressive cilia loss is seen in metastatic melanoma (Snedecor *et al.* 2015) suggesting an ongoing role in tumourigenesis, although this association is not universal and in pancreatic cancer ciliary presence is associated with metastatic risk (Emoto *et al.* 2014). Insight into the timing of ciliary loss in PPGLs is prevented by the lack of a precursor lesion (Korpershoek *et al.* 2014) and the absence of metastatic disease in the studied cohort. VHL haploinsufficiency alone in normal adrenal medulla was insufficient to result in ciliary changes (Figure 4.2A&B).

Ciliary incidence can be markedly different between histological subtypes of medulloblastomas (Han *et al.* 2009), craniopharyngiomas (Coy *et al.* 2016), breast (Menzl *et al.* 2014) and thyroid (Lee *et al.* 2016) cancer. Whilst histological subtypes of PPGLs are of scant clinical relevance (Tischler & deKrijger 2015), distinct subtypes of PPGLs are defined by their genetic and molecular characteristics (Fishbein *et al.* 2017). We observed that ciliary loss was most pronounced in tumours arising in patients with cluster 1 mutations (Figure 4.2) suggesting that cilia could potentially segregate PPGL clusters. A more comprehensive analysis of this is limited by the reliance on clinical genetic testing, meaning only 60% of germline statuses were ascertained. Furthermore, somatic mutation status was unknown in all cases and would be vital to be able to correlate tumoural cilia to the recently described 'Wnt altered' PPGL subtype (Fishbein *et al.* 2017).

Ciliary loss has now been established in two VHL-associated tumours: PPGL (this thesis) and ccRCC (Schraml *et al.* 2009; Basten *et al.* 2013). Whether it is a conserved feature across other VHL-associated pathologies remains to be answered. This could potentially be investigated in other VHL-associated tumours, for example pancreatic NETs and haemangioblastomas.

Despite the importance of ciliary length as a readout for function (Thompson *et al.* 2016) only three studies have attempted to measure cilia length in human cancers with varying results (Table 7.1). Cilia length was reduced in prostate cancer cells (Hassounah *et al.* 2013), unchanged in breast cancer (Menzl *et al.* 2014) and varied depending on thyroid cancer subtype (Lee *et al.* 2016). All three studies used dual-labelled immunofluorescence on formalin fixed paraffin embedded tumour specimens followed by confocal microscopy to identify and measure cilia, although it is unclear whether length was measured from individual z-slices or from MIPs. Ciliary length was longer in phaeochromocytomas and normal adrenal medulla (1.48µm $\pm$ 0.34, 2.02µm $\pm$ 0.39) compared to prostate (median 0.93µm, 1.2µm) and breast (median 0.9µm, 1.2µm) respectively. It is unclear if this is a real biological difference or a result of measurement techniques.

Cancer	Cilia incidence (%) †			Cilia length (µm)‡			Method	n#	Ref
	Normal	**Pre-cursor***	**Tumour**	**Normal**	**Pre-cursor**	**Tumour**			
BCC	'Present'	ND	5/8 ciliated	ND	ND	ND	FFPE IF dual[AO]	8	(Wong *et al.* 2009)
	2.5 ± 2.2	ND	38.5 ± 13.3	ND	ND	ND	FFPE IF dual[GR]	3/0/19	(Yang *et al.* 2017)
Bladder	8-15	ND	2-7	ND	ND	ND	FFPE IF single[A]	10/0/27	(Du *et al.* 2018)
Breast	'Readily identifiable'	'Present'	0.03% of cells in 1 tumour	ND	ND	ND	FFPE IF single[A]	5/NS/26	(Yuan *et al.* 2010)
	Basal 23.6‡ Luminal 1.1‡	0.8/0.8/0.1‡	LG 0.2 HG 0.2	0.9	0.79/1.27	LG 1.1 HG 1.2	FFPE IF dual[AG]	27/39/65	(Menzl *et al.* 2014)
	'Observed'	ND	'Not seen'	ND	ND	ND	FOCT IF dual[AG]	5/0/11	(Nobutani *et al.* 2014)
	5.92	ND	Ductal 1.8 Luminal 4.44	ND	ND	ND	FFPE IF dual[AC]	NS	(Yasar *et al.* 2017)
ccRCC	>90	ND	7.8± 6.0	ND	ND	ND	FFPE IF single[A]	20	(Schraml *et al.* 2009)
	4.97‡	ND	0.41‡	ND	ND	ND	FFPE IF dual[AP] IHC single[A]	89	(Basten *et al.* 2013)
Chondrosarcoma	63.9 ± 8.6	ND	12.4 ± 7.1	ND	ND	ND	FFPE IF dual[AG]	5/0/10	(Ho *et al.* 2013)
Cholangiocarcinoma	'All ducts'	ND	'20% ducts'	ND	ND	ND	FFPE IF dual[AI]	6/0/21	(Gradilone *et al.* 2013)
Colon	2.43‡	ND	3.80‡	ND	ND	ND	FFPE IF dual[AC]	NS	(Yasar *et al.* 2017)
Craniopharyngioma - Papillary - Adamantinomatous	25 ± 13	ND	Basal/Apical 69 ± 12/<1 90 ± 6/82 ± 5	ND	ND	ND	FFPE IHC single[R]	16/0/42	(Coy *et al.* 2016)
Gastric	2.65‡	ND	3.17‡	ND	ND	ND	FFPE IF dual[AC]	NS	(Yasar *et al.* 2017)
Lymphoma	0.83‡	ND	1.18‡	ND	ND	ND	FFPE IF dual[AC]	NS	(Yasar *et al.* 2017)
Lung	1.85‡	ND	2.75‡	ND	ND	ND	FFPE IF dual[AC]	NS	(Yasar *et al.* 2017)
Medulloblastoma - Desmoplastic - Anaplastic - Classic	ND	ND	Ciliated: 5/6 1/9 9/23	ND	ND	ND	FFPE IF dual[AG/P]	0/38	(Han *et al.* 2009)
Melanoma	94 ± 3.06	5 ± 4..3	3 ± 2.9	ND	ND	ND	FFPE IF dual[AG]	22/16/16	(Kim *et al.* 2011b)
	24.9 ± 6.3	4.4 ± 2.1	2.9 ± 2.4	ND	ND	ND	FFPE IF dual[AR]	32/12/43	(Snedecor *et al.* 2015)
Prostate	8.9‡	5.7‡	1.9‡	1.2	0.85	0.93	FFPE IF dual[AP]	10/24/75	(Hassounah *et al.* 2013)
	8.07‡	ND	3.74‡	ND	ND	ND	FFPE IF dual[AC]	NS	(Yasar *et al.* 2017)
PDAC	'Most'	'Devoid'	'Devoid'	ND	ND	ND	FFPE IF single[A]	17	(Seeley *et al.* 2009)
	ND	ND	25% ciliated	ND	ND	ND	FFPE IF dual[AG]	100	(Emoto *et al.* 2014)
	32	18/6/3	1.2	ND	ND	ND	FFPE IF dual[AG]	6/NS/25	(Schimmack *et al.* 2016)

	5.26‡	ND	7.0‡	ND	ND	ND	FFPE IF dual[AC]	NS	(Yasar *et al.* 2017)
pRCC	>90%	ND	44.3 ± 22.3	ND	ND	ND	FFPE IF single[A]	9	(Schraml *et al.* 2009)
Thyroid - PTC - Oncocytic - Hürtle cell	67.8 ± 3.6	ND	 68.7 ± 11.7 17.6 ± 11.7 4.4 ± 2.2	NS	ND	 'Longer' 'Shorter' NS	FFPE IF dual[AR]	5/0/20	(Lee *et al.* 2016)
Phaeochromocytoma	8.42 ± 0.03	ND	3.06 ± 0.14	2.02 ± 0.39	ND	1.48 ± 0.34	FOCT IF dual[AR]	27/0/47	This thesis

Table 7.1: Primary cilia prevalence and length in human tumours

† mean ± standard deviation, ‡ median, # when in form -/-/- represents n for normal/precursor lesion/cancer respectively, * when in form -/-/- represents increasing grades of pre-cursor lesion

BCC – basal cell carcinoma, ccRCC – clear cell renal cell carcinoma, PDAC – pancreatic ductal adenocarcinoma, pRCC – papillary renal cell carcinoma, PTC – papillary thyroid carcinoma, ND – not done, NS – not stated, LG – low grade, HG – high grade, FFPE – formalin fixed paraffin embedded, IF – immunofluorescence, IHC – immunohistochemistry, FOCT – frozen in OCT, A – anti-acetylated α-tubulin, G – anti-gamma tubulin, P –anti-pericentrin, R – anti-Arl13b, I – anti-IFT88, C – anti-CCROC, O – anti-rootetin.

7.1.2 Experimental considerations

The major barrier to examining the role of primary cilia in cancer is the difficulty in identifying them. Primary cilia are small and singular and are not readily visible by standard widefield light microscopy as their diameter, at approximately 0.2µm, approaches its limit of resolution. Furthermore, the entire axoneme would need to lie within a single focal plane – and whilst this may occur within the confines of a 2D cell monolayer – it is less likely within a 3D tissue section. Therefore, alternative approaches to visualise and measure primary cilia are required and are particularly relevant when considering tissue sections.

EM provides a superior limit of resolution (better than 50pm) to light microscopy due to the shortened wavelength of electrons compared to photons and can provide incredible levels of detail and ultrastructural information. This however requires very thin section (around 100nm) meaning the entire ciliary axoneme is rarely captured within a single section, estimated at only 1 in 200 ciliated cells (Farnum & Wilsman 2011). This combined with the time and resource intensive nature of EM severely limits its throughput and it has not gained an established role in large scale ciliary measurement.

Confocal microscopy uses point illumination and a pinhole in an optically conjugate plane to eliminate out-of-focus light. This results in improved optical resolution and contrast and reduction of background fluorescence. In addition, serial optical sections can be collected from thick specimens, allowing the reconstruction of 3D structures. These qualities, alongside its relative ease of use and specimen preparation and relatively short imaging time mean that confocal microscopy is well suited to the identification of large numbers of cilia. This is reflected by the fact that it is the imaging modality of choice for determination of primary cilia in tumour sections (Table 7.1).

One significant shortcoming of confocal microscopy is its inaccuracy in the z-dimension. This occurs because the point spread function of the pinhole is ellipsoid and thus much longer in the z-dimension than in the xy-dimension. This has important implications for imaging 3D structures that are not in a single plane of focus and is particularly pertinent to measuring primary cilia length in tissue sections. Various approaches to limit this problem have been employed.

Maximum intensity projections (MIPs) are 2D representations created by image processing of the original 3D image. They are fast and straightforward to create but can result in shortening of objects not in a single xy plane (Figure 7.1). This technique significantly underestimated synthetic microfiber length in agarose gel as a model of primary cilia, but at lengths (18 and 50µm) that are not

biologically relevant (Saggese *et al.* 2012). When primary cilia themselves were imaged, no significant difference in length was seen in chondrocytes (mean length 1.9µm); however MIPs significantly underestimated length in the longer cilia of renal epithelial cells (mean length 2.2µm) (Saggese *et al.* 2012). This study looked at the entire cilia population and did not differentiate those that were within a single focal plane or those that crossed many. This subpopulation of cilia would be predicted to have the greater inaccuracy in length measurement using the MIP method. Consideration of cilia orientation as either 'flat' or 'angled' based on the number of z-slices they crossed found that 'angled' cilia were significantly shorter than 'flat' cilia in mouse embryonic endothelial cells (mean length 3.28µm) (Dummer *et al.* 2016). A practical approach to this problem can be to simply exclude cilia that are not in a single focal plane. However, this introduces sample bias and reduces population size – a potentially significant problem in tumour sections in which primary cilia may be infrequent and variably orientated.

The main limitation of using MIPs is the loss of depth information from the original dataset. This can be addressed by application of an adaptation of Pythagoras' Theorem (PyT) $a^2 = b^2 + c^2$ in which a is the cilia length on MIP, b is a measure of the depth based on the thickness and number of Z stacks the object traverses and c is the actual length. This approach maintains throughput and is readily and easily calculable using open source software. Although an improvement on MIP for calculation of angled cilia length in mouse embryonic endothelial cells, cilia length remain underestimated (Dummer *et al.* 2016). This is a result of the fact that it does not address the issues of optical distortion in the z-dimension or of a non-linear cilium, which requires a more sophisticated approach.

Deconvolution is a digital filtering technique that aims to reduce optical distortion resulting from the point spread function of the system. Its application to raw images reduces out-of-focus light and improves contrast and resolution, but significant xz axial smear remains (Saggese *et al.* 2012). This can be further addressed by employment of Gaussian blurring, which reduces optical distortion by approximating the z axis optical point spread function to a Gaussian distribution such that the xy resolution approximates the z resolution and thus the previously smeared point spread function becomes spherical. Skeletonization is a digital image processing technique by which a central line skeleton is created of a three dimensional object allowing direct measurement. When combined with deconvolution and Gaussian blurring, this technique accurately measures microfibers of known length. A direct comparison with MIPs did not find a significant difference in chondrocyte cilia (1.8 v 1.9µm), but did in the longer renal epithelial cilia (1.4 v 2.2µm) (Saggese *et al.* 2012).

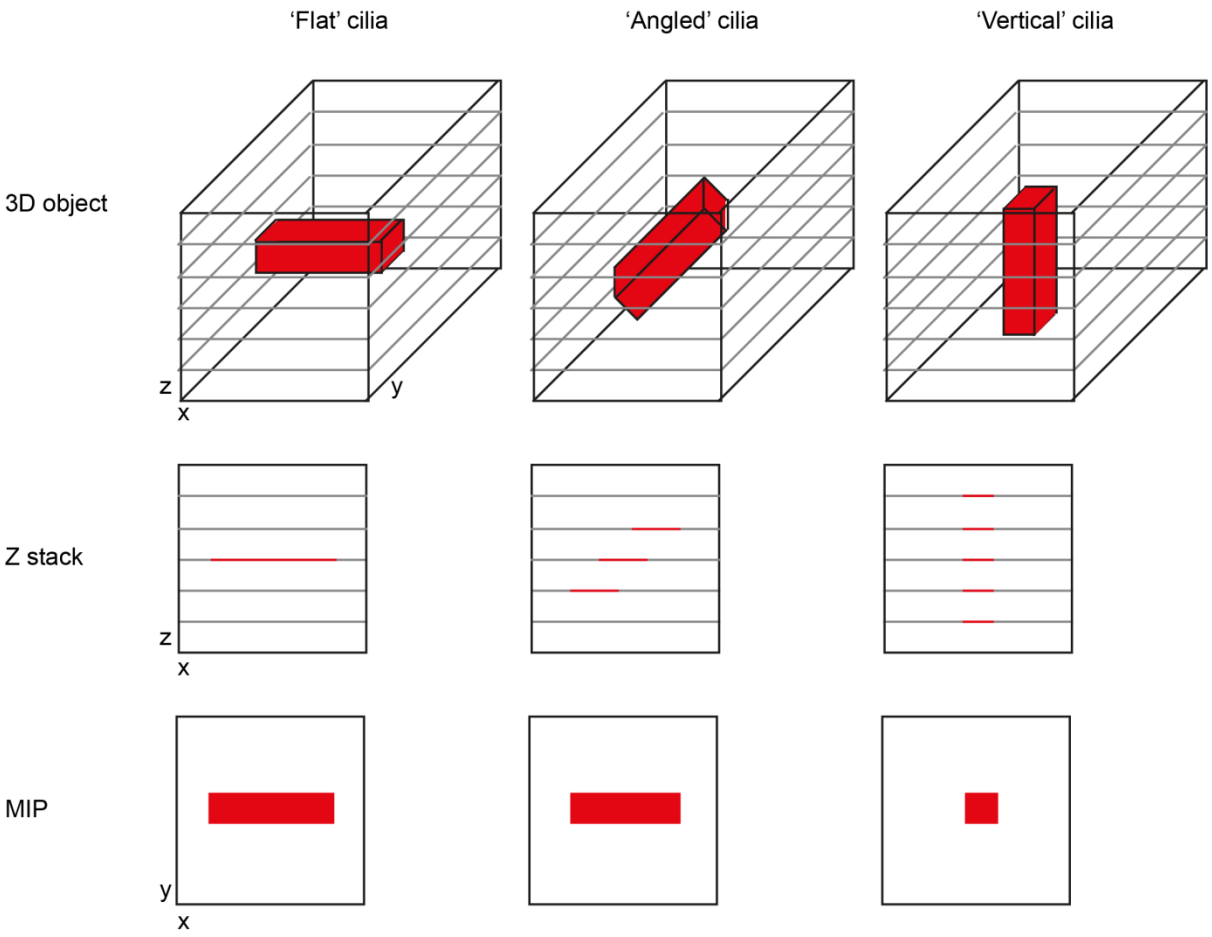

Figure 7.1: Maximum Intensity Projections have the potential to underestimate cilia length

Schematic representation of how three cilia (red) of equal length will have different MIP profiles depending on their three dimensional orientation.

An alternative approach is the use of 3D alternative angled slicing (Dummer *et al.* 2016). In this, a vector through the cilium is defined from the Z-stack and MIP and used to create a slicing plane. Bipolar interpolation of the three dimensional stack generates a new image from which cilia length can be measured. Direct comparison of this technique with MIP and PyT in murine embryonic epithelial cells did not find a significant difference in cilia length in 'flat' cilia, but did with 'angled' cilia (Dummer *et al.* 2016).

Another approach, and the one used for tissue sections in this thesis, was of direct measurement following surface rendering and 3D reconstruction in the surpass module of Imaris 7.1 image processing and analysis software (Bitplane, Belfast, UK). Although time consuming as each axoneme

is individually traced, it ensures accuracy of identification of primary cilia whilst minimising data loss in the vertical dimension. For 2D culture, the higher throughput MIP method was utilised as PC12, MPC and MTT cell primary cilia are predominantly basal (Figure 4.9A).

7.1.3 Primary cilia loss contributes to tumourigenesis in PPGLs

Whether changes in primary cilia in cancer are causative or merely a consequence remains an area of debate and was a focus for investigation in this thesis.

The association between primary cilia and stages of the cell cycle has direct relevance to cellular proliferation, which is one component of tumourigenesis, but does not help to answer this question. No association between the proliferation marker Ki67 and primary cilia was observed in either breast (Menzl *et al.* 2014) or prostate (Hassounah *et al.* 2013) cancer and the authors suggested that this provided evidence that ciliary changes were not simply related to cellular division. We found that ciliary loss was correlated with a higher Ki67 index, using a clinically relevant cut-off (Figure 4.3). This suggests that in PPGLs, cilia loss is related to increased proliferation but does not provide evidence to address the directionality of this relationship. Similarly, alterations in cilia-associated signalling pathways (Figure 4.5) support the observed differences in cilia between phaeochromocytomas and the adrenal medulla but do not resolve this issue.

Loss of primary cilia in PC12 cells, achieved through two distinct mechanisms, results in increased cellular proliferation (Figure 4.10) suggesting that primary cilia loss contributes to, and is not merely a side effect of, proliferation. This is consistent with the observed effects of Ift88 loss in kidney (Delaval *et al.* 2011) and pancreas cells (Cano *et al.* 2004). Although IFT88 has cilia-independent functions (Boehlke *et al.* 2015), the same results were observed following Cep164 knockdown suggesting a cilia-mediated effect. Further evidence for cilia loss contributing to tumourigenesis is presented in the pro-oncogenic transcriptional changes observed following *Ift88* knockdown (Figure 4.11).

Ciliopathies have not traditionally been associated with an increased rate of malignancy; this has been used to argue against a role of primary cilia in tumourigenesis. However, this assertion may not be entirely accurate. A large observational study of patients with ADPKD, the most common ciliopathy, found an increased rate of renal, liver and colon cancer in ADPKD patients compared to matched controls (Yu *et al.* 2016). In addition, malignancy rates may be underestimated in ciliopathy patients due to a combination of their reduced life expectancy and associated intellectual disability reducing diagnosis rates.

7.2 Primary cilia and the tumour microenvironment

Primary cilia, through their cellular location and responsiveness to extracellular stimuli, appear ideal candidate organelles to sense and interact with the complex and multi-faceted tumour microenvironment (Balkwill *et al.* 2012). Hypoxia is a central component of the tumour microenvironment in general and hypoxic signalling is of particular importance in the pathogenesis of cluster 1 PPGLs.

We have shown that hypoxia reduces cilia incidence and length in PPGL cells (Figures 5.1 & 5.3) in a process that is dependent on HIF-signalling (Figures 5.4 & 5.5) and the AURKA/HDAC6 ciliary disassembly pathway (Figure 5.6). Although the response of primary cilia to hypoxia is variable and tissue dependent (summarised in Table 5.1), it is consistent in all three available phaeochromocytoma cell lines examined. That all three contain mutations in cluster 2 PPGL-predisposing genes (Hopewell & Ziff 1995; Powers *et al.* 2000), in which hypoxic signalling is not a salient feature, is intriguing and demonstrates a role for primary cilia in PPGL pathogenesis beyond cluster 1 tumours.

Pseudohypoxia, achieved through loss of function of the cluster 1 PPGL-predisposing genes *SDH* (Figure 5.8 & 5.10), *FH* (Figure 5.12 & 5.13) and *VHL* (Figure 5.14), resulted in the same pattern of ciliary loss and shortening as observed with hypoxia itself. This is consistent with the observations in cluster 1 tumours (Figure 4.2) and although there were no known *FH* cases in the tested cohort, it would be reasonable to predict that this is a shared feature of cluster 1 PPGLs. It raises the question as to whether SDH, like VHL, might be considered a ciliopathy, particularly in view of its association with GISTs, a tumour type in which cilia-mediated signalling pathways (e.g. Wnt and PDGFRα) are important molecular drivers (Janeway *et al.* 2011; Tang *et al.* 2016). This, however, remains to be proved.

In PC12 cells, VHL loss resulted in ciliary loss through HIF and AURKA/HDAC6 dependent mechanisms (Figure 5.17). We also observed that hypoxia itself caused a re-distribution of pVHL out of the cilia, potentially priming it for disassembly (Figure 5.15). This microtubule stabilising function of pVHL (Okuda *et al.* 1999; Hergovich *et al.* 2003, 2006; Schermer *et al.* 2006; Lolkema *et al.* 2007) could potentially explain the development of PPGL in type 2C VHL in which regulation of HIF degradation is unimpaired (Knauth *et al.* 2009; McNeill *et al.* 2009). Further work to address whether there is a genotype-phenotype relationship with respect to primary cilia within VHL-associated PPGLs would be mechanistically informative.

A proposed model to illustrate how hypoxia and pseudohypoxia might result in changes in primary cilia and tumourigenesis in PPGLs is depicted in Figure 7.2.

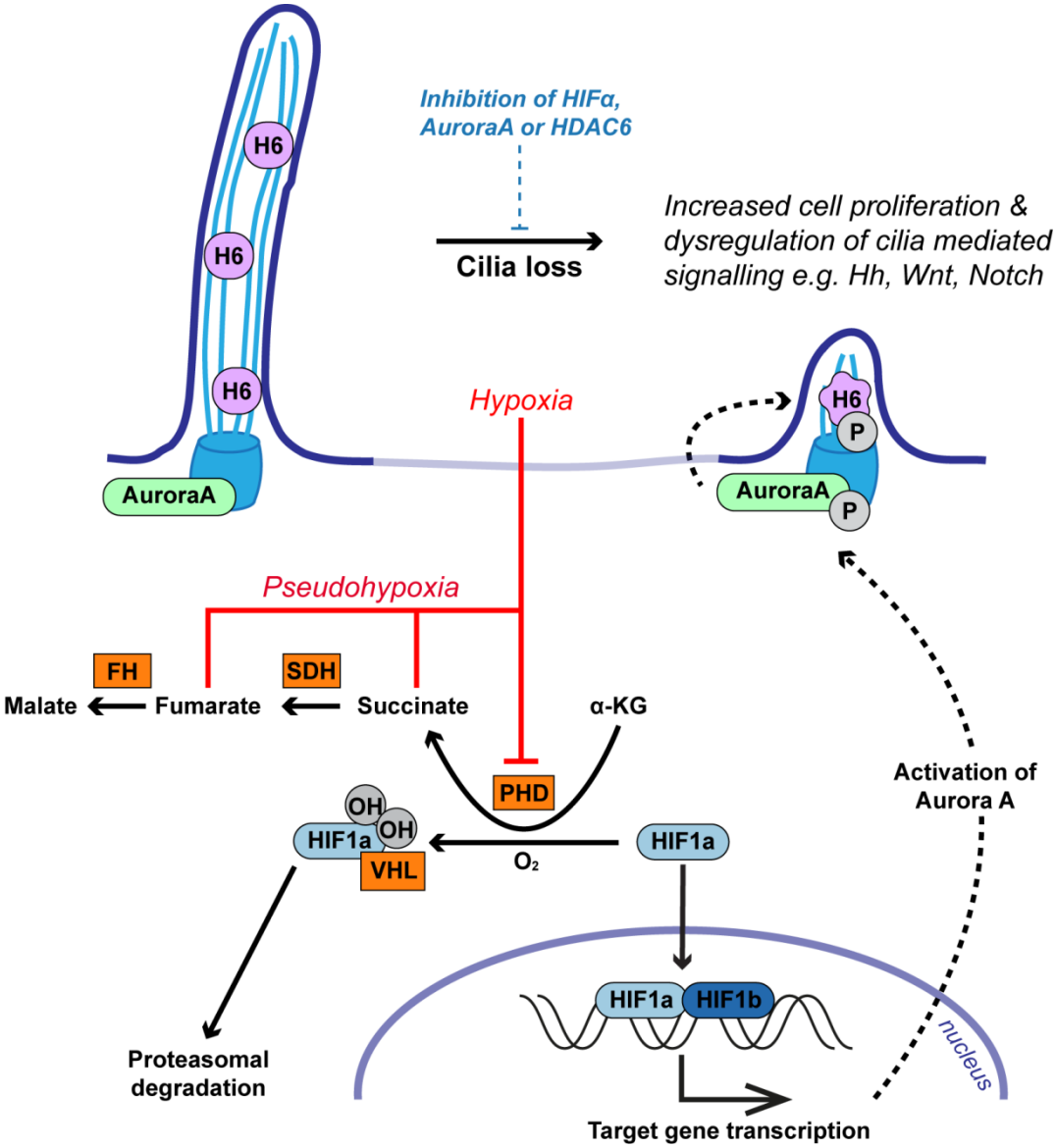

Figure 7.2: Schematic demonstrating the potential role of primary cilia in PPGLs

Model illustrating the potential pathway from pseudohypoxia-induced cilia loss to increased cell proliferation and dysregulation of tumourigenesis relevant cilia-mediated signalling pathways in PPGLs. Proteins where germline mutations in the associated gene predispose to PPGL are in orange.

AuroraA Aurora-A kinase α-KG α-ketoglutarate FH fumarate hydratase, H6 histone deacetylase 6, HIF hypoxia-inducible factor, OH hydroxyl group, P phosphate group, PHD prolyl hydroxylase, SDH succinate dehydrogenase, VHL von Hippel-Lindau.

Catecholamines, the vasoactive secretory product of PPGLs, are at their highest concentrations in PPGLs. However, little is known about whether this specific feature of the PPGL tumour microenvironment plays any role in its tumour biology. We found that adrenaline, noradrenaline and dopamine all promoted ciliary formation *in vitro* (Figures 5.21, 5.24 & 5.25) and that this effect was also seen with metanephrine *in vivo* (Figure 5.19).The responsible mechanism appears to be β-adrenoceptor mediated (Figures 5.22 & 5.23), consistent with the ciliary localisation of this receptor in other neural-derived tissue (Yao *et al.* 2016), although how this results in cilia elongation has yet to be determined.

Unlike hypoxia, catecholamines are a specific feature of the PPGL tumour microenvironment, and so the generalisability to other tumour types is less apparent. However, adrenaline increases ciliary length in pancreatic ductal adenocarcinoma cells (Khan *et al.* 2016) and α_1-adrenoceptor stimulation results in increased proliferation of prostate cancer cells (Thebault *et al.* 2006). How the ciliary effect of catecholamines interacts with other features of the tumour microenvironment which impact on primary cilia, including hypoxia, is not known.

Looking beyond cancer, the primary function of catecholamines is in regulating cardiac output (Figure 2.3). Primary cilia act as mechanosensors in vascular endothelium (Nauli *et al.* 2008) and are lost in areas of high blood flow (Van der Heiden *et al.* 2008). Flow-induced ciliary bending results in cytoskeletal deformation and cellular calcium influx via ciliary-localised polycystins (Talbot *et al.* 2011). Furthermore, vascular endothelial primary cilia are linked with other modulators of vascular tone including nitric oxide and dopamine signalling (Johns *et al.* 1984). The effect of catecholamines on primary cilia in other organs has yet to be investigated with vascular endothelium being of particular interest.

Although somatostatin is not a particular feature of the tumour microenvironment, SSTRs are widely and variably expressed in PPGLs (Kubota *et al.* 1994; Unger *et al.* 2008; Elston *et al.* 2015) and have diagnostic (Taïeb *et al.* 2012) and therapeutic (Kong *et al.* 2017) roles. It is interesting therefore that SSTR activation promotes ciliogenesis in PC12 cells (Figure 5.27). Although this is an early observation with an unknown mechanism, a previous report in a rodent model of PKD suggests that ciliary elongation by SSAs reduced hepatic cyst formation (Lorenzo Pisarello *et al.* 2018).

Taken together, it is apparent that multiple intrinsic and extrinsic factors impact on PPGL primary cilia and that ciliary loss contributes to tumourigenesis. What remains to be resolved, and is the next stage of enquiry, is whether manipulation of primary cilia *in vivo* alters the natural history of the disease as it does for other cancers (Xiang *et al.* 2017).

7.3 Adrenal venous sampling in the diagnosis of phaeochromocytomas

The biochemical diagnosis of functional PPGLs is relatively straightforward, once the condition is suspected, due to the excellent sensitivity and specificity of urine and plasma metanephrine measurement (Raber *et al.* 2000; Lenders *et al.* 2002, 2014). Once catecholamine excess is confirmed, modern cross-sectional and nuclear medicine imaging techniques localise PPGLs in almost all cases (Jalil *et al.* 1998; Lumachi *et al.* 2006; Rufini *et al.* 2011; Gabriel *et al.* 2013), meaning additional localisation techniques are rarely required. This is particularly the case with sporadic and symptomatic disease.

However, the existence of bilateral adrenal lesions can complicate the diagnostic process and has significant therapeutic implications as surgery on the incorrect side could result in hypoadrenalism and its consequent risks. This situation generally arises in the context of patients with a genetic predisposition to PPGL development who are enrolled in screening programmes aiming to diagnose small, pre-symptomatic PPGLs when the risk of disseminated disease is lower (Maher *et al.* 2011; Jasperson *et al.* 2014). In this circumstance, imaging may not be able to confidently define which lesion(s) are phaeochromocytomas and thus there is a potential role for a technique that could assist with anatomical localisation in cases which are unclear following a conventional imaging approach.

AVS has been used as a technique in PPGL localisation, although its utilisation has dramatically fallen as imaging quality has improved. In addition to being an invasive procedure, a lack of normative data to assist interpretation has led to uncertainty in the field (Freel *et al.* 2010).

We have presented reference intervals for side-specific adrenal venous catecholamine concentrations in patients without PPGL (Table 6.7). Using the 97.5th centile as a cut off, there was a 0% false negative rate in six PPGL patients who underwent AVS (Figure 6.7). Five of these patients had VHL (Table 6.8), highlighting the utility of AVS in this syndrome. Whilst it remains unusual for PPGL localisation not to be resolved by imaging, these data facilitate a more robust approach to interpreting AVS for catecholamines.

Having specified a diagnostic cut-off, future work will evaluate its efficacy in a separate cohort of PA patients who underwent AVS between 2015 and 2019 to define the false positive and false negative rates.

7.4 Summary

We have demonstrated that primary cilia loss is a feature of human PPGLs and in particular those with cluster 1 gene mutations; this is the first description of primary cilia in PPGLs. Activation of hypoxic signalling in a phaeochromocytoma-derived cell line through a multitude of disease-relevant mechanisms results in primary cilia loss in a HIF- and AURKA/HDAC6-dependent manner. Primary cilia loss in these cells is associated with increased cellular proliferation and oncogenic transcriptional alterations. Together these results suggest that cilia loss in PPGLs contributes to tumourigenesis and is a potential target for therapeutic intervention.

We have also shown that catecholamines, another feature of the PPGL tumour microenvironment, and SSAs, an existing PPGL therapeutic option, modulate primary cilia. This suggests that other features of the tumour microenvironment might also impact on primary cilia, which could be considered an integrative organelle for these multiple inputs.

Finally, we have presented normative data for adrenal venous catecholamine concentrations to allow their interpretation in instances when PPGL localisation is uncertain via standard techniques.

References

Abdul-Majeed S & Nauli SM 2011 Dopamine receptor type 5 in the primary cilia has dual chemo- and mechano-sensory roles. *Hypertension* **58** 325–331.

Abdul-Majeed S, Moloney BC & Nauli SM 2012 Mechanisms regulating cilia growth and cilia function in endothelial cells. *Cellular and Molecular Life Sciences* **69** 165–173.

Abermil N, Guillaud-Bataille M, Burnichon N, Venisse A, Manivet P, Guignat L, Drui D, Chupin M, Josseaume C, Affres H *et al.* 2012 *TMEM127* Screening in a Large Cohort of Patients with Pheochromocytoma and/or Paraganglioma. *The Journal of Clinical Endocrinology & Metabolism* **97** E805–E809.

Adams M, Simms RJ, Abdelhamed Z, Dawe HR, Szymanska K, Logan C V., Wheway G, Pitt E, Gull K, Knowles MA *et al.* 2012 A meckelin–filamin A interaction mediates ciliogenesis. *Human Molecular Genetics* **21** 1272–1286.

Agarwal G, Sadacharan D, Aggarwal V, Chand G, Mishra A, Agarwal A, Verma AK & Mishra SK 2012 Surgical management of organ-contained unilateral pheochromocytoma: comparative outcomes of laparoscopic and conventional open surgical procedures in a large single-institution series. *Langenbeck's Archives of Surgery* **397** 1109–1116.

Albers J, Rajski M, Schönenberger D, Harlander S, Schraml P, von Teichman A, Georgiev S, Wild PJ, Moch H, Krek W *et al.* 2013 Combined mutation of Vhl and Trp53 causes renal cysts and tumours in mice. *EMBO Molecular Medicine* **5** 949–964.

Algeciras-Schimnich A, Preissner CM, Young WF, Singh RJ & Grebe SKG 2008 Plasma chromogranin A or urine fractionated metanephrines follow-up testing improves the diagnostic accuracy of plasma fractionated metanephrines for pheochromocytoma. *The Journal of Clinical Endocrinology and Metabolism* **93** 91–95.

Alieva IB, Gorgidze LA, Komarova YA, Chernobelskaya OA & Vorobjev IA 1999 Experimental model for studying the primary cilia in tissue culture cells. *Membrane & Cell Biology* **12** 895–905.

Allison DJ, Brown MJ, Jones DH & Timmis JB 1983 Role of venous sampling in locating a phaeochromocytoma. *British Medical Journal (Clinical Research Ed.)* **286** 1122–1124.

Amar L, Baudin E, Burnichon N, Peyrard S, Silvera S, Bertherat J, Bertagna X, Schlumberger M, Jeunemaitre X, Gimenez-Roqueplo A-P *et al.* 2007 Succinate dehydrogenase B gene mutations predict survival in patients with malignant pheochromocytomas or paragangliomas. *The Journal of Clinical Endocrinology and Metabolism* **92** 3822–3828.

Amati B, Brooks MW, Levy N, Littlewood TD, Evan GI & Land H 1993a Oncogenic activity of the c-Myc protein requires dimerization with Max. *Cell* **72** 233–245.

Amati B, Littlewood TD, Evan GI & Land H 1993b The c-Myc protein induces cell cycle progression and apoptosis through dimerization with Max. *The EMBO Journal* **12** 5083–5087.

Amin C, Wagner AJ & Hay N 1993 Sequence-specific transcriptional activation by Myc and repression by Max. *Molecular and Cellular Biology* **13** 383–390.

Anand S, Penrhyn-Lowe S & Venkitaraman AR 2003 AURORA-A amplification overrides the mitotic spindle assembly checkpoint, inducing resistance to Taxol. *Cancer Cell* **3** 51–62.

Anders S & Huber W 2010 Differential expression analysis for sequence count data. *Genome Biol* **11**

R106.

Andrews KA, Ascher DB, Pires DEV, Barnes DR, Vialard L, Casey RT, Bradshaw N, Adlard J, Aylwin S, Brennan P *et al.* 2018 Tumour risks and genotype–phenotype correlations associated with germline variants in succinate dehydrogenase subunit genes SDHB , SDHC and SDHD. *Journal of Medical Genetics* **55** 384–394.

Ansley SJ, Badano JL, Blacque OE, Hill J, Hoskins BE, Leitch CC, Chul Kim J, Ross AJ, Eichers ER, Teslovich TM *et al.* 2003 Basal body dysfunction is a likely cause of pleiotropic Bardet–Biedl syndrome. *Nature* **425** 628–633.

Arias-Stella J & Bustos F 1976 Chronic hypoxia and chemodectomas in bovines at high altitudes. *Archives of Pathology & Laboratory Medicine* **100** 636–639.

Arias-Stella J & Valcarcel J 1976 Chief cell hyperplasia in the human carotid body at high altitudes; physiologic and pathologic significance. *Human Pathology* **7** 361–373.

Asante D, Stevenson NL & Stephens DJ 2014 Subunit composition of the human cytoplasmic dynein-2 complex. *Journal of Cell Science* **127** 4774–4787.

Askew DS, Ashmun RA, Simmons BC & Cleveland JL 1991 Constitutive c-myc expression in an IL-3-dependent myeloid cell line suppresses cell cycle arrest and accelerates apoptosis. *Oncogene* **6** 1915–1922.

Astrom K, Cohen JE, Willett-Brozick JE, Aston CE & Baysal BE 2003 Altitude is a phenotypic modifier in hereditary paraganglioma type 1: evidence for an oxygen-sensing defect. *Human Genetics* **113** 228–237.

Astuti D, Douglas F, Lennard TW, Aligianis IA, Woodward ER, Evans DGR, Eng C, Latif F & Maher ER 2001a Germline SDHD mutation in familial phaeochromocytoma. *The Lancet* **357** 1181–1182.

Astuti D, Latif F, Dallol A, Dahia PL, Douglas F, George E, Sköldberg F, Husebye ES, Eng C & Maher ER 2001b Gene mutations in the succinate dehydrogenase subunit SDHB cause susceptibility to familial pheochromocytoma and to familial paraganglioma. *American Journal of Human Genetics* **69** 49–54.

Avasthi P & Marshall WF 2012 Stages of ciliogenesis and regulation of ciliary length. *Differentiation; Research in Biological Diversity* **83** S30-42.

Avasthi P, Marley A, Lin H, Gregori-Puigjane E, Shoichet BK, von Zastrow M & Marshall WF 2012 A chemical screen identifies class a g-protein coupled receptors as regulators of cilia. *ACS Chemical Biology* **7** 911–919.

Ayala-Ramirez M, Chougnet CN, Habra MA, Palmer JL, Leboulleux S, Cabanillas ME, Caramella C, Anderson P, Al Ghuzlan A, Waguespack SG *et al.* 2012 Treatment with sunitinib for patients with progressive metastatic pheochromocytomas and sympathetic paragangliomas. *The Journal of Clinical Endocrinology and Metabolism* **97** 4040–4050.

Ayer DE, Kretzner L & Eisenman RN 1993 Mad: a heterodimeric partner for Max that antagonizes Myc transcriptional activity. *Cell* **72** 211–222.

van Baars F, Cremers C, van den Broek P, Geerts S & Veldman J 1982 Genetic aspects of nonchromaffin paraganglioma. *Human Genetics* **60** 305–309.

Baba Y, Nakajo M & Hayashi S 2013 Adrenal venous catecholamine concentrations in patients with

adrenal masses other than pheochromocytoma. *Endocrine* **43** 219–224.

Bailey JM, Mohr AM & Hollingsworth MA 2009 Sonic hedgehog paracrine signaling regulates metastasis and lymphangiogenesis in pancreatic cancer. *Oncogene* **28** 3513–3525.

Bailey KL, Bonasera SJ, Wilderdyke M, Hanisch BW, Pavlik JA, DeVasure J, Robinson JE, Sisson JH & Wyatt TA 2014 Aging causes a slowing in ciliary beat frequency, mediated by PKCε. *American Journal of Physiology-Lung Cellular and Molecular Physiology* **306** L584–L589.

Balkwill FR, Capasso M & Hagemann T 2012 The tumor microenvironment at a glance. *Journal of Cell Science* **125** 5591–5596.

Barakat MT, Humke EW & Scott MP 2013 Kif3a is necessary for initiation and maintenance of medulloblastoma. *Carcinogenesis* **34** 1382–1392.

Barnfield PC, Zhang X, Thanabalasingham V, Yoshida M & Hui C 2005 Negative regulation of Gli1 and Gli2 activator function by Suppressor of fused through multiple mechanisms. *Differentiation; Research in Biological Diversity* **73** 397–405.

Basten SG, Willekers S, Vermaat JS, Slaats GG, Voest EE, van Diest PJ & Giles RH 2013 Reduced cilia frequencies in human renal cell carcinomas versus neighboring parenchymal tissue. *Cilia* **2** 2.

Bausch B, Borozdin W, Neumann HPH & European-American Pheochromocytoma Study Group 2006 Clinical and Genetic Characteristics of Patients with Neurofibromatosis Type 1 and Pheochromocytoma. *New England Journal of Medicine* **354** 2729–2731.

Bausch B, Borozdin W, Mautner VF, Hoffmann MM, Boehm D, Robledo M, Cascon A, Harenberg T, Schiavi F, Pawlu C *et al.* 2007 Germline *NF1* Mutational Spectra and Loss-of-Heterozygosity Analyses in Patients with Pheochromocytoma and Neurofibromatosis Type 1. *The Journal of Clinical Endocrinology & Metabolism* **92** 2784–2792.

Bausch B, Schiavi F, Ni Y, Welander J, Patocs A, Ngeow J, Wellner U, Malinoc A, Taschin E, Barbon G *et al.* 2017 Clinical Characterization of the Pheochromocytoma and Paraganglioma Susceptibility Genes SDHA , TMEM127 , MAX , and SDHAF2 for Gene-Informed Prevention. *JAMA Oncology* **3** 1204–1212.

Bay SN, Long AB & Caspary T 2018 Disruption of the ciliary GTPase Arl13b suppresses Sonic hedgehog overactivation and inhibits medulloblastoma formation. *Proceedings of the National Academy of Sciences* **115** 1570–1575.

Baysal BE, Ferrell RE, Willett-Brozick JE, Lawrence EC, Myssiorek D, Bosch A, van der Mey A, Taschner PE, Rubinstein WS, Myers EN *et al.* 2000 Mutations in SDHD, a mitochondrial complex II gene, in hereditary paraganglioma. *Science (New York, N.Y.)* **287** 848–851.

Bellavia S, Dahan K, Terryn S, Cosyns J-P, Devuyst O & Pirson Y 2010 A homozygous mutation in INVS causing juvenile nephronophthisis with abnormal reactivity of the Wnt/beta-catenin pathway. *Nephrology Dialysis Transplantation* **25** 4097–4102.

Benn DE, Gimenez-Roqueplo A-P, Reilly JR, Bertherat J, Burgess J, Byth K, Croxson M, Dahia PLM, Elston M, Gimm O *et al.* 2006 Clinical presentation and penetrance of pheochromocytoma/paraganglioma syndromes. *The Journal of Clinical Endocrinology and Metabolism* **91** 827–836.

Benn DE, Robinson BG & Clifton-Bligh RJ 2015 15 YEARS OF PARAGANGLIOMA: Clinical manifestations of paraganglioma syndromes types 1–5. *Endocrine-Related Cancer* **22** T91–

T103.

Berbari NF, Lewis JS, Bishop GA, Askwith CC & Mykytyn K 2008a Bardet-Biedl syndrome proteins are required for the localization of G protein-coupled receptors to primary cilia. *Proceedings of the National Academy of Sciences of the United States of America* **105** 4242–4246.

Berbari NF, Johnson AD, Lewis JS, Askwith CC & Mykytyn K 2008b Identification of ciliary localization sequences within the third intracellular loop of G protein-coupled receptors. *Molecular Biology of the Cell* **19** 1540–1547.

Berbari NF, O'Connor AK, Haycraft CJ & Yoder BK 2009 The primary cilium as a complex signaling center. *Current Biology : CB* **19** R526-35.

Bergmann C, Fliegauf M, Brüchle NO, Frank V, Olbrich H, Kirschner J, Schermer B, Schmedding I, Kispert A, Kränzlin B *et al.* 2008 Loss of Nephrocystin-3 Function Can Cause Embryonic Lethality, Meckel-Gruber-like Syndrome, Situs Inversus, and Renal-Hepatic-Pancreatic Dysplasia. *The American Journal of Human Genetics* **82** 959–970.

Bertout JA, Patel SA & Simon MC 2008 The impact of O2 availability on human cancer. *Nature Reviews Cancer* **8** 967–975.

Besschetnova TY, Kolpakova-Hart E, Guan Y, Zhou J, Olsen BR & Shah J V. 2010 Identification of Signaling Pathways Regulating Primary Cilium Length and Flow-Mediated Adaptation. *Current Biology* **20** 182–187.

Bhatia KSS, Ismail MM, Sahdev A, Rockall AG, Hogarth K, Canizales A, Avril N, Monson JP, Grossman AB & Reznek RH 2008 123I-metaiodobenzylguanidine (MIBG) scintigraphy for the detection of adrenal and extra-adrenal phaeochromocytomas: CT and MRI correlation. *Clinical Endocrinology* **69** 181–188.

Bishop T, Lau KW, Epstein ACR, Kim SK, Jiang M, O'Rourke D, Pugh CW, Gleadle JM, Taylor MS, Hodgkin J *et al.* 2004 Genetic Analysis of Pathways Regulated by the von Hippel-Lindau Tumor Suppressor in Caenorhabditis elegans. *PLoS Biology* **2** e289.

Bishop GA, Berbari NF, Lewis J & Mykytyn K 2007 Type III adenylyl cyclase localizes to primary cilia throughout the adult mouse brain. *The Journal of Comparative Neurology* **505** 562–571.

Bitgood MJ & McMahon AP 1995 HedgehogandBmpGenes Are Coexpressed at Many Diverse Sites of Cell–Cell Interaction in the Mouse Embryo. *Developmental Biology* **172** 126–138.

Blackwell TK, Kretzner L, Blackwood EM, Eisenman RN & Weintraub H 1990 Sequence-specific DNA binding by the c-Myc protein. *Science (New York, N.Y.)* **250** 1149–1151.

Blackwell TK, Huang J, Ma A, Kretzner L, Alt FW, Eisenman RN & Weintraub H 1993 Binding of myc proteins to canonical and noncanonical DNA sequences. *Molecular and Cellular Biology* **13** 5216–5224.

Blake MA, Krishnamoorthy SK, Boland GW, Sweeney AT, Pitman MB, Harisinghani M, Mueller PR & Hahn PF 2003 Low-density pheochromocytoma on CT: a mimicker of adrenal adenoma. *AJR. American Journal of Roentgenology* **181** 1663–1668.

Blank A, Schmitt AM, Korpershoek E, van Nederveen F, Rudolph T, Weber N, Strebel RT, de Krijger R, Komminoth P & Perren A 2010 SDHB loss predicts malignancy in pheochromocytomas/sympathethic paragangliomas, but not through hypoxia signalling. *Endocrine-Related Cancer* **17** 919–928.

Boehlke C, Janusch H, Hamann C, Powelske C, Mergen M, Herbst H, Kotsis F, Nitschke R & Kuehn EW 2015 A Cilia Independent Role of Ift88/Polaris during Cell Migration. *PLOS ONE* **10** e0140378.

Boisvieux-Ulrich E, Laine MC & Sandoz D 1989 In vitro effects of taxol on ciliogenesis in quail oviduct. *Journal of Cell Science* **92 (Pt 1)** 9–20.

Boutros AR, Bravo EL, Zanettin G & Straffon RA 1990 Perioperative management of 63 patients with pheochromocytoma. *Cleveland Clinic Journal of Medicine* **57** 613–617.

Bowers AJ & Boylan JF 2004 Nek8, a NIMA family kinase member, is overexpressed in primary human breast tumors. *Gene* **328** 135–142.

Brandi ML, Gagel RF, Angeli A, Bilezikian JP, Beck-Peccoz P, Bordi C, Conte-Devolx B, Falchetti A, Gheri RG, Libroia A *et al.* 2001 Guidelines for diagnosis and therapy of MEN type 1 and type 2. *The Journal of Clinical Endocrinology and Metabolism* **86** 5658–5671.

Brauch H, Kishida T, Glavac D, Chen F, Pausch F, Höfler H, Latif F, Lerman MI, Zbar B & Neumann HP 1995 Von Hippel-Lindau (VHL) disease with pheochromocytoma in the Black Forest region of Germany: evidence for a founder effect. *Human Genetics* **95** 551–556.

Bray NL, Pimentel H, Melsted P & Pachter L 2016 Near-optimal probabilistic RNA-seq quantification. *Nature Biotechnology* **34** 525–527.

Brecht HM & Schoeppe W 1978 Relation of plasma noradrenaline to blood pressure, age, sex and sodium balance in patients with stable essential hypertension and in normotensive subjects. *Clinical Science and Molecular Medicine. Supplement* **4** 81s-83s.

Breen W, Bancos I, Young WF, Bible KC, Laack NN, Foote RL & Hallemeier CL 2018 External beam radiation therapy for advanced/unresectable malignant paraganglioma and pheochromocytoma. *Advances in Radiation Oncology* **3** 25–29.

Briggs RS, Birtwell AJ & Pohl JE 1978 Hypertensive response to labetalol in phaeochromocytoma. *Lancet (London, England)* **1** 1045–1046.

Brouwers FM, Eisenhofer G, Tao JJ, Kant JA, Adams KT, Linehan WM & Pacak K 2006 High frequency of SDHB germline mutations in patients with malignant catecholamine-producing paragangliomas: implications for genetic testing. *The Journal of Clinical Endocrinology and Metabolism* **91** 4505–4509.

Brown JAL, Santra T, Owens P, Morrison AM & Barry F 2014 Primary cilium-associated genes mediate bone marrow stromal cell response to hypoxia. *Stem Cell Research* **13** 284–299.

Burke R, Nellen D, Bellotto M, Hafen E, Senti KA, Dickson BJ & Basler K 1999 Dispatched, a novel sterol-sensing domain protein dedicated to the release of cholesterol-modified hedgehog from signaling cells. *Cell* **99** 803–815.

Burnichon N, Brière J-J, Libé R, Vescovo L, Rivière J, Tissier F, Jouanno E, Jeunemaitre X, Bénit P, Tzagoloff A *et al.* 2010 SDHA is a tumor suppressor gene causing paraganglioma. *Human Molecular Genetics* **19** 3011–3020.

Burnichon N, Vescovo L, Amar L, Libé R, de Reynies A, Venisse A, Jouanno E, Laurendeau I, Parfait B, Bertherat J *et al.* 2011 Integrative genomic analysis reveals somatic mutations in pheochromocytoma and paraganglioma. *Human Molecular Genetics* **20** 3974–3985.

Burnichon N, Cascón A, Schiavi F, Morales NP, Comino-Méndez I, Abermil N, Inglada-Pérez L, de

Cubas AA, Amar L, Barontini M *et al.* 2012 MAX mutations cause hereditary and sporadic pheochromocytoma and paraganglioma. *Clinical Cancer Research : An Official Journal of the American Association for Cancer Research* **18** 2828–2837.

Buttitta L, Mo R, Hui C-C & Fan C-M 2003 Interplays of Gli2 and Gli3 and their requirement in mediating Shh-dependent sclerotome induction. *Development (Cambridge, England)* **130** 6233–6243.

Bylund-Fellenius AC, Walker PM, Elander A, Holm S, Holm J & Scherstén T 1981 Energy metabolism in relation to oxygen partial pressure in human skeletal muscle during exercise. *The Biochemical Journal* **200** 247–255.

Calsina B, Currás-Freixes M, Buffet A, Pons T, Contreras L, Letón R, Comino-Méndez I, Remacha L, Calatayud M, Obispo B *et al.* 2018 Role of MDH2 pathogenic variant in pheochromocytoma and paraganglioma patients. *Genetics in Medicine* **20** 1652–1662.

Cameron OG, Starkman MN & Schteingart DE 1995 The effect of elevated systemic cortisol levels on plasma catecholamines in Cushing's syndrome patients with and without depressed mood. *Journal of Psychiatric Research* **29** 347–360.

Cano DA, Murcia NS, Pazour GJ & Hebrok M 2004 Orpk mouse model of polycystic kidney disease reveals essential role of primary cilia in pancreatic tissue organization. *Development (Cambridge, England)* **131** 3457–3467.

Cao M & Zhong Q 2015 Cilia in autophagy and cancer. *Cilia* **5** 4.

Caoili EM, Korobkin M, Francis IR, Cohan RH, Platt JF, Dunnick NR & Raghupathi KI 2002 Adrenal masses: characterization with combined unenhanced and delayed enhanced CT. *Radiology* **222** 629–633.

Caparrós-Martín JA, Valencia M, Reytor E, Pacheco M, Fernandez M, Perez-Aytes A, Gean E, Lapunzina P, Peters H, Goodship JA *et al.* 2013 The ciliary Evc/Evc2 complex interacts with Smo and controls Hedgehog pathway activity in chondrocytes by regulating Sufu/Gli3 dissociation and Gli3 trafficking in primary cilia. *Human Molecular Genetics* **22** 124–139.

Caplin ME, Pavel M, Ćwikła JB, Phan AT, Raderer M, Sedláčková E, Cadiot G, Wolin EM, Capdevila J, Wall L *et al.* 2014 Lanreotide in metastatic enteropancreatic neuroendocrine tumors. *The New England Journal of Medicine* **371** 224–233.

Cappello P, Blaser H, Gorrini C, Lin DCC, Elia AJ, Wakeham A, Haider S, Boutros PC, Mason JM, Miller NA *et al.* 2014 Role of Nek2 on centrosome duplication and aneuploidy in breast cancer cells. *Oncogene* **33** 2375–2384.

Carney JA, Sizemore GW & Tyce GM 1975 Bilateral adrenal medullary hyperplasia in multiple endocrine neoplasia, type 2: the precursor of bilateral pheochromocytoma. *Mayo Clinic Proceedings* **50** 3–10.

Cascón A, Comino-Méndez I, Currás-Freixes M, de Cubas AA, Contreras L, Richter S, Peitzsch M, Mancikova V, Inglada-Pérez L, Pérez-Barrios A *et al.* 2015 Whole-exome sequencing identifies MDH2 as a new familial paraganglioma gene. *Journal of the National Cancer Institute* **107** djv053.

Casey RT, Warren AY, Martin JE, Challis BG, Rattenberry E, Whitworth J, Andrews KA, Roberts T, Clark GR, West H *et al.* 2017 Clinical and Molecular Features of Renal and Pheochromocytoma/Paraganglioma Tumor Association Syndrome (RAPTAS): Case Series and

Literature Review. *The Journal of Clinical Endocrinology and Metabolism* **102** 4013–4022.

Castro-Vega LJ, Buffet A, De Cubas AA, Cascón A, Menara M, Khalifa E, Amar L, Azriel S, Bourdeau I, Chabre O *et al.* 2014 Germline mutations in FH confer predisposition to malignant pheochromocytomas and paragangliomas. *Human Molecular Genetics* **23** 2440–2446.

Cawthon RM, Weiss R, Xu GF, Viskochil D, Culver M, Stevens J, Robertson M, Dunn D, Gesteland R & O'Connell P 1990 A major segment of the neurofibromatosis type 1 gene: cDNA sequence, genomic structure, and point mutations. *Cell* **62** 193–201.

Chailley B & Boisvieux-Ulrich E 1985 Detection of plasma membrane cholesterol by filipin during microvillogenesis and ciliogenesis in quail oviduct. *Journal of Histochemistry & Cytochemistry* **33** 1–10.

Chamoun Z, Mann RK, Nellen D, von Kessler DP, Bellotto M, Beachy PA & Basler K 2001 Skinny hedgehog, an acyltransferase required for palmitoylation and activity of the hedgehog signal. *Science (New York, N.Y.)* **293** 2080–2084.

Chew SL, Dacie JE, Reznek RH, Newbould EC, Sheaves R, Trainer PJ, Lowe DG, Shand WS, Hungerford J & Besser GM 1994 Bilateral phaeochromocytomas in von Hippel-Lindau disease: diagnosis by adrenal vein sampling and catecholamine assay. *The Quarterly Journal of Medicine* **87** 49–54.

Chih B, Liu P, Chinn Y, Chalouni C, Komuves LG, Hass PE, Sandoval W & Peterson AS 2012 A ciliopathy complex at the transition zone protects the cilia as a privileged membrane domain. *Nature Cell Biology* **14** 61–72.

Chizhikov V V., Davenport J, Zhang Q, Shih EK, Cabello OA, Fuchs JL, Yoder BK & Millen KJ 2007 Cilia Proteins Control Cerebellar Morphogenesis by Promoting Expansion of the Granule Progenitor Pool. *Journal of Neuroscience* **27** 9780–9789.

Choi SM, Oh H & Park H 2008 Microarray analyses of hypoxia-regulated genes in an aryl hydrocarbon receptor nuclear translocator (Arnt)-dependent manner. *FEBS Journal* **275** 5618–5634.

Chuang J-Z, Yeh T-Y, Bollati F, Conde C, Canavosio F, Caceres A & Sung C-H 2005 The dynein light chain Tctex-1 has a dynein-independent role in actin remodeling during neurite outgrowth. *Developmental Cell* **9** 75–86.

Clark GR, Sciacovelli M, Gaude E, Walsh DM, Kirby G, Simpson MA, Trembath RC, Berg JN, Woodward ER, Kinning E *et al.* 2014 Germline FH mutations presenting with pheochromocytoma. *The Journal of Clinical Endocrinology and Metabolism* **99** E2046-50.

Clarke MR, Weyant RJ, Watson CG & Carty SE 1998 Prognostic markers in pheochromocytoma. *Human Pathology* **29** 522–526.

Clifford SC, Cockman ME, Smallwood AC, Mole DR, Woodward ER, Maxwell PH, Ratcliffe PJ & Maher ER 2001 Contrasting effects on HIF-1alpha regulation by disease-causing pVHL mutations correlate with patterns of tumourigenesis in von Hippel-Lindau disease. *Human Molecular Genetics* **10** 1029–1038.

Cockcroft JR, Ritter JM, Allison DJ, Causon R & Brown MJ 1987 Location of extra-adrenal catecholamine secreting tumours by selective venous sampling and nuclear magnetic resonance scanning. *Postgraduate Medical Journal* **63** 451–453.

Cockman ME, Masson N, Mole DR, Jaakkola P, Chang G-W, Clifford SC, Maher ER, Pugh CW, Ratcliffe PJ & Maxwell PH 2000 Hypoxia Inducible Factor-α Binding and Ubiquitylation by the von

Hippel-Lindau Tumor Suppressor Protein. *Journal of Biological Chemistry* **275** 25733–25741.

Coene KLM, Mans DA, Boldt K, Gloeckner CJ, van Reeuwijk J, Bolat E, Roosing S, Letteboer SJF, Peters TA, Cremers FPM *et al.* 2011 The ciliopathy-associated protein homologs RPGRIP1 and RPGRIP1L are linked to cilium integrity through interaction with Nek4 serine/threonine kinase. *Human Molecular Genetics* **20** 3592–3605.

Cole DG 1999 Kinesin-II, the heteromeric kinesin. *Cellular and Molecular Life Sciences : CMLS* **56** 217–226.

Comino-Méndez I, Gracia-Aznárez FJ, Schiavi F, Landa I, Leandro-García LJ, Letón R, Honrado E, Ramos-Medina R, Caronia D, Pita G *et al.* 2011 Exome sequencing identifies MAX mutations as a cause of hereditary pheochromocytoma. *Nature Genetics* **43** 663–667.

Comino-Méndez I, de Cubas A a, Bernal C, Álvarez-Escolá C, Sánchez-Malo C, Ramírez-Tortosa CL, Pedrinaci S, Rapizzi E, Ercolino T, Bernini G *et al.* 2013 Tumoral EPAS1 (HIF2A) mutations explain sporadic pheochromocytoma and paraganglioma in the absence of erythrocytosis. *Human Molecular Genetics* **22** 2169–2176.

Conduit SE, Ramaswamy V, Remke M, Watkins DN, Wainwright BJ, Taylor MD, Mitchell CA & Dyson JM 2017 A compartmentalized phosphoinositide signaling axis at cilia is regulated by INPP5E to maintain cilia and promote Sonic Hedgehog medulloblastoma. *Oncogene* **36** 5969–5984.

Corbit KC, Aanstad P, Singla V, Norman AR, Stainier DYR & Reiter JF 2005 Vertebrate Smoothened functions at the primary cilium. *Nature* **437** 1018–1021.

Coupland RE 1965 Electron microscopic observations on the structure of the rat adrenal medulla. *Journal of Anatomy* **99** 231–254.

Coy S, Du Z, Sheu S-H, Woo T, Rodriguez FJ, Kieran MW & Santagata S 2016 Distinct patterns of primary and motile cilia in Rathke's cleft cysts and craniopharyngioma subtypes. *Modern Pathology* **29** 1446–1459.

Crona J, Delgado Verdugo A, Maharjan R, Stålberg P, Granberg D, Hellman P & Björklund P 2013 Somatic Mutations in *H-RAS* in Sporadic Pheochromocytoma and Paraganglioma Identified by Exome Sequencing. *The Journal of Clinical Endocrinology & Metabolism* **98** E1266–E1271.

Cronin C 2008 Charles Sugrue, M.D., of Cork (1775–1816) and the first description of a classical medical condition: phaeochromocytoma. *Irish Journal of Medical Science* **177** 171–175.

Crout JR & Sjoerdsma a 1960 Catecholamines in the localization of pheochromocytoma. *Circulation* **22** 516–525.

Cui S-Y, Huang J-Y, Chen Y-T, Song H-Z, Huang G-C, De W, Wang R & Chen L-B 2013 The role of Aurora A in hypoxia-inducible factor 1α-promoting malignant phenotypes of hepatocelluar carcinoma. *Cell Cycle* **12** 2849–2866.

Cunningham WL, Becker EJ & Kreuzer F 1965 Catecholamines in plasma and urine at high altitude. *Journal of Applied Physiology* **20** 607–610.

Dahia PLM 2014 Pheochromocytoma and paraganglioma pathogenesis : learning from genetic heterogeneity. *Nature Publishing Group* **14** 108–119.

Dai P, Akimaru H, Tanaka Y, Maekawa T, Nakafuku M & Ishii S 1999 Sonic Hedgehog-induced activation of the Gli1 promoter is mediated by GLI3. *The Journal of Biological Chemistry* **274**

8143–8152.

Dajani R, Cleasby A, Neu M, Wonacott AJ, Jhoti H, Hood AM, Modi S, Hersey A, Taskinen J, Cooke RM *et al.* 1999 X-ray crystal structure of human dopamine sulfotransferase, SULT1A3. Molecular modeling and quantitative structure-activity relationship analysis demonstrate a molecular basis for sulfotransferase substrate specificity. *The Journal of Biological Chemistry* **274** 37862–37868.

Dalgard CL, Lu H, Mohyeldin A & Verma A 2004 Endogenous 2-oxoacids differentially regulate expression of oxygen sensors. *The Biochemical Journal* **380** 419–424.

Dannenberg H, Speel EJM, Zhao J, Saremaslani P, van der Harst E, Roth J, Heitz PU, Bonjer HJ, Dinjens WNM, Mooi WJ *et al.* 2000 Losses of Chromosomes 1p and 3q Are Early Genetic Events in the Development of Sporadic Pheochromocytomas. *The American Journal of Pathology* **157** 353–359.

Dar AA, Belkhiri A & El-Rifai W 2009 The aurora kinase A regulates GSK-3β in gastric cancer cells. *Oncogene* **28** 866–875.

Därr R, Eisenhofer G, Kotzerke J, Zöphel K, Stroszczynski C, Deinum J, Schultze Kool LJ, Pistorius S, Neumann H, Bornstein SR *et al.* 2011 Is there still a place for adrenal venous sampling in the diagnostic localization of pheochromocytoma? *Endocrine* **40** 75–79.

Dasgupta B, Dugan LL & Gutmann DH 2003 The neurofibromatosis 1 gene product neurofibromin regulates pituitary adenylate cyclase-activating polypeptide-mediated signaling in astrocytes. *The Journal of Neuroscience : The Official Journal of the Society for Neuroscience* **23** 8949–8954.

Davidson L, Vandongen R, Rouse IL, Beilin LJ & Tunney A 1984 Sex-related differences in resting and stimulated plasma noradrenaline and adrenaline. *Clinical Science (London, England : 1979)* **67** 347–352.

Davies RA, Patt NL & Sole MJ 1979 Localization of pheochromocytoma by selective venous catheterization and assay of plasma catecholamines. *Canadian Medical Association Journal* **120** 539–542.

Dawe HR, Smith UM, Cullinane AR, Gerrelli D, Cox P, Badano JL, Blair-Reid S, Sriram N, Katsanis N, Attie-Bitach T *et al.* 2007 The Meckel–Gruber Syndrome proteins MKS1 and meckelin interact and are required for primary cilium formation. *Human Molecular Genetics* **16** 173–186.

Dawe HR, Adams M, Wheway G, Szymanska K, Logan C V, Noegel AA, Gull K & Johnson CA 2009 Nesprin-2 interacts with meckelin and mediates ciliogenesis via remodelling of the actin cytoskeleton. *Journal of Cell Science* **122** 2716–2726.

Deane JA, Cole DG, Seeley ES, Diener DR & Rosenbaum JL 2001 Localization of intraflagellar transport protein IFT52 identifies basal body transitional fibers as the docking site for IFT particles. *Current Biology : CB* **11** 1586–1590.

Dekkers T, Deinum J, Schultzekool LJ, Blondin D, Vonend O, Hermus ARRM, Peitzsch M, Rump LC, Antoch G, Sweep FCGJ *et al.* 2013 Plasma metanephrine for assessing the selectivity of adrenal venous sampling. *Hypertension* **62** 1152–1157.

Delaval B, Bright A, Lawson ND & Doxsey S 2011 The cilia protein IFT88 is required for spindle orientation in mitosis. *Nature Cell Biology* **13** 461–468.

Delous M, Baala L, Salomon R, Laclef C, Vierkotten J, Tory K, Golzio C, Lacoste T, Besse L, Ozilou C *et*

al. 2007 The ciliary gene RPGRIP1L is mutated in cerebello-oculo-renal syndrome (Joubert syndrome type B) and Meckel syndrome. *Nature Genetics* **39** 875–881.

Dénes J, Swords F, Rattenberry E, Stals K, Owens M, Cranston T, Xekouki P, Moran L, Kumar A, Wassif C *et al.* 2015 Heterogeneous genetic background of the association of pheochromocytoma/paraganglioma and pituitary adenoma – results from a large patient cohort. *The Journal of Clinical Endocrinology & Metabolism* **100** E531-41.

Dere R, Perkins AL, Bawa-Khalfe T, Jonasch D & Walker CL 2015 β-catenin links von Hippel-Lindau to aurora kinase A and loss of primary cilia in renal cell carcinoma. *Journal of the American Society of Nephrology : JASN* **26** 553–564.

DeVaul N, Koloustroubis K, Wang R & Sperry AO 2017 A novel interaction between kinase activities in regulation of cilia formation. *BMC Cell Biology* **18** 33.

Ding Q, Fukami S i, Meng X, Nishizaki Y, Zhang X, Sasaki H, Dlugosz A, Nakafuku M & Hui C c 1999 Mouse suppressor of fused is a negative regulator of sonic hedgehog signaling and alters the subcellular distribution of Gli1. *Current Biology : CB* **9** 1119–1122.

Ding X-F, Zhou J, Hu Q-Y, Liu S-C & Chen G 2015 The tumor suppressor pVHL down-regulates never-in-mitosis A-related kinase 8 via hypoxia-inducible factors to maintain cilia in human renal cancer cells. *The Journal of Biological Chemistry* **290** 1389–1394.

Dishinger JF, Kee HL, Jenkins PM, Fan S, Hurd TW, Hammond JW, Truong YN-T, Margolis B, Martens JR & Verhey KJ 2010 Ciliary entry of the kinesin-2 motor KIF17 is regulated by importin-β2 and RanGTP. *Nature Cell Biology* **12** 703–710.

Domire JS, Green JA, Lee KG, Johnson AD, Askwith CC & Mykytyn K 2011 Dopamine receptor 1 localizes to neuronal cilia in a dynamic process that requires the Bardet-Biedl syndrome proteins. *Cellular and Molecular Life Sciences : CMLS* **68** 2951–2960.

Doobin DJ, Kemal S, Dantas TJ & Vallee RB 2016 Severe NDE1-mediated microcephaly results from neural progenitor cell cycle arrests at multiple specific stages. *Nature Communications* **7** 12551.

Doolin PF & Birge WJ 1966 Ultrastructural organization of cilia and basal bodies of the epithelium of the choroid plexus in the chick embryo. *The Journal of Cell Biology* **29** 333–345.

Dorn K V, Hughes CE & Rohatgi R 2012 A Smoothened-Evc2 complex transduces the Hedgehog signal at primary cilia. *Developmental Cell* **23** 823–835.

Druce MR, Kaltsas GA, Fraenkel M, Gross DJ & Grossman AB 2009 Novel and Evolving Therapies in the Treatment of Malignant Phaeochromocytoma: Experience with the mTOR Inhibitor Everolimus (RAD001). *Hormone and Metabolic Research* **41** 697–702.

Du E, Lu C, Sheng F, Li C, Li H, Ding N, Chen Y, Zhang T, Yang K & Xu Y 2018 Analysis of potential genes associated with primary cilia in bladder cancer. *Cancer Management and Research* **Volume 10** 3047–3056.

van Duinen N, Corssmit EPM, de Jong WHA, Brookman D, Kema IP & Romijn JA 2013 Plasma levels of free metanephrines and 3-methoxytyramine indicate a higher number of biochemically active HNPGL than 24-h urinary excretion rates of catecholamines and metabolites. *European Journal of Endocrinology* **169** 377–382.

Dummer A, Poelma C, DeRuiter MC, Goumans M-JTH & Hierck BP 2016 Measuring the primary cilium length: improved method for unbiased high-throughput analysis. *Cilia* **5** 7.

Dvorak J, Sitorova V, Nikolov DH, Filipova A, Ryska A, Melichar B, Richter I, Buka D, Mokry J, Filip S *et al.* 2014 Primary cilia in gastrointestinal stromal tumors. *Neoplasma* **61** 305–308.

Dvorak J, Hadzi Nikolov D, Dusek L, Filipova A, Richter I, Buka D, Ryska A, Mokry J, Filip S, Melichar B *et al.* 2016 Prognostic significance of the frequency of primary cilia in cells of small bowel and colorectal adenocarcinoma. *Journal of B.U.ON. : Official Journal of the Balkan Union of Oncology* **21** 1233–1241.

Dvorak J, Hadzi Nikolov D, Dusek L, Filipova A, Richter I, Buka D, Ryska A, Mokry J, Filip S, Melichar B *et al.* 2017 Association of the combined parameters including the frequency of primary cilia, CD8+ tumor infiltrating lymphocytes and PD-1 expression with the outcome in intestinal cancer. *Journal of B.U.ON. : Official Journal of the Balkan Union of Oncology* **22** 1477–1487.

Dwight T, Mann K, Benn DE, Robinson BG, McKelvie P, Gill AJ, Winship I & Clifton-Bligh RJ 2013 Familial SDHA mutation associated with pituitary adenoma and pheochromocytoma/paraganglioma. *Journal of Clinical Endocrinology and Metabolism* **98** 1103–1108. (doi:10.1210/jc.2013-1400)

Edwards C, Heath D, Harris P, Castillo Y, Krüger H & Arias-Stella J 1971 The carotid body in animals at high altitude. *The Journal of Pathology* **104** 231–238.

Edwards C, Heath D & Harris P 1972 Ultrastructure of the carotid body in high-altitude guinea-pigs. *The Journal of Pathology* **107** 131–136.

Egeberg DL, Lethan M, Manguso R, Schneider L, Awan A, Jørgensen TS, Byskov AG, Pedersen LB & Christensen ST 2012 Primary cilia and aberrant cell signaling in epithelial ovarian cancer. *Cilia* **1** 15.

Eisenhofer G, Goldstein DS, Stull R, Keiser HR, Sunderland T, Murphy DL & Kopin IJ 1986 Simultaneous liquid-chromatographic determination of 3,4-dihydroxyphenylglycol, catecholamines, and 3,4-dihydroxyphenylalanine in plasma, and their responses to inhibition of monoamine oxidase. *Clinical Chemistry* **32** 2030–2033.

Eisenhofer G, Friberg P, Pacak K, Goldstein DS, Murphy DL, Tsigos C, Quyyumi AA, Brunner HG & Lenders JW 1995a Plasma metadrenalines: do they provide useful information about sympatho-adrenal function and catecholamine metabolism? *Clinical Science (London, England : 1979)* **88** 533–542.

Eisenhofer G, Rundquist B, Aneman A, Friberg P, Dakak N, Kopin IJ, Jacobs MC & Lenders JW 1995b Regional release and removal of catecholamines and extraneuronal metabolism to metanephrines. *The Journal of Clinical Endocrinology and Metabolism* **80** 3009–3017.

Eisenhofer G, Aneman A, Hooper D, Rundqvist B & Friberg P 1996 Mesenteric organ production, hepatic metabolism, and renal elimination of norepinephrine and its metabolites in humans. *Journal of Neurochemistry* **66** 1565–1573.

Eisenhofer G, Keiser H, Friberg P, Mezey E, Huynh TT, Hiremagalur B, Ellingson T, Duddempudi S, Eijsbouts A & Lenders JW 1998 Plasma metanephrines are markers of pheochromocytoma produced by catechol-O-methyltransferase within tumors. *The Journal of Clinical Endocrinology and Metabolism* **83** 2175–2185.

Eisenhofer G, Huynh TT, Hiroi M & Pacak K 2001 Understanding catecholamine metabolism as a guide to the biochemical diagnosis of pheochromocytoma. *Reviews in Endocrine & Metabolic Disorders* **2** 297–311.

Eisenhofer G, Goldstein DS, Walther MM, Friberg P, Lenders JWM, Keiser HR & Pacak K 2003 Biochemical Diagnosis of Pheochromocytoma: How to Distinguish True- from False-Positive Test Results. *The Journal of Clinical Endocrinology & Metabolism* **88** 2656–2666.

Eisenhofer G, Lenders JWM, Timmers H, Mannelli M, Grebe SK, Hofbauer LC, Bornstein SR, Tiebel O, Adams K, Bratslavsky G *et al.* 2011 Measurements of plasma methoxytyramine, normetanephrine, and metanephrine as discriminators of different hereditary forms of pheochromocytoma. *Clinical Chemistry* **57** 411–420.

Eisenhofer G, Lattke P, Herberg M, Siegert G, Qin N, Därr R, Hoyer J, Villringer A, Prejbisz A, Januszewicz A *et al.* 2013 Reference intervals for plasma free metanephrines with an age adjustment for normetanephrine for optimized laboratory testing of phaeochromocytoma. *Annals of Clinical Biochemistry* **50** 62–69.

Elshafie O, Al Badaai Y, Alwahaibi K, Qureshi A, Hussein S, Al Azzri F, Almamari A & Woodhouse N 2014 Catecholamine-secreting carotid body paraganglioma: successful preoperative control of hypertension and clinical symptoms using high-dose long-acting octreotide. *Endocrinology, Diabetes & Metabolism Case Reports* **2014** 140051.

Elston MS, Meyer-Rochow GY, Conaglen HM, Clarkson A, Clifton-Bligh RJ, Conaglen J V & Gill AJ 2015 Increased SSTR2A and SSTR3 expression in succinate dehydrogenase-deficient pheochromocytomas and paragangliomas. *Human Pathology* **46** 390–396.

Elvidge GP, Glenny L, Appelhoff RJ, Ratcliffe PJ, Ragoussis J & Gleadle JM 2006 Concordant Regulation of Gene Expression by Hypoxia and 2-Oxoglutarate-dependent Dioxygenase Inhibition. *Journal of Biological Chemistry* **281** 15215–15226.

Emerson CE & Rainbird A 2003 Use of a 'hospital-at-home' service for patient optimization before resection of phaeochromocytoma. *British Journal of Anaesthesia* **90** 380–382.

Emoto K, Masugi Y, Yamazaki K, Effendi K, Tsujikawa H, Tanabe M, Kitagawa Y & Sakamoto M 2014 Presence of primary cilia in cancer cells correlates with prognosis of pancreatic ductal adenocarcinoma. *Human Pathology* **45** 817–825.

Endicott SJ, Basu B, Khokha M & Brueckner M 2015 The NIMA-like kinase Nek2 is a key switch balancing cilia biogenesis and resorption in the development of left-right asymmetry. *Development* **142** 4068–4079.

Endoh-Yamagami S, Evangelista M, Wilson D, Wen X, Theunissen J-W, Phamluong K, Davis M, Scales SJ, Solloway MJ, de Sauvage FJ *et al.* 2009 The Mammalian Cos2 Homolog Kif7 Plays an Essential Role in Modulating Hh Signal Transduction during Development. *Current Biology* **19** 1320–1326.

Engel BD, Ludington WB & Marshall WF 2009 Intraflagellar transport particle size scales inversely with flagellar length: revisiting the balance-point length control model. *The Journal of Cell Biology* **187** 81–89.

Enríquez-Vega ME, Muñoz-Paredes JG, Cossío-Zazueta A, Ontiveros-Carlos Y, Pacheco-Pittaluga E & Bizueto-Rosas H 2019 SDHD gene mutation in Mexican population with carotid body tumor. *Cirugía y Cirujanos* **86** 38–42.

Esteban-Barragán MA, Ávila P, Álvarez-Tejado M, Gutierrez M, Garcia-Pardo A, Sanchez-Madrid F & Landazuri M 2002 Role of the von Hippel-Lindau tumor suppressor gene in the formation of beta1-integrin fibrillar adhesions. *Cancer Res* **62** 2929–2936.

Esteban MA, Harten SK, Tran MG & Maxwell PH 2006 Formation of primary cilia in the renal epithelium is regulated by the von Hippel-Lindau tumor suppressor protein. *Journal of the American Society of Nephrology : JASN* **17** 1801–1806.

Estus S, Zaks WJ, Freeman RS, Gruda M, Bravo R & Johnson EM 1994 Altered gene expression in neurons during programmed cell death: identification of c-jun as necessary for neuronal apoptosis. *The Journal of Cell Biology* **127** 1717–1727.

Von Euler US, Gemzell CA, Strom G & Westman A 1955 Report of a case of pheochromocytoma, with special regard to preoperative diagnostic problems. *Acta Medica Scandinavica* **153** 127–136.

Evenepoel L, Helaers R, Vroonen L, Aydin S, Hamoir M, Maiter D, Vikkula M & Persu A 2017 KIF1B and NF1 are the most frequently mutated genes in paraganglioma and pheochromocytoma tumors. *Endocrine-Related Cancer* **24** L57–L61.

Ezratty EJ, Stokes N, Chai S, Shah AS, Williams SE & Fuchs E 2011 A Role for the Primary Cilium in Notch Signaling and Epidermal Differentiation during Skin Development. *Cell* **145** 1129–1141.

Ezratty EJ, Pasolli HA & Fuchs E 2016 A Presenilin-2–ARF4 trafficking axis modulates Notch signaling during epidermal differentiation. *The Journal of Cell Biology* **214** 89–101.

Fan S, Fogg V, Wang Q, Chen X-W, Liu C-J & Margolis B 2007 A novel Crumbs3 isoform regulates cell division and ciliogenesis via importin β interactions. *The Journal of Cell Biology* **178** 387–398.

Fan S, Whiteman EL, Hurd TW, McIntyre JC, Dishinger JF, Liu CJ, Martens JR, Verhey KJ, Sajjan U & Margolis B 2011 Induction of Ran GTP drives ciliogenesis. *Molecular Biology of the Cell* **22** 4539–4548.

Farnum CE & Wilsman NJ 2011 Orientation of primary cilia of articular chondrocytes in three-dimensional space. *Anatomical Record (Hoboken, N.J. : 2007)* **294** 533–549.

Favier J, Amar L & Gimenez-Roqueplo A-P 2015 Paraganglioma and phaeochromocytoma: from genetics to personalized medicine. *Nature Reviews Endocrinology* **11** 101–111.

Fawcett D & Porter K 1954 A study of the fine structure of ciliated epitheliae. *J Morphol* **94** 221–281.

Feng Y & Walsh CA 2004 Mitotic Spindle Regulation by Nde1 Controls Cerebral Cortical Size. *Neuron* **44** 279–293.

Fishbein L, Khare S, Wubbenhorst B, DeSloover D, D'Andrea K, Merrill S, Cho NW, Greenberg RA, Else T, Montone K *et al.* 2015 Whole-exome sequencing identifies somatic ATRX mutations in pheochromocytomas and paragangliomas. *Nature Communications* **6** 6140.

Fishbein L, Leshchiner I, Walter V, Danilova L, Robertson AG, Johnson AR, Lichtenberg TM, Murray BA, Ghayee HK, Else T *et al.* 2017 Comprehensive Molecular Characterization of Pheochromocytoma and Paraganglioma. *Cancer Cell* **31** 181–193.

Fleisher DS, Voci G, Cresson SL & Karafin L 1964 Preoperative localization of pheochromocytoma. *The Journal of Pediatrics* **64** 711–715.

Fonte JS, Robles JF, Chen CC, Reynolds J, Whatley M, Ling A, Mercado-Asis LB, Adams KT, Martucci V, Fojo T *et al.* 2012 False-negative ^{123}I-MIBG SPECT is most commonly found in SDHB-related pheochromocytoma or paraganglioma with high frequency to develop metastatic disease. *Endocrine-Related Cancer* **19** 83–93.

Frank V, Habbig S, Bartram MP, Eisenberger T, Veenstra-Knol HE, Decker C, Boorsma RAC, Göbel H,

Nürnberg G, Griessmann A *et al.* 2013 Mutations in NEK8 link multiple organ dysplasia with altered Hippo signalling and increased c-MYC expression. *Human Molecular Genetics* **22** 2177–2185.

Fränkel F 1886 No Ein Fall von doppelseitigem, völlig latent verlaufenen Nebennierentumor und gleichzeitiger Nephritis mit Veränderungen am Circulationsapparat und Retinitis. *Arch Pathol Anat Physiol Klin Med* 244–263.

Freel EM, Stanson AW, Thompson GB, Grant CS, Farley DR, Richards ML & Young WF 2010 Adrenal venous sampling for catecholamines: A normal value study. *Journal of Clinical Endocrinology and Metabolism* **95** 1328–1332.

Frew IJ, Thoma CR, Georgiev S, Minola A, Hitz M, Montani M, Moch H & Krek W 2008 pVHL and PTEN tumour suppressor proteins cooperatively suppress kidney cyst formation. *The EMBO Journal* **27** 1747–1757.

Fukui H, Shiba D, Asakawa K, Kawakami K & Yokoyama T 2012 The ciliary protein Nek8/Nphp9 acts downstream of Inv/Nphp2 during pronephros morphogenesis and left-right establishment in zebrafish. *FEBS Letters* **586** 2273–2279.

Fumoto K, Lee P-C, Saya H & Kikuchi A 2008 AIP regulates stability of Aurora-A at early mitotic phase coordinately with GSK-3β. *Oncogene* **27** 4478–4487.

Funder JW, Carey RM, Mantero F, Murad MH, Reincke M, Shibata H, Stowasser M & Young WF 2016 The Management of Primary Aldosteronism: Case Detection, Diagnosis, and Treatment: An Endocrine Society Clinical Practice Guideline. *The Journal of Clinical Endocrinology & Metabolism* **101** 1889–1916.

Furukawa T, Kanai N, Shiwaku HO, Soga N, Uehara A & Horii A 2006 AURKA is one of the downstream targets of MAPK1/ERK2 in pancreatic cancer. *Oncogene* **25** 4831–4839.

Gaal J, Burnichon N, Korpershoek E, Roncelin I, Bertherat J, Plouin P-F, de Krijger RR, Gimenez-Roqueplo A-P & Dinjens WNM 2010 Isocitrate Dehydrogenase Mutations Are Rare in Pheochromocytomas and Paragangliomas. *The Journal of Clinical Endocrinology & Metabolism* **95** 1274–1278.

Gabriel S, Blanchet EM, Sebag F, Chen CC, Fakhry N, Deveze A, Barlier A, Morange I, Pacak K & Taïeb D 2013 Functional characterization of nonmetastatic paraganglioma and pheochromocytoma by (18) F-FDOPA PET: focus on missed lesions. *Clinical Endocrinology* **79** 170–177.

Gabriel E, Wason A, Ramani A, Gooi LM, Keller P, Pozniakovsky A, Poser I, Noack F, Telugu NS, Calegari F *et al.* 2016 CPAP promotes timely cilium disassembly to maintain neural progenitor pool. *The EMBO Journal* **35** 803–819.

Gaertig J & Wloga D 2008 Chapter 4 Ciliary Tubulin and Its Post-Translational Modifications. In *Current Topics in Developmental Biology*, pp 83–113.

Gagel RF, Tashjian AH, Cummings T, Papathanasopoulos N, Kaplan MM, DeLellis RA, Wolfe HJ & Reichlin S 1988 The clinical outcome of prospective screening for multiple endocrine neoplasia type 2a. An 18-year experience. *The New England Journal of Medicine* **318** 478–484.

Garcia-Gonzalo FR, Corbit KC, Sirerol-Piquer MS, Ramaswami G, Otto EA, Noriega TR, Seol AD, Robinson JF, Bennett CL, Josifova DJ *et al.* 2011 A transition zone complex regulates mammalian ciliogenesis and ciliary membrane composition. *Nature Genetics* **43** 776–784.

García-Zaragoza E, Pérez-Tavarez R, Ballester A, Lafarga V, Jiménez-Reinoso A, Ramírez A, Murillas R & Gallego MI 2012 Intraepithelial paracrine Hedgehog signaling induces the expansion of ciliated cells that express diverse progenitor cell markers in the basal epithelium of the mouse mammary gland. *Developmental Biology* **372** 28–44.

Gerald D, Berra E, Frapart YM, Chan DA, Giaccia AJ, Mansuy D, Pouysségur J, Yaniv M & Mechta-Grigoriou F 2004 JunD reduces tumor angiogenesis by protecting cells from oxidative stress. *Cell* **118** 781–794.

Gerdes JM, Liu Y, Zaghloul NA, Leitch CC, Lawson SS, Kato M, Beachy PA, Beales PL, DeMartino GN, Fisher S *et al.* 2007 Disruption of the basal body compromises proteasomal function and perturbs intracellular Wnt response. *Nature Genetics* **39** 1350–1360.

Gerhardt C, Lier JM, Burmühl S, Struchtrup A, Deutschmann K, Vetter M, Leu T, Reeg S, Grune T & Rüther U 2015 The transition zone protein Rpgrip1l regulates proteasomal activity at the primary cilium. *The Journal of Cell Biology* **210** 115–133.

Gerhardt C, Leu T, Lier JM & Rüther U 2016 The cilia-regulated proteasome and its role in the development of ciliopathies and cancer. *Cilia* **5** 14.

Gerlo EA, Schoors DF & Dupont AG 1991 Age- and sex-related differences for the urinary excretion of norepinephrine, epinephrine, and dopamine in adults. *Clinical Chemistry* **37** 875–878.

Gewirtz GP, Kvetnanský R, Weise VK & Kopin IJ 1971 Effect of hypophysectomy on adrenal dopamine -hydroxylase activity in the rat. *Molecular Pharmacology* **7** 163–168.

Gild ML, Naik N, Hoang J, Hsiao E, McGrath RT, Sywak M, Sidhu S, Delbridge LW, Robinson BG, Schembri G *et al.* 2018 Role of DOTATATE-PET/CT in preoperative assessment of phaeochromocytoma and paragangliomas. *Clinical Endocrinology* **89** 139–147.

Gill AJ, Chou A, Vilain R, Clarkson A, Lui M, Jin R, Tobias V, Samra J, Goldstein D, Smith C *et al.* 2010 Immunohistochemistry for SDHB Divides Gastrointestinal Stromal Tumors (GISTs) into 2 Distinct Types. *The American Journal of Surgical Pathology* **34** 636–644.

Gilula NB & Satir P 1972 The ciliary necklace. A ciliary membrane specialization. *The Journal of Cell Biology* **53** 494–509.

Gimm O, Armanios M, Dziema H, Neumann HP & Eng C 2000 Somatic and occult germ-line mutations in SDHD, a mitochondrial complex II gene, in nonfamilial pheochromocytoma. *Cancer Research* **60** 6822–6825.

Giovanella L, Squin N, Ghelfo A & Ceriani L 2006 Chromogranin A immunoradiometric assay in diagnosis of pheochromocytoma: comparison with plasma metanephrines and 123I-MIBG scan. *Q J Nucl Med Mol Imaging* **50** 344–347.

Gleadle J & Ratcliffe P 2001 *Encyclopedia of Life Sciences: Hypoxia.* John Wiley & Sons, Ltd.

Goetz SC & Anderson K V. 2010 The primary cilium: a signalling centre during vertebrate development. *Nature Reviews Genetics* **11** 331–344.

Gomez-Sanchez EP 1986 Intracerebroventricular infusion of aldosterone induces hypertension in rats. *Endocrinology* **118** 819–823.

Gradilone SA, Radtke BN, Bogert PS, Huang BQ, Gajdos GB & LaRusso NF 2013 HDAC6 inhibition restores ciliary expression and decreases tumor growth. *Cancer Research* **73** 2259–2270.

Grampa V, Delous M, Zaidan M, Odye G, Thomas S, Elkhartoufi N, Filhol E, Niel O, Silbermann F, Lebreton C *et al.* 2016 Novel NEK8 Mutations Cause Severe Syndromic Renal Cystic Dysplasia through YAP Dysregulation. *PLOS Genetics* **12** e1005894.

Graser S, Stierhof Y-D, Lavoie SB, Gassner OS, Lamla S, Le Clech M & Nigg EA 2007 Cep164, a novel centriole appendage protein required for primary cilium formation. *The Journal of Cell Biology* **179** 321–330.

Greene LA & Tischler AS 1976 Establishment of a noradrenergic clonal line of rat adrenal pheochromocytoma cells which respond to nerve growth factor. **73** 2424–2428.

Grim CE, Glenn JF, Wynn JO & Gunnells JC 1967 Bilateral pheochromocytoma: the application of a plasma catecholamine bioassay for tumor localization. *American Heart Journal* **74** 809–815.

Grisanti L, Revenkova E, Gordon RE & Iomini C 2016 Primary cilia maintain corneal epithelial homeostasis by regulation of the Notch signaling pathway. *Development* **143** 2160–2171.

Groeben H, Nottebaum BJ, Alesina PF, Traut A, Neumann HP & Walz MK 2017 Perioperative α-receptor blockade in phaeochromocytoma surgery: an observational case series † †This Article is accompanied by Editorial Aew414. *British Journal of Anaesthesia* **118** 182–189.

Grozinger CM, Hassig CA & Schreiber SL 1999 Three proteins define a class of human histone deacetylases related to yeast Hda1p. *Proceedings of the National Academy of Sciences of the United States of America* **96** 4868–4873.

Grubbs EG, Rich TA, Ng C, Bhosale PR, Jimenez C, Evans DB, Lee JE & Perrier ND 2013 Long-term outcomes of surgical treatment for hereditary pheochromocytoma. *Journal of the American College of Surgeons* **216** 280–289.

Gruber LM, Erickson D, Babovic-Vuksanovic D, Thompson GB, Young WF & Bancos I 2017 Pheochromocytoma and paraganglioma in patients with neurofibromatosis type 1. *Clinical Endocrinology* **86** 141–149.

Guen VJ, Chavarria TE, Kröger C, Ye X, Weinberg RA & Lees JA 2017 EMT programs promote basal mammary stem cell and tumor-initiating cell stemness by inducing primary ciliogenesis and Hedgehog signaling. *Proceedings of the National Academy of Sciences* **114** E10532–E10539.

Guillemot J, Compagnon P, Cartier D, Thouennon E, Bastard C, Lihrmann I, Pichon P, Thuillez C, Plouin P-F, Bertherat J *et al.* 2009 Metoclopramide stimulates catecholamine- and granin-derived peptide secretion from pheochromocytoma cells through activation of serotonin type 4 (5-HT4) receptors. *Endocrine-Related Cancer* **16** 281–290.

Guinot A, Lehmann H, Wild PJ & Frew IJ 2016 Combined deletion of Vhl, Trp53 and Kif3a causes cystic and neoplastic renal lesions. *The Journal of Pathology* **239** 365–373.

Gutmann DH, Aylsworth A, Carey JC, Korf B, Marks J, Pyeritz RE, Rubenstein A & Viskochil D 1997 The diagnostic evaluation and multidisciplinary management of neurofibromatosis 1 and neurofibromatosis 2. *JAMA* **278** 51–57.

Haase VH, Glickman JN, Socolovsky M & Jaenisch R 2001 Vascular tumors in livers with targeted inactivation of the von Hippel-Lindau tumor suppressor. *Proceedings of the National Academy of Sciences of the United States of America* **98** 1583–1588.

Habbig S, Bartram MP, Sägmüller JG, Griessmann A, Franke M, Müller R-U, Schwarz R, Hoehne M, Bergmann C, Tessmer C *et al.* 2012 The ciliopathy disease protein NPHP9 promotes nuclear

delivery and activation of the oncogenic transcriptional regulator TAZ. *Human Molecular Genetics* **21** 5528–5538.

Hadoux J, Favier J, Scoazec J-Y, Leboulleux S, Al Ghuzlan A, Caramella C, Déandreis D, Borget I, Loriot C, Chougnet C *et al.* 2014 SDHB mutations are associated with response to temozolomide in patients with metastatic pheochromocytoma or paraganglioma. *International Journal of Cancer* **135** 2711–2720.

Hagiwara H, Ohwada N, Aoki T, Suzuki T & Takata K 2008 Immunohistochemical and electron microscopic observations of stromal cells in the human oviduct mucosa. *Medical Molecular Morphology* **41** 221–226.

Hammond JW, Huang C-F, Kaech S, Jacobson C, Banker G & Verhey KJ 2010 Posttranslational modifications of tubulin and the polarized transport of kinesin-1 in neurons. *Molecular Biology of the Cell* **21** 572–583.

Han Y-G, Kim HJ, Dlugosz AA, Ellison DW, Gilbertson RJ & Alvarez-Buylla A 2009 Dual and opposing roles of primary cilia in medulloblastoma development. *Nature Medicine* **15** 1062–1065.

Han SJ, Jang H-S, Kim JI, Lipschutz JH & Park KM 2016 Unilateral nephrectomy elongates primary cilia in the remaining kidney via reactive oxygen species. *Scientific Reports* **6** 22281.

Han SJ, Jang H-S, Seu SY, Cho H-J, Hwang YJ, Kim JI & Park KM 2017 Hepatic ischemia/reperfusion injury disrupts the homeostasis of kidney primary cilia via oxidative stress. *Biochimica et Biophysica Acta (BBA) - Molecular Basis of Disease* **1863** 1817–1828.

Han S, Suh CH, Woo S, Kim YJ & Lee JJ 2018 Performance of 68 Ga-DOTA-Conjugated Somatostatin Receptor Targeting Peptide PET in Detection of Pheochromocytoma and Paraganglioma: A Systematic Review and Meta-Analysis. *Journal of Nuclear Medicine* **60** 369–376.

Händel M, Schulz S, Stanarius A, Schreff M, Erdtmann-Vourliotis M, Schmidt H, Wolf G & Höllt V 1999 Selective targeting of somatostatin receptor 3 to neuronal cilia. *Neuroscience* **89** 909–926.

Hao H-X, Khalimonchuk O, Schraders M, Dephoure N, Bayley J-P, Kunst H, Devilee P, Cremers CWRJ, Schiffman JD, Bentz BG *et al.* 2009 SDH5, a gene required for flavination of succinate dehydrogenase, is mutated in paraganglioma. *Science (New York, N.Y.)* **325** 1139–1142.

Harlander S, Schönenberger D, Toussaint NC, Prummer M, Catalano A, Brandt L, Moch H, Wild PJ & Frew IJ 2017 Combined mutation in Vhl, Trp53 and Rb1 causes clear cell renal cell carcinoma in mice. *Nature Medicine* **23** 869–877.

Hartman TR, Liu D, Zilfou JT, Robb V, Morrison T, Watnick T & Henske EP 2009 The tuberous sclerosis proteins regulate formation of the primary cilium via a rapamycin-insensitive and polycystin 1-independent pathway. *Human Molecular Genetics* **18** 151–163.

Hassounah NB, Bunch TA & McDermott KM 2012 Molecular Pathways: The Role of Primary Cilia in Cancer Progression and Therapeutics with a Focus on Hedgehog Signaling. *Clinical Cancer Research* **18** 2429–2435.

Hassounah NB, Nagle R, Saboda K, Roe DJ, Dalkin BL & McDermott KM 2013 Primary cilia are lost in preinvasive and invasive prostate cancer. *PloS One* **8** e68521.

Haycraft CJ, Banizs B, Aydin-Son Y, Zhang Q, Michaud EJ & Yoder BK 2005 Gli2 and Gli3 Localize to Cilia and Require the Intraflagellar Transport Protein Polaris for Processing and Function. *PLoS Genetics* **1** e53.

Hayward DG, Clarke RB, Faragher AJ, Pillai MR, Hagan IM & Fry AM 2004 The centrosomal kinase Nek2 displays elevated levels of protein expression in human breast cancer. *Cancer Research* **64** 7370–7376.

Hearn T, Spalluto C, Phillips VJ, Renforth GL, Copin N, Hanley NA & Wilson DI 2005 Subcellular localization of ALMS1 supports involvement of centrosome and basal body dysfunction in the pathogenesis of obesity, insulin resistance, and type 2 diabetes. *Diabetes* **54** 1581–1587.

Van der Heiden K, Hierck BP, Krams R, de Crom R, Cheng C, Baiker M, Pourquie MJBM, Alkemade FE, DeRuiter MC, Gittenberger-de Groot AC *et al.* 2008 Endothelial primary cilia in areas of disturbed flow are at the base of atherosclerosis. *Atherosclerosis* **196** 542–550.

Hellman NE, Liu Y, Merkel E, Austin C, Le Corre S, Beier DR, Sun Z, Sharma N, Yoder BK & Drummond IA 2010 The zebrafish foxj1a transcription factor regulates cilia function in response to injury and epithelial stretch. *Proceedings of the National Academy of Sciences* **107** 18499–18504.

Hergovich A, Lisztwan J, Barry R, Ballschmieter P & Krek W 2003 Regulation of microtubule stability by the von Hippel-Lindau tumour suppressor protein pVHL. *Nature Cell Biology* **5** 64–70.

Hergovich A, Lisztwan J, Thoma CR, Wirbelauer C, Barry RE & Krek W 2006 Priming-dependent phosphorylation and regulation of the tumor suppressor pVHL by glycogen synthase kinase 3. *Molecular and Cellular Biology* **26** 5784–5796.

Herman B & Albertini DF 1983 Microtubule regulation of cell surface receptor topography during granulosa cell differentiation. *Differentiation; Research in Biological Diversity* **25** 56–63.

Hernandez KG, Ezzat S, Morel CF, Swallow C, Otremba M, Dickson BC, Asa SL & Mete O 2015 Familial pheochromocytoma and renal cell carcinoma syndrome: TMEM127 as a novel candidate gene for the association. *Virchows Archiv* **466** 727–732.

Hewitson KS, Liénard BMR, McDonough MA, Clifton IJ, Butler D, Soares AS, Oldham NJ, McNeill LA & Schofield CJ 2007 Structural and Mechanistic Studies on the Inhibition of the Hypoxia-inducible Transcription Factor Hydroxylases by Tricarboxylic Acid Cycle Intermediates. *Journal of Biological Chemistry* **282** 3293–3301.

Hickman PE, Leong M, Chang J, Wilson SR & McWhinney B 2009 Plasma free metanephrines are superior to urine and plasma catecholamines and urine catecholamine metabolites for the investigation of phaeochromocytoma. *Pathology* **41** 173–177.

von Hippel E 1904 Ueber eine sehr seltene Erkrankung der Netzhaut. *Ophthalmology* **59** 83–106.

Hirano T, Katoh Y & Nakayama K 2017 Intraflagellar transport-A complex mediates ciliary entry and retrograde trafficking of ciliary G protein-coupled receptors. *Molecular Biology of the Cell* **28** 429–439.

Ho L, Ali SA, Al-Jazrawe M, Kandel R, Wunder JS & Alman BA 2013 Primary cilia attenuate hedgehog signalling in neoplastic chondrocytes. *Oncogene* **32** 5388–5396.

Hoekstra AS, de Graaff MA, Briaire-de Bruijn IH, Ras C, Seifar RM, van Minderhout I, Cornelisse CJ, Hogendoorn PCW, Breuning MH, Suijker J *et al.* 2015 Inactivation of SDH and FH cause loss of 5hmC and increased H3K9me3 in paraganglioma/pheochromocytoma and smooth muscle tumors. *Oncotarget* **6** 38777–38788.

Hoff S, Halbritter J, Epting D, Frank V, Nguyen T-MT, van Reeuwijk J, Boehlke C, Schell C, Yasunaga T, Helmstädter M *et al.* 2013 ANKS6 is a central component of a nephronophthisis module linking

NEK8 to INVS and NPHP3. *Nature Genetics* **45** 951–956.

Hoffman MA, Ohh M, Yang H, Klco JM, Ivan M & Kaelin WG 2001 von Hippel-Lindau protein mutants linked to type 2C VHL disease preserve the ability to downregulate HIF. *Human Molecular Genetics* **10** 1019–1027.

Hopewell R & Ziff EB 1995 The nerve growth factor-responsive PC12 cell line does not express the Myc dimerization partner Max. *Molecular and Cellular Biology* **15** 3470–3478.

Hou Y, Qin H, Follit JA, Pazour GJ, Rosenbaum JL & Witman GB 2007 Functional analysis of an individual IFT protein: IFT46 is required for transport of outer dynein arms into flagella. *The Journal of Cell Biology* **176** 653–665.

Hu C-J, Iyer S, Sataur A, Covello KL, Chodosh LA & Simon MC 2006 Differential Regulation of the Transcriptional Activities of Hypoxia-Inducible Factor 1 Alpha (HIF-1) and HIF-2 in Stem Cells. *Molecular and Cellular Biology* **26** 3514–3526.

Huang P & Schier AF 2009 Dampened Hedgehog signaling but normal Wnt signaling in zebrafish without cilia. *Development* **136** 3089–3098.

Huang Y, Zheng J, Chen D, Li F, Wu W, Huang X, Wu Y, Deng Y & Qiu F 2017 Transcriptome profiling identifies a recurrent *CRYL1-IFT88* chimeric transcript in hepatocellular carcinoma. *Oncotarget* **8** 40693–40704.

Huangfu D & Anderson K V 2005 Cilia and Hedgehog responsiveness in the mouse. *Proceedings of the National Academy of Sciences of the United States of America* **102** 11325–11330.

Huangfu D, Liu A, Rakeman AS, Murcia NS, Niswander L & Anderson K V 2003 Hedgehog signalling in the mouse requires intraflagellar transport proteins. *Nature* **426** 83–87.

Hubbert C, Guardiola A, Shao R, Kawaguchi Y, Ito A, Nixon A, Yoshida M, Wang X-F & Yao T-P 2002 HDAC6 is a microtubule-associated deacetylase. *Nature* **417** 455–458.

Huber W, Carey VJ, Gentleman R, Anders S, Carlson M, Carvalho BS, Bravo HC, Davis S, Gatto L, Girke T *et al.* 2015 Orchestrating high-throughput genomic analysis with Bioconductor. *Nat Meth* **12** 115–121.

Hui AS, Striet JB, Gudelsky G, Soukhova GK, Gozal E, Beitner-Johnson D, Guo S-Z, Sachleben LR, Haycock JW, Gozal D *et al.* 2003 Regulation of catecholamines by sustained and intermittent hypoxia in neuroendocrine cells and sympathetic neurons. *Hypertension (Dallas, Tex. : 1979)* **42** 1130–1136.

van Hulsteijn LT, van Duinen N, Verbist BM, Jansen JC, van der Klaauw AA, Smit JWA & Corssmit EPM 2013 Effects of octreotide therapy in progressive head and neck paragangliomas: Case series. *Head & Neck* **35** E391–E396.

van Hulsteijn LT, Niemeijer ND, Dekkers OM & Corssmit EPM 2014 (131)I-MIBG therapy for malignant paraganglioma and phaeochromocytoma: systematic review and meta-analysis. *Clinical Endocrinology* **80** 487–501.

Hurd TW, Fan S & Margolis BL 2011 Localization of retinitis pigmentosa 2 to cilia is regulated by Importin 2. *Journal of Cell Science* **124** 718–726.

Ignatiadis N, Klaus B, Zaugg JB & Huber W 2016 Data-driven hypothesis weighting increases detection power in genome-scale multiple testing. *Nat Meth* **13** 577–580.

Ilias I, Chen CC, Carrasquillo JA, Whatley M, Ling A, Lazúrová I, Adams KT, Perera S & Pacak K 2008 Comparison of 6-18F-fluorodopamine PET with 123I-metaiodobenzylguanidine and 111in-pentetreotide scintigraphy in localization of nonmetastatic and metastatic pheochromocytoma. *Journal of Nuclear Medicine : Official Publication, Society of Nuclear Medicine* **49** 1613–1619.

Inaba H, Goto H, Kasahara K, Kumamoto K, Yonemura S, Inoko A, Yamano S, Wanibuchi H, He D, Goshima N *et al.* 2016 Ndel1 suppresses ciliogenesis in proliferating cells by regulating the trichoplein–Aurora A pathway. *The Journal of Cell Biology* **212** 409–423.

Ingham PW 2001 Hedgehog signaling in animal development: paradigms and principles. *Genes & Development* **15** 3059–3087.

Inoko A, Matsuyama M, Goto H, Ohmuro-Matsuyama Y, Hayashi Y, Enomoto M, Ibi M, Urano T, Yonemura S, Kiyono T *et al.* 2012 Trichoplein and Aurora A block aberrant primary cilia assembly in proliferating cells. *The Journal of Cell Biology* **197** 391–405.

Insel PA 1989 Structure and function of alpha-adrenergic receptors. *The American Journal of Medicine* **87** 12S-18S.

Iomini C, Babaev-Khaimov V, Sassaroli M & Piperno G 2001 Protein particles in Chlamydomonas flagella undergo a transport cycle consisting of four phases. *The Journal of Cell Biology* **153** 13–24.

Isaacs JS, Jung YJ, Mole DR, Lee S, Torres-Cabala C, Chung Y-L, Merino M, Trepel J, Zbar B, Toro J *et al.* 2005 HIF overexpression correlates with biallelic loss of fumarate hydratase in renal cancer: Novel role of fumarate in regulation of HIF stability. *Cancer Cell* **8** 143–153.

Ivan M, Kondo K, Yang H, Kim W, Valiando J, Ohh M, Salic A, Asara JM, Lane WS & Kaelin WG 2001 HIFalpha Targeted for VHL-Mediated Destruction by Proline Hydroxylation: Implications for O2 Sensing. *Science* **292** 464–468.

Iwanaga T, Hozumi Y & Takahashi-Iwanaga H 2011a Immunohistochemical demonstration of dopamine receptor D2R in the primary cilia of the mouse pituitary gland. *Biomedical Research (Tokyo, Japan)* **32** 225–235.

Iwanaga T, Miki T & Takahashi-Iwanaga H 2011b Restricted expression of somatostatin receptor 3 to primary cilia in the pancreatic islets and adenohypophysis of mice. *Biomedical Research (Tokyo, Japan)* **32** 73–81.

Izawa I, Goto H, Kasahara K & Inagaki M 2015 Current topics of functional links between primary cilia and cell cycle. *Cilia* **4** 12.

Jaakkola P, Mole DR, Tian Y-M, Wilson MI, Gielbert J, Gaskell SJ, Kriegsheim A v., Hebestreit HF, Mukherji M, Schofield CJ *et al.* 2001 Targeting of HIF-alpha to the von Hippel-Lindau Ubiquitylation Complex by O2-Regulated Prolyl Hydroxylation. *Science* **292** 468–472.

Jalil ND, Pattou FN, Combemale F, Chapuis Y, Henry JF, Peix JL & Proye CA 1998 Effectiveness and limits of preoperative imaging studies for the localisation of pheochromocytomas and paragangliomas: a review of 282 cases. French Association of Surgery (AFC), and The French Association of Endocrine Surgeons (AFCE). *The European Journal of Surgery* **164** 23–28.

James MF 1989 Use of magnesium sulphate in the anaesthetic management of phaeochromocytoma: a review of 17 anaesthetics. *British Journal of Anaesthesia* **62** 616–623.

Janeway KA, Kim SY, Lodish M, Nose V, Rustin P, Gaal J, Dahia PLM, Liegl B, Ball ER, Raygada M *et al.*

2011 Defects in succinate dehydrogenase in gastrointestinal stromal tumors lacking KIT and PDGFRA mutations. *Proceedings of the National Academy of Sciences* **108** 314–318.

Jang C-Y, Coppinger JA, Seki A, Yates JR & Fang G 2009 Plk1 and Aurora A regulate the depolymerase activity and the cellular localization of Kif2a. *Journal of Cell Science* **122** 1334–1341.

Janssen I, Blanchet EM, Adams K, Chen CC, Millo CM, Herscovitch P, Taieb D, Kebebew E, Lehnert H, Fojo AT *et al.* 2015 Superiority of [68Ga]-DOTATATE PET/CT to Other Functional Imaging Modalities in the Localization of SDHB-Associated Metastatic Pheochromocytoma and Paraganglioma. *Clinical Cancer Research* **21** 3888–3895.

Jasim S, Suman VJ, Jimenez C, Harris P, Sideras K, Burton JK, Worden FP, Auchus RJ & Bible KC 2017 Phase II trial of pazopanib in advanced/progressive malignant pheochromocytoma and paraganglioma. *Endocrine* **57** 220–225.

Jasperson KW, Kohlmann W, Gammon A, Slack H, Buchmann L, Hunt J, Kirchhoff AC, Baskin H, Shaaban A & Schiffman JD 2014 Role of rapid sequence whole-body MRI screening in SDH-associated hereditary paraganglioma families. *Familial Cancer* **13** 257–265.

Jaulin F & Kreitzer G 2010 KIF17 stabilizes microtubules and contributes to epithelial morphogenesis by acting at MT plus ends with EB1 and APC. *The Journal of Cell Biology* **190** 443–460.

Jawed I, Velarde M, Därr R, Wolf KI, Adams K, Venkatesan AM, Balasubramaniam S, Poruchynsky MS, Reynolds JC, Pacak K *et al.* 2018 Continued Tumor Reduction of Metastatic Pheochromocytoma/Paraganglioma Harboring Succinate Dehydrogenase Subunit B Mutations with Cyclical Chemotherapy. *Cellular and Molecular Neurobiology* **38** 1099–1106.

Jenks AD, Vyse S, Wong JP, Kostaras E, Keller D, Burgoyne T, Shoemark A, Tsalikis A, de la Roche M, Michaelis M *et al.* 2018 Primary Cilia Mediate Diverse Kinase Inhibitor Resistance Mechanisms in Cancer. *Cell Reports* **23** 3042–3055.

Jensen CG, Davison EA, Bowser SS & Rieder CL 1987 Primary cilia cycle in PtK1 cells: Effects of colcemid and taxol on cilia formation and resorption. *Cell Motility and the Cytoskeleton* **7** 187–197.

Jimbo T, Kawasaki Y, Koyama R, Sato R, Takada S, Haraguchi K & Akiyama T 2002 Identification of a link between the tumour suppressor APC and the kinesin superfamily. *Nature Cell Biology* **4** 323–327.

Jin H, White SR, Shida T, Schulz S, Aguiar M, Gygi SP, Bazan JF & Nachury M V. 2010 The Conserved Bardet-Biedl Syndrome Proteins Assemble a Coat that Traffics Membrane Proteins to Cilia. *Cell* **141** 1208–1219.

Jin X, Mohieldin AM, Muntean BS, Green JA, Shah J V, Mykytyn K & Nauli SM 2014 Cilioplasm is a cellular compartment for calcium signaling in response to mechanical and chemical stimuli. *Cellular and Molecular Life Sciences : CMLS* **71** 2165–2178.

Johns DW, Ayers CR & Carey RM 1984 The dopamine agonist bromocriptine induces hypotension by venous and arteriolar dilation. *Journal of Cardiovascular Pharmacology* **6** 582–587.

Johnson KA & Rosenbaum JL 1992 Polarity of flagellar assembly in Chlamydomonas. *The Journal of Cell Biology* **119** 1605–1611.

Johnson TS, Young JB & Landsberg L 1983 Sympathoadrenal responses to acute and chronic hypoxia in the rat. *The Journal of Clinical Investigation* **71** 1263–1272.

Johnson ET, Nicola T, Roarty K, Yoder BK, Haycraft CJ & Serra R 2008 Role for primary cilia in the regulation of mouse ovarian function. *Developmental Dynamics : An Official Publication of the American Association of Anatomists* **237** 2053–2060.

Jones DH, Allison DJ, Hamilton CA & Reid JL 1979 Selective venous sampling in the diagnosis and localization of phaeochromocytoma. *Clinical Endocrinology* **10** 179–186.

Jones C, Roper VC, Foucher I, Qian D, Banizs B, Petit C, Yoder BK & Chen P 2008 Ciliary proteins link basal body polarization to planar cell polarity regulation. *Nature Genetics* **40** 69–77.

de Jong WHA, Eisenhofer G, Post WJ, Muskiet FAJ, de Vries EGE & Kema IP 2009 Dietary influences on plasma and urinary metanephrines: implications for diagnosis of catecholamine-producing tumors. *The Journal of Clinical Endocrinology and Metabolism* **94** 2841–2849.

Kaelin WG 2008 The von Hippel-Lindau tumour suppressor protein: O2 sensing and cancer. *Nature Reviews. Cancer* **8** 865–873.

Kahaly G, Krause U, Ritthaler H, Cordes U, Günther R, Schrezenmeir J & Beyer J 1985 Selective blood sampling in adrenal hypertension. *Cardiology* **72 Suppl 1** 179–181.

Kaluza D, Kroll J, Gesierich S, Yao T-P, Boon RA, Hergenreider E, Tjwa M, Rössig L, Seto E, Augustin HG *et al.* 2011 Class IIb HDAC6 regulates endothelial cell migration and angiogenesis by deacetylation of cortactin. *The EMBO Journal* **30** 4142–4156.

Katayama H, Sasai K, Kawai H, Yuan Z-M, Bondaruk J, Suzuki F, Fujii S, Arlinghaus RB, Czerniak BA & Sen S 2004 Phosphorylation by aurora kinase A induces Mdm2-mediated destabilization and inhibition of p53. *Nature Genetics* **36** 55–62.

Kathem SH, Mohieldin AM, Abdul-Majeed S, Ismail SH, Altaei QH, Alshimmari IK, Alsaidi MM, Khammas H, Nauli AM, Joe B *et al.* 2014 Ciliotherapy: a novel intervention in polycystic kidney disease. *Journal of Geriatric Cardiology : JGC* **11** 63–73.

Kawachi Y, Maruyama H, Ishitsuka Y, Fujisawa Y, Furuta J, Nakamura Y, Ichikawa E, Furumura M & Otsuka F 2013 *NF1* gene silencing induces upregulation of vascular endothelial growth factor expression in both Schwann and non-Schwann cells. *Experimental Dermatology* **22** 262–265.

Kee HL, Dishinger JF, Lynne Blasius T, Liu C-J, Margolis B & Verhey KJ 2012 A size-exclusion permeability barrier and nucleoporins characterize a ciliary pore complex that regulates transport into cilia. *Nature Cell Biology* **14** 431–437.

van Keimpema L, Nevens F, Vanslembrouck R, van Oijen MGH, Hoffmann AL, Dekker HM, de Man RA & Drenth JPH 2009 Lanreotide reduces the volume of polycystic liver: a randomized, double-blind, placebo-controlled trial. *Gastroenterology* **137** 1661-8.e1-2.

Keiser HR, Goldstein DS, Wade JL, Douglas FL & Averbuch SD 1985 Treatment of malignant pheochromocytoma with combination chemotherapy. *Hypertension (Dallas, Tex. : 1979)* **7** I18-24.

Kerkhoff E, Bister K & Klempnauer KH 1991 Sequence-specific DNA binding by Myc proteins. *Proceedings of the National Academy of Sciences of the United States of America* **88** 4323–4327.

Khan NA, Willemarck N, Talebi A, Marchand A, Binda MM, Dehairs J, Rueda-Rincon N, Daniels VW, Bagadi M, Raj DBTG *et al.* 2016 Identification of drugs that restore primary cilium expression in cancer cells. *Oncotarget* **7** 9975–9992.

Khorram-Manesh A, Ahlman H, Nilsson O, Odén A & Jansson S 2004 Mortality associated with pheochromocytoma in a large Swedish cohort. *European Journal of Surgical Oncology* **30** 556–559.

Kibel A, Iliopoulos O, DeCaprio JA & Kaelin WG 1995 Binding of the von Hippel-Lindau tumor suppressor protein to Elongin B and C. *Science (New York, N.Y.)* **269** 1444–1446.

Kim WY, Safran M, Buckley MRM, Ebert BL, Glickman J, Bosenberg M, Regan M & Kaelin WG 2006a Failure to prolyl hydroxylate hypoxia-inducible factor alpha phenocopies VHL inactivation in vivo. *The EMBO Journal* **25** 4650–4662.

Kim M, Gans JD, Nogueira C, Wang A, Paik J-H, Feng B, Brennan C, Hahn WC, Cordon-Cardo C, Wagner SN *et al.* 2006b Comparative Oncogenomics Identifies NEDD9 as a Melanoma Metastasis Gene. *Cell* **125** 1269–1281.

Kim S, Zaghloul NA, Bubenshchikova E, Oh EC, Rankin S, Katsanis N, Obara T & Tsiokas L 2011a Nde1-mediated inhibition of ciliogenesis affects cell cycle re-entry. *Nature Cell Biology* **13** 351–360.

Kim J, Dabiri S & Seeley ES 2011b Primary cilium depletion typifies cutaneous melanoma in situ and malignant melanoma. *PloS One* **6** e27410.

Kim JI, Kim J, Jang H-S, Noh MR, Lipschutz JH & Park KM 2013 Reduction of oxidative stress during recovery accelerates normalization of primary cilia length that is altered after ischemic injury in murine kidneys. *American Journal of Physiology-Renal Physiology* **304** F1283–F1294.

Kim S, Lee K, Choi J-H, Ringstad N & Dynlacht BD 2015 Nek2 activation of Kif24 ensures cilium disassembly during the cell cycle. *Nature Communications* **6** 8087.

Kim JH, Ki SM, Joung J-G, Scott E, Heynen-Genel S, Aza-Blanc P, Kwon CH, Kim J, Gleeson JG & Lee JE 2016 Genome-wide screen identifies novel machineries required for both ciliogenesis and cell cycle arrest upon serum starvation. *Biochimica et Biophysica Acta (BBA) - Molecular Cell Research* **1863** 1307–1318.

Kimura N, Schindler M, Kasai N & Kimura I 2001 Immunohistochemical localization of somatostatin receptor type 2A in rat and human tissues. *Endocrine Journal* **48** 95–102.

Kimura N, Takayanagi R, Takizawa N, Itagaki E, Katabami T, Kakoi N, Rakugi H, Ikeda Y, Tanabe A, Nigawara T *et al.* 2014 Pathological grading for predicting metastasis in phaeochromocytoma and paraganglioma. *Endocrine Related Cancer* **21** 405–414.

Kinzel D, Boldt K, Davis EE, Burtscher I, Trümbach D, Diplas B, Attié-Bitach T, Wurst W, Katsanis N, Ueffing M *et al.* 2010 Pitchfork regulates primary cilia disassembly and left-right asymmetry. *Developmental Cell* **19** 66–77.

Kitagawa K, Kotake Y & Kitagawa M 2009 Ubiquitin-mediated control of oncogene and tumor suppressor gene products. *Cancer Science* **100** 1374–1381.

Klein A, Flügel D & Kietzmann T 2008 Transcriptional Regulation of Serine/Threonine Kinase-15 (STK15) Expression by Hypoxia and HIF-1. *Molecular Biology of the Cell* **19** 3667–3675.

Klesse LJ & Parada LF 1998 p21 ras and phosphatidylinositol-3 kinase are required for survival of wild-type and NF1 mutant sensory neurons. *The Journal of Neuroscience : The Official Journal of the Society for Neuroscience* **18** 10420–10428.

Knauth K, Cartwright E, Freund S, Bycroft M & Buchberger A 2009 VHL mutations linked to type 2C

von Hippel-Lindau disease cause extensive structural perturbations in pVHL. *The Journal of Biological Chemistry* **284** 10514–10522.

Kobayashi T, Tsang WY, Li J, Lane W & Dynlacht BD 2011 Centriolar Kinesin Kif24 Interacts with CP110 to Remodel Microtubules and Regulate Ciliogenesis. *Cell* **145** 914–925.

Kobayashi H, Kawauchi D, Hashimoto Y, Ogata T & Murakami F 2013 The control of precerebellar neuron migration by RNA-binding protein Csde1. *Neuroscience* **253** 292–303.

Kobayashi T, Nakazono K, Tokuda M, Mashima Y, Dynlacht BD & Itoh H 2017 HDAC2 promotes loss of primary cilia in pancreatic ductal adenocarcinoma. *EMBO Reports* **18** 334–343.

Kocak S, Aydintug S & Canakci N 2002 Alpha blockade in preoperative preparation of patients with pheochromocytomas. *International Surgery* **87** 191–194.

Koivunen P, Hirsilä M, Remes AM, Hassinen IE, Kivirikko KI & Myllyharju J 2007 Inhibition of Hypoxia-inducible Factor (HIF) Hydroxylases by Citric Acid Cycle Intermediates. *Journal of Biological Chemistry* **282** 4524–4532.

Kong D, Park EJ, Stephen AG, Calvani M, Cardellina JH, Monks A, Fisher RJ, Shoemaker RH & Melillo G 2005 Echinomycin, a Small-Molecule Inhibitor of Hypoxia-Inducible Factor-1 DNA-Binding Activity. *Cancer Research* **65** 9047–9055.

Kong JH, Yang L, Dessaud E, Chuang K, Moore DM, Rohatgi R, Briscoe J & Novitch BG 2015 Notch activity modulates the responsiveness of neural progenitors to sonic hedgehog signaling. *Developmental Cell* **33** 373–387.

Kong G, Grozinsky-Glasberg S, Hofman MS, Callahan J, Meirovitz A, Maimon O, Pattison DA, Gross DJ & Hicks RJ 2017 Efficacy of Peptide Receptor Radionuclide Therapy for Functional Metastatic Paraganglioma and Pheochromocytoma. *The Journal of Clinical Endocrinology & Metabolism* **102** 3278–3287.

Kong MJ, Bak SH, Han K-H, Kim JI, Park J-W & Park KM 2019 Fragmentation of kidney epithelial cell primary cilia occurs by cisplatin and these cilia fragments are excreted into the urine. *Redox Biology* **20** 38–45.

Kontak AC, Wang Z, Arbique D, Adams-Huet B, Auchus RJ, Nesbitt SD, Victor RG & Vongpatanasin W 2010 Reversible sympathetic overactivity in hypertensive patients with primary aldosteronism. *The Journal of Clinical Endocrinology and Metabolism* **95** 4756–4761.

Koriyama N, Kakei M, Yaekura K, Okui H, Yamashita T, Nishimura H, Matsushita S & Tei C 2000 Control of Catecholamine Release and Blood Pressure with Octreotide in a Patient with Pheochromocytoma: A Case Report with in vitro Studies. *Hormone Research in Paediatrics* **53** 46–50.

Korpershoek E, Favier J, Gaal J, Burnichon N, van Gessel B, Oudijk L, Badoual C, Gadessaud N, Venisse A, Bayley J-P *et al.* 2011 SDHA Immunohistochemistry Detects Germline *SDHA* Gene Mutations in Apparently Sporadic Paragangliomas and Pheochromocytomas. *The Journal of Clinical Endocrinology & Metabolism* **96** E1472–E1476.

Korpershoek E, Petri B-J, Post E, van Eijck CHJ, Oldenburg RA, Belt EJT, de Herder WW, de Krijger RR & Dinjens WNM 2014 Adrenal medullary hyperplasia is a precursor lesion for pheochromocytoma in MEN2 syndrome. *Neoplasia (New York, N.Y.)* **16** 868–873.

Korpershoek E, Koffy D, Eussen BH, Oudijk L, Papathomas TG, van Nederveen FH, Belt EJT, Franssen

GJH, Restuccia DFJ, Krol NMG *et al.* 2016 Complex MAX Rearrangement in a Family With Malignant Pheochromocytoma, Renal Oncocytoma, and Erythrocytosis. *The Journal of Clinical Endocrinology & Metabolism* **101** 453–460.

Kovacs JJ, Murphy PJM, Gaillard S, Zhao X, Wu J-T, Nicchitta C V., Yoshida M, Toft DO, Pratt WB & Yao T-P 2005 HDAC6 Regulates Hsp90 Acetylation and Chaperone-Dependent Activation of Glucocorticoid Receptor. *Molecular Cell* **18** 601–607.

Kowal TJ & Falk MM 2015 Primary cilia found on HeLa and other cancer cells. *Cell Biology International* **39** 1341–1347.

Kozminski KG, Johnson KA, Forscher P & Rosenbaum JL 1993 A motility in the eukaryotic flagellum unrelated to flagellar beating. *Proceedings of the National Academy of Sciences of the United States of America* **90** 5519–5523.

Krsek M, Rosická M, Nedvídková J, Kvasnicková H, Hána V, Marek J, Haluzík M, Lai EW & Pacák K 2006 Increased lipolysis of subcutaneous abdominal adipose tissue and altered noradrenergic activity in patients with Cushing's syndrome: an in-vivo microdialysis study. *Physiological Research / Academia Scientiarum Bohemoslovaca* **55** 421–428.

Kubota A, Yamada Y, Kagimoto S, Shimatsu A, Imamura M, Tsuda K, Imura H, Seino S & Seino Y 1994 Identification of somatostatin receptor subtypes and an implication for the efficacy of somatostatin analogue SMS 201-995 in treatment of human endocrine tumors. *The Journal of Clinical Investigation* **93** 1321–1325.

Kuhns S, Schmidt KN, Reymann J, Gilbert DF, Neuner A, Hub B, Carvalho R, Wiedemann P, Zentgraf H, Erfle H *et al.* 2013 The microtubule affinity regulating kinase MARK4 promotes axoneme extension during early ciliogenesis. *The Journal of Cell Biology* **200** 505–522.

Kunst HPM, Rutten MH, de Monnink J-P, Hoefsloot LH, Timmers HJLM, Marres HAM, Jansen JC, Kremer H, Bayley J-P & Cremers CWRJ 2011 SDHAF2 (PGL2-SDH5) and Hereditary Head and Neck Paraganglioma. *Clinical Cancer Research* **17** 247–254.

Kuok C-H, Yen C-R, Huang C-S, Ko Y-P & Tsai P-S 2011 Cardiovascular collapse after labetalol for hypertensive crisis in an undiagnosed pheochromocytoma during cesarean section. *Acta Anaesthesiologica Taiwanica* **49** 69–71.

Lack EE 1977 Carotid body hypertrophy in patients with cystic fibrosis and cyanotic congenital heart disease. *Human Pathology* **8** 39–51.

Lack EE 1978 Hyperplasia of vagal and carotid body paraganglia in patients with chronic hypoxemia. *The American Journal of Pathology* **91** 497–516.

Ladroue C, Carcenac R, Leporrier M, Gad S, Le Hello C, Galateau-Salle F, Feunteun J, Pouysségur J, Richard S & Gardie B 2008 PHD2 mutation and congenital erythrocytosis with paraganglioma. *The New England Journal of Medicine* **359** 2685–2692.

Laidler P & Kay JM 1975 A quantitative morphological study of the carotid bodies of rats living at a simulated altitude of 4300 metres. *The Journal of Pathology* **117** 183–191.

Laidler P & Kay JM 1978 Ultrastructure of carotid body in rats living at a simulated altitude of 4300 metres. *The Journal of Pathology* **124** 27–33.

Lancaster MA, Schroth J & Gleeson JG 2011 Subcellular spatial regulation of canonical Wnt signalling at the primary cilium. *Nature Cell Biology* **13** 700–707.

Landschulz WH, Johnson PF & McKnight SL 1988 The leucine zipper: a hypothetical structure common to a new class of DNA binding proteins. *Science (New York, N.Y.)* **240** 1759–1764.

Latif F, Tory K, Gnarra J, Yao M, Duh FM, Orcutt ML, Stackhouse T, Kuzmin I, Modi W & Geil L 1993 Identification of the von Hippel-Lindau disease tumor suppressor gene. *Science (New York, N.Y.)* **260** 1317–1320.

Lau JHG, Sze WCC, Reznek RH, Matson M, Sahdev A, Carpenter R, Berney DM, Akker SA, Chew SL, Grossman AB *et al.* 2012 A prospective evaluation of postural stimulation testing, computed tomography and adrenal vein sampling in the differential diagnosis of primary aldosteronism. *Clinical Endocrinology* **76** 182–188.

Lavagnino M, Oslapas AN, Gardner KL & Arnoczky SP 2016 Hypoxia inhibits primary cilia formation and reduces cell-mediated contraction in stress-deprived rat tail tendon fascicles. *Muscles, Ligaments and Tendons Journal* **6** 193–197.

Lebuffe G, Dosseh ED, Tek G, Tytgat H, Moreno S, Tavernier B, Vallet B & Proye CAG 2005 The effect of calcium channel blockers on outcome following the surgical treatment of phaeochromocytomas and paragangliomas. *Anaesthesia* **60** 439–444.

Lee S, Nakamura E, Yang H, Wei W, Linggi MS, Sajan MP, Farese R V, Freeman RS, Carter BD, Kaelin WG *et al.* 2005 Neuronal apoptosis linked to EglN3 prolyl hydroxylase and familial pheochromocytoma genes: developmental culling and cancer. *Cancer Cell* **8** 155–167.

Lee KH, Johmura Y, Yu L-R, Park J-E, Gao Y, Bang JK, Zhou M, Veenstra TD, Yeon Kim B & Lee KS 2012a Identification of a novel Wnt5a-CK1ε-Dvl2-Plk1-mediated primary cilia disassembly pathway. *The EMBO Journal* **31** 3104–3117.

Lee JE, Silhavy JL, Zaki MS, Schroth J, Bielas SL, Marsh SE, Olvera J, Brancati F, Iannicelli M, Ikegami K *et al.* 2012b CEP41 is mutated in Joubert syndrome and is required for tubulin glutamylation at the cilium. *Nature Genetics* **44** 193–199.

Lee J, Yi S, Kang YE, Chang JY, Kim JT, Sul HJ, Kim JO, Kim JM, Kim J, Porcelli AM *et al.* 2016 Defective ciliogenesis in thyroid hürthle cell tumors is associated with increased autophagy. *Oncotarget* **7** 79117–79130.

Lee J, Yi S, Won M, Song YS, Yi H-S, Park YJ, Park KC, Kim JT, Chang JY, Lee MJ *et al.* 2018 Loss-of-function of IFT88 determines metabolic phenotypes in thyroid cancer. *Oncogene* **37** 4455–4474.

Légaré S, Chabot C & Basik M 2017 SPEN, a new player in primary cilia formation and cell migration in breast cancer. *Breast Cancer Research* **19** 104.

Lehmann M & Keul J 1986 Urinary excretion of free noradrenaline and adrenaline related to age, sex and hypertension in 265 individuals. *European Journal of Applied Physiology and Occupational Physiology* **55** 14–18.

De Lellis RA, Lloyd R V, Heitz P & Eng C 2004 *World Health Organization Classification of Tumours: Pathology and Genetics of Tumours of Endocrine Organs*. Lyon, France: IARC Press.

Lenders JW, Keiser HR, Goldstein DS, Willemsen JJ, Friberg P, Jacobs MC, Kloppenborg PW, Thien T & Eisenhofer G 1995 Plasma metanephrines in the diagnosis of pheochromocytoma. *Annals of Internal Medicine* **123** 101–109.

Lenders JWM, Pacak K, Walther MM, Linehan WM, Mannelli M, Friberg P, Keiser HR, Goldstein DS &

Eisenhofer G 2002 Biochemical diagnosis of pheochromocytoma: which test is best? *JAMA* **287** 1427–1434.

Lenders JWM, Eisenhofer G, Mannelli M & Pacak K 2005 Phaeochromocytoma. *Lancet (London, England)* **366** 665–675.

Lenders JWM, Willemsen JJ, Eisenhofer G, Ross HA, Pacak K, Timmers HJLM & Sweep CGJF 2007 Is supine rest necessary before blood sampling for plasma metanephrines? *Clinical Chemistry* **53** 352–354.

Lenders JWM, Duh Q-Y, Eisenhofer G, Gimenez-Roqueplo A-P, Grebe SKG, Murad MH, Naruse M, Pacak K, Young WF & Endocrine Society 2014 Pheochromocytoma and Paraganglioma: An Endocrine Society Clinical Practice Guideline. *The Journal of Clinical Endocrinology & Metabolism* **99** 1915–1942.

Lesche S, Lehmann D, Nagel F, Schmid HA & Schulz S 2009 Differential Effects of Octreotide and Pasireotide on Somatostatin Receptor Internalization and Trafficking *in Vitro*. *The Journal of Clinical Endocrinology & Metabolism* **94** 654–661.

Letouzé E, Martinelli C, Loriot C, Burnichon N, Abermil N, Ottolenghi C, Janin M, Menara M, Nguyen AT, Benit P *et al.* 2013 SDH mutations establish a hypermethylator phenotype in paraganglioma. *Cancer Cell* **23** 739–752.

Li ML, Fitzgerald PA, Price DC & Norton JA 2001 Iatrogenic pheochromocytomatosis: a previously unreported result of laparoscopic adrenalectomy. *Surgery* **130** 1072–1077.

Li A, Saito M, Chuang J-Z, Tseng Y-Y, Dedesma C, Tomizawa K, Kaitsuka T & Sung C-H 2011 Ciliary transition zone activation of phosphorylated Tctex-1 controls ciliary resorption, S-phase entry and fate of neural progenitors. *Nature Cell Biology* **13** 402–411.

Li L, Grausam KB, Wang J, Lun MP, Ohli J, Lidov HGW, Calicchio ML, Zeng E, Salisbury JL, Wechsler-Reya RJ *et al.* 2016 Sonic Hedgehog promotes proliferation of Notch-dependent monociliated choroid plexus tumour cells. *Nature Cell Biology* **18** 418–430.

Liberzon A, Birger C, Thorvaldsdóttir H, Ghandi M, Mesirov JP & Tamayo P 2015 The Molecular Signatures Database Hallmark Gene Set Collection. *Cell Systems* **1** 417–425.

Liem KF, He M, Ocbina PJR & Anderson K V. 2009 Mouse Kif7/Costal2 is a cilia-associated protein that regulates Sonic hedgehog signaling. *Proceedings of the National Academy of Sciences* **106** 13377–13382.

Lin F, Hiesberger T, Cordes K, Sinclair AM, Goldstein LSB, Somlo S & Igarashi P 2003 Kidney-specific inactivation of the KIF3A subunit of kinesin-II inhibits renal ciliogenesis and produces polycystic kidney disease. *Proceedings of the National Academy of Sciences* **100** 5286–5291.

Lindau A 1927 Zur Frage der Angiomatosis Retinae und Ihrer Hirncomplikation. *ActaOphthal* **4** 193–226.

Liu Q, Kaneko S, Yang L, Feldman RI, Nicosia S V., Chen J & Cheng JQ 2004 Aurora-A Abrogation of p53 DNA Binding and Transactivation Activity by Phosphorylation of Serine 215. *Journal of Biological Chemistry* **279** 52175–52182.

Liu A, Wang B & Niswander LA 2005 Mouse intraflagellar transport proteins regulate both the activator and repressor functions of Gli transcription factors. *Development* **132** 3103–3111.

Liu YP, Tsai I-C, Morleo M, Oh EC, Leitch CC, Massa F, Lee B-H, Parker DS, Finley D, Zaghloul NA *et al.* 2014 Ciliopathy proteins regulate paracrine signaling by modulating proteasomal degradation of mediators. *Journal of Clinical Investigation* **124** 2059–2070.

Lo CY, Lam KY, Wat MS & Lam KS 2000 Adrenal pheochromocytoma remains a frequently overlooked diagnosis. *American Journal of Surgery* **179** 212–215.

Loh KC, Fitzgerald PA, Matthay KK, Yeo PP & Price DC 1997 The treatment of malignant pheochromocytoma with iodine-131 metaiodobenzylguanidine (131I-MIBG): a comprehensive review of 116 reported patients. *Journal of Endocrinological Investigation* **20** 648–658.

Lolkema MP, Mans DA, Snijckers CM, van Noort M, van Beest M, Voest EE & Giles RH 2007 The von Hippel-Lindau tumour suppressor interacts with microtubules through kinesin-2. *FEBS Letters* **581** 4571–4576.

Lolkema MP, Mans DA, Ulfman LH, Volpi S, Voest EE & Giles RH 2008 Allele-specific regulation of primary cilia function by the von Hippel-Lindau tumor suppressor. *European Journal of Human Genetics : EJHG* **16** 73–78.

López-Jiménez E, de Campos JM, Kusak EM, Landa I, Leskelä S, Montero-Conde C, Leandro-García LJ, Vallejo LA, Madrigal B, Rodríguez-Antona C *et al.* 2008 SDHC mutation in an elderly patient without familial antecedents. *Clinical Endocrinology* **69** 906–910.

Lorenzo FR, Yang C, Ng Tang Fui M, Vankayalapati H, Zhuang Z, Huynh T, Grossmann M, Pacak K & Prchal JT 2013 A novel EPAS1/HIF2A germline mutation in a congenital polycythemia with paraganglioma. *Journal of Molecular Medicine* **91** 507–512.

Lorenzo Pisarello M, Masyuk T V., Gradilone SA, Masyuk AI, Ding JF, Lee P-Y & LaRusso NF 2018 Combination of a Histone Deacetylase 6 Inhibitor and a Somatostatin Receptor Agonist Synergistically Reduces Hepatorenal Cystogenesis in an Animal Model of Polycystic Liver Disease. *The American Journal of Pathology* **188** 981–994.

Loskutov Y V., Griffin CL, Marinak KM, Bobko A, Margaryan N V., Geldenhuys WJ, Sarkaria JN & Pugacheva EN 2018 LPA signaling is regulated through the primary cilium: a novel target in glioblastoma. *Oncogene* **37** 1457–1471.

Love MI, Huber W & Anders S 2014 Moderated estimation of fold change and dispersion for RNA-seq data with DESeq2. *Genome Biology* **15** 550.

Lovejoy CA, Li W, Reisenweber S, Thongthip S, Bruno J, de Lange T, De S, Petrini JHJ, Sung PA, Jasin M *et al.* 2012 Loss of ATRX, Genome Instability, and an Altered DNA Damage Response Are Hallmarks of the Alternative Lengthening of Telomeres Pathway. *PLoS Genetics* **8** e1002772.

Luchetti A, Walsh D, Rodger F, Clark G, Martin T, Irving R, Sanna M, Yao M, Robledo M, Neumann HPH *et al.* 2015 Profiling of Somatic Mutations in Phaeochromocytoma and Paraganglioma by Targeted Next Generation Sequencing Analysis. *International Journal of Endocrinology* **2015** 1–8.

Lumachi F, Tregnaghi A, Zucchetta P, Cristina Marzola M, Cecchin D, Grassetto G & Bui F 2006 Sensitivity and positive predictive value of CT, MRI and 123I-MIBG scintigraphy in localizing pheochromocytomas: a prospective study. *Nuclear Medicine Communications* **27** 583–587.

Luo M, Cao M, Kan Y, Li G, Snell W & Pan J 2011 The Phosphorylation State of an Aurora-Like Kinase Marks the Length of Growing Flagella in Chlamydomonas. *Current Biology* **21** 586–591.

Lutz MS & Burk RD 2006 Primary cilium formation requires von hippel-lindau gene function in renal-derived cells. *Cancer Research* **66** 6903–6907.

Ma W, Tessarollo L, Hong S-B, Baba M, Southon E, Back TC, Spence S, Lobe CG, Sharma N, Maher GW *et al.* 2003 Hepatic vascular tumors, angiectasis in multiple organs, and impaired spermatogenesis in mice with conditional inactivation of the VHL gene. *Cancer Research* **63** 5320–5328.

MacKenzie ED, Selak MA, Tennant DA, Payne LJ, Crosby S, Frederiksen CM, Watson DG & Gottlieb E 2007 Cell-permeating alpha-ketoglutarate derivatives alleviate pseudohypoxia in succinate dehydrogenase-deficient cells. *Molecular and Cellular Biology* **27** 3282–3289.

Maher ER, Neumann HP & Richard S 2011 von Hippel-Lindau disease: a clinical and scientific review. *Eur J Hum Genet* **19** 617–623.

Mahjoub MR, Qasim Rasi M & Quarmby LM 2004 A NIMA-related Kinase, Fa2p, Localizes to a Novel Site in the Proximal Cilia of *Chlamydomonas* and Mouse Kidney Cells. *Molecular Biology of the Cell* **15** 5172–5186.

Mahoney NM, Goshima G, Douglass AD & Vale RD 2006 Making Microtubules and Mitotic Spindles in Cells without Functional Centrosomes. *Current Biology* **16** 564–569.

Mannelli M, Lanzillotti R, Pupilli C, Ianni L, Conti A & Serio M 1994 Adrenal medulla secretion in Cushing's syndrome. *The Journal of Clinical Endocrinology and Metabolism* **78** 1331–1335.

Manning DK, Sergeev M, van Heesbeen RG, Wong MD, Oh J-H, Liu Y, Henkelman RM, Drummond I, Shah J V. & Beier DR 2013 Loss of the Ciliary Kinase *Nek8* Causes Left-Right Asymmetry Defects. *Journal of the American Society of Nephrology* **24** 100–112.

Mans DA, Voest EE & Giles RH 2008 All along the watchtower: is the cilium a tumor suppressor organelle? *Biochimica et Biophysica Acta* **1786** 114–125.

Mansini AP, Lorenzo Pisarello MJ, Thelen KM, Cruz-Reyes M, Peixoto E, Jin S, Howard BN, Trussoni CE, Gajdos GB, LaRusso NF *et al.* 2018 MicroRNA (miR)-433 and miR-22 dysregulations induce histone-deacetylase-6 overexpression and ciliary loss in cholangiocarcinoma. *Hepatology* **68** 561–573.

Mansini AP, Peixoto E, Jin S, Richard S & Gradilone SA 2019 The chemosensory function of primary cilia regulates cholangiocyte migration, invasion and tumor growth. *Hepatology* **69** 1582–1598.

Mansmann G, Lau J, Balk E, Rothberg M, Miyachi Y & Bornstein SR 2004 The clinically inapparent adrenal mass: update in diagnosis and management. *Endocrine Reviews* **25** 309–340.

Manu P & Runge LA 1984 Biochemical screening for pheochromocytoma. Superiority of urinary metanephrines measurements. *American Journal of Epidemiology* **120** 788–790.

Marchand F 1883 Ueber die accessorischen Nebennieren im Ligamentum latum. *Virchows Archiv Für Pathologische Anatomie Und Physiologie Und Fur Klinische Medizin* 11–19.

Marley A & von Zastrow M 2012 A simple cell-based assay reveals that diverse neuropsychiatric risk genes converge on primary cilia. *PloS One* **7** e46647.

Marley A, Choy RW-Y & von Zastrow M 2013 GPR88 reveals a discrete function of primary cilia as selective insulators of GPCR cross-talk. *PloS One* **8** e70857.

Marshall WF, Qin H, Brenni MR & Rosenbaum JL 2005 Flagellar Length Control System: Testing a

Simple Model Based on Intraflagellar Transport and Turnover. *Molecular Biology of the Cell* **16** 270–278.

Martin GA, Viskochil D, Bollag G, McCabe PC, Crosier WJ, Haubruck H, Conroy L, Clark R, O'Connell P & Cawthon RM 1990 The GAP-related domain of the neurofibromatosis type 1 gene product interacts with ras p21. *Cell* **63** 843–849.

Martiniova L, Lai EW, Elkahloun AG, Abu-Asab M, Wickremasinghe A, Solis DC, Perera SM, Huynh T-T, Lubensky IA, Tischler AS *et al.* 2009 Characterization of an animal model of aggressive metastatic pheochromocytoma linked to a specific gene signature. *Clinical & Experimental Metastasis* **26** 239–250.

Maskey D, Marlin MC, Kim S, Kim S, Ong E-C, Li G & Tsiokas L 2015 Cell cycle-dependent ubiquitylation and destruction of NDE1 by CDK5-FBW7 regulates ciliary length. *The EMBO Journal* **34** 2424–2440.

Maxwell PH, Wiesener MS, Chang G-W, Clifford SC, Vaux EC, Cockman ME, Wykoff CC, Pugh CW, Maher ER & Ratcliffe PJ 1999 The tumour suppressor protein VHL targets hypoxia-inducible factors for oxygen-dependent proteolysis. *Nature* **399** 271–275.

May-Simera HL, Petralia RS, Montcouquiol M, Wang Y-X, Szarama KB, Liu Y, Lin W, Deans MR, Pazour GJ & Kelley MW 2015 Ciliary proteins Bbs8 and Ift20 promote planar cell polarity in the cochlea. *Development* **142** 555–566.

Mazzeo RS, Wolfel EE, Butterfield GE & Reeves JT 1994 Sympathetic response during 21 days at high altitude (4,300 m) as determined by urinary and arterial catecholamines. *Metabolism: Clinical and Experimental* **43** 1226–1232.

McDermott KM, Liu BY, Tlsty TD & Pazour GJ 2010 Primary cilia regulate branching morphogenesis during mammary gland development. *Current Biology : CB* **20** 731–737.

McGlashan SR, Cluett EC, Jensen CG & Poole CA 2008 Primary cilia in osteoarthritic chondrocytes: From chondrons to clusters. *Developmental Dynamics* **237** 2013–2020.

McNeil AR, Blok BH, Koelmeyer TD, Burke MP & Hilton JM 2000 Phaeochromocytomas discovered during coronial autopsies in Sydney, Melbourne and Auckland. *Australian and New Zealand Journal of Medicine* **30** 648–652.

McNeill A, Rattenberry E, Barber R, Killick P, MacDonald F & Maher ER 2009 Genotype-phenotype correlations in VHL exon deletions. *American Journal of Medical Genetics Part A* **149A** 2147–2151.

McWhinney SR, Pasini B & Stratakis CA 2007 Familial gastrointestinal stromal tumors and germ-line mutations. *The New England Journal of Medicine* **357** 1054–1056.

Melmon KL & Rosen SW 1964 Lindau's disease. Review of the literature and study of a liarge kindred. *The American Journal of Medicine* **36** 595–617.

Menzl I, Lebeau L, Pandey R, Hassounah NB, Li FW, Nagle R, Weihs K & McDermott KM 2014 Loss of primary cilia occurs early in breast cancer development. *Cilia* **3** 7.

Mihailovich M, Militti C, Gabaldón T & Gebauer F 2010 Eukaryotic cold shock domain proteins: highly versatile regulators of gene expression. *BioEssays* **32** 109–118.

Mikule K, Delaval B, Kaldis P, Jurcyzk A, Hergert P & Doxsey S 2007 Loss of centrosome integrity

induces p38-p53-p21-dependent G1-S arrest. *Nature Cell Biology* **9** 160–170.

Miller JL, Immelman EJ, Roman TE & Mervis B 1983 Phaeochromocytoma of the urinary bladder localized by selective venous sampling and computed tomography. *Postgraduate Medical Journal* **59** 533–535.

Minn AJ, Gupta GP, Siegel PM, Bos PD, Shu W, Giri DD, Viale A, Olshen AB, Gerald WL & Massagué J 2005 Genes that mediate breast cancer metastasis to lung. *Nature* **436** 518–524.

Miyajima E, Yamada Y, Yoshida Y, Matsukawa T, Shionoiri H, Tochikubo O & Ishii M 1991 Muscle sympathetic nerve activity in renovascular hypertension and primary aldosteronism. *Hypertension* **17** 1057–1062.

Miyamoto T, Hosoba K, Ochiai H, Royba E, Izumi H, Sakuma T, Yamamoto T, Dynlacht BD & Matsuura S 2015 The Microtubule-Depolymerizing Activity of a Mitotic Kinesin Protein KIF2A Drives Primary Cilia Disassembly Coupled with Cell Proliferation. *Cell Reports* **10** 664–673.

Miyoshi K, Kasahara K, Miyazaki I & Asanuma M 2009 Lithium treatment elongates primary cilia in the mouse brain and in cultured cells. *Biochemical and Biophysical Research Communications* **388** 757–762.

Miyoshi K, Kasahara K, Murakami S, Takeshima M, Kumamoto N, Sato A, Miyazaki I, Matsuzaki S, Sasaoka T, Katayama T *et al.* 2014 Lack of dopaminergic inputs elongates the primary cilia of striatal neurons. *PloS One* **9** e97918.

Montani M, Heinimann K, von Teichman A, Rudolph T, Perren A & Moch H 2010 VHL-gene deletion in single renal tubular epithelial cells and renal tubular cysts: further evidence for a cyst-dependent progression pathway of clear cell renal carcinoma in von Hippel-Lindau disease. *The American Journal of Surgical Pathology* **34** 806–815.

Moore LE, Nickerson ML, Brennan P, Toro JR, Jaeger E, Rinsky J, Han SS, Zaridze D, Matveev V, Janout V *et al.* 2011 Von Hippel-Lindau (VHL) inactivation in sporadic clear cell renal cancer: associations with germline VHL polymorphisms and etiologic risk factors. *PLoS Genetics* **7** e1002312.

Moreno-Manzano V, Rodríguez-Jiménez FJ, Aceña-Bonilla JL, Fustero-Lardíes S, Erceg S, Dopazo J, Montaner D, Stojkovic M & Sánchez-Puelles JM 2010 FM19G11, a New Hypoxia-inducible Factor (HIF) Modulator, Affects Stem Cell Differentiation Status. *Journal of Biological Chemistry* **285** 1333–1342.

Moser JJ, Fritzler MJ & Rattner JB 2009 Primary ciliogenesis defects are associated with human astrocytoma/glioblastoma cells. *BMC Cancer* **9** 448.

Moser SC, Bensaddek D, Ortmann B, Maure J-F, Mudie S, Blow JJ, Lamond AI, Swedlow JR & Rocha S 2013 PHD1 links cell-cycle progression to oxygen sensing through hydroxylation of the centrosomal protein Cep192. *Developmental Cell* **26** 381–392.

Moss S, Greenbaum R & Sever PS 1980 Preoperative localization of a phaeochromocytoma using plasma noradrenaline concentrations in multiple-site samples. *Journal of the Royal Society of Medicine* **73** 139–141.

Mucha L, Leidig-Bruckner G, Frank-Raue K, Bruckner T, Kroiss M, Raue F & German study group for rare thyroid cancer 2017 Phaeochromocytoma in multiple endocrine neoplasia type 2: RET codon-specific penetrance and changes in management during the last four decades. *Clinical Endocrinology* **87** 320–326.

Muller M, Ferlicot S, Guillaud-Bataille M, Le Teuff G, Genestie C, Deveaux S, Slama A, Poulalhon N, Escudier B, Albiges L *et al.* 2017 Reassessing the clinical spectrum associated with hereditary leiomyomatosis and renal cell carcinoma syndrome in French *FH* mutation carriers. *Clinical Genetics* **92** 606–615.

Müller M, Padberg W, Schindler E, Sticher J, Osmer C, Friemann S & Hempelmann G 1998 Renocortical tissue oxygen pressure measurements in patients undergoing living donor kidney transplantation. *Anesthesia and Analgesia* **87** 474–476.

Mulligan LM, Kwok JB, Healey CS, Elsdon MJ, Eng C, Gardner E, Love DR, Mole SE, Moore JK, Papi L *et al.* 1993 Germ-line mutations of the RET proto-oncogene in multiple endocrine neoplasia type 2A. *Nature* **363** 458–460.

Mullins F, O'Shea P, FitzGerald R & Tormey W 2012 Enzyme-linked immunoassay for plasma-free metanephrines in the biochemical diagnosis of phaeochromocytoma in adults is not ideal. *Clinical Chemistry and Laboratory Medicine* **50** 105–110.

Murata Y, Tsuji M & Tani M 1984 Ultrastructure of multiple glomus tumor. *Journal of Cutaneous Pathology* **11** 53–58.

Murre C, McCaw PS & Baltimore D 1989 A new DNA binding and dimerization motif in immunoglobulin enhancer binding, daughterless, MyoD, and myc proteins. *Cell* **56** 777–783.

Nachury M V., Loktev A V., Zhang Q, Westlake CJ, Peränen J, Merdes A, Slusarski DC, Scheller RH, Bazan JF, Sheffield VC *et al.* 2007 A Core Complex of BBS Proteins Cooperates with the GTPase Rab8 to Promote Ciliary Membrane Biogenesis. *Cell* **129** 1201–1213.

Nagatsu T, Levitt M & Udenfriend S 1964 Tyrosine hydroxylase. The initial step in norepinephrine biosynthesis. *The Journal of Biological Chemistry* **239** 2910–2917.

Najafi M, Maza NA & Calvert PD 2012 Steric volume exclusion sets soluble protein concentrations in photoreceptor sensory cilia. *Proceedings of the National Academy of Sciences* **109** 203–208.

Nakajo M, Shapiro B, Copp J, Kalff V, Gross MD, Sisson JC & Beierwaltes WH 1983 The normal and abnormal distribution of the adrenomedullary imaging agent m-[I-131]iodobenzylguanidine (I-131 MIBG) in man: evaluation by scintigraphy. *Journal of Nuclear Medicine : Official Publication, Society of Nuclear Medicine* **24** 672–682.

Nangaku M, Sato-Yoshitake R, Okada Y, Noda Y, Takemura R, Yamazaki H & Hirokawa N 1994 KIF1B, a novel microtubule plus end-directed monomeric motor protein for transport of mitochondria. *Cell* **79** 1209–1220.

Nastos K, Cheung VTF, Toumpanakis C, Navalkissoor S, Quigley A-M, Caplin M & Khoo B 2017 Peptide Receptor Radionuclide Treatment and (131)I-MIBG in the management of patients with metastatic/progressive phaeochromocytomas and paragangliomas. *Journal of Surgical Oncology* **115** 425–434.

Natarajan M, Stewart JE, Golemis EA, Pugacheva EN, Alexandropoulos K, Cox BD, Wang W, Grammer JR & Gladson CL 2006 HEF1 is a necessary and specific downstream effector of FAK that promotes the migration of glioblastoma cells. *Oncogene* **25** 1721–1732.

National Toxicology Progam 1993 NTP Toxicology and Carcinogenesis Studies of Talc (CAS No. 14807-96-6)(Non-Asbestiform) in F344/N Rats and B6C3F1 Mice (Inhalation Studies). *National Toxicology Program Technical Report Series* **421** 1–287.

National Toxicology Progam 1996a NTP Toxicology and Carcinogenesis Studies of Nickel Subsulfide (CAS No. 12035-72-2) in F344 Rats and B6C3F1 Mice (Inhalation Studies). *National Toxicology Program Technical Report Series* **453** 1–365.

National Toxicology Progam 1996b NTP Toxicology and Carcinogenesis Studies of Nickel Oxide (CAS No. 1313-99-1) in F344 Rats and B6C3F1 Mice (Inhalation Studies). *National Toxicology Program Technical Report Series* **451** 1–381.

National Toxicology Progam 1998 NTP Toxicology and Carcinogenesis Studies of Cobalt Sulfate Heptahydrate (CAS No. 10026-24-1) in F344/N Rats and B6C3F1 Mice (Inhalation Studies). *National Toxicology Program Technical Report Series* **471** 1–268.

Nauli SM, Alenghat FJ, Luo Y, Williams E, Vassilev P, Li X, Elia AEH, Lu W, Brown EM, Quinn SJ *et al.* 2003 Polycystins 1 and 2 mediate mechanosensation in the primary cilium of kidney cells. *Nature Genetics* **33** 129–137.

Nauli SM, Kawanabe Y, Kaminski JJ, Pearce WJ, Ingber DE & Zhou J 2008 Endothelial Cilia Are Fluid Shear Sensors That Regulate Calcium Signaling and Nitric Oxide Production Through Polycystin-1. *Circulation* **117** 1161–1171.

van Nederveen FH, Gaal J, Favier J, Korpershoek E, Oldenburg RA, de Bruyn EM, Sleddens HF, Derkx P, Rivière J, Dannenberg H *et al.* 2009 An immunohistochemical procedure to detect patients with paraganglioma and phaeochromocytoma with germline SDHB, SDHC, or SDHD gene mutations: a retrospective and prospective analysis. *The Lancet Oncology* **10** 764–771.

Neumann HP & Wiestler OD 1991 Clustering of features of von Hippel-Lindau syndrome: evidence for a complex genetic locus. *Lancet (London, England)* **337** 1052–1054.

Neumann HP, Pawlu C, Peczkowska M, Bausch B, McWhinney SR, Muresan M, Buchta M, Franke G, Klisch J, Bley T *et al.* 2004 Distinct clinical features of paraganglioma syndromes associated with SDHB and SDHD gene mutations. *JAMA* **292** 943–951.

Neumann HPH, Vortmeyer A, Schmidt D, Werner M, Erlic Z, Cascon A, Bausch B, Januszewicz A & Eng C 2007 Evidence of MEN-2 in the Original Description of Classic Pheochromocytoma. *New England Journal of Medicine* **357** 1311–1315.

Neumann HPH, Sullivan M, Winter A, Malinoc A, Hoffmann MM, Boedeker CC, Bertz H, Walz MK, Moeller LC, Schmid KW *et al.* 2011 Germline Mutations of the *TMEM127* Gene in Patients with Paraganglioma of Head and Neck and Extraadrenal Abdominal Sites. *The Journal of Clinical Endocrinology & Metabolism* **96** E1279–E1282.

Newbould EC, Ross GA, Dacie JE, Bouloux PM, Besser GM & Grossman A 1991 The use of venous catheterization in the diagnosis and localization of bilateral phaeochromocytomas. *Clinical Endocrinology* **35** 55–59.

Ng SSM, Cheung Y-T, An X-M, Chen YC, Li M, Hoi-Yee Li G, Cheung W, Sze J, Lai L, Peng Y *et al.* 2007 Cell Cycle-Related Kinase: A Novel Candidate Oncogene in Human Glioblastoma. *JNCI Journal of the National Cancer Institute* **99** 936–948.

Ni Y, Zbuk KM, Sadler T, Patocs A, Lobo G, Edelman E, Platzer P, Orloff MS, Waite KA & Eng C 2008 Germline mutations and variants in the succinate dehydrogenase genes in Cowden and Cowden-like syndromes. *American Journal of Human Genetics* **83** 261–268.

Nielsen SK, Møllgård K, Clement CA, Veland IR, Awan A, Yoder BK, Novak I & Christensen ST 2008 Characterization of primary cilia and Hedgehog signaling during development of the human

pancreas and in human pancreatic duct cancer cell lines. *Developmental Dynamics : An Official Publication of the American Association of Anatomists* **237** 2039–2052.

Niemann S & Müller U 2000 Mutations in SDHC cause autosomal dominant paraganglioma, type 3. *Nature Genetics* **26** 268–270.

Niemeijer ND, Alblas G, van Hulsteijn LT, Dekkers OM & Corssmit EPM 2014 Chemotherapy with cyclophosphamide, vincristine and dacarbazine for malignant paraganglioma and pheochromocytoma: systematic review and meta-analysis. *Clinical Endocrinology* **81** 642–651.

Nobin A, Karp W, Lunderquist A, Rosengren E, Sandén G & Sundler F 1982 Localization of carcinoids and pheochromocytomas with vein catheterization and amine determination. *Brain Research Bulletin* **9** 781–797.

Nobutani K, Shimono Y, Yoshida M, Mizutani K, Minami A, Kono S, Mukohara T, Yamasaki T, Itoh T, Takao S *et al.* 2014 Absence of primary cilia in cell cycle-arrested human breast cancer cells. *Genes to Cells : Devoted to Molecular & Cellular Mechanisms* **19** 141–152.

Novarino G, Akizu N & Gleeson JG 2011 Modeling Human Disease in Humans: The Ciliopathies. *Cell* **147** 70–79.

O'Connor AK, Malarkey EB, Berbari NF, Croyle MJ, Haycraft CJ, Bell PD, Hohenstein P, Kesterson RA & Yoder BK 2013 An inducible CiliaGFP mouse model for in vivo visualization and analysis of cilia in live tissue. *Cilia* **2** 8.

Ocbina PJR & Anderson K V. 2008 Intraflagellar transport, cilia, and mammalian Hedgehog signaling: Analysis in mouse embryonic fibroblasts. *Developmental Dynamics* **237** 2030–2038.

Ocbina PJR, Tuson M & Anderson K V. 2009 Primary Cilia Are Not Required for Normal Canonical Wnt Signaling in the Mouse Embryo. *PLoS ONE* **4** e6839.

Oh EC & Katsanis N 2013 Context-Dependent Regulation of Wnt Signaling through the Primary Cilium. *Journal of the American Society of Nephrology* **24** 10–18.

Ohh M, Yauch RL, Lonergan KM, Whaley JM, Stemmer-Rachamimov a O, Louis DN, Gavin BJ, Kley N, Kaelin WG & Iliopoulos O 1998 The von Hippel-Lindau tumor suppressor protein is required for proper assembly of an extracellular fibronectin matrix. *Molecular Cell* **1** 959–968.

Okuda H, Hirai S, Takaki Y, Kamada M, Baba M, Sakai N, Kishida T, Kaneko S, Yao M, Ohno S *et al.* 1999 Direct interaction of the beta-domain of VHL tumor suppressor protein with the regulatory domain of atypical PKC isotypes. *Biochemical and Biophysical Research Communications* **263** 491–497.

Omori Y, Chaya T, Yoshida S, Irie S, Tsujii T & Furukawa T 2015 Identification of G Protein-Coupled Receptors (GPCRs) in Primary Cilia and Their Possible Involvement in Body Weight Control. *PloS One* **10** e0128422.

Omura M, Saito J, Yamaguchi K, Kakuta Y & Nishikawa T 2004 Prospective study on the prevalence of secondary hypertension among hypertensive patients visiting a general outpatient clinic in Japan. *Hypertension Research : Official Journal of the Japanese Society of Hypertension* **27** 193–202.

Opotowsky AR, Moko LE, Ginns J, Rosenbaum M, Greutmann M, Aboulhosn J, Hageman A, Kim Y, Deng LX, Grewal J *et al.* 2015 Pheochromocytoma and Paraganglioma in Cyanotic Congenital Heart Disease. *The Journal of Clinical Endocrinology & Metabolism* **100** 1325–1334.

Ortiz-Barahona A, Villar D, Pescador N, Amigo J & del Peso L 2010 Genome-wide identification of hypoxia-inducible factor binding sites and target genes by a probabilistic model integrating transcription-profiling data and in silico binding site prediction. *Nucleic Acids Research* **38** 2332–2345.

Ostrowski LE, Blackburn K, Radde KM, Moyer MB, Schlatzer DM, Moseley A & Boucher RC 2002 A proteomic analysis of human cilia: identification of novel components. *Molecular & Cellular Proteomics : MCP* **1** 451–465.

Ou Y, Ruan Y, Cheng M, Moser JJ, Rattner JB, Hoorn FA Van Der, Tn C & Tn C 2009 Adenylate cyclase regulates elongation of mammalian primary cilia. *Experimental Cell Research* **315** 2802–2817.

Ozaki K, Haseman JK, Hailey JR, Maronpot RR & Nyska A 2002 Association of adrenal pheochromocytoma and lung pathology in inhalation studies with particulate compounds in the male F344 rat--the National Toxicology Program experience. *Toxicologic Pathology* **30** 263–270.

Pacak K 2007 Preoperative Management of the Pheochromocytoma Patient. *The Journal of Clinical Endocrinology & Metabolism* **92** 4069–4079.

Pacak K, Goldstein DS, Doppman JL, Shulkin BL, Udelsman R & Eisenhofer G 2001 A 'Pheo' lurks: Novel approaches for locating occult pheochromocytoma. *Journal of Clinical Endocrinology and Metabolism* **86** 3641–3646.

Pacak K, Eisenhofer G & Ilias I 2009 Diagnosis of pheochromocytoma with special emphasis on MEN2 syndrome. *Hormones (Athens, Greece)* **8** 111–116.

Pacheco-Ojeda L, Durango E, Rodriquez C & Vivar N 1988 Carotid body tumors at high altitudes: Quito, Ecuador, 1987. *World Journal of Surgery* **12** 856–860.

Palmer KJ, MacCarthy-Morrogh L, Smyllie N & Stephens DJ 2011 A role for Tctex-1 (DYNLT1) in controlling primary cilium length. *European Journal of Cell Biology* **90** 865–871.

Palublnskas J, Roizen MF & Conte FA 1980 Localization of functioning pheochromocytomas by venous sampling and radioenzymatic analysis. *Radiology* **136** 495–496.

Pampliega O, Orhon I, Patel B, Sridhar S, Díaz-Carretero A, Beau I, Codogno P, Satir BH, Satir P & Cuervo AM 2013 Functional interaction between autophagy and ciliogenesis. *Nature* **502** 194–200.

Papathomas TG, Gaal J, Corssmit EPM, Oudijk L, Korpershoek E, Heimdal K, Bayley JP, Morreau H, Van Dooren M, Papaspyrou K *et al.* 2014 Non-pheochromocytoma (PCC)/paraganglioma (PGL) tumors in patients with succinate dehydrogenase-related PCC-PGL syndromes: A clinicopathological and molecular analysis. *European Journal of Endocrinology* **170** 1–12.

Papathomas TG, Oudijk L, Persu A, Gill AJ, van Nederveen F, Tischler AS, Tissier F, Volante M, Matias-Guiu X, Smid M *et al.* 2015 SDHB/SDHA immunohistochemistry in pheochromocytomas and paragangliomas: a multicenter interobserver variation analysis using virtual microscopy: a Multinational Study of the European Network for the Study of Adrenal Tumors (ENS@T). *Modern Pathology* **28** 807–821.

Park TJ, Mitchell BJ, Abitua PB, Kintner C & Wallingford JB 2008 Dishevelled controls apical docking and planar polarization of basal bodies in ciliated epithelial cells. *Nature Genetics* **40** 871–879.

Pasquali D, Rossi V, Conzo G, Pannone G, Bufo P, De Bellis A, Renzullo A, Bellastella G, Colao A,

Vallone G *et al.* 2008 Effects of somatostatin analog SOM230 on cell proliferation, apoptosis, and catecholamine levels in cultured pheochromocytoma cells. *Journal of Molecular Endocrinology* **40** 263–271.

Pazour GJ, Dickert BL & Witman GB 1999 The DHC1b (DHC2) isoform of cytoplasmic dynein is required for flagellar assembly. *The Journal of Cell Biology* **144** 473–481.

Pazour GJ, Dickert BL, Vucica Y, Seeley ES, Rosenbaum JL, Witman GB & Cole DG 2000 Chlamydomonas IFT88 and its mouse homologue, polycystic kidney disease gene tg737, are required for assembly of cilia and flagella. *The Journal of Cell Biology* **151** 709–718.

Perera RM, Stoykova S, Nicolay BN, Ross KN, Fitamant J, Boukhali M, Lengrand J, Deshpande V, Selig MK, Ferrone CR *et al.* 2015 Transcriptional control of autophagy–lysosome function drives pancreatic cancer metabolism. *Nature* **524** 361–365.

Perry RR, Keiser HR, Norton JA, Wall RT, Robertson CN, Travis W, Pass HI, Walther MM & Linehan WM 1990 Surgical management of pheochromocytoma with the use of metyrosine. *Annals of Surgery* **212** 621–628.

Piperno G, LeDizet M & Chang XJ 1987 Microtubules containing acetylated alpha-tubulin in mammalian cells in culture. *The Journal of Cell Biology* **104** 289–302.

Piperno G, Siuda E, Henderson S, Segil M, Vaananen H & Sassaroli M 1998 Distinct mutants of retrograde intraflagellar transport (IFT) share similar morphological and molecular defects. *The Journal of Cell Biology* **143** 1591–1601.

Plotnikova O V., Pugacheva EN, Dunbrack RL & Golemis EA 2010 Rapid calcium-dependent activation of Aurora-A kinase. *Nature Communications* **1** 1–8.

Plotnikova O V., Pugacheva EN & Golemis EA 2011 Aurora A kinase activity influences calcium signaling in kidney cells. *The Journal of Cell Biology* **193** 1021–1032.

Plotnikova O V, Nikonova AS, Loskutov Y V, Kozyulina PY, Pugacheva EN & Golemis EA 2012 Calmodulin activation of Aurora-A kinase (AURKA) is required during ciliary disassembly and in mitosis. *Molecular Biology of the Cell* **23** 2658–2670.

Plotnikova O V., Seo S, Cottle DL, Conduit S, Hakim S, Dyson JM, Mitchell CA & Smyth IM 2015 INPP5E interacts with AURKA, linking phosphoinositide signaling to primary cilium stability. *Journal of Cell Science* **128** 364–372.

Plouin P-F, Fitzgerald P, Rich T, Ayala-Ramirez M, Perrier ND, Baudin E & Jimenez C 2012 Metastatic pheochromocytoma and paraganglioma: focus on therapeutics. *Hormone and Metabolic Research* **44** 390–399.

Podlasek CA, Barnett DH, Clemens JQ, Bak PM & Bushman W 1999 Prostate development requires Sonic hedgehog expressed by the urogenital sinus epithelium. *Developmental Biology* **209** 28–39.

Podrini C, Rowe I, Pagliarini R, Costa ASH, Chiaravalli M, Di Meo I, Kim H, Distefano G, Tiranti V, Qian F *et al.* 2018 Dissection of metabolic reprogramming in polycystic kidney disease reveals coordinated rewiring of bioenergetic pathways. *Communications Biology* **1** 194.

Ponder BA, Ponder MA, Coffey R, Pembrey ME, Gagel RF, Telenius-Berg M, Semple P & Easton DF 1988 Risk estimation and screening in families of patients with medullary thyroid carcinoma. *Lancet (London, England)* **1** 397–401.

Poopalalingam R & Chin EY 2001 Rapid preparation of a patient with pheochromocytoma with labetolol and magnesium sulfate. *Canadian Journal of Anaesthesia = Journal Canadien d'anesthesie* **48** 876–880.

Porter JA, Ekker SC, Park WJ, von Kessler DP, Young KE, Chen CH, Ma Y, Woods AS, Cotter RJ, Koonin E V *et al.* 1996 Hedgehog patterning activity: role of a lipophilic modification mediated by the carboxy-terminal autoprocessing domain. *Cell* **86** 21–34.

Pouysségur J, Dayan F & Mazure NM 2006 Hypoxia signalling in cancer and approaches to enforce tumour regression. *Nature* **441** 437–443.

Powers JF, Evinger MJ, Tsokas P, Bedri S, Alroy J, Shahsavari M & Tischler AS 2000 Pheochromocytoma cell lines from heterozygous neurofibromatosis knockout mice. *Cell and Tissue Research* **302** 309–320.

Praskova M, Xia F & Avruch J 2008 MOBKL1A/MOBKL1B phosphorylation by MST1 and MST2 inhibits cell proliferation. *Current Biology : CB* **18** 311–321.

Prodromou N V, Thompson CL, Osborn DPS, Cogger KF, Ashworth R, Knight MM, Beales PL & Chapple JP 2012 Heat shock induces rapid resorption of primary cilia. *Journal of Cell Science* **125** 4297–4305.

Proulx-Bonneau S & Annabi B 2011 The primary cilium as a biomarker in the hypoxic adaptation of bone marrow-derived mesenchymal stromal cells: a role for the secreted frizzled-related proteins. *Biomarker Insights* **6** 107–118.

Prys-Roberts C & Farndon JR 2002 Efficacy and safety of doxazosin for perioperative management of patients with pheochromocytoma. *World Journal of Surgery* **26** 1037–1042.

Pugacheva EN & Golemis EA 2005 The focal adhesion scaffolding protein HEF1 regulates activation of the Aurora-A and Nek2 kinases at the centrosome. *Nature Cell Biology* **7** 937–946.

Pugacheva EN, Jablonski SA, Hartman TR, Henske EP & Golemis EA 2007 HEF1-dependent Aurora A activation induces disassembly of the primary cilium. *Cell* **129** 1351–1363.

Qin H, Diener DR, Geimer S, Cole DG & Rosenbaum JL 2004 Intraflagellar transport (IFT) cargo. *The Journal of Cell Biology* **164** 255–266.

Qin Y, Yao L, King EE, Buddavarapu K, Lenci RE, Chocron ES, Lechleiter JD, Sass M, Aronin N, Schiavi F *et al.* 2010 Germline mutations in TMEM127 confer susceptibility to pheochromocytoma. *Nature Genetics* **42** 229–233.

Qin Y, Deng Y, Ricketts CJ, Srikantan S, Wang E, Maher ER & Dahia PLM 2014 The tumor susceptibility gene TMEM127 is mutated in renal cell carcinomas and modulates endolysosomal function. *Human Molecular Genetics* **23** 2428–2439.

Raber W, Raffesberg W, Bischof M, Scheuba C, Niederle B, Gasic S, Waldhäusl W & Roden M 2000 Diagnostic efficacy of unconjugated plasma metanephrines for the detection of pheochromocytoma. *Archives of Internal Medicine* **160** 2957–2963.

Radford R, Slattery C, Jennings P, Blacque O, Pfaller W, Gmuender H, Van Delft J, Ryan MP, McMorrow T & McMorrow T 2012 Carcinogens induce loss of the primary cilium in human renal proximal tubular epithelial cells independently of effects on the cell cycle. *American Journal of Physiology-Renal Physiology* **302** F905–F916.

Razumilava N, Gradilone SA, Smoot RL, Mertens JC, Bronk SF, Sirica AE & Gores GJ 2014 Non-canonical Hedgehog signaling contributes to chemotaxis in cholangiocarcinoma. *Journal of Hepatology* **60** 599–605.

von Recklinghausen F 1882 *Ueber Die Multiplen Fibrome Der Haut Und Ihre Beziehung Zu Den Multiplen Neuromen*.

Reed NA, Cai D, Blasius TL, Jih GT, Meyhofer E, Gaertig J & Verhey KJ 2006 Microtubule Acetylation Promotes Kinesin-1 Binding and Transport. *Current Biology* **16** 2166–2172.

Remacha L, Comino-Méndez I, Richter S, Contreras L, Currás-Freixes M, Pita G, Letón R, Galarreta A, Torres-Pérez R, Honrado E *et al.* 2017 Targeted Exome Sequencing of Krebs Cycle Genes Reveals Candidate Cancer–Predisposing Mutations in Pheochromocytomas and Paragangliomas. *Clinical Cancer Research* **23** 6315–6324.

Resnick A 2016 HIF Stabilization Weakens Primary Cilia. *PloS One* **11** e0165907.

Resnick A & Hopfer U 2007 Force-response considerations in ciliary mechanosensation. *Biophysical Journal* **93** 1380–1390.

Reubi JC, Waser B, Liu Q, Laissue JA & Schonbrunn A 2000 Subcellular distribution of somatostatin sst2A receptors in human tumors of the nervous and neuroendocrine systems: membranous versus intracellular location. *The Journal of Clinical Endocrinology and Metabolism* **85** 3882–3891.

Reubi JC, Waser B, Schaer JC & Laissue JA 2001 Somatostatin receptor sst1-sst5 expression in normal and neoplastic human tissues using receptor autoradiography with subtype-selective ligands. *European Journal of Nuclear Medicine* **28** 836–846.

Richardson DS, Lai AZ & Mulligan LM 2006 RET ligand-induced internalization and its consequences for downstream signaling. *Oncogene* **25** 3206–3211.

Richter S, Gieldon L, Pang Y, Peitzsch M, Huynh T, Leton R, Viana B, Ercolino T, Mangelis A, Rapizzi E *et al.* 2019 Metabolome-guided genomics to identify pathogenic variants in isocitrate dehydrogenase, fumarate hydratase, and succinate dehydrogenase genes in pheochromocytoma and paraganglioma. *Genetics in Medicine* **21** 705–717.

Ricketts CJ, Forman JR, Rattenberry E, Bradshaw N, Lalloo F, Izatt L, Cole TR, Armstrong R, Kumar VKA, Morrison PJ *et al.* 2010 Tumor risks and genotype-phenotype-proteotype analysis in 358 patients with germline mutations in SDHB and SDHD. *Human Mutation* **31** 41–51.

Rieder CL, Jensen CG & Jensen LC 1979 The resorption of primary cilia during mitosis in a vertebrate (PtK1) cell line. *Journal of Ultrastructure Research* **68** 173–185.

Rinke A, Muller H-H, Schade-Brittinger C, Klose K-J, Barth P, Wied M, Mayer C, Aminossadati B, Pape U-F, Blaker M *et al.* 2009 Placebo-Controlled, Double-Blind, Prospective, Randomized Study on the Effect of Octreotide LAR in the Control of Tumor Growth in Patients With Metastatic Neuroendocrine Midgut Tumors: A Report From the PROMID Study Group. *Journal of Clinical Oncology* **27** 4656–4663.

Ritter A, Friemel A, Kreis N-N, Hoock SC, Roth S, Kielland-Kaisen U, Brüggmann D, Solbach C, Louwen F & Yuan J 2018 Primary Cilia Are Dysfunctional in Obese Adipose-Derived Mesenchymal Stem Cells. *Stem Cell Reports* **10** 583–599.

Robert A, Margall-Ducos G, Guidotti J-E, Bregerie O, Celati C, Brechot C & Desdouets C 2007 The

intraflagellar transport component IFT88/polaris is a centrosomal protein regulating G1-S transition in non-ciliated cells. *Journal of Cell Science* **120** 628–637.

Robinson MD & Oshlack A 2010 A scaling normalization method for differential expression analysis of RNA-seq data. *Genome Biology* **11** R25.

Rocha C, Papon L, Cacheux W, Marques Sousa P, Lascano V, Tort O, Giordano T, Vacher S, Lemmers B, Mariani P *et al.* 2014 Tubulin glycylases are required for primary cilia, control of cell proliferation and tumor development in colon. *The EMBO Journal* **33** 2247–2260.

Rodriguez-Cuevas H, Lau I & Rodriguez HP 1986 High-altitude paragangliomas diagnostic and therapeutic considerations. *Cancer* **57** 672–676.

Rodríguez-Cuevas S, López-Garza J & Labastida-Almendaro S 1998 Carotid body tumors in inhabitants of altitudes higher than 2000 meters above sea level. *Head & Neck* **20** 374–378.

Roe J-S, Kim H, Lee S-M, Kim S-T, Cho E-J & Youn H-D 2006 p53 Stabilization and Transactivation by a von Hippel-Lindau Protein. *Molecular Cell* **22** 395–405.

Rohatgi R, Milenkovic L & Scott MP 2007 Patched1 Regulates Hedgehog Signaling at the Primary Cilium. *Science* **317** 372–376.

Romain C V, Paul P, Lee S, Qiao J & Chung DH 2014 Targeting aurora kinase A inhibits hypoxia-mediated neuroblastoma cell tumorigenesis. *Anticancer Research* **34** 2269–2274.

Rosenbaum JL & Child FM 1967 Flagellar regeneration in protozoan flagellates. *The Journal of Cell Biology* **34** 345–364.

Rosenbaum JL, Moulder JE & Ringo DL 1969 Flagellar elongation and shortening in Chlamydomonas. The use of cycloheximide and colchicine to study the synthesis and assembly of flagellar proteins. *The Journal of Cell Biology* **41** 600–619.

Rufini V, Treglia G, Castaldi P, Perotti G, Calcagni ML, Corsello SM, Galli G, Fanti S & Giordano A 2011 Comparison of 123I-MIBG SPECT-CT and 18F-DOPA PET-CT in the evaluation of patients with known or suspected recurrent paraganglioma. *Nuclear Medicine Communications* **32** 575–582.

Saggese T, Young A a, Huang C, Braeckmans K & McGlashan SR 2012 Development of a method for the measurement of primary cilia length in 3D. *Cilia* **1** 11.

Saito M, Otsu W, Hsu K, Chuang J, Yanagisawa T, Shieh V, Kaitsuka T, Wei F, Tomizawa K & Sung C 2017 Tctex-1 controls ciliary resorption by regulating branched actin polymerization and endocytosis. *EMBO Reports* **18** 1460–1472.

Saldana MJ, Salem LE & Travezan R 1973 High altitude hypoxia and chemodectomas. *Human Pathology* **4** 251–263.

Sang L, Miller JJ, Corbit KC, Giles RH, Brauer MJ, Otto EA, Baye LM, Wen X, Scales SJ, Kwong M *et al.* 2011 Mapping the NPHP-JBTS-MKS Protein Network Reveals Ciliopathy Disease Genes and Pathways. *Cell* **145** 513–528.

Sasaki H, Nishizaki Y, Hui C, Nakafuku M & Kondoh H 1999 Regulation of Gli2 and Gli3 activities by an amino-terminal repression domain: implication of Gli2 and Gli3 as primary mediators of Shh signaling. *Development (Cambridge, England)* **126** 3915–3924.

Schaefer CF, Anthony K, Krupa S, Buchoff J, Day M, Hannay T & Buetow KH 2009 PID: the Pathway Interaction Database. *Nucleic Acids Research* **37** D674–D679.

Schermer B, Ghenoiu C, Bartram M, Müller RU, Kotsis F, Höhne M, Kühn W, Rapka M, Nitschke R, Zentgraf H *et al.* 2006 The von Hippel-Lindau tumor suppressor protein controls ciliogenesis by orienting microtubule growth. *The Journal of Cell Biology* **175** 547–554.

Schiavi F, Boedeker CC, Bausch B, Peçzkowska M, Gomez CF, Strassburg T, Pawlu C, Buchta M, Salzmann M, Hoffmann MM *et al.* 2005 Predictors and prevalence of paraganglioma syndrome associated with mutations of the SDHC gene. *JAMA* **294** 2057–2063.

Schiavi F, Milne RL, Anda E, Blay P, Castellano M, Opocher G, Robledo M & Cascón A 2010 Are we overestimating the penetrance of mutations in SDHB? *Human Mutation* **31** 761–762.

Schimmack S, Kneller S, Dadabaeva N, Bergmann F, Taylor A, Hackert T, Werner J & Strobel O 2016 Epithelial to Stromal Re-Distribution of Primary Cilia during Pancreatic Carcinogenesis. *PLOS ONE* **11** e0164231.

Schlisio S, Kenchappa RS, Vredeveld LCW, George RE, Stewart R, Greulich H, Shahriari K, Nguyen N V, Pigny P, Dahia PL *et al.* 2008 The kinesin KIF1Bbeta acts downstream from EglN3 to induce apoptosis and is a potential 1p36 tumor suppressor. *Genes & Development* **22** 884–893.

Schmid KW, Schröder S, Dockhorn-Dworniczak B, Kirchmair R, Tötsch M, Böcker W & Fischer-Colbrie R 1994 Immunohistochemical demonstration of chromogranin A, chromogranin B, and secretogranin II in extra-adrenal paragangliomas. *Modern Pathology : An Official Journal of the United States and Canadian Academy of Pathology, Inc* **7** 347–353.

Schneider L, Clement CA, Teilmann SC, Pazour GJ, Hoffmann EK, Satir P & Christensen ST 2005 PDGFRalpha signaling is regulated through the primary cilium in fibroblasts. *Current Biology : CB* **15** 1861–1866.

Schodel J, Oikonomopoulos S, Ragoussis J, Pugh CW, Ratcliffe PJ & Mole DR 2011 High-resolution genome-wide mapping of HIF-binding sites by ChIP-seq. *Blood* **117** e207–e217.

Schraml P, Frew IJ, Thoma CR, Boysen G, Struckmann K, Krek W & Moch H 2009 Sporadic clear cell renal cell carcinoma but not the papillary type is characterized by severely reduced frequency of primary cilia. *Mod Pathol* **22** 31–36.

Schwab M, Praml C & Amler LC 1996 Genomic instability in Ip and human malignancies. *Genes, Chromosomes and Cancer* **16** 211–229.

Sciacovelli M, Gonçalves E, Johnson TI, Zecchini VR, da Costa ASH, Gaude E, Drubbel AV, Theobald SJ, Abbo SR, Tran MGB *et al.* 2016 Fumarate is an epigenetic modifier that elicits epithelial-to-mesenchymal transition. *Nature* **537** 544–547.

Seeley ES, Carrière C, Goetze T, Seeley ES, Carrie C, Goetze T, Longnecker DS & Korc M 2009 Pancreatic Cancer and Precursor Pancreatic Intraepithelial Neoplasia Lesions Are Devoid of Primary Cilia Lesions Are Devoid of Primary Cilia. 422–430.

Selak M a, Armour SM, MacKenzie ED, Boulahbel H, Watson DG, Mansfield KD, Pan Y, Simon MC, Thompson CB & Gottlieb E 2005 Succinate links TCA cycle dysfunction to oncogenesis by inhibiting HIF-alpha prolyl hydroxylase. *Cancer Cell* **7** 77–85.

Seo S, Baye LM, Schulz NP, Beck JS, Zhang Q, Slusarski DC & Sheffield VC 2010 BBS6, BBS10, and BBS12 form a complex with CCT/TRiC family chaperonins and mediate BBSome assembly. *Proceedings of the National Academy of Sciences* **107** 1488–1493.

Shamloo K, Chen J, Sardar J, Sherpa RT, Pala R, Atkinson KF, Pearce WJ, Zhang L & Nauli SM 2017

Chronic Hypobaric Hypoxia Modulates Primary Cilia Differently in Adult and Fetal Ovine Kidneys. *Frontiers in Physiology* **8** 677.

Sharma N, Kosan ZA, Stallworth JE, Berbari NF & Yoder BK 2011 Soluble levels of cytosolic tubulin regulate ciliary length control. *Molecular Biology of the Cell* **22** 806–816.

Shen WT, Grogan R, Vriens M, Clark OH & Duh Q-Y 2010 One hundred two patients with pheochromocytoma treated at a single institution since the introduction of laparoscopic adrenalectomy. *Archives of Surgery (Chicago, Ill. : 1960)* **145** 893–897.

Shih SM, Engel BD, Kocabas F, Bilyard T, Gennerich A, Marshall WF & Yildiz A 2013 Intraflagellar transport drives flagellar surface motility. *ELife* **2** e00744.

Shpak M, Goldberg MM & Cowperthwaite MC 2014 Cilia gene expression patterns in cancer. *Cancer Genomics & Proteomics* **11** 13–24.

Shulkin BL, Thompson NW, Shapiro B, Francis IR & Sisson JC 1999 Pheochromocytomas: Imaging with 2-[Fluorine-18]fluoro-2-deoxy- d -glucose PET. *Radiology* **212** 35–41.

Sibal L, Jovanovic A, Agarwal SC, Peaston RT, James RA, Lennard TWJ, Bliss R, Batchelor A & Perros P 2006 Phaeochromocytomas presenting as acute crises after beta blockade therapy. *Clinical Endocrinology* **65** 186–190.

Simons M, Gloy J, Ganner A, Bullerkotte A, Bashkurov M, Krönig C, Schermer B, Benzing T, Cabello OA, Jenny A *et al.* 2005 Inversin, the gene product mutated in nephronophthisis type II, functions as a molecular switch between Wnt signaling pathways. *Nature Genetics* **37** 537–543.

Sipple JH 1961 The association of pheochromocytoma with carcinoma of the thyroid gland. *Am. J. Med.* **31** 163–166.

Sjoblom T, Jones S, Wood LD, Parsons DW, Lin J, Barber TD, Mandelker D, Leary RJ, Ptak J, Silliman N *et al.* 2006 The Consensus Coding Sequences of Human Breast and Colorectal Cancers. *Science* **314** 268–274.

Smith LA, Bukanov NO, Husson H, Russo RJ, Barry TC, Taylor AL, Beier DR & Ibraghimov-Beskrovnaya O 2006 Development of Polycystic Kidney Disease in Juvenile Cystic Kidney Mice: Insights into Pathogenesis, Ciliary Abnormalities, and Common Features with Human Disease. *Journal of the American Society of Nephrology* **17** 2821–2831.

Smith EH, Janknecht R & Maher LJ 2007 Succinate inhibition of alpha-ketoglutarate-dependent enzymes in a yeast model of paraganglioma. *Human Molecular Genetics* **16** 3136–3148.

Snedecor ER, Sung CC, Moncayo A, Rothstein BE, Mockler DC, Tonnesen MG, Jones EC, Fujita M, Clark RA, Shroyer KR *et al.* 2015 Loss of primary cilia in melanoma cells is likely independent of proliferation and cell cycle progression. *The Journal of Investigative Dermatology* **135** 1456–1458.

Snouffer A, Brown D, Lee H, Walsh J, Lupu F, Norman R, Lechtreck K, Ko HW & Eggenschwiler J 2017 Cell Cycle-Related Kinase (CCRK) regulates ciliogenesis and Hedgehog signaling in mice. *PLoS Genetics* **13** e1006912.

Sohara E, Luo Y, Zhang J, Manning DK, Beier DR & Zhou J 2008 Nek8 Regulates the Expression and Localization of Polycystin-1 and Polycystin-2. *Journal of the American Society of Nephrology* **19** 469–476.

Solanki KK, Bomanji J, Moyes J, Mather SJ, Trainer PJ & Britton KE 1992 A pharmacological guide to medicines which interfere with the biodistribution of radiolabelled meta-iodobenzylguanidine (MIBG). *Nuclear Medicine Communications* **13** 513–521.

Soneson C, Love MI & Robinson MD 2015 Differential analyses for RNA-seq: transcript-level estimates improve gene-level inferences. *F1000Research* **4** 1521.

Song L & Dentler WL 2001 Flagellar Protein Dynamics in *Chlamydomonas*. *Journal of Biological Chemistry* **276** 29754–29763.

Sorokin S 1962 Centrioles and the formation of rudimentary cilia by fibroblasts and smooth muscle cells. *The Journal of Cell Biology* **15** 363–377.

Sorokin SP 1968 Reconstructions of centriole formation and ciliogenesis in mammalian lungs. *Journal of Cell Science* **3** 207–230.

Spalluto C, Wilson DI & Hearn T 2012 Nek2 localises to the distal portion of the mother centriole/basal body and is required for timely cilium disassembly at the G2/M transition. *European Journal of Cell Biology* **91** 675–686.

Spann AL, Yuan K, Goliwas KF, Steg AD, Kaushik DD, Kwon Y-J & Frost AR 2015 The presence of primary cilia in cancer cells does not predict responsiveness to modulation of smoothened activity. *International Journal of Oncology* **47** 269–279.

Spektor A, Tsang WY, Khoo D & Dynlacht BD 2007 Cep97 and CP110 Suppress a Cilia Assembly Program. *Cell* **130** 678–690.

Srirangalingam U, Walker L, Khoo B, MacDonald F, Gardner D, Wilkin TJ, Skelly RH, George E, Spooner D, Monson JP *et al.* 2008 Clinical manifestations of familial paraganglioma and phaeochromocytomas in succinate dehydrogenase B (SDH-B) gene mutation carriers. *Clinical Endocrinology* **69** 587–596.

Srirangalingam U, Khoo B, Walker L, MacDonald F, Skelly RH, George E, Spooner D, Johnston LB, Monson JP, Grossman AB *et al.* 2009 Contrasting clinical manifestations of SDHB and VHL associated chromaffin tumours. *Endocrine-Related Cancer* **16** 515–525.

Srirangalingam U, Khoo B, Matson M, Carpenter R, Reznek R, Maher ER, Chew SL & Drake WM 2010 SDHD-related chromaffin tumours: disease localisation to genetic dysfunction. *Hormone Research in Pædiatrics* **73** 135–139.

Stasiulewicz M, Gray SD, Mastromina I, Silva JC, Bjorklund M, Seymour PA, Booth D, Thompson C, Green RJ, Hall EA *et al.* 2015 A conserved role for Notch signaling in priming the cellular response to Shh through ciliary localisation of the key Shh transducer Smo. *Development* **142** 2291–2303.

Steinsapir J, Carr AA, Prisant LM & Bransome ED 1997 Metyrosine and pheochromocytoma. *Archives of Internal Medicine* **157** 901–906.

Stene M, Panagiotis N, Tuck ML, Sowers JR, Mayes D & Berg G 1980 Plasma norepinephrine levels are influenced by sodium intake, glucocorticoid administration, and circadian changes in normal man. *The Journal of Clinical Endocrinology and Metabolism* **51** 1340–1345.

Stephens RE 1997 Synthesis and turnover of embryonic sea urchin ciliary proteins during selective inhibition of tubulin synthesis and assembly. *Molecular Biology of the Cell* **8** 2187–2198.

Storey JD & Tibshirani R 2003 Statistical significance for genomewide studies. *Proceedings of the National Academy of Sciences* **100** 9440–9445.

Sugiyama N, Tsukiyama T, Yamaguchi TP & Yokoyama T 2011 The canonical Wnt signaling pathway is not involved in renal cyst development in the kidneys of inv mutant mice. *Kidney International* **79** 957–965.

Sugrue C 1800 Dr. Sugrue's Case of Gastrodynia. *The Medical and Physical Journal* **4** 228–231.

Sun X, Haley J, Bulgakov O V, Cai X, McGinnis J & Li T 2012 Tubby is required for trafficking G protein-coupled receptors to neuronal cilia. *Cilia* **1** 21.

Suzuki S 1910 Ueber zwei Tumoren aus Nebennierenmarkgewebe. *Berliner Klinische Wochenschrift* **47** 1623–1625.

Sze WCC, Grossman AB, Goddard I, Amendra D, Shieh SCC, Plowman PN, Drake WM, Akker SA & Druce MR 2013 Sequelae and survivorship in patients treated with (131)I-MIBG therapy. *British Journal of Cancer* **109** 565–572.

Sze WCC, Soh LM, Lau JH, Reznek R, Sahdev A, Matson M, Riddoch F, Carpenter R, Berney D, Grossman AB *et al.* 2014 Diagnosing unilateral primary aldosteronism - comparison of a clinical prediction score, computed tomography and adrenal venous sampling. *Clinical Endocrinology* **81** 25–30.

Taïeb D, Timmers HJ, Hindié E, Guillet BA, Neumann HP, Walz MK, Opocher G, de Herder WW, Boedeker CC, de Krijger RR *et al.* 2012 EANM 2012 guidelines for radionuclide imaging of phaeochromocytoma and paraganglioma. *European Journal of Nuclear Medicine and Molecular Imaging* **39** 1977–1995.

Talbot JJ, Shillingford JM, Vasanth S, Doerr N, Mukherjee S, Kinter MT, Watnick T & Weimbs T 2011 Polycystin-1 regulates STAT activity by a dual mechanism. *Proceedings of the National Academy of Sciences* **108** 7985–7990.

Tang N, Mack F, Haase VH, Simon MC & Johnson RS 2006 pVHL Function Is Essential for Endothelial Extracellular Matrix Deposition. *Molecular and Cellular Biology* **26** 2519–2530.

Tang Z, Lin MG, Stowe TR, Chen S, Zhu M, Stearns T, Franco B & Zhong Q 2013 Autophagy promotes primary ciliogenesis by removing OFD1 from centriolar satellites. *Nature* **502** 254–257.

Tang C-M, Lee TE, Syed SA, Burgoyne AM, Leonard SY, Gao F, Chan JC, Shi E, Chmielecki J, Morosini D *et al.* 2016 Hedgehog pathway dysregulation contributes to the pathogenesis of human gastrointestinal stromal tumors via GLI-mediated activation of KIT expression. *Oncotarget* **7** 78226–78241.

Teilmann SC & Christensen ST 2005 Localization of the angiopoietin receptors Tie-1 and Tie-2 on the primary cilia in the female reproductive organs. *Cell Biology International* **29** 340–346.

Teilmann SC, Byskov AG, Pedersen PA, Wheatley DN, Pazour GJ & Christensen ST 2005 Localization of transient receptor potential ion channels in primary and motile cilia of the female murine reproductive organs. *Molecular Reproduction and Development* **71** 444–452.

Thebault S, Flourakis M, Vanoverberghe K, Vandermoere F, Roudbaraki M, Lehen'kyi V, Slomianny C, Beck B, Mariot P, Bonnal J-L *et al.* 2006 Differential Role of Transient Receptor Potential Channels in Ca^{2+} Entry and Proliferation of Prostate Cancer Epithelial Cells. *Cancer Research* **66** 2038–2047.

Thiel C, Kessler K, Giessl A, Dimmler A, Shalev SA, von der Haar S, Zenker M, Zahnleiter D, Stöss H, Beinder E *et al.* 2011 NEK1 Mutations Cause Short-Rib Polydactyly Syndrome Type Majewski. *The American Journal of Human Genetics* **88** 106–114.

Thoenen H, Mueller RA & Axelrod J 1969 Trans-synaptic induction of adrenal tyrosine hydroxylase. *The Journal of Pharmacology and Experimental Therapeutics* **169** 249–254.

Thoma CR, Frew IJ, Hoerner CR, Montani M, Moch H & Krek W 2007 pVHL and GSK3beta are components of a primary cilium-maintenance signalling network. *Nature Cell Biology* **9** 588–595.

Thompson LDR 2002 Pheochromocytoma of the Adrenal gland Scaled Score (PASS) to separate benign from malignant neoplasms: a clinicopathologic and immunophenotypic study of 100 cases. *The American Journal of Surgical Pathology* **26** 551–566.

Thompson CL, Wiles A, Poole CA & Knight MM 2016 Lithium chloride modulates chondrocyte primary cilia and inhibits Hedgehog signaling. *FASEB Journal : Official Publication of the Federation of American Societies for Experimental Biology* **30** 716–726.

Timmers HJLM, Kozupa A, Eisenhofer G, Raygada M, Adams KT, Solis D, Lenders JWM & Pacak K 2007a Clinical presentations, biochemical phenotypes, and genotype-phenotype correlations in patients with succinate dehydrogenase subunit B-associated pheochromocytomas and paragangliomas. *The Journal of Clinical Endocrinology and Metabolism* **92** 779–786.

Timmers HJLM, Kozupa A, Chen CC, Carrasquillo JA, Ling A, Eisenhofer G, Adams KT, Solis D, Lenders JWM & Pacak K 2007b Superiority of fluorodeoxyglucose positron emission tomography to other functional imaging techniques in the evaluation of metastatic SDHB-associated pheochromocytoma and paraganglioma. *Journal of Clinical Oncology : Official Journal of the American Society of Clinical Oncology* **25** 2262–2269.

Tischler AS 2000 Divergent differentiation in neuroendocrine tumors of the adrenal gland. *Seminars in Diagnostic Pathology* **17** 120–126.

Tischler AS & deKrijger RR 2015 15 YEARS OF PARAGANGLIOMA: Pathology of pheochromocytoma and paraganglioma. *Endocrine-Related Cancer* **22** T123–T133.

Tobin JL & Beales PL 2009 The nonmotile ciliopathies. *Genetics in Medicine : Official Journal of the American College of Medical Genetics* **11** 386–402.

Toledo SPA, Lourenço DM, Sekiya T, Lucon AM, Baena MES, Castro CC, Bortolotto LA, Zerbini MCN, Siqueira SAC, Toledo RA *et al.* 2015 Penetrance and Clinical Features of Pheochromocytoma in a Six-Generation Family Carrying a Germline *TMEM127* Mutation. *The Journal of Clinical Endocrinology & Metabolism* **100** E308–E318.

Tonyukuk V, Emral R, Temizkan S, Sertçelik A, Erden I & Corapçioğlu D 2003 Case report: patient with multiple paragangliomas treated with long acting somatostatin analogue. *Endocrine Journal* **50** 507–513.

Traiffort E, Dubourg C, Faure H, Rognan D, Odent S, Durou M-R, David V & Ruat M 2004 Functional Characterization of Sonic Hedgehog Mutations Associated with Holoprosencephaly. *Journal of Biological Chemistry* **279** 42889–42897.

Traina G, Lanneau C, Arnoux A, Porokhov B, Bagnoli P & Epelbaum J 1998 Expression and coupling of somatostatin receptors in rat adrenal (PC12) and pituitary (GC) cell lines. *Neuroscience Letters* **252** 131–134.

Tucker RW, Scher CD & Stiles CD 1979 Centriole deciliation associated with the early response of 3T3 cells to growth factors but not to SV40. *Cell* **18** 1065–1072.

van der Tuin K, Mensenkamp AR, Tops CMJ, Corssmit EPM, Dinjens WN, van de Horst-Schrivers AN, Jansen JC, de Jong MM, Kunst HPM, Kusters B *et al.* 2018 Clinical Aspects of SDHA-Related Pheochromocytoma and Paraganglioma: A Nationwide Study. *The Journal of Clinical Endocrinology & Metabolism* **103** 438–445.

Tukachinsky H, Kuzmickas RP, Jao CY, Liu J & Salic A 2012 Dispatched and Scube Mediate the Efficient Secretion of the Cholesterol-Modified Hedgehog Ligand. *Cell Reports* **2** 308–320.

Turner JA, Bolen CR & Blankenship DM 2015 Quantitative gene set analysis generalized for repeated measures, confounder adjustment, and continuous covariates. *BMC Bioinformatics* **16** 272.

Tuson M, He M & Anderson K V. 2011 Protein kinase A acts at the basal body of the primary cilium to prevent Gli2 activation and ventralization of the mouse neural tube. *Development* **138** 4921–4930.

Tyler KM, Fridberg A, Toriello KM, Olson CL, Cieslak JA, Hazlett TL & Engman DM 2009 Flagellar membrane localization via association with lipid rafts. *Journal of Cell Science* **122** 859–866.

Udager AM, Magers MJ, Goerke DM, Vinco ML, Siddiqui J, Cao X, Lucas DR, Myers JL, Chinnaiyan AM, McHugh JB *et al.* 2018 The utility of SDHB and FH immunohistochemistry in patients evaluated for hereditary paraganglioma-pheochromocytoma syndromes. *Human Pathology* **71** 47–54.

Uetake Y, Loncarek J, Nordberg JJ, English CN, La Terra S, Khodjakov A & Sluder G 2007 Cell cycle progression and de novo centriole assembly after centrosomal removal in untransformed human cells. *The Journal of Cell Biology* **176** 173–182.

Unger N, Serdiuk I, Sheu S-Y, Walz MK, Schulz S, Saeger W, Schmid KW, Mann K & Petersenn S 2008 Immunohistochemical localization of somatostatin receptor subtypes in benign and malignant adrenal tumours. *Clinical Endocrinology* **68** 850–857.

Unger N, Ueberberg B, Schulz S, Saeger W, Mann K & Petersenn S 2012 Differential Expression of Somatostatin Receptor Subtype 1–5 Proteins in Numerous Human Normal Tissues. *Experimental and Clinical Endocrinology & Diabetes* **120** 482–489.

Upadhyay VS, Muntean BS, Kathem SH, Hwang JJ, Aboualaiwi W a & Nauli SM 2014 Roles of dopamine receptor on chemosensory and mechanosensory primary cilia in renal epithelial cells. *Frontiers in Physiology* **5** 72.

Valenta LJ, Elias AN & Eisenberg H 1986 ACTH stimulation of adrenal epinephrine and norepinephrine release. *Hormone Research* **23** 16–20.

Valente EM, Logan C V, Mougou-Zerelli S, Lee JH, Silhavy JL, Brancati F, Iannicelli M, Travaglini L, Romani S, Illi B *et al.* 2010 Mutations in TMEM216 perturb ciliogenesis and cause Joubert, Meckel and related syndromes. *Nature Genetics* **42** 619–625.

van Veelen W, Klompmaker R, Gloerich M, van Gasteren CJR, Kalkhoven E, Berger R, Lips CJM, Medema RH, Höppener JWM & Acton DS 2009 *P18* is a tumor suppressor gene involved in human medullary thyroid carcinoma and pheochromocytoma development. *International Journal of Cancer* **124** 339–345.

Verghese E, Zhuang J, Saiti D, Ricardo SD & Deane JA 2011 In vitro investigation of renal epithelial injury suggests that primary cilium length is regulated by hypoxia-inducible mechanisms. *Cell*

Biology International **35** 909–913.

Vézina A, Vaillancourt-Jean E, Albarao S & Annabi B 2014 Mesenchymal stromal cell ciliogenesis is abrogated in response to tumor necrosis factor-α and requires NF-κB signaling. *Cancer Letters* **345** 100–105.

Vortkamp A, Lee K, Lanske B, Segre G V, Kronenberg HM & Tabin CJ 1996 Regulation of rate of cartilage differentiation by Indian hedgehog and PTH-related protein. *Science (New York, N.Y.)* **273** 613–622.

Wallingford JB, Rowning BA, Vogeli KM, Rothbächer U, Fraser SE & Harland RM 2000 Dishevelled controls cell polarity during Xenopus gastrulation. *Nature* **405** 81–85.

Wallukat G 2002 The β-Adrenergic Receptors. *Herz* **27** 683–690.

Walz MK, Alesina PF, Wenger FA, Koch JA, Neumann HPH, Petersenn S, Schmid KW & Mann K 2006 Laparoscopic and Retroperitoneoscopic Treatment of Pheochromocytomas and Retroperitoneal Paragangliomas: Results of 161 Tumors in 126 Patients. *World Journal of Surgery* **30** 899–908.

Wang B-E, Shou J, Ross S, Koeppen H, De Sauvage FJ & Gao W-Q 2003 Inhibition of epithelial ductal branching in the prostate by sonic hedgehog is indirectly mediated by stromal cells. *The Journal of Biological Chemistry* **278** 18506–18513.

Wang W, Wu T & Kirschner MW 2014 The master cell cycle regulator APC-Cdc20 regulates ciliary length and disassembly of the primary cilium. *ELife* **3** e03083.

Wann AKT, Zuo N, Haycraft CJ, Jensen CG, Poole CA, McGlashan SR & Knight MM 2012 Primary cilia mediate mechanotransduction through control of ATP-induced Ca^{2+} signaling in compressed chondrocytes. *The FASEB Journal* **26** 1663–1671.

Wann AKT, Thompson CL, Chapple JP & Knight MM 2013 Interleukin-1 β sequesters hypoxia inducible factor 2 α to the primary cilium. *Cilia* **2** 17.

Warrell D, Cox T, Firth J & Benz E 2003 *Oxford Textbook of Medicine*. Oxford: Oxford University Press.

Weatherbee SD, Niswander LA & Anderson K V. 2009 A mouse model for Meckel syndrome reveals Mks1 is required for ciliogenesis and Hedgehog signaling. *Human Molecular Genetics* **18** 4565–4575.

Webb JL 1966 *Enzyme and Metabolic Inhibitors Vol II*. New York and London: Academic Press.

Webb R, Mathur A, Chang R, Baid S, Nilubol N, Libutti SK, Stratakis CA & Kebebew E 2012 What is the best criterion for the interpretation of adrenal vein sample results in patients with primary hyperaldosteronism? *Annals of Surgical Oncology* **19** 1881–1886.

Weingarten TN, Cata JP, O'Hara JF, Prybilla DJ, Pike TL, Thompson GB, Grant CS, Warner DO, Bravo E & Sprung J 2010 Comparison of two preoperative medical management strategies for laparoscopic resection of pheochromocytoma. *Urology* **76** 508.e6-11.

Weiterer S, Kohlen T, Veit F, Sachs L, Uhle F, Lichtenstern C, Weigand MA & Henrich M 2015 Galactomannan and Zymosan Block the Epinephrine-Induced Particle Transport in Tracheal Epithelium. *PLOS ONE* **10** e0143163.

Welander J, Łysiak M, Brauckhoff M, Brunaud L, Söderkvist P & Gimm O 2018 Activating FGFR1 Mutations in Sporadic Pheochromocytomas. *World Journal of Surgery* **42** 482–489.

Wenger RH, Stiehl DP & Camenisch G 2005 Integration of Oxygen Signaling at the Consensus HRE. *Science Signaling* **2005** re12.

Wheatley D, Wang AM & Strugnell GE 1996 Expression of primary cilia in mammalian cells. *Cell Biology International* **20** 73–81.

Whelton PK, Carey RM, Aronow WS, Casey DE, Collins KJ, Dennison Himmelfarb C, DePalma SM, Gidding S, Jamerson KA, Jones DW *et al.* 2018 2017 ACC/AHA/AAPA/ABC/ACPM/AGS/APhA/ASH/ASPC/NMA/PCNA Guideline for the Prevention, Detection, Evaluation, and Management of High Blood Pressure in Adults: Executive Summary: A Report of the American College of Cardiology/American Heart Association Task Force on Clinical Practice Guidelines. *Hypertension* **71** 1269–1324.

Wheway G, Abdelhamed Z, Natarajan S, Toomes C, Inglehearn C & Johnson CA 2013 Aberrant Wnt signalling and cellular over-proliferation in a novel mouse model of Meckel–Gruber syndrome. *Developmental Biology* **377** 55–66.

Wiens CJ, Tong Y, Esmail MA, Oh E, Gerdes JM, Wang J, Tempel W, Rattner JB, Katsanis N, Park H-W *et al.* 2010 Bardet-Biedl Syndrome-associated Small GTPase ARL6 (BBS3) Functions at or near the Ciliary Gate and Modulates Wnt Signaling. *Journal of Biological Chemistry* **285** 16218–16230.

Wilkinson SE, Furic L, Buchanan G, Larsson O, Pedersen J, Frydenberg M, Risbridger GP & Taylor RA 2013 Hedgehog signaling is active in human prostate cancer stroma and regulates proliferation and differentiation of adjacent epithelium. *The Prostate* **73** 1810–1823.

Williams CL, Li C, Kida K, Inglis PN, Mohan S, Semenec L, Bialas NJ, Stupay RM, Chen N, Blacque OE *et al.* 2011 MKS and NPHP modules cooperate to establish basal body/transition zone membrane associations and ciliary gate function during ciliogenesis. *The Journal of Cell Biology* **192** 1023–1041.

Wilson CW, Nguyen CT, Chen M-H, Yang J-H, Gacayan R, Huang J, Chen J-N & Chuang P-T 2009 Fused has evolved divergent roles in vertebrate Hedgehog signalling and motile ciliogenesis. *Nature* **459** 98–102.

Wiseman GA, Pacak K, O'Dorisio MS, Neumann DR, Waxman AD, Mankoff DA, Heiba SI, Serafini AN, Tumeh SS, Khutoryansky N *et al.* 2009 Usefulness of 123I-MIBG scintigraphy in the evaluation of patients with known or suspected primary or metastatic pheochromocytoma or paraganglioma: results from a prospective multicenter trial. *Journal of Nuclear Medicine : Official Publication, Society of Nuclear Medicine* **50** 1448–1454.

Wong SY, Seol AD, So P-L, Ermilov AN, Bichakjian CK, Epstein EH, Dlugosz AA & Reiter JF 2009 Primary cilia can both mediate and suppress Hedgehog pathway-dependent tumorigenesis. *Nature Medicine* **15** 1055–1061.

Wood LD, Parsons DW, Jones S, Lin J, Sjoblom T, Leary RJ, Shen D, Boca SM, Barber T, Ptak J *et al.* 2007 The Genomic Landscapes of Human Breast and Colorectal Cancers. *Science* **318** 1108–1113.

Wu K-S & Tang TK 2012 CPAP is required for cilia formation in neuronal cells. *Biology Open* **1** 559–565.

Wu D, Tischler AS, Lloyd R V, DeLellis RA, de Krijger R, van Nederveen F & Nosé V 2009 Observer variation in the application of the Pheochromocytoma of the Adrenal Gland Scaled Score. *The American Journal of Surgical Pathology* **33** 599–608. (doi:10.1097/PAS.0b013e318190d12e)

Wurtman RJ & Axelrod J 1965 Adrenaline synthesis: control by the pituitary gland and adrenal glucocorticoids. *Science (New York, N.Y.)* **150** 1464–1465.

Xekouki P, Pacak K, Almeida M, Wassif C a., Rustin P, Nesterova M, De La Luz Sierra M, Matro J, Ball E, Azevedo M *et al.* 2012 Succinate dehydrogenase (SDH) D subunit (SDHD) inactivation in a growth-hormone-producing pituitary tumor: A new association for SDH? *Journal of Clinical Endocrinology and Metabolism* **97** 357–366.

Xia P, Chu S, Liu G, Chen G, Yi T, Feng S & Zhou H 2018 High expression of KIF3A is a potential new parameter for the diagnosis and prognosis of breast cancer. *Biomedical Reports* **8** 343–349.

Xiang W, Jiang T, Guo F, Xu T, Gong C, Cheng P, Zhao L, Cheng W & Xu K 2014 Evaluating the Role of PTH in Promotion of Chondrosarcoma Cell Proliferation and Invasion by Inhibiting Primary Cilia Expression. *International Journal of Molecular Sciences* **15** 19816–19831.

Xiang W, Guo F, Cheng W, Zhang J, Huang J, Wang R, Ma Z & Xu K 2017 HDAC6 inhibition suppresses chondrosarcoma by restoring the expression of primary cilia. *Oncology Reports* **38** 229–236.

Xu J, Li H, Wang B, Xu Y, Yang J, Zhang X, Harten SK, Shukla D, Maxwell PH, Pei D *et al.* 2010 VHL Inactivation Induces HEF1 and Aurora Kinase A. *Journal of the American Society of Nephrology* **21** 2041–2046.

Yaari G, Bolen CR, Thakar J & Kleinstein SH 2013 Quantitative set analysis for gene expression: a method to quantify gene set differential expression including gene-gene correlations. *Nucleic Acids Research* **41** e170–e170.

Yang H, Minamishima YA, Yan Q, Schlisio S, Ebert BL, Zhang X, Zhang L, Kim WY, Olumi AF & Kaelin WG 2007 pVHL Acts as an Adaptor to Promote the Inhibitory Phosphorylation of the NF-κB Agonist Card9 by CK2. *Molecular Cell* **28** 15–27.

Yang C, Chen W, Chen Y & Jiang J 2012 Smoothened transduces Hedgehog signal by forming a complex with Evc/Evc2. *Cell Research* **22** 1593–1604.

Yang Y, Roine N & Mäkelä TP 2013 CCRK depletion inhibits glioblastoma cell proliferation in a cilium-dependent manner. *EMBO Reports* **14** 741–747.

Yang C, Zhuang Z, Fliedner SMJ, Shankavaram U, Sun MG, Bullova P, Zhu R, Elkahloun AG, Kourlas PJ, Merino M *et al.* 2015 Germ-line PHD1 and PHD2 mutations detected in patients with pheochromocytoma/paraganglioma-polycythemia. *Journal of Molecular Medicine* **93** 93–104.

Yang N, Leung EL-H, Liu C, Li L, Eguether T, Jun Yao X-J, Jones EC, Norris DA, Liu A, Clark RA *et al.* 2017 INTU is essential for oncogenic Hh signaling through regulating primary cilia formation in basal cell carcinoma. *Oncogene* **36** 4997–5005.

Yao L, Schiavi F, Cascon A, Qin Y, Inglada-Pérez L, King EE, Toledo RA, Ercolino T, Rapizzi E, Ricketts CJ *et al.* 2010 Spectrum and Prevalence of FP/TMEM127 Gene Mutations in Pheochromocytomas and Paragangliomas. *JAMA* **304** 2611.

Yao G, Luo C, Harvey M, Wu M, Schreiber TH, Du Y, Basora N, Su X, Contreras D & Zhou J 2016 Disruption of polycystin-L causes hippocampal and thalamocortical hyperexcitability. *Human Molecular Genetics* **25** 448–458.

Yasar B, Linton K, Slater C & Byers R 2017 Primary cilia are increased in number and demonstrate structural abnormalities in human cancer. *Journal of Clinical Pathology* **70** 571–574.

Yeap PM, Tobias ES, Mavraki E, Fletcher A, Bradshaw N, Freel EM, Cooke A, Murday VA, Davidson HR, Perry CG *et al.* 2011 Molecular Analysis of Pheochromocytoma after Maternal Transmission of SDHD Mutation Elucidates Mechanism of Parent-of-Origin Effect. *The Journal of Clinical Endocrinology & Metabolism* **96** E2009–E2013.

Yeh I-T, Lenci RE, Qin Y, Buddavarapu K, Ligon AH, Leteurtre E, Cao C Do, Cardot-Bauters C, Pigny P & Dahia PLM 2008 A germline mutation of the KIF1Bβ gene on 1p36 in a family with neural and nonneural tumors. *Human Genetics* **124** 279–285.

Yeh C, Li A, Chuang J-Z, Saito M, Cáceres A & Sung C-H 2013 IGF-1 Activates a Cilium-Localized Noncanonical Gβγ Signaling Pathway that Regulates Cell-Cycle Progression. *Developmental Cell* **26** 358–368.

You N, Tan Y, Zhou L, Huang X, Wang W, Wang L, Wu K, Mi N, Li J & Zheng L 2017 Tg737 acts as a key driver of invasion and migration in liver cancer stem cells and correlates with poor prognosis in patients with hepatocellular carcinoma. *Experimental Cell Research* **358** 217–226.

Young AP, Schlisio S, Minamishima YA, Zhang Q, Li L, Grisanzio C, Signoretti S & Kaelin WG 2008 VHL loss actuates a HIF-independent senescence programme mediated by Rb and p400. *Nature Cell Biology* **10** 361–369.

Yu T-M, Chuang Y-W, Yu M-C, Chen C-H, Yang C-K, Huang S-T, Lin C-L, Shu K-H & Kao C-H 2016 Risk of cancer in patients with polycystic kidney disease: a propensity-score matched analysis of a nationwide, population-based cohort study. *The Lancet. Oncology* **17** 1419–1425.

Yuan K, Frolova N, Xie Y, Wang D, Cook L, Kwon Y, Steg AD, Serra R & Frost A 2010 Primary cilia are decreased in breast cancer: analysis of a collection of human breast cancer cell lines and tissues. *J Histochem Cytochem* **58** 857–870.

Zalli D, Bayliss R & Fry AM 2012 The Nek8 protein kinase, mutated in the human cystic kidney disease nephronophthisis, is both activated and degraded during ciliogenesis. *Human Molecular Genetics* **21** 1155–1171.

Zanconato F, Forcato M, Battilana G, Azzolin L, Quaranta E, Bodega B, Rosato A, Bicciato S, Cordenonsi M & Piccolo S 2015 Genome-wide association between YAP/TAZ/TEAD and AP-1 at enhancers drives oncogenic growth. *Nature Cell Biology* **17** 1218–1227.

Zbar B, Kishida T, Chen F, Schmidt L, Maher ER, Richards FM, Crossey PA, Webster AR, Affara NA, Ferguson-smith MA *et al.* 1996 Germline Mutations in the n Hippel-Lindau Disease (VHL) Gene in Families From North America, Euope and Japan. *Human Mutation* **357** 348–357.

Zelinka T, Petrák O, Turková H, Holaj R, Strauch B, Kršek M, Vránková AB, Musil Z, Dušková J, Kubinyi J *et al.* 2012 High incidence of cardiovascular complications in pheochromocytoma. *Hormone and Metabolic Research* **44** 379–384.

Zervos AS, Gyuris J & Brent R 1993 Mxi1, a protein that specifically interacts with Max to bind Myc-Max recognition sites. *Cell* **72** 223–232.

Zhang X, Yuan Z, Zhang Y, Yong S, Salas-Burgos A, Koomen J, Olashaw N, Parsons JT, Yang X-J, Dent SR *et al.* 2007 HDAC6 Modulates Cell Motility by Altering the Acetylation Level of Cortactin. *Molecular Cell* **27** 197–213.

Zhang J, Lipinski RJ, Gipp JJ, Shaw AK & Bushman W 2009 Hedgehog pathway responsiveness correlates with the presence of primary cilia on prostate stromal cells. *BMC Developmental Biology* **9** 50.

Zhao C, Takita J, Tanaka Y, Setou M, Nakagawa T, Takeda S, Yang HW, Terada S, Nakata T, Takei Y *et al.* 2001 Charcot-Marie-Tooth disease type 2A caused by mutation in a microtubule motor KIF1Bbeta. *Cell* **105** 587–597.

Zhao X, Pak E, Ornell KJ, Pazyra-Murphy MF, MacKenzie EL, Chadwick EJ, Ponomaryov T, Kelleher JF & Segal RA 2017 A Transposon Screen Identifies Loss of Primary Cilia as a Mechanism of Resistance to SMO Inhibitors. *Cancer Discovery* **7** 1436–1449.

Zheng X, Ramani A, Soni K, Gottardo M, Zheng S, Ming Gooi L, Li W, Feng S, Mariappan A, Wason A *et al.* 2016 Molecular basis for CPAP-tubulin interaction in controlling centriolar and ciliary length. *Nature Communications* **7** 11874.

Zhu D, Shi S, Wang H & Liao K 2009 Growth arrest induces primary-cilium formation and sensitizes IGF-1-receptor signaling during differentiation induction of 3T3-L1 preadipocytes. *Journal of Cell Science* **122** 2760–2768.

Zhuang Z, Yang C, Lorenzo F, Merino M, Fojo T, Kebebew E, Popovic V, Stratakis C a., Prchal JT & Pacak K 2012 Gain-of-Function Mutations in Paraganglioma with Polycythemia. *New England Journal of Medicine* **367** 922–930.

Ziegler CG, Brown JW, Schally A V, Erler A, Gebauer L, Treszl A, Young L, Fishman LM, Engel JB, Willenberg HS *et al.* 2009 Expression of neuropeptide hormone receptors in human adrenal tumors and cell lines: antiproliferative effects of peptide analogues. *Proceedings of the National Academy of Sciences of the United States of America* **106** 15879–15884.

Zilber Y, Babayeva S, Seo JH, Liu JJ, Mootin S & Torban E 2013 The PCP effector Fuzzy controls cilial assembly and signaling by recruiting Rab8 and Dishevelled to the primary cilium. *Molecular Biology of the Cell* **24** 555–565.

Zimmermann KW 1898 Beitrage zur Kenntniss einiger Drusen und Epithelien. *Arch. Mikrosk. Anat.* **52** 552–706.

Zuber S, Wesley R, Prodanov T, Eisenhofer G, Pacak K & Kantorovich V 2014 Clinical utility of chromogranin A in *SDHx*- related paragangliomas. *European Journal of Clinical Investigation* **44** 365–371.

List of publications arising from this thesis

Journal articles

C.W.C. Sze*, S.M. O'Toole*, R.K. Tirador, S.A. Akker, M. Matson, L. Perry, M.R. Druce, T. Dekkers, J. Deinum, J.W.M. Lenders, G. Eisenhofer, W.M. Drake (2017) *Hormone and Metabolic Research* 49(6):418-423.

* Joint first author

S.M. O'Toole, D.S. Watson, T.V. Novoselova, L.E.L. Romano, P.J. King, T.Y. Bradshaw, C.L. Thompson, M.M. Knight, T.V. Sharp, M.R. Barnes, U. Srirangalingam, W.M. Drake, J.P. Chapple (2019) Oncometabolite induced primary cilia loss in pheochromocytoma. *Endocrine Related Cancer* 26(1):165-180.

Conference abstracts

S.M. O'Toole, C. Sze, K. Tirador, S. Akker, M. Matson, L. Perry, M.R. Druce, T. Dekkers, J. Deinum, J. Lenders, G. Eisenhofer, W.M. Drake. Adrenal vein catecholamine levels and ratios: reference intervals derived from patients with primary aldosteronism

Oral communication at Society for Endocrinology BES 2015, Edinburgh, 2-4/11/15

S.M. O'Toole, U. Srirangalingam, W.M. Drake, J.P. Chapple. The role of primary cilia in the molecular pathogenesis of phaeochromocytoma

Oral communication at Cilia, Cytoskeleton and Cancer, a Biochemical Society Focused Meeting, Edinburgh, 25-6/4/16

Oral communication at UK Cilia Network Meeting, London, 7/7/16

Oral communication at ENDO, Orlando, Florida, USA, 1-4/4/17

Appendix

Adrenal Vein Catecholamine Levels and Ratios: Reference Intervals Derived from Patients with Primary Aldosteronism

Authors
Candy W.C. Sze[1*], Samuel Matthew O'Toole[1*], Roger Kent Tirador[1], Scott A. Akker[1], Matthew Matson[2], Leslie Perry[3], Maralyn Rose Druce[1], Tanja Dekkers[4], Jaap Deinum[4], Jacques W.M. Lenders[4, 5], Graeme Eisenhofer[5, 6], William Martyn Drake[1]

Affiliations
1 Department of Endocrinology, St Bartholomew's Hospital, London, UK
2 Department of Radiology, St Bartholomew's Hospital, London, UK
3 Department of Biochemistry, St Bartholomew's Hospital, London, UK
4 Department of Internal Medicine, Radboud University Medical Center, Nijmegen, The Netherlands
5 Department of Internal Medicine III, University Hospital Carl Gustav Carus, Technische Universität Dresden, Dresden, Germany
6 Institute of Clinical Chemistry and Laboratory Medicine, University Hospital Carl Gustav Carus, Technische Universität Dresden, Dresden, Germany

Key words
adrenal venous sampling, catecholamines, phaeochromocytoma, hypertension, reference interval

received 17.06.2016
accepted 13.12.2016

Bibliography
DOI http://dx.doi.org/10.1055/s-0042-124419
Horm Metab Res 2017; 49: 1–7

ISSN 0018-5043

Correspondence
Professor William Martyn Drake
Department of Endocrinology
St Bartholomew's Hospital
London EC1A 7BE, UK
Tel.: +44/203/465 7264, Fax: +44/203/465 6148
w.m.drake@qmul.ac.uk

Supporting Information for this article is available online at http://www.thieme-connect.de/products

ABSTRACT

Phaeochromocytoma localisation is generally reliably achieved with modern imaging techniques, particularly in sporadic cases. On occasion, however, there can be diagnostic doubt due to the presence of bilateral adrenal abnormalities, particularly in patients with mutations in genes predisposing them to the development of multiple phaeochromocytomas. In such cases, surgical intervention is ideally limited to large or functional lesions due to the long-term consequences associated with hypoadrenalism. Adrenal venous sampling (AVS) for catecholamines has been used in this situation to guide surgery, although there are few data available to support diagnostic thresholds. Retrospective analyses of AVS results from 2 centres were carried out. A total of 172 patients (88 men, 84 women) underwent AVS under cosyntropin stimulation for the diagnosis of established primary aldosteronism (PA) with measurement of adrenal and peripheral venous cortisol, aldosterone and catecholamines. Six patients (3 men, 3 women) with phaeochromocytoma underwent AVS for diagnostic purposes with subsequent histological confirmation. Reference intervals for the adrenal venous norepinephrine to epinephrine ratio were created from the PA group. Using the 97.5th centile (1.21 on the left, 1.04 on the right), the false negative rate in the phaeochromocytoma group was 0 %. In conclusion, this study describes the largest dataset of adrenal venous catecholamine measurements and provides reference intervals in patients without phaeochromocytoma. This strengthens the certainty with which conclusions related to adrenal venous sampling for catecholamines can be drawn, acknowledging the procedure is not part of the routine diagnostic workup and is an adjunct for use only in difficult clinical cases.

Introduction

Phaeochromocytomas are rare, catecholamine producing tumours of the adrenal medulla that, if undiagnosed or untreated, may cause considerable morbidity and mortality [1, 2]. Diagnosis requires the demonstration of abnormal biochemistry (fractionated metanephrines in the blood and/or urine) prior to attempted localisation by imaging techniques such as computed tomography (CT), magnetic resonance imaging (MRI) and meta-^{123}iodobenzylguanidine (MIBG) scintigraphy [3]. Using these techniques, uncertainty regarding localisation in most patients with a sporadic phaeochromocytoma is unusual. The situation is different, however, in patients with inherited endocrine tumour syndromes [e. g., von Hippel–Lindau syndrome (VHL), multiple endocrine neoplasia type 2 (MEN2), mutations of the various subunits of succinate dehydrogenase (SDHx)]. Such patients are often asymptomatic and enrolled within screening programs [4–6] in which biochemical and radiological surveillance runs concurrently – the aim being to detect and treat tumours before they give rise to symptoms or haemodynamic instability. On occasion, this leads to the finding of bilateral radiological abnormalities in association with elevated urine

* Denotes equal contribution

or plasma levels of metanephrines and/or catecholamines. This presents difficulties for decision-making. Correct identification of one or other adrenal gland as being the source of catecholamine excess would be treated by a unilateral adrenalectomy (thereby avoiding, for a time, the need for adrenal replacement therapy); whereas a secure diagnosis of bilateral phaeochromocytomata could facilitate surgery at a single sitting.

The most commonly used for the localisation of primary aldosteronism (PA), adrenal venous sampling (AVS), was originally developed for the diagnosis and localisation of catecholamine-producing tumours [7]. Although a number of reports [8–25] have highlighted the use of AVS in the diagnosis of phaeochromocytoma, there remains uncertainty in the field [26], largely because of the lack of robust reference intervals for catecholamine values in adrenal venous effluent. Here, we report a large series of patients being investigated for PA in whom adrenal vein catecholamine concentrations were also measured, with the aim of producing reference intervals for use when AVS is utilized in challenging phaeochromocytoma cases.

Patients and Methods

Patients

Successive patients underwent AVS for the localisation of established PA at one of 2 centres: St Bartholomew's Hospital, London, UK and the Radboud University Medical Center, Nijmegen, The Netherlands between 2006 and 2015. A second group of 6 patients at St Bartholomew's Hospital were identified who had undergone AVS for the diagnosis and localisation of phaeochromocytoma; with subsequent histological confirmation of the diagnosis. The protocol received institutional board review at both centres.

Adrenal venous catheterisation

An intravenous infusion of cosyntropin 50 µg/h was commenced one hour before samples were obtained from each adrenal vein and the low inferior vena cava (IVC; as a peripheral sample) as previously described [27, 28]. Successful cannulation of each adrenal vein was defined by an adrenal vein to peripheral cortisol ratio exceeding 5–1 [29]. Aldosterone antagonists and potassium sparing diuretics were discontinued for at least 4 weeks, whilst beta-blockers and angiotensin converting enzyme inhibitors were withheld for at least 2 weeks prior to AVS.

At each centre it is standard practice to obtain a duplicate sample from each site for the potential future measurement of cortisol, aldosterone and catecholamines in order to provide extra reassurance regarding successful cannulation in the event of any technical shortcomings. It is these catecholamine values that have been used for this analysis; only those from patients satisfying the strict ≥ 5:1 cortisol ratio are included.

Biochemical analysis

Plasma catecholamines were measured using high performance liquid chromatography with electrochemical detection at both St Bartholomew's Hospital (Chromsystems, Gräfelfing, Germany) and at the University of Dresden (in house method [30]) for the Nijmegen samples.

Serum cortisol was measured by electrochemiluminescence immunoassay at both St Bartholomew's Hospital (Roche, Basel, Switzerland) and at Nijmegen (Modular E170 analyzer, Roche diagnostics Woerden, the Netherlands).

Statistical analysis

Data are presented as mean ± standard error of the mean or median with interquartile ranges. The Wilcoxon signed rank test was used to compare between adrenal veins. Centile values of the left and right norepinephrine to epinephrine ratio was calculated by counting. Analyses were performed using Stata version 13 (StatCorp, College Station, Texas, USA).

Results

Normal adrenal catecholamine levels in patients with PA

One hundred and seventy-two patients (88 males, 84 females) underwent AVS for localisation of biochemically confirmed PA. Their details are summarized in **Table 1S**. Samples for catecholamine analysis were available from 289 adrenal veins (130 right, 159 left).

Adrenal vein catecholamine concentrations are shown in ▶ **Table 1** and **Table 2S**. The median epinephrine (61.4 nmol/l compared to 35.1) and norepinephrine (16.3 nmol/l compared to 10.6) concentrations were higher in the right adrenal vein than in the left. The norepinephrine to epinephrine ratio was greater on the left (0.31) than the right (0.26).

▶ **Table 1** Adrenal vein catecholamine concentrations in patients who underwent adrenal venous sampling for the diagnosis of primary aldosteronism.

Catecholamine	Median (interquartile range)		p-Value
	Left adrenal vein	Right adrenal vein	
Epinephrine (nmol/l)	35.1 (19.5–72.8)	61.4 (31.5–126.7)	<0.001
Norepinephrine (nmol/l)	10.6 (6.6–18.7)	16.3 (8.8–31.8)	<0.001
Norepinephrine:epinephrine ratio	0.31 (0.20–0.51)	0.26 (0.18–0.38)	<0.001

Data are presented from the 113 patients with successful bilateral adrenal vein cannulation as median and interquartile ranges. p-Values were calculated using the Wilcoxon signed rank test.

Centile values of the left and right adrenal venous norepinephrine to epinephrine ratio were calculated and are shown in ▶ **Table 2**. The ratio for the 97.5th centile was 1.21 on the left and 1.04 on the right.

Adrenal catecholamine levels in patients with phaeochromocytoma

Six patients (3 males, 3 females) with the clinical and biochemical suspicion of catecholamine excess but with equivocal imaging underwent AVS as part of the diagnostic process. The mean age of these patients was 31.3 ± 6.9 years (range 13–67 years) and 5 had a genetic predisposition to phaeochromocytoma development (all VHL). AVS data guided surgical decision making and adrenalectomy was undertaken in all 6 patients (bilateral in 4) with the diagnosis confirmed histologically in all cases. The clinical details and AVS data for these patients are shown in ▶ **Table 3**. All 6 patients were alpha blocked prior to AVS and there were no haemodynamic or other adverse effects following AVS.

The lowest adrenal vein norepinephrine to epinephrine ratio in confirmed phaeochromocytoma was 2.96 on the left and 1.75 on the right.

Adrenal vein norepinephrine to epinephrine ratios for patients with PA and those with phaeochromocytomas are displayed in ▶ **Fig. 1**. Using a cut-off defined by the 97.5th centile of the PA cohort the false negative rate in the phaeochromocytoma cohort was 0 %.

Discussion

Historically, caval catheters and AVS have been used for the diagnosis [7, 12, 14, 16] and lateralization of adrenal phaeochromocytomas [11, 15, 21, 23] as well as the localisation of abdominal [8–10, 13, 21–23], bladder [17] and head and neck paragangliomas [8, 19]. Interpretation of these venous sampling studies depended either on the use of non-standardized concentration gradient cut-offs, comparisons with the contralateral adrenal or assumptions surrounding the norepinephrine to epinephrine ratio. Epinephrine is the predominantly secreted adrenal catecholamine [31] and an excess of norepinephrine, expressed as a norepinephrine to epinephrine ratio exceeding one, has been proposed as being pathological [20], although there are limited normative data to support this.

This series is the largest reported to date of catecholamine concentrations in the adrenal veins. In keeping with previous studies [26, 32, 33], we observed wide variation in absolute catecholamine concentrations (up to a factor of 178 on the right and 106 on the left); a fact that has been used to argue against the utility of AVS in the diagnosis of phaeochromocytoma [26]. This variation was reduced when considering the norepinephrine to epinephrine ratio in each adrenal vein (variation up to a factor of 54 on the right and 34 on the left) but not by 'correcting' for adrenal vein cortisol (**Table 3S**).

We have generated reference intervals for the adrenal vein norepinephrine to epinephrine ratio in individuals with PA. A ratio exceeding one has previously been suggested to be pathological, although this was based on data from only 3 patients with phaeochromocytoma and 5 without [20]. This previously proposed cut-off is close to what were observed in the PA cohort, particularly on the left. In the phaeochromocytoma cases the ratio was usually significantly higher.

A limitation of this study is the use of patients with PA to define reference intervals, but the use of healthy normotensive subjects would not be justifiable given the invasive nature, contrast and radiation exposure of AVS. Aldosterone stimulates the central nervous system in animals [34] but there is contradictory evidence as to whether sympathetic nervous system activity is increased [35] or attenuated [36] in individuals with PA, and whether this alters adrenal venous catecholamine levels is unknown. Alpha blockade has the potential to elevate circulating norepinephrine [3]; however both the PA and phaeochromocytoma groups were treated with alpha receptor antagonists prior to AVS (in the PA group for blood pressure control whilst not interfering with aldosterone measurement). Subgroup analysis (**Table 4S**) suggests that doxazosin treatment at the time of AVS increases norepinephrine in the left adrenal vein and the norepinephrine: epinephrine ratio on the right. It is unclear why this asymmetry should occur but the differential alpha blocker use at the time of AVS may partly explain the observed differences between the 2 cohorts (**Table 2S**).Prior to this report, the group at the Mayo Clinic reported AVS catecholamine results in 18 patients being evaluated for autonomous cortisol production [26]. These patients had cortisol excess, suppressed adrenocorticotrophin releasing hormone (ACTH) in all but one case and the AVS was performed under dexamethasone suppression. All of these factors have the potential to influence adrenal catecholamine production via effects on enzymes of the catecholamine synthesis pathway [31, 37–39]. The evidence for this in humans is limited and conflicting with reports of reduced peripheral epinephrine [40], norepinephrine [41] or both epinephrine and norepinephrine [42] in patients with Cushing's syndrome. One study found that chronic administration of ACTH to normal subjects did not affect peripheral norepinephrine, whilst dexamethasone at a dose of 6 mg over 3 days reduced norepinephrine [43]. Another study found no significant difference between the adrenal venous epinephrine to norepinephrine ratio in 8 patients with Cushing's compared to 12 controls [42]. Our patients were also hypercortisolaemic, albeit tem-

▶ **Table 2** Centile values for the norepinephrine:epinephrine ratio in the right and left adrenal veins in patients with primary aldosteronism.

Centile	Left	Right
1	0.09	0.07
2.5	0.10	0.09
5	0.11	0.10
10	0.13	0.11
25	0.20	0.17
50	0.31	0.26
75	0.51	0.40
90	0.74	0.62
95	0.88	0.77
97.5	1.21	1.04
99	2.41	3.38

HMR/2016-06-0197/27.12.2016/MPS

Thieme

▶ **Table 3** Patients who underwent AVS for the diagnosis of phaeochromocytoma.

Patient	Age	Sex	Genetic syndrome	Radiology *		MIBG		NE:E ratio		Operation	Histology
				Right	Left	Right	Left	Right	Left		
1	13	M	VHL	45	0	+	–	NC	2.96	Bilateral adrenalectomy	Bilateral phaeochromocytoma
2	67	F	Nil	19	14	+	–	1.75†	0.85	Right adrenalectomy	Phaeochromocytoma
3‡	29	M	VHL	45	10	+	–	210	9	Bilateral adrenalectomy	Bilateral phaeochromocytoma
4‡	25	F	VHL	25	5	+	–	26	11	Bilateral adrenalectomy	Bilateral phaeochromocytoma
5‡	24	F	VHL	10	50	–	+	11	26	Bilateral adrenalectomy	Bilateral phaeochromocytoma
6‡	30	M	VHL	0	0	–	–	0.8	0.5	Resection of left kidney, adrenal and para-aortic mass	Renal carcinoma, para-aortic paraganglioma Normal adrenal histology

MIBG: Metaiodobenzylguanidine; NE: Norepinephrine; E: Epinephrine; VHL: von Hippel-Lindau; +: positive; –: Negative; NC: Not cannulated; AVS: Adrenal Venous Sampling.

* Maximum dimension (mm) of an adrenal abnormality visualised by any imaging modality.

†This is the minimum possible ratio as unfortunately insufficient sample was available for further determination of the norepinephrine concentration.

‡These patients have been reported previously [21].

Patient 2's left adrenal lesion was indeterminate on imaging and underwent a unilateral right adrenalectomy based on the AVS result with subsequent histological confirmation of a phaeochromocytoma. Post-operative metanephrine measurements were normal excluding the presence of a pheochromocytoma in the left adrenal gland which remained in situ. Patient 6 underwent resection of his left kidney (for renal cell carcinoma) and a left-sided para-aortic mass (paraganglioma) that was not possible to be distinguished from the left adrenal gland on imaging. Anatomically it was impossible to preserve the left adrenal gland which was histologically normal (corresponding adrenal vein NE:E ratio 0.5).

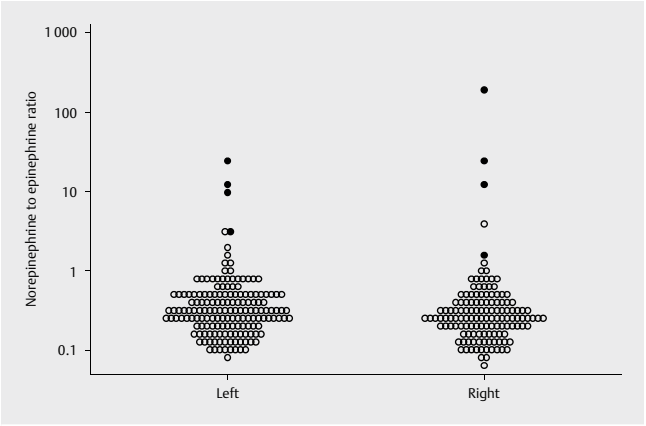

▶ **Fig. 1** Adrenal venous norepinephrine to epinephrine ratios in patients undergoing AVS for PA (open circles) or with histologically confirmed phaeochromocytoma (solid circles).

porarily, due to infusion of cosyntropin at the time of AVS and this has been shown to increase adrenal vein epinephrine and norepinephrine in one small series [44].

In keeping with the results of Freel et al. [26] we also observed a difference between left and right adrenal veins, necessitating different reference intervals. This differential is presumed to arise due to the anatomical differences between the 2 sides. They found no histological evidence of phaeochromocytoma in 4 patients who underwent adrenalectomy with a norepinephrine to epinephrine ratio exceeding one. The maximum observed ratio was 1.2 on the right and 2.1 on the left and it would be interesting to know how many of these patients had ratios exceeding our proposed cut offs. In addition, the applicability of their data to patients without Cushing's who did not undergo dexamethasone suppression is unclear.

The bulk of the published literature surrounding venous sampling for the diagnosis of phaeochromocytoma heralds from a time when cross-sectional and nuclear medicine imaging quality and availability were much more limited than in contemporary practice. As a result AVS has a more limited role in the diagnosis of phaeochromocytoma and paraganglioma than previously. One situation in which we believe it may still play a role is in patients with predisposing genetic syndromes such as VHL and SDHx. Participation in modern screening programs means that catecholamine excess may be identified early, often in asymptomatic individuals who might have bilateral radiological abnormalities. In this context, identification of a single adrenal gland as the source of catecholamine excess would facilitate a unilateral adrenalectomy, postponing the need for adrenal replacement therapy and its associated morbidity and mortality. Conversely, a secure diagnosis of bilateral phaeochromocytoma would allow surgery at a single sitting. In the context of bilateral disease or a predisposing syndrome, adrenal preserving surgery is an option, but long term follow-up data are limited and there is a significant risk of recurrence [45] and a more difficult second operation.

Previous reports from our centre illustrate these benefits. Chew et al. [21] described 4 patients with VHL and catecholamine excess, 3 of whom proceeded to bilateral adrenalectomy on the basis of elevated norepinephrine to epinephrine ratios bilaterally (range 9–210) with subsequent histological confirmation. The fourth patient had non-suggestive ratios (0.8 on the right, 0.5 on the left) and a diagnosis of a para-aortic paraganglioma which could not be delineated from the adjacent adrenal gland on cross-sectional imaging and so was not subjected to bilateral adrenalectomy. Srirangalingam et al. [23] reported a 15 year-old with an SDHD mutation in whom data from AVS led to a surgical approach that allowed preservation of his left adrenal gland when a right phaeochromocytoma and left abdominal paraganglioma were resected.

An advantage of the use of the adrenal vein norepinephrine to epinephrine ratio is that it does not rely on comparison with the contralateral adrenal gland, which, in the clinical settings outlined, has a high pre-test probability of being abnormal.

One disadvantage is the issue of a purely epinephrine secreting phaeochromocytoma which would not be identified using the norepinephrine to epinephrine ratio. However such cases are rare, particularly within the context of VHL and SDHx [46, 47] and would be identified prior to AVS by urine and plasma catecholamine and metanephrine analysis. It should be noted that epinephrine secreting phaeochromocytoma are a feature of both MEN2 and neurofibromatosis type 1 (NF1) [48] and this should be borne in mind when interpreting AVS results in these syndromes.

In summary, we have presented data from a large group of patients with PA and suggest that it could serve as a reference interval for adrenal vein catecholamines in non-phaeochromocytoma patients. We acknowledge that with advanced cross-sectional and nuclear medicine imaging, AVS is not required in the routine diagnosis of phaeochromocytoma. However, in some patients with known germline mutations of genes that predispose to the formation of phaeochromocytomas, screening programs may detect the presence of bilateral radiological abnormalities (with or without abnormal urine/plasma biochemistry) that presents diagnostic difficulties. In such selected situations, AVS, performed in an experienced centre and interpreted in the context of the reference intervals presented here, remains a useful complementary tool for determining treatment strategies in this challenging group of patients.

Acknowledgements

We thank Mr Jonathan Bestwick for his expert statistical assistance.

Conflict of Interest

The authors declare no conflict of interest.

References

[1] Khorram-Manesh A, Ahlman H, Nilsson O, Odén A, Jansson S. Mortality associated with pheochromocytoma in a large Swedish cohort. Eur J Surg Oncol 2004; 30: 556–559

[2] Zelinka T, Petrák O, Turková H, Holaj R, Strauch B, Kršek M, Vránková AB, Musil Z, Dušková J, Kubinyi J, Michalský D, Novák K, Widimský J. High incidence of cardiovascular complications in pheochromocytoma. Horm Metab Res 2012; 44: 379–384

[3] JWM Lenders, Duh Q-Y, Eisenhofer G, Gimenez-Roqueplo A-P, Grebe SKG, Murad MH, Naruse M, Pacak K, Young WF. Pheochromocytoma and paraganglioma: an endocrine society clinical practice guideline. J Clin Endocrinol Metab 2014; 99: 1915–1942

[4] Maher ER, Neumann HP, Richard S. von Hippel-Lindau disease: a clinical and scientific review. Eur J Hum Genet 2011; 19: 617–623

[5] Brandi ML, Gagel RF, Angeli A, Bilezikian JP, Beck-Peccoz P, Bordi C, Conte-Devolx B, Falchetti A, Gheri RG, Libroia A, Lips CJ, Lombardi G, Mannelli M, Pacini F, Ponder BA, Raue F, Skogseid B, Tamburrano G, Thakker RV, Thompson NW, Tomassetti P, Tonelli F, Wells SA, Marx SJ. Guidelines for diagnosis and therapy of MEN type 1 and type 2. J Clin Endocrinol Metab 2001; 86: 5658–5671

[6] Jasperson KW, Kohlmann W, Gammon A, Slack H, Buchmann L, Hunt J, Kirchhoff AC, Baskin H, Shaaban A, Schiffman JD. Role of rapid sequence whole-body MRI screening in SDH-associated hereditary paraganglioma families. Fam Cancer 2014; 13: 257–265

[7] Von Euler US, Gemzell CA, Strom G, Westman A. Report of a case of pheochromocytoma, with special regard to preoperative diagnostic problems. Acta Med Scand 1955; 153: 127–136

[8] Crout JR, Sjoerdsma A. Catecholamines in the localization of pheochromocytoma. Circulation 1960; 22: 516–525

[9] Fleisher DS, Voci G, Cresson SL, Karafin L. Preoperative localization of pheochromocytoma. J Pediatr 1964; 64: 711–715

[10] Grim CE, Glenn JF, Wynn JO, Gunnells JC. Bilateral pheochromocytoma: the application of a plasma catecholamine bioassay for tumor localization. Am Heart J 1967; 74: 809–815

[11] Davies RA, Patt NL, Sole MJ. Localization of pheochromocytoma by selective venous catheterization and assay of plasma catecholamines. Can Med Assoc J 1979; 120: 539–542

[12] Jones DH, Allison DJ, Hamilton CA, Reid JL. Selective venous sampling in the diagnosis and localization of phaeochromocytoma. Clin Endocrinol (Oxf) 1979; 10: 179–186

[13] Moss S, Greenbaum R, Sever PS. Preoperative localization of a phaeochromocytoma using plasma noradrenaline concentrations in multiple-site samples. J R Soc Med 1980; 73: 139–141

[14] Palublnskas J, Roizen MF, Conte FA. Localization of functioning pheochromocytomas by venous sampling and radioenzymatic analysis. Radiology 1980; 136: 495–496

[15] Nobin A, Karp W, Lunderquist A, Rosengren E, Sandén G, Sundler F. Localization of carcinoids and pheochromocytomas with vein catheterization and amine determination. Brain Res Bull 1982; 9: 781–797

[16] Allison DJ, Brown MJ, Jones DH, Timmis JB. Role of venous sampling in locating a phaeochromocytoma. Br Med J (Clin Res Ed) 1983; 286: 1122–1124

[17] Miller JL, Immelman EJ, Roman TE, Mervis B. Phaeochromocytoma of the urinary bladder localized by selective venous sampling and computed tomography. Postgrad Med J 1983; 59: 533–535

[18] Bomanji J, Bouloux PMG, Levison DA, Flatman WD, Horne T, Britton KE, Ross G, Besser GM. Observations on the function of normal adrenomedullary tissue in patients with phaeochromocytomas and other paragangliomas. Eur J Nucl Med 1987; 13: 86–89

[19] Cockcroft JR, Ritter JM, Allison DJ, Causon R, Brown MJ. Location of extra-adrenal catecholamine secreting tumours by selective venous sampling and nuclear magnetic resonance scanning. Postgrad Med J 1987; 63: 451–453

[20] Newbould EC, Ross GA, Dacie JE, Bouloux PM, Besser GM, Grossman A. The use of venous catheterization in the diagnosis and localization of bilateral phaeochromocytomas. Clin Endocrinol (Oxf) 1991; 35: 55–59

[21] Chew SL, Dacie JE, Reznek RH, Newbould EC, Sheaves R, Trainer PJ, Lowe DG, Shand WS, Hungerford J, Besser GM. Bilateral phaeochromocytomas in von Hippel-Lindau disease: diagnosis by adrenal vein sampling and catecholamine assay. Q J Med 1994; 87: 49–54

[22] Pacak K, Goldstein DS, Doppman JL, Shulkin BL, Udelsman R, Eisenhofer G. A "Pheo" lurks: Novel approaches for locating occult pheochromocytoma. J Clin Endocrinol Metab 2001; 86: 3641–3646

[23] Srirangalingam U, Khoo B, Matson M, Carpenter R, Reznek R, Maher ER, Chew SL, Drake WM. SDHD-related chromaffin tumours: disease localisation to genetic dysfunction. Horm Res pædiatrics 2010; 73: 135–139

[24] Därr R, Eisenhofer G, Kotzerke J, Zöphel K, Stroszczynski C, Deinum J, Schultze Kool LJ, Pistorius S, Neumann H, Bornstein SR, Hofbauer LC. Is there still a place for adrenal venous sampling in the diagnostic localization of pheochromocytoma? Endocrine 2011; 40: 75–79

[25] Mercado-Asis LB, Tingcungco AG, Bolong DT, Lopez Ra, Caguioa EV, Yamamoto ME, Marcos J, Mercado AB, Zacarias MB. Diagnosis of small adrenal pheochromocytomas by adrenal venous sampling with glucagon stimulation test. Int J Endocrinol Metab 2011; 9: 323–329

[26] Freel EM, Stanson AW, Thompson GB, Grant CS, Farley DR, Richards ML, Young WF. Adrenal venous sampling for catecholamines: A normal value study. J Clin Endocrinol Metab 2010; 95: 1328–1332

[27] Lau JHG, Sze WCC, Reznek RH, Matson M, Sahdev A, Carpenter R, Berney DM, Akker SA, Chew SL, Grossman AB, Monson JP, Drake WM. A prospective evaluation of postural stimulation testing, computed tomography and adrenal vein sampling in the differential diagnosis of primary aldosteronism. Clin Endocrinol (Oxf) 2012; 76: 182–188

[28] Sze WCC, Soh LM, Lau JH, Reznek R, Sahdev A, Matson M, Riddoch F, Carpenter R, Berney D, Grossman AB, Chew SL, Akker SA, Druce MR, Waterhouse M, Monson JP, Drake WM. Diagnosing unilateral primary aldosteronism - comparison of a clinical prediction score, computed tomography and adrenal venous sampling. Clin Endocrinol (Oxf) 2014; 81: 25–30

[29] Webb R, Mathur A, Chang R, Baid S, Nilubol N, Libutti SK, Stratakis CA, Kebebew E. What is the best criterion for the interpretation of adrenal vein sample results in patients with primary hyperaldosteronism? Ann Surg Oncol 2012; 19: 1881–1886

[30] Eisenhofer G, Goldstein DS, Stull R, Keiser HR, Sunderland T, Murphy DL, Kopin IJ. Simultaneous liquid-chromatographic determination of 3,4-dihydroxyphenylglycol, catecholamines, and 3,4-dihydroxyphenylalanine in plasma, and their responses to inhibition of monoamine oxidase. Clin Chem 1986; 32: 2030–2033

[31] Wurtman RJ, Axelrod J. Adrenaline synthesis: control by the pituitary gland and adrenal glucocorticoids. Science 1965; 150: 1464–1465

[32] Kahaly G, Krause U, Ritthaler H, Cordes U, Günther R, Schrezenmeir J, Beyer J. Selective blood sampling in adrenal hypertension. Cardiology 1985; 72 (Suppl 1): 179–181

[33] Baba Y, Nakajo M, Hayashi S. Adrenal venous catecholamine concentrations in patients with adrenal masses other than pheochromocytoma. Endocrine 2013; 43: 219–224

[34] Gomez-Sanchez EP. Intracerebroventricular infusion of aldosterone induces hypertension in rats. Endocrinology 1986; 118: 819–823

[35] Kontak AC, Wang Z, Arbique D, Adams-Huet B, Auchus RJ, Nesbitt SD, Victor RG, Vongpatanasin W. Reversible sympathetic overactivity in hypertensive patients with primary aldosteronism. J Clin Endocrinol Metab 2010; 95: 4756–4761

[36] Miyajima E, Yamada Y, Yoshida Y, Matsukawa T, Shionoiri H, Tochikubo O, Ishii M. Muscle sympathetic nerve activity in renovascular hypertension and primary aldosteronism. Hypertension 1991; 17: 1057–1062

[37] Wurtman RJ, Axelrod J. Control of enzymatic synthesis of adrenaline in the adrenal medulla by adrenal cortical steroids. J Biol Chem 1966; 241: 2301–2305

[38] Gewirtz GP, Kvetnanský R, Weise VK, Kopin IJ. Effect of hypophysectomy on adrenal dopamine -hydroxylase activity in the rat. Mol Pharmacol 1971; 7: 163–168

[39] Thoenen H, Mueller RA, Axelrod J. Trans-synaptic induction of adrenal tyrosine hydroxylase. J Pharmacol Exp Ther 1969; 169: 249–254

[40] Cameron OG, Starkman MN, Schteingart DE. The effect of elevated systemic cortisol levels on plasma catecholamines in Cushing's syndrome patients with and without depressed mood. J Psychiatr Res 1995; 29: 347–360

[41] Krsek M, Rosická M, Nedvídková J, Kvasnicková H, Hána V, Marek J, Haluzík M, Lai EW, Pacák K. Increased lipolysis of subcutaneous abdominal adipose tissue and altered noradrenergic activity in patients with Cushing's syndrome: an in-vivo microdialysis study. Physiol Res 2006; 55: 421–428

[42] Mannelli M, Lanzillotti R, Pupilli C, Ianni L, Conti A, Serio M. Adrenal medulla secretion in Cushing's syndrome. J Clin Endocrinol Metab 1994; 78: 1331–1335

[43] Stene M, Panagiotis N, Tuck ML, Sowers JR, Mayes D, Berg G. Plasma norepinephrine levels are influenced by sodium intake, glucocorticoid administration, and circadian changes in normal man. J Clin Endocrinol Metab 1980; 51: 1340–1345

[44] Valenta LJ, Elias AN, Eisenberg H. ACTH stimulation of adrenal epinephrine and norepinephrine release. Horm Res 1986; 23: 16–20

[45] Srirangalingam U, Walker L, Khoo B, MacDonald F, Gardner D, Wilkin TJ, Skelly RH, George E, Spooner D, Monson JP, Grossman AB, Akker SA, Pollard PJ, Plowman N, Avril N, Berney DM, Burrin JM, Reznek RH, Kumar VKA, Maher ER, Chew SL. Clinical manifestations of familial paraganglioma and phaeochromocytomas in succinate dehydrogenase B (SDH-B) gene mutation carriers. Clin Endocrinol (Oxf) 2008; 69: 587–596

[46] Srirangalingam U, Khoo B, Walker L, MacDonald F, Skelly RH, George E, Spooner D, Johnston LB, Monson JP, Grossman AB, Drake WM, Akker SA, Pollard PJ, Plowman N, Avril N, Berney DM, Burrin JM, Reznek RH, Kumar VKA, Maher ER, Chew SL. Contrasting clinical manifestations of SDHB and VHL associated chromaffin tumours. Endocr Relat Cancer 2009; 16: 515–525

[47] Eisenhofer G, Lenders JWM, Timmers H, Mannelli M, Grebe SK, Hofbauer LC, Bornstein SR, Tiebel O, Adams K, Bratslavsky G, Linehan WM, Pacak K. Measurements of plasma methoxytyramine, normetanephrine, and metanephrine as discriminators of different hereditary forms of pheochromocytoma. Clin Chem 2011; 57: 411–420

[48] ■■■

Dear Authors,
Please complete reference [48] (cited in line 247) in the reference list by providing full details of the citation.
Thank you.

RESEARCH

Oncometabolite induced primary cilia loss in pheochromocytoma

Samuel M O'Toole[1,2], David S Watson[1], Tatiana V Novoselova[1], Lisa E L Romano[1], Peter J King[1], Teisha Y Bradshaw[1], Clare L Thompson[3], Martin M Knight[3], Tyson V Sharp[4], Michael R Barnes[1], Umasuthan Srirangalingam[1,2,5], William M Drake[2] and **J Paul Chapple[1]**

[1]William Harvey Research Institute, Barts and the London School of Medicine, Queen Mary University of London, London, UK
[2]Department of Endocrinology, St Bartholomew's Hospital, Barts Health NHS Trust, London, UK
[3]Institute of Bioengineering and School of Engineering and Material Sciences, Queen Mary University of London, London, UK
[4]Barts Cancer Institute, Queen Mary University of London, London, UK
[5]Department of Diabetes and Endocrinology, University College London Hospital, London, UK

Correspondence should be addressed to J P Chapple: j.p.chapple@qmul.ac.uk

Abstract

Primary cilia are sensory organelles involved in regulation of cellular signaling. Cilia loss is frequently observed in tumors; yet, the responsible mechanisms and consequences for tumorigenesis remain unclear. We demonstrate that cilia structure and function is disrupted in human pheochromocytomas – endocrine tumors of the adrenal medulla. This is concomitant with transcriptional changes within cilia-mediated signaling pathways that are associated with tumorigenesis generally and pheochromocytomas specifically. Importantly, cilia loss was most dramatic in patients with germline mutations in the pseudohypoxia-linked genes *SDHx* and *VHL*. Using a pheochromocytoma cell line derived from rat, we show that hypoxia and oncometabolite-induced pseudohypoxia are key drivers of cilia loss and identify that this is dependent on activation of an Aurora-A/HDAC6 cilia resorption pathway. We also show cilia loss drives dramatic transcriptional changes associated with proliferation and tumorigenesis. Our data provide evidence for primary cilia dysfunction contributing to pathogenesis of pheochromocytoma by a hypoxic/pseudohypoxic mechanism and implicates oncometabolites as ciliary regulators. This is important as pheochromocytomas can cause mortality by mechanisms including catecholamine production and malignant transformation, while hypoxia is a general feature of solid tumors. Moreover, pseudohypoxia-induced cilia resorption can be pharmacologically inhibited, suggesting potential for therapeutic intervention.

Key Words

- pheochromocytoma
- primary cilia
- hypoxia
- succinate dehydrogenase
- von Hippel–Lindau protein

Endocrine-Related Cancer (2019) **26**, 165–180

Introduction

Pheochromocytomas (PCCs) are neuroendocrine tumors that originate from chromaffin cells of the adrenal medulla or autonomic nervous system, where they are termed paragangliomas (PGLs). The majority of the morbidity associated with PCC/PGLs is consequent upon their production of catecholamines, leading to severe, life-threatening hypertension, but they may also cause local mass effect and have the potential for metastatic spread (Fishbein & Nathanson 2012, Burnichon *et al.* 2016). Understanding of the pathogenesis of PCC/PGLs is incomplete, with limited ability to predict malignant potential and at present the response to conventional cancer therapies is disappointing.

Approximately 30% of PCC/PGLs are associated with inherited germline mutations in more than 15

https://erc.bioscientifica.com
https://doi.org/10.1530/ERC-18-0134

different susceptibility genes (Dahia 2017). These include causative genes for inherited cancer syndromes, where, relative to other tumor types, there is a high incidence of PCC/PGL. Recent analyses of germline and somatic mutations have classified PCC/PGL into four molecularly defined groups, including a pseudohypoxia-linked subtype (Fishbein *et al.* 2017). These pseudohypoxic tumors occur due to mutations that impact regulation of the hypoxia transcription factors HIF1α and HIF2α. This can be through germline or somatic mutation of the ubiquitin E3 ligase pVHL (von Hippel–Lindau protein), which targets HIFα for degradation by the ubiquitin proteasome system (Dannenberg *et al.* 2003, Gossage *et al.* 2015, Crespigio *et al.* 2017). Increased HIF activity also results from germline mutation in genes that encode the succinate dehydrogenase (SDH) complex subunits (SDHA, SDHB, SDHC, SDHD), succinate dehydrogenase complex assembly factor 2 (SDHAF2), fumarate hydratase (FH) and malate dehydrogenase (MDH2) (Fishbein & Nathanson 2012). This is because loss of their function leads to accumulation of oncometabolites that inhibit pVHL-mediated degradation of HIFα (Selak *et al.* 2005).

Although pseudohypoxic mechanisms account, at least in part, for angiogenesis-facilitated growth, they do not, of themselves, satisfactorily explain PCC/PGL tumorigenesis. Mutations in the *VHL* gene are known to be important in renal cancers; this includes the occurrence of clear cell renal cell carcinoma (ccRCC) as part of the inherited cancer syndrome von Hippel–Lindau disease, in which *VHL* is mutated and PCC/PGL can occur (Gossage *et al.* 2015, Crespigio *et al.* 2017). One of the hallmark features of ccRCC is the loss of primary cilia (Basten *et al.* 2013), which act as flow sensors on renal epithelial cells. Cilia are cellular organelles that consist of a microtubule-based core structure, known as the axoneme, which elongates from a basal body and is covered by the ciliary membrane. Cilia function as signaling platforms involved in the transduction of extracellular stimuli, through mechanisms including regulating the spatial compartmentalization of signaling components (Berbari *et al.* 2009, Goetz & Anderson 2010). For example, primary cilia are modulators of WNT signaling and have an essential role in mammalian hedgehog (Hh) signaling (Berbari *et al.* 2009, Wong *et al.* 2009, Goetz & Anderson 2010, Lancaster *et al.* 2011, Oh & Katsanis 2013).

The coordination of cilia-mediated signaling is influenced by the dynamic nature of cilia, which elongate and shorten in response to cell cycle stage and other stimuli. This requires the process of intraflagellar transport (IFT) to traffic ciliary components in both anterograde and retrograde directions along axonemal microtubules. Cilia are assembled when cells enter stationary phase and are normally resorbed prior to cell division. This occurs as the basal body, which acts as a nucleation site for the growth of axoneme microtubules during ciliogenesis, is derived from a mother centriole and is required for mitotic spindle pole formation. Importantly, the mother centriole has this dual role means that the presence of a primary cilium potentially acts as a checkpoint within the cell cycle (Izawa *et al.* 2015). Thus, cilia might oppose cell division and proliferation; however, it should be noted that there are instances where cilia are present on mitotic cells (Goto *et al.* 2013). Dysregulation of normal restraints on cellular proliferation is required for neoplastic progression, and it is hypothesized that disruption of a ciliary cell cycle checkpoint may promote tumorigenesis (Mans *et al.* 2008), although ciliopathy patients have not been identified as having an increased risk of cancer (Johnson & Collis 2016).

Here, we address key questions regarding the loss of cilia in tumor cells in the context of PCC/PGLs. These include whether cilia loss is correlated with changes in cilia-mediated signaling *in vivo*. We also consider whether cilia loss increases cellular proliferation or is a consequence of it. We demonstrate that primary cilia loss is a feature of PCC/PGL and in particular those that are driven by germline mutations in pseudohypoxia-linked genes. This finding is consistent with transcriptome-based evidence from PCCs for dysregulation of cilia maintenance and cilia-mediated signaling pathways. Using a rat PCC-derived cell line (PC12), we define the molecular mechanism of primary cilia loss, demonstrating that axonemal resorption is dependent on both HIF signaling and Aurora-A kinase activation. Moreover, loss of primary cilia in PC12, induced by ciliary protein knockdown, leads to increased proliferation and alterations in expression of genes associated with pathways involved in proliferation and cancer. We also show that knockdown of pseudohypoxia-causing PCC/PGL genes and treatment with inhibitors that trigger accumulation of oncometabolites result in primary cilia loss.

Materials and methods

Tissue sample collection and preparation for immunolabeling and RNA extraction

Samples of tumor and adjacent adrenal medulla, where available, were collected at the time of adrenalectomy (for PCC) or PGL resection (patient recruitment and

https://erc.bioscientifica.com
https://doi.org/10.1530/ERC-18-0134

ethical approval is described in the Supplementary data, see section on supplementary data given at the end of this article). PCC and normal adrenal medulla were differentiated at the time of surgery with subsequent pathology analysis. For immunofluorescence, samples were fixed in 4% paraformaldehyde, resuspended in 30% sucrose and embedded in OCT compound (VWR) prior to storage at −80°C. For RNA extraction, tissue samples were placed directly into RNAlater (Thermo Fisher Scientific) and stored at −20°C. Samples were subsequently homogenized in RLT buffer and purified using RNeasy Mini Kit (Qiagen).

Cell culture and experimental treatments

Cell lines were cultured and treated with drugs as described in Supplementary data. PC-12 Adh (ATCC CRL-1721.1) cells were obtained from the American Type Culture Collection; for cilia assembly experiments, cells were plated and grown in complete media for 24 h prior to serum starvation for a further 24 h or otherwise specified. For cilia disassembly experiments serum-containing media was reintroduced for 24 h after starvation or as otherwise specified.

Immunofluorescent detection and quantification of primary cilia

The immmunostaining protocols and antibodies used are described in Supplementary data. Confocal microscopy was performed using an LSM510 or LSM880 laser scanning confocal microscope (Zeiss). Quantification of cilia incidence and length was performed blinded to experimental status. Cilia incidence was defined as the number of cells with a cilium (identified by two axonemal markers) divided by the number of nuclei in a given field. Cilia length was measured from maximum intensity projections created from confocal Z-stacks using Zen (Zeiss) and ImageJ (NIH) software. The surpass module of Imaris 7.1 image processing and analysis software (Bitplane) was used to surface render 3D images.

siRNA-mediated knockdown

PC12 cells were transfected with either targeted or non-targeted control siRNAs (Silencer Select, Ambion) using Lipofectamine 3000 (Thermo Fisher Scientific), according to the manufacturer's instructions. For knockdown of *VHL*, *SDHB* and *FH*, *IFT88* and *Cep164* – two distinct siRNAs each targeting distinct exons – were used at a total concentration of 30 nM (sequences available on request).

RNA-sequence data and pathway analyses

RNA extraction and sequencing is described in Supplementary data. All analyses were conducted in the R statistical environment, version 3.4.0, using software from the Bioconductor repository (Huber *et al.* 2015). Functional analysis of differential gene expression between control and *Ift88*-knockdown cells was performed using Ingenuity Pathways Analysis (IPA; Ingenuity Systems), using all genes with log fold change ≥2 and q-value was <0.01, as input. For all gene set enrichment analyses, a right-tailed Fisher's exact test was used to calculate a pathway P-value determining the probability that each biological function assigned to that data set was due to chance alone. All enrichment scores were calculated in IPA using all transcripts that passed QC as the background data set. For more details of transcriptome and pathway analyses, see our supplemental R Markdown document (https://github.com/C4TB/markdown-chapple_pcc).

Results

The incidence and length of primary cilia is reduced in PCCs relative to adjacent normal adrenal medulla

We collected paired tissue samples from PCCs and adjacent macroscopically normal adrenal medulla from 25 patients who underwent adrenalectomy. Two individuals had bilateral disease giving a total of 27 paired samples (Table 1 and Supplementary Table 1). The tissues were immunostained for the axonemal proteins acetylated α-tubulin and ADP-ribosylation factor-like protein 13B (Arl13b) and analyzed for the incidence of cells with a primary cilium (Fig. 1A). This showed that the occurrence of a primary cilium was lower ($P=4.74\times10^{-11}$) in PCCs (3.06±0.14% of cells) compared to adrenal medulla (8.42±0.03% of cells) (Fig. 1B). The length of the ciliary axoneme was also reduced ($P=8.24\times10^{-11}$) in PCC cells that still had cilia (1.48±0.34 µm) relative to cells in adjacent adrenal medulla (2.02±0.39 µm) (Fig. 1C). The incidence and length of primary cilia measured in individuals correlated in both PCCs and adjacent adrenal medulla, although this relationship was stronger in PCCs than adjacent adrenal medulla (PCC $P<0.001$, $r^2=0.66$; adrenal $P=0.001$, $r^2=0.36$) (Fig. 1D). We also observed that in every instance cilia incidence was lower in the PCC than its adjacent adrenal medulla (Supplementary Fig. 1A). This was also the case for cilia length in all but one of the paired samples (Supplementary Fig. 1B). Together, these data established that loss of primary cilia is a feature of PCC.

https://erc.bioscientifica.com
https://doi.org/10.1530/ERC-18-0134

Table 1 Clinical details – summary table.

	Paired	Unpaired	All
Samples (*n*)	27	20	47
Patients (*n*)	25	15	40
Sex			
Male; *n* (%)	12 (48)	7 (47)	19 (47.5)
Female; *n* (%)	13 (52)	8 (53)	21 (52.5)
Age (years)			
Mean ± S.E.M.	46.8 ± 4.0	46.2 ± 3.4	46.6 ± 2.8
Range	12–78	15–68	12–78
Size (mm)			
Mean ± S.E.M.	49 ± 4	47 ± 7	48 ± 4
Range	8–87	13–120	8–120
Location			
Adrenal (%)	27 (100)	7 (35)	34 (72)
PGL (%)	0 (0)	13 (65)	13 (28)
Mode of diagnosis			
Symptomatic (%)	9 (33)	9 (45)	18 (38)
Incidental (%)	14 (52)	7 (35)	21 (45)
Screening (%)	4 (15)	4 (20)	8 (17)
Germline mutation (patients) (%)	5 (25)	8 (53)	13 (33.5)
SDHA	0	1	1
SDHB	1	4	5
VHL	3	2	5
MEN2	1	1	2
Germline mutation (tumors) (%)	7 (26)	13 (65)	20 (42.6)
SDHA	0	3	3
SDHB	1	5	6
VHL	5	4	9
MEN2	1	1	2

Incidental, diagnosis due to investigation for another unrelated condition; MEN2, multiple endocrine neoplasia 2; mode of diagnosis – symptomatic, diagnosis due to symptoms or signs of catecholamine excess leading to diagnosis; PGL, paraganglioma; screening, diagnosis during a screening program in individuals with known pheo/PGL predisposition; SDH, succinate dehydrogenase; S.E.M., standard error of the mean; VHL, von Hippel–Lindau.

It has previously been reported that the tumor suppressor pVHL plays a role in ciliogenesis (Schermer *et al.* 2006). Thus, we next compared cilia loss and length reduction in PCC from patients with germline mutations in *VHL* compared to those without. We found that both cilia incidence (1.40±0.01% vs 3.43±0.02) and length (1.15±0.35 µm vs 1.58±0.31 µm) were reduced in VHL-PCCs compared to non-VHL-PCCs (P=0.010 for incidence, P=0.010 for length) (Fig. 1E and F). There was no significant difference in either cilia incidence or length in adjacent adrenal medulla from *VHL* and non-*VHL* patients (Fig. 1E and F). This suggests that cilia loss and shortening in VHL-PCCs occurs during tumorigenesis and is not a pre-existing/pre-malignant feature.

In order to further evaluate whether this finding was specific to VHL or a feature of other pseudohypoxic PCCs, we extended our analysis to include an additional 20 tumors from 15 patients from whom a paired adrenal sample was unavailable (total 47 PCC/PGL from 40 patients; Table 1 and Supplementary Table 2). We compared PCC/PGLs from patients with germline mutations in VHL, to tumors from patients with germline mutations in SDHx and those without a known germline mutation in a pseudohypoxia-linked gene. Cilia incidence was reduced in PCC/PGLs from patients with germline mutations in VHL (P=0.0007) and SDHx (P=0.0103 for incidence), relative to PCC/PGLs from patients that were not of a pseudohypoxia-linked subtype (Fig. 1G). Cilia length was also reduced in VHL- and SDHx-PCC/PGLs relative to the non-pseudohypoxia tumors, although this was only significant for VHL (P=0.0013) (Fig. 1H).

We also examined if there was any correlation between cilia loss and clinical disease parameters in patients with PCC/PGL. Patients under 18 years of age at the time of surgery had tumor cells with fewer and shorter cilia than patients who were over the age of 18 years (Supplementary Fig. 1C and D), suggesting an association between cilia loss

https://erc.bioscientifica.com
https://doi.org/10.1530/ERC-18-0134

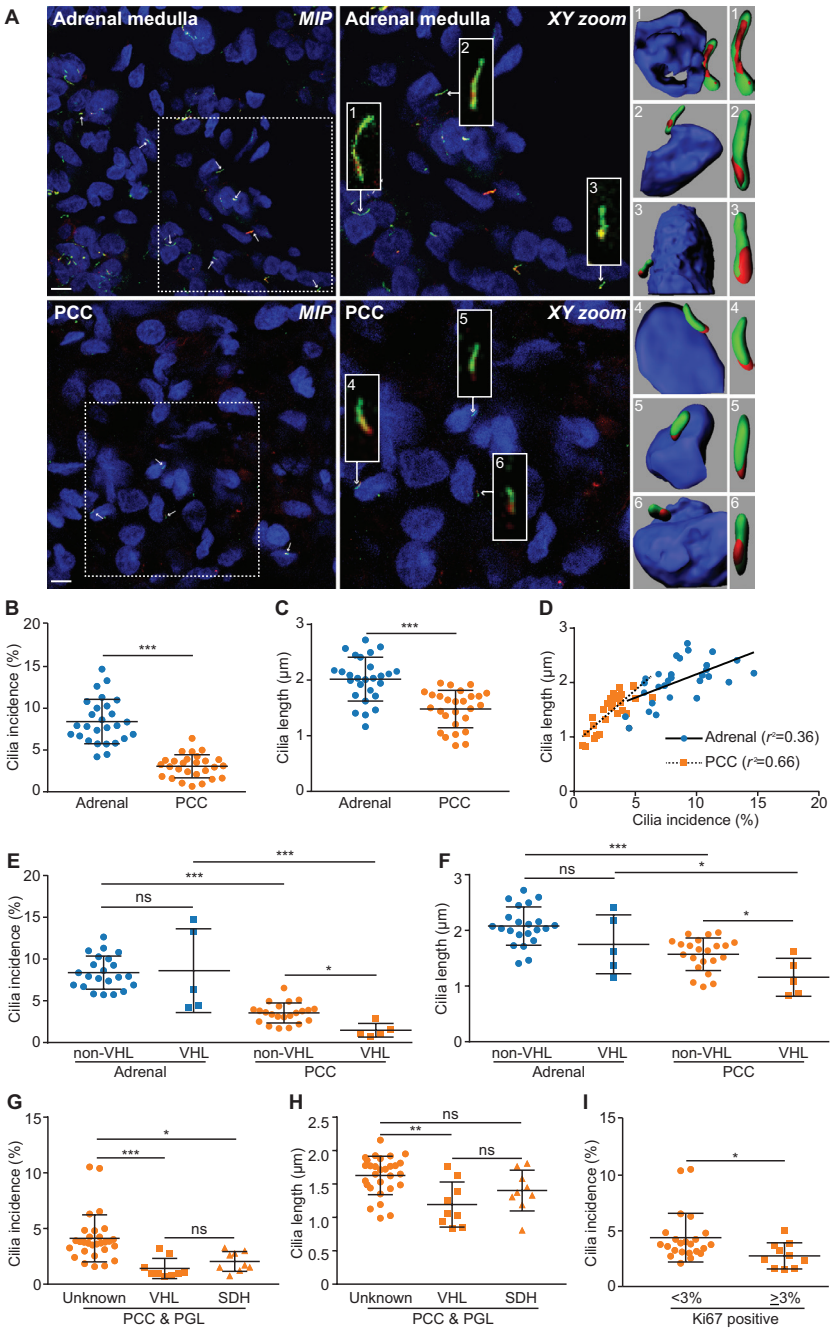

Figure 1

Primary cilia incidence and length is reduced in PCCs relative to adjacent adrenal medulla. (A) Maximum intensity projections (*MIP*) of confocal Z-stacks of PCC and adjacent adrenal medulla. Tissue sections were processed for dual-immunofluorescent detection of the ciliary markers acetylated α-tubulin (green) and Arl13b (red). They were then counterstained with DAPI (blue) to detect nuclei. A single confocal section from the area demarked by the dashed box is shown zoomed (*XY zoom*). Individual cilia, indicated by arrows, are further enlarged in insets 1–6 and are shown as surface rendered 3D images in the panels on the right. Scale bars = 10 µm. (B) Quantification of primary cilium incidence in 27 paired PCC and adjacent adrenal medulla tissue samples. (C) Quantification of axoneme length (from confocal Z-stacks) from cells that had a primary cilium in PCC and adjacent adrenal medulla. (D) Cilia incidence and length correlate in both PCCs and adjacent adrenal medulla, with a more significant relationship in tumor than normal tissue. (E and F) Cilia incidence and length in 27 paired PCCs and adrenal medulla samples comparing individuals with (n = 5) and without (n = 22) germline mutations in VHL. (G and H) Cilia incidence and length in 47 PCC/PGL comparing those with a germline mutations in VHL (n = 9), to tumors from patients with germline mutations in *SDHx* (n = 9) and those without a known germline mutation in a pseudohypoxia-linked gene (Con, n = 29). (I) Cilia incidence in 33 PCC where more or less than 3% of cells labeled positively for Ki67. The number of cilia and nuclei were counted in 15 randomly selected fields for each sample. Mean axonemal length was quantified from at least 50 ciliated cells for each sample. Error bars indicate S.D. Statistical tests: *t*-test (B, C, E, F and I), ANOVA (G and H), linear regression (D). $*P < 0.05$, $**P < 0.01$, $***P < 0.001$.

https://erc.bioscientifica.com
https://doi.org/10.1530/ERC-18-0134

and age (at time of surgery). As the presence of a primary cilium is potentially a checkpoint for cell division, we next tested if cilia loss correlated with cellular proliferation in PCC/PGLs. This was by quantifying the percentage of cells that labeled positively for Ki67 (quantified by routine clinical immunohistochemistry), a marker of proliferative activity that has previously been correlated with malignant potential in PCCs (Clarke *et al.* 1998, Kimura *et al.* 2014). Cilia incidence was reduced in PCCs/PGLs that had a Ki67 index of 3% or higher (P=0.0159) compared to PCC /PGLs with a lower Ki67 index (P=0.0159) (Fig. 1I). These data indicate that degree of cilia loss is linked to clinical parameters in PCC/PGLs.

Dysregulation of cilia-mediated signaling pathways in PCCs

We hypothesized that the reduced incidence and length of primary cilia in PCCs, relative to adrenal medulla, may result in alterations in cilia-mediated signaling. This was examined using RNA-Seq transcriptome analysis of 12 PCCs and adjacent adrenal medulla (Supplementary Table 1) to identify differentially expressed cilia-linked gene networks. We performed principal component analysis (PCA) on the filtered, normalized and transformed count matrix to explore the data's latent structure (Fig. 2A). This revealed that

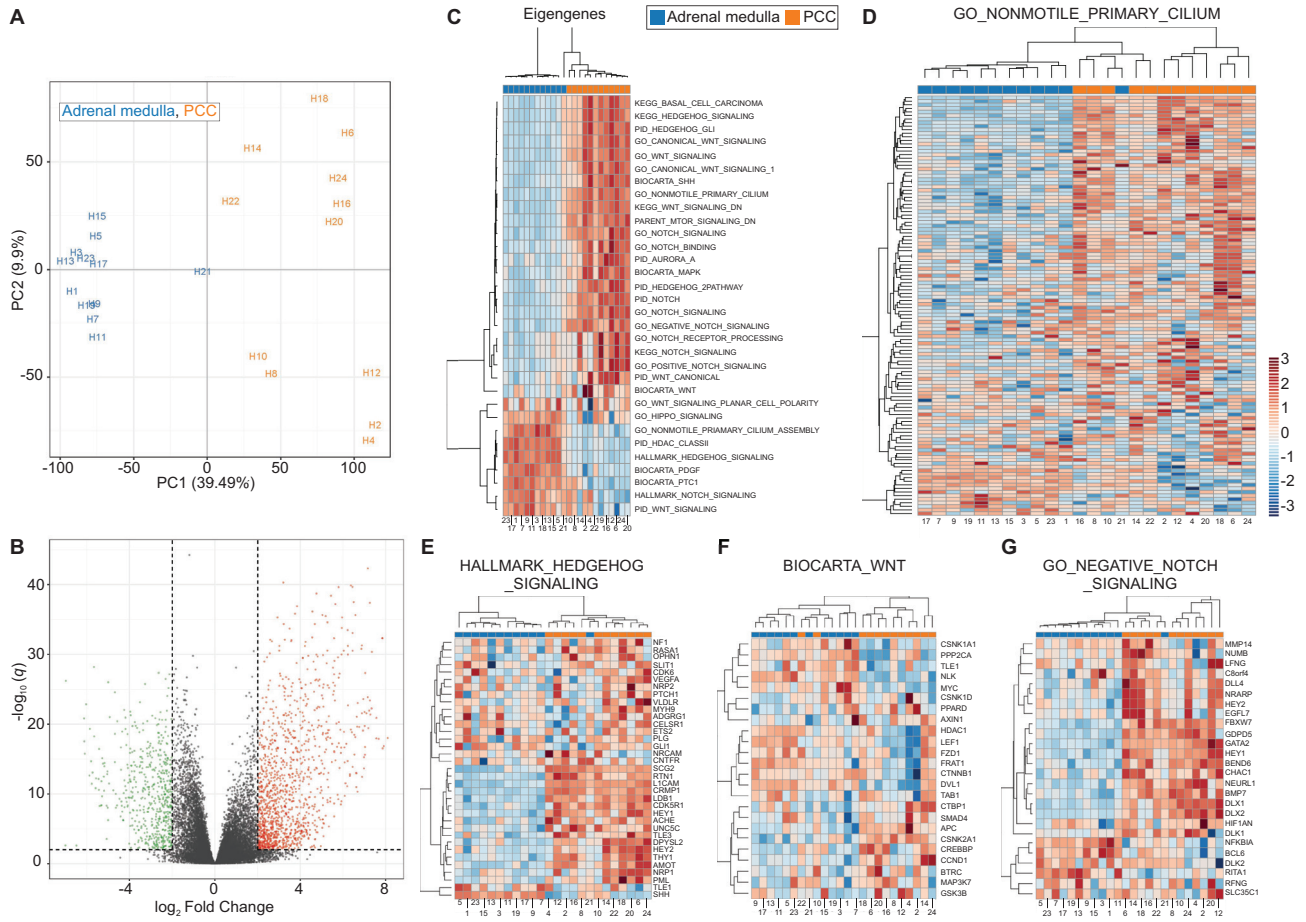

Figure 2
Changes in expression of cilia-linked genes in the transcriptomes of PCCs relative to adrenal medulla. (A) Principal component analysis (PCA) of RNA-seq expression data from 12 paired PCC and adjacent adrenal medulla tissue samples. (B) Volcano plot showing $\log_{10}$ FDR-adjusted q values versus $\log_2$ fold change between PCC and adjacent adrenal medulla. The vertical and horizontal dotted lines indicate 2× or −2× fold change and q = 0.01, respectively. (C) Heat map and hierarchical clustering depiction of all differentially expressed module eigengenes, from a collection of 32 gene sets known to be associated with cilia structure and cilia-mediated signaling, that are altered between PCCs and adjacent adrenal medulla. (D) Heat map and hierarchical clustering depiction of differentially expressed genes in the GO_NONMOTILE_PRIMARY_CILIUM pathway, comparing PCC and adjacent adrenal medulla samples. (E, F and G) Heat map and hierarchical clustering depictions of differentially expressed genes in three cilia-associated signaling pathways that are altered in PCCs relative to adjacent adrenal medulla: (E) HALLMARK_HEDGEHOG_SIGNALING; (F) BIOCARTA_WNT_PATHWAY; (G) GO_NEGATIVE_REGULATION_OF_NOTCH_SIGNALING_PATHWAY. Numbers shown at the bottom of the heat maps correspond to the sample IDs shown in the PCA (but are not prefixed with 'H').

https://erc.bioscientifica.com
https://doi.org/10.1530/ERC-18-0134

principal component 1, which accounts for nearly 40% of all variation in the counts, separated the PCC samples from adjacent adrenal medulla. PCC samples were spread along principal component 2, which accounts for over 10% of data variance, indicating a heterogeneity in this group that is absent in adjacent adrenal medulla, where samples cluster together more closely.

Our unsupervised analysis suggested a strong transcriptomic signal differentiating tumor and adrenal medulla samples. To quantify this and identify relevant biomarkers, we conducted differential expression analysis using the DESeq2 software package (Love *et al.* 2014). We defined a gene as differentially expressed if its absolute log fold change ≥2 and its q-value was ≤0.01, imposing a false discovery rate of 1%. This strict threshold ensured high specificity. Overall, 1839 genes met these criteria, representing some 8% of the transcriptome after filtering (Fig. 2B).

To test if cilia function was altered in PCC relative to adjacent adrenal medulla, we curated a collection of 32 gene sets known to be associated with cilia structure and cilia-mediated signaling. We found considerable enrichment among these pathways (14 out of 32 at $q \leq 0.1$). Eigengenes for all modules are depicted in Fig. 2C. Altered gene modules included those associated with cilia structure. For example, the GO_NONMOTILE_PRIMARY_CILIUM module showed altered expression in PCC tissue relative to adrenal medulla ($q=0.0519$) (Fig. 2D), suggesting changes in gene expression may contribute to cilia loss in PCCs. We also observed changes in the Aurora-A Gene module ($q=0.2365$), which is of interest as activation of Aurora-A pathway plays a role in regulation of cilia disassemble.

We also identified that gene modules associated with Hedgehog, Wnt and NOTCH signaling were altered between PCCs and adrenal medulla e.g. HALLMARK_HEDGEHOG_SIGNALING ($q=1.66\times10^{-7}$), BIOCARTA_WNT_PATHWAY ($q=0.0519$) and GO_NEGATIVE_REGULATION_OF_NOTCH_SIGNALING_PATHWAY ($q=1.58\times10^{-6}$). Analyses of these gene modules revealed significant upregulation and downregulation of individual genes (absolute log fold change ≥2, $q \leq 0.01$), while hierarchical clustering analyses separately grouped tumor and adrenal medulla samples in each of these pathways, with the exception of one medulla sample (H21) in the Hedgehog and Notch pathways, and two tumor samples (H10 and H22) in the Wnt pathway (Fig. 2D, E, F and G). These data are consistent with cilia-mediated signaling pathways being disrupted in PCC, but could also be explained by other potential mechanisms.

Disruption of primary cilia function in the PCC-derived PC12 cell line promotes proliferation and alters expression of tumorigenesis-linked gene networks

It is not fully resolved whether cilia loss is a driver or consequence of tumorigenesis. To address this question, in the context of PCC, we first established that PCC-derived cultured cell lines are able to form primary cilia. This was confirmed in the rat tumor-derived PC12 cell line, with cilia incidence and length increasing after serum starvation, such that 55.4 ± 5.98% of cells had a detectable cilium with a mean axonemal length of 2.17 ± 0.69 µm after 24 h (Fig. 3A, B, C and Supplementary Fig. 2A, B, C). Cilia were also present and responsive to serum starvation in two mouse PCC cell lines, MPC and MTT (Supplementary Fig. 2D, E and F). It should be noted that PC12 cells do not express the Myc dimerization partner MAX, while MPC and MTT lines were derived from the neurofibromatosis type 1 (NF1)-knockout mouse (Hopewell & Ziff 1995, Burnichon *et al.* 2012, Korpershoek *et al.* 2012).

We next disrupted cilia function in PC12 cells through siRNA-mediated knockdown of either the IFT88, a central component of the intraflagellar transport complex (Pazour *et al.* 2000), or Cep164, which plays a role in microtubule organization and/or maintenance for the formation of cilia (Graser *et al.* 2007). IFT88 knockdown was confirmed by immunoblot (Supplementary Fig. 3A and B), while knockdown of Cep164 was confirmed at the level of transcript (Supplementary Fig. 3C). Knockdown cells were then immunolabeled to detect cilia and stained with the proliferation marker Ki67 (Fig. 3D). Quantitative analysis confirmed, compared to control cells transfected with a non-targeting siRNA, that cilia incidence was reduced in both IFT88 ($P=0.02577$) and Cep 164-knockdown cells ($P=0.0.00222$) (Fig. 3E and H). Cilia length was also reduced in both instances (Supplementary Fig. 3D and E). Moreover, the percentage of Ki67-positive cells was increased after both IFT88 knockdown ($P=4.35\times10^{-12}$) and Cep164 knockdown ($P=0.03937$) (Fig. 3F and I). Increased proliferation of IFT88 and Cep164 knockdown PC12 cell, relative to controls, was further confirmed by quantification of cell numbers 48 h after siRNA transfection (Fig. 3G and J).

To further understand how disruption of cilia function impacts on cellular proliferation, we compared the transcriptomes of IFT88 knockdown and control cells (transfected with non-targeting siRNA) by RNA-Seq. Reads were pseudo-aligned (using the same pipeline as described for PCC and adrenal medulla) and

https://erc.bioscientifica.com
https://doi.org/10.1530/ERC-18-0134

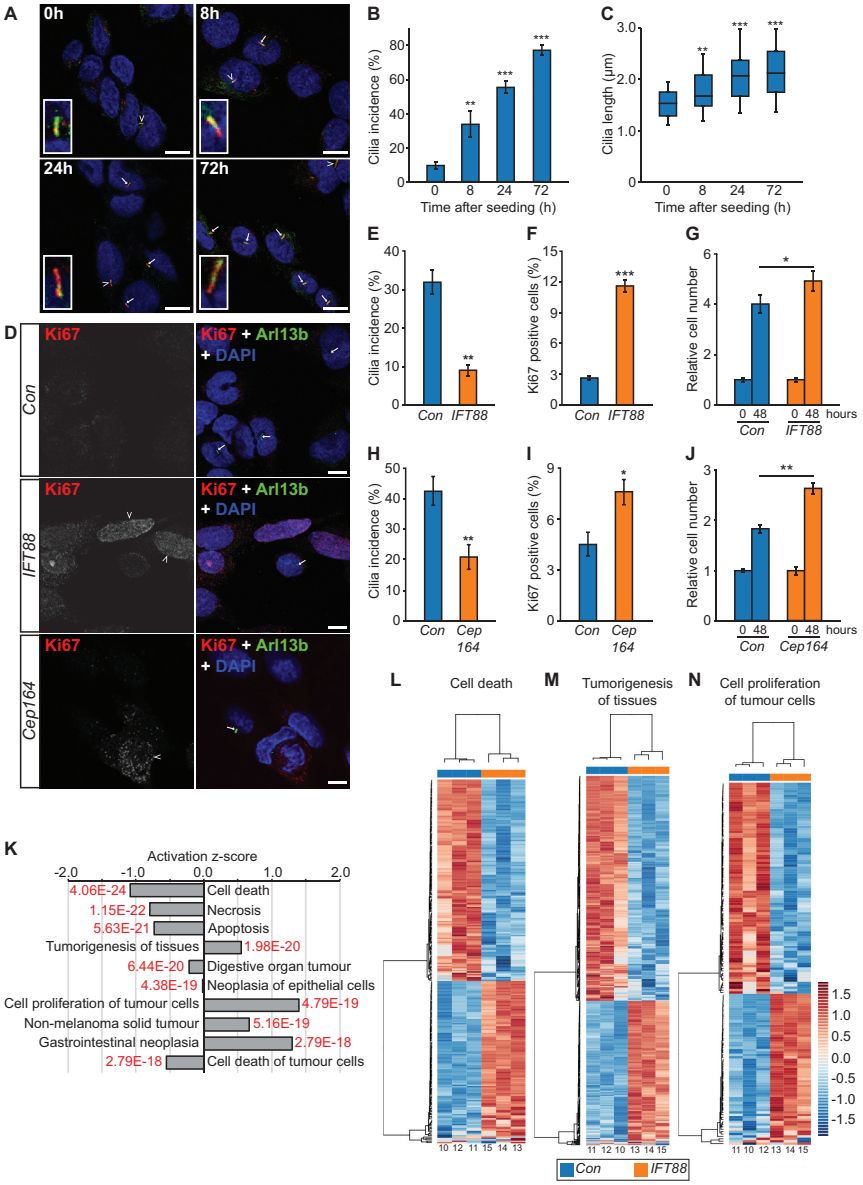

Figure 3

Loss of primary cilia in PC12 cells promotes proliferation and alters gene expression. (A) Confocal images of PC12 cells cultured in the absence of serum for between 0 and 72 h. Cells were immunolabeled with anti-acetylated α-tubulin (green) and anti-Arl13b (red) for detection of primary cilia. Nuclei were stained with DAPI (blue). Cilia are indicated by arrows, or arrowheads where they are also shown zoomed in the insets. Scale bars = 10μm. (B and C) Quantification of primary cilia incidence (B) and axonemal length (C) under conditions of serum starvation. (D) Confocal images of PC12 cells cultured for 48 h after transfection with siRNA targeting IFT88, Cep164, or non-targeting control siRNAs (Con). Cells were immunolabeled to detect cilia (Arl13b, green) and the proliferation marker Ki67 (red). Nuclei were stained with DAPI (blue). Cilia are indicated by arrows and Ki67 positive cells by arrowheads. Scale bars = 10 μm. (E, F, G and H) Quantification of primary cilia incidence (E), the percentage of Ki67 positive cells (F), and relative cell numbers (G), 48 h after transfection with siRNA targeting IFT88. (H, I and J) Quantification of primary cilia incidence (H), the percentage of Ki67 positive cells (I) and relative cell numbers (J), 48 h after transfection with siRNA targeting Cep164. Cilia and Ki67 scoring were performed in ten randomly selected fields for each experimental condition in three biological replicates. Mean axonemal length was quantified from at least 50 ciliated cells for each experimental condition. Cell counting was performed on six samples from three biological replicates. Error bars indicate 2× S.E.M. In box and whisker plots, the box represents median, upper and lower quartiles and the whiskers the 10th and 90th centiles. Statistical tests: ANOVA (B and C), *t*-test (E, F and G). $*P < 0.05$, $**P < 0.01$, $***P < 0.001$. (K) Gene Ontology (GO) analysis of the transcriptome of PC12 cells transfected with siRNA targeting IFT88 or non-targeting control siRNAs, showing the top-ranking altered biological processes identified by Ingenuity Pathways Analysis. *q* values are depicted in red ($E = 10$ to the power of the following number). (L and M) Heat map and hierarchical clustering depictions of differentially expressed genes in altered pathways with the GO terms cell death (L), tumorigenesis of tissues (M) and cell proliferation of tumor cells (N). Numbers shown at the bottom of the heat maps correspond to sample IDs shown in Supplementary Fig. 3.

https://erc.bioscientifica.com
https://doi.org/10.1530/ERC-18-0134

PCA performed. PC1 separated IFT88 knockdown and control cells, accounting for over 30% of the variation in the counts (Supplementary Fig. 3F). We found 662 genes differentially expressed at $q \leq 0.01$ (Supplementary Fig. 3G), representing some 6% of the transcriptome after filtering. Ingenuity pathways analysis was then used to identify statistically significant functions of the differentially regulated genes. This gene ontology (GO) analysis revealed that the top ten biological processes of these genes were related to cell death, cell proliferation and tumorigenesis. Moreover, activation *z*-scores suggested that cell death pathways were inhibited while proliferation and tumorigenesis pathways were induced (Fig. 3K). Hierarchical cluster analysis of gene modules described by the GO terms 'cell death', 'tumorigenesis of tissues', and 'cell proliferation of tumor cells' clearly separated IFT88-knockdown samples from controls (Fig. 3L, M and N). These data suggest that cilia loss promotes proliferation of PC12 cells.

PC12 cells resorb primary cilia under hypoxic conditions

Primary cilia incidence was most reduced in tumors with germline mutations in *VHL* and *SDHx* (Fig. 1G). This suggested that hypoxic signaling may be a driver of cilia loss. To test this hypothesis, we exposed ciliated PC12 cells (grown in serum-free conditions for 24 h) to normal cell culture oxygen levels (21% O_2) and hypoxic conditions (1% O_2). Cells were then immunolabeled to detect cilia. Subsequent confocal imaging and quantitative analysis demonstrated that culture of ciliated PC12 cells in 1% O_2 caused a reduction in cilia incidence ($P = 3.75 \times 10^{-15}$) and length ($P = 0.0106$) (Fig. 4A, B and C). This cilia resorption was shown to be transient, with PC12 cells able to reform primary cilia within 24 h of return to 21% O_2 (Fig. 4B and C). We also looked at the effect of oxygen levels on ciliogenesis. Cilia formation, induced by culture in serum-free conditions, was compared in cells maintained under normoxic (21% O_2) and hypoxic conditions (1% O_2). Lowered oxygen levels again resulted in cells having a reduction in cilia incidence ($P = 1.27 \times 10^{-5}$) and length ($P = 0.0075$) (Fig. 4D and E). To further confirm cilia loss occurred in PCC-derived cell lines cultured under hypoxic conditions, we immunolabeled MPC and MTT cells to detect cilia. In MPC and MTT cell lines, primary cilia incidence (MPC $P = 0.002$; MTT $P = 0.0351$) and length (MPC $P = 1.00 \times 10^{-15}$; MTT $P = 0.0001$) was reduced after transfer to 1% O_2 for 24 h (Supplementary Fig. 4).

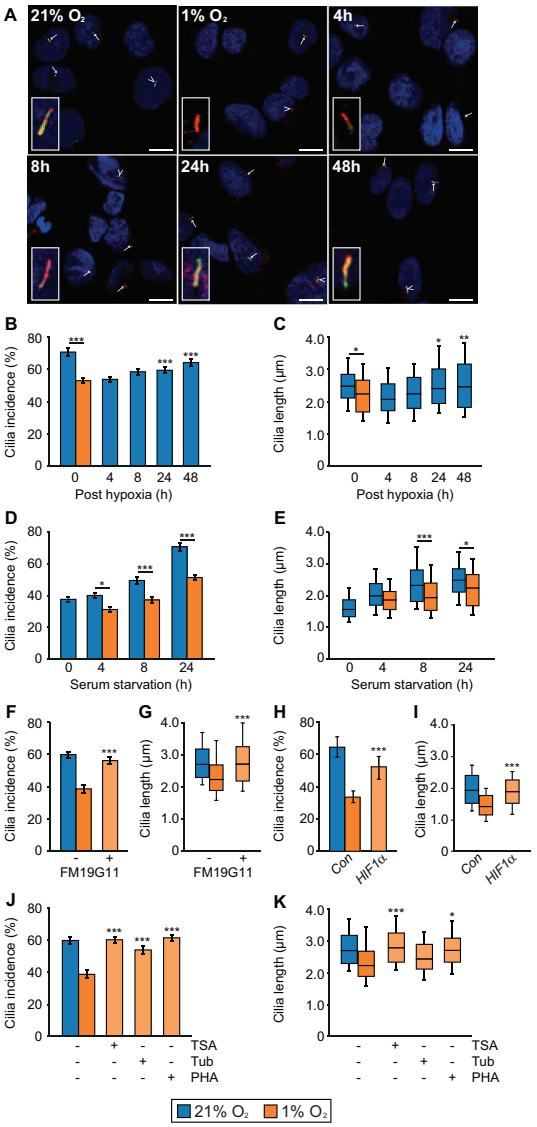

Figure 4
Primary cilia are lost from PC12 cells when oxygen levels are reduced. (A) Confocal images of PC12 cells cultured in 21% or 1% oxygen for 24 h, prior to return to 21% oxygen for 4, 8, 24 or 48 h before processing for the detection of primary cilia as in Fig. 3A. Scale bars = 10 μm. (B and C) Quantification of primary cilia incidence (B) and axonemal length (C) after 24 hours of culture in 21% and 1% oxygen and subsequent recovery in 21% oxygen. (D and E) Comparison of primary cilia incidence (D) and axonemal length (E) upon serum starvation after culture in 21% or 1% oxygen. (F and G) Quantification of primary cilia incidence (F) and axonemal length (G) after 24 h of culture in 1% oxygen in the presence of the HIFα inhibitor FM19G11 or vehicle only control. (H and I) Quantification of primary cilia incidence (H) and axonemal length (I) after 24 h of culture in 1% oxygen in cells transfected with non-targeting control siRNAs or siRNA targeting HIF1α. (J and K) Quantification of primary cilia incidence (J) and axonemal length (K) after 24 h of culture in 1% oxygen in the presence of the inhibitors trichostatin A (TSA), tubacin, PHA-680632 or vehicle only control. Cilia scoring was performed in ten randomly selected fields for each experimental condition in three biological replicates. Mean axonemal length was quantified from at least 50 ciliated cells for each experimental condition. Error bars indicate 2× S.E.M. Box and whisker plots are as in Fig. 3. Statistical tests: ANOVA. $*P < 0.05$, $**P < 0.01$, $***P < 0.001$.

https://erc.bioscientifica.com
https://doi.org/10.1530/ERC-18-0134

To investigate if the loss of primary cilia under hypoxic conditions was dependent on HIF-mediated signaling, we added the HIFα inhibitor FM19G11 (Moreno-Manzano *et al.* 2010) to culture media prior to transfer of cells to 1% O_2. Compared to vehicle-only-treated control cells, FM19G11 prevented hypoxia-induced cilia loss ($P=8.68\times10^{-5}$ for incidence, $P=7.08\times10^{-6}$ for length) (Fig. 4F, G and Supplementary Fig. 4D). We further tested a role for HIF1α signaling in hypoxia-induced cilia loss by targeting with siRNA. This showed that HIF1α knockdown was able to rescue cilia loss in PC12 cells cultured in 1% O_2 (Fig. 4H, I and Supplementary Fig. 4E, F). To further understand the mechanism of hypoxia-induced cilia loss, we next tested for involvement of the Aurora-A kinase /histone deacetylase 6 (HDAC6) pathway. Activation of Aurora-A has been shown to cause phosphorylation of HDAC6, which deacetylates ciliary tubulin and destabilizes the axonemal microtubules (Pugacheva *et al.* 2007). Inhibition of Aurora-A, with the specific inhibitor PHA-680632, prevented cilia loss ($P=1.85\times10^{-7}$) and shortening ($P=2.94\times10^{-6}$) in cells exposed to 1% O_2 (Fig. 4J, K and Supplementary Fig. 4D). Hypoxia-induced cilia loss was also inhibited by the mammalian class I and II HDAC inhibitor trichostatin A (TSA) ($P=3.22\times10^{-8}$ for incidence, $P=3.29\times10^{-8}$ for length) and the selective HDAC6 inhibitor tubacin ($P=1.11\times10^{-4}$ for incidence, $P=0.0487$ for length) (Fig. 4J, K and Supplementary Fig. 4D). These data suggest that reduced oxygen levels lead to cilia resorption in PC12 cells by a mechanism that includes HIF signaling and activation of the Aurora-A kinase/HDAC6 pathway.

In addition to degradation of HIF, pVHL stabilizes microtubules and plays a role in cilia maintenance. It is reported that loss of pVHL alone does not affect cilia structure but may sensitize cells to lose pre-established cilia (Thoma *et al.* 2007). pVHL has been shown to localize to the ciliary axoneme, and this was also the case in PC12 cells (Supplementary Fig. 4G). We thus investigated if activation of hypoxic signaling affected localization of pVHL by quantifying levels of the protein in the axoneme. Ciliary axonemes were detected by immunolabeling for acetylated tubulin and levels of pVHL that localized within the region of the cilia determined by analyses of fluorescent intensity. This showed that pVHL levels were reduced ($P=0.0234$) in the cilium of cells maintained at 1% O_2 relative to cells maintained at 21% O_2 (Supplementary Fig. 4H). Thus, activation of hypoxic signaling may also destabilize cilia through a mechanism where pVHL is reduced in the ciliary axoneme.

Pseudohypoxia in PC12 cells results in primary cilia loss and shortening

Under normoxic conditions HIFα is hydroxylated at conserved proline residues by HIF prolyl-hydroxylases (HIF-PHDs). This leads to recognition of HIFα by VHL, facilitating their ubiquitination and subsequent proteasomal degradation. Thus, direct inactivation of either HIF-PHDs or VHL can result in persistence of HIFα and transcription of HIF target genes even in the presence of oxygen – pseudohypoxia. Moreover, succinate, which accumulates as a result of loss of SDH function, inhibits HIF-PHDs, again resulting in pseudohypoxia (Fig. 5A). To establish if pseudohypoxia impacted primary cilia, we firstly targeted HIF-PHs by treating PC12 cells with the inhibitor dimethyloxalylglycine, N-(methoxyoxoacetyl)-glycine methyl ester (DMOG). This resulted in reduced cilia incidence ($P=3.86\times10^{-11}$) and length ($P=8.00\times10^{-14}$) (Fig. 5B, C and Supplementary Fig. 5A). We next tested if drivers of the pseudohypoxic PCC/PGL phenotype resulted in cilia loss. For SDHB, siRNA-mediated knockdown (Supplementary Fig. 5B, C and D) again leads to a reduction in cilia incidence ($P=1.20\times10^{-8}$) and length ($P=0.00124$) (Fig. 5D and E). Cilia loss also occurred in the presence of malonate, which competes with succinate for active sites of SDH (Fig. 5F, G and Supplementary Fig. 5E). Malonate inhibition of SDH can be reversed by pharmacologically elevating intracellular α-ketoglutarate (MacKenzie *et al.* 2007). Consistent with this, we observed that addition of α-ketoglutarate to PC12 cells rescued the cilia loss phenotype observed in cells treated with malonate alone (Fig. 5H, I and Supplementary Fig. 5E). Similar to succinate, accumulation of fumarate, another citric acid cycle intermediate, inhibits HIF-PHDs (this is also linked to disease as germline mutations in FH cause PCC/PGL). We inhibited FH using the cell-permeable derivative of fumarate, monomethyl fumarate. This again resulted in the reduction in cilia incidence ($P=1.67\times10^{-5}$) and length ($P=2.28\times10^{-17}$) (Fig. 5J, K and Supplementary Fig. 5F). The same pattern of reduced cilia incidence ($P=4.11\times10^{-6}$) and length ($P=5.75\times10^{-19}$) was observed when siRNA-mediated knockdown of FH (Supplementary Fig. 5G, H and I) was performed (Fig. 5L and M).

Finally, we investigated the effect of siRNA-mediated knockdown of VHL (Supplementary Fig. 5J, K and L) on primary cilia. Quantification of cilia incidence and length showed that VHL knockdown resulted in fewer cells exhibiting a cilium ($P=6.93\times10^{-13}$) and that mean cilia length was decreased ($P=8.12\times10^{-14}$) (Fig. 5N and O). In summary, these data show cilia loss was induced

https://erc.bioscientifica.com
https://doi.org/10.1530/ERC-18-0134

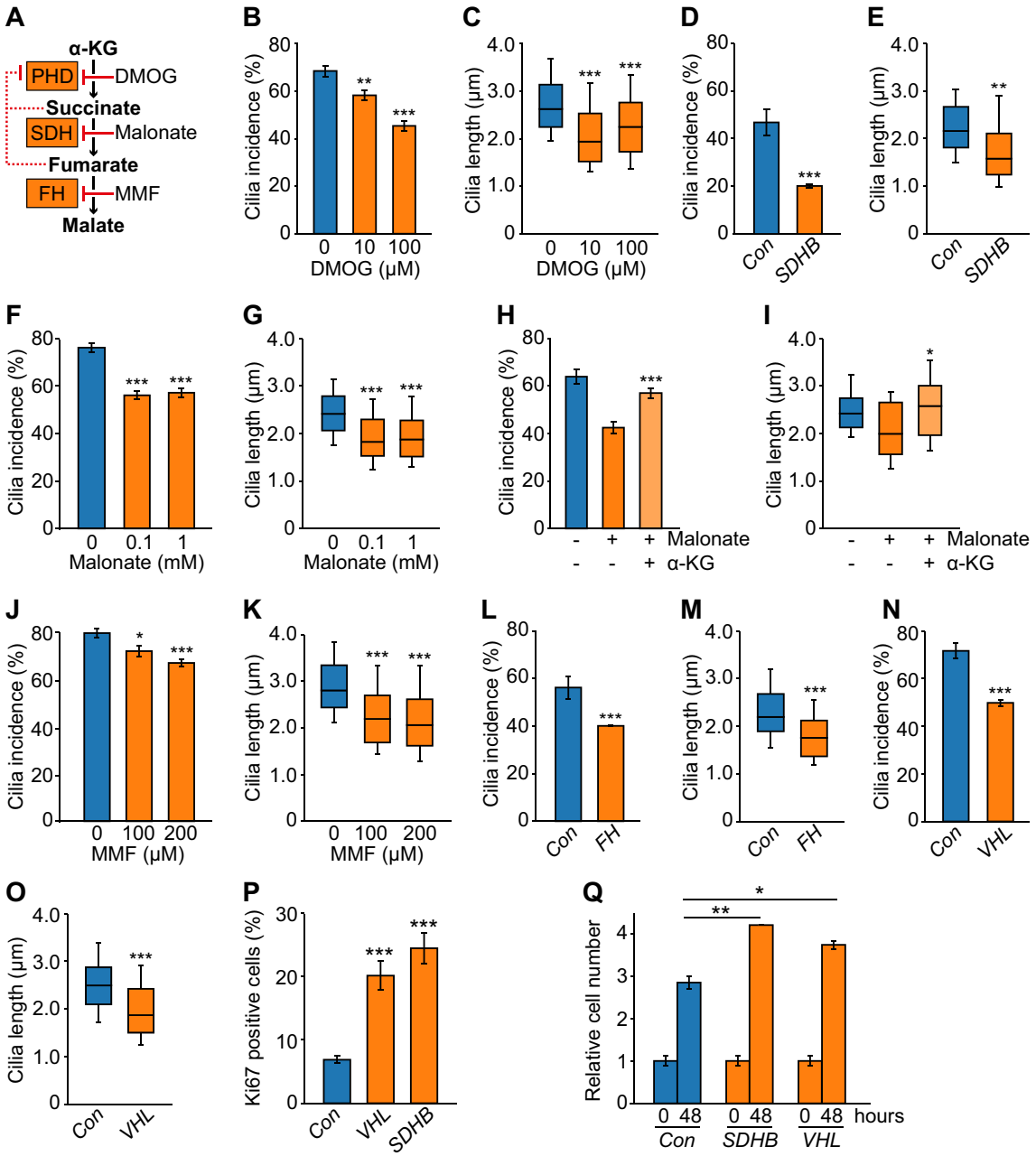

Figure 5

Inducers of pseudohypoxia cause primary cilia loss and shortening in PC12 cells. (A) Schematic showing PCC linked enzymes and inhibitors used to block their action. (B and C) Quantification of primary cilia incidence (B) and axonemal length (C) after 24 h of culture in the presence or absence of DMOG. (D and E) Quantification of primary cilia incidence (D) and axonemal length (E) 48 h after transfection with siRNAs targeting SDHB or non-targeting control siRNAs (*Con*). (F and G) Quantification of primary cilia incidence (F) and axonemal length (G) after 24 h of culture in the presence or absence of malonate. (H and I) Quantification of primary cilia incidence (H) and axonemal length (I) after 24 h of culture in the presence or absence of malonate (0.1 mM), with or without α-ketoglutarate (α-KG). (J and K) Quantification of primary cilia incidence (J) and axonemal length (K) after 24 h of culture in the presence or absence of monomethyl fumarate (MMF). (L, M, N and O) Quantification of primary cilia incidence (L and N) and axonemal length (M and O) 48 h after transfection with siRNAs targeting FH (L and M) or VHL (N and O) compared to non-targeting control siRNAs (*Con*). (P and Q) Quantification of the percentage of Ki67 positive cells (P) and of relative cell numbers (Q), 48 h after transfection with siRNAs targeting SDHB, VHL or control siRNAs. Cilia and Ki67 scoring was performed in ten randomly selected fields for each experimental condition in three biological replicates. Mean axonemal length was quantified from at least 50 ciliated cells for each experimental condition. Cell counting was performed on six samples from three biological replicates. Error bars indicate 2× S.E.M. Box and whisker plots are as in Fig. 3. Statistical tests: ANOVA (B, C, F, G, H, I, J, K, P, Q), *t*-test (D, E, L, M, N, O). $*P < 0.05$, $**P < 0.01$, $***P < 0.001$.

https://erc.bioscientifica.com
https://doi.org/10.1530/ERC-18-0134

by a number of different conditions that impair HIFα degradation, including those that lead to accumulation of oncometabolites. Importantly, knockdown of *Sdhb* and *Vhl* also resulted in increased Ki67 labeling and cell number, relative to control cells transfected with a non-targeting siRNA (Fig. 5P and Q). This is consistent with pseudohypoxia-induced cilia loss correlating with increased cellular proliferation.

Inhibition of both the Aurora-A/HDAC6 cilia resorption pathways and of hypoxic signaling prevents cilia loss in SDHB and VHL-knockdown cells

To understand why cilia incidence and length was reduced upon depletion of *SDHB* or *VHL*, we tested whether inhibition of the Aurora-A/HDAC6 pathway prevented cilia loss. PC12 cells were transfected with siRNAs targeting *Sdhb* or *Vhl* and then cultured in media containing PHA-680632, TSA, tubacin or vehicle only as a control. Forty-eight hours after transfection, cells were fixed and cilia were immunolabeled for confocal microscopy. Quantification of cilia incidence and length showed that treatment with the Aurora-A inhibitor PHA-680632 and the HDAC inhibitors TSA and tubacin reduced cilia loss and shortening in response to pVHL and SDHB (Fig. 6A, B, C, D and Supplementary Fig. 6) knockdown. Inhibition of HIF signaling with FM19G11 also reduced cilia loss in both *Sdhb*- and *Vhl*-depleted cells (Fig. 6A, B, C, D and Supplementary Fig. 6). Together, these data indicate that the Aurora-A/HDAC6 pathway is a modulator of cilia loss in PC12 cells depleted for SDHB or pVHL.

Discussion

Data presented here are the first to show that primary cilia are lost from PCCs compared to normal adjacent adrenal medulla. This corresponds with observations that primary cilia structure and function is disrupted in a broad range of cancers (O'Toole & Chapple 2016). These include breast, prostate, renal, pancreatic, melanoma, cholangiocarcinoma, glioblastoma, chondrosarcoma and colon cancer (Moser *et al.* 2009, Schraml *et al.* 2009, Seeley *et al.* 2009, Yuan *et al.* 2010, Kim *et al.* 2011, Gradilone *et al.* 2013, Hassounah *et al.* 2013, Ho *et al.* 2013, Rocha *et al.* 2014). In PCCs, the degree of cilia loss was more pronounced in tumors from patients with germline mutations in pseudohypoxia-linked genes *VHL* and *SDHB*. For pVHL, this may be partly explained by its reported non-canonical function in ciliogenesis, by orienting growth of microtubules toward the cell periphery (Schermer *et al.* 2006). Cilia frequency is also reduced relative to neighboring tissue in ccRCC. The *VHL* gene is inactivated in the majority (87%) of sporadic clear-cell RCCs (Moore *et al.* 2011), with ccRCCs also occurring as part of

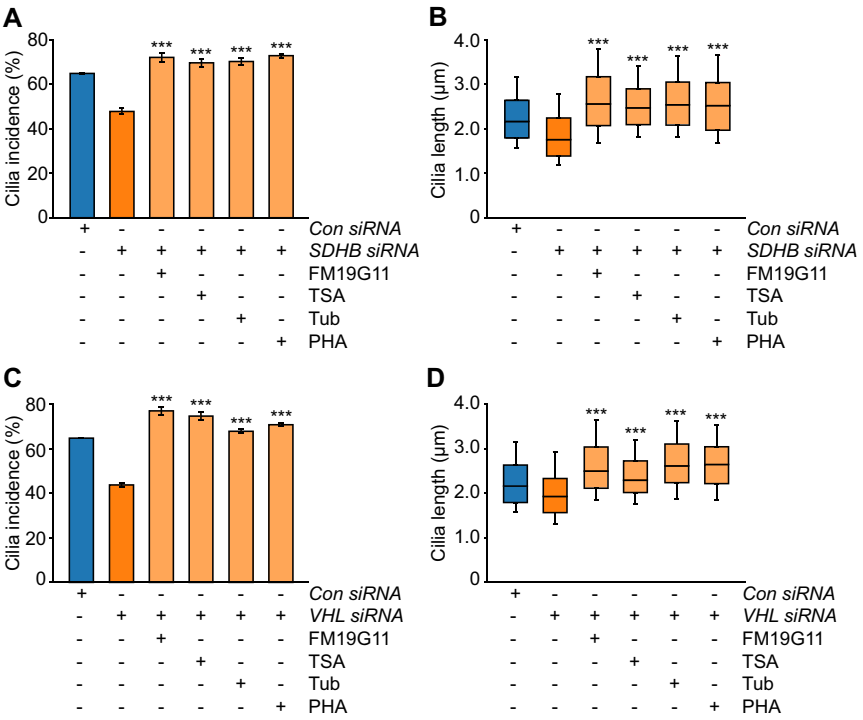

Figure 6
Inhibition of cilia resorption and hypoxic signaling prevents cilia loss caused by knockdown of SDHB and VHL. (A and B) Quantification of primary cilia incidence (A) and axonemal length (B) 48 h after transfection with siRNAs targeting SDHB in the presence or absence of the inhibitors FM19G11, TSA, tubacin (Tub) and PHA-680632 (PHA), or vehicle only controls. Cells transfected with non-targeting control siRNAs (*Con*) were treated with the same inhibitors. (C and D) Quantification of primary cilia incidence (C) and axonemal length (D) 48 h after transfection with siRNAs targeting VHL in the presence or absence of the inhibitors used in Fig. 6A and B. Cilia scoring was performed in ten randomly selected fields for each experimental condition in three biological replicates. Mean axonemal length was quantified from at least 50 ciliated cells for each experimental condition. Error bars indicate 2× S.E.M. Box and whisker plots are as in Fig. 3. Statistical tests: ANOVA. $*P < 0.05$, $**P < 0.01$, $***P < 0.001$.

https://erc.bioscientifica.com
https://doi.org/10.1530/ERC-18-0134

von Hippel–Lindau disease (Gossage *et al.* 2015, Crespigio *et al.* 2017). Contrasting ccRCC, *VHL* inactivation is a much less common feature of sporadic PCCs (Dannenberg *et al.* 2003, Burnichon *et al.* 2011). In the context of our data, this suggests that although disruption of a cilia-specific function of VHL may contribute to loss of cilia in PCC, it is not the main mechanism responsible for cilia loss.

Using the PCC-derived PC12 cell line, we found that siRNA-mediated depletion of SDHB, FH and VHL, all resulted in reduction of cilia frequency. We also observed that treatment of cells with drugs that inhibit HIF-PHs, SDH and FH, leading to accumulation of oncometabolites for SDH and FH, caused cilia loss. Culture of PC12 cells in conditions of reduced oxygen similarly reduced the incidence of cilia, although it should be noted the change in oxygen concentration from 21% (standard for cell culture) to 1% is greater than will to occur *in vivo*, where physiological levels of oxygen range from 2 to 9% (Tiede *et al.* 2011). Together, these data implicate pseudohypoxic /hypoxic signaling as a regulator of cilia dynamics. This is further supported by the finding that inhibition of HIF signaling reduced cilia loss in response to hypoxia and inducers of pseudohypoxia and is consistent with studies that show axoneme length is influenced by hypoxia-inducible mechanisms (Proulx-Bonneau & Annabi 2011, Wann *et al.* 2013). Hypoxia is not just a driver of PCC/PGL formation (Rodriguez-Cuevas *et al.* 1986, Opotowsky *et al.* 2015), but is also a salient feature of many solid tumors, and may therefore modulate cilia presence in cancers more generally.

There are a number of potential pathways through which HIF signaling could influence ciliogenesis and resorption. These include that stabilization of HIF promotes transcription of Aurora-A kinase, which functions in regulation of ciliary resorption with HDAC6 (Pugacheva *et al.* 2007, Xu *et al.* 2010). Inhibition of the Aurora-A/HDAC6 pathway in PC12 cells prevented cilia loss in response to hypoxia and induction of pseudohypoxia. Collectively, these findings suggest that the reduction in cilia frequency in pseudohypoxic PCC is likely to be mediated by both HIF signaling and the Aurora-A/HDAC6 cilia resorption pathway, although involvement of other regulators of cilia dynamics is also possible.

Transcriptome analyses identified altered expression of gene modules associated with cilia-mediated signaling in PCCs relative to adjacent adrenal medulla. Altered cilia-mediated signaling pathways included Hh, WNT and Notch signaling. The role of cilia in the regulation of cancer-linked signaling pathways is complex and context dependent (Oh & Katsanis 2013). For example, WNT signaling, which is generally considered to be attenuated by the presence of a cilium, can be decreased in cells with shortened cilia yet activated by ablation of cilia (Lancaster *et al.* 2011, Oh & Katsanis 2013), while for Hh signaling, the cilium activates the pathway in the presence of the sonic hedgehog ligand (SHH) and restrains signaling when SHH is absent (Wong *et al.* 2009, Hassounah *et al.* 2012). There is also crosstalk between cilia-mediated signaling pathways, such as Notch signaling modulating SHH signaling, by regulating the ciliary localization of the Hh signal transduction proteins patched and smoothened (Kong *et al.* 2015). This complexity makes it difficult to interpret how alterations in cilia incidence and length may impact on specific pathways. Nevertheless, hierarchical clustering analyses separately grouped tumor and adrenal medulla samples based on changes of gene expression in multiple cilia-linked signaling pathways. This is consistent with loss of cilia correlating with dysregulation of cilia-mediated signaling in PCCs. Disruption of WNT signaling is particularly relevant to PCC/PGLs, with WNT-altered tumors classified as one of four molecularly defined PCC/PGL subtypes (Fishbein *et al.* 2017).

In addition to modulating signaling pathways that are dysregulated in tumorigenesis and cancer, the presence of a primary cilium may act as a checkpoint for cell division. We observed that disruption of cilia structure and function, by knockdown of *Ift88* or *Cep164*, correlated with increased cellular proliferation of PC12 cells. This was accompanied by changes in gene expression that inhibited cell death pathways, while activating cell proliferation and tumor-linked pathways. Together, our data are concordant with cilia acting as a checkpoint for cell division in PC12 cells and suggest cilia loss promotes proliferation and perhaps tumorigenesis in PCC/PGL. Interestingly, we also observed that in PCC tissue, there was a correlation between degree of cilia loss and Ki67 staining implying *in vivo* relevance of our findings in PC12 cells.

In summary, we propose that in PCC/PGLs oncometabolite-induced pseudohypoxia drives cilia loss through activation of the Aurora-A kinase/HDAC6 cilia resorption pathway. In PCCs, this cilia loss causes dysregulation of cilia-mediated signaling pathways including SHH, WNT and Notch signaling and is also likely to promote increased cellular proliferation (Fig. 7). Hypoxia-induced cilia resorption may be a feature of cancers more generally and represents a potential target to slow tumor progression.

https://erc.bioscientifica.com
https://doi.org/10.1530/ERC-18-0134

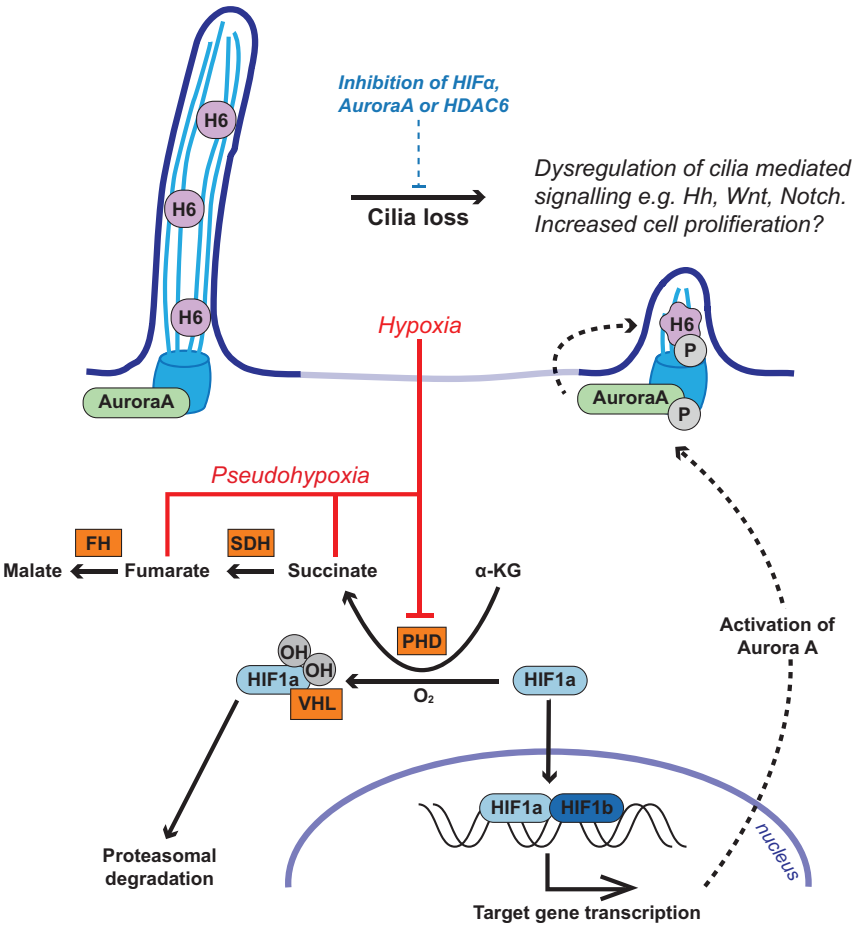

Figure 7
Model illustrating the potential pathway from pseudohypoxia-induced cilia loss to increased cell proliferation and dysregulation of tumorigenesis relevant cilia-mediated signaling pathways in PCCs. Proteins where germline mutations in the gene predispose to PCC are in orange boxes. Aurora-A, Aurora-A kinase; FH, fumarate hydratase; H6, HDAC6; HIF, hypoxia-inducible factor; OH, hydroxyl group; P, phosphate group; PH, prolyl-hydroxylases; SDH, succinate dehydrogenase; VHL, von Hippel–Lindau protein.

Supplementary data
This is linked to the online version of the paper at https://doi.org/10.1530/ERC-18-0134.

Declaration of interest
The authors declare that there is no conflict of interest that could be perceived as prejudicing the impartiality of the research reported.

Funding
This work was funded by a Barts and the London Charity Clinical Research Training Fellowships awarded to Samuel M O'Toole (grant number MRD0191) and by a project grant from the UK Medical Research Council (MRC) (grant number MR/L002876/1). Dr Tyson V Sharp is funded by grants from the UK Biotechnology and Biological Sciences Research Council (grant number BB/M0020611) and MRC (grant number MR/N009185/1). The LSM880 confocal used in these studies was purchased through a Barts and the London Charity award (grant number MGU0293). The RNA-Seq analyses were in part funded by a grant from The Medical College of Saint Bartholomew's Hospital Trust and were performed at the Barts and the London Genome Centre. This work also forms part of the research themes contributing to the translational research portfolio of Barts and the London Cardiovascular Biomedical Research Centre, which is supported and funded by the National Institute of Health Research. This project was enabled through access to the MRC eMedLab Medical Bioinformatics infrastructure, supported by the MRC (grant number MR/L016311/1).

Author contribution statement
S M O, P J K, M M K, T V S, U S, W M D and J P C conceived and planned the experiments. S M O, L E L R, T V N, T Y B and C L T carried out the experiments. S M O, D S W, M R B and J P C analyzed and interpreted the data. S M O and J P C wrote the draft manuscript. All authors provided critical feedback, which shaped the research, analysis and the manuscript.

Acknowledgements
The authors would like to thank the following clinical colleagues for collection of PCC and adrenal samples: Mr Robert Carpenter and Ms Laila Parvanta (St Bartholomew's Hospital, London); Mr Tom Kurzawinski and Mr Tarek Abdel-Aziz (University College London Hospitals, London); Prof. Michael Gleeson (National Hospital for Neurology and Neurosurgery). They are also extremely grateful to the patients who donated these tissues. The MPC and MTT cell lines where a gift from Dr Karel Pacak (NIH), via Professor Marta Korbonits (Queen Mary University of London). Prof. Korbonits was also principal investigator for ethical approvals related to this work. They would also like to thank Profs. Morris Brown, Jacky Burrin and Adrian Clark (Queen Mary University of London) for their constructive comments on the manuscript.

References

Basten SG, Willekers S, Vermaat JS, Slaats GG, Voest EE, van Diest PJ & Giles RH 2013 Reduced cilia frequencies in human renal cell carcinomas versus neighboring parenchymal tissue. *Cilia* **2** 2. (https://doi.org/10.1186/2046-2530-2-2)

Berbari NF, O'Connor AK, Haycraft CJ & Yoder BK 2009 The primary cilium as a complex signaling center. *Current Biology* **19** R526–R535. (https://doi.org/10.1016/j.cub.2009.05.025)

Burnichon N, Vescovo L, Amar L, Libe R, de Reynies A, Venisse A, Jouanno E, Laurendeau I, Parfait B, Bertherat J, *et al*. 2011 Integrative genomic analysis reveals somatic mutations in pheochromocytoma and paraganglioma. *Human Molecular Genetics* **20** 3974–3985. (https://doi.org/10.1093/hmg/ddr324)

Burnichon N, Cascon A, Schiavi F, Morales NP, Comino-Mendez I, Abermil N, Inglada-Perez L, de Cubas AA, Amar L, Barontini M, *et al*. 2012 MAX mutations cause hereditary and sporadic pheochromocytoma and paraganglioma. *Clinical Cancer Research* **18** 2828–2837. (https://doi.org/10.1158/1078-0432.CCR-12-0160)

Burnichon N, Buffet A & Gimenez-Roqueplo AP 2016 Pheochromocytoma and paraganglioma: molecular testing and personalized medicine. *Current Opinion in Oncology* **28** 5–10. (https://doi.org/10.1097/CCO.0000000000000249)

Clarke MR, Weyant RJ, Watson CG & Carty SE 1998 Prognostic markers in pheochromocytoma. *Human Pathology* **29** 522–526. (https://doi.org/10.1016/S0046-8177(98)90070-3)

Crespigio J, Berbel LCL, Dias MA, Berbel RF, Pereira SS, Pignatelli D & Mazzuco TL 2017 Von Hippel-Lindau disease: a single gene, several hereditary tumors. *Journal of Endocrinological Investigation* **41** 21–31. (https://doi.org/10.1007/s40618-017-0683-1)

Dahia PL 2017 Pheochromocytomas and paragangliomas, genetically diverse and minimalist, all at once! *Cancer Cell* **31** 159–161. (https://doi.org/10.1016/j.ccell.2017.01.009)

Dannenberg H, De Krijger RR, van der Harst E, Abbou M, Ijzendoorn Y, Komminoth P & Dinjens WN 2003 Von Hippel-Lindau gene alterations in sporadic benign and malignant pheochromocytomas. *International Journal of Cancer* **105** 190–195. (https://doi.org/10.1002/ijc.11060)

Fishbein L & Nathanson KL 2012 Pheochromocytoma and paraganglioma: understanding the complexities of the genetic background. *Cancer Genetics* **205** 1–11. (https://doi.org/10.1016/j.cancergen.2012.01.009)

Fishbein L, Leshchiner I, Walter V, Danilova L, Robertson AG, Johnson AR, Lichtenberg TM, Murray BA, Ghayee HK, Else T, *et al*. 2017 Comprehensive molecular characterization of pheochromocytoma and paraganglioma. *Cancer Cell* **31** 181–193. (https://doi.org/10.1016/j.ccell.2017.01.001)

Goetz SC & Anderson KV 2010 The primary cilium: a signalling centre during vertebrate development. *Nature Reviews Genetics* **11** 331–344. (https://doi.org/10.1038/nrg2774)

Gossage L, Eisen T & Maher ER 2015 VHL, the story of a tumour suppressor gene. *Nature Reviews Cancer* **15** 55–64. (https://doi.org/10.1038/nrc3844)

Goto H, Inoko A & Inagaki M 2013 Cell cycle progression by the repression of primary cilia formation in proliferating cells. *Cellular and Molecular Life Sciences* **70** 3893–3905. (https://doi.org/10.1007/s00018-013-1302-8)

Gradilone SA, Radtke BN, Bogert PS, Huang BQ, Gajdos GB & LaRusso NF 2013 HDAC6 inhibition restores ciliary expression and decreases tumor growth. *Cancer Research* **73** 2259–2270. (https://doi.org/10.1158/0008-5472.CAN-12-2938)

Graser S, Stierhof YD, Lavoie SB, Gassner OS, Lamla S, Le Clech M & Nigg EA 2007 Cep164, a novel centriole appendage protein required for primary cilium formation. *Journal of Cell Biology* **179** 321–330. (https://doi.org/10.1083/jcb.200707181)

Hassounah NB, Bunch TA & McDermott KM 2012 Molecular pathways: the role of primary cilia in cancer progression and therapeutics with a focus on Hedgehog signaling. *Clinical Cancer Research* **18** 2429–2435. (https://doi.org/10.1158/1078-0432.CCR-11-0755)

Hassounah NB, Nagle R, Saboda K, Roe DJ, Dalkin BL & McDermott KM 2013 Primary cilia are lost in preinvasive and invasive prostate cancer. *PLoS ONE* **8** e68521. (https://doi.org/10.1371/journal.pone.0068521)

Ho L, Ali SA, Al-Jazrawe M, Kandel R, Wunder JS & Alman BA 2013 Primary cilia attenuate hedgehog signalling in neoplastic chondrocytes. *Oncogene* **32** 5388–5396. (https://doi.org/10.1038/onc.2012.588)

Hopewell R & Ziff EB 1995 The nerve growth factor-responsive PC12 cell line does not express the Myc dimerization partner Max. *Molecular and Cellular Biology* **15** 3470–3478. (https://doi.org/10.1128/MCB.15.7.3470)

Huber W, Carey VJ, Gentleman R, Anders S, Carlson M, Carvalho BS, Bravo HC, Davis S, Gatto L, Girke T, *et al*. 2015 Orchestrating high-throughput genomic analysis with bioconductor. *Nature Methods* **12** 115–121. (https://doi.org/10.1038/nmeth.3252)

Izawa I, Goto H, Kasahara K & Inagaki M 2015 Current topics of functional links between primary cilia and cell cycle. *Cilia* **4** 12. (https://doi.org/10.1186/s13630-015-0021-1)

Johnson CA, Collis SJ 2016 Ciliogenesis and the DNA damage response: a stressful relationship. *Cilia* **5** 19. (https://doi.org/10.1186/s13630-016-0040-6)

Kim J, Dabiri S & Seeley ES 2011 Primary cilium depletion typifies cutaneous melanoma in situ and malignant melanoma. *PLoS ONE* **6** e27410. (https://doi.org/10.1371/journal.pone.0027410)

Kimura N, Takayanagi R, Takizawa N, Itagaki E, Katabami T, Kakoi N, Rakugi H, Ikeda Y, Tanabe A, Nigawara T, *et al*. 2014 Pathological grading for predicting metastasis in phaeochromocytoma and paraganglioma. *Endocrine-Related Cancer* **21** 405–414. (https://doi.org/10.1530/ERC-13-0494)

Kong JH, Yang L, Dessaud E, Chuang K, Moore DM, Rohatgi R, Briscoe J & Novitch BG 2015 Notch activity modulates the responsiveness of neural progenitors to sonic hedgehog signaling. *Developmental Cell* **33** 373–387. (https://doi.org/10.1016/j.devcel.2015.03.005)

Korpershoek E, Pacak K & Martiniova L 2012 Murine models and cell lines for the investigation of pheochromocytoma: applications for future therapies? *Endocrine Pathology* **23** 43–54. (https://doi.org/10.1007/s12022-012-9194-y)

Lancaster MA, Schroth J & Gleeson JG 2011 Subcellular spatial regulation of canonical Wnt signalling at the primary cilium. *Nature Cell Biology* **13** 700–707. (https://doi.org/10.1038/ncb2259)

Love MI, Huber W & Anders S 2014 Moderated estimation of fold change and dispersion for RNA-seq data with DESeq2. *Genome Biology* **15** 550. (https://doi.org/10.1186/s13059-014-0550-8)

MacKenzie ED, Selak MA, Tennant DA, Payne LJ, Crosby S, Frederiksen CM, Watson DG & Gottlieb E 2007 Cell-permeating alpha-ketoglutarate derivatives alleviate pseudohypoxia in succinate dehydrogenase-deficient cells. *Molecular and Cellular Biology* **27** 3282–3289. (https://doi.org/10.1128/MCB.01927-06)

Mans DA, Voest EE & Giles RH 2008 All Along the Watchtower: is the cilium a tumor suppressor organelle? *Biochimica et Biophysica Acta* **1786** 114–125. (https://doi.org/10.1016/j.bbcan.2008.02.002)

Moore LE, Nickerson ML, Brennan P, Toro JR, Jaeger E, Rinsky J, Han SS, Zaridze D, Matveev V, Janout V, *et al*. 2011 Von Hippel-Lindau (VHL) inactivation in sporadic clear cell renal cancer: associations with germline VHL polymorphisms and etiologic risk factors. *PLoS Genetics* **7** e1002312. (https://doi.org/10.1371/journal.pgen.1002312)

Moreno-Manzano V, Rodriguez-Jimenez FJ, Acena-Bonilla JL, Fustero-Lardies S, Erceg S, Dopazo J, Montaner D, Stojkovic M & Sanchez-Puelles JM 2010 FM19G11, a new hypoxia-inducible factor (HIF) modulator, affects stem cell differentiation status. *Journal of Biological Chemistry* **285** 1333–1342. (https://doi.org/10.1074/jbc.M109.008326)

Moser JJ, Fritzler MJ & Rattner JB 2009 Primary ciliogenesis defects are associated with human astrocytoma/glioblastoma cells. *BMC Cancer* **9** 448. (https://doi.org/10.1186/1471-2407-9-448)

Oh EC & Katsanis N 2013 Context-dependent regulation of Wnt signaling through the primary cilium. *Journal of the American Society of Nephrology* **24** 10–18. (https://doi.org/10.1681/ASN.2012050526)

https://erc.bioscientifica.com
https://doi.org/10.1530/ERC-18-0134

Opotowsky AR, Moko LE, Ginns J, Rosenbaum M, Greutmann M, Aboulhosn J, Hageman A, Kim Y, Deng LX, Grewal J, *et al*. 2015 Pheochromocytoma and paraganglioma in cyanotic congenital heart disease. *Journal of Clinical Endocrinology and Metabolism* **100** 1325–1334. (https://doi.org/10.1210/jc.2014-3863)

O'Toole SM & Chapple JP 2016 Primary cilia: a link between hormone signalling and endocrine-related cancers? *Biochemical Society Transactions* **44** 1227–1234. (https://doi.org/10.1042/BST20160149)

Pazour GJ, Dickert BL, Vucica Y, Seeley ES, Rosenbaum JL, Witman GB & Cole DG 2000 Chlamydomonas IFT88 and its mouse homologue, polycystic kidney disease gene tg737, are required for assembly of cilia and flagella. *Journal of Cell Biology* **151** 709–718. (https://doi.org/10.1083/jcb.151.3.709)

Proulx-Bonneau S & Annabi B 2011 The primary cilium as a biomarker in the hypoxic adaptation of bone marrow-derived mesenchymal stromal cells: a role for the secreted frizzled-related proteins. *Biomark Insights* **6** 107–118. (https://doi.org/10.4137/BMI.S8247)

Pugacheva EN, Jablonski SA, Hartman TR, Henske EP & Golemis EA 2007 HEF1-dependent Aurora A activation induces disassembly of the primary cilium. *Cell* **129** 1351–1363. (https://doi.org/10.1016/j.cell.2007.04.035)

Rocha C, Papon L, Cacheux W, Marques Sousa P, Lascano V, Tort O, Giordano T, Vacher S, Lemmers B, Mariani P, *et al*. 2014 Tubulin glycylases are required for primary cilia, control of cell proliferation and tumor development in colon. *EMBO Journal* **33** 2247–2260. (https://doi.org/10.15252/embj.201488466)

Rodriguez-Cuevas H, Lau I & Rodriguez HP 1986 High-altitude paragangliomas diagnostic and therapeutic considerations. *Cancer* **57** 672–676. (https://doi.org/10.1002/1097-0142(19860201)57:3<672::AID-CNCR2820570346>3.0.CO;2-C)

Schermer B, Ghenoiu C, Bartram M, Muller RU, Kotsis F, Hohne M, Kuhn W, Rapka M, Nitschke R, Zentgraf H, *et al*. 2006 The von Hippel-Lindau tumor suppressor protein controls ciliogenesis by orienting microtubule growth. *Journal of Cell Biology* **175** 547–554. (https://doi.org/10.1083/jcb.200605092)

Schraml P, Frew IJ, Thoma CR, Boysen G, Struckmann K, Krek W & Moch H 2009 Sporadic clear cell renal cell carcinoma but not the papillary type is characterized by severely reduced frequency of primary cilia. *Modern Pathology* **22** 31–36. (https://doi.org/10.1038/modpathol.2008.132)

Seeley ES, Carriere C, Goetze T, Longnecker DS & Korc M 2009 Pancreatic cancer and precursor pancreatic intraepithelial neoplasia lesions are devoid of primary cilia. *Cancer Research* **69** 422–430. (https://doi.org/10.1158/0008-5472.CAN-08-1290)

Selak MA, Armour SM, MacKenzie ED, Boulahbel H, Watson DG, Mansfield KD, Pan Y, Simon MC, Thompson CB & Gottlieb E 2005 Succinate links TCA cycle dysfunction to oncogenesis by inhibiting HIF-alpha prolyl hydroxylase. *Cancer Cell* **7** 77–85. (https://doi.org/10.1016/j.ccr.2004.11.022)

Thoma CR, Frew IJ, Hoerner CR, Montani M, Moch H & Krek W 2007 pVHL and GSK3beta are components of a primary cilium-maintenance signalling network. *Nature Cell Biology* **9** 588–595. (https://doi.org/10.1038/ncb1579)

Tiede LM, Cook EA, Morsey B & Fox HS 2011 Oxygen matters: tissue culture oxygen levels affect mitochondrial function and structure as well as responses to HIV viroproteins. *Cell Death and Disease* **2** e246. (https://doi.org/10.1038/cddis.2011.128)

Wann AK, Thompson CL, Chapple JP & Knight MM 2013 Interleukin-1beta sequesters hypoxia inducible factor 2alpha to the primary cilium. *Cilia* **2** 17. (https://doi.org/10.1186/2046-2530-2-17)

Wong SY, Seol AD, So PL, Ermilov AN, Bichakjian CK, Epstein EH, Jr., Dlugosz AA & Reiter JF 2009 Primary cilia can both mediate and suppress Hedgehog pathway-dependent tumorigenesis. *Nature Medicine* **15** 1055–1061. (https://doi.org/10.1038/nm.2011)

Xu J, Li H, Wang B, Xu Y, Yang J, Zhang X, Harten SK, Shukla D, Maxwell PH, Pei D, *et al*. 2010 VHL inactivation induces HEF1 and Aurora kinase A. *Journal of the American Society of Nephrology* **21** 2041–2046. (https://doi.org/10.1681/ASN.2010040345)

Yuan K, Frolova N, Xie Y, Wang D, Cook L, Kwon YJ, Steg AD, Serra R & Frost AR 2010 Primary cilia are decreased in breast cancer: analysis of a collection of human breast cancer cell lines and tissues. *Journal of Histochemistry and Cytochemistry* **58** 857–870. (https://doi.org/10.1369/jhc.2010.955856)

Received in final form 27 August 2018
Accepted 5 September 2018
Accepted Preprint published online 7 September 2018

Assay Class: Eukaryote Total RNA Nano
Data Path: C:\...Data\2016-09-15\Eukaryote Total RNA Nano_2016-09-15_001.xad

Created: 15/09/2016 14:43:44
Modified: 15/09/2016 15:07:37

Electrophoresis File Run Summary

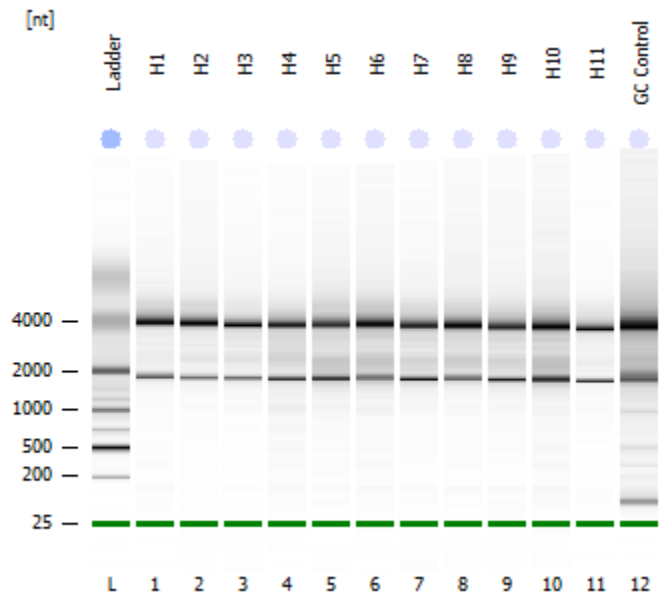

Instrument Information:

Instrument Name: DE72901262 Firmware: C.01.069
Serial#: DE72901262 Type: G2939A

Assay Information:

Assay Origin Path: C:\Program Files (x86)\Agilent\2100 bioanalyzer\2100 expert\assays\RNA\Eukaryote Total RNA Nano Series II.xsy

Assay Class: Eukaryote Total RNA Nano

Version: 2.6

Assay Comments: Total RNA Analysis ng sensitivity (Eukaryote)

Chip Information:

Chip Lot #:

Reagent Kit Lot #:

Chip Comments:

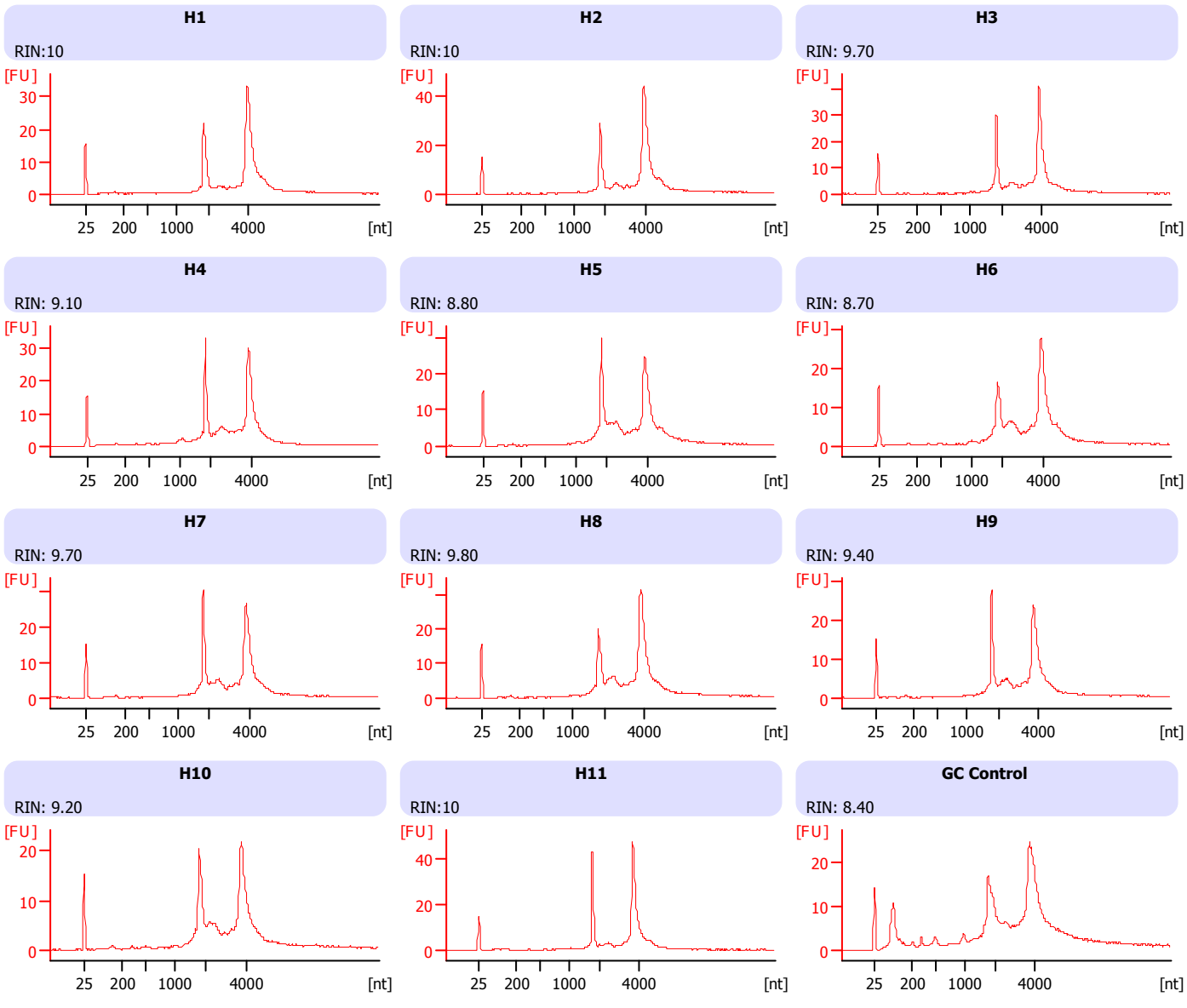

  Printed: 15/09/2016 15:07:50

Assay Class: Eukaryote Total RNA Nano
Data Path: C:\...Data\2016-09-15\Eukaryote Total RNA Nano_2016-09-15_001.xad

Created: 15/09/2016 14:43:44
Modified: 15/09/2016 15:07:37

Electrophoresis File Run Summary (Chip Summary)

Sample Name	Sample Comment	Status	Result Label	Result Color
H1		✓	RIN:10	
H2		✓	RIN:10	
H3		✓	RIN: 9.70	
H4		✓	RIN: 9.10	
H5		✓	RIN: 8.80	
H6		✓	RIN: 8.70	
H7		✓	RIN: 9.70	
H8		✓	RIN: 9.80	
H9		✓	RIN: 9.40	
H10		✓	RIN: 9.20	
H11		✓	RIN:10	
GC Control		✓	RIN: 8.40	
Ladder		✓	All Other Samples	

Chip Lot #

Reagent Kit Lot #

Chip Comments :

Assay Class: Eukaryote Total RNA Nano Created: 15/09/2016 14:43:44
Data Path: C:\...Data\2016-09-15\Eukaryote Total RNA Nano_2016-09-15_001.xad Modified: 15/09/2016 15:07:37

Electrophoresis Assay Details

General Analysis Settings

Number of Available Sample and Ladder Wells (Max.) : 13
Minimum Visible Range [s] : 17
Maximum Visible Range [s] : 70
Start Analysis Time Range [s] : 19
End Analysis Time Range [s] : 69
Ladder Concentration [ng/µl] : 150
Lower Marker Concentration [ng/µl] : 0
Upper Marker Concentration [ng/µl] : 0
Used Lower Marker for Quantitation
Standard Curve Fit is Logarithmic
Show Data Aligned to Lower Marker

Integrator Settings

Integration Start Time [s] : 19
Integration End Time [s] : 69
Slope Threshold : 0.6
Height Threshold [FU] : 0.5
Area Threshold : 0.2
Width Threshold [s] : 0.5
Baseline Plateau [s] : 6

Filter Settings

Filter Width [s] : 0.5
Polynomial Order : 4

Ladder

Ladder Peak	Size
1	25
2	200
3	500
4	1000
5	2000
6	4000

Assay Class: Eukaryote Total RNA Nano
Data Path: C:\...Data\2016-09-19\Eukaryote Total RNA Nano_2016-09-19_002.xad

Created: 19/09/2016 15:25:55
Modified: 19/09/2016 15:49:01

Electrophoresis File Run Summary

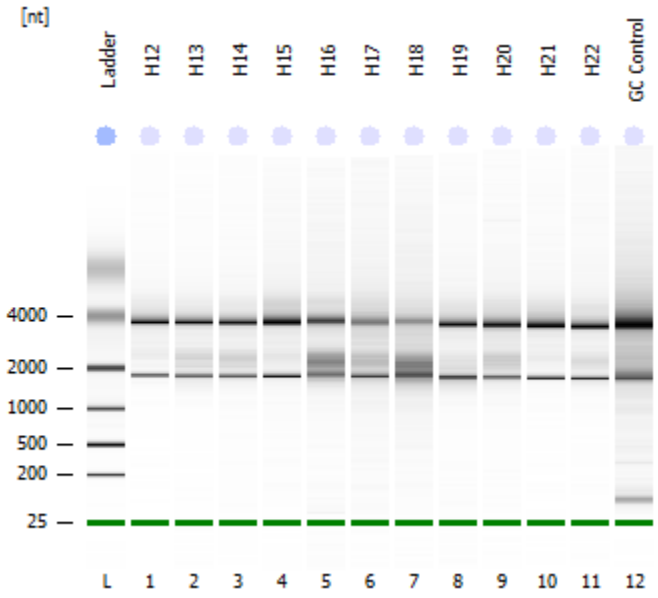

Instrument Information:

Instrument Name: DE72901262 Firmware: C.01.069
Serial#: DE72901262 Type: G2939A

Assay Information:

Assay Origin Path: C:\Program Files (x86)\Agilent\2100 bioanalyzer\2100 expert\assays\RNA\Eukaryote Total RNA Nano Series II.xsy

Assay Class: Eukaryote Total RNA Nano

Version: 2.6

Assay Comments: Total RNA Analysis ng sensitivity (Eukaryote)

Chip Information:

Chip Lot #:

Reagent Kit Lot #:

Chip Comments:

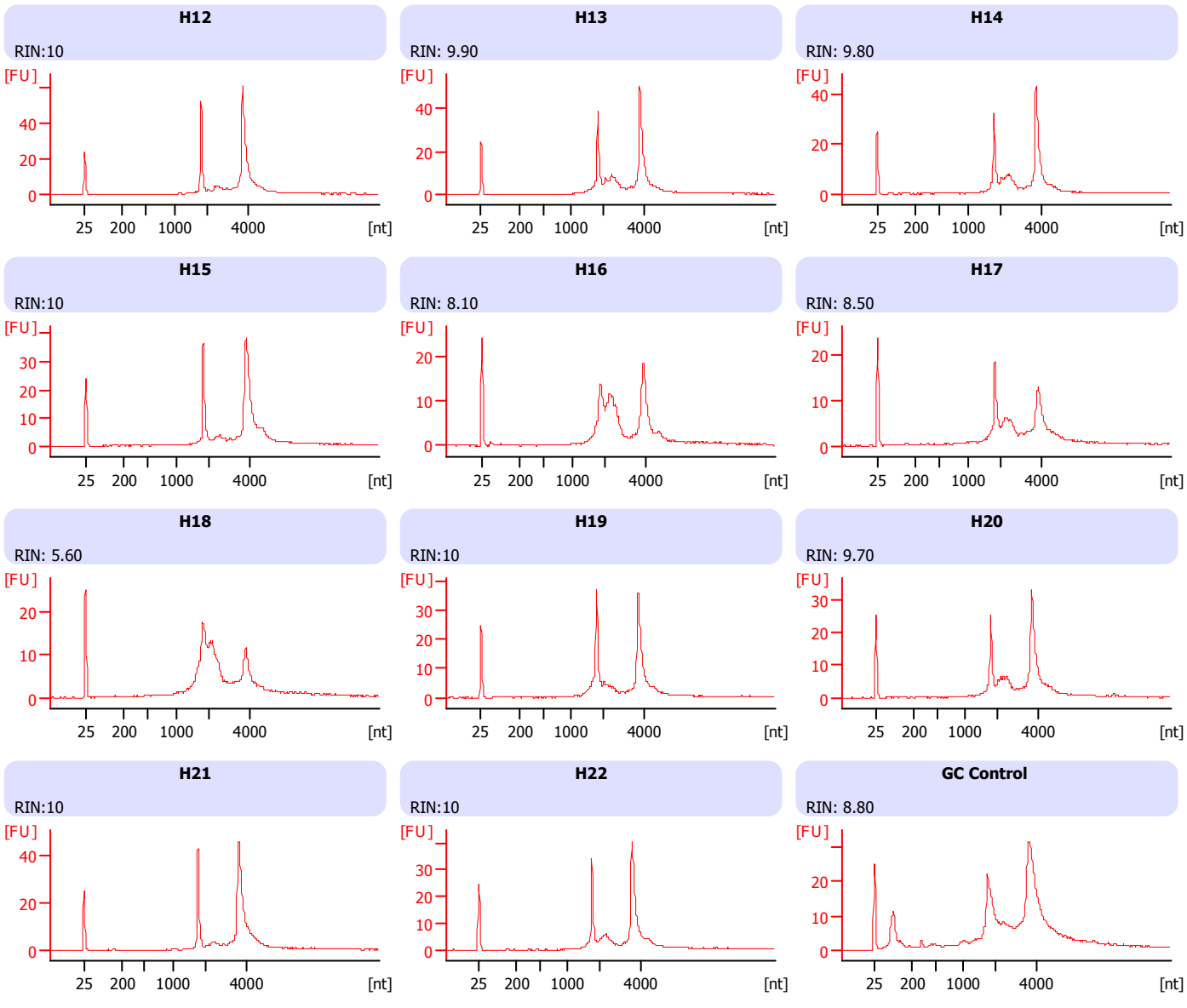

Assay Class: Eukaryote Total RNA Nano
Data Path: C:\...Data\2016-09-19\Eukaryote Total RNA Nano_2016-09-19_002.xad

Created: 19/09/2016 15:25:55
Modified: 19/09/2016 15:49:01

Electrophoresis File Run Summary (Chip Summary)

Sample Name	Sample Comment	Status	Result Label	Result Color
H12		✓	RIN:10	
H13		✓	RIN: 9.90	
H14		✓	RIN: 9.80	
H15		✓	RIN:10	
H16		✓	RIN: 8.10	
H17		✓	RIN: 8.50	
H18		✓	RIN: 5.60	
H19		✓	RIN:10	
H20		✓	RIN: 9.70	
H21		✓	RIN:10	
H22		✓	RIN:10	
GC Control		✓	RIN: 8.80	
Ladder		✓	All Other Samples	

Chip Lot #

Reagent Kit Lot #

Chip Comments :

Assay Class: Eukaryote Total RNA Nano
Data Path: C:\...Data\2016-09-19\Eukaryote Total RNA Nano_2016-09-19_002.xad

Created: 19/09/2016 15:25:55
Modified: 19/09/2016 15:49:01

Electrophoresis Assay Details

General Analysis Settings

Number of Available Sample and Ladder Wells (Max.) : 13
Minimum Visible Range [s] : 17
Maximum Visible Range [s] : 70
Start Analysis Time Range [s] : 19
End Analysis Time Range [s] : 69
Ladder Concentration [ng/µl] : 150
Lower Marker Concentration [ng/µl] : 0
Upper Marker Concentration [ng/µl] : 0
Used Lower Marker for Quantitation
Standard Curve Fit is Logarithmic
Show Data Aligned to Lower Marker

Integrator Settings

Integration Start Time [s] : 19
Integration End Time [s] : 69
Slope Threshold : 0.6
Height Threshold [FU] : 0.5
Area Threshold : 0.2
Width Threshold [s] : 0.5
Baseline Plateau [s] : 6

Filter Settings

Filter Width [s] : 0.5
Polynomial Order : 4

Ladder

Ladder Peak	Size
1	25
2	200
3	500
4	1000
5	2000
6	4000

Assay Class: Eukaryote Total RNA Nano
Data Path: C:\...Data\2016-09-19\Eukaryote Total RNA Nano_2016-09-19_003.xad

Created: 19/09/2016 16:04:16
Modified: 19/09/2016 16:27:23

Electrophoresis File Run Summary

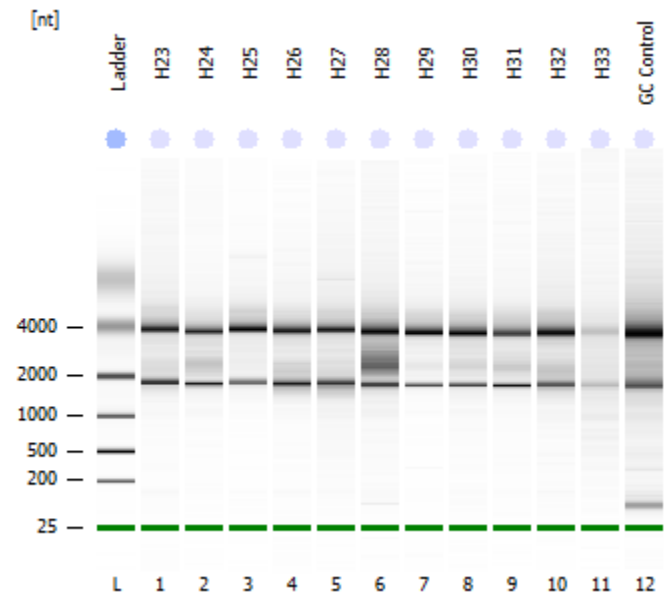

Instrument Information:

Instrument Name: DE72901262 Firmware: C.01.069
Serial#: DE72901262 Type: G2939A

Assay Information:

Assay Origin Path: C:\Program Files (x86)\Agilent\2100 bioanalyzer\2100 expert\assays\RNA\Eukaryote Total RNA Nano Series II.xsy

Assay Class: Eukaryote Total RNA Nano

Version: 2.6

Assay Comments: Total RNA Analysis ng sensitivity (Eukaryote)

Chip Information:

Chip Lot #:

Reagent Kit Lot #:

Chip Comments:

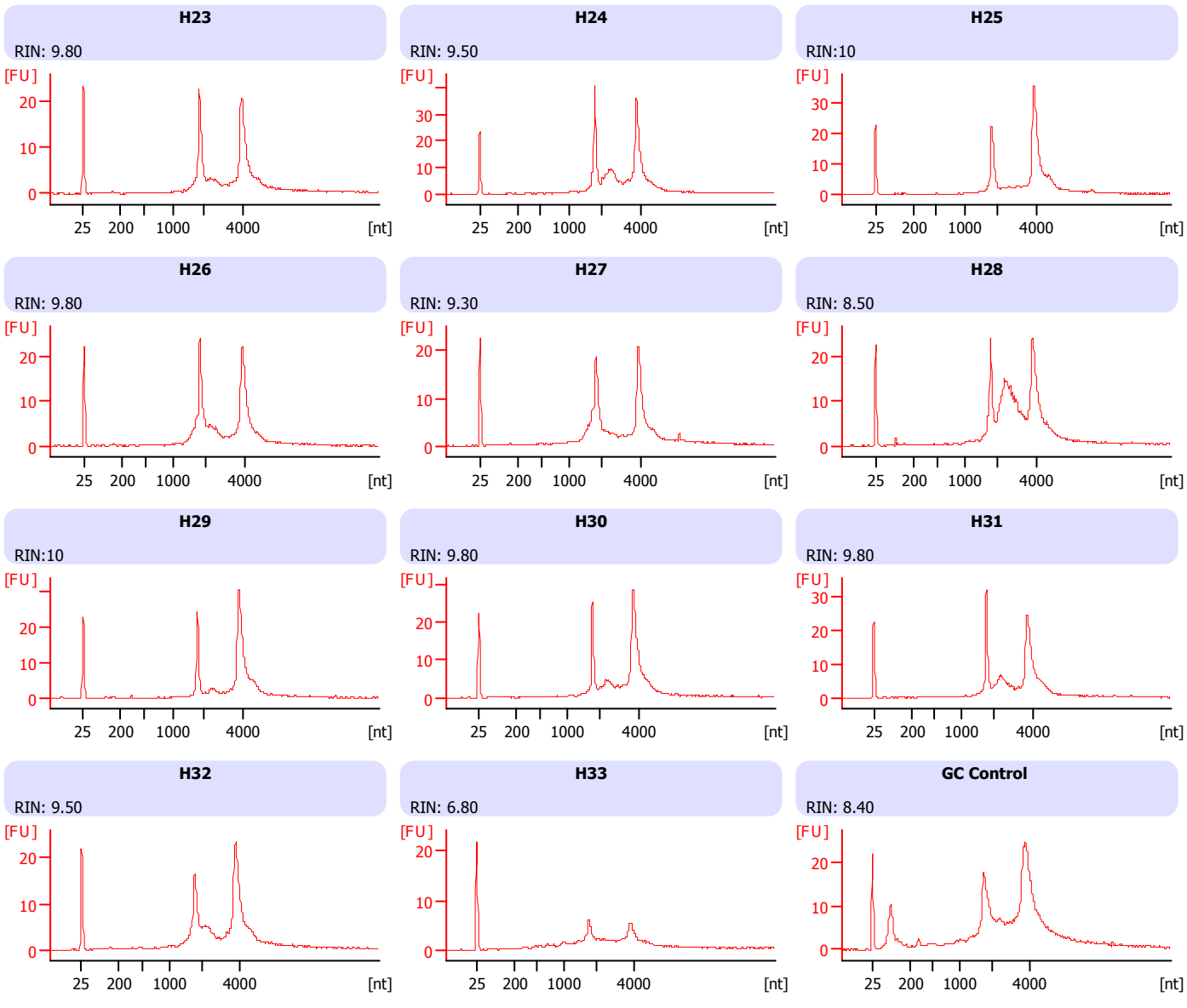

Assay Class: Eukaryote Total RNA Nano
Data Path: C:\...Data\2016-09-19\Eukaryote Total RNA Nano_2016-09-19_003.xad

Created: 19/09/2016 16:04:16
Modified: 19/09/2016 16:27:23

Electrophoresis File Run Summary (Chip Summary)

Sample Name	Sample Comment	Status	Result Label	Result Color
H23		✓	RIN: 9.80	
H24		✓	RIN: 9.50	
H25		✓	RIN:10	
H26		✓	RIN: 9.80	
H27		✓	RIN: 9.30	
H28		✓	RIN: 8.50	
H29		✓	RIN:10	
H30		✓	RIN: 9.80	
H31		✓	RIN: 9.80	
H32		✓	RIN: 9.50	
H33		✓	RIN: 6.80	
GC Control		✓	RIN: 8.40	
Ladder		✓	All Other Samples	

Chip Lot #

Reagent Kit Lot #

Chip Comments :

Assay Class: Eukaryote Total RNA Nano Created: 19/09/2016 16:04:16
Data Path: C:\...Data\2016-09-19\Eukaryote Total RNA Nano_2016-09-19_003.xad Modified: 19/09/2016 16:27:23

Electrophoresis Assay Details

General Analysis Settings

Number of Available Sample and Ladder Wells (Max.) : 13
Minimum Visible Range [s] : 17
Maximum Visible Range [s] : 70
Start Analysis Time Range [s] : 19
End Analysis Time Range [s] : 69
Ladder Concentration [ng/µl] : 150
Lower Marker Concentration [ng/µl] : 0
Upper Marker Concentration [ng/µl] : 0
Used Lower Marker for Quantitation
Standard Curve Fit is Logarithmic
Show Data Aligned to Lower Marker

Integrator Settings

Integration Start Time [s] : 19
Integration End Time [s] : 69
Slope Threshold : 0.6
Height Threshold [FU] : 0.5
Area Threshold : 0.2
Width Threshold [s] : 0.5
Baseline Plateau [s] : 6

Filter Settings

Filter Width [s] : 0.5
Polynomial Order : 4

Ladder

Ladder Peak	Size
1	25
2	200
3	500
4	1000
5	2000
6	4000

Assay Class: Eukaryote Total RNA Nano
Data Path: C:\...Data\2016-09-19\Eukaryote Total RNA Nano_2016-09-19_004.xad

Created: 19/09/2016 16:55:05
Modified: 19/09/2016 17:18:15

Electrophoresis File Run Summary

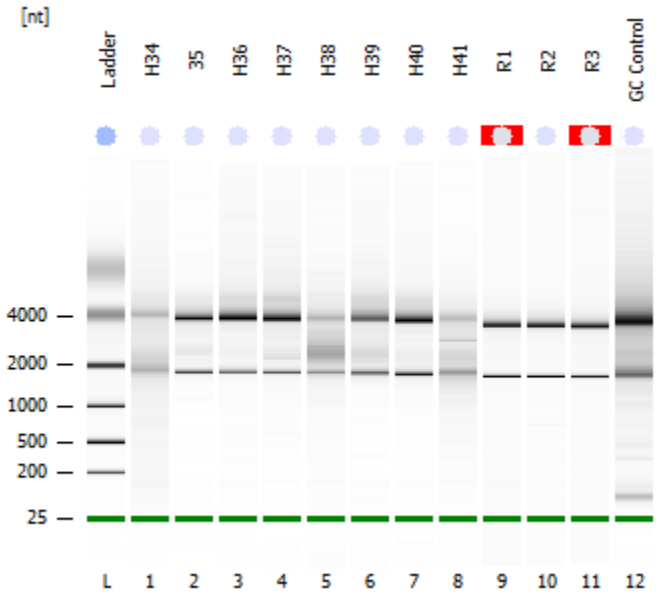

Instrument Information:

Instrument Name: DE72901262
Firmware: C.01.069
Serial#: DE72901262
Type: G2939A

Assay Information:

Assay Origin Path: C:\Program Files (x86)\Agilent\2100 bioanalyzer\2100 expert\assays\RNA\Eukaryote Total RNA Nano Series II.xsy
Assay Class: Eukaryote Total RNA Nano
Version: 2.6
Assay Comments: Total RNA Analysis ng sensitivity (Eukaryote)

Chip Information:

Chip Lot #:
Reagent Kit Lot #:
Chip Comments:

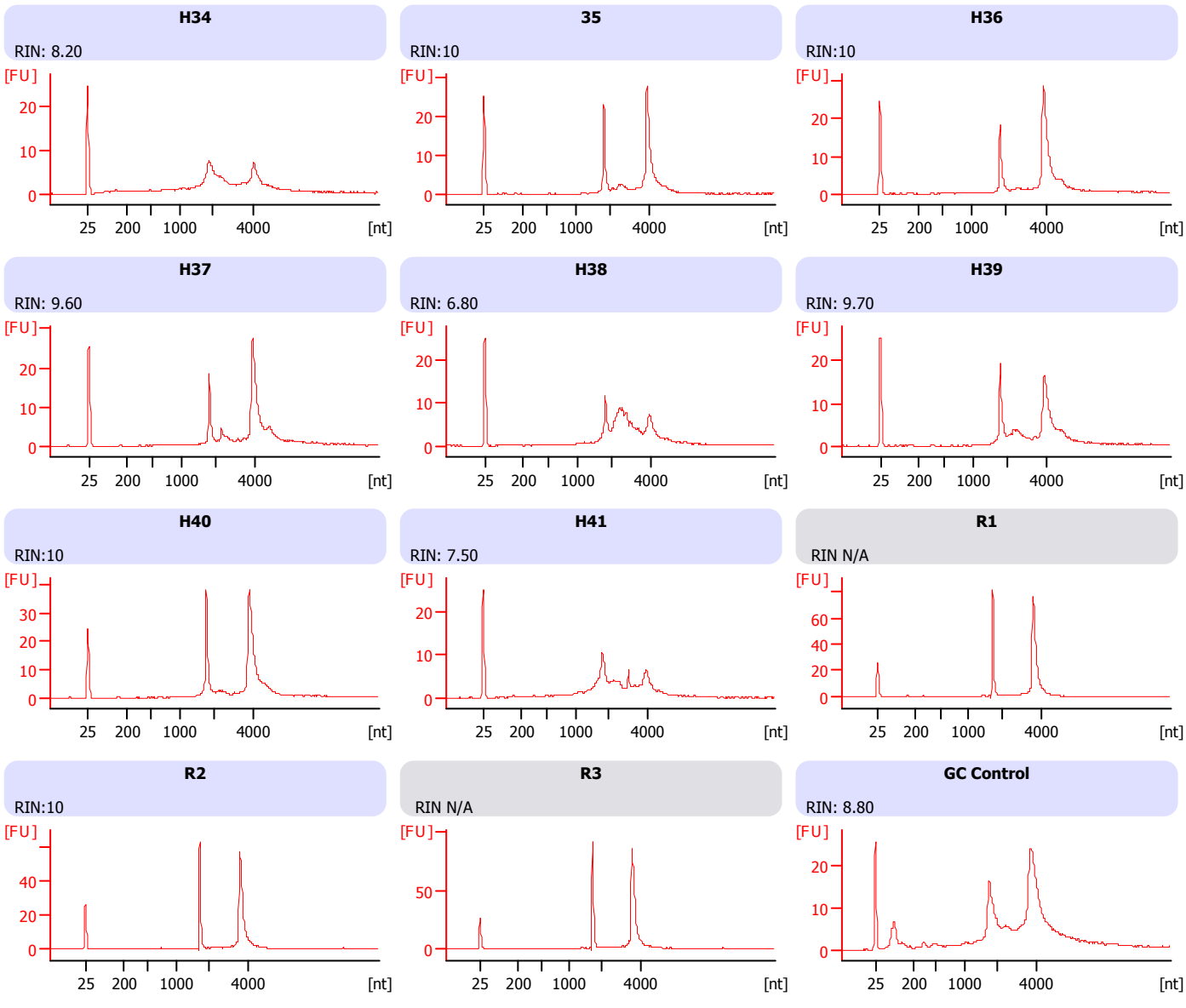

Assay Class: Eukaryote Total RNA Nano
Data Path: C:\...Data\2016-09-19\Eukaryote Total RNA Nano_2016-09-19_004.xad

Created: 19/09/2016 16:55:05
Modified: 19/09/2016 17:18:15

Electrophoresis File Run Summary (Chip Summary)

Sample Name	Sample Comment	Status	Result Label	Result Color
H34		✓	RIN: 8.20	
35		✓	RIN:10	
H36		✓	RIN:10	
H37		✓	RIN: 9.60	
H38		✓	RIN: 6.80	
H39		✓	RIN: 9.70	
H40		✓	RIN:10	
H41		✓	RIN: 7.50	
R1		✓	RIN N/A	
R2		✓	RIN:10	
R3		✓	RIN N/A	
GC Control		✓	RIN: 8.80	
Ladder		✓	All Other Samples	

Chip Lot #

Reagent Kit Lot #

Chip Comments :

Assay Class: Eukaryote Total RNA Nano Created: 19/09/2016 16:55:05
Data Path: C:\...Data\2016-09-19\Eukaryote Total RNA Nano_2016-09-19_004.xad Modified: 19/09/2016 17:18:15

Electrophoresis Assay Details

General Analysis Settings

Number of Available Sample and Ladder Wells (Max.) : 13
Minimum Visible Range [s] : 17
Maximum Visible Range [s] : 70
Start Analysis Time Range [s] : 19
End Analysis Time Range [s] : 69
Ladder Concentration [ng/µl] : 150
Lower Marker Concentration [ng/µl] : 0
Upper Marker Concentration [ng/µl] : 0
Used Lower Marker for Quantitation
Standard Curve Fit is Logarithmic
Show Data Aligned to Lower Marker

Integrator Settings

Integration Start Time [s] : 19
Integration End Time [s] : 69
Slope Threshold : 0.6
Height Threshold [FU] : 0.5
Area Threshold : 0.2
Width Threshold [s] : 0.5
Baseline Plateau [s] : 6

Filter Settings

Filter Width [s] : 0.5
Polynomial Order : 4

Ladder

Ladder Peak	Size
1	25
2	200
3	500
4	1000
5	2000
6	4000

Assay Class: Eukaryote Total RNA Nano
Data Path: C:\...Data\2016-09-20\Eukaryote Total RNA Nano_2016-09-20_001.xad

Created: 20/09/2016 15:55:50
Modified: 20/09/2016 16:27:15

Electrophoresis File Run Summary

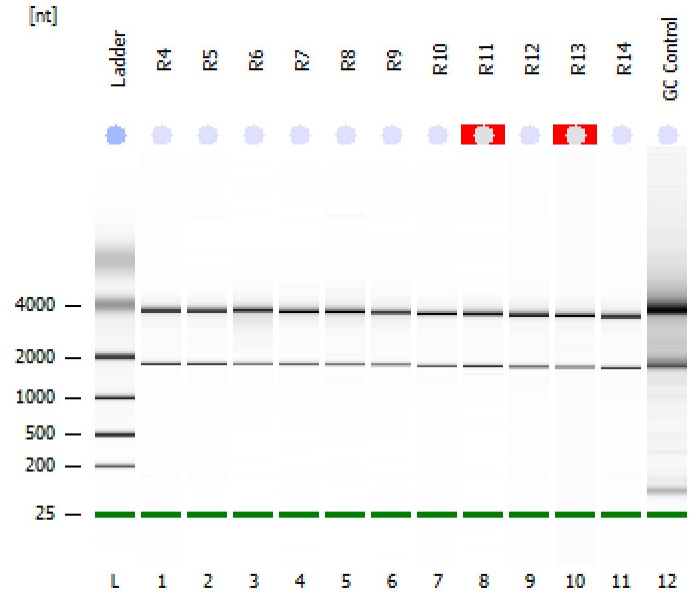

Instrument Information:

Instrument Name: DE72901262 Firmware: C.01.069
Serial#: DE72901262 Type: G2939A

Assay Information:

Assay Origin Path: C:\Program Files (x86)\Agilent\2100 bioanalyzer\2100 expert\assays\RNA\Eukaryote Total RNA Nano Series II.xsy

Assay Class: Eukaryote Total RNA Nano

Version: 2.6

Assay Comments: Total RNA Analysis ng sensitivity (Eukaryote)

Chip Information:

Chip Lot #:

Reagent Kit Lot #:

Chip Comments:

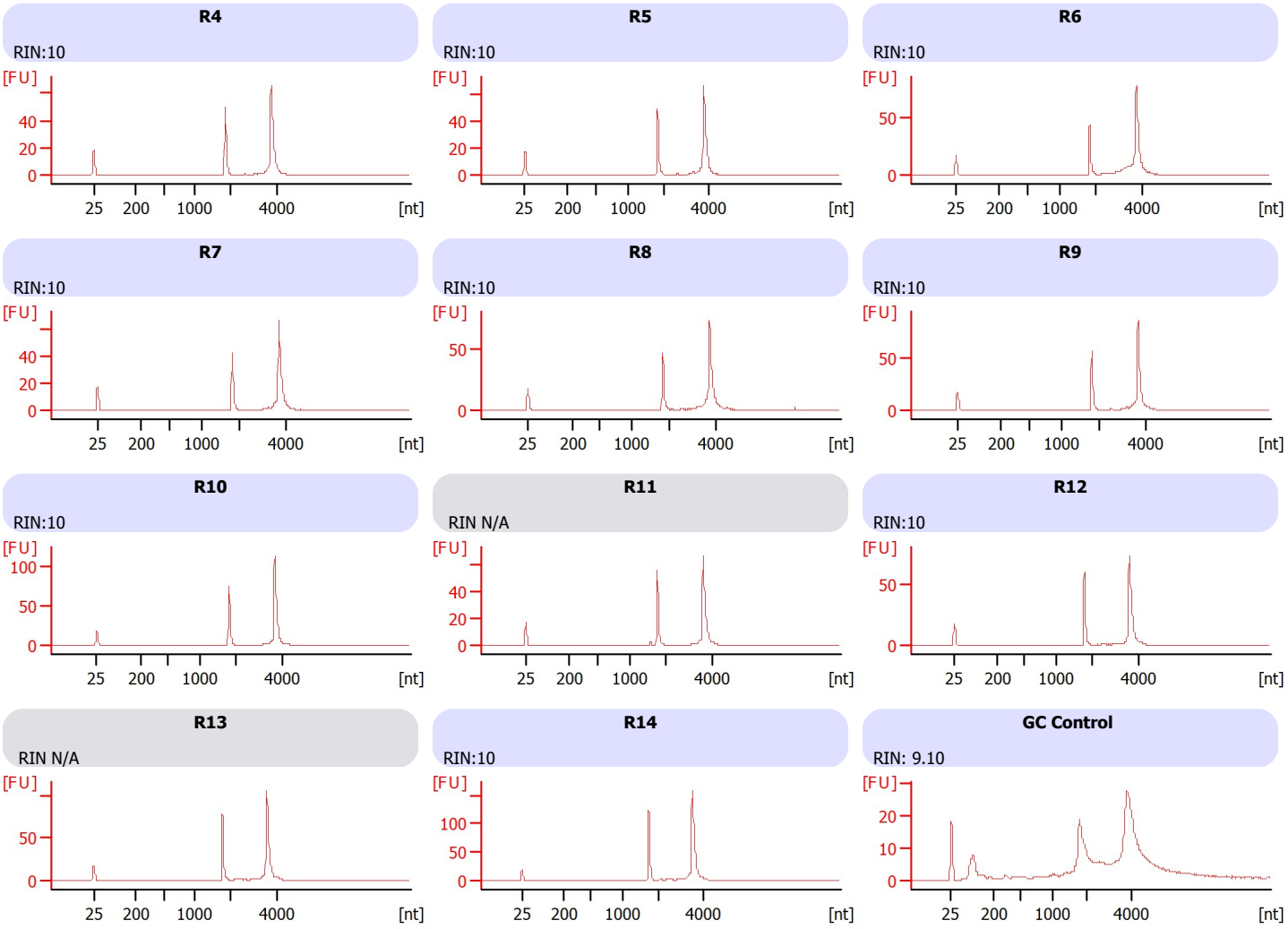

Assay Class: Eukaryote Total RNA Nano
Data Path: C:\...Data\2016-09-20\Eukaryote Total RNA Nano_2016-09-20_001.xad

Created: 20/09/2016 15:55:50
Modified: 20/09/2016 16:27:15

Electrophoresis File Run Summary (Chip Summary)

Sample Name	Sample Comment	Status	Result Label	Result Color
R4		✓	RIN:10	
R5		✓	RIN:10	
R6		✓	RIN:10	
R7		✓	RIN:10	
R8		✓	RIN:10	
R9		✓	RIN:10	
R10		✓	RIN:10	
R11		✓	RIN N/A	
R12		✓	RIN:10	
R13		✓	RIN N/A	
R14		✓	RIN:10	
GC Control		✓	RIN: 9.10	
Ladder		✓	All Other Samples	

Chip Lot #

Reagent Kit Lot #

Chip Comments :

Assay Class: Eukaryote Total RNA Nano
Data Path: C:\...Data\2016-09-20\Eukaryote Total RNA Nano_2016-09-20_001.xad

Created: 20/09/2016 15:55:50
Modified: 20/09/2016 16:27:15

Electrophoresis Assay Details

General Analysis Settings

Number of Available Sample and Ladder Wells (Max.) : 13
Minimum Visible Range [s] : 17
Maximum Visible Range [s] : 70
Start Analysis Time Range [s] : 19
End Analysis Time Range [s] : 69
Ladder Concentration [ng/µl] : 150
Lower Marker Concentration [ng/µl] : 0
Upper Marker Concentration [ng/µl] : 0
Used Lower Marker for Quantitation
Standard Curve Fit is Logarithmic
Show Data Aligned to Lower Marker

Integrator Settings

Integration Start Time [s] : 19
Integration End Time [s] : 69
Slope Threshold : 0.6
Height Threshold [FU] : 0.5
Area Threshold : 0.2
Width Threshold [s] : 0.5
Baseline Plateau [s] : 6

Filter Settings

Filter Width [s] : 0.5
Polynomial Order : 4

Ladder

Ladder Peak	Size
1	25
2	200
3	500
4	1000
5	2000
6	4000